Oxidative Medicine and Cellular Longevity

Yeast Stress, Aging, and Death

Guest Editors: Cristina Mazzoni, Sergio Giannattasio, Joris Winderickx, and Paula Ludovico

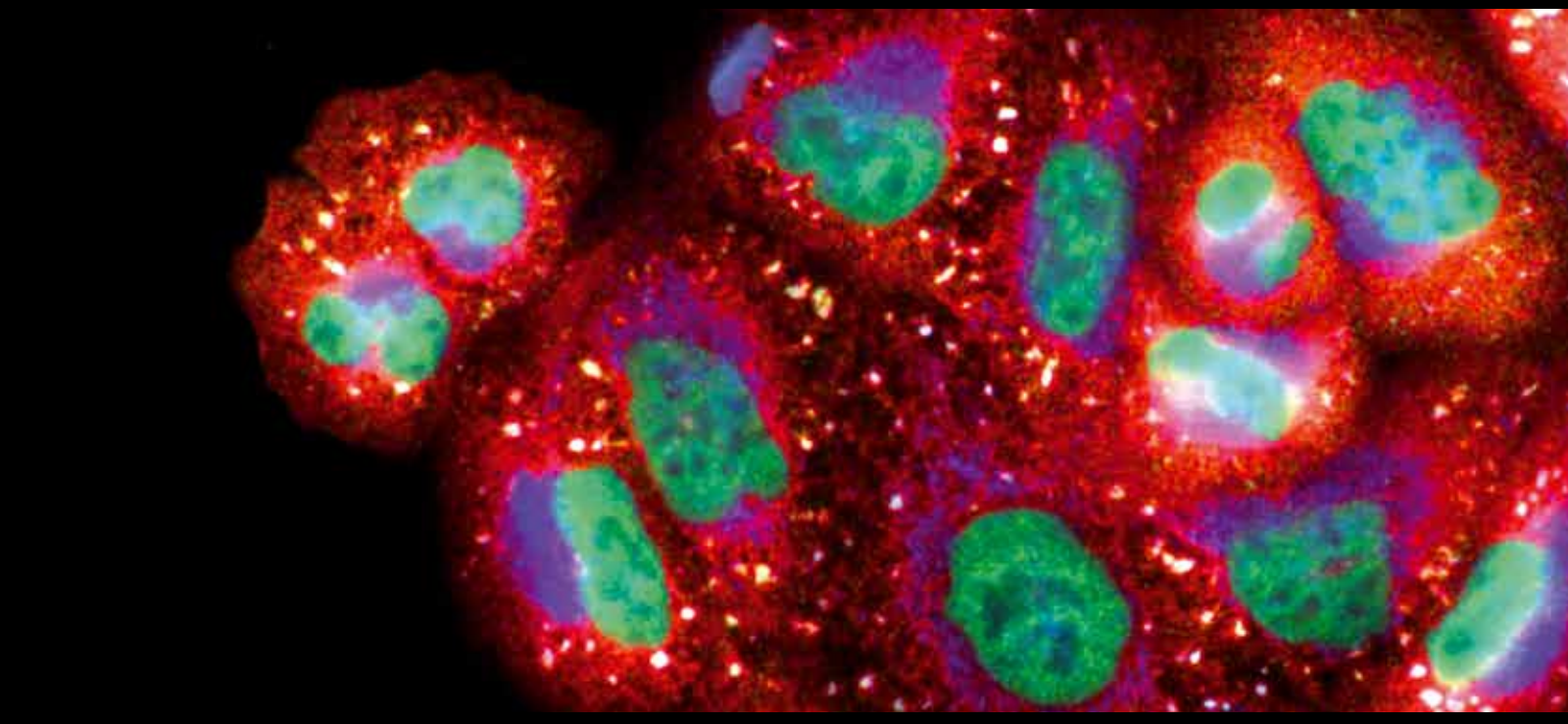

Yeast Stress, Aging, and Death

Oxidative Medicine and Cellular Longevity

Yeast Stress, Aging, and Death

Guest Editors: Cristina Mazzoni, Sergio Giannattasio, Joris Winderickx, and Paula Ludovico

Editorial Board

Contents

Hindawi Publishing Corporation
Oxidative Medicine and Cellular Longevity
Volume 2013, Article ID 684395, 3 pages
http://dx.doi.org/10.1155/2013/684395

Editorial

Yeast Stress, Aging, and Death

Cristina Mazzoni,[1] Sergio Giannattasio,[2] Joris Winderickx,[3] and Paula Ludovico[4,5]

[1] *Pasteur Institute-Cenci Bolognetti Foundation, Department of Biology and Biotechnology Charles Darwin Sapienza, University of Rome, 00185 Rome, Italy*
[2] *National Research Council-Institute of Biomembranes and Bioenergetics, Via Amendola 165/a, 70126 Bari, Italy*
[3] *Functional Biology, KU Leuven, Kasteelpark Arenberg 31, 3001 Heverlee, Belgium*
[4] *Life and Health Sciences Research Institute, School of Health Sciences, University of Minho, 4710-057 Braga, Portugal*
[5] *ICVS/3B's–PT Government Associate Laboratory, Braga, Guimarães, Portugal*

Correspondence should be addressed to Cristina Mazzoni; cristina.mazzoni@uniroma1.it

Received 7 October 2013; Accepted 7 October 2013

Until about 15 years ago, programmed cell death (PCD), at that time mainly defined as apoptosis, was believed to be a feature occurring only in metazoans to ensure proper embryonic development, cell differentiation, and regulation of the immune response. However, the discovery that single-celled organisms, such as yeast, also undergo PCD challenged this idea. Meanwhile, several key regulators and cell death executers were shown to be highly conserved in yeast and other unicellular organisms, and it is now generally accepted that at least part of the molecular cell death machinery originated early in evolution.

Approximately 31% of the yeast genes have a mammalian homologue, and an additional 30% of yeast genes show domain similarity. This, combined with the ease of manipulation of yeast and the elegance of yeast genetics, has turned this lower eukaryote into an ideal system to study more complex phenomena that occur in metazoan cells, including stress responses, mechanisms governing life span and cell death, and processes contributing to aging or human diseases like cancers and neurodegenerative disorders.

In this special issue, we collected both original research and review articles, which combined give a nice overview on the current status of the field.

Several papers relate to mitochondrial functions and mitochondrial dynamics, thereby documenting the pivotal role of this organelle in aging processes and life span determination. In their review article, Y. Liu and X. J. Chen discuss a novel form of mitochondria-induced cell death in yeast cells tentatively referred to as degenerative cell death (DCD). Mutations in the adenine nucleotide translocase (Ant) cause aging-dependent DCD in yeast, which is sequentially manifested by inner membrane stress, mitochondrial DNA (mtDNA) loss, and progressive loss of cell viability. Recent work revealed that the Ant-induced DCD is suppressed by reduced cytosolic protein synthesis, suggesting a proteostatic crosstalk between mitochondria and the cytosol, which may play an important role in cell survival during aging.

Maintenance of mtDNA is important for cell growth and survival. Oxidative damage to mtDNA causes respiratory deficiency and human disease. In higher eukaryotes, the mechanisms for maintenance and transmission of the mitochondrial genome are still elusive. However, studies using the budding yeast *Saccharomyces cerevisiae* have generated an abundance of data on how its mitochondrial genome is maintained, and many nuclear-encoded proteins of diverse functions appear to be involved. As such, mutations in TCA cycle enzyme-encoding genes lead to variable defects in mtDNA maintenance and respiratory deficiency. The most severe phenotype is caused by mutations in the *ACO1* gene encoding aconitase, which has been shown to have a novel function in mediating mtDNA maintenance by directly binding mtDNA. In this issue, Z. Liu and co-workers come with an alternative model to account for mtDNA loss due to an

*aco1*Δ mutation. On the basis of genetic evidence they found that intracellular iron-citrate complex toxicity contributes to *aco1*Δ mutant phenotypes.

Mitochondrial morphology also changes during aging and similar changes are also observed when yeast cells switch their metabolism from the use of fermentative carbon sources to nonfermentative ones and vice versa. I. W. Dawes and co-workers studied this in more detail, which led them to a correlation between carbon source availability, mitochondrial dynamics, and autophagy. In particular, they show that increasing autophagy prevents mitochondrial fragmentation and that this relates directly to the determination of life span.

F. F. Severin and co-workers provide an overview and discussion on the role and delicate balance between mitochondrial fission and fusion events as an ingenious mechanism for the removal of defective mitochondria, a topic which directly links to the pathophysiological role of mitochondrial dynamics.

It is well known that genotoxic stress contributes to aging. Also, changes in the organization of chromatin are of particular importance. In their research paper, G. Miloshev and co-workers examined the role of the linker histone Hho1 on chromatin organization and found this histone to be essential for the maintenance of the chromatin loop structures during chronological aging.

Significant progress has also been made in understanding how metabolism impacts on aging and the determination of life span. In an interesting study, M. Barile and co-workers investigated the potential metabolic regulation of FAD by metabolites such as NAD, and they propose a novel role of mitochondrial NAD redox status in regulating FAD homeostasis in yeast.

M. J. Sousa and co-workers report that ammonium ion shortens the chronological life span (CLS) of *S. cerevisiae* cells when they are starved for different auxotrophy-complementing amino acids (leucine, lysine, and histidine). Interestingly, this effect of ammonium is mediated through different pathways depending on the amino acid that is missing. Therefore, this study provides interesting new insights on the underlying signalling network and as such gives new clues for the development of environmental interventions that extend CLS or for the identification of new therapeutic targets in diseases associated with hyperammonemia.

M. Vai and co-workers show that products of acetic acid and ethanol metabolism, rather than the compounds themselves, influence CLS. In particular, they show that inhibition of ethanol metabolism by pyrazole prevents CLS.

J. A. Bárcena and colleagues address two critical processes within the cell, that is, heme biosynthesis and the nonoxidative part of the pentose phosphate pathway (PPP). Particularly, the authors investigated the key enzymes uroporphyrinogen decarboxylase (Hem12p) and transketolase (Tkl1p) and proposed a redox control mechanism for heme biosynthesis that might be important in the context of tumour progression.

K. F. Cooper and colleagues reveal that Mtl1, a cell wall stress sensor protein that activates the cell wall integrity pathway (CWI) upon exposure to hydrogen peroxide, plays an important role in the pathways leading to destruction of cyclin C, which is involved in PCD.

S. Colombo and co-workers further investigated the involvement of the Ras proteins in PCD. They found that Ras-GFP relocalizes to mitochondria after abrogation of the glycolytic enzyme hexokinase 2. As this renders yeast cells more susceptible to acetic acid, their data suggest that this enzyme confers protection against apoptosis in *S. cerevisiae*.

R. Schaffrath and co-workers investigated how ceramides trigger stress responses in yeast. Besides being building blocks for complex sphingolipids in the plasma membrane, ceramides are known to play a crucial role in the regulation of cell proliferation and apoptosis. Here, the authors describe a novel Sit4-dependent regulatory mechanism in the ceramide stress response.

That metabolic changes play a crucial role not only at the cellular level, but also at the level of colonies is nicely documented in an elegant study by Z. Palkova and co-workers. Colonies represent a well-structured and differentiated multicellular community. During aging, cells within the colony produce ammonia as signal for metabolic reprogramming to support long term survival. Here, the authors reveal that aging giant colonies and rapidly developing microcolonies pass through similar developmental phases, which indicates that the age of colony is not crucial for colony differentiation.

Finally, three papers report how yeast can be used as a model to study human disease or to screen for drugs and decipher their mode of action.

V. Franssens and co-workers present an elegant review on the benefits of using humanized yeast models to study fundamental aspects related to protein folding diseases. The authors discuss the most important findings and recent advances that assign new roles for cell wall integrity signaling, Ca^{2+} homeostasis, mitophagy, and cytoskeleton-mediated transport processes in the pathobiology underlying Parkinson's disease.

The research article by K. Thevissen and colleagues demonstrates a role for superoxide dismutases in governing tolerance of the pathogenic yeast *Candida albicans* to the antifungal drug Amphotericin B.

The review article by G. Farrugia and R. Balzan illustrates how yeast research contributes to our understanding of the proapoptotic effects and the mode of action of traditional novel nonsteroidal anti-inflammatory drugs such as aspirin. The authors give an overview of the various proapoptotic pathways activated by these drugs and show the remarkable similarity of the effects triggered in yeast and mammalian cells.

In the opinion of the editors, the contributions published in this special issue highlight many novel features on the interplay between metabolism, stress responses, aging, and PCD pathways and how this determines the life span of yeast cells. Insight into the matter is not only important to better understand fundamental aspects of yeast physiology, but it is also of direct relevance in the context of human health, as nicely documented in several reviews.

Acknowledgments

We, the editors, are convinced that the different contributions shaped this special issue into an interesting and informative document for the readers and explicitly want to thank all authors for sharing their data and ideas.

Cristina Mazzoni
Sergio Giannattasio
Joris Winderickx
Paula Ludovico

Hindawi Publishing Corporation
Oxidative Medicine and Cellular Longevity
Volume 2013, Article ID 320823, 15 pages
http://dx.doi.org/10.1155/2013/320823

Research Article

The Cell Wall Sensors Mtl1, Wsc1, and Mid2 Are Required for Stress-Induced Nuclear to Cytoplasmic Translocation of Cyclin C and Programmed Cell Death in Yeast

Chunyan Jin,[1] Andrey V. Parshin,[2] Ira Daly,[3] Randy Strich,[1] and Katrina F. Cooper[4]

[1] *Department of Molecular Biology, Graduate School of Biomedical Sciences, Rowan University, Stratford, NJ 08055, USA*
[2] *Department of Cell Biology, Graduate School of Biomedical Sciences, Rowan University, Stratford, NJ 08055, USA*
[3] *Quintiles Transnational Corp., Morris Plains, NI 07950, USA*
[4] *Department of Molecular Biology, Graduate School of Biomedical Sciences, Rowan University, Two Medical Center Drive, Stratford, NJ 08084, USA*

Correspondence should be addressed to Katrina F. Cooper; cooperka@rowan.edu

Received 11 June 2013; Revised 14 August 2013; Accepted 16 August 2013

Academic Editor: Cristina Mazzoni

Mtl1 is a member of a cell wall sensor family that monitors cell wall integrity in budding yeast. In response to cell wall stress, Mtl1 activates the cell wall integrity (CWI) MAP kinase pathway which transmits this signal to the nucleus to effect changes in gene expression. One target of the CWI MAP kinase is cyclin C, a negative regulator of stress response genes. CWI activation results in cyclin C relocalization from the nucleus to the cytoplasm where it stimulates programmed cell death (PCD) before it is destroyed. This report demonstrates that under low oxidative stress conditions, a combination of membrane sensors, Mtl1 and either Wsc1 or Mid2, are required jointly to transmit the oxidative stress signal to initiate cyclin C destruction. However, when exposed to elevated oxidative stress, additional pathways independent of these three sensor proteins are activated to destroy cyclin C. In addition, *N*-glycosylation is important for Mtl1 function as mutating the receptor residue (Asn42) or an enzyme required for synthesis of *N*-acetylglucosamine (Gfa1) reduces sensor activity. Finally, combining *gfa1-1* with the cyclin C null allele induces a severe synthetic growth defect. This surprising result reveals a previously unknown genetic interaction between cyclin C and plasma membrane integrity.

1. Introduction

The yeast cell wall is the first level of defense against environmental stress. Embedded in this cell wall are sensors that detect damage and transduce this signal to the nucleus to change gene expression. In addition, this stress signal must then be disseminated throughout the cell to elicit changes in organelle function and morphology. For example, exposure to oxidative stress induces the transcription of protein chaperones and antioxidant enzymes, alters ribosome assembly in the nucleolus, and triggers extensive fragmentation of the mitochondria [1]. All three examples help inform the cell on deciding whether to arrest cell growth and repair the damage or execute the programmed cell death pathway.

In yeast, the cell wall integrity pathway (CWI) responds to a variety of stresses, including oxidative stress [2], heat shock [3], and any other stress that alters the cell wall integrity. In brief, the CWI pathway senses the stress via a family of cell-surface sensors (Wsc1, Mid2, and Mtl1 [4]). These sensors transmit the stress to a small G protein Rho1, which in turn activates protein kinase C (Pkc1). The activated Pkc1 transmits the intracellular signals to the MAPK Slt2/Mpk1 via the MAPK module (see Figure 1(a)). Finally, the transcription factors (Rlm1, Swi4/Swi6) regulating the corresponding gene expression act as the output of the CWI pathway (Figure 1(a) and reviewed in [5]). In addition, oxidative stress activation of this pathway triggers the Slt2-dependent cytoplasmic translocation and consequent degradation of cyclin C [6, 7].

The cell wall sensor proteins are members of either the Mid2 or Wsc subfamily [4]. The Wsc sensor subfamily includes Wsc1, the main Wsc senor [8], Wsc2, and Wsc3 [9].

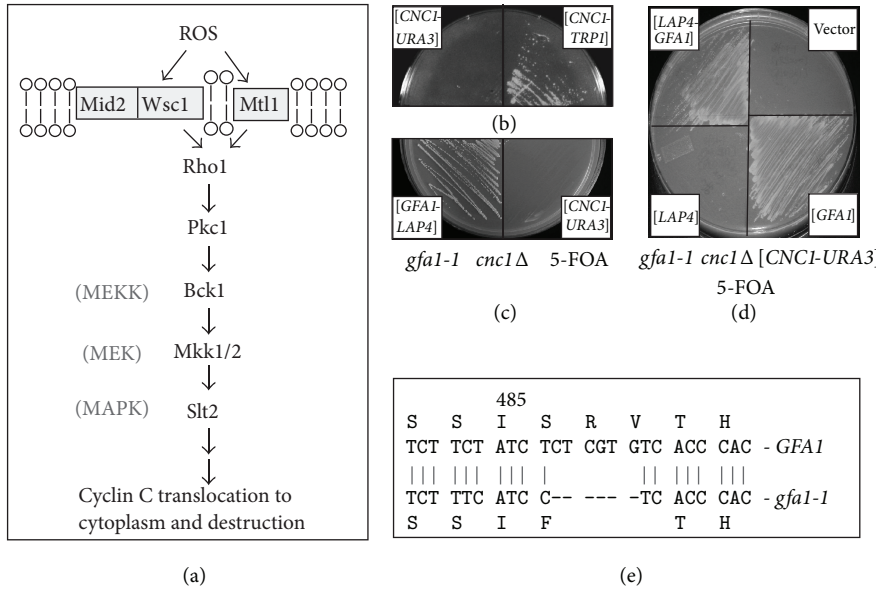

Figure 1: Negative synthetic growth defect in a *cnc1*Δ *gfa1-1* mutant. (a) Model of the cell wall signaling pathway that regulates cyclin C cytoplasmic translocation and consequent degradation. Adapted from [5] and data presented in [6, 7, 25] and this report. (b) An isolate following EMS mutagenesis harboring either a *URA3* (left half) or *TRP1* (right half) marked *CNC1* expression plasmid was streaked on medium containing 5-FOA. (c) and (d) The *gfa1-1 cnc1*Δ double mutant strain was transformed with the indicated plasmids then streaked on 5-FOA medium. All plates were incubated for 3 days at 30° before the image was taken. (e) Sequence analysis of the *gfa1-1* allele is shown. The six nucleotide deletion is indicated by the hash marks. The predicted amino acid sequences for the wild type and *gfa1-1* encoded proteins are indicated in single amino acid code.

The Mid2 subfamily contains Mid2 and Mtl1 that shares 50% homology with Mid2 [10]. Although these cell wall sensors share structural similarity, their sequences are not conserved. The Wsc subfamily contains an N-terminal cysteine-rich region, termed the CRD domain, which is not present in Mid2 or Mtl1. The CRD domain transiently interacts with the glucan chains in the cell wall, while the transmembrane domain anchors the sensor in the plasma membrane. In response to cell wall stress, the glucan chains are stretched, exerting a force on the nanospring-like Ser/Thr-rich domain. This results in a conformational change within the cytoplasmic domain, which triggers the interaction with Rom2 and activates the downstream signaling cascade (reviewed in [11]). Intermolecular interactions of the CRD domains promote sensor clustering, with a concomitant increase of the downstream signaling. This local accumulation enhances the stress signal and the cellular response [12].

Posttranslational modification is required for proper function of these cell wall sensors. The *N*-glycosylation of Asn35 is required for Mid2-dependent Slt2 activation [13]. However, this modification is not necessary for deposition of Mid2 to the plasma membrane suggesting that glycosylation is important for the protein to initiate the stress signal. The production of UDP-*N*-acetyl-D-glucosamine (UDP-GlcNAc), a building block for *N*- and *O*-linked glycosylation, as well as the formation of GPI-anchors and chitin (reviewed in [14]) is controlled by both extra- and intracellular cues. For example, *GFA1,* which encodes glutamine fructose-6-phosphate aminotransferase, an enzyme that catalyzes the first and rate-limiting step in UDP-GlcNAc production, is regulated in response to mating pheromones [15], cell cycle progression [16, 17], and cell wall damage [18]. Defects in this pathway result in hypersensitivity to cell wall damage induced by heat shock [19] or spore wall morphogenesis [20]. Defects in glycosylation also result in cell death [21, 22] via Kex1, a protease involved in programmed cell death induced by acetic acid or chronological aging [23]. These results suggest an intimate relationship between glycosylation, stress signaling, and the execution of cell death programs in yeast.

The mechanisms underlying transcription factor activation by signal transduction pathways have garnered much of the attention when studying how exogenous cues are converted into changes in the gene expression program [24]. The other side of the coin, that is, removal of repressor proteins, is not as well understood. In budding yeast, repression of many stress response genes (SRG) including the *HSP70* member *SSA1* [25], *CIT1,* and *DDR2* [6] is mediated by the cyclin C-cyclin-dependent kinase 8 (Cdk8) module [26, 27]. This complex associates with the mediator component of the RNA polymerase holoenzyme and plays both a positive and negative roles in transcription depending on the specific locus [28–30]. Unlike cyclins that regulate the cell cycle, cyclin C levels do not vary significantly during the cell cycle in yeast or human cells [25, 31]. To relieve cyclin C-Cdk8-dependent repression in yeast, cyclin C is destroyed by a Not4-dependent process in cultures subjected to a variety of stressors [6]. Before it is destroyed, cyclin C (but not Cdk8) translocates to the cytoplasm [6] where it is required for stress-induced mitochondrial hyperfission (unpublished data; K. F. Cooper, S. Khakhina, S. K. Kim, and R. Strich).

Table 1: Yeast strains used in this study.

Strain	Genotype	Source
RSY10[a]	*MAT***a** *ade2 ade6 can1-100 his3-11, 15 leu2-3, 112 trp1-1 ura3-1*	[41]
W303-1B[b]	*MAT*$\boldsymbol{\alpha}$ *ade2 can1-100 his3-11, 15 leu2-3, 112 trp1-1 ura3-1*	[42]
RSY391[a]	*cnc1::LEU2*	[25]
RSY397[b]	*cnc1::LEU2*	This study
RSY1543[b]	*cnc1::LEU2 gfa1-1*	This study
RSY1539[a]	*chs3::KANMX4*	This study
RSY1538[b]	*mid2::HIS3*	This study
RSY1547[a]	*wsc1::KANMX4 mid2::HIS3*	This study
RSY1659[a]	*MTL1-3HA::HIS3*	This study
RSY1608[a]	*cnc1::LEU2 mtl1::TRP1*	This study
RSY1660[a]	*mtl1::HIS3*	This study
RSY1661[b]	*cnc1::LEU2 gfa1-1 MTL1-3HA::TRP1*	This study
RSY1707[b]	*wsc1::KANMX4 mid2::HIS3 mtl1::TRP1*	This study
RSY1844[b]	*wsc1::KANMX4 mid2::HIS3 pGAL-MTL1*	This study

[a]Genotype: *MAT***a** *ade2 ade6 can1-100 his3-11, 15 leu2-3, 112 trp1-1 ura3-1.*
[b]Genotype: *MAT*$\boldsymbol{\alpha}$ *ade2 can1-100 his3-11, 15 leu2-3, 112 trp1-1 ura3-1.*

Mitochondrial hyper-fission is a conserved hallmark of the stress response in higher eukaryotes [32–34] as well as yeast [35–37] (see [38] for review). In many examples, mitochondrial fission is an early event in the PCD pathway [39, 40]. Thus, the resistance to ROS-induced programmed cell death (PCD) exhibited by cyclin C null cells [6, 7] is likely due to a defect in the extensive mitochondrial fragmentation associated with cellular damage. These results indicate that the normal cellular response to oxidative stress requires the proper function of cell wall sensors that transduce the signal to the nucleus to mediate translocation of cyclin C to the cytoplasm. This study connects a complex sensor system requiring proper *N*-glycosylation through Gfa1 function to cyclin C relocalization, destruction, and programmed cell death.

2. Materials and Methods

2.1. Yeast Strains, Plasmids, and Cell Culturing Conditions. The strains used in this study are listed in Table 1 and most are derived from W303-related strains RSY10 (*MAT***a** *ade2 ade6 can1-100 his3-11, 15 leu2-3, 112 trp1-1 ura3-1*) [41] or W303-1B [42]. In accordance with the Mediator nomenclature unification effort [43] cyclin C *(SSN8/UME3/SRB11)* and *Cdk8 (SSN3/UME5/SRB10)* we will use *CNC1* and *CDK8* gene designations, respectively. *KANMX4* deletion strains were constructed by integrating the PCR amplified *KANMX4* deleted alleles obtained from the Research Genetics deletion strain collection. Deletion alleles using other auxotrophic markers or the Mtl1-3HA and *pGAL-MTL1* strains were constructed using gene replacement methodology [44]. The *cnc1*Δ strains have been previously described [25]. All primers used are listed in Table 2. Details about the plasmids used in this study can be found in Table 3. The *CNC1* ORF was tagged with one copy of the myc epitope placed immediately downstream of initiator methionine and creates a functional protein [25]. The functional YFP-cyclin C fusion expression plasmid construct (pBK37) was made by replacing the GFP allele in the functional GFP-cyclin C construct, pBK1 [6] with PCR amplified YFP. pID301 was created in two steps. First, a 2.5 kbp *Eco*R1 fragment containing the *CNC1* minimal subclone [25] was cloned into *Eco*R1 digested pRS316 [45] to form pKC311. Second, *ADE2* was inserted into pKC311 by cloning the *Bam*HI fragment from pAZ11 [46] into *Bgl*II cut pKC311 to form pID301. pJB323 was made by cloning the *CNC1* minimal subclone that contains its own promotor and terminator sequences into *ECOR1* cut pRS314 [45]. Further details are available upon request. The 3HA-tagged *MTL1* plasmids (pCJ3 and pCJ4) were made by PCR amplification using Phusion Taq (Denville Scientific) of the chromosomally tagged *MTL1* ORF, promotor and terminator from RSY1659. The PCR fragment was cut with *Sac*II and *Eco*R1 and the resulting fragment cloned into pRS423 or pRS426 [45], respectively, digested with the same enzymes. The $MTL1^{N42A}$ and $MTL1^{N547A}$ constructs were generated using site-directed mutagenesis on pCJ3 or pCJ4 according to the manufacturers direction (Stratagene) with oligonucleotides listed in Table 2. The remaining plasmids were gifts: pYO964 containing hyperactive *RHO1* allele (*G19V*) was provided by Y. Ohya. *BCK1-20* containing the constitutively active *BCK1* allele and the *SLT2*-HA expression plasmids were from D. Levin. Cells were grown in either rich, nonselective medium (YPDA) or synthetic minimal medium (SC) to allow for plasmid selection as previously described [25]. Galactose inducible gene expression was achieved by adding galactose (2% final concentration) to cultures grown in SC with raffinose as a carbon source.

2.2. Synthetic Lethality Screen. The colony color-sectoring method was used as previously described [47]. Strain (RSY397, *ade2 cnc1::LEU2 ura3*) harboring the *CNC1* gene on a plasmid with the *ADE2* and *URA3* selectable markers (pID301) was grown to midlog phase (8×10^6), mutagenized with ethylmethane sulfonate (EMS) as previously

Table 2: Primers used in this study.

Name	Mutation created	Oligonucleotide
MID2 F1	*mid2*Δ	5′ TCGTTGAAGATTGGACATATAAAATACGCAAATCATAGTCGGATCCCCGGGTTAATTAA 3′
MID2 R1	*mid2*Δ	5′ AGGAATGAAAAGTAGCCATAAGCACTAAATGATATCAATGAATTCGAGCTCGTTTAAAC 3′
WSC1 F	*wsc1*Δ	5′ GTA AAC TCG ACC AGG CAC 3′
WSC1 R	*wsc1*Δ	5′ TATATCGTCTTTCAACGCGG 3′
MTL1 F1	*mtl1*Δ	5′ TTAACTTACTCCCAGTTAGTATAATATAAGTAGTTAAGGTCGGATCCCCGGGTTAATTAA 3′
MTL1 R1	*mtl1*Δ	5′ TTAAGAAGAAAAGTTATGGCAAAGCTGCTTTCGCTATGATGAATTCGAGCTCGTTTAAAC 3′
MTL1 F2	*MTL1-3HA*	5′ TATTACACGAAACCAAACAACGGCTTAAATATCACGAACTATCGGATCCCCGGGTTAATTAA 3′
MTL1 F4	*PGAL-MTL1*	5′ TTTAAACACTTCTAGTTCATTTCGGGTTGGTTCGATCTTGGAATTCGAGCTCGTTTAAAC 3′
MTL1 R2	*PGAL-MTL1*	5′ TTGAAGCAGAGCTCTTCTTCCTGGTCGGATTGCAGCTTGCCATTTTGAGATCCGGGTTTT 3′
N42A-F	$Mtl1^{N42A}$	5′ GCAGGAGTTGGTTCCAGCTGCTAGCACAACATCGAGCAC 3′
N42A-R	$Mtl1^{N42A}$	5′ GTGCTCGATGTTGTGCTAGCAGCTGGAACCAACTCCTGC 3′
N547A-F	$Mtl1^{N547A}$	5′ GAAACCAAACAACGGCTTAGCTATCACGAACTATTAAATC 3′
N547A-R	$Mtl1^{N547A}$	5′ GATTTAATAGTTCGTGATAGCTAAGCCGTTGTTTGGTTTC 3′
KCO1234	Amplify *gfa1-1*	5′ CGCTTACAAGAAAGCATTC 3′
KCO1235	Amplify *gfa1-1*	5′ GTCTAATTTAGGGCTGCAAC 3′

Oligonucleotides used in this study with their accompanying mutation identified.

Table 3: Plasmids used in this study.

Plasmid name	Gene	Epitope tag	Marker	Promotor	2μ or CEN	Reference
pYO964	$RHO1^{G19V}$	No	*URA3*	*ADH1*	CEN	[66]
pKC311	*CNC1*	No	*URA3*	*CNC1*	CEN	This study
pKC800	*GFA1* and *LAP4*	No	*TRP1*	*GFA1* and *LAP4*	CEN	This study
pKC811	*LAP4*	No	*TRP1*	*LAP4*	CEN	This study
pKC812	*GFA1*	No	*TRP1*	*GFA1*	CEN	This study
pID301	*CNC1*	No	*URA3* and *ADE2*	*CNC1*	CEN	This study
pBK37	*CNC1*	YFP	*TRP1*	*ADH1*	CEN	This study
pLR106	*BCK1-20*	No	*HIS3*	*ADH1*	CEN	[7]
pLR337	*CNC1*	1 myc	*TRP1*	*ADH1*	CEN	[25]
MPK1-HA	*SLT2*	HA	*LEU2*	*MPK1*	2μ	[67]
pCJ3	*MTL1*	3HA	*HIS3*	*ADH1*	CEN	This study
pCJ4	*MTL1*	3HA	*URA3*	*ADH1*	CEN	This study
pCJ11	$MTL1^{N42A}$	3HA	*URA3*	*ADH1*	CEN	This study
pCJ12	$MTL1^{N42A}$	3HA	*HIS3*	*ADH1*	CEN	This study
pCJ13	$MTL1^{N547A}$	3HA	*HIS3*	*ADH1*	CEN	This study

described [41], and then plated on solid medium with limiting adenine (6 mg/mL). Colonies that were unable to lose pID301 (as demonstrated by an unsectored colony) were selected as candidates for further study. To further screen these candidates, the colonies were transferred to solid medium containing 5-fluoroorotic acid (5-FOA), an analog in the uracil biosynthetic pathway. Colonies able to lose the *CNC1* plasmid with the *URA3* gene would continue to grow. We identified thirteen colonies unable to lose the *CNC1* expression plasmid suggesting that *CNC1* was now required for growth. From this double screen, one individual (RSY1543) was chosen for further study as described in the text due to strength of the slow growth phenotype. Verification of the requirement for cyclin C was achieved by swapping pID301 for pJB323 and plating these cells on limiting adenine and 5-FOA medium. The mutant allele responsible for this synthetic phenotype was isolated by transforming RSY1543 harboring pID301 with the pRS200 (*TRP1-marked*) genomic library (ATCC 77164) and identifying cells that could grow on 5-FOA medium. Plasmid DNA (pKC800) was recovered by *E. coli* transformation from 5-FOA resistant cells that formed white colonies and retransformed back into RSY1543 to verify the complementation phenotype. pKC800 was sequenced and determined to contain two ORFS, *GFA1* and *LAP4*. pKC811 (*LAP4* ORF, promotor and terminator) and pKC812 (*GFA1* ORF promotor and terminator) were created from pKC800.

2.3. Identification of the gfa1-1 Mutation. The *gfa1-1* mutation was identified by sequencing a PCR fragment generated from the chromosomal copy of the mutant allele in strain RSY1543. In brief, yeast DNA from RSY1543 was made as previously

described [25] and amplified using KCO1234 and KCO1235 which map 200 bp upstream and 200 bp downstream of the *GFA1* ORF, respectively. This PCR fragment was then sequenced (Eurofins MWG Operon) and the results were aligned with wild type *GFA1* ORF. Further details of primers used for sequencing are available upon request.

2.4. Survival and Stress Assays. For all stress assays, cells were grown to midlog phase (6×10^6 cells/mL) and then treated with H_2O_2 or acetic acid at the concentrations described in the text. Clonogenic viability studies were conducted with midlog phase (6×10^6 cells/mL) treated with 100 mM acetic acid for 200 min and then serially diluted (1 : 10) and plated on minimal complete medium with or without plasmid selection as indicated in the text. Caspase assays were conducted with three independent cultures as described [48] except that the cells were incubated with the caspase substrate (CaspSCREEN BioVision Inc.) at 37° for 24 h in the dark. At least 20,000 cells were counted per sample. Statistical analysis was performed using the unpaired Student's *t*-test with *P* values <0.05 being considered significant.

2.5. Western Blot Analysis. Extracts prepared for analyzing myc-cyclin C levels were prepared from midlog cultures (6×10^6 cells/mL) as described previously [25] except that the lysis buffer used was 150 mM NaCl, 50 mM Tris-HCl pH 8.0, 1% NP-40, 0.15% deoxycholic acid sodium salt, 1 μg/mL pepstatin, 1 μg/mL leupeptin, and 0.2% protease inhibitor cocktail (Sigma). In brief, 500 μg of soluble extract was immunoprecipitated using either anti-myc or anti-HA antibodies (Roche), collected on agarose A beads, and then analyzed by Western blot. For monitoring Mtl1 glycosylation, a gradient acrylamide gel was used (5–10%) to allow resolution of both modified and unmodified signals on the same gel. Western blot signals were detected using goat α-mouse secondary antibodies conjugated to alkaline phosphatase (Sigma) and the CDP-Star chemiluminescence kit (Tropix). Signals were quantitated by phosphorimaging (Kodak Inc.). Half-life determinations were calculated by linear regression analysis with curves possessing r values >0.9. Relative cyclin C concentrations were standardized internally to Tub1 levels before comparing to other values. Slt2-HA phosphorylation was detected using α-phospho-p44/42 antibodies (Cell Signaling) as previously described [7]. Tub1 was visualized using α-tubulin antibodies (12G10) were obtained from the Developmental Studies Hybridoma Bank (University of Iowa).

2.6. N-Glycosylation Assay. Mtl1 *N*-glycosylation was monitored as described previously [13]. Briefly, crude membrane extracts were prepared from 250 mL midlog cultures harboring the Mtl1-3HA plasmid indicated (5×10^6 cells/mL in minimal medium). An equal volume of glass beads to the cell pellet was added, and the cells lysed with 500 μL lysis buffer (150 mM NaCl, 50 mM Tris-HCl pH 8.0, 1% NP-40, 0.15% deoxycholic acid sodium salt, 1 μg/mL pepstatin, 1 μg/mL leupeptin, and 0.2% protease inhibitor cocktail (Sigma)) by vortexing four times for 1 min (with 1 min intervals on ice). Cell debris was removed by centrifugation for 5 min at 3500 ×g at 4°C. Crude membranes were collected from the supernatant by centrifugation for 30 min at 18,000 ×g at 4°C (Beckman TLA-55 rotor) and resuspended in 100 μL lysis buffer. The crude membranes were digested with 2,500 units of Endo H (New England Biolabs) for 2 h at 37°C. Mock incubations were carried out without Endo H. Reactions were stopped by adding 3X SDS sample buffer and analyzed by Western blot.

2.7. Immunofluorescence Microscopy. Localization studies of chimeric fusion proteins were performed on cells fixed in 3.7% paraformaldehyde and stained with 4′,6-diamidino-2-phenylindole (DAPI). For all experiments, the cells were grown to midlog (5×10^6 cells/mL), treated with the H_2O_2 concentrations and timepoints indicated in the figures, and then analyzed by fluorescence microscopy. Images were obtained using a Nikon microscope (model E800) with a 60X objective (Plan Fluor Oil, NA 1.3) and a CCD camera (RETIGA Exi). Data were collected using NIS software and processed using Image Pro software. All images of individual cells were optically sectioned (0.2 μ slices at 0.6 μ spacing) and deconvolved.

3. Results

3.1. Gfa1 and Cyclin C Display a Negative Genetic Interaction. Cyclin C is a target of the cell wall integrity pathway and required for programmed cell death [7]. To identify additional components of this regulatory network, a synthetic lethality screen was undertaken (see Section 2 for details). These studies identified a mutant that was unable to grow in the presence of the counterselection drug 5-FOA when cyclin C was expressed from a plasmid containing the *URA3* selectable marker (Figure 1(b), left panel). However, introduction of *CNC1* on a plasmid with the *TRP1* selectable marker was able to lose the *URA3* based plasmid indicating the cyclin C expression was required for normal cell growth (Figure 1(b), right panel). Continued incubation of these plates did permit limited growth of the double mutant strain (data not shown). This indicates that the phenotype observed was not due to synthetic lethality but rather a severe growth defect.

To identify the gene corresponding to the mutant allele responsible for this synthetic phenotype, a genomic library was introduced into this strain and transformants were identified that were now able to grow in the absence of cyclin C. One transformant was identified that contained a genomic contig with two intact genes, *GFA1* and *APE1/LAP4* (Figure 1(c), left panel). To determine which of these genes possessed the complementation activity, plasmids were introduced into the mutant strain expressing either *GFA1* or *APE1*. This experiment revealed that *GFA1* complemented the synthetic growth phenotype (Figure 1(d)). Since *GFA1* is an essential gene, our allele (*gfa1-1*) must be hypomorphic but still possessing sufficient activity for survival. To determine the nature of this allele, DNA sequence analysis was performed on PCR products specific to the *GFA1* coding region generated from the *gfa1-1* strain. This analysis revealed a six nucleotide deletion which changed S486 to a phenylalanine

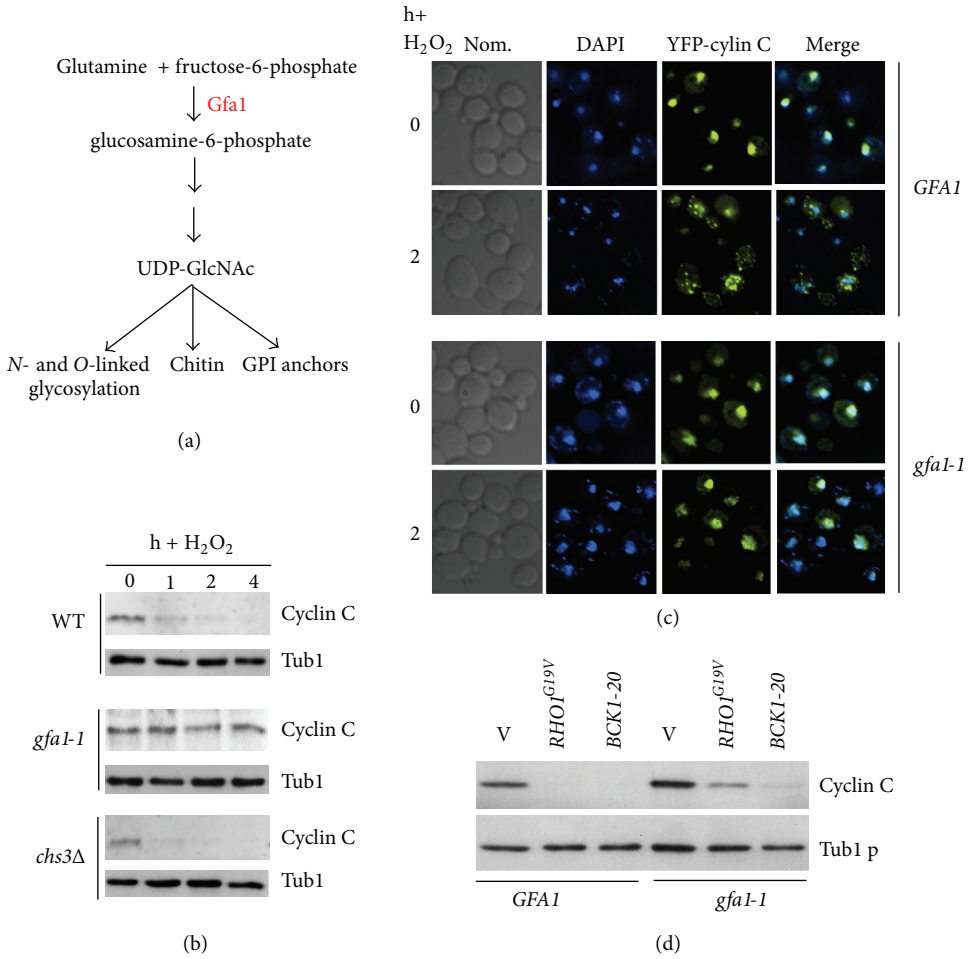

Figure 2: Gfa1 is required for cyclin C relocalization and destruction. (a) Diagram of Gfa1 functions in the cell. (b) Gfa1 is required for cyclin C destruction. Wild type (RSY10), *gfa1-1 cnc1*Δ (RSY1543), and *chs3*Δ (RSY1539) midlog phase cultures expressing myc-cyclin C (pLR337) were treated with 0.4 mM H_2O_2 for the indicated times in hours. Cyclin C levels were determined by Western blot analysis of immunoprecipitates. Tub1 levels were used as a loading control. (c) YFP-cyclin C subcellular localization was monitored in a wild type and *gfa1-1 cnc1*Δ strains harboring pBK37 before and following H_2O_2 treatment. DAPI staining was used to identify the nucleus. (d) Gfa1 functions upstream of the CWI pathway. Cyclin C levels were determined by Western blot analysis of immunoprecipitates in a midlog phase wild type (RSY10) or *gfa1-1 cnc1*Δ (RSY1543) cultures expressing myc-cyclin C (pLR337) and either a vector control (v), *BCK1-20* or $RHO1^{G19V}$. Tub1 levels were used as a loading control.

and deleted R487 and V488 (Figure 1(e)). The remainder of the protein appears unaltered. This small deletion resides in one of two sugar isomerase (SIS) domains found in many sugar binding proteins [49]. This result suggests that the small deletion in Gfa1 reduces, but does not eliminate, Gfa1 activity.

3.2. Gfa1 Is Required for Cyclin C Destruction in Response to Oxidative Stress. *GFA1* encodes an essential glutamine-fructose-6-phosphate aminotransferase that catalyzes the first step in GlcNAc biosynthesis [15]. GlcNAc is involved in several biological processes including GPI anchor formation, chitin biosynthesis, and the substrate for *N*- and *O*-linked glycosylation (Figure 2(a)). Given the established role of Gfa1 in cell wall maintenance and our previous findings that cell wall stressors induce cyclin C destruction, we next determined if Gfa1 is required for oxidative stress-induced degradation of cyclin C. A *CNC1* myc tagged allele under the control of the *ADH1* promoter was placed on a single copy plasmid and introduced into the *gfa1-1* mutant. Myc-cyclin C levels were monitored by Western blot analysis following exposure to hydrogen peroxide (0.4 mM). Compared to wild type, myc-cyclin C levels were not reduced in the *gfa1-1* strain (Figure 2(b)). These results indicate that Gfa1 is required for normal cyclin C destruction. However, chitin synthase (*CHS3*) is not required for cyclin C destruction (Figure 2(b)). Although other chitin synthases are present in the cell, *chs3* mutants display several phenotypes similar to *gfa1* mutants including spore wall assembly and temperature sensitive growth [50]. Taken together, these results suggest that Gfa1 functions other than stimulating chitin formation are involved in regulating cyclin C destruction.

Our previous report indicated that cyclin C relocalization from the nucleus to the cytoplasm was required for both cyclin C destruction and programmed cell death

execution [6]. Therefore, we next asked whether Gfa1 was also required for cyclin C relocalization. A wild type and *gfa1-1* strain was transformed with a plasmid expressing YFP-cyclin C. We have previously demonstrated that this reporter protein was functional and recapitulated normal cyclin C regulation [6]. In response to H_2O_2 treatment, YFP-cyclin C foci were observed in the cytoplasm in the wild-type strain (Figure 2(c)). However, YFP-cyclin C remained predominantly nuclear in the *gfa1-1* strain. These results indicate that Gfa1 is required for ROS-induced nuclear to cytoplasmic translocation of cyclin C.

The results just described indicate that Gfa1 is required for the oxidative stress signal to induce cyclin C relocalization and destruction. We have reported that the cell wall integrity MAP kinase pathway is necessary for this process (see Figure 1(a) and [7]). To determine if Gfa1 functions upstream or downstream of this signaling pathway, epistasis experiments were conducted. Plasmids expressing either constitutively active alleles of *RHO1* (*RHO1*^{G19V}) or *BCK1* (*BCK1-20*) were introduced into a wild type strain and the *gfa1-1* mutant. Cyclin C levels were monitored in these cultures in the absence of stress. As previously reported [7] constitutive activation of Bck1 or Rho1 (this study) can induce cyclin C destruction in the absence of stress (Figure 2(d)). A similar result was obtained in the *gfa1-1* strain. The low level retention of cyclin C in the *gfa1-1* culture expressing Rho1^{G19V} was reproducible suggesting that Gfa1 function is partially required for Rho1^{G19V}-induced cyclin C destruction. These results indicate that Gfa1 mediates stress-induced cyclin C relocalization and destruction. These results suggest that Gfa1 may regulate cyclin C destruction through glycosylation of a CWI pathway component.

3.3. Mtl1, Mid2, and Wsc1 Are Required for Cyclin C Degradation in Response to Moderate Oxidative Stress. *N*-Glycosylation is required for the proper function of Mid2, a cell wall sensor that is required to transduce the cell wall stress signal [13]. To determine which cell wall sensor (or sensors) is required to transmit the stress signal to cyclin C, we examined cyclin C levels in sensor mutants following exposure to H_2O_2 (0.4 mM). Cyclin C was protected from destruction in the *mtl1*Δ strain indicating that Mtl1 is required for this process (Figure 3(a), quantitated in Figure 3(c)). However, deleting *MID2* did not significantly alter cyclin C degradation kinetics (Figure 3(b)) suggesting that a functional specialization exists between these two members of the *N*-glucosamine modified family. Previous studies have shown that Mid2 and Wsc1 have redundant functions as oxidative stress sensors [2]. Consistent with this finding, cyclin C was not destroyed following H_2O_2 stress in *mid2*Δ *wsc1*Δ cells (Figure 2(b)) indicating that these proteins perform overlapping functions controlling cyclin C destruction. Interestingly, the prestress cyclin C levels were lower in the double mutant compared to the wild type. This observation may reflect the activation of another stress pathway that recognizes instability in the cell wall due to the loss of these sensors (reviewed in [11]) resulting in partial cyclin C destruction. A similar reduction in cyclin C levels was observed in unstressed *slt2*Δ mutants [7]. Taken together, these data suggest that two sensor groups, Mid2/Wsc1 and Mtl1, mediate H_2O_2-induced cyclin C destruction.

Previous studies indicated that the CWI MAPK Slt2 is required for H_2O_2 induced cyclin C destruction [7]. To determine if the Mid2/Wsc1 and Mtl1 sensor groups signal cyclin C destruction through Slt2, its activation was monitored by Thr and Tyr T-loop phosphorylation [51]. T-loop phosphorylation specific antibodies were used to probe Western blots of Slt2 immunoprecipitated from extracts prepared from wild type, *mtl1*Δ, or *mid2*Δ *wsc1*Δ strains before and after exposure to 0.4 mM H_2O_2. As previously reported [7] a transient elevation in phosphorylated Slt2 was detected in wild-type cells (Figure 3(d)). A similar result was obtained in the *mtl1*Δ strain while the *mid2*Δ *wsc1*Δ double mutant displayed a reduction in total Slt2 activation. To determine if both sensor groups contributed to Slt2 activation, the experiment was repeated in the *mid2*Δ *wsc1*Δ *mtl1*Δ triple mutant. This analysis revealed no detectable Slt2 phosphorylation under these conditions (Figure 3(e)). These results suggest that both Mid2/Wsc1 and Mtl1 groups are required for normal Slt2 activation in response to low-level H_2O_2 exposure.

3.4. Mtl1 Is N-Glycosylated on Asn42 in a Gfa1-Dependent Manner. Our results indicating that both Mtl1 and Gfa1 are required for ROS-induced cyclin C destruction prompted further experiments to determine if these proteins were functionally related. Given the role of Gfa1 in production of GlcNAc, we tested whether Mtl1 was *N*-glycosylated. The *MTL1* gene was tagged in the chromosome with three HA epitopes (3HA). Mtl1-3HA was immunoprecipitated and this immunoprecipitate was split and one half was treated with Endo H to remove glycosylation. Western blot analysis revealed that most of the Mtl1-3HA signal migrated at an apparent molecular weight of 56 kDa close to its predicted size (arrowhead, Figure 4(a)). A significantly slower species was also observed (open arrow) that shifted to a faster mobility upon Endo H treatment (solid arrow). The remaining high molecular weight Mtl1 species was most likely due to *O*-mannosylation. These results indicate that, as recently reported [52], Mtl1 is *N*-glycosylated. Inspection of the Mtl1 sequence for consensus *N*-glycosylation recognition sites (NxS/T, x ≠ P) revealed two motifs at Asn42 and Asn547. Site-directed mutagenesis was used to substitute alanines for these Asn residues and the experiments were repeated. Unlike the N547A mutant, Mtl1^{N47A} did not display the characteristic shift in mobility upon Endo H treatment (Figure 4(b)). These results indicate that Mtl1 is modified on N42.

Finally, Mtl1 modification was examined in the *gfa1-1* mutant. In these experiments, two differences were observed compared to the wild-type control. First, Mtl1 mobility was enhanced following PAGE in the untreated mutant extract compared to wild type (Figure 4(c), compare open and dark grey arrows). Treatment of these samples with Endo H resulted in further mobility enhancement (compare solid and light grey arrows) although to a lesser extent. These results suggest that Mtl1 is still *N*-glycosylated to some extent, most likely due to residual Gfa1-1 activity. The second result was

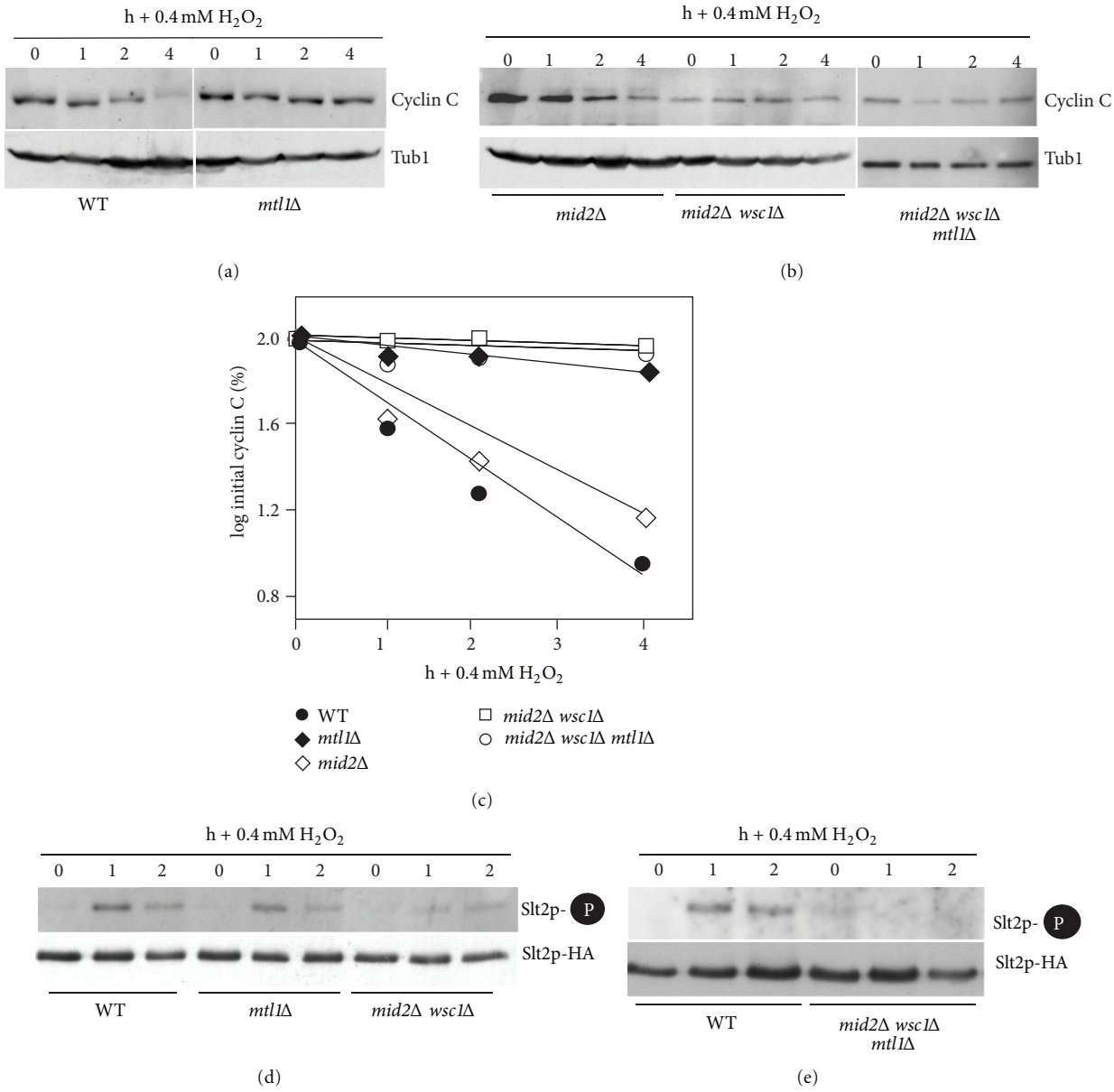

Figure 3: Mtl1 and Mid2/Wsc1 membrane sensors are required for cyclin C destruction following 0.4 mM H_2O_2 stress. (a) Wild type (RSY10) and *mtl1*Δ (RSY1660) expressing myc-cyclin C (pLR337) were grown to midlog phase (0 h) and then treated with 0.4 mM H_2O_2 for the indicated times in hours. Cyclin C levels were determined by Western blot analysis of immunoprecipitates. Tub1 levels were used as a loading control. (b) Cyclin C levels were monitored in *mid2*Δ (RSY1538), *mid2*Δ *wsc1*Δ (RSY1547), and *mid2*Δ *wsc1*Δ *mtl1*Δ (RSY1707) strains as described in (a). (c) Quantification of the results obtained in (a) and (b). (d) T-loop phosphorylation (top panel) and immunoprecipitations (bottom panel) of Slt2-HA in wild type, *mtl1*Δ, *mid2*Δ *wsc1*Δ, and (e) *mid2*Δ *wsc1*Δ *mtl1*Δ following 0.4 mM H_2O_2 treatment for the times indicated (h).

that the total amount of modified Mtl1 was reduced in the *gfa1-1* mutant with a corresponding increase in the unmodified form compared to wild-type extracts. In this experiment, twice the amount of the *gfa1-1* extract was required to visualize modified Mtl1. These results indicate that Mtl1 is *N*-glycosylated on Asn42 and that this modification requires Gfa1. In addition, the loss of Gfa1 activity reduces the steady state levels of modified Mtl1.

3.5. Mtl1 N-Glycosylation Is Required for Normal ROS-Induced PCD and Cyclin C Degradation. Previous studies have found that mutants lacking Mtl1 are hypersensitive to H_2O_2 treatment [53]. To determine whether this loss in viability was due to PCD or necrosis, an *mtl1*Δ strain was transformed with plasmids expressing wild-type *MTL1* or the vector control. Three independent transformants were grown to midlog phase and subjected to 0.4 mM H_2O_2 for 4 h. These cells were

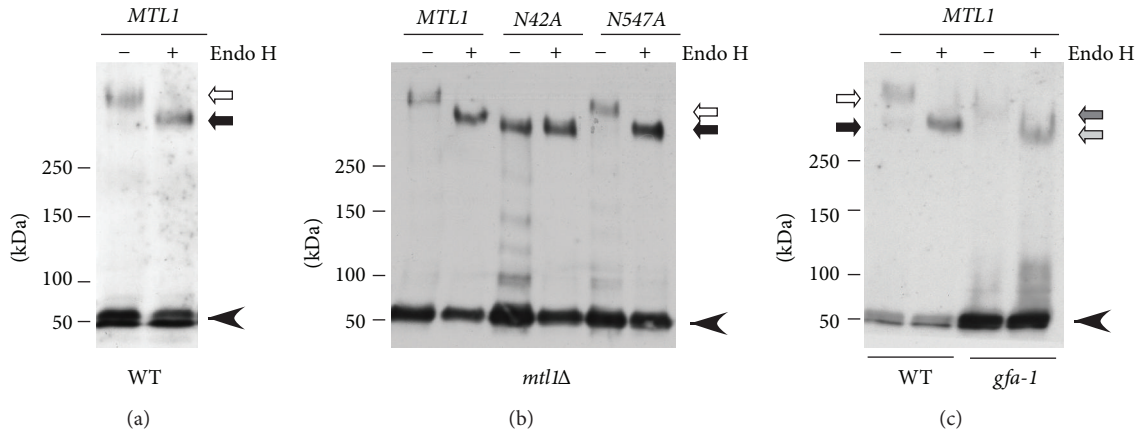

Figure 4: Mtl1 is glycosylated on Asn42. Immunoprecipitates from extracts prepared from a wild-type strain expressing Mtl1-3HA from its normal promoter were either subjected (+) or not (−) to Endo H treatment. Molecular weight standards (kDa) are given on the left. The arrowhead indicates the migration of the unmodified Mtl1-3HA. Open and closed arrows indicate modified Mtl1-3HA before and after Endo H treatment, respectively. (b) Site directed mutagenesis was used to substitute alanine for asparagine at position 42 or 547. The experiments described in (a) were repeated with the modified forms of Mtl1. (c) The experiment described in (a) was repeated with a wild type and *gfa1-1* mutant. Open and dark grey arrows indicated fully modified form in wild type and *gfa1-1* mutant, respectively. Closed and light grey arrows indicate the Endo H treated samples in wild type and the *gfa1-1* mutant, respectively.

analyzed for caspase activity using a fluorescent substrate and flow cytometry (see Section 2 for details). These studies revealed a significant increase in caspase active cells in the cells lacking *MTL1* expression (Figure 5(a)) indicating that at least a portion of the enhanced cell death observed in *mtl1*Δ mutants is due to PCD. To determine if *N*-glycosylation was required for this activity, the experiment was repeated with the *mtl1*Δ strain harboring a plasmid expressing $mtl1^{N42A}$. This study revealed an intermediate elevation in PCD compared to the wild type and the null strain values. These results suggest that loss of *N*-glycosylation reduces, but does not eliminate, Mtl1 function with respect to H_2O_2-induced PCD execution.

We next determined whether this intermediate phenotype was observed under two additional stress conditions known to induce PCD, namely, higher H_2O_2 concentrations or exposure to acetic acid. Surprisingly, exposing these cultures to higher H_2O_2 levels did not significantly change caspase activation between the three cultures. Conversely, the acetic acid treated $mtl1^{N42A}$ expressing strain exhibited similar levels of caspase activation compared to the vector control. This hypersensitivity to acetic acid was also observed in plating assays (Figure 5(b)) indicating that *N*-glycosylation is important for Mtl1 function following acetic acid treatment. These results indicate that Gfa1-dependent *N*-glycosylation of Mtl1 is required for the normal cellular response to low levels of H_2O_2 and acetic acid. However, this activity is dispensable in cells exposed to higher concentrations of peroxide. These results suggest that the cell can modulate the signal transduction configuration based on the extent and type of damage encountered.

3.6. Increasing H_2O_2 Concentrations Elevates CWI Pathway Activation. The results just described indicated that Mtl1 is important for transducing a low-level ROS signal but not that of a higher concentration. To examine this question further, we investigated the role of the Mtl1 and Mid2-Wsc1 sensor groups in transducing high-level H_2O_2 exposure. Western blot analysis was used to monitor cyclin C levels before and following the addition of 0.8 mM H_2O_2 to wild type, *mtl1*Δ, *mid2*Δ *wsc1*Δ, and *mtl1*Δ *mid2*Δ *wsc1*Δ midlog-phase cultures. Unlike the results obtained with lower H_2O_2 concentration, loss of either the Mtl1 or Mid2/Wsc1 groups did not protect cyclin C from destruction (Figure 6(a)). Consistent with this finding, Slt2 activation was readily observed in both *mtl1*Δ and *mid2*Δ *wsc1*Δ mutants (Figure 6(b)). However, eliminating both groups (*mtl1*Δ *mid2*Δ *wsc1*Δ) stabilized cyclin C and suppressed Slt2 activation. These results suggest that as ROS exposure increases, either Mtl1 or Mid2/Wsc1 can initiate a signal sufficient to trigger cyclin C destruction. However, cyclin C destruction still occurs in the triple sensor mutant when the H_2O_2 concentration is raised to 1.2 mM (Figure 6(a)). These findings suggest that an additional pathway(s) is now enabled that can initiate cyclin C destruction under severe stress exposure (see Section 4).

The above results suggest a model in which H_2O_2-mediated cyclin C destruction is regulated differently depending on the ROS dose. Two models seem most likely to describe these results. First, there may be a linear relationship between the amount of ROS applied and the effective rate for cyclin C destruction. Alternatively, there may be separate pathways whose activation occurs under specified stress conditions. To begin testing these possibilities, cyclin C levels were monitored in a wild-type strain exposed to increasing concentrations of H_2O_2. For these experiments, a single poststress timepoint of one hour was chosen as it represents an intermediate time so that changes in destruction kinetics can be identified. In wild-type cells, the addition of H_2O_2 up to 0.4 mM does not induce an appreciable decline in cyclin C levels after 1 h (Figure 6(c), quantitated Figure 6(d)).

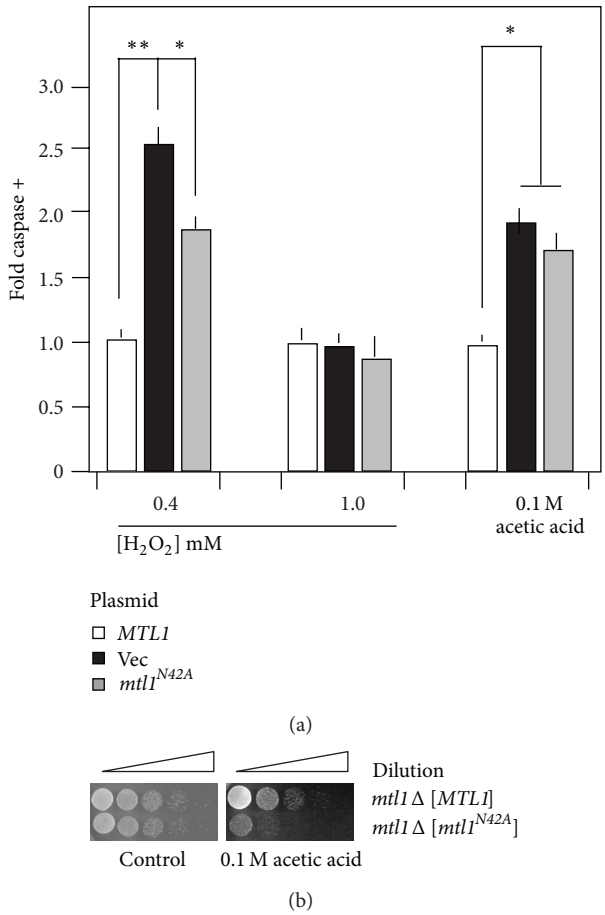

Figure 5: Mtl1 *N*-glycosylation is required for efficient stress-induced PCD execution. (a) The *mtl1*Δ strain (RSY1660) transformed with plasmids expressing *MTL1* (pCJ4), $MTL1^{N42A}$ (pCJ10), or the vector control was subjected to H_2O_2 or acetic acid at the indicated concentrations for 240, 200, and 200 m, respectively. Caspase assays were performed on three independent cultures and the mean ± S.E.M. is indicated. $^{*}P < 0.05$, $^{**}P < 0.01$. (b) Strains described in (a) were grown to midlog phase and then either treated or not with 100 mM acetic acid for 200 min. The cells were serially diluted (1 : 10) and then spotted onto growth medium. The images were obtained following 2 days incubation at 30°C.

However, a significant reduction in cyclin C levels is observed at 0.6 mM H_2O_2. A continued reduction in cyclin C levels is observed at 0.8 mM but they remain relatively constant through 1.2 mM. These results are more consistent with the second model that additional pathways able to trigger cyclin C destruction are enabled in the 0.8–1.2 mM H_2O_2 concentrations. To further test this model, the experiment was repeated with the *mtl1*Δ mutant. Interestingly, following a delay in cyclin C destruction until 0.6 mM, a very similar profile was observed except that the 0.8 to 1.2 mM plateau occurred around 50% of cyclin C remaining versus approximately 15% for the wild-type strain. These results suggest that Mtl1 contributes to the oxidative stress signal regardless of the level of ROS and that additional pathways are activated to destroy cyclin C as ROS exposure increases (see Section 4).

3.7. Sensor Concentration Regulates the Cyclin C Destruction Signal. The results just described suggest a model that increased oxidative stress is able to induce more rapid destruction of cyclin C. To determine if this difference in destruction kinetics could be explained by elevated Slt2 activation, the extent of T-loop phosphorylation was monitored in cultures exposed to low (0.4 mM) or high (0.8 mM) H_2O_2 concentrations. These concentrations were chosen as they represent the two steps observed with cyclin C destruction (see Figure 6(d)). These experiments revealed that Slt2 activation was elevated in cultures subjected to 0.8 mM H_2O_2 compared to 0.4 mM (Figure 7(a)). In addition, cyclin C destruction kinetics are enhanced in response to high ROS conditions (compare cyclin C degradation kinetics between Figures 3(a) and 6(a)). Taken together, these results suggest that activation of multiple stress pathways leads to heightened Slt2 activation and more rapid cyclin C destruction.

Since elevated H_2O_2 concentrations are able to increase Slt2 stimulation, we next asked if the different stress sensors generated a specific signal or Slt2 was simply responding to overall signal intensity. To test these possibilities, a plasmid containing *MTL1* under the control of the galactose inducible promoter (*GAL1*) was introduced into a *mid2*Δ *wsc1*Δ double mutant. In the presence of the repressing carbon source glucose, cyclin C was not destroyed in response to low H_2O_2 levels in the double mutant (Figure 7(b)) as we observed previously (see Figure 3(b)). Growing this culture in galactose medium, which induced Mtl1 overexpression, allowed normal cyclin C destruction to occur. These results indicate that overexpression of Mtl1 can compensate for the loss of the Mid2/Wsc1 signal. This finding is consistent with a model that overall sensor activity, and not a sensor-specific signal, mediates cyclin C destruction. Taken together, these results indicate that elevated sensor signaling, either by increasing the sensor or H_2O_2 concentrations, can more efficiently induce cyclin C destruction.

4. Discussion

ROS generated by oxidative phosphorylation in the mitochondria are normally neutralized by the intrinsic antioxidant system. The addition of exogenous prooxidants (peroxides, heavy metals) triggers the oxidative stress response. Low-level oxidative stress induces cell cycle arrest until the damage has been repaired. Conversely, extensive ROS-induced damage activates the programmed cell death pathway. Our previous studies found that oxidative stress induces the nuclear to cytoplasmic relocalization and destruction of the stress response gene transcriptional repressor cyclin C. In addition, cyclin C translocation is required for efficient PCD execution making the signaling pathway that transmits the ROS signal critical for the decision to enter PCD. In this report, we describe the sensor array that transmits the cyclin C destruction signal following H_2O_2 treatment. Using cyclin C relocalization and destruction as readouts, this study revealed that the cell wall sensors Mtl1 and either Mid2 or Wsc1 combinations are required for low-level ROS signaling to cyclin C. However, our data suggest that the cell is sensing the total signal, not a specific activity derived from each

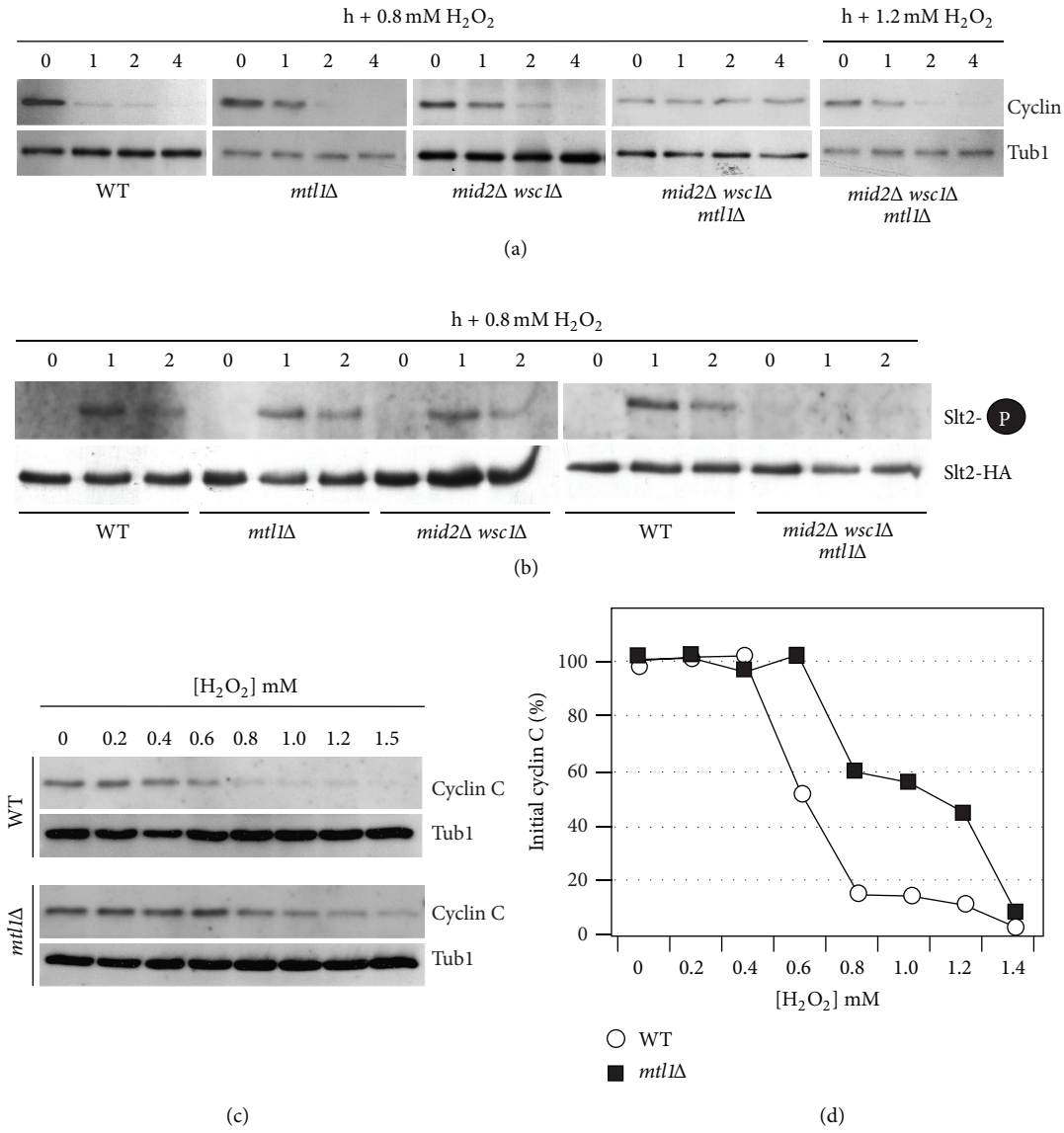

Figure 6: Membrane sensors are not required for cyclin C destruction following 0.8 mM H_2O_2 stress. (a) Wild type (RSY10), *mtl1*Δ (RSY1660), *mids2*Δ *wsc1*Δ (RSY1547), and *mid2*Δ *wsc1*Δ *mtl1*Δ (RSY1707) strains expressing myc-cyclin C (pLR337) were grown to midlog phase (0 hr) and then treated with 0.8 mM or 1.2 mM H_2O_2 for the indicated times. Cyclin C levels were determined by Western blot analysis of immunoprecipitates. Tub1 levels were used as a loading control. (b) Phosphorylation (top panels) and immunoprecipitation (bottom panels) of Slt2-HA in wild type, *mtl1*Δ, *mids2*Δ *wsc1*Δ, and *mid2*Δ *wsc1*Δ *mtl1*Δ strains following 0.8 mM H_2O_2 treatment. (c) Kinetics of cyclin C degradation are dependent upon the H_2O_2 dose. Wild type (RSY10) and *mtl1*Δ (RSY1600) strains expressing myc-cyclin C (pLR337) were grown to midlog phase (0 hr) and then treated with increasing amounts of H_2O_2 for 1 hour. Cyclin C levels were determined by Western blot analysis of immunoprecipitates. Tub1 levels were used as a loading control. (d) Quantification of cyclin C levels in (c).

of these sensors. In addition, Mtl1 signaling requires *N*-glycosylated via a Gfa1-dependent process. In response to higher concentrations of prooxidant, additional pathways are activated that do not require these sensors. These findings indicate that the cell is able to respond to differing levels of oxidative stress through activation of multiple signaling pathways.

This study was initiated by the finding that a mutation in *GFA1* caused cells deleted for cyclin C to grow very slowly. This synthetic growth defect suggested that these factors somehow functioned in similar or redundant pathways. However, our data indicate that Gfa1 is required for the ROS-induced destruction of cyclin C indicating opposing functions. Thus, why are *cnc1*Δ *gfa1-1* mutants synthetically sick? One possibility takes into consideration that cyclin C is part of the Cdk8 module that represses over 100 genes [55, 56] while Gfa1 controls the modification of proteins through the production of GlcNAc and GPI anchors. Therefore, there are multiple opportunities for these two mutations to interact. For example, cyclin C-Cdk8 represses the transcription of *GIP2* [55], an activator of the protein phosphatase Glc7 [57]. Hyperactivation of Glc7 displays a

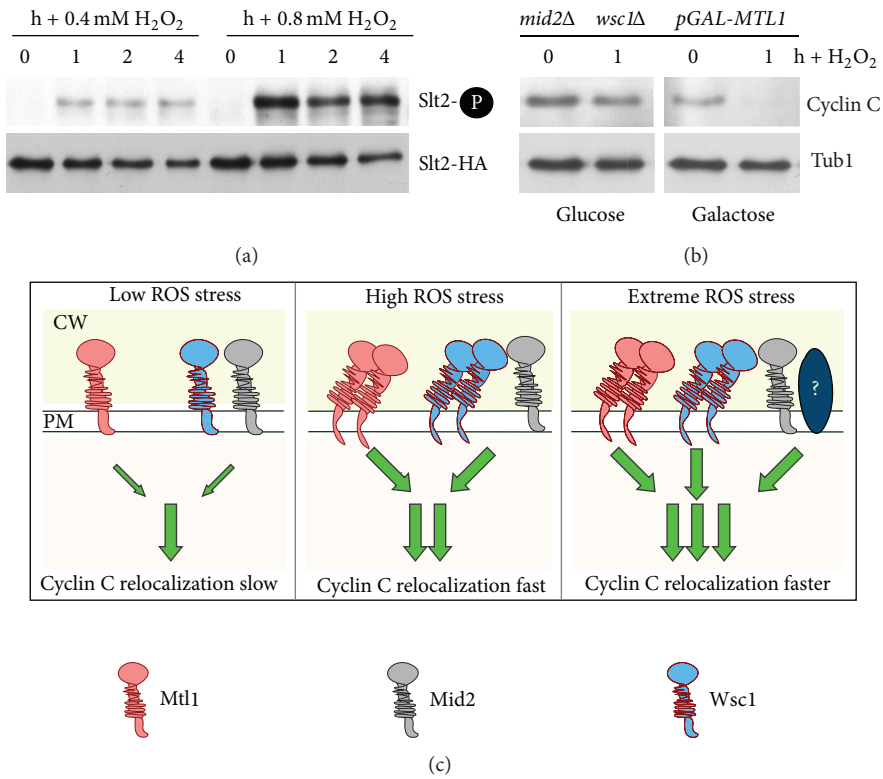

FIGURE 7: Mtl1 overexpression suppresses *mid2*Δ *wsc1*Δ signaling defect. (a) Phosphorylation (top panels) and immunoprecipitation (bottom panels) of Slt2-HA in wild-type strain (RSY10) following 0.4 mM and 0.8 mM H_2O_2 treatment as indicated. (b) A *mid2*Δ *wsc1*Δ mutant (RSY1844) harboring an integrated copy of *MTL1* under the control of the *GAL1* promoter and cyclin C-myc (pLR337) was grown to midlog in raffinose. The culture was split and treated with either 2% galactose or glucose for 2 h before the addition of 0.4 mM H_2O_2. Cyclin C levels were monitored by Western blot analysis of immunoprecipitates. Tub1 levels were used as a loading control. (c) Model of combinatorial signal transduction pathway control for cyclin C regulation. Sensors associated with the plasma membrane (PM) and cell wall (CW) are indicated. Sensor activity in response to low, high, and extreme ROS exposure is indicated. Under low stress conditions, the combined signals from both Mtl1 and Mid2/Wsc1 are required to trigger cyclin C relocalization and destruction. High stress conditions generate more signal from each group, perhaps through sensor clustering as proposed for Wsc1 [12, 54]. Extreme stress environment proposes the existence of another pathway, represented here by the question mark, that contributes to the overall stress. The location of this pathway at the plasma membrane was done for convenience and does not imply another cell wall sensor system per se.

growth defect in combination with mutations in the CWI pathway [58], which requires glycosylated Mlt1 for normal activity. Therefore, although the interactions may not be direct, the proper function of both cyclin C and Gfa1 as regulators of the stress response is important for normal cell growth.

An important question is how the cell responds to differences in stress signal intensities. The Wsc group is proposed to function as a mechanosensor in which the transmembrane domain anchors the protein in the plasma membrane while the head groups provide a dynamic interaction with the cell wall [24, 54, 59]. Here, we have identified specific sensor combinations that are required for cyclin C destruction. A current model in the field suggests that sensor concentration is an important factor for relaying the intensity of the damage signal [54, 59]. Our results can also be viewed in this overall framework. At low ROS levels, the combined activity of the Mtl1 and Wsc1/Mid2 sensor array is necessary to generate a signal sufficient to induce cyclin C destruction (Figure 7(c)). In response to elevated oxidative stress, each sensor group generates a signal on its own sufficient to induce cyclin C translocation to the cytoplasm. This ability may be partially explained by a clustering mechanism just described. At high stress levels, inactivating either Mtl1 or Mid2/Wsc1 still permits the generation of a signal sufficient to induce cyclin C relocalization and destruction. Our finding that simply increasing the levels of Mtl1 can suppress the requirement for Mid2 and Wsc1 suggests that overall signal intensity, not a specific signal generated by each senor type, is being read by the cell. By sensing the increased overall signal, the cell could respond by a more intense and sustained Slt2 activation, which in turn promotes a more rapid translocation of cyclin C to the cytoplasm. Thus, the rate of cyclin C appearance in the cytoplasm may represent a measure for the extent of the cellular damage encountered.

Since cyclin C is still destroyed in the absence of Mtl1 and Mid2/Wsc1 at extreme stress levels, this model would require that an additional, yet undefined, pathway (or pathways) activated is able to contribute cyclin C translocation. One possible pathway would involve the additional Wsc family

members Wsc2 and Wsc3. Wsc2 overexpression is able to suppress the requirement for Mid2 [10] suggesting that a functional overlap exists between these sensors. An alternative, but not mutually exclusive, possibility is that as exogenously added H_2O_2 increases, lipids, protein, and finally DNA are oxidized [60]. Oxidized proteins are selectively degraded by the proteasome [61] while DNA damage is sensed by several well-characterized pathways [62]. Maintenance of the redox state in the ER is critical for proper disulfide bond formation by Ero1 during nascent peptide folding (see [63] for review). An oxidized ER environment restricts Ero1 function resulting in misfolded proteins and ultimately ER stress. In addition, a product of Ero1 function is H_2O_2, which can add to the oxidative stress load especially under condition of elevated protein synthesis and/or defects in the protein folding system. For example, *N*-glycan addition is important for the folding of secretory proteins. Inactivation of this *N*-glycosylation step through the use of tunicamycin can initiate ER stress which involves an ER to nuclear translocation of a transcription factor [64]. Interestingly, cyclin C is partially destroyed in cells treated with tunicamycin [65] although Slt2 was not activated. These observations suggest that ER stress induced by protein folding deficiencies can also trigger cyclin C destruction. Therefore, depending on the level of ROS exposure, the signaling repertoire of the cell is altered to reflect detected damage at different cellular compartments. By having these pathways conflating their respective signals at cyclin C, the cell could detect and respond to significant damage even if one pathway is defective.

Acknowledgments

The authors thank David Levin and Yoshikazu Ohya for plasmids. This work was supported by Grants from the National Institutes of Health (CA099003, GM086788) to Randy Strich and the WW Smith Charitable Trust (no.CO604) to Katrina F. Cooper.

References

[1] K. A. Morano, C. M. Grant, and W. S. Moye-Rowley, "The response to heat shock and oxidative stress in *Saccharomyces cerevisiae*," *Genetics*, vol. 190, no. 4, pp. 1157–1195, 2012.

[2] F. Vilella, E. Herrero, J. Torres, and M. A. de la Torre-Ruiz, "Pkc1 and the upstream elements of the cell integrity pathway in *Saccharomyces cerevisiae*, Rom2 and Mtl1, are required for cellular responses to oxidative stress," *Journal of Biological Chemistry*, vol. 280, no. 10, pp. 9149–9159, 2005.

[3] Y. Kamada, U. S. Jung, J. Piotrowski, and D. E. Levin, "The protein kinase C-activated MAP kinase pathway of *Saccharomyces cerevisiae* mediates a novel aspect of the heat shock response," *Genes and Development*, vol. 9, no. 13, pp. 1559–1571, 1995.

[4] R. Rodicio and J. J. Heinisch, "Together we are strong—cell wall integrity sensors in yeasts," *Yeast*, vol. 27, no. 8, pp. 531–540, 2010.

[5] D. E. Levin, "Regulation of cell wall biogenesis in *Saccharomyces cerevisiae*: the cell wall integrity signaling pathway," *Genetics*, vol. 189, no. 4, pp. 1145–1175, 2011.

[6] K. F. Cooper, M. S. Scarnati, E. Krasley et al., "Oxidative-stress-induced nuclear to cytoplasmic relocalization is required for Not4-dependent cyclin C destruction," *Journal of Cell Science*, vol. 125, pp. 1015–1026, 2012.

[7] E. Krasley, K. F. Cooper, M. J. Mallory, R. Dunbrack, and R. Strich, "Regulation of the oxidative stress response through Slt2p-dependent destruction of cyclin C in *Saccharomyces cerevisiae*," *Genetics*, vol. 172, no. 3, pp. 1477–1486, 2006.

[8] J. V. Gray, J. P. Ogas, Y. Kamada, M. Stone, D. E. Levin, and I. Herskowitz, "A role for the Pkc1 MAP kinase pathway of *Saccharomyces cerevisiae* in bud emergence and identification of a putative upstream regulator," *The EMBO Journal*, vol. 16, no. 16, pp. 4924–4937, 1997.

[9] J. Verna, A. Lodder, K. Lee, A. Vagts, and R. Ballester, "A family of genes required for maintenance of cell wall integrity and for the stress response in *Saccharomyces cerevisiae*," *Proceedings of the National Academy of Sciences of the United States of America*, vol. 94, no. 25, pp. 13804–13809, 1997.

[10] M. Rajavel, B. Philip, B. M. Buehrer, B. Errede, and D. E. Levin, "Mid2 is a putative sensor for cell integrity signaling in *Saccharomyces cerevisiae*," *Molecular and Cellular Biology*, vol. 19, no. 6, pp. 3969–3976, 1999.

[11] A. Jendretzki, J. Wittland, S. Wilk, A. Straede, and J. J. Heinisch, "How do I begin? Sensing extracellular stress to maintain yeast cell wall integrity," *European Journal of Cell Biology*, vol. 90, no. 9, pp. 740–744, 2011.

[12] J. J. Heinisch, V. Dupres, D. Alsteens, and Y. F. Dufrêne, "Measurement of the mechanical behavior of yeast membrane sensors using single-molecule atomic force microscopy," *Nature Protocols*, vol. 5, no. 4, pp. 670–677, 2010.

[13] F. Hutzler, R. Gerstl, M. Lommel, and S. Strahl, "Protein N-glycosylation determines functionality of the *Saccharomyces cerevisiae* cell wall integrity sensor Mid2p," *Molecular Microbiology*, vol. 68, no. 6, pp. 1438–1449, 2008.

[14] T. R. Gemmill and R. B. Trimble, "Overview of N- and O-linked oligosaccharide structures found in various yeast species," *Biochimica et Biophysica Acta*, vol. 1426, no. 2, pp. 227–237, 1999.

[15] G. Watzele and W. Tanner, "Cloning of the glutamine:fructose-6-phosphate amidotransferase gene from yeast. Pheromonal regulation of its transcription," *Journal of Biological Chemistry*, vol. 264, no. 15, pp. 8753–8758, 1989.

[16] D. A. Bulik, M. Olczak, H. A. Lucero, B. C. Osmond, P. W. Robbins, and C. A. Specht, "Chitin synthesis in *Saccharomyces cerevisiae* in response to supplementation of growth medium with glucosamine and cell wall stress," *Eukaryotic Cell*, vol. 2, no. 5, pp. 886–900, 2003.

[17] M.-H. Kuo and E. Grayhack, "A library of yeast genomic *MCM1* binding sites contains genes involved in cell cycle control, cell wall and membrane structure, and metabolism," *Molecular and Cellular Biology*, vol. 14, no. 1, pp. 348–359, 1994.

[18] A. Boorsma, H. de Nobel, B. ter Riet et al., "Characterization of the transcriptional response to cell wall stress in *Saccharomyces cerevisiae*," *Yeast*, vol. 21, no. 5, pp. 413–427, 2004.

[19] L. Ballou, J. R. Grove, R. J. Roon, J. Wiggs, and C. E. Ballou, "Temperature-sensitive glucosamine auxotroph of *Saccharomyces cerevisiae*," *Molecular and Cellular Biology*, vol. 1, no. 1, pp. 9–12, 1981.

[20] W. L. Whelan and C. E. Ballou, "Sporulation in D glucosamine auxotrophs of *Saccharomyces cerevisiae*: meiosis with defective ascospore wall formation," *Journal of Bacteriology*, vol. 124, no. 3, pp. 1545–1557, 1975.

[21] P. Hauptmann, C. Riel, L. A. Kunz-Schughart, K.-U. Fröhlich, F. Madeo, and L. Lehle, "Defects in N-glycosylation induce apoptosis in yeast," *Molecular Microbiology*, vol. 59, no. 3, pp. 765–778, 2006.

[22] M. Sugiura and H. Takagi, "Yeast cell death caused by mutation of the *OST2* gene encoding the ε-subunit of *Saccharomyces cerevisiae* oligosaccharyltransferase," *Bioscience, Biotechnology and Biochemistry*, vol. 70, no. 5, pp. 1234–1241, 2006.

[23] P. Hauptmann and L. Lehle, "Kex1 protease is involved in yeast cell death induced by defective N-glycosylation, acetic acid, and chronological aging," *Journal of Biological Chemistry*, vol. 283, no. 27, pp. 19151–19163, 2008.

[24] D. E. Levin, "Cell wall integrity signaling in *Saccharomyces cerevisiae*," *Microbiology and Molecular Biology Reviews*, vol. 69, no. 2, pp. 262–291, 2005.

[25] K. F. Cooper, M. J. Mallory, J. B. Smith, and R. Strich, "Stress and developmental regulation of the yeast C-type cyclin *Ume3p (Srb11p/Ssn8p)*," *The EMBO Journal*, vol. 16, no. 15, pp. 4665–4675, 1997.

[26] S.-M. Liao, J. Zhang, D. A. Jeffery et al., "A kinase-cyclin pair in the RNA polymerase II holoenzyme," *Nature*, vol. 374, no. 6518, pp. 193–196, 1995.

[27] K. F. Cooper and R. Strich, "Functional analysis of the Ume3p/Srb11p-RNA polymerase II holoenzyme interaction," *Gene Expression*, vol. 8, no. 1, pp. 43–57, 1999.

[28] M. Hirst, M. S. Kobor, N. Kuriakose, J. Greenblatt, and I. Sadowski, "GAL4 is regulated by the RNA polymerase II holoenzyme-associated cyclin-dependent protein kinase *SRB10/CDK8*," *Molecular Cell*, vol. 3, no. 5, pp. 673–678, 1999.

[29] O. Vincent, S. Kuchin, S.-P. Hong, R. Townley, V. K. Vyas, and M. Carlson, "Interaction of the Srb10 kinase with Sip4, a transcriptional activator of gluconeogenic genes in *Saccharomyces cerevisiae*," *Molecular and Cellular Biology*, vol. 21, no. 17, pp. 5790–5796, 2001.

[30] Y. Chi, M. J. Huddleston, X. Zhang et al., "Negative regulation of Gcn4 and Msn2 transcription factors by Srb10 cyclin-dependent kinase," *Genes and Development*, vol. 15, no. 9, pp. 1078–1092, 2001.

[31] D. J. Lew, V. Dulić, and S. I. Reed, "Isolation of three novel human cyclins by rescue of G1 cyclin (Cln) function in yeast," *Cell*, vol. 66, no. 6, pp. 1197–1206, 1991.

[32] T. Igaki, H. Kanuka, N. Inohara et al., "Drob-1, a Drosophila member of the Bcl-2/CED-9 family that promotes cell death," *Proceedings of the National Academy of Sciences of the United States of America*, vol. 97, no. 2, pp. 662–667, 2000.

[33] M. Karbowski, Y.-J. Lee, B. Gaume et al., "Spatial and temporal association of Bax with mitochondrial fission sites, Drp1, and Mfn2 during apoptosis," *Journal of Cell Biology*, vol. 159, no. 6, pp. 931–938, 2002.

[34] H. L. A. Vieira, P. Boya, I. Cohen et al., "Cell permeable BH3-peptides overcome the cytoprotective effect of Bcl-2 and Bcl-XL," *Oncogene*, vol. 21, no. 13, pp. 1963–1977, 2002.

[35] A. Bink, G. Govaert, I. E. J. A. François et al., "A fungicidal piperazine-1-carboxamidine induces mitochondrial fission-dependent apoptosis in yeast," *FEMS Yeast Research*, vol. 10, no. 7, pp. 812–818, 2010.

[36] C. Q. Scheckhuber, N. Erjavec, A. Tinazli, A. Hamann, T. Nyström, and H. D. Osiewacz, "Reducing mitochondrial fission results in increased life span and fitness of two fungal ageing models," *Nature Cell Biology*, vol. 9, no. 1, pp. 99–105, 2007.

[37] I. Ivanovska and J. M. Hardwick, "Viruses activate a genetically conserved cell death pathway in a unicellular organism," *Journal of Cell Biology*, vol. 170, no. 3, pp. 391–399, 2005.

[38] N. Guaragnella, M. Zdralevic, L. Antonacci, S. Passarella, E. Marra, and S. Giannattasio, "The role of mitochondria in yeast programmed cell death," *Frontiers in Oncology*, vol. 2, article 70, 2012.

[39] D. G. Breckenridge, M. Stojanovic, R. C. Marcellus, and G. C. Shore, "Caspase cleavage product of *BAP31* induces mitochondrial fission through endoplasmic reticulum calcium signals, enhancing cytochrome c release to the cytosol," *Journal of Cell Biology*, vol. 160, no. 7, pp. 1115–1127, 2003.

[40] S. Frank, B. Gaume, E. S. Bergmann-Leitner et al., "The role of dynamin-related protein 1, a mediator of mitochondrial fission, in apoptosis," *Developmental Cell*, vol. 1, no. 4, pp. 515–525, 2001.

[41] R. Strich, M. R. Slater, and R. E. Esposito, "Identification of negative regulatory genes that govern the expression of early meiotic genes in yeast," *Proceedings of the National Academy of Sciences of the United States of America*, vol. 86, no. 24, pp. 10018–10022, 1989.

[42] B. J. Thomas and R. Rothstein, "Elevated recombination rates in transcriptionally active DNA," *Cell*, vol. 56, no. 4, pp. 619–630, 1989.

[43] H.-M. Bourbon, "Comparative genomics supports a deep evolutionary origin for the large, four-module transcriptional mediator complex," *Nucleic Acids Research*, vol. 36, no. 12, pp. 3993–4008, 2008.

[44] M. S. Longtine, A. McKenzie, D. J. Demarini et al., "Additional modules for versatile and economical PCR-based gene deletion and modification in *Saccharomyces cerevisiae*," *Yeast*, vol. 14, pp. 953–961, 1998.

[45] T. W. Christianson, R. S. Sikorski, M. Dante, J. H. Shero, and P. Hieter, "Multifunctional yeast high-copy-number shuttle vectors," *Gene*, vol. 110, no. 1, pp. 119–122, 1992.

[46] A. Stotz and P. Linder, "The *ADE2* gene from *Saccharomyces cerevisiae*: sequence and new vectors," *Gene*, vol. 95, no. 1, pp. 91–98, 1990.

[47] A. Bender and J. R. Pringle, "Use of a screen for synthetic lethal and multicopy suppressee mutants to identify two new genes involved in morphogenesis in *Saccharomyces cerevisiae*," *Molecular and Cellular Biology*, vol. 11, no. 3, pp. 1295–1305, 1991.

[48] L. Váchová and Z. Palková, "Physiological regulation of yeast cell death in multicellular colonies is triggered by ammonia," *Journal of Cell Biology*, vol. 169, no. 5, pp. 711–717, 2005.

[49] A. Bateman, "The SIS domain: a phosphosugar-binding domain," *Trends in Biochemical Sciences*, vol. 24, no. 3, pp. 94–95, 1999.

[50] J. A. Shaw, P. C. Mol, B. Bowers et al., "The function of chitin synthases 2 and 3 in the *Saccharomyces cerevisiae* cell cycle," *Journal of Cell Biology*, vol. 114, no. 1, pp. 111–123, 1991.

[51] J. J. Heinisch, A. Lorberg, H.-P. Schmitz, and J. J. Jacoby, "The protein kinase C-mediated MAP kinase pathway involved in the maintenance of cellular integrity in *Saccharomyces cerevisiae*," *Molecular Microbiology*, vol. 32, no. 4, pp. 671–680, 1999.

[52] M. I. Petkova, N. Pujol-Carrion, and M. A. de la Torre-Ruiz, "Mtl1 O-mannosylation mediated by both Pmt1 and Pmt2 is important for cell survival under oxidative conditions and TOR blockade," *Fungal Genetics and Biology*, vol. 49, no. 11, pp. 903–914, 2012.

[53] M. I. Petkova, N. Pujol-Carrion, J. Arroyo, J. García-Cantalejo, and M. A. de la Torre-Ruiz, "Mtl1 is required to activate general

stress response through TOR1 and RAS2 inhibition under conditions of glucose starvation and oxidative stress," *Journal of Biological Chemistry*, vol. 285, no. 25, pp. 19521–19531, 2010.

[54] J. J. Heinisch, V. Dupres, S. Wilk, A. Jendretzki, and Y. F. Dufrêne, "Single-molecule atomic force microscopy reveals clustering of the yeast plasma-membrane sensor Wsc1," *PLoS One*, vol. 5, no. 6, Article ID e11104, 2010.

[55] F. C. P. Holstege, E. G. Jennings, J. J. Wyrick et al., "Dissecting the regulatory circuitry of a eukaryotic genome," *Cell*, vol. 95, no. 5, pp. 717–728, 1998.

[56] J. van de Peppel, N. Kettelarij, H. van Bakel, T. T. J. P. Kockelkorn, D. van Leenen, and F. C. P. Holstege, "Mediator expression profiling epistasis reveals a signal transduction pathway with antagonistic submodules and highly specific downstream targets," *Molecular Cell*, vol. 19, no. 4, pp. 511–522, 2005.

[57] J. P. Bharucha, J. R. Larson, L. Gao, L. K. Daves, and K. Tatchell, "Ypi1, a positive regulator of nuclear protein phosphatase type 1 activity in *Saccharomyces cerevisiae*," *Molecular Biology of the Cell*, vol. 19, no. 3, pp. 1032–1045, 2008.

[58] M. A. García-Gimeno, I. Muñoz, J. Ariño, and P. Sanz, "Molecular characterization of Ypi1, a novel *Saccharomyces cerevisiae* type 1 protein phosphatase inhibitor," *Journal of Biological Chemistry*, vol. 278, no. 48, pp. 47744–47752, 2003.

[59] V. Dupres, D. Alsteens, S. Wilk, B. Hansen, J. J. Heinisch, and Y. F. Dufrêne, "The yeast Wsc1 cell surface sensor behaves like a nanospring in vivo," *Nature Chemical Biology*, vol. 5, no. 11, pp. 857–862, 2009.

[60] P. Moradas-Ferreira, V. Costa, P. Piper, and W. Mager, "The molecular defences against reactive oxygen species in yeast," *Molecular Microbiology*, vol. 19, no. 4, pp. 651–658, 1996.

[61] D. Poppek and T. Grune, "Proteasomal defense of oxidative protein modifications," *Antioxidants and Redox Signaling*, vol. 8, no. 1-2, pp. 173–184, 2006.

[62] S. Boiteux and S. Jinks-Robertson, "DNA repair mechanisms and the bypass of DNA damage in *Saccharomyces cerevisiae*," *Genetics*, vol. 193, pp. 1025–1064, 2013.

[63] C. S. Sevier and C. A. Kaiser, "Ero1 and redox homeostasis in the endoplasmic reticulum," *Biochimica et Biophysica Acta*, vol. 1783, no. 4, pp. 549–556, 2008.

[64] L. W. Ruddock and M. Molinari, "N-glycan processing in ER quality control," *Journal of Cell Science*, vol. 119, no. 21, pp. 4373–4380, 2006.

[65] T. J. Cohen, M. J. Mallory, R. Strich, and T.-P. Yao, "Hos2p/Set3p deacetylase complex signals secretory stress through the Mpk1p cell integrity pathway," *Eukaryotic Cell*, vol. 7, no. 7, pp. 1191–1199, 2008.

[66] M. Sekiya-Kawasaki, M. Abe, A. Saka et al., "Dissection of upstream regulatory components of the Rho1p effector, 1,3-β-glucan synthase, in *Saccharomyces cerevisiae*," *Genetics*, vol. 162, no. 2, pp. 663–676, 2002.

[67] K. Irie, M. Takase, K. S. Lee et al., "*MKK1* and *MKK2*, which encode *Saccharomyces cerevisiae* mitogen-activated protein kinase-kinase homologs, function in the pathway mediated by protein kinase C," *Molecular and Cellular Biology*, vol. 13, no. 5, pp. 3076–3083, 1993.

Hindawi Publishing Corporation
Oxidative Medicine and Cellular Longevity
Volume 2013, Article ID 678473, 10 pages
http://dx.doi.org/10.1155/2013/678473

Research Article

Lack of *HXK2* Induces Localization of Active Ras in Mitochondria and Triggers Apoptosis in the Yeast *Saccharomyces cerevisiae*

Loredana Amigoni,[1,2] Enzo Martegani,[1,2] and Sonia Colombo[1,2]

[1] *Department of Biotechnology and Biosciences, University of Milano-Bicocca, Piazza Della Scienza 2, 20126 Milan, Italy*
[2] *SysBio Centre of Systems Biology, Piazza Della Scienza 2, 20126 Milan, Italy*

Correspondence should be addressed to Sonia Colombo; sonia.colombo@unimib.it

Received 12 June 2013; Revised 18 July 2013; Accepted 24 July 2013

Academic Editor: Paula Ludovico

We recently showed that activated Ras proteins are localized to the plasma membrane and in the nucleus in wild-type cells growing exponentially on glucose, while in the *hxk2*Δ strain they accumulated mainly in mitochondria. An aberrant accumulation of activated Ras in these organelles was previously reported and correlated to mitochondrial dysfunction, accumulation of ROS, and cell death. Here we show that addition of acetic acid to wild-type cells results in a rapid recruitment of Ras-GTP from the nucleus and the plasma membrane to the mitochondria, providing a further proof that Ras proteins might be involved in programmed cell death. Moreover, we show that Hxk2 protects against apoptosis in *S. cerevisiae*. In particular, cells lacking *HXK2* and showing a constitutive accumulation of activated Ras at the mitochondria are more sensitive to acetic-acid-induced programmed cell death compared to the wild type strain. Indeed, deletion of *HXK2* causes an increase of apoptotic cells with several morphological and biochemical changes that are typical of apoptosis, including DNA fragmentation, externalization of phosphatidylserine, and ROS production. Finally, our results suggest that apoptosis induced by lack of Hxk2 may not require the activation of Yca1, the metacaspase homologue identified in yeast.

1. Introduction

In *Saccharomyces cerevisiae* the highly homologous genes *RAS1* and *RAS2* encode small G-proteins that are activated by the guanine nucleotide exchange factors (GEFs), Cdc25 and Sdc25 [1, 2] and inactivated by the GTPase-activating proteins (GAPs), Ira1 and Ira2 [3]. GEFs and GAPs control the switch of the two small monomeric proteins between the active GTP-bound and the inactive GDP-bound state. The Ras proteins and the GPCR system [4–6] constitute two branches that modulate the activity of adenylate cyclase (Cyr1), according to the glucose availability in the environment. In turn Cyr1 [7] activates cAMP-dependent protein kinase (PKA) through cAMP. The amount of this second messenger is also regulated at the level of degradation by the two phosphodiesterases, Pde1 and Pde2. PKA plays a major role in the modulation of metabolism, stress resistance, cell growth, proliferation, morphogenesis, and aging [8].

Recently, our group expressed a probe consisting of a GFP fusion with a trimeric Ras Binding Domain of Raf1 (eGFP-RBD3), which binds Ras-GTP with a much higher affinity than Ras-GDP, to investigate the localization of active Ras in wild-type and in mutant strains in the cAMP/PKA pathway [9]. Our results showed that in W303-1A wild-type cells the probe is localized essentially at the plasma membrane and in the nucleus, while in *hxk2*Δ cells the fluorescent signal accumulated in internal membranes and mitochondria [9]. This peculiar localization of activated Ras2 was previously found in *S. cerevisiae* cells lacking Whi2p function, a protein known to influence cell cycle exit under conditions of nutritional stress [10]. The loss of Whi2p function led to accumulation of damaging ROS and cell death that displayed the hallmarks of apoptosis. More recently, it has been shown that also in mammalian cells, translocation of activated K-RAS protein to mitochondria caused mitochondrial dysfunction and increased ROS generation [11].

Apoptosis plays a crucial role in embryogenesis, development, tissue homeostasis, and disease control in multicellular organisms. In the last two decades the budding yeast *S. cerevisiae* has become a useful model organism for studying this process [12–15]. The basic molecular machinery executing programmed cell death is phylogenetically conserved in yeast as well as animals. Yeast orthologues of mammalian genes related to apoptosis coding for caspase (Yca1), the apoptosis-inducing factor (Aif1), the AIF-homologous mitochondrion-associated inducer of death (Ndi1), the serine protease OMI (Nma111), the endonuclease G (Nuc1), and the endo-/exonuclease Tat-D (scTat-D) [12, 15–20] have been characterized. The apoptotic pathway in *S. cerevisiae* can be activated by several mutations, including *cdc48-S565G* [13], the inactivation of the UBP10 gene coding for a deubiquitinating enzyme [21] or by overexpression of the mammalian apoptotic cell death regulator Bax [22]. Moreover apoptotic cell death is also induced by exogenous toxic agents such as hydrogen peroxide [23], formic acid [24], acetic acid [25], and others. In particular, acetic-acid-induced apoptosis has been investigated in detail, and it has been shown that ROS accumulation and release of cytochrome c to the cytosol take place and that H_2O_2 is a trigger for acetic-acid-induced apoptosis [26–29]. In addition, at least two death pathways can be activated in yeast acetic-acid-induced apoptosis, one is dependent on cyt c release, which requires *YCA1* and the other(s) is independent of it [16, 30]. The yeast caspase Yca1 can protect yeast cells against multiple distinct forms of lethal insults, such as exposure to metals (iron, manganese, cadmium), to low doses of valpronic acid and the previous mentioned acetic acid, to toxins produced by virus killer toxins and others [31]. On the other side, in many instances, Yca1 is not necessary for cell death. For example, external stimuli such as formic acid or copper, or apoptosis derived from defective N-glycosylation in cells lacking Ost2p, the yeast homolog of the mammalian defender of apoptosis-1, are independent of *YCA1* [31].

In this work we provide data indicating that a correlation exists between programmed cell death and localization of active Ras proteins to mitochondria. First of all, we show that addition of acetic acid to wild-type cells causes within five minutes a delocalization of the eGFP-RBD3 probe from plasma membrane and nucleus to mitochondria. Furthermore, we show that in *hxk2*Δ cells, showing a constitutive localization of active Ras at the mitochondria, addition of acetic acid causes an increase of ROS accumulation, mitochondrial dysfunction, and cell death compared with the wild-type strain. It is known that hexokinase 2 functions as a glycolytic enzyme in the cytoplasm and as a regulator of gene transcription of several Mig1-regulated genes in the nucleus [32, 33]. In this paper, we provide data showing a new role for hexokinases 2 as an antiapoptotic factor in this microorganism.

2. Materials and Methods

2.1. Yeast Strains and Media. Strains used in this study: W303-1A (*MATa ade2-1 can1-100 his3-11,15 leu2-3112 trp1-1 ura3-1*) [34]; YSH310 (*MATa* W303-1A with *hxk2::LEU2*) [34]; *yca1*Δ (*MATa* W303-1A with *yca1::URA3*) (this study); *hxk2*Δ *yca1*Δ (YSH310 with *yca1::URA3*) (this study); W303-1A [peGFP-RBD3] [9]; YSH310 [YCp*RAS2*^{Val19}], are obtained by transforming YSH310 with plasmid YCp*RAS2*^{Val19} [35]. The *yca1*Δ and the *hxk2*Δ *yca1*Δ strains were generated by one-step gene disruption [36] from the wild-type W303-1A and the YSH310 strains, respectively, using specific primers previously described [37] and kindly provided by M. Vai, University of Milano-Bicocca.

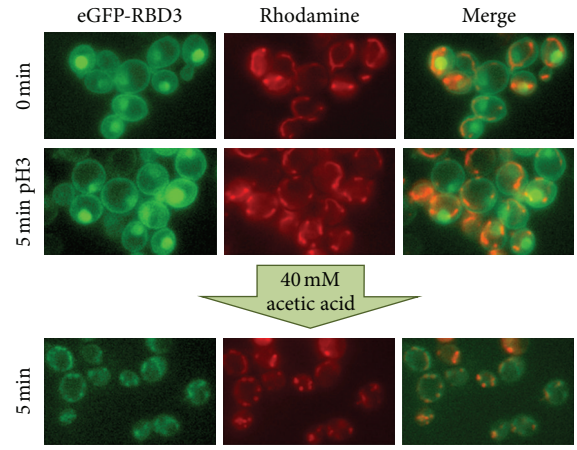

Figure 1: Localization of active Ras in the W303-1A wild-type strain after addition of 40 mM acetic acid. Cells transformed with YEpeGFP-RBD3 were grown in 2% glucose medium at 30°C until exponential phase, collected by centrifugation, and resuspended in medium adjusted to pH 3.0. Cells were then photographed with a Nikon fluorescence microscope, before and after addition of 40 Mm acetic acid. Colocalization of eGFP fluorescence and the red-fluorescent Rhodamine B hexyl ester is clearly visible five minutes after addition of the apoptotic stimulus.

Synthetic complete media (SD) contained 2% glucose, 6.7 g/L YNB w/o aminoacids (Becton and Dickinson Italia, Buccinasco) and the proper selective drop-out CSM (Complete Synthetic Medium, supplied by BIO101, California, USA). Culture density was measured with a Coulter Counter (Coulter mod. Z2) on mildly sonicated, diluted samples. YEPD plates contained 2% w/v glucose, 2% w/v peptone, 1% yeast extract, and 2% agar.

2.2. Acetic Acid Treatment. Cells were grown at 30°C to exponential phase (1-2 × 10^7 cells/mL) in SD medium, harvested, resuspended (10^7 cells/mL) in fresh SD medium adjusted to pH 3.0 (set with HCl), and treated with acetic acid (Riedel-deHaen) at the indicated concentration (between 0 and 120 mM). Cells were incubated for up to 200 minutes at 30°C with shaking (160 rpm).

2.3. Fluorescence Microscopy to Detect Active Ras Localization. W303-1A cells were grown in SD medium at 30°C until exponential phase and treated with 40 mM acetic acid as described previously. Both treated and untreated cells were incubated with the mitochondrial marker Rhodamine B hexyl ester perchlorate (Molecular Probes, Eugene, OR, USA) 100 nM final concentration for about 5 min before imaging. Subsequently,

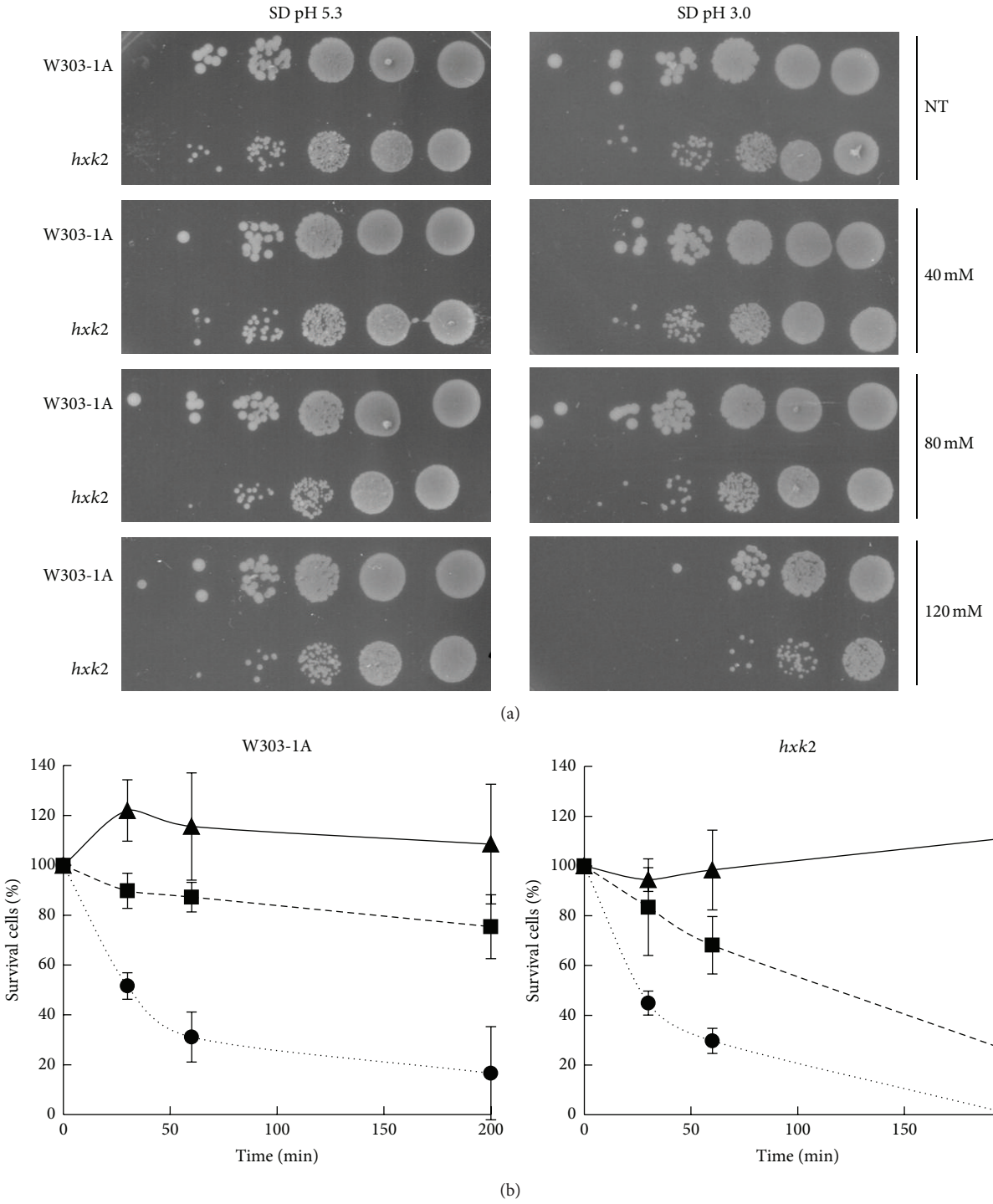

Figure 2: *hxk2*Δ cells exhibit inhibition of cell growth and hypersensitivity to acetic acid. (a) W303-1A and *hxk2*Δ cells were harvested and resuspended (1-2 × 10^7 cells/mL) in SD medium adjusted either at pH 5.3 or at pH 3.0 (set with HCl) in the absence (NT) or in the presence of 40, 80, or 120 mM acetic acid. Cells were incubated for 200 min at 30°C with shaking (160 rpm). After treatment, cells were harvested and resuspended at the same concentration (10^8 cells/mL) in milliQ water. 5 microliter from a concentrated suspension and from 10-fold dilutions of each culture was spotted onto YEPD plates and incubated at 30°C for 3 days. (b) Cell survival of W303-1A and *hxk2*Δ strains. Cell viability of W303-1A and *hxk2*Δ untreated cells (▲) or treated with 80 mM (■) and 120 mM (●) acetic acid was analyzed at indicated times by measuring colony-forming units (cfu) after 2 days of growth at 30°C. Cell survival (100%) corresponds to the cfu at time zero. The means of 4 independent experiments with standard deviations are reported.

40 μL of cells suspension was seeded on concanavalin A (Sigma-Aldrich, Milano, Italy) coated cover glass for 10 min (100 μg/mL). The cover glass was washed 4 times using the proper medium and put on top of a Thoma chamber. Images were acquired with a Nikon Eclipse E600 microscope equipped with a 60X, 1.4 oil Plan-Apochromat objective and a standard FITC filter set for GFP fluorescence. Images were recorded digitally using a Leica DC 350F camera and processed using Adobe Photoshop (Adobe Systems, Inc.).

2.4. Acetic Acid Sensitivity. This assay was performed essentially as described by Casatta et al. [38]. Exponential-phase cells were harvested and resuspended (10^7 cells/mL) in SD medium adjusted either at pH 5.3 or at pH 3.0 (set with HCl) and containing 0, 40, 80, or 120 mM acetic acid. Cells were incubated for 200 min at 30°C with shaking (160 rpm). After treatment, cells (10-fold serial dilutions) were spotted onto YEPD plates and incubated at 30°C for 3 days.

2.5. Viability Assay. Cells were grown in SD medium at 30°C until exponential phase and treated with acetic acid as described previously. At different times (0, 30, 60, and 200 minutes) during acetic acid treatment, cell number was calculated and 400 cells were plated. Viability was determined by measuring colony-forming units (cfu) after 2 days of growth on YEPD agar plates at 30°C. The percentage of viable cells resulted in dividing the number of surviving colonies of the treated sample by the number of surviving colonies of the same culture before acid acetic addition.

2.6. Dihydrorhodamine 123 (DHR123) Staining. ROS (reactive oxygen species) were detected with DHR123 (Sigma Aldrich) essentially as described by Madeo et al. [23]. Cells were grown in SD medium at 30°C until exponential phase and treated with acetic acid as described previously. DHR123 was added directly to the culture medium at the final concentration of 5 μg/mL from a 2.5 μg/μL stock solution. After 2 hours of incubation, cells were diluted to 10^6 cells/mL and analyzed using a FACScan instrument (Becton Dickinson) at low flow rate with excitation and emission settings of 488 and 525–550 nm (filter FL 1). A total of 20.000 events were acquired for each sample and data were processed using WinMDI 2.9 software.

2.7. 4′,6-Diamidino-2-phenylindole (DAPI) Staining. Cells were fixed with 3.7% formaldehyde for 30 minutes, stained with 2 μg/mL of DAPI for 10 minutes, washed with distilled water, and resuspended in 50% glycerol solution. Images were acquired with a Nikon Eclipse E600 fluorescence microscope using a DAPI filter, recorded digitally using a Leica DC 350F camera, and processed using Adobe Photoshop (Adobe Systems, Inc.).

2.8. Annexin V and Propidium Iodide (PI) Staining. (FITC) conjugated recombinant Annexin V (Immuno Tools) was used for the detection of phosphatidylserine exposed in the membrane of apoptotic cells. Cells were harvested after 200 minutes of acetic acid treatment, as reported previously, washed with sorbitol buffer (1 M sorbitol, 0.1 M NaH_2PO_4, pH 8.0), and the cell wall was digested with Zymolyase 20T (Seikagaku Biobusiness Corporation) for about 35 minutes at 37°C. Cells were then washed two times with binding buffer (10 mM Hepes/NaOH pH 7.4, 140 mM NaCl, 2.5 mM $CaCl_2$, 1.2 M sorbitol). Spheroplasts were resuspended in 35 μL of binding buffer and incubated with 2.5 μL of Annexin V and 2 μL of a PI (Fluka) working solution (50 μg/mL) for 15 minutes in the dark at room temperature. After staining, the samples were resuspended in binding buffer and analyzed using a FACScan instrument (Becton Dickinson) using FL 1-H filter on x-axis and FL 2-H filter on y-axis. A total of 30.000 events were acquired for each sample, and data were processed using WinMDI 2.9 software.

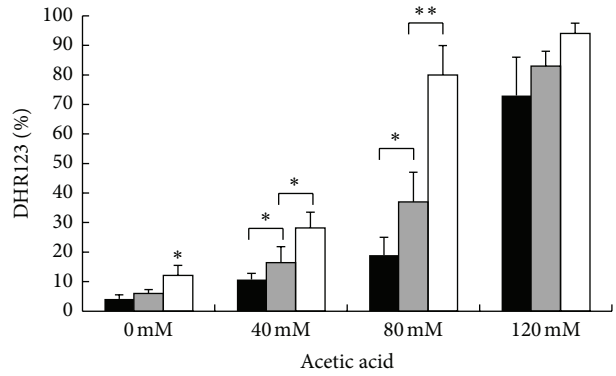

Figure 3: ROS accumulation in W303-1A, *hxk2*Δ, and *hxk2*Δ cells expressing the activated *Ras2*^{Val19} allele after treatment with acetic acid. W303-1A (black bars), *hxk2*Δ (gray bars), and *hxk2*Δ cells expressing the activated Ras2^{Val19} allele (white bars) exponentially growing cells were treated with different concentrations (40–80–120 mM) of acetic acid for 200 minutes at 30°C. ROS accumulation was assayed using the dye dihydrorhodamine 123 (DHR123) by flow cytometry. The means of 3 independent experiments with standard deviations are reported. Student's t-test $^*P < 0.05$ and $^{**}P < 0.01$.

2.9. 3,3′-Dihexyloxacarbocyanine Iodide (DiOC6) Staining. The mitochondrial morphology and membrane potential were assessed by staining with $DiOC_6$ (Molecular Probes, Invitrogen). Cells were grown in SD medium at 30°C until exponential phase and treated with acetic acid as described previously. DiOC6 was added directly to the culture medium at the final concentration of 175 nM for 15 minutes in the dark at room temperature. After staining, the cells were analyzed using a FACScan instrument (Becton Dickinson) using FL1-H filter. A total of 20.000 events were acquired for each sample, and data were processed using WinMDI 2.9 software. Images were also acquired with a Nikon Eclipse E600 microscope equipped with a 60X, 1.4 oil Plan-Apochromat objective, and a standard FITC filter set.

3. Results and Discussion

3.1. Effect of Acetic Acid on the Localization of Active Ras in Glucose-Growing Cells. In a recent study we showed that

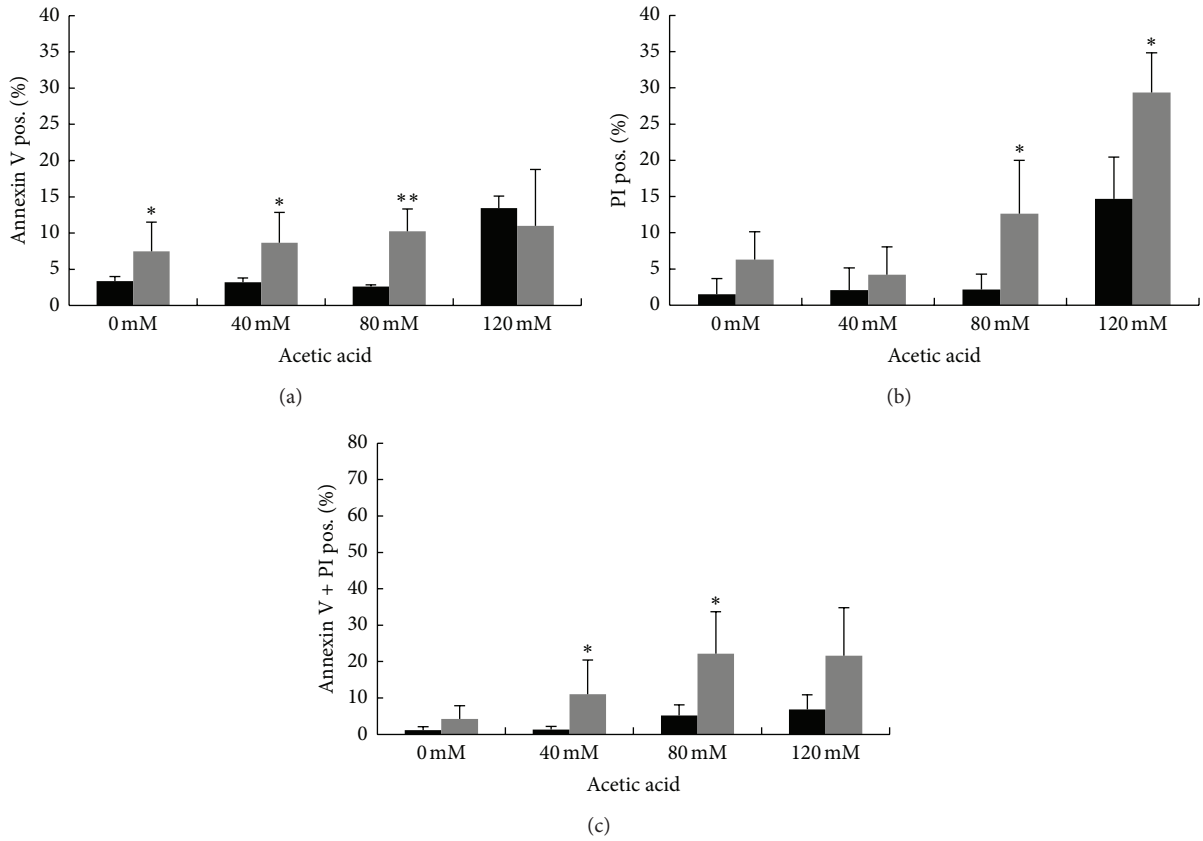

Figure 4: The occurrence of acetic-acid-induced cell death in *hxk2*Δ cells is characterized by markers of both apoptosis and necrosis. Assessment of cell death by FITC-coupled annexin V and PI staining. W303-1A (black bars) and *hxk2*Δ (gray bars) exponentially growing cells were treated with different concentrations (40–80–120 mM) of acetic acid for 200 minutes at 30°C, before being processed for determination of phosphatidylserine externalization and membrane integrity by flow cytometry. 30000 events have been evaluated. The means of 3 independent experiments with standard deviations are reported. Student's *t*-test $^{*}P < 0.05$ and $^{**}P < 0.01$.

active Ras proteins accumulated mainly in the plasma membrane and in the nucleus in exponentially growing wild-type cells, while they accumulated in mitochondria in cells deleted in the *HXK2* gene, indicating that this enzyme was involved in the proper localization of these small GTPases [9]. The role played by active Ras in mitochondria is not known, although other reports have found Ras-GTP associated with these organelles, both in mammals and lower eukaryotes, and have linked it to cancer and apoptosis. Leadsham et al. [10] demonstrated that in *S. cerevisiae* loss of Whi2p function, a protein known to influence cell cycle exit under conditions of nutritional depletion determined an aberrant accumulation of activated Ras at the mitochondria. In this mutant, the failure to shut down Ras signalling by addressing Ras to the vacuole would lead to mitochondrial dysfunction, accumulation of damaging ROS, and cell death. More recently, Hu et al. [11], using a tetracycline inducible model, demonstrated that in mammalian cells association of K-ras^{G12V} proteins with mitochondria induced mitochondrial dysfunction, increased ROS accumulation, and a metabolic switch from oxidative phosphorylation to glycolysis.

To investigate whether a correlation exists between the mitochondrial localization of active Ras and programmed cell death, we evaluated the effect of the addition of acetic acid, a well-known apoptotic stimulus [25], to wild-type cells expressing the eGFP-RBD3 probe on the localization of Ras-GTP proteins. To this aim, exponentially growing cells were collected by centrifugation, resuspended in low pH medium (pH 3.0), and pictures were taken at the fluorescence microscope, before and after addition of 40 mM acetic acid. Our results showed that within 5 minutes this apoptotic stimulus caused the localization of active Ras proteins exclusively to the mitochondria, reinforcing the hypothesis of the involvement of these proteins in programmed cell death (Figure 1). In wild-type cells resuspended in low pH medium for 5 minutes without acetic acid added, active Ras proteins accumulated mainly in the plasma membrane and in the nucleus, indicating that acidification of the medium did not influence the localization of these small G proteins (Figure 1). A mitochondrial localization of Ras-GTP was also observed when a low concentration of H_2O_2 was added to the medium (data not shown), indicating that delocalization of active Ras to these organelles is a more general response to different apoptotic stimuli and suggesting that mitochondrial localization of Ras2-GTP is actually important for the induction of apoptosis in yeast.

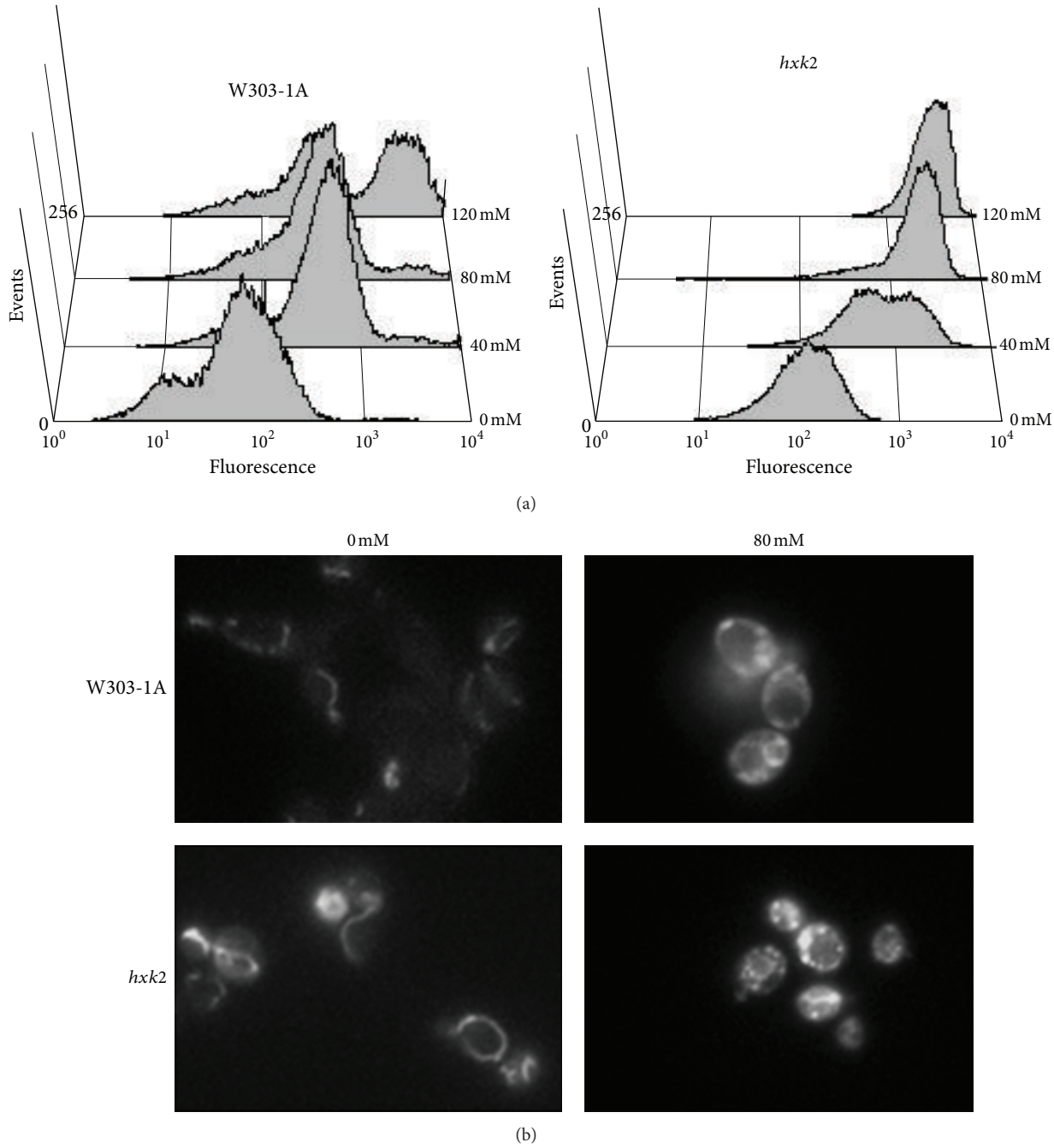

Figure 5: Mitochondrial membrane potential and morphology in W303-1A and *hxk2*Δ strains upon acetic acid treatment. W303-1A and *hxk2*Δ exponentially growing cells were treated with different concentrations (40–80–120 mM) of acetic acid for 200 minutes at 30°C. $DiOC_6$ uptake was assessed using both flow cytometry (a) and fluorescence microscopy (b). Photomicrographs illustrate the alteration of the tubular mitochondrial network to clustered mitochondrial morphology, particularly exacerbated in *hxk2*Δ cells after acetic acid treatment.

3.2. Deletion of HXK2 Enhances Cell Death and Increases Intracellular ROS Levels. The results presented previously suggest that localization of active Ras proteins to mitochondria might be involved in programmed cell death, since these proteins are localized to mitochondria following addition of acetic acid. Since in glucose-growing *hxk2*Δ cells, active Ras is constitutively located in mitochondria [9], we next analyzed the behavior of the *hxk2*Δ mutant under conditions that caused apoptosis. While the growth of *hxk2*Δ mutant was almost indistinguishable from the wild-type strain at pH 5.3, it exhibited an increased sensitivity to acetic acid stress at low pH (Figure 2(a)), suggesting that Hxk2 is required for normal tolerance to acetic acid treatment. Cell survival of wild-type and *hxk2*Δ cells after induction of apoptosis with acetic acid was further tested in a plating assay. After treatment with different concentrations (80 and 120 mM) of acetic acid for

up to 200 minutes at 30°C, *hxk2*Δ cells showed a significant dose-dependent reduction in cell survival when compared with wild-type cells (Figure 2(b)). Taken together these data suggest that Hxk2 is required for normal tolerance to acetic acid treatment.

Since an aberrant accumulation of activated Ras in mitochondria accompanied to accumulation of ROS has already been reported both in mammals and yeast [10, 11] and since ROS play a pivotal role in apoptotic cell death, FACS analyses were performed to evaluate the accumulation of ROS in wild-type and *hxk2*Δ cells treated with different concentrations of acetic acid for 200 min at 30°C. In particular, DHR123 was used to determine the accumulation of ROS in the cells, since this compound can easily permeate them and can be quantitatively oxidized to a green fluorescent product in the presence of ROS. The percentage of oxidized R123 was about the double for *hxk2*Δ cells compared to wild-type cells, 200 min after treatment with either 40 or 80 mM acetic acid (Figure 3). To substantiate the hypothesis that an aberrant accumulation of activated Ras in mitochondria might lead to mitochondrial dysfunction and accumulation of damaging ROS, we expressed the dominant active $RAS2^{Val19}$ allele, which was reported to show a much higher level of Ras2-GTP [39], in *hxk2*Δ cells. Our results showed that indeed the expression of this allele in the *hxk2*Δ background caused a further increase in the level of ROS, both in growing cells and after treatment with acetic acid (Figure 3). These data suggest that conditions that presumably cause a higher mitochondrial accumulation of active Ras may contribute to accumulation of ROS and cell death.

3.3. Loss of Hxk2 Causes an Increase of Both Apoptosis and Necrosis. The results presented previously suggest that Hxk2 might have an antiapoptotic activity. To better characterize the nature of cell death triggered by addition of acetic acid to *hxk2*Δ cells, we quantified phenotypic changes indicative of apoptosis. While apoptotic DNA condensation was detected by DAPI staining, combined Annexin V/propidium iodide (PI) staining was used to discriminate between early apoptotic (Annexin V+/PI−), late apoptotic/secondary necrotic (Annexin V+/PI+), and necrotic (Annexin V−/PI+) deaths. DAPI staining showed that nuclei of untreated cells were round, while the nuclear DNA was condensed in both wild-type and *hxk2*Δ cells treated with 80 mM acetic acid, being the extent of this phenotype more pronounced for the mutant strain compared to the wild-type strain (data not shown). Annexin V/propidium iodide (PI) staining revealed that *hxk2*Δ-facilitated cell death was accompanied by an increase in both apoptotic and necrotic markers (Figure 4). In particular, untreated *hxk2*Δ cells showed a higher percentage of both early apoptotic and necrotic cells compared with the wild-type strain, which further increased upon treatment with acetic acid.

3.4. Deletion of HXK2 Causes Hyperpolarization of Mitochondria. Mitochondrial membrane potential ($\Delta\Psi_m$) is a useful indicator of mitochondrial function. To measure $\Delta\Psi_m$, we used the cationic lipophylic dye $DiOC_6$, which accumulates

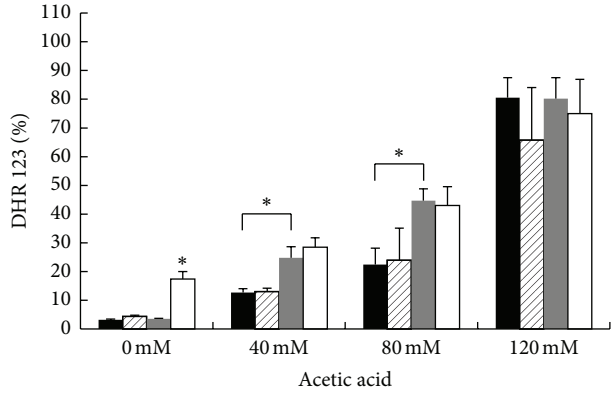

Figure 6: Effect of *YCA1* deletion on ROS accumulation after treatment with acetic acid. W303-1A (black bars), *yca1*Δ (black hatched bars), *hxk2*Δ (gray bars), and *hxk2*Δ-*yca1*Δ (white bars) exponentially growing cells were treated with different concentrations (40–80–120 mM) of acetic acid for 200 minutes at 30°C. ROS accumulation was assayed by flow cytometry using the dye dihydrorhodamine 123 (DHR123). Student's t-test $^{*}P < 0.05$.

in mitochondria in accordance with $\Delta\Psi_m$. Wild-type and *hxk2*Δ cells were treated with different concentration of acetic acid (40–80–120 mM) for 200 min at 30°C, collected, and stained with this dye. FACS analysis showed that mitochondrial membrane potential clearly increased in both wild-type and *hxk2*Δ cells after treatment with acetic acid, compared with untreated control cells, with the hyperpolarization of mitochondria being much stronger in the mutant cells compared with wild-type cells (Figure 5(a)). In parallel, mitochondrial morphology was assessed by using $DiOC_6$, both in wild-type and *hxk2*Δ cells. At low concentration, this dye specifically stains the mitochondrial membranes in a manner that depends on membrane potential and can be observed by fluorescence microscopy. Before treatment with acetic acid, both wild-type and *hxk2*Δ cells displayed a tubular mitochondrial morphology, indicating that these mitochondria were healthy and possessed a membrane potential (Figure 5(b)). By contrast, the mitochondrial membranes present in both wild-type and *hxk2*Δ cells appeared rounded and highly fragmented after treatment with acetic acid (Figure 5(b)). This conversion of mitochondrial morphology from tubular to punctuate structures is likely to occur by excessive mitochondrial fission and has already been observed in yeast apoptosis induced by acetic acid treatment [40]. Importantly, $DiOC_6$ staining was greatly increased and more pronounced in *hxk2*Δ cells compared to wild-type cells after treatment with acetic acid, confirming the increase of fluorescence observed in these mutant cells by FACS analysis. These data indicate that both in wild-type and *hxk2*Δ cells, acetic acid treatment caused hyperpolarization of mitochondrial membrane with consequent damage of these organelles and loss of functionality. This effect was more pronounced in *hxk2*Δ cells compared to wild-type cells.

*3.5. Acetic-Acid-Induced Cell Death in the hxk2*Δ *Strain Is Yca1 Independent.* At least two death pathways can be activated

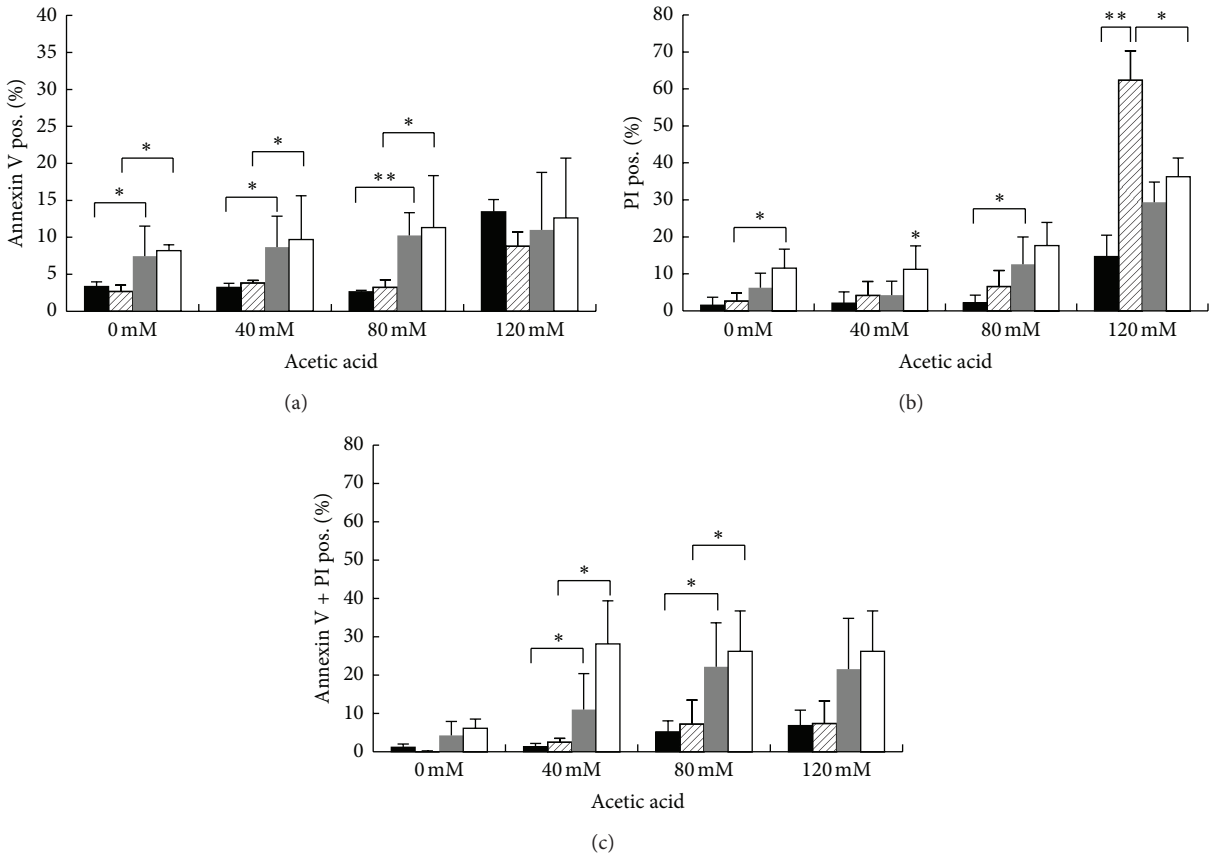

Figure 7: Effect of *YCA1* deletion on cell death after treatment with acetic acid. W303-1A (black bars), *yca1*Δ (black hatched bars), *hxk2*Δ (gray bars) and *hxk2*Δ-*yca1*Δ (white bars) exponentially growing cells were treated with different concentrations (40–80–120 mM) of acetic acid for 200 minutes at 30°C. Cell death was assessed by flow cytometry using FITC-coupled annexin V and PI co-staining to determinate the externalization of phosphatidylserine and the membrane integrity. The means of 3 independent experiments with standard deviations are reported. Student's *t*-test $^{*}P < 0.05$ and $^{**}P < 0.01$.

in yeast acetic-acid-induced apoptosis, one dependent on cytochromec release, which requires *YCA1*, and the other(s) independent of it [16, 30]. Consequently, we next investigated whether the yeast caspase Yca1 might be involved in acetic-acid-induced cell death in *hxk2*Δ cells. In particular, to assess whether Yca1 plays a role in acetic-acid-induced ROS accumulation in *hxk2*Δ cells, we treated *hxk2*Δ and *hxk2*Δ *yca1*Δ cells with different concentration of acetic acid (40–80–120 mM) for 200 min at 30°C and measured the ROS accumulation. Our results showed that deletion of *YCA1* in *hxk2*Δ cells had no effect on acetic-acid-induced ROS accumulation (Figure 6), suggesting that the generation of ROS in *hxk2*Δ cells upon acetic acid stress is Yca1 independent. However, the level of intracellular ROS was consistently higher in the *hxk2*Δ *yca1*Δ double mutant growing on glucose medium compared with the *hxk2*Δ mutant. Similarly, Du et al. [24] showed that formic acid induced Yca1-independent apoptosis-like cell death and that the burst of ROS during cell death occurred earlier and at a higher level in the *yca1*Δ strain than in the wild-type strain. Moreover, Khan et al. [41] determined the level of oxidized proteins in yeast cells under H_2O_2 stress and showed that lack of Yca1 abrogated apoptosis but elevated intracellular oxidized proteins compared with wild-type cells. Consequently, both our results and data in the literature [24, 41] clearly suggest a linkage between ROS production and Yca1 activation during apoptosis in yeast. Finally, cytofluorometric quantification of phosphatidylserine externalization and/or membrane permeabilization (annexin V/PI costaining) further confirmed that Yca1p did not influence the acetic-acid-induced cell death in *hxk2*Δ cells (Figure 7). These results strongly suggest that apoptosis induced by acetic acid in *hxk2*Δ cells is largely Yca1 independent.

4. Conclusion

Several studies indicate that the Ras protein may be physically associated with mitochondria, both in yeast and mammals [10, 11, 42–44]. This study provides results indicating that association of active Ras to these organelles might be linked to apoptosis. First of all, we show that addition of acetic acid, a well-known apoptotic stimulus in *S. cerevisiae*, to growing wild-type cells determined a delocalization of active Ras proteins from nuclei and plasma membrane to mitochondria. Furthermore, we show that addition of acetic acid to *hxk2*Δ cells, showing a constitutive localization of active Ras in mitochondria [9], enhanced ROS production and cell death

compared with wild-type cells. Moreover, expression of the dominant active *RAS2*^{Val19} allele in the *hxk2*Δ background caused an even higher increase in the level of ROS, both in growing cells and after treatment with acetic acid, providing a further proof to the hypothesis that conditions that presumably cause a higher mitochondrial accumulation of active Ras may contribute to accumulation of ROS and cell death. We also show that, in *hxk2*Δ cells, addition of acetic acid increased cell death compared with the wild-type strain with the typical markers of apoptosis, highlighting a new role for Hexokinase 2, as an antiapoptotic factor in *S. cerevisiae* cells. However at this stage we cannot exclude a correlation between the well-known functions of Hxk2 in glucose repression and signalling and the role of Ras in inducing apoptosis.

Finally, in this study we show that lack of Hxk2 induces apoptosis via a mitochondria-mediated pathway without metacaspase Yca1 involvement, since deletion of *YCA1* in the *hxk2*Δ background did not abrogate the acetic-acid-induced accumulation of ROS and did not decrease the percentage of both apoptotic and necrotic cells.

Acknowledgments

The authors thank J. Winderickx, University of Leuven, Belgium, for the gift of strains and M. Vai, Università Milano-Bicocca, Milan, for the gift of primers. This work was supported by FAR grant to Sonia Colombo and by founding of Program SysBioNet, Italian Roadmap Research Infrastructure 2012.

References

[1] S. Jones, M.-L. Vignais, and J. R. Broach, "The CDC25 protein of *Saccharomyces cerevisiae* promotes exchange of guanine nucleotides bound to Ras," *Molecular and Cellular Biology*, vol. 11, no. 5, pp. 2641–2646, 1991.

[2] S. Rudoni, S. Colombo, P. Coccetti, and E. Martegani, "Role of guanine nucleotides in the regulation of the Ras/cAMP pathway in *Saccharomyces cerevisiae*," *Biochimica et Biophysica Acta*, vol. 1538, no. 2-3, pp. 181–189, 2001.

[3] K. Tanaka, M. Nakafuku, T. Satoh et al., "S. cerevisiae genes IRA1 and IRA2 encode proteins that may be functionally equivalent to mammalian ras GTPase activating protein," *Cell*, vol. 60, no. 5, pp. 803–807, 1990.

[4] S. Zaman, S. I. Lippman, X. Zhao, and J. R. Broach, "How *Saccharomyces* responds to nutrients," *Annual Review of Genetics*, vol. 42, pp. 27–81, 2008.

[5] J. M. Thevelein and J. H. De Winde, "Novel sensing mechanisms and targets for the cAMP-protein kinase A pathway in the yeast *Saccharomyces cerevisiae*," *Molecular Microbiology*, vol. 33, no. 5, pp. 904–918, 1999.

[6] F. Rolland, J. Winderickx, and J. M. Thevelein, "Glucose-sensing and -signalling mechanisms in yeast," *FEMS Yeast Research*, vol. 2, no. 2, pp. 183–201, 2002.

[7] G. F. Casperson, N. Walker, and H. R. Bourne, "Isolation of the gene encoding adenylate cyclase in *Saccharomyces cerevisiae*," *Proceedings of the National Academy of Sciences of the United States of America*, vol. 82, no. 15, pp. 5060–5063, 1985.

[8] B. Smets, R. Ghillebert, P. De Snijder et al., "Life in the midst of scarcity: adaptations to nutrient availability in *Saccharomyces cerevisiae*," *Current Genetics*, vol. 56, no. 1, pp. 1–32, 2010.

[9] S. Broggi, E. Martegani, and S. Colombo, "Live-cell imaging of endogenous Ras-GTP shows predominant Ras activation at the plasma membrane and in the nucleus in *Saccharomyces cerevisiae*," *The International Journal of Biochemistry & Cell Biology*, vol. 45, no. 2, pp. 384–394, 2013.

[10] J. E. Leadsham, K. Miller, K. R. Ayscough et al., "Whi2p links nutritional sensing to actin-dependent Ras-cAMP-PKA regulation and apoptosis in yeast," *Journal of Cell Science*, vol. 122, no. 5, pp. 706–715, 2009.

[11] Y. Hu, W. Lu, G. Chen et al., "K-rasG12V transformation leads to mitochondrial dysfunction and a metabolic switch from oxidative phosphorylation to glycolysis," *Cell Research*, vol. 22, no. 2, pp. 399–412, 2012.

[12] S. Büttner, T. Eisenberg, D. Carmona-Gutierrez et al., "Endonuclease G regulates budding yeast life and death," *Molecular Cell*, vol. 25, no. 2, pp. 233–246, 2007.

[13] F. Madeo, E. Fröhlich, and K.-U. Fröhlich, "A yeast mutant showing diagnostic markers of early and late apoptosis," *Journal of Cell Biology*, vol. 139, no. 3, pp. 729–734, 1997.

[14] F. Madeo, E. Herker, S. Wissing, H. Jungwirth, T. Eisenberg, and K.-U. Fröhlich, "Apoptosis in yeast," *Current Opinion in Microbiology*, vol. 7, no. 6, pp. 655–660, 2004.

[15] F. Madeo, E. Herker, C. Maldener et al., "A caspase-related protease regulates apoptosis in yeast," *Molecular Cell*, vol. 9, no. 4, pp. 911–917, 2002.

[16] N. Guaragnella, C. Pereira, M. J. Sousa et al., "YCA1 participates in the acetic acid induced yeast programmed cell death also in a manner unrelated to its caspase-like activity," *FEBS Letters*, vol. 580, no. 30, pp. 6880–6884, 2006.

[17] W. Li, L. Sun, Q. Liang, J. Wang, W. Mo, and B. Zhou, "Yeast AMID homologue Ndi1p displays respiration-restricted apoptotic activity and is involved in chronological aging," *Molecular Biology of the Cell*, vol. 17, no. 4, pp. 1802–1811, 2006.

[18] S. Wissing, P. Ludovico, E. Herker et al., "An AIF orthologue regulates apoptosis in yeast," *Journal of Cell Biology*, vol. 166, no. 7, pp. 969–974, 2004.

[19] B. Fahrenkrog, U. Sauder, and U. Aebi, "The S. cerevisiae HtrA-like protein Nma111p is a nuclear serine protease that mediates yeast apoptosis," *Journal of Cell Science*, vol. 117, no. 1, pp. 115–126, 2004.

[20] J. Qiu, J.-H. Yoon, and B. Shen, "Search for apoptotic nucleases in yeast: role of Tat-D nuclease in apoptotic DNA degradation," *The Journal of Biological Chemistry*, vol. 280, no. 15, pp. 15370–15379, 2005.

[21] I. Orlandi, M. Bettiga, L. Alberghina, and M. Vai, "Transcriptional profiling of ubp10 null mutant reveals altered subtelomeric gene expression and insurgence of oxidative stress response," *The Journal of Biological Chemistry*, vol. 279, no. 8, pp. 6414–6425, 2004.

[22] M. Ligr, F. Madeo, E. Fröhlich, W. Hilt, K.-U. Fröhlich, and D. H. Wolf, "Mammalian Bax triggers apoptotic changes in yeast," *FEBS Letters*, vol. 438, no. 1-2, pp. 61–65, 1998.

[23] F. Madeo, E. Fröhlich, M. Ligr et al., "Oxygen stress: a regulator of apoptosis in yeast," *Journal of Cell Biology*, vol. 145, no. 4, pp. 757–767, 1999.

[24] L. Du, Y. Su, D. Sun et al., "Formic acid induces Yca1p-independent apoptosis-like cell death in the yeast *Saccharomyces cerevisiae*," *FEMS Yeast Research*, vol. 8, no. 4, pp. 531–539, 2008.

[25] P. Ludovico, M. J. Sousa, M. T. Silva, C. Leão, and M. Côrte-Real, "*Saccharomyces cerevisiae* commits to a programmed cell death process in response to acetic acid," *Microbiology*, vol. 147, no. 9, pp. 2409–2415, 2001.

[26] P. Ludovico, F. Rodrigues, A. Almeida, M. T. Silva, A. Barrientos, and M. Côrte-Real, "Cytochrome c release and mitochondria involvement in programmed cell death induced by acetic acid in *Saccharomyces cerevisiae*," *Molecular Biology of the Cell*, vol. 13, no. 8, pp. 2598–2606, 2002.

[27] N. Guaragnella, L. Antonacci, S. Passarella, E. Marra, and S. Giannattasio, "Hydrogen peroxide and superoxide anion production during acetic acid-induced yeast programmed cell death," *Folia Microbiologica*, vol. 52, no. 3, pp. 237–240, 2007.

[28] S. Giannattasio, A. Atlante, L. Antonacci et al., "Cytochrome c is released from coupled mitochondria of yeast en route to acetic acid-induced programmed cell death and can work as an electron donor and a ROS scavenger," *FEBS Letters*, vol. 582, no. 10, pp. 1519–1525, 2008.

[29] N. Guaragnella, L. Antonacci, S. Giannattasio, E. Marra, and S. Passarella, "Catalase T and Cu, Zn-superoxide dismutase in the acetic acid-induced programmed cell death in *Saccharomyces cerevisiae*," *FEBS Letters*, vol. 582, no. 2, pp. 210–214, 2008.

[30] N. Guaragnella, A. Bobba, S. Passarella, E. Marra, and S. Giannattasio, "Yeast acetic acid-induced programmed cell death can occur without cytochrome c release which requires metacaspase YCA1," *FEBS Letters*, vol. 584, no. 1, pp. 224–228, 2010.

[31] F. Madeo, D. Carmona-Gutierrez, J. Ring, S. Büttner, T. Eisenberg, and G. Kroemer, "Caspase-dependent and caspase-independent cell death pathways in yeast," *Biochemical and Biophysical Research Communications*, vol. 382, no. 2, pp. 227–231, 2009.

[32] D. Ahuatzi, A. Riera, R. Peláez, P. Herrero, and F. Moreno, "Hxk2 regulates the phosphorylation state of Mig1 and therefore its nucleocytoplasmic distribution," *The Journal of Biological Chemistry*, vol. 282, no. 7, pp. 4485–4493, 2007.

[33] F. Moreno, D. Ahuatzi, A. Riera, C. A. Palomino, and P. Herrero, "Glucose sensing through the Hxk2-dependent signalling pathway," *Biochemical Society Transactions*, vol. 33, no. 1, pp. 265–268, 2005.

[34] B. J. Thomas and R. Rothstein, "Elevated recombination rates in transcriptionally active DNA," *Cell*, vol. 56, no. 4, pp. 619–630, 1989.

[35] L. C. Robinson, J. B. Gibbs, M. S. Marshall, I. S. Sigal, and K. Tatchell, "CDC25: a component of the RAS-adenylate cyclase pathway in *Saccharomyces cerevisiae*," *Science*, vol. 235, no. 4793, pp. 1218–1221, 1987.

[36] R. J. Rothstein, "One-step gene disruption in yeast," *Methods in Enzymology*, vol. 101, pp. 202–211, 1983.

[37] M. Bettiga, L. Calzari, I. Orlandi, L. Alberghina, and M. Vai, "Involvement of the yeast metacaspase Yca1 in *ubp10*Δ-programmed cell death," *FEMS Yeast Research*, vol. 5, no. 2, pp. 141–147, 2004.

[38] N. Casatta, A. Porro, I. Orlandi, L. Brambilla, and M. Vai, "Lack of Sir2 increases acetate consumption and decreases extracellular pro-aging factors," *Biochimica et Biophysica Acta*, vol. 1833, no. 3, pp. 593–601, 2013.

[39] S. Colombo, D. Ronchetti, J. M. Thevelein, J. Winderickx, and E. Martegani, "Activation state of the Ras2 protein and glucose-induced signaling in *Saccharomyces cerevisiae*," *The Journal of Biological Chemistry*, vol. 279, no. 45, pp. 46715–46722, 2004.

[40] P. Fabrizio and V. D. Longo, "Chronological aging-induced apoptosis in yeast," *Biochimica et Biophysica Acta*, vol. 1783, no. 7, pp. 1280–1285, 2008.

[41] M. A. S. Khan, P. B. Chock, and E. R. Stadtman, "Knockout of caspase-like gene, YCA1, abrogates apoptosis and elevates oxidized proteins in *Saccharomyces cerevisiae*," *Proceedings of the National Academy of Sciences of the United States of America*, vol. 102, no. 48, pp. 17326–17331, 2005.

[42] J. C. Wolfman, S. M. Planchon, J. Liao, and A. Wolfman, "Structural and functional consequences of c-N-Ras constitutively associated with intact mitochondria," *Biochimica et Biophysica Acta*, vol. 1763, no. 10, pp. 1108–1124, 2006.

[43] T. G. Bivona, S. E. Quatela, B. O. Bodemann et al., "PKC regulates a farnesyl-electrostatic switch on K-Ras that promotes its association with Bcl-XL on mitochondria and induces apoptosis," *Molecular Cell*, vol. 21, no. 4, pp. 481–493, 2006.

[44] A. Rebollo, D. Pérez-Sala, and C. Martínez-A, "Bcl-2 differentially targets K-, N-, and H-Ras to mitochondria in IL-2 supplemented or deprived cells: implications in prevention of apoptosis," *Oncogene*, vol. 18, no. 35, pp. 4930–4939, 1999.

Hindawi Publishing Corporation
Oxidative Medicine and Cellular Longevity
Volume 2013, Article ID 129645, 9 pages
http://dx.doi.org/10.1155/2013/129645

Research Article

A Novel Sit4 Phosphatase Complex Is Involved in the Response to Ceramide Stress in Yeast

Alexandra Woodacre,[1] Museer A. Lone,[2] Daniel Jablonowski,[1,3] Roger Schneiter,[2] Flaviano Giorgini,[1] and Raffael Schaffrath[1,3]

[1] *Department of Genetics, University of Leicester, Leicester, LE1 7RH, UK*
[2] *Division of Biochemistry, Department of Biology, University of Fribourg, CH-1700 Fribourg, Switzerland*
[3] *Institut für Biologie, FG Mikrobiologie, Universität Kassel, 34132 Kassel, Germany*

Correspondence should be addressed to Flaviano Giorgini; fg36@le.ac.uk and Raffael Schaffrath; schaffrath@uni-kassel.de

Received 10 May 2013; Revised 28 June 2013; Accepted 25 July 2013

Academic Editor: Joris Winderickx

Ceramide is a building block for complex sphingolipids in the plasma membrane, but it also plays a significant role in secondary signalling pathways regulating cell proliferation and apoptosis in response to stress. Ceramide activated protein phosphatase activity has been previously observed in association with the Sit4 protein phosphatase. Here we find that *sit4*Δ mutants have decreased ceramide levels and display resistance to exogenous ceramides and phytosphingosine. Mutants lacking *SIT4* or *KTI12* display a shift towards nonhydroxylated forms of long chain bases and sphingolipids, suggesting regulation of hydroxylase (*SUR2*) or ceramide synthase by Sit4p. We have identified novel subunits of the Sit4 complex and have also shown that known Sit4 regulatory subunits—SAP proteins—are not involved in the ceramide response. This is the first observation of separation of function between Sit4 and SAP proteins. We also find that the Sit4p target Elongator is not involved in the ceramide response but that cells deficient in Kti12p—an accessory protein with an undefined regulatory role—have similar ceramide phenotypes to *sit4*Δ mutants. Therefore, Kti12p may play a similar secondary role in the ceramide response. This evidence points to a novel Sit4-dependent regulatory mechanism in response to ceramide stress.

1. Introduction

Ceramide is a building block for complex sphingolipids which comprise an important structural component of the plasma membrane. It is also a secondary signalling molecule that accumulates in response to stresses such as heat shock [1]. It is therefore important for sphingolipid metabolism to be tightly regulated, and the damaging effects of dysregulation are apparent in patients with Tay-Sachs disease, Fabry disease, and other inherited sphingolipidosis disorders [2]. Ceramide mediates controlled cell death by triggering several signalling cascades to initiate caspase-dependent and independent apoptosis [3]. In contrast, the phosphorylated ceramide precursors dihydrosphingosine (DHSP) and phytosphingosine (PHSP) are signals for pathways that promote cell proliferation [4].

Although it is known that the cellular response to ceramide is important for the regulation of cell proliferation and cell death pathways, the precise molecular mechanisms for this regulation still remain elusive. It is vital to further understand the way cells respond to stress in order to develop strategies to modify them, either to accelerate cell death using targeted anticancer drugs or to prevent accumulation of toxic products in sphingolipidoses [5–7].

Saccharomyces cerevisiae has been used effectively as a model to study sphingolipid metabolism, and Figure 1 shows a detailed summary of the sphingolipid biosynthetic pathway in yeast [8]. Many of the genes involved are conserved from yeast to higher eukaryotes, with diversion in the synthesis of complex sphingolipids occurring only after the production of ceramides, resulting in the production of different end products in the pathway. The addition of inositol to ceramide in

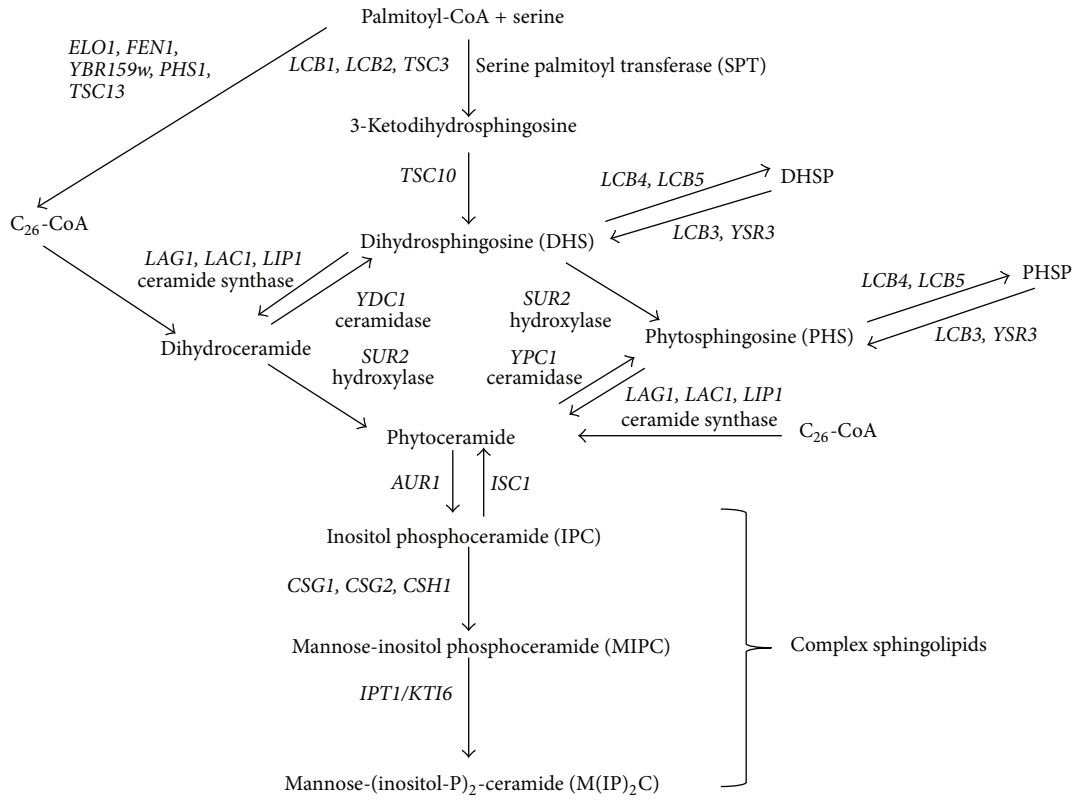

Figure 1: Biosynthesis of sphingolipids in *Saccharomyces cerevisiae*. Key enzymes discussed in the text are highlighted and genes encoding all relevant parts of the pathway are included. The directions of arrows indicate the end products of enzymatic reactions.

yeast forms inositol phosphoceramide, and glucose, galactose or phosphorylcholine is added to ceramide in mammalian cells to generate glycosphingolipids and sphingomyelin [9].

Early work by Nickels and Broach showed that a ceramide-activated phosphatase activity was present in *Saccharomyces cerevisiae*, which is separate from the activity of the major PP2A phosphatases Pph21p and Pph22p [10]. The ceramide resistance of a *sit4*Δ mutant strain suggested that the PP2A-like phosphatase Sit4p is responsible for this activity. *SIT4* is an essential gene in the absence of the suppressor allele *SSD1-v* and has important roles in the progression of the cell cycle, cell integrity, nutrient responses via TORC1, drug resistance via efflux pumps, and tRNA modification [11–16]. Diverse regulatory subunits of Sit4p are partially responsible for the different specificities of Sit4p; for example, Tap42p is phosphorylated by Tor and binds Sit4p [17] and Sap185p and Sap190p subunits are essential for correct phosphoregulation of Elongator and tRNA modification [18]. Mutation of the SAPs (Sit4 associated proteins) can confer different specificities on Sit4p but a deletion of all four SAPs always results in the same phenotypes as deletion of *SIT4*, for example resistance to the tRNAse toxin zymocin, cell cycle arrest, and sensitivity to rapamycin [19, 20]. The accessory protein Kti12p is also essential for the phosphoregulation of the Elongator subunit Elp1p by the Sit4p/Sap185p/Sap190p complex. Kti12p interacts with the casein kinase Hrr25p in an Elongator-dependent manner but the mechanism by which Kti12p regulates phosphorylation remains unclear [21].

The aim of this study was to further investigate the role of Sit4 as the ceramide-activated protein phosphatase (CAPP) in yeast. We identify *KTI12* as an important gene mediating ceramide toxicity and show that ceramide toxicity is independent of Elongator function. Mutants lacking *SIT4* or *KTI12* have decreased levels of ceramide and the balance of hydroxylated and nonhydroxylated sphingolipids is altered. The confirmation that Tpd3p and Cdc55p can interact with Sit4p and a separation of function between *SIT4* and the regulatory SAP subunits indicates that the CAPP is likely to be an alternative Sit4 complex operating via a novel mechanism.

2. Methods

2.1. Yeast Strains and Media. Yeast were routinely grown in yeast extract peptone dextrose medium (YPD; 1% yeast extract, 1% peptone, 2% glucose) at 30°C with shaking. Glucose was replaced with 2% galactose to induce expression of *SIT4* and *PPH21* from the *GAL1* promoter. Synthetic defined medium without inositol (0.67% yeast nitrogen base, 2% glucose, supplemented with essential amino acids) was used for labelling with [^{3}H]*myo*-inositol. Yeast strains used in this study are listed in Table 1.

Table 1: Yeast strains used in this study.

Strain	Genotype	Reference
CY4029	Mat a *ade2-1 his3-11,15 leu2-3,112 trp1-1 ura3-1 can1-100 SSD1-v1 gal+*	[20]
CY3938	CY4029, *sit4Δ::HIS3*	[20]
CY5236	CY4029, *sap4Δ::LEU2 sap155Δ::HIS3 sap185Δ::ADE2 sap190Δ::TRP1*	[20]
CY5220	CY4029, *sap4Δ::LEU2 sap155Δ::HIS3*	[20]
CY5224	CY4029, *sap185Δ::ADE2 sap190Δ::TRP1*	[20]
CY4917	CY4029, *sap185Δ::ADE2*	[20]
CY4380	CY4029, *sap190Δ::TRP1*	[20]
DJY101	CY4029, *sit4Δ::HIS3 kti12ΔKlLEU2*	[18]
LFY3	Mat a *ade2-1 his3-11,15 leu2-3,112, ura3-1 can1-100, elp1Δ::TRP1*	[18]
LFY4	Mat a *ade2-1 his3-11,15 leu2-3,112, ura3-1 can1-100, elp2Δ::TRP1*	[18]
LFY5	Mat a *ade2-1 his3-11,15 leu2-3,112, ura3-1 can1-100, elp3Δ::TRP1*	[22]
LFY6	Mat a *ade2-1 his3-11,15 leu2-3,112, ura3-1 can1-100, kti12Δ::TRP1*	[22]
AWY1	CY4029 *TRP1::GAL1::$(HA)_3$-SIT4 CDC55-$(c\text{-}myc)_3$::HIS3MX6*	This study
AWY2	CY4029, *kanMX6::PGAL1::$(HA)_3$-PPH21, CDC55-$(c\text{-}myc)_3$::HIS3MX6*	This study
AWY3	CY4029, *CDC55-$(c\text{-}myc)_3$::HIS3MX6*	This study

2.2. Growth Tests Using Ceramide and Long Chain Bases. C2-ceramide, C2-phytoceramide, dihydrosphingosine (DHS), and phytosphingosine (PHS) powders were purchased from Enzo Life Sciences and resuspended in 100% ethanol. Stock solutions (5 mg/mL) were stored at −20°C for a maximum of 1 week. Yeast cultures were diluted from a starter culture to 5×10^3 cells/mL in YPD containing ceramides/long chain bases or an equal volume of ethanol as an untreated control. Cultures were grown until the untreated control reached exponential phase (from 15–36 hours depending on the strain) and the OD_{600} measured for both treated and untreated cultures. After 24 hours, an additional dose of ceramide/long chain base was added to counteract the effects of compound degradation. The amount of growth in each concentration of ceramide/long chain base was then expressed as a percentage of the growth in untreated media. This method of standardising growth enables the comparison of slow-growing mutants such as *sit4*Δ to a faster-growing wild-type strain. Raw OD_{600} data is provided in Supplementary Tables 1 and 2 (see Supplementary Material available online at http://dx.doi.org/10.1155/2013/129645). A minimum of three biological replicates were performed for each strain and a one-way ANOVA with Bonferroni post-test was used to determine if growth was significantly different from the wild type (CY4029).

2.3. Immunoprecipitation. Dynabeads (Invitrogen) were coupled with 5 μg of anti-HA antibody per mg of beads, following the manufacturer's instructions. Total protein extracts were prepared from 50 mL cultures grown for 8 hours in YPD supplemented with galactose. Cell pellets were resuspended in 400 μL B60 buffer (50 mM HEPES pH 7.3, 60 mM sodium acetate, 5 mM magnesium acetate, 0.1% Triton X-100, 10% glycerol, 1 mM sodium fluoride, 20 mM glycerophosphate, 1 mM DTT, 1X Complete Mini Protease Inhibitor Cocktail (Roche)). An equal volume of glass beads was added and cells disrupted using a bead beater for 1 minute, followed by centrifugation at 15700 g, 4°C for 5 minutes. The supernatant was transferred to a new tube and centrifuged at 15700 g, 4°C for 20 minutes. The cleared protein extract was quantified using spectrophotometry and 3.5 mg of total protein extract was incubated with 1.5 mg of antibody-coated beads for 30 minutes at 4°C. Unbound proteins were removed by three washes with 1 mL B60 buffer, and antibody-bound proteins were eluted with 50 μL of 10% (v/v) SDS for 10 minutes at room temperature. The beads were then removed with a magnet and the supernatant used for Western blot analysis. SDS-PAGE of 100 μg of total protein from each strain and immunoprecipitation supernatants (equal volumes) was carried out using 12% acrylamide gels and then Western blotted at 100 V for 1 hour. Blots were probed with anti-HA (F7 Santa Cruz), anti-c-myc (A14 Santa Cruz), or anti-Tpd3 (Y. Jiang, University of Pittsburg School of Medicine, USA) and secondary antibodies conjugated to horseradish peroxidase (Roche Diagnostics) were detected by chemiluminescence and exposed to X-ray film.

2.4. Sphingolipid Analysis by ESI-MS. Overnight cultures grown at 24°C in YPD media were diluted to OD_{600} 0.2 and grown until they reached OD_{600} of 2. A total of 10 OD units of cells were collected and washed once with sterile water. Lipid extraction was performed by a two-step lipid extraction method [23]. Cells were resuspended in 1 mL of 150 mM ammonium bicarbonate (NH_4HCO_3) and 600 μL of glass beads were added. After cell lysis using a Precellys 24 homogenizer ((Bertin technologies) 5000 rpm, 3x 30 sec on 30 sec off), lysates were diluted in 5 mL of 150 mM NH_4HCO_3 solution and internal standards were added. Long chain bases and ceramides were quantified relative to respective lipid standards, and inositol phosphoceramides were measured relative to a phosphoinositol standard. Lipid standards were purchased from Avanti Polar Lipids. ESI-MS analysis was performed using a Bruker Esquire HCT ion trap mass spectrometer in positive or negative ion mode. Peaks

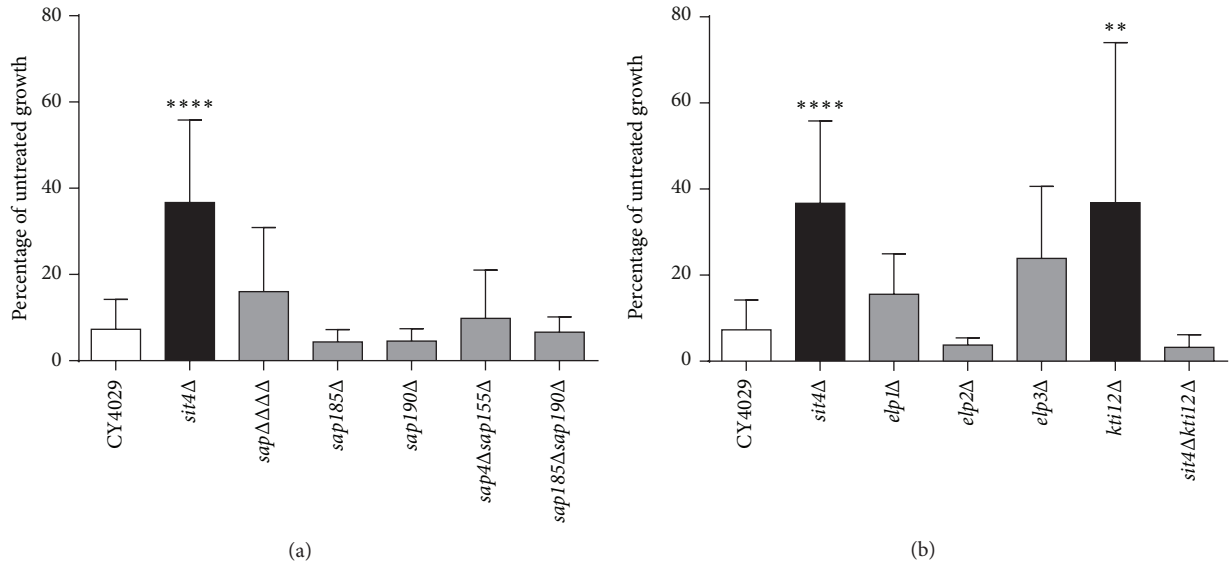

Figure 2: Deletion of *SIT4* or *KTI12* confers resistance to excess dihydroceramide. (a) Ceramide growth tests in Sit4 associated protein (SAP) mutants. (b) Ceramide growth tests in Elongator-associated mutants. Yeast cultures were diluted to 5×10^3 cells/mL in YPD with the addition of either 15 μM C-2 dihydroceramide or an equal volume of ethanol. Cells were grown until the untreated culture reached exponential phase and the OD_{600} of all cultures was determined. Growth in 15 μM dihydroceramide is expressed as a percentage of untreated growth. Raw OD_{600} values are given in Supplementary Table 1. A minimum of three replicates are shown and error bars represent the standard deviation above and below the mean. A one-way ANOVA with a Bonferroni post-test was used to determine if mutants showed a significant difference in growth compared to the wild type (CY4029) ($^{**}P < 0.01$, $^{***}P < 0.001$, and $^{****}P < 0.0001$).

were identified based on their fragmentation pattern and by comparison to commercially available standards. Three biological replicates were included in each analysis.

2.5. Incorporation of [^{3}H]-Labelled Inositol. Overnight cultures grown at 24°C in YPD were diluted to OD_{600} 1.0 in synthetic defined media containing 40 μCi [^{3}H] *myo*-inositol (American Radiolabelled Chemicals, MO, USA) and grown at 24°C for 4 h until they reached OD_{600} of approximately 2. A total of 10 OD units were harvested, and lipids were extracted using chloroform/methanol/water (10 : 10 : 3) and analysed as previously described [24] by thin layer chromatography with or without mild-base treatment. Mild-base treatment to remove inositol phosphate and leave only N-acetylated sphingolipids was performed by incubating lipids in 0.1 M NaOH at 30°C for 1 hour. Radioactivity was detected using a phosphorimager (Typhoon FLA9500, GE Healthcare) and a representative image of two biological replicates is shown.

3. Results

3.1. Deletion of Sit4-Associated Proteins (SAPs) Does Not Confer Resistance to Exogenous Dihydroceramide. As previously described [10], deletion of *SIT4* leads to significant resistance to 15 μM dihydroceramide (Figure 2, $P < 0.0001$). However, mutation of the four SAP regulatory proteins, either individually or in combination, does not confer resistance to dihydroceramide (Figure 2(a)). In previous studies, the phenotype of the quadruple *sap* mutant has been indistinguishable from that of *sit4*Δ [19, 20]. Thus, the ceramide sensitivity of the *sap* mutant is the first observed separation of function between *sit4*Δ and *sap*ΔΔΔΔ.

3.2. Kti12p Appears to Be the Only Elongator-Associated Protein Involved in the Ceramide Response. As Sit4p plays a major role in the phosphoregulation of the Elongator complex [18, 21] and previous studies suggested that Elongator mutants were resistant to ceramide, Elongator components were investigated as potential targets of Sit4p in the response to excess dihydroceramide. Although deletion of Elongator subunits did not confer statistically significant resistance to 15 μM dihydroceramide, deletion of the Elongator accessory protein Kti12p did confer resistance (Figure 2(b)) to some extent, though the obtained data were rather variable (Supplementary Table 1). Interestingly, deletion of *SIT4* and *KTI12* in tandem restored sensitivity to dihydroceramide, whereas in a previous study mutants lacking one or both of these genes had the same phenotype that resulted in hyperphosphorylation of Elp1p and zymocin resistance [18]. In addition, phosphorylation of Elp1p was unchanged in the presence of dihydroceramide, and this was not affected by deletion of *SIT4* and/or *KTI12* (data not shown). Therefore, our data suggest that Kti12p might play a regulatory role in the ceramide response that is independent of Elongator.

*3.3. PHS Resistance of sit4*Δ *Indicates Separation of Function from kti12*Δ. Growth in phytoceramide decreases in a concentration-dependent manner in both wild-type and mutant strains; however, *sit4*Δ and *kti12*Δ mutants show significantly more growth ($P < 0.005$) than the parental

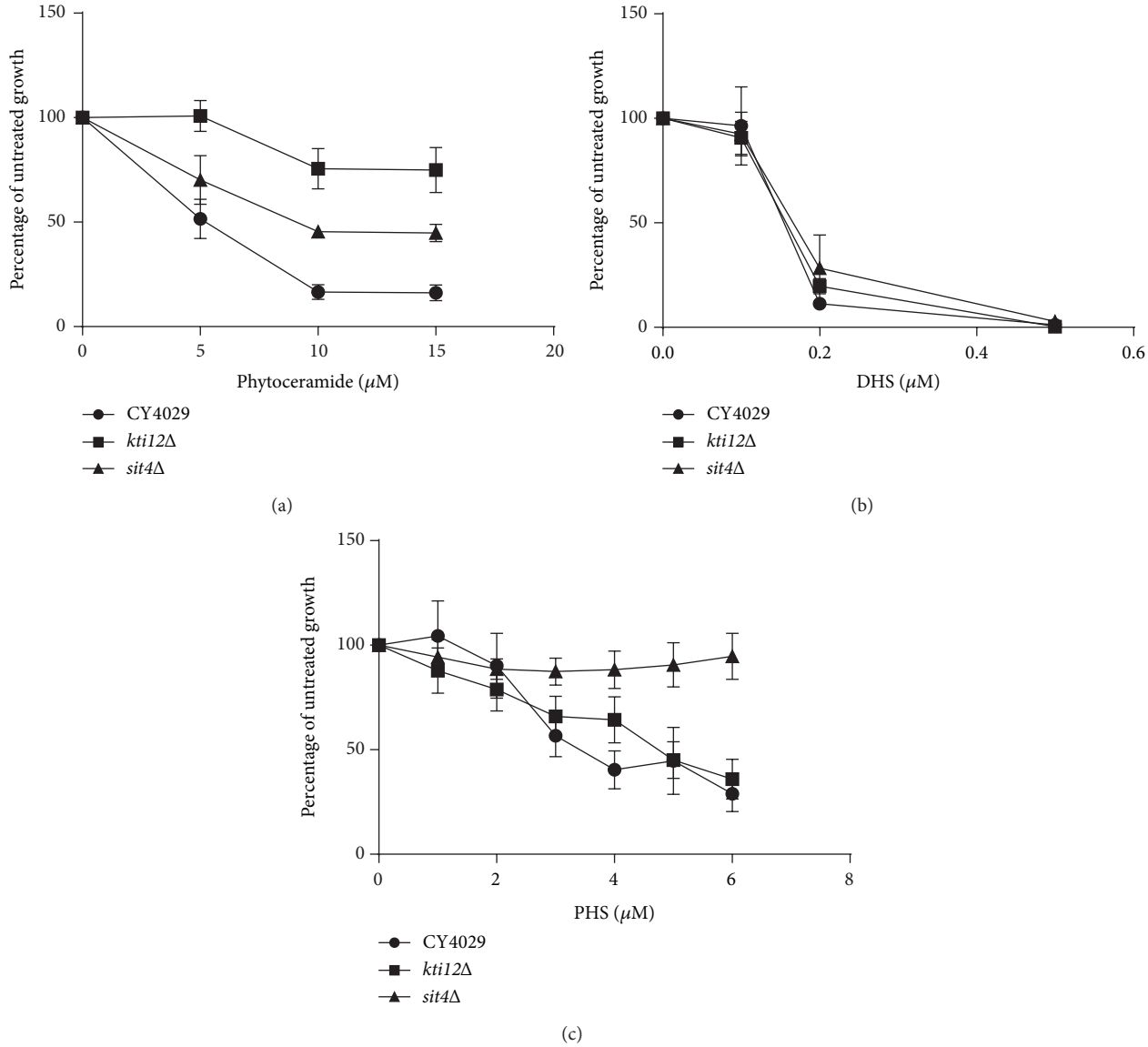

Figure 3: Response of *sit4*Δ and *kti12*Δ mutants to phytoceramide and long chain bases. Yeast cultures were diluted to 5×10^3 cells/mL in YPD with the addition of the indicated concentrations of (a) phytoceramide, (b) dihydrosphingosine (DHS), (c) phytosphingosine (PHS), or an equal volume of ethanol. Cells were grown until the untreated culture reached exponential phase and then the OD_{600} of both treated and untreated cells was measured and plotted as a percentage of untreated growth. Raw OD_{600} values are given in Supplementary Table 2. A minimum of three replicates are shown and error bars represent the standard error above and below the mean. A Student's *t*-test was used to determine if the mutants showed a significant difference in growth compared to the wild type (CY4029) at each concentration shown.

CY4029 strain at concentrations of 10–15 μM (Figure 3(a)). In contrast, growth of *sit4*Δ and *kti12*Δ mutants in excess dihydrosphingosine (DHS) is indistinguishable from CY4029 (Figure 3(b)). The most striking result is that while *kti12*Δ is also sensitive to phytosphingosine (PHS), *sit4*Δ shows significant ($P < 0.05$) resistance to 3–6 μM PHS (Figure 3(c)), suggesting divergence of function between Kti12p and Sit4p in the response to long chain bases.

*3.4. Ceramide and Long Chain Base Levels Are Reduced in sit4*Δ *and kti12*Δ *Mutants.* To investigate the possibility that Sit4p and Kti12p regulate the sphingolipid biosynthesis pathway, we measured steady state levels of ceramides, long chain bases, and inositol phosphate in *sit4*Δ and *kti12*Δ strains relative to wild-type yeast cells. Deletion of *SIT4* or *KTI12* reduces the intracellular levels of phytoceramide by approximately 50% (Figure 4(a)). Levels of dihydroceramide are also reduced in both mutants, but the decrease is only statistically significant in *sit4*Δ (Figure 4(a)). This suggests that the mutants may be able to tolerate otherwise toxic levels of exogenous ceramides due to the constitutively lower levels present within the cell. The reduction of PHS levels by approximately two-thirds in the *sit4*Δ mutant could permit the strain to survive excess concentrations of PHS

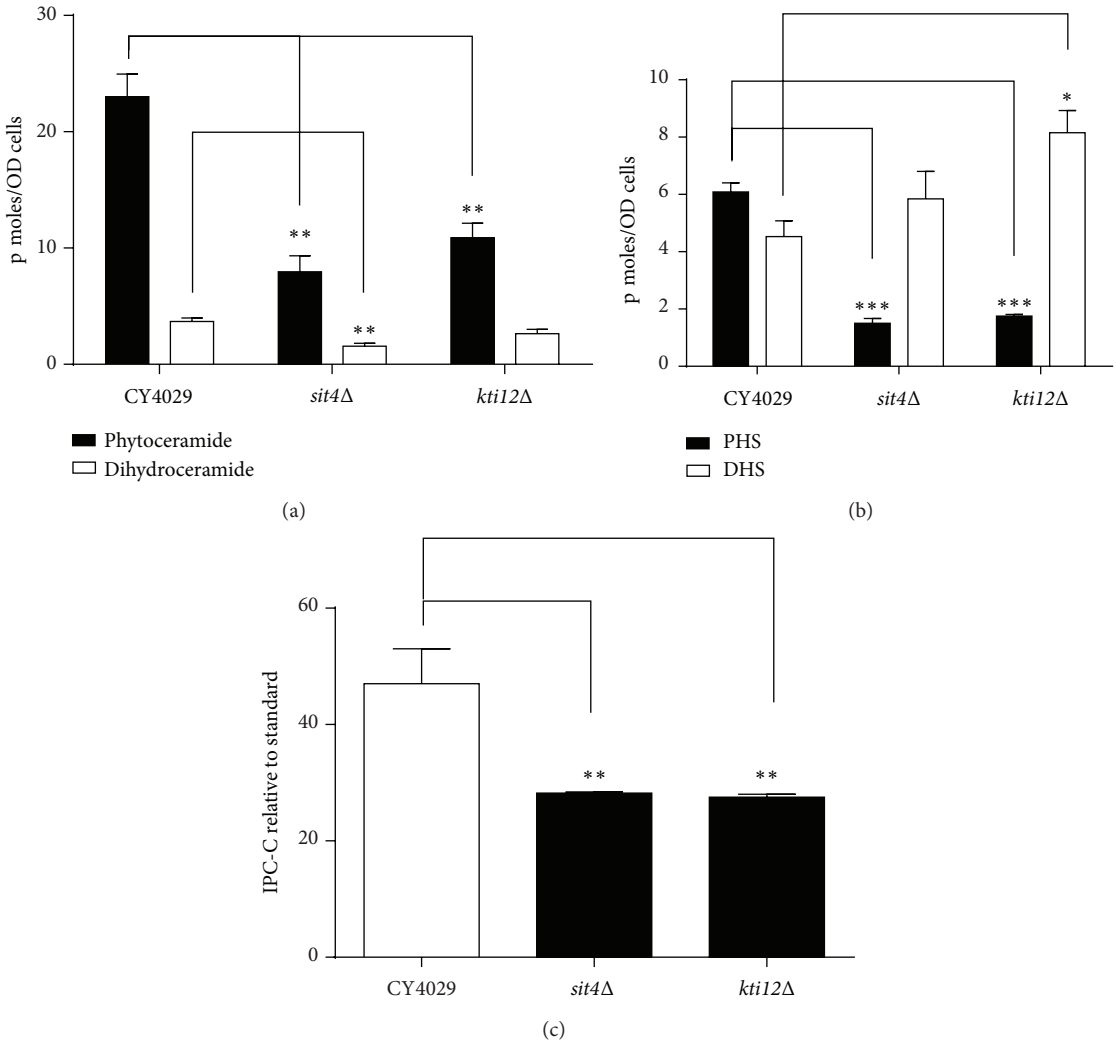

FIGURE 4: Mass spectrometric analysis of sphingolipid species. Yeast cultures were diluted to an OD_{600} of 0.2 in YPD and grown for 8 hours at 24°C. A total of 10 OD_{600} units of cells were removed and lipids extracted for mass spectrometry analysis. (a) Ceramides, (b) long chain bases phytosphingosine (PHS) and dihydrosphingosine (DHS), and (c) Inositol phosphoceramide-C (IPC-C) were quantified using relevant internal standards. Average values for a minimum of three biological replicates are shown and error bars represent the standard error above and below the mean. A Student's *t*-test was used to determine if the mutants showed a significant difference from the wild type CY4029. ($^{*}P < 0.05$, $^{**}P < 0.01$, and $^{***}P < 0.005$).

(Figure 4(b)). However, a similar decrease in PHS levels in the *kti12*Δ mutant does not correlate with resistance to exogenous PHS (Figures 4(b) and 3(c)), suggesting that a more complex mechanism underlies PHS resistance. There is a small increase in the levels of DHS in *sit4*Δ and *kti12*Δ mutants (Figure 4(b)) which is unlikely to affect the toxicity of DHS seen in Figure 3(b).

3.5. Sit4 Mutants Show an Increase in the Proportion of Dihydro Sphingolipids and a Corresponding Decrease in the Proportion of Hydroxylated Sphingolipids. Tritium labelled inositol incorporation was used to analyse the maturation of complex sphingolipid species formed from both dihydroceramide and phytoceramide. Dihydroceramide B′ (18:0;2/26:0;0) and phytoceramide C (18:0;3/26:0;0) form inositol phosphoceramide B (IPC-B) and inositol phosphoceramide C (IPC-C) respectively. IPC-C and the corresponding MIPC-C generated from it form the relatively more abundant species of their sphingolipid class in the wild type (Figure 5). Interestingly, the *sit4*Δ mutant contains increased levels of IPC-B and MIPC-B compared to the wild type, with a decrease in the levels of IPC-C and MIPC-C (Figure 5). The *kti12*Δ mutant also shows a similar trend in the relative levels of sphingolipid species, but the differences from the wild type are less pronounced than those for *sit4*Δ. This indicates a shift towards more sphingolipids being synthesised from dihydroceramide/DHS precursors than from the hydroxylated phytoceramide/PHS precursors. Figure 4(c) provides additional evidence for this shift and quantification of IPC-C levels shows a significant decrease in both *sit4*Δ and *kti12*Δ mutants. This also correlates with the increase in DHS and

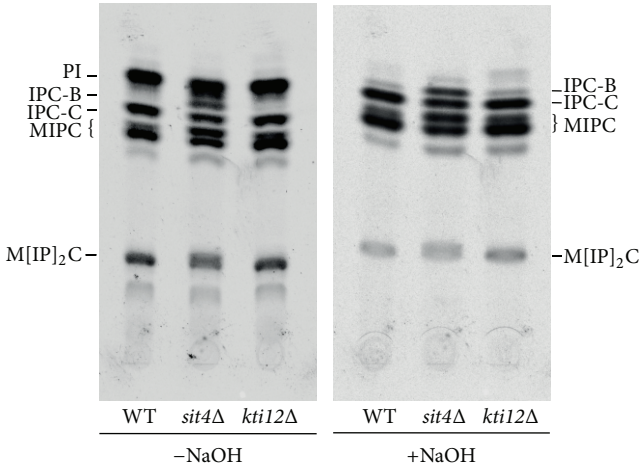

Figure 5: Tritium labelled inositol incorporation into yeast cells. CY4029 (WT), *sit4*Δ, and *kti12*Δ were incubated with [^{3}H]-inositol for 4 hours, and lipids were extracted and analysed by thin layer chromatography, before and after mild-base treatment to remove inositol phosphate (PI). Equal CPMs were loaded for all the samples. A representative image of two biological replicates is shown.

decrease in PHS levels observed in *sit4*Δ and *kti12*Δ mutants (Figure 4(b)).

3.6. Novel Interactions of Sit4p with Tpd3p and Cdc55p Suggest a Role for an Alternative Phosphatase Complex in the Response to Ceramide. Previous studies suggested that Tpd3p and Cdc55p could be part of the CAPP complex as deletion of these genes conferred resistance to ceramide [10]. Indeed, we found via immunoprecipitation experiments with HA-labelled Sit4p that Tpd3p and Cdc55p-c-myc interact with Sit4p, forming a minor complex compared to the Pph21p/Tpd3p/Cdc55p complex (Figure 6). As this novel Sit4p/Tpd3p/Cdc55p trimer is formed constitutively and is not induced by the presence of ceramide (data not shown), the mechanism by which the phosphatase is activated in response to an increase in ceramide levels remains unclear.

4. Discussion

The aim of this study was to further investigate the role of the Sit4 phosphatase in response to ceramide and to determine if this signalling pathway is directly related to the biosynthesis of ceramides and sphingolipids. The phosphorylation status of Orm1p regulates the activity of serine palmitoyltransferase and therefore the production of all downstream products of the sphingolipid pathway. Orm1p is phosphorylated by Ypk1p and evidence suggests that dephosphorylation may involve Sit4p and/or its TOR-dependent subunit Tap42p [25, 26]. However, Orm1p is unlikely to be the direct substrate for the Sit4p or Tap42p phosphatases as mutation of these genes leads to decreased phosphorylation of Orm1p [25].

The Sit4 phosphatase is a well-characterised regulator of tRNA modification via the Elongator complex [18, 21, 27–29]. However, here we show that the role of Sit4p in the ceramide response is independent of Elongator yet still involves the multifunctional and Elongator-related accessory protein Kti12p. Although previous work suggested that Elongator may be involved in ceramide resistance [18], more detailed analysis in this current study indicates that Elongator mutants are sensitive to ceramide. Although Kti12p is essential for the phosphoregulation of Elongator, its precise role remains unclear [18, 21]. Kti12p also has diverse roles in other cellular processes including the cell cycle [30] and transcription [31], and regulation of the ceramide response can now be added to this list.

The Sit4 phosphatase has multiple regulatory subunits including the Sit4 associated proteins (SAPs) Sap4p, Sap155p, Sap185p, and Sap190p. A quadruple deletion of all SAPs is sensitive to excess ceramide, in contrast to the resistant *sit4*Δ mutant. Importantly, this is the first separation of function observed between the *sit4*Δ and *sap*ΔΔΔΔ mutants. This suggests that an alternative Sit4 phosphatase complex is involved in the regulation of the ceramide response, supporting the idea that this process is independent of Elongator functions that require Sit4/Sap complexes. The identification of a Sit4p/Tpd3p/Cdc55p trimer also supports the theory that the ceramide activated protein phosphatase could be acting via a previously unknown mechanism.

The alteration of the sphingolipid makeup in *sit4*Δ and *kti12*Δ mutants and the decreased levels of ceramide and long chain bases indicate that there is regulation of the biosynthetic pathway at some level by Sit4p and/or Kti12p. The decreased level of endogenous ceramide and PHS in the mutants presumably enables them to survive an otherwise toxic concentration of these compounds. This suggests that deletion of *SIT4* and *KTI12* mediates a downregulation or partial inactivation of ceramide synthesis rather than a complete block, as there are clearly sufficient precursors available for effective biosynthesis of sphingolipids. The presence of multiple genes encoding enzymes for synthesis and degradation of ceramides is a key way in which sphingolipid metabolism can be maintained when the pathway is partially blocked. Phosphoregulation of ceramide synthases has not been previously observed, but three phosphorylated serine residues are conserved in both Lag1p and Lac1p ceramide synthases and could be potential targets for dephosphorylation by Sit4p [32, 33]. In common with *sit4*Δ and *kti12*Δ mutants, *lac1*Δ*lag1*Δ mutants are resistant to the tRNase toxin zymocin, but the mechanism of action is due to a defect in plasma membrane integrity caused by decreased levels of the sphingolipid M(IP)$_2$C and not via Elongator [34].

In *sit4*Δ and *kti12*Δ mutants, the relative proportion of lipids synthesised from dihydroceramides/DHS is higher than those synthesised from phytoceramides/PHS, suggesting that there could be a defect in the Sur2 hydroxylase which hydroxylates both long chain bases and ceramides [35]. This is also reflected in the increased levels of DHS seen in the mutants and is therefore unlikely to simply be a defect in the synthesis of ceramide or downregulation at an earlier stage in the pathway, as not all components of the pathway are downregulated. The ceramidases Ypc1p and Ydc1p also have a minor ceramide synthase activity and show specificity for

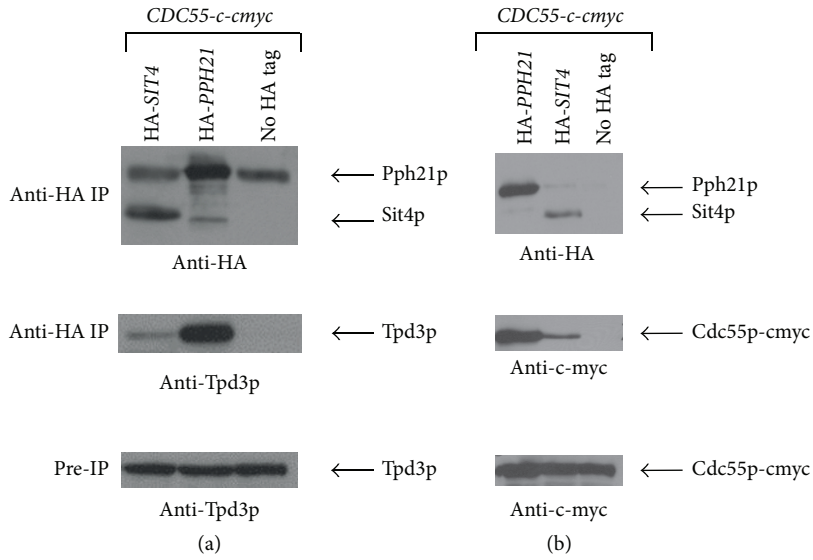

Figure 6: Immunoprecipitation of HA-Sit4p reveals novel interactors. Equal amounts of protein extracts were immunoprecipitated with magnetic beads coated with anti-HA antibodies, and the precipitates were then subjected to Western blotting and probed with anti-HA and anti-Tpd3 (a) or anti-c-myc (b) antibodies. Equal amounts of total protein extracts (without immunoprecipitation) were also probed with anti-Tpd3 or anti-c-myc antibodies.

hydroxylated and nonhydroxylated forms of long chain bases, respectively. [36] Dysregulation in *sit4*Δ could cause a shift towards the synthesis of nonhydroxylated sphingolipids by these enzymes. However, these enzymes contribute a minor level of ceramide synthase activity compared to Lag1p, Lac1p, and Lip1p [37], so a change in their regulation is unlikely to have any detrimental effects on the overall sphingolipid composition of the plasma membrane, even if the balance of individual components is altered.

These new insights into the novel ceramide-associated functions of Sit4p and Kti12p are helpful in understanding the diverse roles these proteins play in the cell and expand our knowledge of their importance beyond their association with the Elongator complex. Relatively little is known about the human orthologues of Sit4p and Kti12p, and thus yeast studies are vital in unravelling the essential role they play in regulating cell proliferation and cell death in both healthy and malignant cells.

5. Conclusions

This study indicates that the roles of Sit4p and Kti12p in the ceramide response are distinct from their roles in the regulation of the Elongator complex and are therefore likely to be mediated via a novel mechanism. The separation of function between *sit4*Δ and *sap*ΔΔΔ mutants and the interaction of Sit4p with the alternative regulatory subunits Cdc55p and Tpd3p also support this theory. Alterations in the levels of ceramides, long chain bases, and complex sphingolipids in *sit4*Δ and *kti12*Δ mutants indicate that these proteins are also likely to regulate the sphingolipid biosynthesis pathway. Future work will be targeted at delineating the underlying mechanism(s) underlying these observations.

Acknowledgments

This work was funded by The Wellcome Trust (Grant no. WT088104MA). The authors would like to thank Yu Jiang for the donation of anti-Tpd3p antibody and Michael Stark and Robert Mason for helpful discussions.

References

[1] G. M. Jenkins and Y. A. Hannun, "Role for *de Novo* sphingoid base biosynthesis in the heat-induced transient cell cycle arrest of *Saccharomyces cerevisiae*," *Journal of Biological Chemistry*, vol. 276, no. 11, pp. 8574–8581, 2001.

[2] T. Kolter, "A view on sphingolipids and disease," *Chemistry and Physics of Lipids*, vol. 164, no. 6, pp. 590–606, 2011.

[3] P. P. Ruvolo, "Intracellular signal transduction pathways activated by ceramide and its metabolites," *Pharmacological Research*, vol. 47, no. 5, pp. 383–392, 2003.

[4] S. A. Saddoughi, P. Song, and B. Ogretmen, "Roles of bioactive sphingolipids in cancer biology and therapeutics," *Sub-Cellular Biochemistry*, vol. 49, pp. 413–440, 2008.

[5] S. Gatt and A. Dagan, "Cancer and sphingolipid storage disease therapy using novel synthetic analogs of sphingolipids," *Chemistry and Physics of Lipids*, vol. 165, no. 4, pp. 462–474, 2012.

[6] S. Ponnusamy, M. Meyers-Needham, C. E. Senkal et al., "Sphingolipids and cancer: ceramide and sphingosine-1-phosphate in the regulation of cell death and drug resistance," *Future Oncology*, vol. 6, no. 10, pp. 1603–1624, 2010.

[7] L. K. Ryland, T. E. Fox, X. Liu, T. P. Loughran, and M. Kester, "Dysregulation of sphingolipid metabolism in cancer," *Cancer Biology and Therapy*, vol. 11, no. 2, pp. 138–149, 2011.

[8] R. C. Dickson, "New insights into sphingolipid metabolism and function in budding yeast," *Journal of Lipid Research*, vol. 49, no. 5, pp. 909–921, 2008.

[9] N. Bartke and Y. A. Hannun, "Bioactive sphingolipids: metabolism and function," *Journal of Lipid Research*, vol. 50, supplement, pp. S91–96, 2009.

[10] J. T. Nickels and J. R. Broach, "A ceramide-activated protein phosphatase mediates ceramide-induced G1 arrest of *Saccharomyces cerevisiae*," *Genes and Development*, vol. 10, no. 4, pp. 382–394, 1996.

[11] M. A. de la Torre-Ruiz, J. Torres, J. Ariño, and E. Herrero, "Sit4 is required for proper modulation of the biological functions mediated by Pkc1 and the cell integrity pathway in *Saccharomyces cerevisiae*," *Journal of Biological Chemistry*, vol. 277, no. 36, pp. 33468–33476, 2002.

[12] A. R. Butler, R. W. O'Donnell, V. J. Martin, G. W. Gooday, and M. J. R. Stark, "*Kluyveromyces lactis* toxin has an essential chitinase activity," *European Journal of Biochemistry*, vol. 199, no. 2, pp. 483–488, 1991.

[13] B. Huang, J. Lu, and A. S. Byström, "A genome-wide screen identifies genes required for formation of the wobble nucleoside 5-methoxycarbonylmethyl-2-thiouridine in *Saccharomyces cerevisiae*," *RNA*, vol. 14, no. 10, pp. 2183–2194, 2008.

[14] Y. Jiang and J. R. Broach, "Tor proteins and protein phosphatase 2A reciprocally regulate Tap42 in controlling cell growth in yeast," *EMBO Journal*, vol. 18, no. 10, pp. 2782–2792, 1999.

[15] M. N. Miranda, C. A. Masuda, A. Ferreira-Pereira, E. Carvajal, M. Ghislain, and M. Montero-Lomelí, "The serine/threonine protein phosphatase Sit4p activates multidrug resistance in *Saccharomyces cerevisiae*," *FEMS Yeast Research*, vol. 10, no. 6, pp. 674–686, 2010.

[16] A. Sutton, D. Immanuel, and K. T. Arndt, "The *SIT4* protein phosphatase functions in late G1 for progression into S phase," *Molecular and Cellular Biology*, vol. 11, no. 4, pp. 2133–2148, 1991.

[17] C. J. Di Como and K. T. Arndt, "Nutrients, via the Tor proteins, stimulate the association of Tap42 with type 2A phosphatases," *Genes and Development*, vol. 10, no. 15, pp. 1904–1916, 1996.

[18] D. Jablonowski, L. Fichtner, M. J. R. Stark, and R. Schaffrath, "The yeast elongator histone acetylase requires Sit4-dependent dephosphorylation for toxin-target capacity," *Molecular Biology of the Cell*, vol. 15, no. 3, pp. 1459–1469, 2004.

[19] D. Jablonowski, J.-E. Täubert, C. Bär, M. J. R. Stark, and R. Schaffrath, "Distinct subsets of Sit4 holophosphatases are required for inhibition of *Saccharomyces cerevisiae* growth by rapamycin and zymocin," *Eukaryotic Cell*, vol. 8, no. 11, pp. 1637–1647, 2009.

[20] M. M. Luke, F. D. Seta, C. J. Di Como, H. Sugimoto, R. Kobayashi, and K. T. Arndt, "The SAPs, a new family of proteins, associate and function positively with the *SIT4* phosphatase," *Molecular and Cellular Biology*, vol. 16, no. 6, pp. 2744–2755, 1996.

[21] C. Mehlgarten, D. Jablonowski, K. D. Breunig, M. J. R. Stark, and R. Schaffrath, "Elongator function depends on antagonistic regulation by casein kinase Hrr25 and protein phosphatase Sit4," *Molecular Microbiology*, vol. 73, no. 5, pp. 869–881, 2009.

[22] D. Jablonowski, F. Frohloff, L. Fichtner, M. J. R. Stark, and R. Schaffrath, "*Kluyveromyces lactis* zymocin mode of action is linked to RNA polymerase II function via Elongator," *Molecular Microbiology*, vol. 42, no. 4, pp. 1095–1105, 2001.

[23] S. Han, M. A. Lone, R. Schneiter, and A. Chang, "Orm1 and Orm2 are conserved endoplasmic reticulum membrane proteins regulating lipid homeostasis and protein quality control," *Proceedings of the National Academy of Sciences of the United States of America*, vol. 107, no. 13, pp. 5851–5856, 2010.

[24] F. Reggiori, E. Canivenc-Gansel, and A. Conzelmann, "Lipid remodeling leads to the introduction and exchange of defined ceramides on GPI proteins in the ER and Golgi of *Saccharomyces cerevisiae*," *EMBO Journal*, vol. 16, no. 12, pp. 3506–3518, 1997.

[25] M. Liu, C. Huang, S. R. Polu, R. Schneiter, and A. Chang, "Regulation of sphingolipid synthesis through Orm1 and Orm2 in yeast," *Journal of Cell Science*, vol. 125, no. 10, pp. 2428–2435, 2012.

[26] F. M. Roelants, D. K. Breslow, A. Muir, J. S. Weissman, and J. Thorner, "Protein kinase Ypk1 phosphorylates regulatory proteins Orm1 and Orm2 to control sphingolipid homeostasis in *Saccharomyces cerevisiae*," *Proceedings of the National Academy of Sciences of the United States of America*, vol. 108, no. 48, pp. 19222–19227, 2011.

[27] B. Huang, M. J. O. Johansson, and A. S. Byström, "An early step in wobble uridine tRNA modification requires the Elongator complex," *RNA*, vol. 11, no. 4, pp. 424–436, 2005.

[28] D. Jablonowski, S. Zink, C. Mehlgarten, G. Daum, and R. Schaffrath, "tRNAGlu wobble uridine methylation by Trm9 identifies Elongator's key role for zymocin-induced cell death in yeast," *Molecular Microbiology*, vol. 59, no. 2, pp. 677–688, 2006.

[29] C. Mehlgarten, D. Jablonowski, U. Wrackmeyer et al., "Elongator function in tRNA wobble uridine modification is conserved between yeast and plants," *Molecular Microbiology*, vol. 76, no. 5, pp. 1082–1094, 2010.

[30] A. R. Butler, J. H. White, Y. Folawiyo, A. Edlin, D. Gardiner, and M. J. R. Stark, "Two *Saccharomyces cerevisiae* genes which control sensitivity to G1 arrest induced by *Kluyveromyces lactis* toxin," *Molecular and Cellular Biology*, vol. 14, no. 9, pp. 6306–6316, 1994.

[31] T. G. Petrakis, T. M. M. Søgaard, H. Erdjument-Bromage, P. Tempst, and J. Q. Svejstrup, "Physical and functional interaction between elongator and the chromatin-associated Kti12 protein," *Journal of Biological Chemistry*, vol. 280, no. 20, pp. 19454–19460, 2005.

[32] B. Bodenmiller, D. Campbell, B. Gerrits et al., "PhosphoPep: a database of protein phosphorylation sites in model organisms," *Nature Biotechnology*, vol. 26, no. 12, pp. 1339–1340, 2008.

[33] A. Huber, B. Bodenmiller, A. Uotila et al., "Characterization of the rapamycin-sensitive phosphoproteome reveals that Sch9 is a central coordinator of protein synthesis," *Genes and Development*, vol. 23, no. 16, pp. 1929–1943, 2009.

[34] S. Zink, C. Mehlgarten, H. K. Kitamoto et al., "Mannosyldiinositolphospho-ceramide, the major yeast plasma membrane sphingolipid, governs toxicity of *Kluyveromyces lactis* zymocin," *Eukaryotic Cell*, vol. 4, no. 5, pp. 879–889, 2005.

[35] M. M. Grilley, S. D. Stock, R. C. Dickson, R. L. Lester, and J. Y. Takemoto, "Syringomycin action gene *SYR2* is essential for sphingolipid 4- hydroxylation in *Saccharomyces cerevisiae*," *Journal of Biological Chemistry*, vol. 273, no. 18, pp. 11062–11068, 1998.

[36] C. Mao, R. Xu, A. Bielawska, and L. M. Obeid, "Cloning of an alkaline ceramidase from *Saccharomyces cerevisiae*. An enzyme with reverse (CoA-independent) ceramide synthase activity," *Journal of Biological Chemistry*, vol. 275, no. 10, pp. 6876–6884, 2000.

[37] C. Mao, R. Xu, A. Bielawska, Z. M. Szulc, and L. M. Obeid, "Cloning and characterization of a *Saccharomyces cerevisiae* alkaline ceramidase with specificity for dihydroceramide," *Journal of Biological Chemistry*, vol. 275, no. 40, pp. 31369–31378, 2000.

Hindawi Publishing Corporation
Oxidative Medicine and Cellular Longevity
Volume 2013, Article ID 704654, 7 pages
http://dx.doi.org/10.1155/2013/704654

Research Article

Potentiation of Antibiofilm Activity of Amphotericin B by Superoxide Dismutase Inhibition

Katrijn De Brucker,[1] Anna Bink,[1] Els Meert,[1] Bruno P. A. Cammue,[1,2] and Karin Thevissen[1]

[1] *Centre of Microbial and Plant Genetics, KU, Leuven, 3001 Heverlee, Belgium*
[2] *CMPG, Kasteelpark Arenberg 20, 3001 Heverlee, Belgium*

Correspondence should be addressed to Bruno P. A. Cammue; bruno.cammue@biw.kuleuven.be

Received 8 May 2013; Accepted 23 July 2013

Academic Editor: Cristina Mazzoni

This study demonstrates a role for superoxide dismutases (Sods) in governing tolerance of *Candida albicans* biofilms to amphotericin B (AmB). Coincubation of *C. albicans* biofilms with AmB and the Sod inhibitors N,N′-diethyldithiocarbamate (DDC) or ammonium tetrathiomolybdate (ATM) resulted in reduced viable biofilm cells and increased intracellular reactive oxygen species levels as compared to incubation of biofilm cells with AmB, DDC, or ATM alone. Hence, Sod inhibitors can be used to potentiate the activity of AmB against *C. albicans* biofilms.

1. Introduction

Candida albicans biofilms are responsible for device-related infections in most nosocomial diseases [1]. Such infections are particularly serious because biofilm-associated *Candida* cells are relatively resistant to a wide spectrum of antifungal drugs, including amphotericin B (AmB) [2]. The cause of this increased resistance is not yet fully elucidated but could be due to a combined action of different mechanisms including (i) expression of resistance genes, (ii) drug binding to the extracellular matrix, (iii) the change in membrane composition, or (iv) the presence of persister cells, which are cells that can survive high doses of an antimicrobial agent [3]. Due to this increased resistance, biofilm eradication and treatment of associated infections are challenging. The recalcitrance to antifungal therapy remains the biggest threat to patients with fungal biofilms and is an increasingly significant clinical problem [4]. Understanding the role of fungal biofilms during infection should help the clinical management of these recalcitrant infections. Until now, no vaccines are available to combat fungal infections, despite the considerable growth in the research field [5]. Therefore, the use of antimycotics is currently the only clinical solution for these infections. Among the current antimycotics in clinical use, only the liposomal formula of AmB and echinocandins has shown consistent *in vitro* and *in vivo* activity against *C. albicans* biofilms [6–8]. AmB is a fungicidal polyene and, apart from its interaction with ergosterol and subsequent pore formation, induces accumulation of reactive oxygen species (ROS) and apoptosis in planktonic and biofilm *C. albicans* cells [9, 10]. Despite its high efficacy as an antimycotic, the effective concentrations of AmB required for elimination of *Candida* biofilms are often hepatoxic and/or nephrotoxic [11, 12]. Therefore, in order to improve the potential of AmB for treatment of such biofilms, it is recommended to search for new approaches in which the effective concentration of AmB against *C. albicans* biofilms and consequently also its negative side effects are reduced.

In this study, we aimed at identifying compounds that lead to increased antibiofilm activity of AmB. Recently, we reported that superoxide dismutases (Sods) are involved in *C. albicans* biofilm persistence to the ROS-inducing antifungal miconazole. *C. albicans* contains 6 different Sods, which are involved in the detoxification of ROS by converting O_2^- into molecular oxygen and hydrogen peroxide [13, 14]. Sod1, Sod4, Sod5, and Sod6 of *C. albicans* are Cu,Zn-containing superoxide dismutases [14] that can be inhibited using the Cu,Zn-Sod inhibitor N,N′-diethyldithiocarbamate (DDC),

which chelates copper [15]. We previously demonstrated that this inhibitor potentiates the activity of miconazole against *C. albicans* persister cells within biofilms, thereby allowing ROS build-up and intensive killing of the persister cells [16]. Ammonium tetramolybdate (ATM) is another copper chelator which is used in clinical applications. For example, ATM is used therapeutically in the treatment of copper metabolism disorders (e.g., Wilson's disease) where it reduces copper adsorption or removes excess copper from the body [17–19]. ATM inhibits activities of a variety of Cu-utilizing enzymes, including Cu,Zn-Sod1 [20–22]. In the present study, we investigated a putative effect of DDC or ATM on the activity of AmB against *C. albicans* biofilms and planktonic cells.

2. Materials and Methods

2.1. Materials, Yeast Strains, Plasmids, and Growth Media. *C. albicans* CA-IF100 [13], *C. albicans* clinical isolates F17, G6 [23], and 2CA [16] were used in this study. Growth medium was YPD (1% yeast extract, 2% peptone, and 2% glucose) and SC (1% CSM, complete amino acid supplement mixture, 1% YNB, yeast nitrogen base; 2% glucose). N-N′-diethyldithiocarbamate (DDC) (stock = 1 M in water), ammonium tetrathiomolybdate (ATM) (stock = 1 M in DMSO) and AmB (stock = 5 mM in DMSO), were purchased from Sigma (St. Louis, MO, USA). DHE was purchased from Life technologies (Paisley, UK). Phosphate-buffered saline (PBS) was prepared by combining 8 gl^{-1} NaCl, 0.2 gl^{-1} KCl, 1.44 gl^{-1} Na_2HPO_4, and 0.24 gl^{-1} KH_2PO_4 (pH 7.4).

2.2. Drug Susceptibility Testing against Planktonic C. albicans Cells. Overnight cultures of *C. albicans* were washed in PBS and diluted in SC medium to 1×10^6 cells/mL. Cultures were treated with 0.156 μM AmB, 10 mM DDC or 0.156 μM AmB, and 10 mM DDC and incubated for 24 hours at 37°C. DMSO (2%) was used as a control treatment. Next, cells were diluted in PBS and plated on YPD agar plates. Afterwards, the number of colony-forming units was determined and the percentage of surviving *C. albicans* cells was calculated relative to the DMSO control treatment.

2.3. Drug Susceptibility Testing on C. albicans Biofilms. The activity of AmB (final DMSO concentration = 2%) in the absence or presence of 10 mM DDC or 10 mM ATM against 16 h old *C. albicans* biofilms was assessed in PBS as described previously [16]. DMSO (2%) was used as a control treatment. Briefly, after incubation for 24 h, biofilms were washed, resuspended in PBS by vigorous vortexing, and plated on YPD agar plates. The fraction of viable biofilm cells was determined by counting the colonies and calculating the percentage of surviving *Candida* cells, relative to the control treatment.

2.4. ROS Accumulation Assay in C. albicans Biofilm Cells. Quantification of ROS using 2′,7′-dichlorodihydrofluorescein diacetate (DCFHDA) was performed as previously described [16]. Quantification of ROS was additionally determined using dihydroethidium (DHE). To this end, *C. albicans* biofilms were treated with 1 μM AmB in presence or absence of 10 mM DDC or 10 mM ATM (final DMSO concentration = 2%). As a control treatment, 2% DMSO was used. After 24 h incubation at 37°C, biofilms were washed and resuspended in PBS by vigorous vortexing. A sample was taken for colony counting, after which the biofilm cells were incubated for 20 minutes at 37°C with 20 μM DHE. After washing, fluorescence was measured (510 nm/595 nm) using a fluorescence spectrometer and values were normalized to the number of CFUs.

2.5. Statistical Analysis. Statistical analysis was performed using unpaired t-test. Differences were considered significant if $^{*}P < 0.05$; $^{**}P < 0.01$; $^{***}P < 0.001$. Data of all experiments are represented by the mean ± SEM.

3. Results and Discussion

3.1. DDC Increases the Antibiofilm Activity of AmB against C. albicans. First we investigated the effect of N-N′-diethyldithiocarbamate (DDC) on the activity of Amphotericin B (AmB) against *C. albicans* CA_IF-100 biofilms. To this end, a concentration of AmB that had no significant effect on the viability of *C. albicans* biofilm cells was used. Treatment of *C. albicans* biofilms with 1 μM AmB did not result in a statistically significant reduction of viable biofilm cells compared to control treatment (Figure 1). We used these concentrations of AmB to further investigate the potential of DDC on potentiating the antibiofilm activity of AmB against *C. albicans* biofilms. Since Lushchak and colleagues previously demonstrated that treatment of *Saccharomyces cerevisiae* with DDC caused a dose-dependent inhibition of Sod activity *in vivo*, with 75% inhibition occurring at 10 mM DDC [15], we used a similar concentration in our experiments. Coincubation of *C. albicans* biofilms with 1 μM AmB and 10 mM DDC resulted in an approximately 10,000-fold reduction of viable biofilm cells as compared to AmB or DDC treatment alone. More specifically, treatment of *C. albicans* biofilms with 1 μM AmB and 10 mM DDC resulted in only 0.008 ± 0.002% viable biofilm cells ($P < 0.001$), whereas treatment of biofilms with 1 μM AmB alone resulted in 84.80 ± 9.66% viable biofilm cells. Treatment of *C. albicans* biofilms with 10 mM DDC alone resulted only in a 2-fold reduction of the viable biofilm cells ($P < 0.05$) (Figure 1), pointing to a clearly enhanced antibiofilm activity of AmB when combined with DDC.

3.2. The Antibiofilm Activity of AmB against C. albicans Clinical Isolates is Enhanced by DDC. To evaluate the above findings further, we assessed the antibiofilm activity of AmB and DDC using 3 *C. albicans* clinical isolates. Clinical isolates F17 and G6 are characterized by increased levels of AmB-tolerant persisters [23] whereas strain 2CA was isolated from the voice prosthesis of different laryngectomized patients [16]. The percentage of viable biofilm cells upon treatment of *C. albicans* F17, G6, or 2CA biofilms is represented in

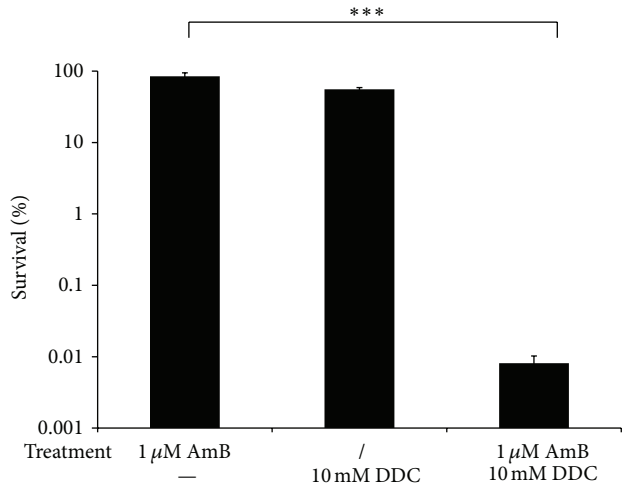

Figure 1: Effect of N-N′-diethyldithiocarbamate (DDC) on AmB-tolerant cells in *C. albicans* CA-IF100 biofilms. Biofilms were treated with or without (/) 1 μM AmB in presence or absence (−) of 10 mM DDC. After 24 hours, biofilms were washed with PBS and the percentage survival of *C. albicans* cells, relative to the control treatment (2% DMSO), was determined by plating the biofilm cells on YPD plates. Data represent the mean and SEM for one representative experiment out of two, each consisting of triplicate measurements. $^{***}P < 0.001$.

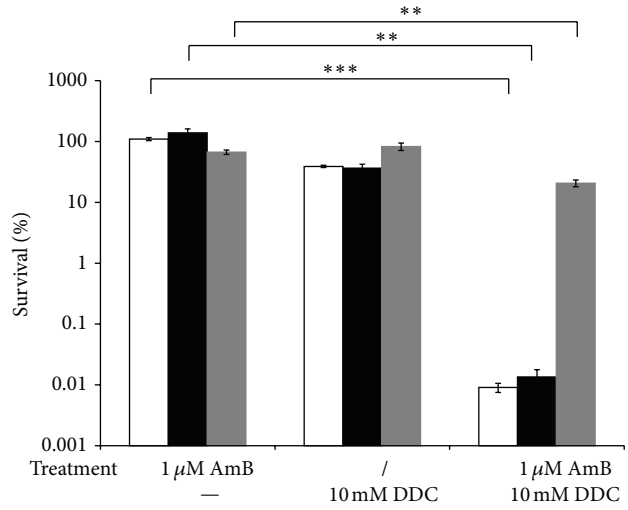

Figure 2: Effect of DDC on AmB-tolerant cells in biofilms of *C. albicans* clinical isolates F17, G6, and 2CA. *C. albicans* biofilms of F17, G6, or 2CA were treated with or without (/) 1 μM AmB in presence or absence (−) of 10 mM DDC. Afterwards, biofilms were washed with PBS and survival of *Candida* cells was determined by plating the biofilm cells on YPD plates. The AmB-tolerant fraction in presence or absence of 10 mM DDC was determined relative to DMSO treatment. Data represent the mean and SEM for one representative experiment out of two, each consisting of triplicate measurements. F16 (white bars), G6 (black bars), 2CA (grey bars). $^{**}P < 0.01$; $^{***}P < 0.001$.

Figure 2. Coincubation of F17 or G6 biofilms with 1 μM AmB and 10 mM DDC resulted in an approximately 10,000-fold reduction of viable biofilm cells as compared to AmB treatment alone. More specifically, treatment of biofilms of F17 or G6 with 1 μM AmB and 10 mM DDC resulted in only 0.009 ± 0.002% ($P < 0.001$) or 0.01 ± 0.004% ($P < 0.01$) of viable biofilm cells, respectively, whereas treatment of biofilms of F17 or G6 with 1 μM AmB alone had no effect on the viability of these biofilm cells. Treatment of these biofilms with 10 mM DDC alone resulted in a 3-fold reduction of viable biofilm cells ($P < 0.05$) (Figure 2). Treatment of 2CA biofilms with 1 μM AmB and 10 mM DDC resulted in an approximately 3-fold reduction of viable cells compared to AmB treatment alone. More specifically, coincubated 2CA biofilms resulted in 20.6 ± 2.6% ($P < 0.01$) of viable cells, whereas treatment of these biofilms with 1 μM AmB alone resulted in 66.8 ± 5.7% of viable cells. Treatment of 2CA biofilms with 10 mM DDC alone resulted in 82.7 ± 11.5% viable cells (Figure 2). These results confirm that inhibition of Sod activity by DDC can potentiate the antibiofilm activity of AmB against various *C. albicans* clinical isolates. The extent of potentiation of the AmB antibiofilm activity seems strain dependent.

3.3. Potentation of Antifungal Activity of AmB by DDC is Not Biofilm Specific. The activity of AmB in the presence of DDC against planktonic *C. albicans* CA_IF-100 cells was determined. Also here, concentrations of AmB (0.156 μM) and DDC (1.25 mM) were used that had no or limited effect on the viability of planktonic *C. albicans* cells. The percentage of viable *C. albicans* planktonic cells after treatment with or without AmB in presence or absence of DDC is shown in Figure 3. Combined treatment of AmB and DDC resulted in an 8-fold reduction of the percentage of viable *C. albicans* cells compared to planktonic cells treated with AmB only. The percentage of viable planktonic cells after combined

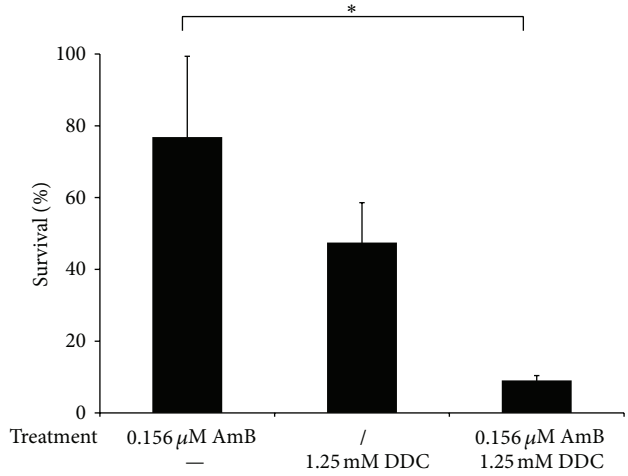

Figure 3: Effect of combined treatment of DDC and AmB on planktonic *C. albicans* cell cultures. Planktonic *C. albicans* cultures were treated with or without (/) 0.156 μM AmB in presence of absence (−) of 1.25 mM DDC for 24 hours and afterwards plated on YPD plates. The percentage survival relative to the control treatment (2% DMSO) is shown. Data represent the mean of 2 independent biological experiments, each consisting of two measurements. $^{*}P < 0.05$.

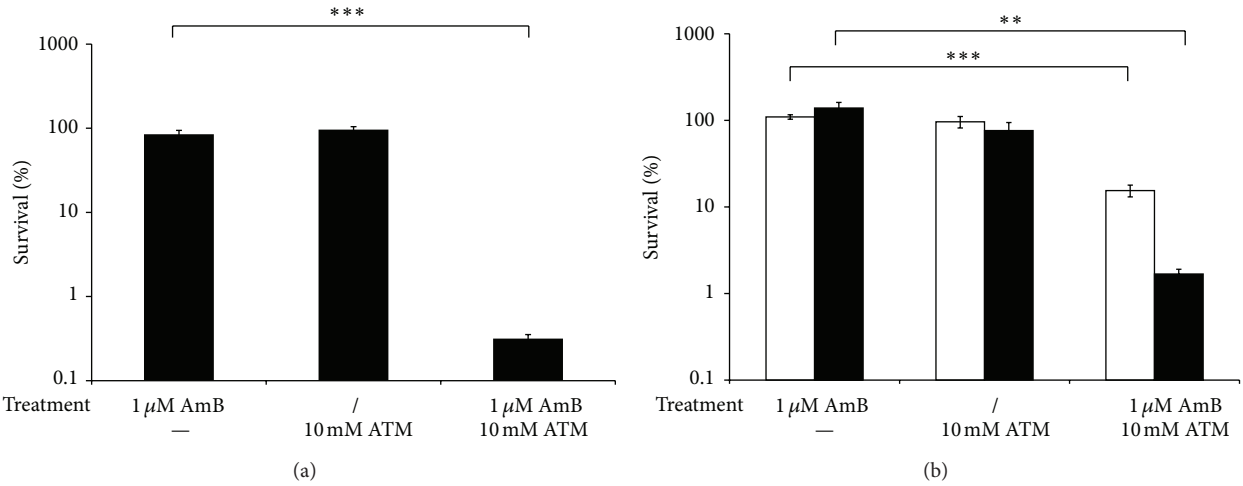

Figure 4: Effect of ATM on AmB-tolerant cells in biofilms of *C. albicans* CA-IF100 (a) and clinical isolates F17 and G6 (b). *C. albicans* biofilms were treated without (/) or with 1 μM AmB in the absence (−) or presence of 10 mM ATM. Afterwards, biofilms were washed with PBS and survival of *Candida* cells was determined by plating the biofilm cells on YPD plates. The AmB-tolerant fraction in presence or absence of 10 mM DDC was determined relative to DMSO treatment. Data represent the mean and SEM for one representative experiment out of two, each consisting of triplicate measurements. (a) CA-IF100 and (b) clinical isolates F17 (white bars) and G6 (black bars). $^{**}P < 0.01$; $^{***}P < 0.001$.

treatment of AmB and DDC (9 ± 1%) was significantly reduced ($P < 0.05$) compared to treatment with AmB (77 ± 20%) or DDC (47 ± 11%) alone (Figure 3). This result shows that DDC-dependent potentiation of the activity of AmB is not biofilm specific, as DDC also potentiates the activity of AmB against planktonic cells, albeit to a lesser extent.

3.4. ATM, a Clinical Used Copper Chelator, Increases the Activity of AmB against C. albicans Biofilm Cells. As DDC is associated with neurotoxicity [24], which might limit its clinical potential, we also determined the effect of ATM, a therapeutically used copper chelator [17, 18], on the antibiofilm activity of AmB. Coincubation of *C. albicans* CA_IF-100 biofilms with 1 μM AmB and 10 mM ATM led to an approximately 300-fold reduction of viable biofilm cells, resulting in only 0.32 ± 0.04% ($P < 0.001$) of viable biofilm cells, compared to AmB treatment alone. Treatment of *C. albicans* biofilms with 10 mM ATM alone did not result in a significant reduction of the viable biofilm cells (Figure 4(a)). In addition, the percentage of viable *C. albicans* cells of two clinical isolates, F17 and G6, was also determined after treatment without or with 1 μM AmB in the presence or absence of 10 mM ATM (Figure 4(b)). Co-incubation of F17 or G6 biofilms with 1 μM AmB and 10 mM ATM resulted in a 7- or 80-fold significant reduction of viable biofilm cells, respectively, as compared to AmB treatment alone (Figure 4(b)). Treatment of biofilms of F17 or G6 with 1 μM AmB and 10 mM ATM resulted in 15.47 ± 2.40% ($P < 0.001$) or 1.68 ± 0.22% ($P < 0.01$) viable biofilm cells, respectively, whereas treatment of biofilms of F17 or G6 with 1 μM AmB alone had no effect on the viability of these biofilm cells. Treatment of these biofilms with 10 mM ATM alone resulted in no significant reduction of the viable biofilm cells (Figure 4(b)). These results indicate that ATM also increases the activity of AmB against clinical isolates, albeit to a lesser extent compared to the wild-type CA-IF100, in contrast to DDC. This might indicate that DDC is more effective in inhibiting Sods compared to ATM. However, additional studies are necessary to investigate this further.

3.5. Treatment with DDC and ATM Increases Endogenous Reactive Oxygen Species Levels in AmB-Treated Biofilms. To determine if treatment with the Sod inhibitors DDC or ATM enhances endogenous reactive oxygen species (ROS) levels in AmB-treated biofilms, the accumulation of ROS was quantified using 2′,7′-dichlorodihydrofluorescein diacetate (DCFHDA) or dihydroethidium (DHE). DCF, the conversion product of DCFHDA, indicates the presence of several types of ROS, including hydrogen peroxide and peroxyl radicals, whereas DHE is a specific superoxide detection reagent [25]. In a first series of experiments, we used DCFHDA as detection reagent. Coincubation of CA-IF100 biofilms with AmB and DDC resulted in significantly increased endogenous ROS levels in *C. albicans* biofilm cells as compared to AmB or DDC treatment alone. CA-IF100 biofilms, treated with a combination of 1 μM AmB and 10 mM DDC and incubated with H2DCFA, resulted in an approximately 10,000-fold increase of endogenous ROS levels ($P < 0.05$), compared to biofilms treated with AmB or DDC alone (Figure 5(a)). Also coincubation of *C. albicans* biofilms with 1 μM AmB and 10 mM ATM resulted in an approximately 50-fold increase of endogenous ROS levels in *C. albicans* biofilm cells (Figure 5(a)) ($P < 0.001$), indicating again that DDC seems more effective in inhibiting Sods compared to ATM. As Sods convert superoxide to hydrogen peroxide, we have set up additional experiments in which we specifically

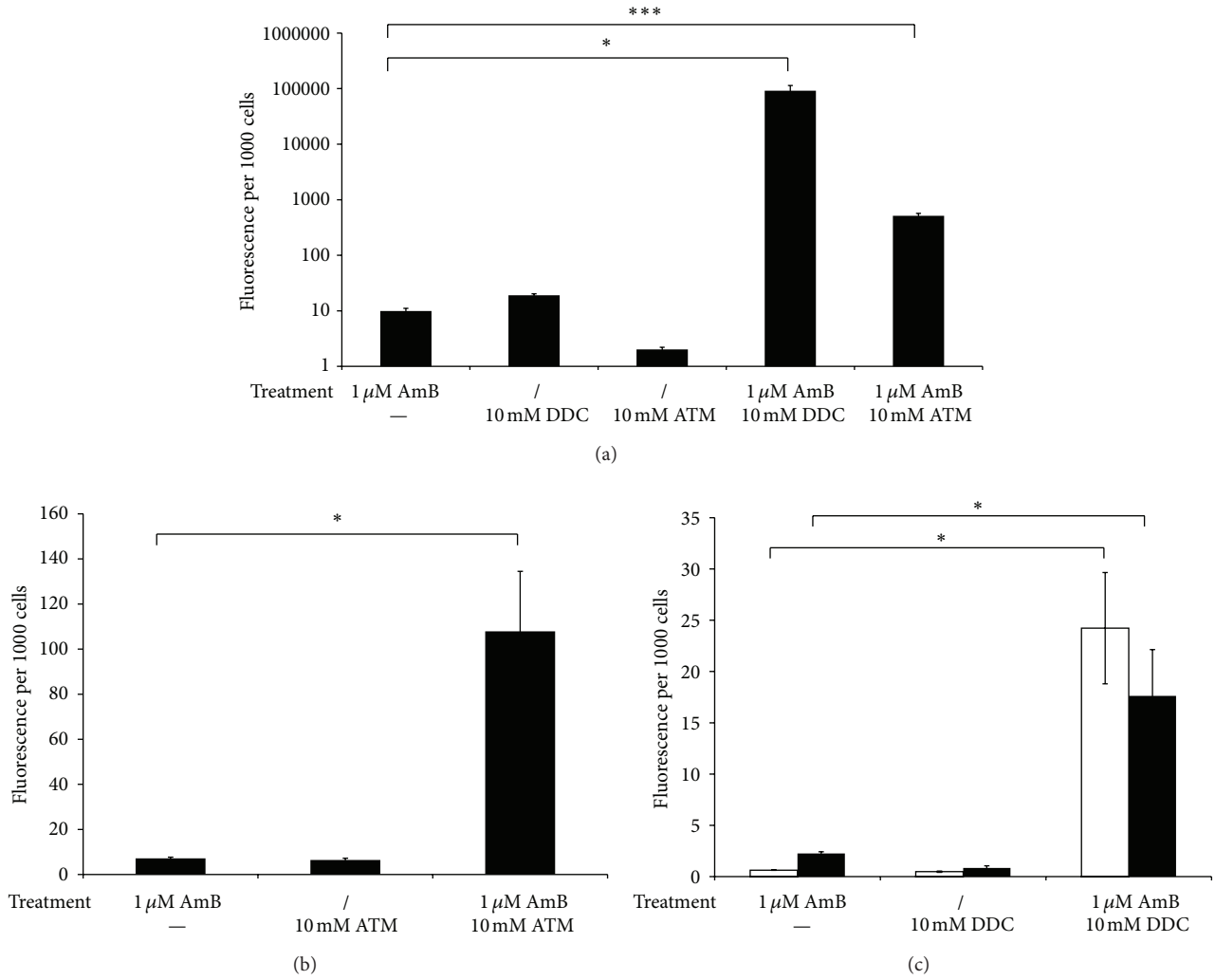

Figure 5: Effect of DDC and ATM on ROS levels in *C. albicans* biofilms. (a) *C. albicans* CA-IF100 biofilms were treated with or without (/) 1 μM AmB in presence or absence (−) of 10 mM DDC or 10 mM ATM. Biofilms were washed with PBS and a sample was taken for CFU determination. Afterwards, 10 μM DCFDA was added. Fluorescence was normalized to the number of CFUs after treatment. (b) and (c). Effect of DDC on peroxide levels on *C. albicans* biofilm cells. *C. albicans* biofilms were treated with or without (/) 1 μM AmB in presence or absence (−) of 10 mM DDC. Biofilms were washed with PBS and a sample was taken for CFU determination. Afterwards, 20 μM DHE was added. Fluorescence was normalized to the number of CFUs after treatment. (b) CA-IF100, (c) F17 (white bars), and G6 (black bars). Data represent the mean and SEM for one representative experiment out of two, each consisting of triplicate measurements. $^{*}P < 0.05$, $^{***}P < 0.001$.

monitored superoxide accumulation, using DHE staining, in *C. albicans* CA-IF100, G6, and F17 biofilms cells upon various treatments. Co-incubation of CA-IF100 biofilm cells with AmB and DDC resulted in an approximately 15-fold increased superoxide accumulation ($P < 0.05$), compared to biofilms treated with AmB or DDC alone (Figure 5(b)). Moreover, also biofilms of clinical isolates F17 and G6, treated with AmB and DDC, accumulated, respectively, 40- or 8-fold more superoxide compared to F17 or G6 biofilms treated with AmB alone ($P < 0.05$) (Figure 5(c)). These results show that inhibition of Sod activity by DDC in the presence of AmB results in a significantly increased superoxide accumulation. Hence, it seems that AmB specifically induces superoxide as a means to kill fungal cells, including biofilm cells.

4. Conclusions

All above data indicate that, in *C. albicans* biofilm cells, Sods are not only involved in protection of *C. albicans* biofilms to miconazole [16] but also to AmB, probably via detoxification of AmB-induced superoxide.

These results are in line with results of Seneviratne and coworkers [26]. They demonstrated that *C. albicans* biofilm formation is associated with increased antioxidative capacities. Several proteins involved in oxidative stress defenses, including thioredoxin peroxidase and alkyl hydroperoxide reductase, are upregulated in biofilms, which may contribute to the higher resistance to ROS-inducing antifungals like AmB and miconazole [25]. In addition, several reports document the possibility of enhancing the fungicidal activity

of ROS-inducing antifungals by targeting the oxidative stress response system of fungi. For example, Kim and coworkers demonstrated that different redox-potent chemosensitizing agents like natural dihydroxybenzaldehydes, thymol, or salicylaldehyde could enhance the antifungal activity of different ROS-inducing antifungals [27–29]. One of their studies specifically demonstrates that chemically targeting the oxidative stress response system of fungi effectively augments antimycotic potency of AmB [28]. Based on our data, it seems that Sod inhibitors can reduce the antioxidative capacities of *C. albicans* biofilm cells, resulting in increased efficacy of ROS-inducing antifungals. In a report of Walker and coworkers, it was demonstrated that the combination of DDC and AmB is effective in treating systemic *Candida* infections [30]. We now demonstrated that the combination of DDC and AmB displayed potent *in vitro* activity against biofilms of various *C. albicans* strains, including AmB-tolerant clinical isolates. However, as DDC is associated with neurotoxicity, ATM or other nontoxic and specific Sod inhibitors might lead to a novel antibiofilm combination therapy, consisting of a ROS-inducing antifungal with such inhibitor.

Conflict of Interests

The authors declare that they have no conflict of interests.

Authors' Contribution

Katrijn De Brucker and Anna Bink contributed equally to this paper.

Acknowledgments

This work was supported by grants from FWO-Vlaanderen (W0.026.11N, G.0896.10N) and the Industrial Research Fund (IOF) of KU Leuven (knowledge platform IOF/KP/11/007). Furthermore, the research leading to these results has received funding from the European Commission's Seventh Framework Programme (FP7/2007–2013) under the grant agreement COATIM (Project no. 278425). Karin Thevissen acknowledges the receipt of a postdoctoral fellowship from the Industrial Research Fund and KU Leuven (IOFm/05/022) and Anna Bink a predoctoral fellowship from FWO-Vlaanderen.

References

[1] G. Ramage, E. Mowat, B. Jones, C. Williams, and J. Lopez-Ribot, "Our current understanding of fungal biofilms fungal biofilms," *Critical Reviews in Microbiology*, vol. 35, no. 4, pp. 340–355, 2009.

[2] N. N. Mishra, T. Prasad, N. Sharma et al., "Pathogenicity and drug resistance in *Candida albicans* and other yeast species," *Acta Microbiologica et Immunologica Hungarica*, vol. 54, no. 3, pp. 201–235, 2007.

[3] C. J. Seneviratne, L. Jin, and L. P. Samaranayake, "Biofilm lifestyle of *Candida*: a mini review," *Oral Diseases*, vol. 14, no. 7, pp. 582–590, 2008.

[4] G. Ramage, J. P. Martínez, and J. L. López-Ribot, "*Candida* biofilms on implanted biomaterials: a clinically significant problem," *FEMS Yeast Research*, vol. 6, no. 7, pp. 979–986, 2006.

[5] A. Cassone, "Fungal vaccines: real progress from real challenges," *The Lancet Infectious Diseases*, vol. 8, no. 2, pp. 114–124, 2008.

[6] L. Didone, D. Oga, and D. J. Krysan, "A novel assay of biofilm antifungal activity reveals that amphotericin B and caspofungin lyse *Candida albicans* cells in biofilms," *Yeast*, vol. 28, no. 8, pp. 561–568, 2011.

[7] D. M. Kuhn, T. George, J. Chandra, P. K. Mukherjee, and M. A. Ghannoum, "Antifungal susceptibility of *Candida* biofilms: unique efficacy of amphotericin B lipid formulations and echinocandins," *Antimicrobial Agents and Chemotherapy*, vol. 46, no. 6, pp. 1773–1780, 2002.

[8] J. A. Shuford, M. S. Rouse, K. E. Piper, J. M. Steckelberg, and R. Patel, "Evaluation of caspofungin and amphotericin B deoxycholate against *Candida albicans* biofilms in an experimental intravascular catheter infection model," *The Journal of Infectious Diseases*, vol. 194, no. 5, pp. 710–713, 2006.

[9] R. S. Al-Dhaheri and L. J. Douglas, "Apoptosis in *Candida* biofilms exposed to amphotericin B," *Journal of Medical Microbiology*, vol. 59, no. 2, pp. 149–157, 2010.

[10] A. J. Phillips, I. Sudbery, and M. Ramsdale, "Apoptosis induced by environmental stresses and amphotericin B in *Candida albicans*," *Proceedings of the National Academy of Sciences of the United States of America*, vol. 100, no. 2, pp. 14327–14332, 2003.

[11] K. V. Clemons, J. A. Schwartz, and D. A. Stevens, "Therapeutic and toxicologic studies in a murine model of invasive pulmonary aspergillosis," *Medical Mycology*, vol. 49, no. 8, pp. 834–847, 2011.

[12] G. P. Patel, C. W. Crank, and J. B. Leikin, "An evaluation of hepatotoxicity and nephrotoxicity of liposomal amphotericin B (L-AMB)," *Journal of Medical Toxicology*, vol. 7, no. 1, pp. 12–15, 2011.

[13] I. E. Frohner, C. Bourgeois, K. Yatsyk, O. Majer, and K. Kuchler, "*Candida albicans* cell surface superoxide dismutases degrade host-derived reactive oxygen species to escape innate immune surveillance," *Molecular Microbiology*, vol. 71, no. 1, pp. 240–252, 2009.

[14] M. Martchenko, A.-M. Alarco, D. Harcus, and M. Whiteway, "Superoxide dismutases in *Candida albicans*: transcriptional regulation and functional characterization of the hyphal-induced sod5 gene," *Molecular Biology of the Cell*, vol. 15, no. 2, pp. 456–467, 2004.

[15] V. Lushchak, H. Semchyshyn, O. Lushchak, and S. Mandryk, "Diethyldithiocarbamate inhibits in vivo Cu,Zn-superoxide dismutase and perturbs free radical processes in the yeast *Saccharomyces cerevisiae* cells," *Biochemical and Biophysical Research Communications*, vol. 338, no. 4, pp. 1739–1744, 2005.

[16] A. Bink, D. Vandenbosch, T. Coenye, H. Nelis, B. P. A. Cammue, and K. Thevissen, "Superoxide dismutases are involved in *Candida albicans* biofilm persistence against miconazole," *Antimicrobial Agents and Chemotherapy*, vol. 55, no. 9, pp. 4033–4037, 2011.

[17] G. J. Brewer, F. Askari, R. B. Dick et al., "Treatment of Wilson's disease with tetrathiomolybdate: V. control of free copper by tetrathiomolybdate and a comparison with trientine," *Translational Research*, vol. 154, no. 2, pp. 70–77, 2009.

[18] C. F. Mills, T. T. El-Gallad, and I. Bremner, "Effects of molybdate, sulfide, and tetrathiomolybdate on copper metabolism in

rats," *Journal of Inorganic Biochemistry*, vol. 14, no. 3, pp. 189–207, 1981.

[19] P. V. E. Van Den Berghe and L. W. J. Klomp, "New developments in the regulation of intestinal copper absorptionn," *Nutrition Reviews*, vol. 67, no. 11, pp. 658–672, 2009.

[20] M. V. Chidambaram, G. Barnes, and E. Frieden, "Inhibition of ceruloplasmin and other copper oxidases by thiomolybdate," *Journal of Inorganic Biochemistry*, vol. 22, no. 4, pp. 231–239, 1984.

[21] J. C. Juarez, O. Betancourt Jr., S. R. Pirie-Shepherd et al., "Copper binding by tetrathiomolybdate attenuates angiogenesis and tumor cell proliferation through the inhibition of superoxide dismutase 1," *Clinical Cancer Research*, vol. 12, no. 16, pp. 4974–4982, 2006.

[22] V. Medici and G. C. Sturniolo, "Tetrathiomolybdate, a copper chelator for the treatment of Wilson disease, pulmonary fibrosis and other indications," *IDrugs*, vol. 11, no. 8, pp. 592–606, 2008.

[23] M. D. LaFleur, Q. Qi, and K. Lewis, "Patients with long-term oral carriage harbor high-persister mutants of *Candida albicans*," *Antimicrobial Agents and Chemotherapy*, vol. 54, no. 1, pp. 39–44, 2010.

[24] O. M. Viquez, H. L. Valentine, K. Amarnath, D. Milatovic, and W. M. Valentine, "Copper accumulation and lipid oxidation precede inflammation and myelin lesions in N,N-diethyldithiocarbamate peripheral myelinopathy," *Toxicology and Applied Pharmacology*, vol. 229, no. 1, pp. 77–85, 2008.

[25] Invitrogen, The molecular probes handbook, 11th edition, chapter 18, section 18. 2.

[26] C. J. Seneviratne, Y. Wang, L. Jin, Y. Abiko, and L. P. Samaranayake, "*Candida albicans* biofilm formation is associated with increased anti-oxidative capacities," *Proteomics*, vol. 8, no. 14, pp. 2936–2947, 2008.

[27] J. H. Kim, K. L. Chan, N. Mahoney, and B. C. Campbell, "Antifungal activity of redox-active benzaldehydes that target cellular antioxidation," *Annals of Clinical Microbiology and Antimicrobials*, vol. 10, article 23, 2011.

[28] J. H. Kim, N. C. Faria, M. L. Martins, K. L. Chan, and B. C. Campbell, "Enhancement of antimycotic activity of amphotericin B by targeting the oxidative stress response of *Candida* and *Cryptococcus* with natural dihydroxybenzaldehydes," *Frontiers in Microbiology*, vol. 3, p. 261, 2012.

[29] J. H. Kim, K. L. Chan, N. C. Faria, M. L. Martins, and B. C. Campbell, "Targeting the oxidative stress response system of fungi with redox-potent chemosensitizing agents," *Frontiers in Microbiology*, vol. 3, p. 88, 2012.

[30] E. M. Walker Jr., D. J. Cannon, and M. E. Reifsteck, "Effects of diethyldithiocarbamate and structural analogs in mice with systemic candidial infections," *Research Communications in Chemical Pathology and Pharmacology*, vol. 56, no. 2, pp. 253–263, 1987.

Hindawi Publishing Corporation
Oxidative Medicine and Cellular Longevity
Volume 2013, Article ID 612784, 16 pages
http://dx.doi.org/10.1155/2013/612784

Research Article

A Regulatory Role of NAD Redox Status on Flavin Cofactor Homeostasis in *S. cerevisiae* Mitochondria

Teresa Anna Giancaspero,[1] Vittoria Locato,[2] and Maria Barile[1,3]

[1] *Istituto di Biomembrane e Bioenergetica, CNR, Via Orabona 4, 70126 Bari, Italy*
[2] *Centro Integrato di Ricerca, Università Campus Bio-Medico di Roma, Via Alvaro del Portillo 21, 00128 Roma, Italy*
[3] *Dipartimento di Bioscienze, Biotecnologie e Biofarmaceutica, Università degli Studi di Bari "Aldo Moro", Via Orabona 4, 70126 Bari, Italy*

Correspondence should be addressed to Maria Barile; maria.barile@uniba.it

Received 21 May 2013; Accepted 18 July 2013

Academic Editor: Cristina Mazzoni

Flavin adenine dinucleotide (FAD) and nicotinamide adenine dinucleotide (NAD) are two redox cofactors of pivotal importance for mitochondrial functionality and cellular redox balance. Despite their relevance, the mechanism by which intramitochondrial NAD(H) and FAD levels are maintained remains quite unclear in *Saccharomyces cerevisiae*. We investigated here the ability of isolated mitochondria to degrade externally added FAD and NAD (in both its reduced and oxidized forms). A set of kinetic experiments demonstrated that mitochondrial FAD and NAD(H) destroying enzymes are different from each other and from the already characterized NUDIX hydrolases. We studied here, in some detail, FAD pyrophosphatase (EC 3.6.1.18), which is inhibited by NAD^+ and NADH according to a noncompetitive inhibition, with *Ki* values that differ from each other by an order of magnitude. These findings, together with the ability of mitochondrial FAD pyrophosphatase to metabolize endogenous FAD, presumably deriving from mitochondrial holoflavoproteins destined to degradation, allow for proposing a novel possible role of mitochondrial NAD redox status in regulating FAD homeostasis and/or flavoprotein degradation in *S. cerevisiae*.

1. Introduction

Flavin adenine dinucleotide (FAD) and nicotinamide adenine dinucleotide (NAD) are two molecules of pivotal importance for mitochondrial functionality, given their role as redox cofactors of a large number of dehydrogenases, reductases, and oxidases mainly involved in energy production and redox homeostasis [1–4]. Additional emerging regulatory roles are linked to a number of additional cofactor-dependent events, such as protein folding, apoptosis, gene silencing, transcriptional regulation, DNA repairs and calcium-dependent signaling pathways. In many of these processes NAD and FAD are also involved in nonredox reactions (for recent reviews see [2, 5, 6]). In particular, NAD homeostasis and NAD-dependent modification of target proteins play a crucial role in calorie-restriction-induced lifespan extension and in age-related metabolic diseases [7–9]. Consistently, NAD- and FAD-dependent enzymes deficiency and/or impairment in flavin and NAD homeostasis in humans and experimental animals have been linked to several diseases, such as cancer, cardiovascular diseases, anemia, abnormal fetal development, and different neuromuscular and neurological disorders [10–14].

The relevance of such processes merits further research aimed to better describe NAD and FAD homeostasis and flavoenzyme biogenesis, especially in those organisms that can be simple and suitable model for human diseases. The conserved biological processes with all eukaryotic cells, together with the possibility of simple and quick genetic manipulation, allowed for proposing the budding yeast, *Saccharomyces cerevisiae*, as the premier model to understand the biochemistry and molecular biology of mammalian cells and to decipher molecular mechanisms underlying human diseases [15–17].

In yeast and most other organisms, besides *de novo* synthesis of NAD, the regeneration of NAD from its nicotinamide degradation products has been described in some detail [8, 18, 19]. This salvage pathway accompanies NAD^+-dependent signaling processes which, differently from those in which NAD works as redox cofactor, require constant replenishment of cellular NAD pools. NAD^+ salvage pathway takes place in the nucleus [20]. Differently from mammals [21, 22], NAD^+ is not synthesized in yeast mitochondria; consistently, two mitochondrial carriers (NDT1/2) seem to be responsible for replenishing mitochondrial NAD^+ level in yeasts [23, 24].

As regards NAD^+ into nicotinamide degradation products conversion, which occurs in many NAD^+-dependent signaling processes, the NAD^+ glycoside bound is potentially cleaved via reactions catalyzed by transferases (EC 2.4.2.-), like poly(ADP-ribose)polymerase; deacetylases (EC 3.5.1.-), like sirtuins; or hydrolases (EC 3.2.2.5) to produce nicotinamide and a variety of ADP-ribosyl products [5, 25]. From this wide spectrum of NAD^+ consuming enzymes, only sirtuins (SIRTs) have been identified in yeasts [26]. No member, out of the five *S. cerevisiae* sirtuins, seems to be localized into mitochondria.

Another way to cleave the pyridine nucleotide molecule is at the level of pyrophosphate bond via hydrolytic enzymes. A diphosphatase (pyrophosphatase), performing an enzymatic activity towards NADH, as preferred substrate, and giving NMNH and AMP as products, has been characterized in yeast as belonging to the NUDIX hydrolase family (EC 3.6.1.-) [27]. This enzyme, namely, Npy1p encoded by *YGL067W*, is able to catalyze NAD^+ hydrolysis and also very weakly FAD hydrolysis; it was reported to be located in peroxisomes, active at alkaline pH, and strongly inhibited by F^-. The existence of a mitochondrial isoenzyme has not been reported so far [28].

Turning to FAD, it is synthesized starting from riboflavin (Rf, vitamin B_2) via the sequential action of riboflavin kinase or ATP: riboflavin 5′-phosphotransferase (RFK, EC 2.7.1.26) and FAD synthase or FMN: ATP adenylyltransferase (FADS, EC 2.7.7.2). The first eukaryotic genes encoding for RFK [29] and FADS [30] have been identified and cloned in *S. cerevisiae*. Besides in the cytosol, FAD synthesis occurs also in yeast mitochondria [31, 32], thus necessitating Rf uptake into the organelle. The same mitochondrial pathway operates also in mammals and plants [33–35].

The knowledge of FAD cleavage events in yeast is rather poor, as opposed to its biosynthesis. The first investigation on FAD hydrolysis was carried out on cellular extracts obtained by the flavinogenic yeast *Pichia guilliermondii* [36, 37]. Following the demonstration of the existence of a mitochondrial FAD pyrophosphatase (FADppase, EC 3.6.1.18) and FMN phosphohydrolase (EC 3.1.3.2) in rat liver mitochondria [38], further functional evidence of FAD cleaving enzymes has been obtained in *S. cerevisiae* mitochondria (SCM) [39, 40]. The molecular identification of FADppase is still lacking, while a gene encoding for a specific FADppase so far has been cloned and identified in *Arabidopsis* and named *AtNUDX23*. It belongs to the NUDIX hydrolase family and is distributed in plastids [41, 42]. The possibility that some members of *S. cerevisiae* NUDIX hydrolase family were able to hydrolyze FAD remains to be investigated, in the frame of characterization of a putative mitochondrial FADppase [40].

Here we studied the ability of SCM to catalyze NAD and FAD hydrolysis via enzymatic activities which are different from the already characterized NUDIX hydrolases. The differential inhibition by the oxidized and reduced form of NAD, together with the ability of mitochondrial FADppase to metabolize endogenous FAD, presumably deriving from mitochondrial holoflavoproteins destined to degradation, allows for proposing a novel possible role of mitochondrial NAD redox status in regulating FAD homeostasis and, possibly, flavoprotein degradation in *S. cerevisiae*.

2. Materials and Methods

2.1. Materials. All reagents and enzymes were from Sigma-Aldrich (St. Luis, MO, USA), Zymolyase was from ICN (Abingdon, UK), and Bacto Yeast Extract was from Difco (Franklin Lakes, NJ, USA). Mitochondrial substrates were used as Tris salts at pH 7.0. Solvents and salts used for HPLC were from J.T.Baker (Center Valley, PA, USA).

2.2. Yeast Strain, Media, and Growth Conditions. The wild-type *S. cerevisiae* strain (EBY157A, genotype *MATα ura 3–52 MAL2-8^c SUC2 p426MET25*) used in this work was derived from the CEN.PK series of yeast strain and was obtained from P. Kotter (Instituet fuer Mikrobiologie, Goethe-Universitaet Frankfurt, Frankfurt, Germany), as already described in [31]. Cells were grown aerobically at 28°C with constant shaking in a semisynthetic liquid medium (3 g/L yeast extract, 1 g/L KH_2PO_4, 1 g/L NH_4Cl, 0.5 g/L NaCl, 0.5 g/L $CaCl_2{\cdot}2H_2O$, $MgCl_2{\cdot}6H_2O$, 20 mg/L uracil, 0.05% glucose) supplemented with 2% ethanol as carbon source. The pH of the medium was adjusted to 5.5 with HCl.

2.3. Mitochondria Isolation and Purification. Crude *S. cerevisiae* mitochondria (SCM) were isolated according to [31]. For pure SCM preparation, the final mitochondrial pellet was resuspended in the isolation medium, consisting of 0.6 M Mannitol and 20 mM HEPES pH 7.4, to obtain 5 mg mitochondrial protein/mL and subsequently purified from extramitochondrial contaminations using a sucrose gradient basically as described in [43]. The intactness of mitochondrial inner membrane was checked measuring the latency of release of the mitochondrial matrix enzyme fumarase (FUM) as in [34, 44] by treating SCM with the nonionic detergent Triton X-100 (TX100, 0.1%) at 0°C for 1 min. The mitochondrial functionality was assessed by oxygen uptake measurements carried out using a Gilson oxygraph as in [31]. The SCM purity was checked by measuring in SCM and spheroplasts (sphero) the activities of different marker enzymes such as cytosolic pyruvate decarboxylase (PDC), vacuolar alkaline phosphatase (AP), peroxisomal D-amino-acid oxidase (D-AAOX), and mitochondrial citrate synthase (CS) via spectrophotometric assays, essentially as described in [31, 45]. Mitochondrial protein concentration was determined according to [46].

2.4. FAD Hydrolysis. FAD externally added or endogenous FAD metabolism in *S. cerevisiae* was monitored by means of fluorimetric and HPLC measurements, essentially as in [38, 47]. In the case of fluorimetric measurements, flavin derivative emission spectra (excitation wavelength at 450 nm) and time drive measurements (excitation and emission wavelengths at 450 nm and 520 nm, resp.) were carried out at 25°C in 2 mL of a standard medium consisting of 0.6 M Mannitol, 50 mM TRIS-HCl, pH 7.5, and 5 mM $MgCl_2$ by means of a LS50B Perkin Elmer spectrofluorimeter. Flavin fluorescence emission spectra were corrected as in [48] by adding a few crystals of sodium dithionite to the mitochondrial suspension. When externally added FAD hydrolysis was measured, the endogenous flavin fluorescence was not considered since it was found to be negligible compared to that measured in subcellular suspension.

In each experiment, FAD, FMN, and Rf fluorescence was calibrated individually using standard solutions whose concentrations were calculated by using ε_{450} of 12.2 $mM^{-1} \cdot cm^{-1}$ for FMN and Rf, and 11.3 $mM^{-1} \cdot cm^{-1}$ for FAD. Under the experimental conditions used here, FAD fluorescence constant (K_{FAD}) proved to be about ten times lower than those of FMN and Rf ($K_{FMN/Rf}$) which did not differ significantly from each other [33, 49]. Thus, the rate of FAD hydrolysis, that is, the rate of FMN + Rf formation, expressed as nmol FAD hydrolyzed $\cdot$ $min^{-1} \cdot mg^{-1}$ protein, was calculated from the rate of fluorescence increase, measured as tangent to the initial part of the experimental curve by applying the following equation:

$$v_o = \frac{\left(\Delta F / \Delta K \times V_f\right)}{\Delta t \times m}, \tag{1}$$

where ΔF is expressed in fluorescence arbitrary units, V_f is expressed in mL, $\Delta K = K_{FMN/RF} - K_{FAD}$ is expressed as μM^{-1}, Δt is expressed in min, and m is the mass of protein in mg.

In the case of HPLC measurements, from aliquots of the subcellular suspension (100 μL), taken at various times, perchloric extracts were obtained and neutralized with KOH [33]. FAD, FMN, and Rf were analyzed by means of HPLC, as in [31, 47]. FAD, FMN, and Rf were measured in each experiment, with a quantitative determination carried out by measuring peak areas by means of a calibration curve. It should be noted that, in externally added FAD experiments, the contribution of endogenous flavins to the measured chromatographic peak area was proved to be negligible with respect to that due to flavin derivatives found in the subcellular suspension. Since the rate of FMN/Rf appearance measured fluorimetrically o via HPLC showed no significant difference, these experimental approaches were used in this work indifferently.

2.5. NADH Oxidation and Hydrolysis. NADH metabolism in *S. cerevisiae* was monitored by means of fluorimetric measurements, using a LS50B Perkin Elmer spectrofluorimeter. NADH excitation spectra (emission wavelength at 456 nm) and time drive measurements (excitation and emission wavelength pairs at 260/456 and 340/456 nm, resp.) were carried out at 25°C in 2 mL of a standard medium.

NADH oxidation to give the nonfluorescence NAD^+ can be revealed (when it is the sole process responsible for NADH disappearance) as a fluorescence decrease at 260/456 nm and 340/456 nm as tangent to the linear part of the experimental curve as

$$v_{ox} = \left[\frac{\left(\Delta F_{260/456}/\Delta t\right)}{K_{NADH260}}\right] \times V_f = \left[\frac{\left(\Delta F_{340/456}/\Delta t\right)}{K_{NADH340}}\right] \times V_f, \tag{2}$$

where $\Delta F_{ecc/em}$ is expressed in fluorescence arbitrary units, V_f is expressed in mL, $K_{NADH260}$ and $K_{NADH340}$ are expressed as μM^{-1}, and Δt is expressed in min.

Differently from oxidation, NADH hydrolysis results in products which are not fluorescent at 260/456 nm but still fluorescent at 340/456 nm (with a constant value 1.25-fold lower). Therefore, when hydrolysis is the sole process responsible for NADH disappearance, it can be revealed as a fluorescence decrease at 260/456 nm and 340/456 nm as tangent to the linear part of the experimental curve as

$$v_{idr} = \left[\frac{\left(\Delta F_{260/456}/\Delta t\right)}{K_{NADH260}}\right] \times V_f = \left[\frac{\left(\Delta F_{340/456}/\Delta t\right)}{\Delta K_{340}}\right] \times V_f \tag{3}$$

with $\Delta F_{260/456}/\Delta t$ higher than $\Delta F_{340/456}/\Delta t$.

Rearranging (2) and (3), it is possible to calculate the two components of the NADH disappearance in a complex system, where oxidation is significantly reduced with respect to hydrolysis (i.e., in the presence of KCN 1 mM).

The rate of NADH hydrolysis in the presence of residual NADH oxidation, expressed as nmol NADH hydrolyzed $\cdot$ $min^{-1} \cdot mg^{-1}$ protein, can be calculated by applying the following equation:

$$v_{idr} = \frac{\left[\left(\Delta F_{260/456}/\Delta t\right)/K_{NADH340} - \left(\Delta F_{340/456}/\Delta t\right)/K_{NADH260}\right]}{K_{NADH260} \cdot \left(K_{NADH340} - \Delta K_{340}\right)} \cdot V_f \tag{4}$$

with $\Delta F_{260/456}/\Delta t$ higher or equal to $\Delta F_{340/456}/\Delta t$.

The rate of NADH oxidation in the mixed system can be calculated as

$$v_{ox} = \frac{\left[\left(\Delta F_{340/456}/\Delta t\right)/K_{NADH260} - \left(\Delta F_{260/456}/\Delta t\right)/\Delta K_{340}\right]}{K_{NADH260} \cdot \left(K_{NADH340} - \Delta K_{340}\right)} \cdot V_f. \tag{5}$$

In each experiment, the $K_{NADH260}$ and $K_{NADH340}$ values were determined by calibrating NADH fluorescence with standard solutions, whose concentrations were spectrophotometrically defined (ε_{340} was 6.2 $mM^{-1} \cdot cm^{-1}$). NMNH fluorescence was calibrated using a standard curve produced by incubating NADH (at concentrations ranging from 1 to 10 μM) with excess amounts of commercial nucleotide pyrophosphatase (EC 3.6.1.9) to determine the ΔK_{340} value.

2.6. NAD^+ Hydrolysis. NAD^+ hydrolysis was measured by fluorimetrically monitoring the hydrolysis of nicotinamide $1,N^6$-ethenoadenine dinucleotide (ε-NAD^+), essentially as described in [50, 51]. Fluorescence measurements were performed using a Perkin Elmer LS5 spectrofluorimeter (excitation and emission wavelengths set at 310 nm and 410 nm) at 25°C in 2 mL of a standard medium. The fluorescence changes produced by subcellular suspensions were calibrated by using a standard curve produced by incubating ε-NAD^+ (at concentrations ranging from 1 to 6 μM) with excess amounts of commercial NADase [50]. The concentration of ε-NAD^+ was determined by the conversion of ε-NAD^+ to ε-NADH using the commercial alcohol dehydrogenase reaction and assuming a molar extinction coefficient for ε-NADH of $6.2\,mM^{-1} \cdot cm^{-1}$ at 340 nm.

2.7. Kinetic Data Analysis. Data fitting was performed according to the Michaelis-Menten equation:

$$v = V_{max} \cdot \frac{[S]}{K_m} + [S]. \quad (6)$$

To fit the experimental data and to obtain estimates of the kinetic parameters use was made of the GraFit software (v. 3.00, 1992, by R. J. Leatherbarrow, Erithacus Software).

2.8. Statistical Analysis. All experiments were repeated at least 3 times with different mitochondrial preparations. Results are presented as mean ± standard deviation. Statistical significance was evaluated by Student's t-test. Values of $P < 0.05$ were considered statistically significant.

3. Results and Discussion

In order to study NAD(H) mitochondrial metabolism we isolated functionally active SCM, as described before [31, 32], and further purified them, basically as in [43]. To control that SCM were significantly depleted by extramitochondrial contaminations; in Figure 1(a) we measured the distribution of the cytosolic marker enzyme (pyruvate decarboxylase, PDC), the vacuolar marker enzyme (alkaline phosphatase, AP), and the peroxisomal marker enzyme (D-aminoacid oxidase, DAAOX), with their specific activities being about tenfold (for the cytosolic and vacuolar markers) and fivefold (for the peroxisomal marker) lower in the mitochondrial fraction than those in spheroplasts (sphero). The purity of mitochondrial preparations was also assessed, by following the enrichment of the mitochondrial matrix marker enzymes citrate synthase (CS) in Figure 1(a) and fumarase (FUM) in Figure 1(b) whose specific activities were about sixfold enriched in the mitochondrial fraction. The intactness of mitochondrial suspension was also checked by following the latency of release of the mitochondrial matrix enzyme FUM, following the rupture of the inner mitochondrial membrane by Triton X-100 (TX100). An integrity of 81 ± 3% was measured in three different mitochondrial preparations (Figure 1(b)), as described in Section 2. Then, in the frame of assessing mitochondrial functionality, NADH (1 mM) was externally added to purified SCM, to induce respiration, via the two external NADH dehydrogenases (namely, Nde1p and Nde2p), as schematized in Figure 1(c). In the typical experiment reported, SCM respired NADH (1 mM) with a rate equal to 700 ngatoms $O \cdot min^{-1} \cdot mg^{-1}$ protein. When ADP (0.1 mM) was added, the oxygen uptake rate increased up to 1240 ngatoms $O \cdot min^{-1} \cdot mg^{-1}$ protein, with a respiratory control index (RCI) value equal to 1.8. Under this ADP limiting concentration a P/O value equal to 1.4 was measured. Addition of ADP at higher concentration (1 mM) increased the oxygen consumption rate up to 1730 ngatoms $O \cdot min^{-1} \cdot mg^{-1}$ protein, with a RCI value equal to 2.5. In three experiments, performed with different mitochondrial preparations, SCM showed RCI values ranging from 2.0 to 3.0. As expected, NADH-induced respiration was almost totally inhibited by KCN (1 mM), thus excluding a significant contribution by alternative oxidase pathway [52].

To better investigate the fate of externally added NADH, SCM were ruptured by freezing-thawing cycles and added to NADH (5 μM) in the absence and in the presence of KCN (1 mM) (Figure 2(a)). Fluorescence excitation spectra of the suspension were registered for 10 min, with the emission wavelength set at 456 nm. As expected, two major emission fluorescence peaks are found (at 260 and 340 nm, resp.) due to the reduced form of the coenzyme, with the corresponding fluorescence intensities decreasing concomitantly in the course of NADH oxidation at both 260 nm and 340 nm. From the values of fluorescence decrease, a NADH oxidation rate of 520 $nmol \cdot min^{-1} \cdot mg^{-1}$ protein was calculated as reported in Section 2 (data not shown). KCN (1 mM) addition to ruptured SCM reduced the rate of NADH disappearance to less than 8% of that measured in its absence (Figure 2(a)). Under this experimental conditions, the rate of fluorescence decrease at wavelength pairs 340/456 nm (essentially due to the KCN-insensitive NADH oxidation rate) became lower than that measured at 260/456 nm.

A possible explanation for this asymmetry derived from the hypothesis that oxidation is not the sole process responsible for NADH disappearance in the suspension, with a possible contribution due to putative hydrolytic processes. In this case a NADH hydrolysis rate equal to 14 nmol NADH hydrolyzed $\cdot min^{-1} \cdot mg^{-1}$ protein was calculated by applying (4) reported in Section 2, while NADH oxidation rate was reduced at 48 $nmol \cdot min^{-1} \cdot mg^{-1}$ protein. In three independent experiments using different mitochondrial preparations, a mean rate of 14.6 ± 1.1 nmol NADH hydrolyzed $\cdot min^{-1} \cdot mg^{-1}$ protein was calculated (with NADH oxidation rate of 34 ± 12 $nmol \cdot min^{-1} \cdot mg^{-1}$ protein). Similar results were obtained when the fluorescence decrease was continuously measured at both the wavelength pairs 260/456 nm and 340/456 nm, respectively. Typical traces are reported in Figure 2(b) (straight lines).

The specific NADH hydrolytic activity measured in the mitochondrial fraction resulted almost equal to that found in whole sphero (14.1 ± 1.6 $nmol \cdot min^{-1} \cdot mg^{-1}$ protein); this allows us to propose a mitochondrial localization for NADH destroying enzyme, even if not exclusive. The already characterized hydrolase which is known to cleave NADH, namely, Npy1p (see Section 1), seemed to be peroxisomal [28].

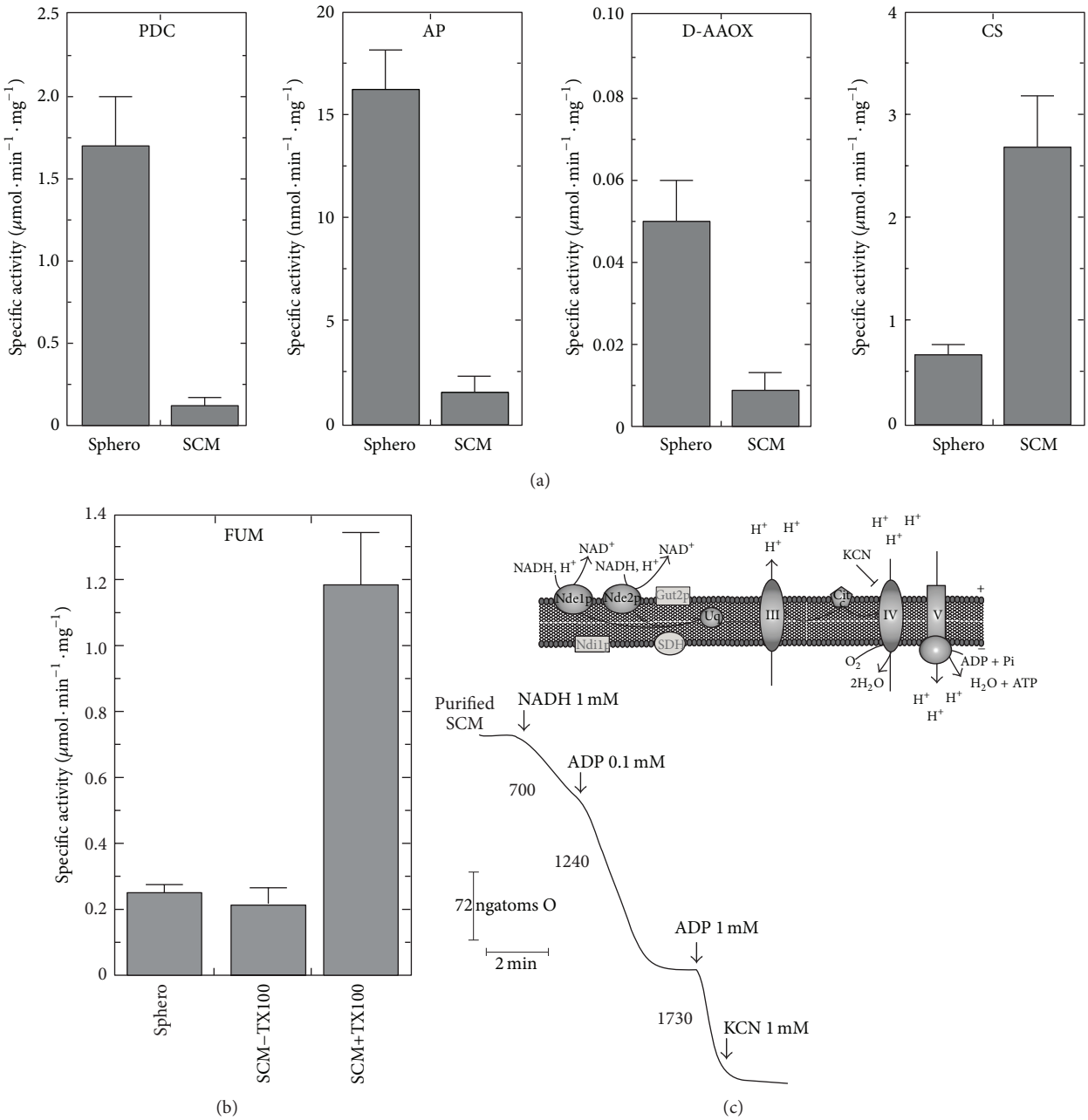

Figure 1: Purity, integrity, and functionality of SCM. (a) The amount of PDC, AP, D-AAOX, and CS activities in sphero and SCM (0.05–0.1 mg protein) were measured, as reported in Section 2. The values of the enzymatic activities are the mean (±SD) of three experiments performed with different cellular preparations. (b) FUM activity was measured in sphero, intact SCM (SCM − TX100), and solubilized SCM (SCM + TX100) (0.05 mg protein each) as reported in Section 2. The values are the mean (±SD) of three experiments performed with different cellular preparations. (c) A schematic representation of the electron transport along the respiratory chain starting from the external NADH dehydrogenases (*Nde1p* and *Nde2p*) is reported. Polarographic measurements of the NADH-dependent oxygen uptake rate in SCM (0.1 mg protein) were carried out as described in Section 2. The arrows indicate when the additions were made. The numbers along the trace refer to the oxygen uptake rate expressed as ngatoms O · min^{-1} · mg^{-1} mitochondrial protein.

With the aim of identifing the NADH destroying enzyme, we queried a number of protein sorting signal prediction programs (i.e., iPSORT, TargetP, and MITOPROT), thus finding a possible mitochondrial localization for this protein.

To understand whether the mitochondrial NADH hydrolytic activity was due to the NUDIX hydrolase Npy1p, the effects of both NaF (1 mM) and $CaCl_2$ (1 mM), powerful inhibitors of the peroxisomal enzyme, were tested (Figure 2(b)). Since they clearly did not inhibit the NADH hydrolysis rate (dotted lines), we exclude that the activity we revealed was due to a putative mitochondrial isoform of this enzyme. Independently from an auspicial protein

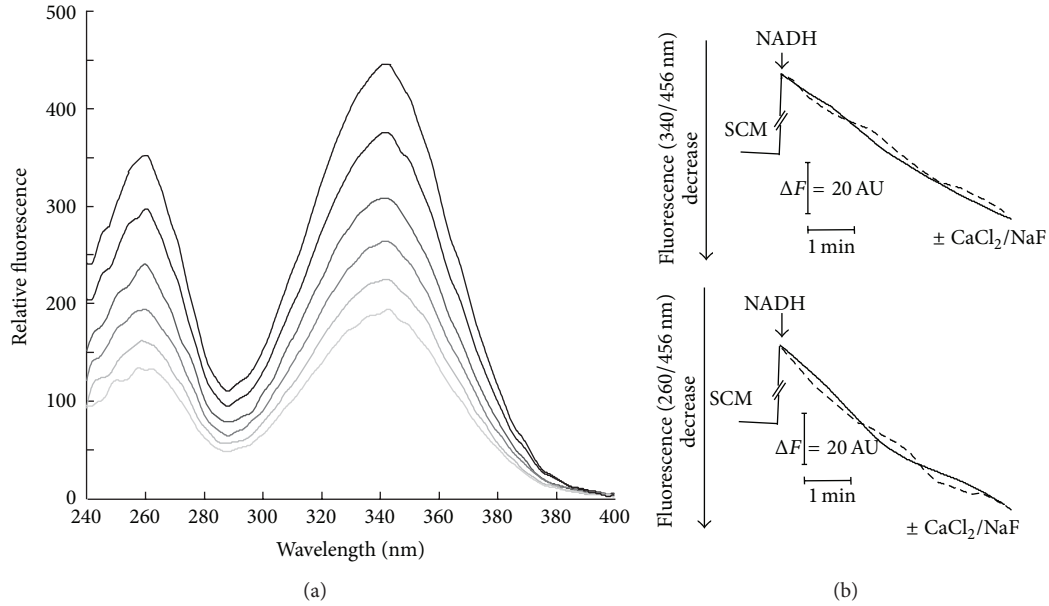

Figure 2: Fluorimetric evidence of NADH cleavage catalyzed by solubilized SCM. (a) SCM (0.025 mg protein) were added to NADH (5 μM) in the standard medium supplemented with KCN (1 mM) and the reaction followed at 25°C, essentially as described in Section 2. NADH fluorescence excitation spectra (emission wavelength set at 456 nm) were recorded at different incubation times. (b) NADH fluorescence decrease, induced by freezing-thawing rupture of SCM, was continuously measured at both the wavelength pairs 260/456 and 340/456 nm, under the experimental condition described in (a). Where indicated NaF or $CaCl_2$ (1 mM each) were added (dotted lines).

identification, these experiments represent the first evidence in favor of the existence of a novel mitochondrial NAD(H) destroying activity. Nevertheless, the rapid fluorimetric method used prevents a detailed kinetic characterization.

A simpler investigation of NAD-destroying activities makes use of a NAD^+ fluorescent analog, namely, nicotinamide $1,N^6$-ethenoadenine dinucleotide (ε-NAD^+) [50, 51]. This assay was specifically useful to investigate whether purified SCM can hydrolyze also the oxidized form of the pyridine coenzyme. In Figure 3(a) a typical ε-NAD^+ (50 μM) emission spectrum is reported, as revealed at pH 7.5, in the 340–500 nm range, with excitation wavelength set a 310 nm. As expected, it reveals a characteristic peak at 410 nm, whose intensity linearly depends on ε-NAD^+ concentration. Addition of SCM (previously solubilized with TX100) induced an increase in fluorescence emission at 410 nm, as a linear function of time up to 20 min. Since the ε-adenine ring specific fluorescence constant is about ten-fold higher than that of the ε-NAD^+, the observed fluorescence increase strongly suggests that ε-NAD^+ was cleaved with a rate equal to 0.23 nmol ε-NAD^+ cleaved $\cdot$ min^{-1} $\cdot$ mg^{-1} protein. In Figure 3(b) the fluorescence changes of ε-NAD^+ (50 μM) suspensions, following the addition of solubilized SCM, were continuously measured, at the fixed excitation and emission wavelengths (set at 310 nm and 410 nm, resp.), corresponding to an initial rate of hydrolysis equal to 0.25 nmol $\cdot$ min^{-1} $\cdot$ mg^{-1} protein (+TX100). No increase was observed when freshly isolated intact SCM were used (−TX100), thus suggesting an intramitochondrial localization for NAD^+-cleaving activity.

The dependence of the rate of cleavage of ε-NAD^+ catalyzed by solubilized SCM was determined in the pH range 4.5–10, using 100 mM acetate/acetic acid and 50 mM Tris/HCl buffering mixtures (Figure 4(a)). ε-NAD^+ cleavage was found to occur with a bell-shaped profile with the maximum rate measured at pH 5.5.

To gain some insights into the substrate affinity, the dependence of the rate of ε-NAD^+ was studied at pH 6 as a function of the substrate concentration (Figure 4(b)). Hyperbolic characteristic was found, with saturation kinetics analyzed by the Michaelis-Menten equation, using the *GraFit* software (see Section 2). Thus, K_m and V_{max} values equal to 56 ± 8.9 μM and 1.7 ± 0.1 nmol $\cdot$ min^{-1} $\cdot$ mg^{-1} of mitochondrial protein, respectively, were calculated from the data in Figure 4(b). In three independent experiments using different mitochondrial preparations, a mean rate of 1.6 ± 0.2 nmol ε-NAD^+ hydrolyzed $\cdot$ min^{-1} $\cdot$ mg^{-1} protein was found, using ε-NAD^+ (200 μM).

The specific ε-NAD^+ hydrolytic activity was also measured in solubilized sphero, under the same experimental conditions. As reported in Figure 4(c), the specific ε-NAD^+ hydrolytic activity in sphero is similar to that measured in SCM. This finding, as previously observed for NADH hydrolytic activity, suggests a preferential, but not exclusive, mitochondrial localization for this enzyme.

As previously observed for NADH hydrolyzing activity, the mitochondrial ε-NAD^+ hydrolytic activity was not inhibited by both NaF (1 mM) and $CaCl_2$ (1 mM) (Figure 4(d)), thus again excluding that a NUDIX hydrolase was responsible for this activity. Conversely, the mitochondrial NAD^+-cleavage activity was totally inhibited by AMP (1 mM) but also significantly inhibited by nicotinamide, with an IC_{50} of about 5 mM (Figure 4(d)).

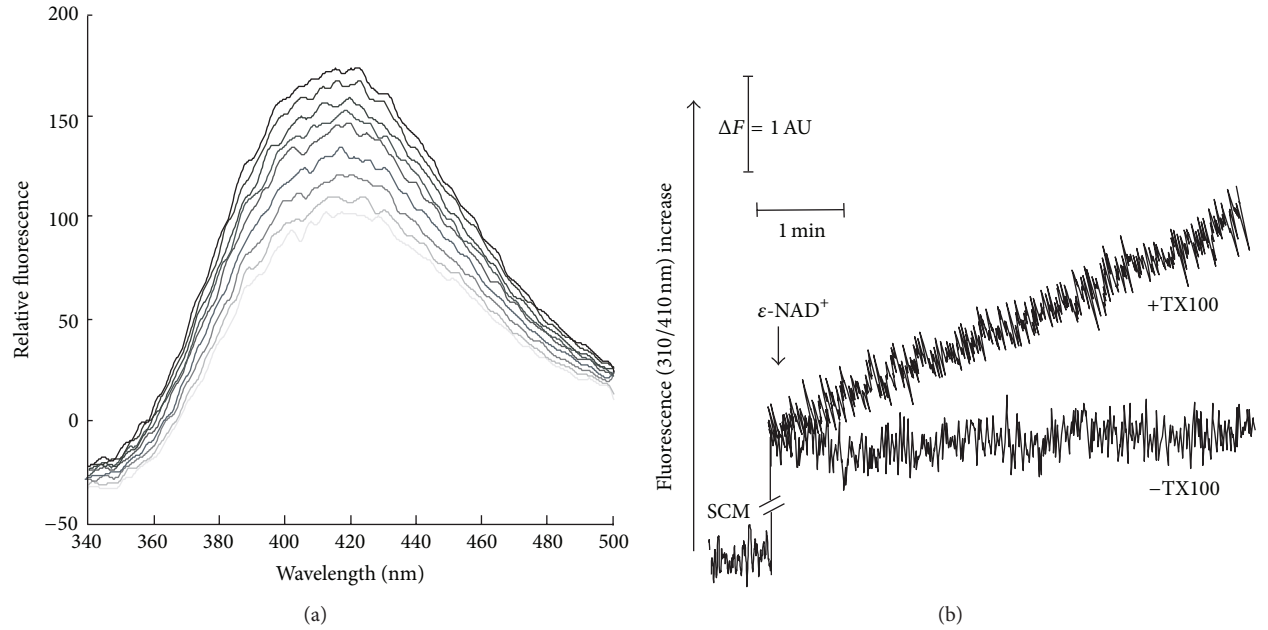

Figure 3: Fluorimetric evidence of ε-NAD^+ cleavage catalyzed by solubilized SCM. (a) SCM (0.3 mg protein), solubilized with TX100, were added to ε-NAD^+ (50 μM) in the standard medium and the reaction followed at 25°C, essentially as described in Section 2. ε-NAD^+ emission spectra (at excitation wavelength 310) were monitored at different incubation times. (b) ε-NAD^+ fluorescence decrease was continuously monitored at 310/410 nm under the same experimental condition described in (a) using intact (−TX100) or solubilized SCM (+TX100).

This last experiment strongly supports the proposal that a nicotinamide-sensitive pyridine nucleotide-destroying enzyme is enriched in SCM, even if, unfortunately, it did not allow to precisely identify the product of mitochondrial NAD(H) hydrolysis. Nevertheless, the strong inhibition by AMP allows us to postulate that the dinucleotide was broken at the level of pyrophosphate bond, as already demonstrated for certain animal and plants FAD pyrophosphatases (FADppase, EC 3.6.1.18) [54, 55].

Particular attention merits the finding that NAD^+ degradation, as well as FAD degradation (see below), strictly depends on pH, which in yeast is highly dynamic [56]; thus, we expect that local changes in intramitochondrial pH may have profound influence on the availability of intramitochondrial pyridine and flavin cofactors. Under respiratory conditions, an intramitochondrial pH value ranging from 7.7 to 7.3 during the different growth phases was experimentally evaluated [57], presumably accompanied by a very low cofactor degradation, as shown by measurements performed here. Thus, under physiological conditions, respiratory-chain-driven proton pumping prevents cofactor hydrolysis by generating a transmembrane pH gradient, negative inside.

Mild uncoupling [58] or various stress conditions [57] induce a severe decrease in intramitochondrial pH value, which plays a central role, together with vacuoles, in controlling cytosolic pH [56, 59, 60]. Under these conditions we expected an increase in the rate of NAD^+, as well as FAD degradation (see below), which in turn may regulate redox homeostasis, cell growth, and defense responses [61, 62].

Since the contribution of mitochondrial NAD(H) degrading enzyme activity on the economy of NAD(H) homeostasis and, in turn, on cell longevity and stress resistance is still unexplored, our future goal will be to identify acidic mitochondrial NAD pyrophosphatase in yeast.

As far as FAD degradation is concerned, the occurrence of AMP-inhibited FAD hydrolysis in isolated intact mitochondria was for the first time demonstrated in rat liver [38] and, more recently, in *S. cerevisiae* [40]. In order to understand whether FADppase, described in [40], could also be responsible for the mitochondrial NAD(H) hydrolyzing activity observed in our mitochondrial preparation, FADppase was characterized in some detail. Thus, FAD (3 μM) was added to solubilized SCM and flavin fluorescence emission spectra (with excitation wavelength set at 450 nm) registered at pH 7.5, as a function of time. As expected, an increase in the 500–600 nm wavelength range with a peak at 520 nm was observed in Figure 5(a), due to the conversion of FAD into FMN/Rf, with a rate of fluorescence increase, measured as described in Section 2, corresponding to 0.28 nmol FAD hydrolyzed · min^{-1} · mg^{-1} protein.

In Figure 5(b), FAD (3 μM) fluorescence was continuously measured at the fixed excitation and emission wavelengths (set at 450 nm and 520 nm, resp.). No fluorescence increase was observed after addition of intact and coupled SCM (−TX100). When FAD was added to solubilized SCM an increase was observed with a rate equal to 0.30 nmol FAD hydrolyzed · min^{-1} · mg^{-1} protein (+TX100). In seven experiments performed with different mitochondrial preparations, a mean rate of 0.32 ± 0.05 nmol FAD hydrolyzed · min^{-1} · mg^{-1} protein was measured. FAD hydrolysis could be revealed only when SCM were solubilized by TX100 and in this aspect SCM are different from rat liver mitochondria.

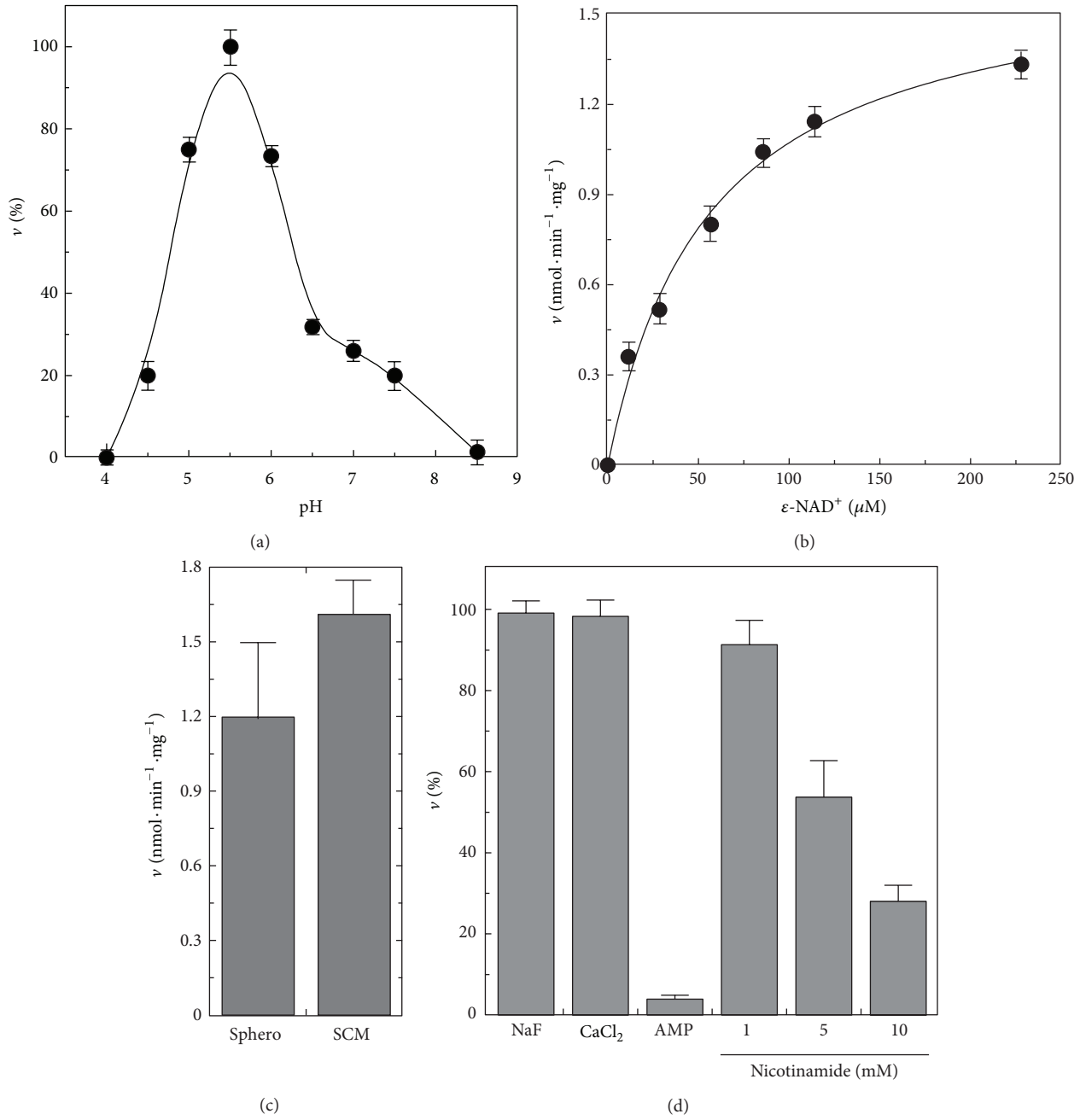

FIGURE 4: Some features of ε-NAD^+ cleavage. (a) The pH profile of the rate of ε-NAD^+ (100 μM) cleavage, catalyzed by solubilized SCM (0.3 mg protein), was fluorimetrically measured as described in Section 2. Use was made of 100 mM acetate/acetic acid and 50 mM Tris/HCl buffering mixtures (supplemented with 5 mM $MgCl_2$), whose pH was adjusted to the desired value. A specific calibration curve was obtained at each pH value as described in Section 2. The values are reported as percentage of the maximum rate (i.e., 1.6 nmol $\cdot$ min^{-1} $\cdot$ mg^{-1}), arbitrarily set equal to 100%. (b) The dependence of the rate of ε-NAD^+ cleavage on substrate concentration was measured using solubilized SCM (0.3 mg protein) at pH 6. (c) The rate of ε-NAD^+ (200 μM) cleavage catalyzed by TX100-solubilized sphero and SCM (0.3 mg protein each) was measured at pH 6. (d) The sensitivity of ε-NAD^+ (50 μM) cleavage (catalyzed by solubilized SCM, 0.3 mg protein) towards NaF, $CaCl_2$, AMP (1 mM each), and nicotinamide (at the indicated concentrations) was measured at pH 6.

In order to characterize the products of FAD hydrolysis catalyzed by solubilized mitochondria, under the same experimental conditions described in Figure 5(a), extracts of the suspension were taken at different incubation times and analyzed via HPLC, as described in Section 2, with measurements made of FAD, FMN, and Rf amount in the suspension.

Solubilized SCM added with FAD (3 μM) were incubated either in the absence (panel (A)) or in the presence of AMP (panel (B)). In a parallel assay the effect of NaPPi (panel (C)),

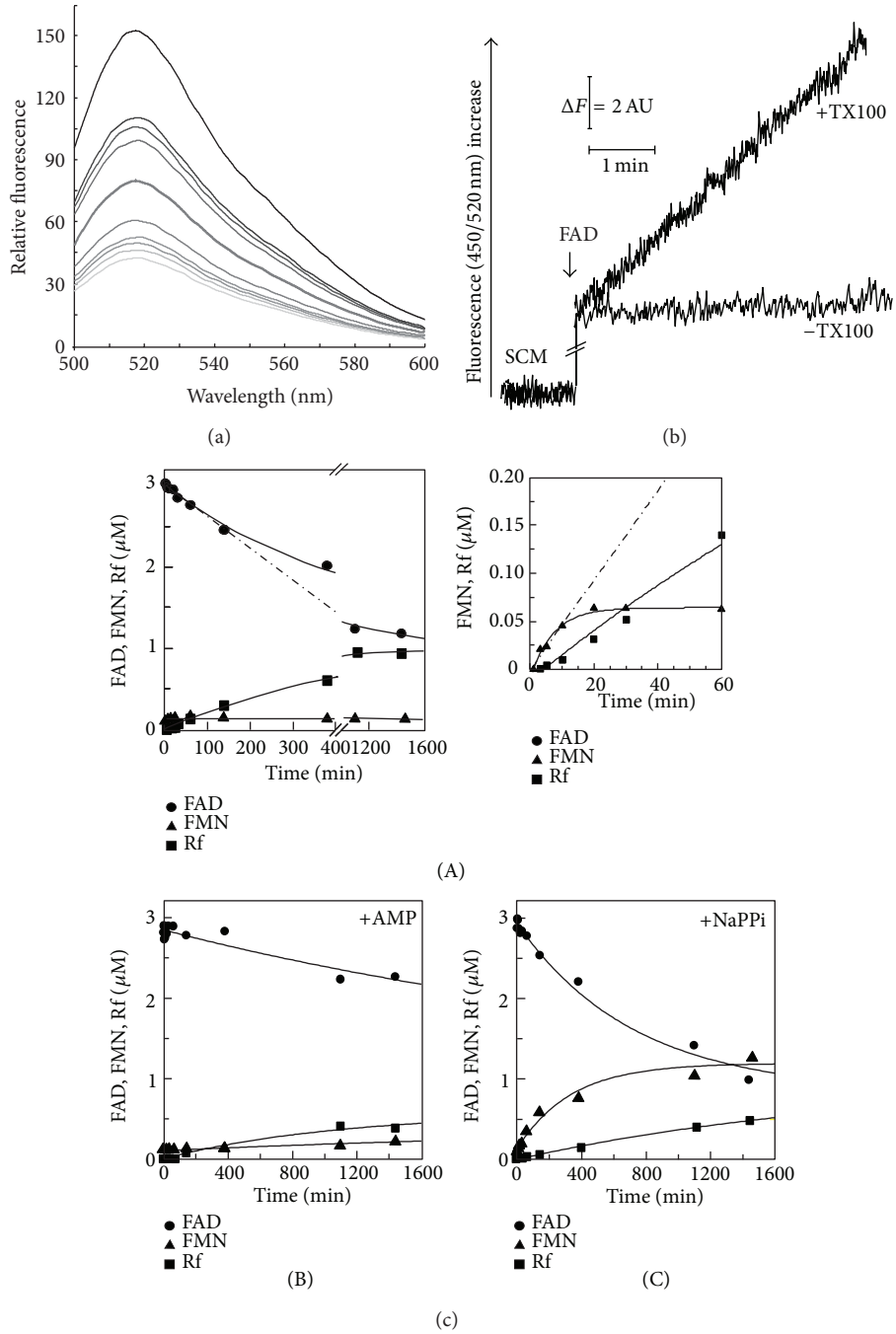

Figure 5: FAD pyrophosphatase in solubilized SCM. (a) SCM (0.05 mg protein), solubilized with TX100, were incubated under the experimental conditions described in Section 2. The reaction was started by FAD (3 μM) addition to the mitochondrial suspension and followed at 25°C. FAD emission spectra (at excitation wavelength 450 nm) were monitored at different incubation times. (b) FAD fluorescence decrease was continuously monitored at 450/520 nm under the same experimental condition described in (a) using intact (−TX100) or solubilized SCM (+TX100). (c) Extracts of the FAD hydrolysis reaction mixture were taken at different incubation times and analyzed via HPLC, as described in Section 2 with measurements of FAD, FMN, and Rf concentrations. The value obtained were plotted against the incubation time after FAD addition. FAD hydrolysis reaction was carried in the absence (panel (A)) or in the presence of AMP (1 mM) (panel (B)) or NaPPi (1 mM) (panel (C)). The inset in (panel (A)) is an enlargement of the first 60 min of the plot reported in the same panel.

which was proved to prevent FMN hydrolysis in SCM [31], was also tested.

As shown in Figure 5(c) (panel (A)), FAD amount was found to decrease with a constant initial rate of 0.29 nmol FAD hydrolyzed · min^{-1} · mg^{-1} protein, in agreement with the fluorimetric measurements, and then it reached a plateau. Concomitantly with FAD disappearance, a significant increase in FMN amount was initially observed with a constant rate of 0.30 nmol · min^{-1} · mg^{-1} protein in the first 10 min, in a fairly good agreement with a stoichiometric ratio of 1 : 1 with the FAD amount decrease (see inset). At longer incubation time, Rf, that was not initially detectable, appeared in the suspension (see inset) and it increased linearly up to 60 min (with a rate of 0.10 · min^{-1} · mg^{-1} protein), thus prevailing over FMN (panel (A)) which remained relatively constant (at about 0.06 μM). Since FAD hydrolysis rate does not depend on the rate of FMN into Rf conversion in the first 10 min (that is, the step catalyzed by FADppase is the limiting step of mitochondrial FAD degradation pathway), kinetics measurements of FADppase reaction were performed consistently by fluorimetric method.

As expected, the rate of FAD hydrolysis was totally inhibited by AMP (1 mM); neither FMN nor Rf was found to appear during the incubation time (panel (B)). Conversely, in the presence of NaPPi (1 mM), the rate of FAD hydrolysis resulted unchanged, with a notable increase in FMN (with an initial rate of 0.30 nmol · min^{-1} · mg^{-1} proteins), which was slowly accompanied by Rf appearance with an 85% reduced rate, in comparison to the rate measured in the absence of NaPPi (panel (C)).

When the mitochondrial FAD (3 μM) hydrolysis was studied at pH 6 (i.e., the optimum of ε-NAD^+ hydrolytic activity), FAD disappearance was found to occur with a 2.5-fold higher rate and to be still in a good agreement with a stoichiometric ratio of 1 : 1 with the appearance of FMN, that is the preeminent species at this pH value, whereas the rate of Rf appearance is extremely low (0.02 nmol · min^{-1} · mg^{-1} mitochondrial proteins).

Consistently, the rate of FAD cleavage catalyzed by solubilized SCM, fluorimetrically determined in the pH range 4.0–10 in Figure 6(a), was found to occur with a bell-shaped profile with the maximum rate measured at pH 6 (being equal to 1.05 nmol · min^{-1} · mg^{-1} protein, when FAD 10 μM was used as substrate). This pH profile is quite different from that described in [40], whose optimum activity was at alkaline pH. Thus, the dependence of FAD hydrolysis rate on substrate concentration was studied at pH 6 (Figure 6(b)). Hyperbolic characteristic was found with saturation kinetic, analyzed by the Michaelis-Menten equation, using the *GraFit* software (see Section 2). Thus, K_m and V_{max} values equal to 5.9 ± 0.5 μM and 1.6 ± 0.1 nmol · min^{-1} · mg^{-1} of mitochondrial protein, respectively, were calculated from the data in Figure 6(b). A K_m value equal to 10 ± 2 μM was determined at pH 7.5 (data not shown).

These results confirm that in SCM, a FADppase exists and it is able to catalyze the cleavage of the diphosphate bound in dinucleotides. This enzyme is inhibited by AMP and stimulated by acidic pH value. A putative mitochondrial FMN phosphohydrolase activity is involved in FMN dephosphorylation; it is specifically inhibited by NaPPi and its activity is significantly reduced at acidic pH value.

As regards inhibition of FAD hydrolysis, the inorganic compounds NaF (1 mM) and $CaCl_2$ (1 mM), differently from AMP (1 mM), did not reduce FAD hydrolytic activity in SCM (Figure 6(c)), as already observed for ε-NAD^+ hydrolysis, thus excluding that FMN is produced by a putative mitochondrial NUDIX hydrolase.

Quite interestingly, differently from ε-NAD^+ hydrolysis, nicotinamide (as well as NMN) did not affect FAD hydrolysis rate. Therefore, we may conclude that mitochondrial NAD(H) and FAD destroying activities are different. Another difference between mitochondrial NAD(H) and FAD destroying activities resides in the observation that specific FAD hydrolytic activity catalyzed by solubilized SCM corresponded to about only 27% of that measured in the sphero (Figure 6(d)). Taking into account the extramitochondrial contaminations present in our mitochondrial preparations (see Figure 1(a)), it represents about 10% of the total activity detectable in the sphero. A similar distribution ratio was also found for other mitochondrial enzymes, that is, RFK and FADS [29, 31]. Presumably, other quite active FADppases are localized in the extramitochondrial compartments.

In a first attempt to determine the physiological role for the intramitochondrial FADppase, the possibility that this enzyme can play a major role in the intramitochondrial FAD degradation was studied by both fluorescence and HPLC experiments. A typical fluorimetric experiment is reported in Figure 7(a). At initial time, intact mitochondria showed a typical endogenous flavin emission spectrum with a peak at 520 nm (excitation wavelength set at 450 nm) (−TX100, dotted line). No increase in flavin fluorescence was observed when coupled and intact SCM were used. When SCM were solubilized with TX100 an increase in the 500–600 nm wavelength range was observed (−NAD^+). This strongly suggests that endogenous FAD has been hydrolyzed to FMN/Rf. Endogenous flavin fluorescence was found to increase as a linear function of time up to 30 min with a rate equal to 7 pmol endogenous FAD hydrolyzed · min^{-1} · mg^{-1} protein (see inset). It should be noted that under our experimental conditions less that 20% of total mitochondrial FAD amount was hydrolyzed, presumably due to an inhibition by FAD hydrolysis product(s) or because the remaining FAD was bound to holoflavoprotein and thus protected by hydrolytic activity.

Since FADppase is located inside mitochondria the stimulatory effect of the detergent could not be easy explained, unless some internal metabolite, whose concentration is high in the matrix of intact organelles and diluted following membrane rupture, is able to inhibit FADppase. In this hypothesis we tested a possible inhibitory effect by NAD^+ (1 mM), which was found to completely inhibit endogenous FAD to FMN conversion (+NAD^+).

In the same experiment, the hydrolysis of endogenous FAD was confirmed by HPLC measurements of FAD, FMN, and Rf amounts before and after TX100 addition (Figure 7(b)). In the absence of TX100 the mitochondrial

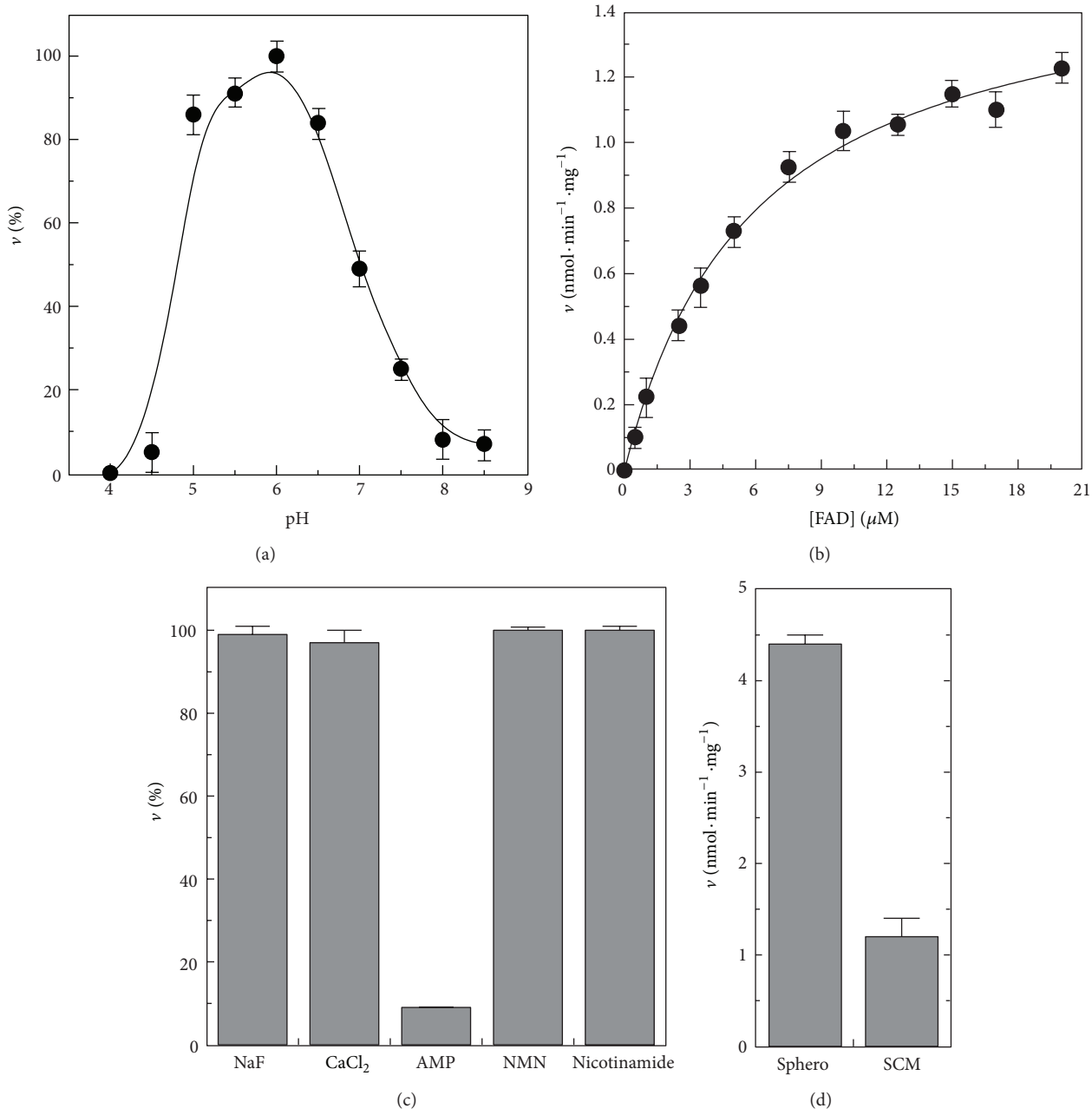

Figure 6: Some features of FAD pyrophosphatase. (a) The pH profile of the rate of FADppase, catalyzed by solubilized SCM (0.1 mg protein) in the presence of FAD (10 μM), was fluorimetrically measured as described in Section 2. Use was made of 100 mM acetate/acetic acid and 50 mM Tris/HCl buffering mixtures (with 5 mM $MgCl_2$), whose pH was adjusted to the desired value. A specific calibration curve was obtained at each pH value in Section 2. The values are reported as percentage of the maximum rate (i.e., 1.05 nmol · min^{-1} · mg^{-1} protein), arbitrarily set equal to 100%. (b) The dependence of the rate of FADppase on substrate concentration was measured at pH 6 using solubilized SCM (0.1 mg protein). (c) The sensitivity of FADppase, catalyzed by solubilized SCM (0.1 mg) in the presence of FAD (10 μM), towards NaF, $CaCl_2$, AMP, NMN (1 mM each), and nicotinamide (5 mM) was measured at pH 6. (d) The rate of FAD (10 μM) cleavage, catalyzed by solubilized sphero and SCM (0.1 mg protein each), was measured at pH 6.

amounts of FAD and FMN were about 172 and 26 pmol · mg^{-1} protein, respectively, and no Rf was detected (panel (A)). As a result of TX100 addition, FAD and FMN were found to decrease, with significant appearance of Rf (panel (B)). Rf content was found to increase up to 20 min in a fairly good stoichiometric ratio (1 : 1) with FAD decrease (data not shown). The rate of FAD hydrolysis (i.e., Rf appearance) was equal to 7.2 pmol · min^{-1} · mg^{-1} protein, in good agreement with fluorescence measurements. Rf appearance was strongly prevented by NAD^+ (panel (C)).

The effect of NAD^+ was confirmed on exogenous FAD hydrolysis by HPLC (data not shown) and the nature of

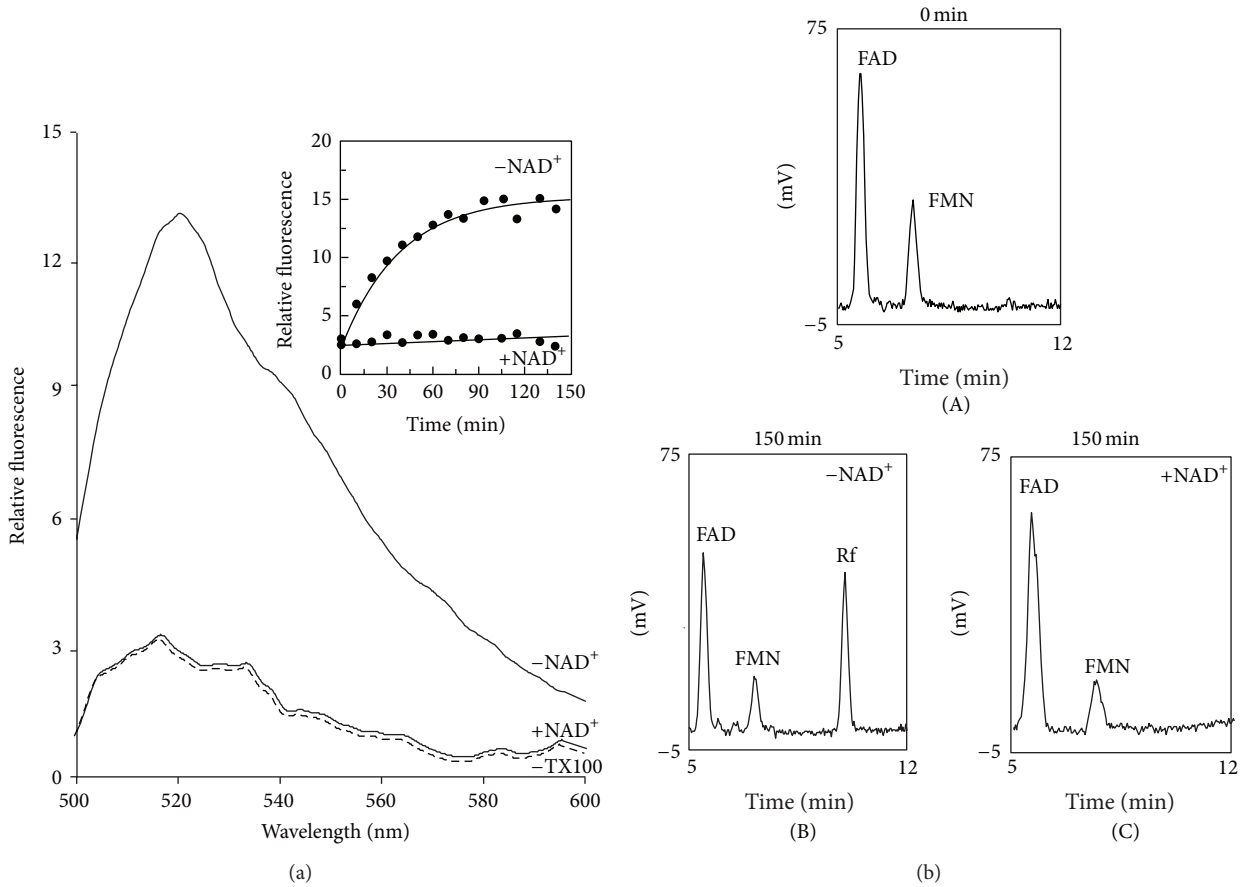

Figure 7: Endogenous FAD hydrolysis by isolated SCM induced by TX100; inhibition by NAD^+. (a) SCM (0.1 mg protein) were incubated under the experimental conditions described in Section 2. Fluorescence emission spectra (excitation wavelength at 450 nm) of the suspension were recorded after 150 min in the absence (−TX100, dotted line) or in the presence of TX100 (0.1%). Where indicated, NAD^+ (1 mM) was also added. In the inset, the fluorescence intensity, measured at 520 nm, as obtained after TX100 addition, either in the absence or in the presence of NAD^+, was plotted against the incubation time. (b) FAD, FMN, and Rf in TX100 treated mitochondrial suspension extracts were revealed by means of HPLC measurements, performed as described in Section 2, following 0 (panel (A)) or 150 min incubation time in the absence (panel (B)) or presence (panel (C)) of NAD^+ (1 mM).

the inhibition studied fluorimetrically (Figure 8(a)). FAD hydrolysis sensitivity to NAD^+ was consistent with a noncompetitive inhibition, as shown in the Dixon plot with a Ki value equal to 10 μM, calculated from the data in Figure 8(a).

Adenosine and derived compounds (i.e., ADP-ribose, Ap_5A, and CoA) and guanosine nucleotides, but not nicotinamide and NMN, are able to reduce FAD hydrolysis rate (data not shown); therefore we feel that the purine moiety is relevant for inhibitor recognition by FADppase. Consistently, NADH is also able to inhibit in a noncompetitive way the rate of FAD hydrolysis, but, interestingly, the Ki differed for an order magnitude, being equal to 100 μM for NADH, as calculated from the data reported in Figure 8(b).

These results demonstrate that FAD hydrolyzing enzyme could discriminate between the redox status of pyridine nucleotides, as depicted in Figure 9. It is well known that a high electron pressure, namely, an increase in NADH/NAD^+ ratio, is a condition favoring ROS generation which can be contrasted by an efficient respiratory chain (which is flavin dependent) and by defense systems (some of which are flavoenzymes) [6]. According to the measurements performed here, reduction of NAD^+ to NADH is expected to favor hydrolysis of free FAD, since the oxidized form of the pyridine cofactor is more powerful as inhibitor (lower Ki) than the reduced form (higher Ki), at least in ruptured SCM. Thus, we can speculate that reducing conditions are accompanied by a more rapid local "recycling" of FAD, presumably deriving from holoflavoprotein turnover. This situation could allow a more rapid intramitochondrial assembly of novel flavoproteins (mainly components of the respiratory chain, like SDH [32, 63]) and saving of cytosolic Rf level which is necessary for enzymatic ROS defense.

Whether or not flavin-coenzymes homeostasis is modulated *in vivo* by pyridine nucleotide redox status inside SCM as postulated and summarized in the scheme in Figure 9, is an interesting interrogative that we would like to address in the next future.

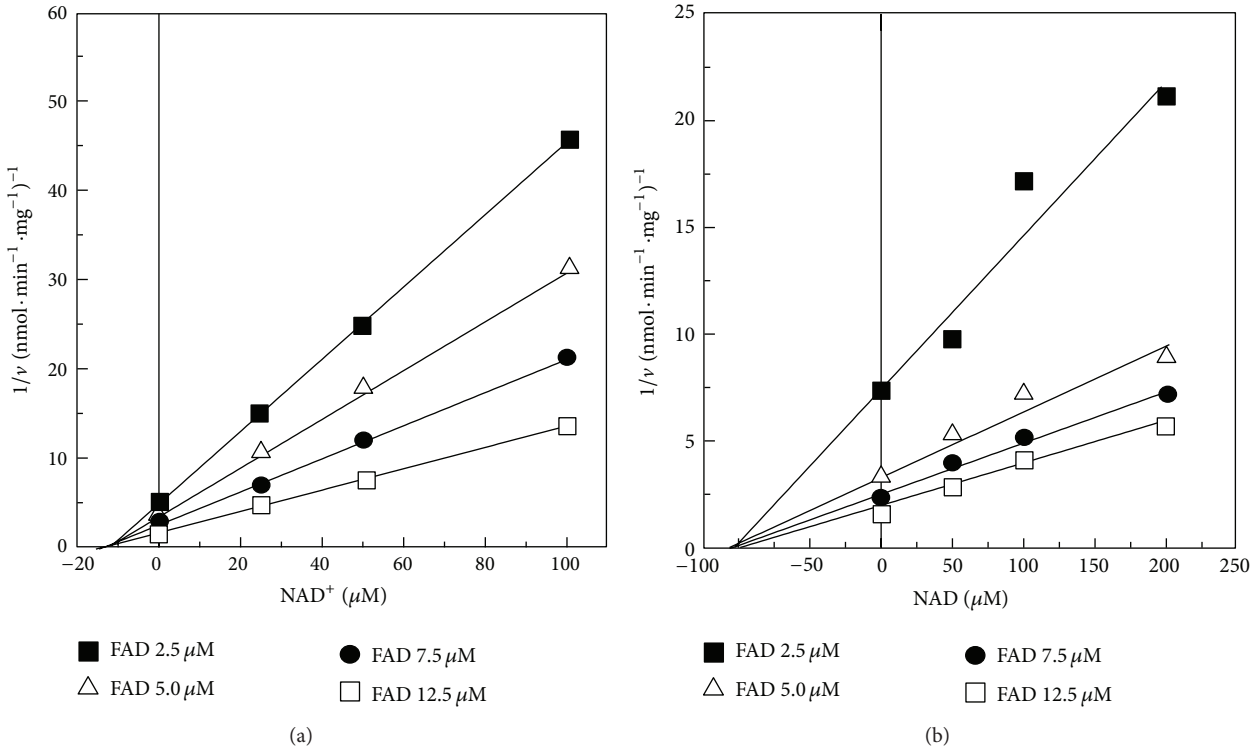

FIGURE 8: NAD^+ and NADH inhibition of FAD pyrophosphatase. The rate of FAD hydrolysis (v) was fluorimetrically measured in the standard medium at pH 7.5 with FAD at the indicated concentrations (2.5, 5, 7.5, or 12.5 μM) and solubilized SCM (0.05 mg protein). NAD^+ or NADH was added in the FAD degradation reaction mixture at the concentration indicated. When NADH sensitivity was tested, KCN (1 mM) was added to the reaction mixture. The Dixon plots of the inhibition by NAD^+ and NADH are reported in panels (a) and (b), respectively.

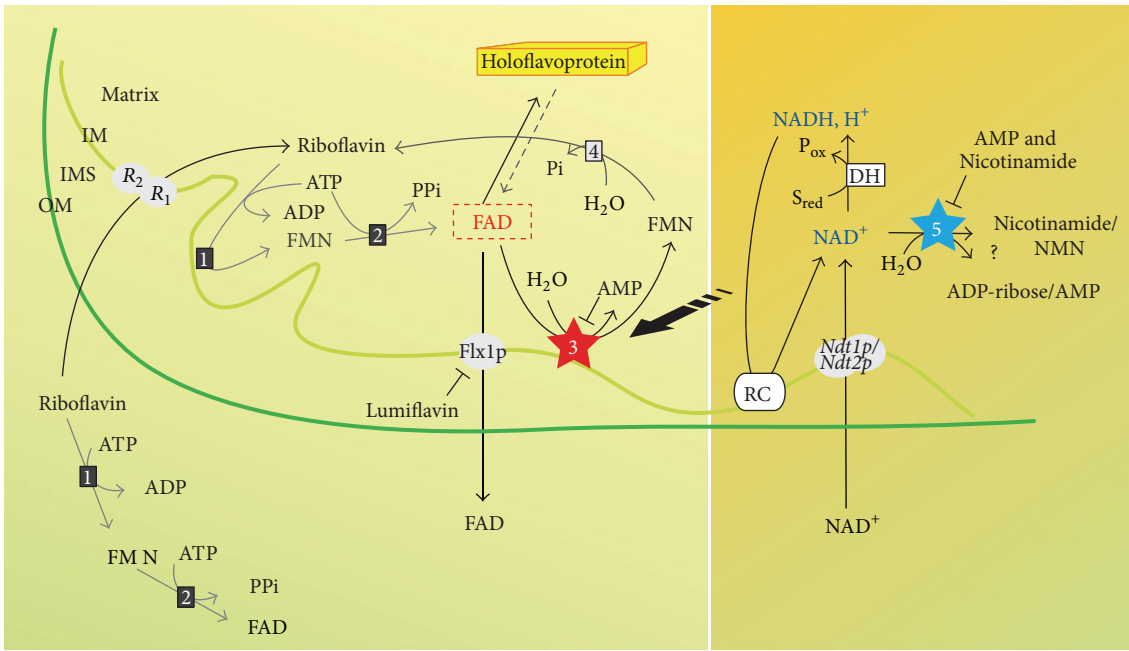

FIGURE 9: FAD and NAD homeostasis in SCM. The scheme summarized the functional studies described in this and other previous papers [23, 31, 32, 53]. R_1/R_2, mitochondrial Rf transporter; Flx1p, mitochondrial FAD exporter; *Ndt1p/Ndt2p*, mitochondrial NAD^+ transporter; (1), riboflavin kinase (EC 2.7.1.26); (2), FAD synthase (EC 2.7.7.2); (3), FAD pyrophosphatase (EC 3.6.1.18); (4), FMN phosphohydrolase (EC 3.1.3.2); (5), NAD(H) cleaving enzyme; DH, NAD(H)-dependent dehydrogenase; RC, respiratory chain.

4. Conclusions

Here we proved the ability of SCM to catalyze NAD(H) and FAD hydrolysis, via enzymatic activities which are different from the already characterized NUDIX hydrolases.

The differential inhibition by the oxidized and reduced form of NAD toward the mitochondrial FADppase, together with the ability of mitochondrial FADppase to metabolize endogenous FAD, presumably deriving from mitochondrial holoflavoproteins destined to degradation, allows for proposing a novel possible role of mitochondrial NAD redox status in regulating FAD homeostasis and, possibly, flavoprotein degradation in *S. cerevisiae*.

Abbreviations

FAD:	Flavin adenine dinucleotide
NAD:	Nicotinamide adenine dinucleotide
Rf:	Riboflavin
RFK:	Riboflavin kinase
FADS:	FAD synthase
SCM:	*Saccharomyces cerevisiae* mitochondria
sphero:	Spheroplasts
PDC:	Pyruvate decarboxylase
AP:	Alkaline phosphatase
D-AAOX:	D-amino acid oxidase
CS:	Cytrate synthase
FUM:	Fumarase
TX100:	Triton X-100
RCI:	Respiratory control index
FADppase:	FAD pyrophosphatase.

Conflict of Interests

The authors declare no conflict of interests.

Acknowledgment

This work was supported by grants from PON-Ricerca e Competitività 2007–2013 (PON Project 01_00937: "Modelli sperimentali biotecnologici integrati per la produzione ed il monitoraggio di biomolecole di interesse per la salute dell'uomo") to Maria Barile.

References

[1] V. Joosten and W. J. van Berkel, "Flavoenzymes," *Current Opinion in Chemical Biology*, vol. 11, no. 2, pp. 195–202, 2007.

[2] P. MacHeroux, B. Kappes, and S. E. Ealick, "Flavogenomics—a genomic and structural view of flavin-dependent proteins," *FEBS Journal*, vol. 278, no. 15, pp. 2625–2634, 2011.

[3] D. B. McCormick, "Two interconnected B vitamins: riboflavin and pyridoxine," *Physiological Reviews*, vol. 69, no. 4, pp. 1170–1198, 1989.

[4] T. I. Gossmann, M. Ziegler, P. Puntervoll, L. F. De Figueiredo, S. Schuster, and I. Heiland, "NAD^+ biosynthesis and salvage—a phylogenetic perspective," *FEBS Journal*, vol. 279, pp. 3355–3363, 2012.

[5] A. Chiarugi, C. Dolle, R. Felici, and M. Ziegler, "The NAD metabolome—a key determinant of cancer cell biology," *Nature Reviews Cancer*, vol. 12, pp. 741–752, 2012.

[6] M. Barile, T. A. Giancaspero, C. Brizio et al., "Biosynthesis of flavin cofactors in man: implications in health and disease," *Current Pharmaceutical Design*, vol. 19, pp. 2649–2675, 2013.

[7] P. Belenky, K. L. Bogan, and C. Brenner, "NAD^+ metabolism in health and disease," *Trends in Biochemical Sciences*, vol. 32, no. 1, pp. 12–19, 2007.

[8] S.-P. Lu and S.-J. Lin, "Regulation of yeast sirtuins by NAD^+ metabolism and calorie restriction," *Biochimica et Biophysica Acta*, vol. 1804, no. 8, pp. 1567–1575, 2010.

[9] L. Guarente, "Sirtuins, aging, and metabolism," *Cold Spring Harbor Symposia on Quantitative Biology*, vol. 76, pp. 81–90, 2011.

[10] R. H. Houtkooper, E. Pirinen, and J. Auwerx, "Sirtuins as regulators of metabolism and healthspan," *Nature Reviews Molecular Cell Biology*, vol. 13, no. 4, pp. 225–238, 2012.

[11] H. J. Powers, "Riboflavin (vitamin B-2) and health," *American Journal of Clinical Nutrition*, vol. 77, no. 6, pp. 1352–1360, 2003.

[12] R. Horvath, "Update on clinical aspects and treatment of selected vitamin-responsive disorders II (riboflavin and CoQ10)," *Journal of Inherited Metabolic Disease*, vol. 35, no. 4, pp. 679–687, 2011.

[13] F. Depeint, W. R. Bruce, N. Shangari, R. Mehta, and P. J. O'Brien, "Mitochondrial function and toxicity: role of the B vitamin family on mitochondrial energy metabolism," *Chemico-Biological Interactions*, vol. 163, no. 1-2, pp. 94–112, 2006.

[14] L. Guarente, "Mitochondria—a nexus for aging, calorie restriction, and sirtuins?" *Cell*, vol. 132, no. 2, pp. 171–176, 2008.

[15] C. Pimentel, L. Batista-Nascimento, C. Rodrigues-Pousada, and R. A. Menezes, "Oxidative stress in Alzheimer's and Parkinson's diseases: insights from the yeast *Saccharomyces cerevisiae*," *Oxidative Medicine and Cellular Longevity*, vol. 2012, Article ID 132146, 9 pages, 2012.

[16] D. Botstein and G. R. Fink, "Yeast: an experimental organism for 21st century biology," *Genetics*, vol. 189, no. 3, pp. 695–704, 2011.

[17] S. Tenreiro and T. F. Outeiro, "Simple is good: yeast models of neurodegeneration," *FEMS Yeast Research*, vol. 10, no. 8, pp. 970–979, 2010.

[18] R. M. Anderson, K. J. Bitterman, J. G. Wood, O. Medvedik, and D. A. Sinclair, "Nicatinamide and PNC1 govern lifespan extension by calorie restriction in *Saccharomyces cerevisiae*," *Nature*, vol. 423, no. 6936, pp. 181–185, 2003.

[19] S.-J. Lin and L. Guarente, "Nicotinamide adenine dinucleotide, a metabolic regulator of transcription, longevity and disease," *Current Opinion in Cell Biology*, vol. 15, no. 2, pp. 241–246, 2003.

[20] J. J. Sandmeier, I. Celic, J. D. Boeke, and J. S. Smith, "Telomeric and rDNA silencing in *Saccharomyces cerevisiae* are dependent on a nuclear NAD^+ salvage pathway," *Genetics*, vol. 160, no. 3, pp. 877–889, 2002.

[21] M. Barile, S. Passarella, G. Danese, and E. Quagliariello, "Rat liver mitochondria can synthesize nicotinamide adenine dinucleotide from nicotinamide mononucleotide and ATP via a putative matrix nicotinamide mononucleotide adenylyltransferase," *Biochemistry and Molecular Biology International*, vol. 38, no. 2, pp. 297–306, 1996.

[22] A. Nikiforov, C. Dölle, M. Niere, and M. Ziegler, "Pathways and subcellular compartmentation of NAD biosynthesis in human cells: from entry of extracellular precursors to mitochondrial

NAD generation," *Journal of Biological Chemistry*, vol. 286, no. 24, pp. 21767–21778, 2011.

[23] S. Todisco, G. Agrimi, A. Castegna, and F. Palmieri, "Identification of the mitochondrial NAD^+ transporter in *Saccharomyces cerevisiae*," *Journal of Biological Chemistry*, vol. 281, no. 3, pp. 1524–1531, 2006.

[24] L. R. Stein and S. Imai, "The dynamic regulation of NAD metab olism in mitochondria," *Trends in Endocrinology & Metabolism*, vol. 23, pp. 420–428, 2012.

[25] L. F. De Figueiredo, T. I. Gossmann, M. Ziegler, and S. Schuster, "Pathway analysis of NAD^+ metabolism," *Biochemical Journal*, vol. 439, no. 2, pp. 341–348, 2011.

[26] S. Imai, F. B. Johnson, R. A. Marciniak, M. McVey, P. U. Park, and L. Guarante, "Sir2: an NAD-dependent histone deacetylase that connects chromatin silencing, metabolism, and aging," *Cold Spring Harbor Symposia on Quantitative Biology*, vol. 65, pp. 297–302, 2000.

[27] A. G. McLennan, "The Nudix hydrolase superfamily," *Cellular and Molecular Life Sciences*, vol. 63, no. 2, pp. 123–143, 2006.

[28] S. R. AbdelRaheim, J. L. Cartwright, L. Gasmi, and A. G. McLennan, "The NADH diphosphatase encoded by the *Saccharomyces cerevisiae* NPY1 nudix hydrolase gene is located in peroxisomes," *Archives of Biochemistry and Biophysics*, vol. 388, no. 1, pp. 18–24, 2001.

[29] M. A. Santos, A. Jimenez, and J. L. Revuelta, "Molecular characterization of FMN1, the structural gene for the monofunctional flavokinase of *Saccharomyces cerevisiae*," *Journal of Biological Chemistry*, vol. 275, no. 37, pp. 28618–28624, 2000.

[30] M. Wu, B. Repetto, D. M. Glerum, and A. Tzagoloff, "Cloning and characterization of FAD1, the structural gene for flavin adenine dinucleotide synthetase of *Saccharomyces cerevisiae*," *Molecular and Cellular Biology*, vol. 15, no. 1, pp. 264–271, 1995.

[31] V. Bafunno, T. A. Giancaspero, C. Brizio et al., "Riboflavin uptake and FAD synthesis in *Saccharomyces cerevisiae* mitochondria. Involvement of the flx1p carrier in fad export," *Journal of Biological Chemistry*, vol. 279, no. 1, pp. 95–102, 2004.

[32] T. A. Giancaspero, R. Wait, E. Boles, and M. Barile, "Succinate dehydrogenase flavoprotein subunit expression in *Saccharomyces cerevisiae*—involvement of the mitochondrial FAD transporter, Flx1p," *FEBS Journal*, vol. 275, no. 6, pp. 1103–1117, 2008.

[33] M. Barile, S. Passarella, A. Bertoldi, and E. Quagliariello, "Flavin adenine dinucleotide synthesis in isolated rat liver mitochondria caused by imported flavin mononucleotide," *Archives of Biochemistry and Biophysics*, vol. 305, no. 2, pp. 442–447, 1993.

[34] T. A. Giancaspero, V. Locato, M. C. De Pinto, L. De Gara, and M. Barile, "The occurrence of riboflavin kinase and FAD synthetase ensures FAD synthesis in tobacco mitochondria and maintenance of cellular redox status," *FEBS Journal*, vol. 276, no. 1, pp. 219–231, 2009.

[35] E. M. Torchetti, C. Brizio, M. Colella et al., "Mitochondrial localization of human FAD synthetase isoform 1," *Mitochondrion*, vol. 10, no. 3, pp. 263–273, 2010.

[36] A. A. Sibirnyi and G. M. Shavlovskii, "Inhibition of alkaline phosphatase I of Pichia guilliermondii yeast in vitro and in vivo," *Ukrainskii Biokhimicheskii Zhurnal*, vol. 50, no. 2, pp. 212–217, 1978.

[37] V. I. Iatsishin, D. V. Fedorovich, and A. A. Sibirnyĭ, "The microbial synthesis of flavin nucleotides: a review," *Prikladnaia Biokhimiia i Mikrobiologiia*, vol. 45, no. 2, pp. 133–142, 2009.

[38] M. Barile, C. Brizio, C. De Virgilio, S. Delfine, E. Quagliariello, and S. Passarella, "Flavin adenine dinucleotide and flavin mononucleotide metabolism in rat liver. The occurrence of FAD pyrophosphatase and FMN phosphohydrolase in isolated mitochondria," *European Journal of Biochemistry*, vol. 249, no. 3, pp. 777–785, 1997.

[39] T. Giancaspero, V. Bafunno, C. Brizio, M. Barile, and S. Passarella, "Flavin Adenine Dinucleotide metabolism in *S. cerevisiae* The occurrence of a FAD pyrophosphatase in isolated mitochondria," *Italian Journal of Biochemistry*, vol. 52, p. 240, 2003.

[40] M. L. Pallotta, "Evidence for the presence of a FAD pyrophosphatase and a FMN phosphohydrolase in yeast mitochondria: a possible role in flavin homeostasis," *Yeast*, vol. 28, no. 10, pp. 693–705, 2011.

[41] T. Ogawa, K. Yoshimura, H. Miyake et al., "Molecular characterization of organelle-type nudix hydrolases in Arabidopsis," *Plant Physiology*, vol. 148, no. 3, pp. 1412–1424, 2008.

[42] F. J. Sandoval, Y. Zhang, and S. Roje, "Flavin nucleotide metabolism in plants: monofunctional enzymes synthesize FAD in plastids," *Journal of Biological Chemistry*, vol. 283, no. 45, pp. 30890–30900, 2008.

[43] C. Meisinger, T. Sommer, and N. Pfanner, "Purification of Saccharomcyes cerevisiae mitochondria devoid of microsomal and cytosolic contaminations," *Analytical Biochemistry*, vol. 287, no. 2, pp. 339–342, 2000.

[44] M. Neuburger, E.-P. Journet, R. Bligny, J.-P. Carde, and R. Douce, "Purification of plant mitochondria by isopycnic centrifugation in density gradients of Percoll," *Archives of Biochemistry and Biophysics*, vol. 217, no. 1, pp. 312–323, 1982.

[45] G. Tedeschi, L. Pollegioni, and A. Negri, "Assays of d-amino acid oxidases," *Methods in Molecular Biology*, vol. 794, pp. 381–395, 2012.

[46] M. M. Bradford, "A rapid and sensitive method for the quantitation of microgram quantities of protein utilizing the principle of protein dye binding," *Analytical Biochemistry*, vol. 72, no. 1-2, pp. 248–254, 1976.

[47] E. M. Torchetti, F. Bonomi, M. Galluccio et al., "Human FAD synthase (isoform 2): a component of the machinery that delivers FAD to apo-flavoproteins," *FEBS Journal*, vol. 278, no. 22, pp. 4435–4449, 2011.

[48] W. S. Kunz, "Evaluation of electron-transfer flavoprotein and α-lipoamide dehydrogenase redox states by two-channel fluorimetry and its application to the investigation of β-oxidation," *Biochimica et Biophysica Acta*, vol. 932, no. 1, pp. 8–16, 1988.

[49] T. E. King, R. L. Howard, D. F. Wilson, and J. C. Li, "The partition of flavins in the heart muscle preparation and heart mitochondria," *The Journal of Biological Chemistry*, vol. 237, pp. 2941–2946, 1962.

[50] J. R. Barrio, J. A. Secrist III, and N. J. Leonard, "A fluorescent analog of nicotinamide adenine dinucleotide," *Proceedings of the National Academy of Sciences of the United States of America*, vol. 69, no. 8, pp. 2039–2042, 1972.

[51] F. Di Lisa, R. Menabò, M. Canton, M. Barile, and P. Bernardi, "Opening of the mitochondrial permeability transition pore causes depletion of mitochondrial and cytosolic NAD^+ and is a causative event in the death of myocytes in postischemic reperfusion of the heart," *Journal of Biological Chemistry*, vol. 276, no. 4, pp. 2571–2575, 2001.

[52] E. Rosenfeld and B. Beauvoit, "Role of the non-respiratory pathways in the utilization of molecular oxygen by *Saccharomyces cerevisiae*," *Yeast*, vol. 20, no. 13, pp. 1115–1144, 2003.

[53] A. Tzagoloff, J. Jang, D. M. Glerum, and M. Wu, "FLX1 codes for a carrier protein involved in maintaining a proper balance of flavin nucleotides in yeast mitochondria," *Journal of Biological Chemistry*, vol. 271, no. 13, pp. 7392–7397, 1996.

[54] M. H. Ragab, R. Brightwell, and A. L. Tappel, "Hydrolysis of flavin-adenine dinucleotide by rat liver lysosomes," *Archives of Biochemistry and Biophysics*, vol. 123, no. 1, pp. 179–185, 1968.

[55] H. J. Shin and J. L. Mego, "A rat liver lysosomal membrane flavin-adenine dinucleotide phosphohydrolase: purification and characterization," *Archives of Biochemistry and Biophysics*, vol. 267, no. 1, pp. 95–103, 1988.

[56] R. Orij, M. L. Urbanus, F. J. Vizeacoumar et al., "Genome-wide analysis of intracellular pH reveals quantitative control of cell division rate by pH(c) in *Saccharomyces cerevisiae*," *Genome Biology*, vol. 13, p. R80, 2012.

[57] A. Ayer, J. Sanwald, B. A. Pillay, A. J. Meyer, G. G. Perrone, and I. W. Dawes, "Distinct redox regulation in sub-cellular compartments in response to various stress conditions in *Saccharomyces cerevisiae*," *PLoS ONE*, vol. 8, Article ID e65240, 2013.

[58] D. Dikov, A. Aulbach, B. Muster, S. Dröse, M. Jendrach, and J. Bereiter-Hahn, "Do UCP2 and mild uncoupling improve longevity?" *Experimental Gerontology*, vol. 45, no. 7-8, pp. 586–595, 2010.

[59] A. L. Hughes and D. E. Gottschling, "An early age increase in vacuolar pH limits mitochondrial function and lifespan in yeast," *Nature*, vol. 492, pp. 261–265, 2012.

[60] R. Dechant, M. Binda, S. S. Lee, S. Pelet, J. Winderickx, and M. Peter, "Cytosolic pH is a second messenger for glucose and regulates the PKA pathway through V-ATPase," *EMBO Journal*, vol. 29, no. 15, pp. 2515–2526, 2010.

[61] H. Yang, T. Yang, J. A. Baur et al., "Nutrient-sensitive mitochondrial NAD^+ levels dictate cell survival," *Cell*, vol. 130, no. 6, pp. 1095–1107, 2007.

[62] T. Maruta, T. Yoshimoto, D. Ito et al., "An Arabidopsis FAD pyrophosphohydrolase, AtNUDX23, is involved in the flavin homeostasis," *Plant and Cell Physiology*, 2012.

[63] H.-X. Hao, O. Khalimonchuk, M. Schraders et al., "SDH5, a gene required for flavination of succinate dehydrogenase, is mutated in paraganglioma," *Science*, vol. 325, no. 5944, pp. 1139–1142, 2009.

Hindawi Publishing Corporation
Oxidative Medicine and Cellular Longevity
Volume 2013, Article ID 493536, 10 pages
http://dx.doi.org/10.1155/2013/493536

Research Article

Mitochondrial DNA Instability in Cells Lacking Aconitase Correlates with Iron Citrate Toxicity

Muhammad A. Farooq,[1] Tammy M. Pracheil,[1] Zhejun Dong,[1,2] Fei Xiao,[2] and Zhengchang Liu[1]

[1] *Department of Biological Sciences, University of New Orleans, New Orleans, LA 70148, USA*
[2] *Key Laboratory of Geriatrics, Beijing Institute of Geriatrics, Beijing Hospital, Ministry of Health, Beijing 100730, China*

Correspondence should be addressed to Zhengchang Liu; zliu5@uno.edu

Received 15 May 2013; Revised 12 July 2013; Accepted 24 July 2013

Academic Editor: Sergio Giannattasio

Aconitase, the second enzyme of the tricarboxylic acid cycle encoded by *ACO1* in the budding yeast *Saccharomyces cerevisiae*, catalyzes the conversion of citrate to isocitrate. *aco1*Δ results in mitochondrial DNA (mtDNA) instability. It has been proposed that Aco1 binds to mtDNA and mediates its maintenance. Here we propose an alternative mechanism to account for mtDNA loss in *aco1*Δ mutant cells. We found that *aco1*Δ activated the RTG pathway, resulting in increased expression of genes encoding citrate synthase. By deleting *RTG1*, *RTG3*, or genes encoding citrate synthase, mtDNA instability was prevented in *aco1*Δ mutant cells. Increased activity of citrate synthase leads to iron accumulation in the mitochondria. Mutations in *MRS3* and *MRS4*, encoding two mitochondrial iron transporters, also prevented mtDNA loss due to *aco1*Δ. Mitochondria are the main source of superoxide radicals, which are converted to H_2O_2 through two superoxide dismutases, Sod1 and Sod2. H_2O_2 in turn reacts with Fe^{2+} to generate very active hydroxyl radicals. We found that loss of Sod1, but not Sod2, prevents mtDNA loss in *aco1*Δ mutant cells. We propose that mtDNA loss in *aco1*Δ mutant cells is caused by the activation of the RTG pathway and subsequent iron citrate accumulation and toxicity.

1. Introduction

Respiratory metabolism in eukaryotes requires proteins encoded in both the nuclear genome and the mitochondrial genome (mtDNA). Mitochondrial genomes generally encode a small number of proteins, many of which are involved in respiratory metabolism [1, 2]. Maintenance of mtDNA is important for cell growth and survival. Oxidative damage to mtDNA causes respiratory deficiency and human diseases [3–5]. In higher eukaryotes, how the mitochondrial genome is maintained and transmitted is not well understood. However, studies using the budding yeast *Saccharomyces cerevisiae* have generated an abundance of data on how its mitochondrial genome is maintained [6, 7]. Many nuclear-encoded proteins of diverse functions are required for mtDNA maintenance. When mtDNA is mutated, yeast cells form the so-called "petite" mutants. Yeast can be categorized as those with wild type (rho^+ cells), extensively deleted (rho^- petites), or with complete loss of (rho^0 petites) mtDNA. How mutations in nuclear genes cause defects in mtDNA maintenance is complex and often indirect. For example, mutations in the yeast homolog of frataxin, Yfh1, lead to iron overload in mitochondria, defects in maturation of proteins containing iron-sulfur clusters such as the TCA cycle enzyme aconitase, mtDNA instability and respiratory deficiency, and so forth [8–10]. Yeast studies have suggested that iron citrate toxicity may be responsible for *yfh1* mutant phenotypes [11, 12]. Respiratory metabolism generates reactive oxygen species such as superoxide radicals. Superoxide dismutases, Sod1 and Sod2, localized in the cytoplasm and mitochondria, respectively, are responsible for converting superoxide radicals to relatively harmless hydrogen peroxide [13], which can react with ferrous iron (Fe^{2+}) to generate highly reactive hydroxyl radicals through the Fenton reaction. Hydrogen peroxide is detoxified by enzymes such as catalases, converting hydrogen peroxide to oxygen and water [14]. Mutations in yeast catalases and

superoxide dismutase lead to oxidative damage and reduced resistance to oxidants [14–16].

Besides resulting in respiratory deficiency, mutations in TCA cycle enzyme encoding genes also lead to variable defects in mtDNA maintenance [17, 18]. The most severe phenotype is caused by mutations in the *ACO1* gene encoding aconitase, followed by the *IDH1* gene encoding a subunit of mitochondrial isocitrate dehydrogenase [19]. It has been proposed that Aco1 has a novel function in mediating mtDNA maintenance by directly binding mtDNA [20, 21]. Mutations in *ACO1* and *IDH1* share several growth defect phenotypes, which can be partially rescued by mutations in *CIT1*, encoding the mitochondrial isoform of citrate synthase [17]. Expression of *CIT1*, *ACO1*, *IDH1*, and *IDH2* is under dual control of two transcriptional regulatory complexes, Rtg1/3 and Hap2/3/4/5 [22]. In cells with reduced or defective respiratory functions, expression of these genes is under increased control of Rtg1/3. Rtg1 and Rtg3 are two basic helix-loop-helix transcription factors in the retrograde response pathway that mediates signaling from mitochondria to the nucleus [23]. Activation of Rtg1/3 requires a cytoplasmic protein, Rtg2, which has an N-terminal ATP binding domain in the Hsp70/actin/sugar kinase ATP binding domain superfamily [24]. The retrograde response pathway, also known as the RTG pathway, is activated in response to defects in mitochondrial respiratory function. Cit1, Aco1, and Idh1/2 promote synthesis of α-ketoglutarate, a precursor of glutamate, which is a potent repressor of the RTG pathway [23]. Mutations in *ACO1*, which lead to both a block in mitochondrial respiratory function and glutamate auxotrophy [25–27], therefore, likely activate the RTG pathway. However, it is not clear whether the *RTG* pathway contributes to the phenotypes of aco1 mutants.

Mutations in *RTG2* and *CIT2* have been reported to suppress mtDNA instability due to mutations in *YFH1* [12]. In this study, we provide an alternative model to account for mtDNA loss due to an *aco1*Δ mutation. We found that mutations in either *RTG* genes, genes encoding citrate synthases, genes encoding mitochondrial iron transporters, or *SOD1* suppress *aco1*Δ-induced mtDNA loss. Therefore, we propose that iron citrate toxicity contributes to *aco1*Δ mutant phenotypes.

2. Materials and Methods

2.1. Strains, Plasmids, Growth Media, and Growth Conditions. Yeast strains and plasmids used in this study are listed in Tables 1 and 2, respectively. Yeast mutant strains were created by either direct transformation with gene knockout cassettes or through meiotic segregation analysis of heterozygous diploids. Mutations were confirmed by PCR-genotyping, standard genotyping based on selection markers, phenotypic analysis, and/or immunoblotting using antibody against Aco1. The BY4741 rho^0 strain was generated by one passage of rho$^+$ cells grown in YPD medium supplemented with 15 μg/mL ethidium bromide. Yeast cells were grown in SD (0.67% yeast nitrogen base plus 2% dextrose), YNBCasD (SD medium plus 1% casamino acids), YNBcasR (0.67% yeast nitrogen base, 1% casamino acids, and 2% raffinose), YPD (1% yeast extract, 2% peptone, 2% dextrose), or YPEthanol (1% yeast extract, 2% peptone, 2% ethanol) medium at 30°C. When necessary, amino acids, adenine, and/or uracil were added to the growth medium at standard concentrations to cover auxotrophic requirements [28].

2.2. Yeast Transformation and β-Galactosidase Activity Assays. Plasmids were transformed into yeast strains using the high-efficiency lithium acetate-PEG method and β-galactosidase assays were carried out as described [28]. For each plasmid and strain combination, assays were conducted in duplicates, and independent experiments were carried out two times. Specific activity of β-galactosidase is expressed as nmols of *o*-nitrophenol generated from substrate *o*-nitrophenyl-β-D-galactoside per min per mg protein.

2.3. DAPI Staining of Nuclear and Mitochondrial DNA and FLuorescence Microscopy. DAPI (4′6,-diamidino-2-phenylindole) staining of nuclear and mitochondrial DNA was carried out as described [28]. Briefly, yeast strains were grown in liquid YPD or YNBcasD medium at 30°C overnight to $A_{600} \sim 0.8$. Cells were collected by centrifugation and treated with 1 μg/mL DAPI in 95% ethanol for 30 min and cell pellets were washed with sterile water three times. DAPI-stained DNA molecules in fixed cells were observed by fluorescence microscopy using a Nikon Eclipse E800 microscope equipped with an HBO 100 W/2 mercury arc lamp, a Nikon Plan Fluor 100X objective lens, and epifluorescence with a Nikon UV-2E/C filter set (excitation 340–380 nm and emission 435–485 nm). Digital images were acquired with Photometrics Coolsnap fx CCD camera and Metamorph Imaging Software (Molecular Devices, Sunnyvale, CA) and processed using ImageJ (National Institutes of Health) and Adobe Photoshop (Mountain View, CA).

2.4. Citrate Analysis. Cells were grown in 10 mL YPD medium overnight to ~OD_{600} 1.0. Cultures were chilled in ice-cold water for 22 min and cells were collected by centrifugation at 4°C. Cell pellets were then washed twice in chilled water. Citrate levels were determined using a citrate assay kit (BioVision, CA, USA). Cells were disrupted in 500 μL Assay Buffer in the kit using glass beads method. Cell extract was clarified by centrifugation at 21,000 g at 4°C for 15 min. 20 uL cell extract was analyzed for protein concentration using Bradford assay and the rest of cell extract (~350) was deproteinized in Amicon Ultra 4 column (10 kDa cutoff). Deproteinized extract was analyzed for citrate levels according to the protocol provided by the manufacturer. Citrate levels in different strains were normalized by protein concentration of cellular extract prior to deproteinization. Citrate concentration in the wild-type strain was 7.97 nmols/mg proteins, which was arbitrarily set as 1 unit. Citrate concentration in the wild-type strain determined in this study is similar to ~1.1 nmols/10^7 cells reported previously [12].

Table 1: Strains used in this study.

Strain	Genotype	Source
BY4741	*MATa ura3 leu2 his3 met15*	Research genetics
BY4731	*MATa ura3 leu2 met15*	Research genetics
BY4742	*MATa ura3 leu2 his3 lys2*	Research genetics
BY4741 (rho^0)	BY4741 rho^0 derivative	This study
ZLY2630	BY4741 *aco1::kanMX4*	This study
ZLY1264	BY4741 *rtg1::kanMX4*	Research genetics
ZLY1267	BY4741 *rtg2::kanMX4*	Research genetics
ZLY1273	BY4741 *rtg3::kanMX4*	Research genetics
ZLY2568	BY4742 *rtg1::LEU2*	This study
ZLY143	BY4731 *rtg2::LEU2*	This study
ZLY2570	BY4742 *rtg3::URA3*	This study
ZLY2648	BY4741 *rtg1::LEU2 aco1::kanMX4*	This study
ZLY2631	BY4741 *rtg2::LEU2 aco1::kanMX4*	This study
ZLY2652	BY4741 *rtg3::URA3 aco1::kanMX4*	This study
ZLY3206	*MATα met? [rho^0]*	This study
CS725-3A	*MATa ura3 leu2 his3 met15 cit1/2/3::kanMX4*	[21]
ZLY2545	CS725-3A *aco1::HIS3*	[21]
RBY353	BY4741 *cit1::kanMX4*	Research genetics
RBY355	BY4741 *cit2::kanMX4*	Research genetics
RBY356	BY4741 *cit3::kanMX4*	Research genetics
ZLY2603	*MATa ura3 leu2 met15 aco1::kanMX4*	This study
RBY469	BY4741 *cit1::kanMX4 aco1::kanMX4*	This study
RBY277	BY4741 *cit2::kanMX4 aco1::kanMX4*	This study
RBY363	BY4741 *cit3::kanMX4 aco1::kanMX4*	This study
ZLY854	BY4741 *cit1/2::kanMX4 aco1::kanMX4*	This study
BY4741 (*mrs3 mrs4*)	BY4741 *mrs3::kanMX4 mrs4::kanMX4*	[29]
ZLY3505	BY4741 *mrs3::kanMX4 mrs4::kanMX4 aco1::HIS3*	This study
ZLY4603	BY4741 *sod1::kanMX4*	This study
BY4741 (*sod2*)	BY4741 *sod2::kanMX4*	Research genetics
TPY1507	BY4741 *sod1::kanMX4 aco1::kanMX4*	This study
ZLY3973	BY4741 *sod2::kanMX4 aco1::kanMX4*	This study

Table 2: Plasmids used in this study.

Plasmid	Description	Source
pRS416	A yeast centromeric plasmid carrying *URA3* selection marker	[30]
pUC-rtg1::LEU2	An *rtg1::LEU2* disruption cassette in pUC19	[31]
pUC-rtg2::LEU2	An *rtg2::LEU2* disruption cassette in pUC19	[31]
pUC-rtg3::URA3	An *rtg3::URA3* disruption cassette in pUC19	[32]
pBS-aco1::HIS3	An *aco1::HIS3*disruption cassette in pBluescript	This study
pCIT2-lacZ	A *CIT2-lacZ* reporter gene on the plasmid pWCJ (*CEN URA3*)	This study
pRS303-SOD1	The *SOD1* gene was cloned into the integrative plasmid pRS303	This study

3. Results and Discussion

3.1. aco1Δ Activates the RTG Pathway. Mutations in *ACO1* lead to both respiratory deficiency and glutamate starvation, which are expected to activate the RTG pathway. To test this possibility, we determined the effect of an *aco1*Δ mutation on the expression of a *CIT2-lacZ* reporter gene, which has been used extensively as a readout of the activity of the RTG pathway [22, 24, 33–35]. Expression of *CIT2-lacZ* was assessed in wild-type rho^+ and *aco1*Δ mutant cells using β-galactosidase assays. Since *aco1*Δ cells are rho^0 petites, we also determined *CIT2-lacZ* expression in otherwise wild-type rho^0 cells. Cells were grown in rich media with either raffinose or dextrose (D-glucose) as the sole carbon source, which have been used in studies on the *RTG* pathway and mitochondrial genome maintenance, respectively [12, 20, 21, 36]. In cells grown in raffinose medium, *CIT2-lacZ* expression was 4-fold higher in rho^0 cells compared to rho^+ cells, consistent with previous

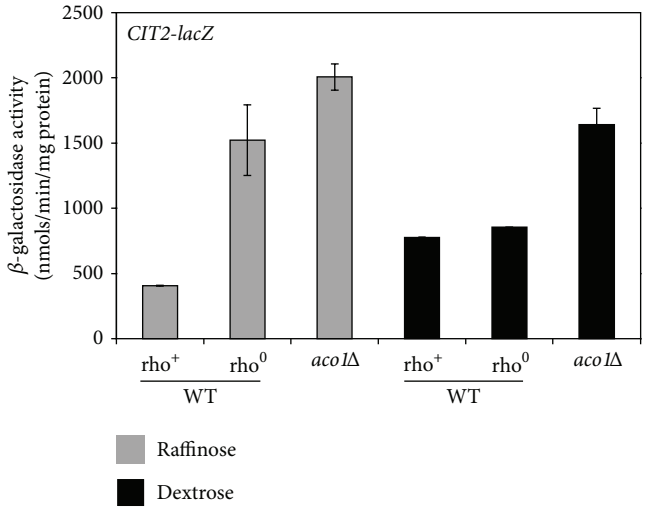

Figure 1: The RTG pathway is activated in *aco1*Δ mutant cells grown in dextrose medium. Wild-type rho$^+$ (WT, BY4741), its rho^0 derivative, and *aco1*Δ (ZLY2603) mutant strains were transformed with a centromeric plasmid encoding a *CIT2-lacZ* reporter gene (pCIT2-lacZ) and transformants were grown in YNBcasR (Raffinose) and YNBcasD (Dextrose) medium to mid-logarithmic phase. Cells were collected and β-galactosidase assays were conducted as described in Section 2.

reports that the *RTG* pathway is activated in rho^0 cells [33, 36]. An *aco1*Δ mutation induced *CIT2-lacZ* expression slightly higher than in wild-type rho^0 cells (Figure 1). In cells grown in dextrose medium, *CIT2-lacZ* expression in rho^0 cells is only marginally higher than in rho$^+$ cells, whereas an *aco1*Δ mutation almost doubled *CIT2-lacZ* expression. Activation of the RTG pathway is strain dependent [37]. The lack of induction of the RTG pathway due to loss of mtDNA in dextrose-grown BY4741 background strains used in this study can be partly attributed to a doubling of *CIT2-lacZ* expression in rho$^+$ cells grown in this medium compared to raffinose medium, which is consistent with activation of the RTG pathway due to compromised mitochondrial respiratory function since dextrose suppresses respiratory metabolism in yeast. Altogether, these data indicate that an *aco1*Δ mutation leads to activation of the RTG pathway.

3.2. Mutations in RTG Genes Prevent mtDNA Loss due to aco1Δ. To determine whether activation of the RTG pathway in *aco1*Δ mutant cells contributes to mtDNA loss, *rtg1*Δ *aco1*Δ, *rtg2*Δ *aco1*Δ, and *rtg3*Δ *aco1*Δ double mutants were constructed and examined for the presence or absence of mtDNA. These double mutant strains were created by crossing respective haploid mutant strains to form heterozygous diploid mutants, which were then sporulated to generate desired haploid segregants. Seven *rtg1*Δ *aco1*Δ, seven *rtg2*Δ *aco1*Δ, and six *rtg3*Δ *aco1*Δ double mutant segregants were obtained. Eight *aco1*Δ single mutant segregants were also isolated similarly. DAPI, a DNA-specific probe that forms a fluorescent complex [38], was then used to visualize mtDNA using fluorescence microscopy in these mutants along with wild-type rho$^+$ and rho^0 strains. In addition to nuclear DNA, DAPI staining revealed punctate cytoplasmic structures of mtDNA in wild-type rho$^+$ cells grown in YPD medium (Figure 2(a)) [38]. In contrast, mtDNA was absent in both wild-type rho^0 and *aco1*Δ mutant cells, consistent with previous reports that Aco1 is required for mtDNA maintenance [17, 18, 21]. Interestingly, mtDNA was maintained in *rtg1*Δ *aco1*Δ, *rtg2*Δ *aco1*Δ, and *rtg3*Δ *aco1*Δ double mutant strains, indicating that Rtg proteins mediate mtDNA instability in *aco1*Δ mutant cells. The percentage of rho^0 cells was quantified from DAPI-stained images and a large majority of *rtg*Δ *aco1*Δ double mutant cells were found to contain mtDNA (Figure 2(b)). Among seven *rtg2*Δ *aco1*Δ double mutant segregants from heterozygous *rtg2*Δ*/RTG2 aco1*Δ*/ACO1* diploid mutant cells, all were found to maintain mtDNA. Similarly, all of the seven *rtg1*Δ *aco1* and six *rtg3*Δ *aco1*Δ double mutant segregants were also found to be rho$^+$ cells. In contrast, all of the eight *aco1*Δ single mutant segregants from a heterozygous *aco1*Δ*/ACO1* diploid mutant have lost mtDNA. Together, our data suggest that mtDNA instability in *aco1*Δ mutant cells may result from activation of the RTG pathway.

Damages to mtDNA can lead to extensive deletions (rho$^-$) or point mutations (*mit*$^-$) [6, 7]. Yeast strains that carry these two types of mutant mitochondrial genomes are respiratory deficient. To determine whether the mtDNA in the *rtg*Δ *aco1*Δ double mutant strains is functional, we conducted a complementation assay by crossing wild-type rho$^+$, wild-type rho^0, *rtg1*Δ, *rtg2*Δ, *rtg3*Δ, *rtg1*Δ *aco1*Δ, *rtg2*Δ *aco1*Δ, and *rtg3*Δ *aco1*Δ mutant strains to a rho^0 tester strain of opposite mating type with wild-type nuclear *ACO1* gene and analyzing the respiratory capacity of the resultant diploid strains. *rtg1*Δ *aco1*Δ, *rtg2*Δ *aco1*Δ, and *rtg3*Δ *aco1*Δ mutant strains were unable to utilize carbon sources that require respiratory metabolism such as ethanol because they are defective in the TCA cycle (data not shown), and Figure 2(c) shows that diploids generated from crossing wild-type rho$^+$, *rtg1*Δ, *rtg2*Δ, and *rtg3*Δ strains with the rho^0 tester strain were able to grow on ethanol medium. In contrast, diploids from crosses involving wild-type rho^0 or the *aco1*Δ single mutant were unable to grow on ethanol medium, consistent with the absence of mtDNA in these diploids. Remarkably, diploids generated from the rho^0 tester strain and *rtg*Δ *aco1*Δ double mutants were able to grow on ethanol medium, indicating that mtDNA in *rtg*Δ *aco1*Δ cells are functional.

3.3. Mutations in Genes Encoding Citrate Synthase, Primarily CIT1, Prevent mtDNA Loss due to aco1Δ. What is the mechanism of *aco1*Δ suppression by mutations in *RTG* genes? The *RTG* pathway is required for glutamate biosynthesis in cells with reduced respiratory function by regulating expression of *CIT1*, *CIT2*, *ACO1*, *IDH1*, and *IDH2* [23]. It has been shown previously that a *cit1*Δ mutation partially suppresses mtDNA loss in *aco1*Δ mutant cells and that mutations in *CIT2* and *RTG2* rescue respiratory deficiency in *yfh1*Δ mutant cells [12, 17]. Three genes, *CIT1*, *CIT2*, and *CIT3*, encode citrate synthase in yeast, with *CIT1* and *CIT3* encoding the two mitochondrial isoforms and *CIT2* encoding the peroxisomal isoform [39–41]. Therefore, suppression of mtDNA loss in

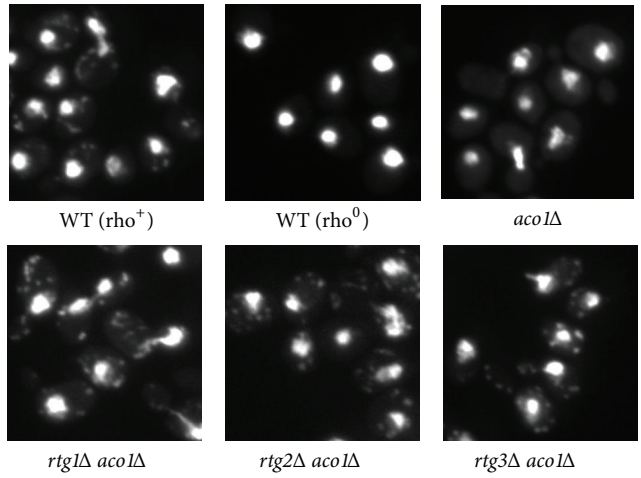

(a)

Strains	rho^0 cells (%)	Number of cells analyzed
WT (rho^+)	2.5%	551
WT (rho^0)	100.0%	433
*aco1*Δ	100.0%	440
*rtg1*Δ *aco1*Δ	4.7%	406
*rtg2*Δ *aco1*Δ	18.3%	454
*rtg3*Δ *aco1*Δ	6.0%	399

(b)

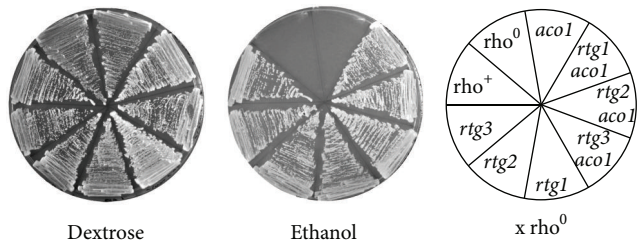

(c)

Figure 2: mtDNA is maintained in *rtg1*Δ *aco1, rtg2*Δ *aco1*Δ, *and rtg3*Δ *aco1*Δ mutant cells. (a) Cells grown exponentially in YPD medium were stained with DAPI and then examined using fluorescence microscopy. WT (rho^+), BY4741; WT (rho^0), BY4741 rho^0; *aco1*Δ, ZLY2630; *rtg1*Δ *aco1*Δ, ZLY2648; *rtg2*Δ *aco1*Δ, ZLY2631; *rtg3*Δ *aco1*Δ, ZLY2652. (b) Quantitative analysis of the percentage of rho^0 cells in yeast strains based on DAPI-staining images. (c) mtDNA in *rtg*Δ *aco1*Δ double mutant cells is functional. Strains as described in (a) as well as *rtg1*Δ, *rtg2*Δ, and *rtg3*Δ single mutants were crossed to a rho^0 tester strain (X rho^0) of opposite mating type. Diploids were selected and grown on YPD (Dextrose) and YPEthanol (Ethanol) medium. Pictures of cells were taken after 3 days' growth at 30°C.

*rtg1*Δ *aco1*Δ, *rtg2*Δ *aco1*Δ, and *rtg3*Δ *aco1*Δ double mutant cells may be due to reduced expression of genes encoding citrate synthase. To confirm this possibility, we introduced an *aco1*Δ mutation into a *cit1*Δ *cit2*Δ *cit3*Δ triple mutant in the BY4741 strain background generated by Chen et al. [21]. The presence or absence of mtDNA in the resultant quadruple mutant cells was examined by DAPI staining and fluorescence microscopy. Figure 3(a) shows that the *cit1*Δ *cit2*Δ *cit3*Δ *aco1*Δ quadruple mutant maintained mtDNA. To determine which citrate synthase-encoding gene(s) is responsible for mtDNA loss in *aco1*Δ mutant cells, we generated *cit1*Δ *aco1*Δ, *cit2*Δ *aco1*Δ, and *cit3*Δ *aco1*Δ double mutants, as well as an *aco1*Δ *cit1*Δ *cit2*Δ triple mutant by crossing respective haploid mutant strains followed by meiotic segregation analysis. Using DAPI staining and fluorescence microscopy, we found that six out of eight *cit1*Δ *aco1*Δ double mutants, zero out of six *cit2*Δ *aco1*Δ double mutants, zero out of six *cit3*Δ *aco1*Δ double mutants, and six out of six *cit1*Δ *cit2*Δ *aco1*Δ triple mutant strains maintained mtDNA (Figure 3 and data not shown). We also calculated the percentage of rho^0 cells in a *cit1*Δ *aco1*Δ double, a *cit1*Δ *cit2*Δ *aco1*Δ triple, and a *cit1*Δ *cit2*Δ *cit3*Δ *aco1*Δ quadruple mutant and found that over 90%

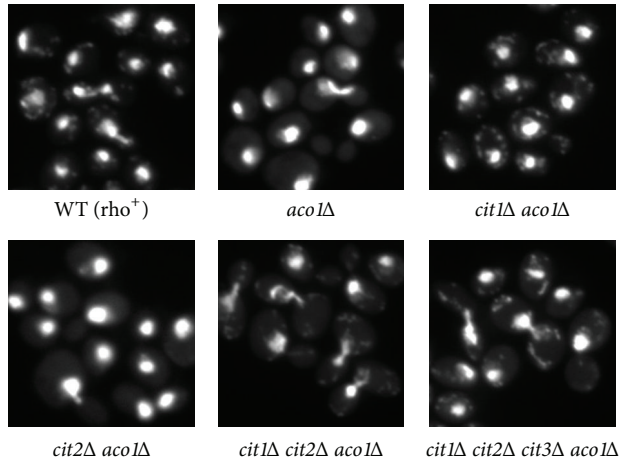

(a)

Strains	rho^0 cells (%)	Number of cells analyzed
*aco1*Δ	100.0%	440
*cit1*Δ *aco1*Δ	6.5%	432
*cit1*Δ *cit2*Δ *aco1*Δ	9.9%	444
*cit1*Δ *cit2*Δ *cit3*Δ *aco1*Δ	8.2%	454

(b)

Figure 3: Mutations in genes encoding citrate synthase prevent mtDNA loss due to *aco1*Δ. (a) Cells grown in YPD medium to mid-logarithmic phase were stained with DAPI and examined using fluorescence microscopy. WT (rho$^+$), BY4741; *aco1*Δ, ZLY2630; *cit1*Δ *aco1*Δ, RBY469; *cit2*Δ *aco1*Δ, RBY277; *cit1*Δ *cit2*Δ *aco1*Δ, ZLY854; *cit1*Δ *cit2*Δ *cit3*Δ *aco1*Δ, ZLY854; *rtg2*Δ *aco1*Δ, ZLY2545. (b) Quantitative analysis of the percentage of rho^0 cells in yeast strains based on DAPI-staining images.

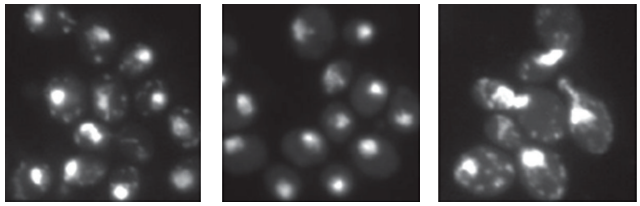

Figure 4: Mutations in *MRS3* and *MRS4*, encoding mitochondrial iron transporters, prevent mtDNA loss due to *aco1*Δ. Cells grown in YPD medium to mid-logarithmic phase were stained with DAPI and examined using fluorescence microscopy. WT (rho$^+$), BY4741; *aco1*Δ, ZLY2630; *mrs3*Δ *mrs4*Δ *aco1*Δ, ZLY3505.

cells from these mutants maintained mtDNA (Figure 3(b)). Taken together, these data suggest that citrate synthase is the target of the RTG pathway that mediates mtDNA instability in *aco1*Δ mutant cells and that Cit1 is primarily responsible for this phenotype in the BY4741 strain background.

*3.4. Mutations in Genes Encoding Mitochondrial Iron Transporters Mrs3 and Mrs4 Prevent mtDNA Loss due to aco1*Δ. It has been proposed that iron citrate toxicity contributes to oxidative damage and mtDNA loss in *yfh1*Δ mutant cells, which have higher levels of cellular and mitochondrial iron [8, 12]. Mutations in *RTG2* and *CIT2* reduce petite formation in *yfh1*Δ mutants by lowering cellular citrate and iron levels. Suppression of mtDNA loss in *aco1*Δ mutant cells by mutations in *RTG* genes and genes encoding citrate synthase prompted us to test whether mitochondrial iron overload is responsible for mtDNA instability in *aco1*Δ mutants. Mitochondrial iron transport is mediated by iron transporters Mrs3 and Mrs4 [11, 29, 42, 43], mutations of which rescue mtDNA loss in *yfh1*Δ mutants. To this end, we generated an *mrs3*Δ *mrs4*Δ *aco1*Δ triple mutant by introducing an *aco1*Δ mutation into an *mrs3*Δ *mrs4*Δ double mutant. DAPI staining of the triple mutant showed that mtDNA was maintained (Figure 4). Furthermore, quantitative analysis showed that the percentage of rho^0 cells in the triple mutant was 0.4%, slightly lower than 2.5% in wild-type rho$^+$ cells. The *mrs3*Δ *mrs4*Δ *aco1*Δ triple mutant was also mated to a rho^0 tester strain and the resulting diploids were streaked onto plates with ethanol as the sole carbon source. We found that the diploids could grow on ethanol medium, indicating that mtDNA in the *mrs3*Δ *mrs4*Δ *aco1*Δ triple mutant is functional (data not shown). Together, this data supports the notion that mtDNA loss in *aco1*Δ mutant cells is due to iron citrate toxicity.

It has been reported that the supplementation of exogenous iron (1 mM $FeSO_4$) or raising pH of the growth medium reduces petite frequency in *aco1*Δ mutant cells grown in YPGalactose medium [17]. Thus, Lin et al. proposed that some of the effects of elevated citrate levels in *aco1*Δ are

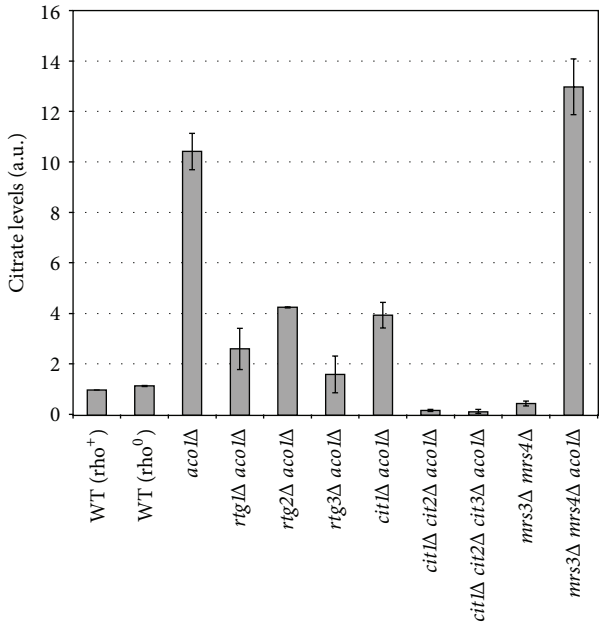

Figure 5: Citrate levels in wild-type (WT) and indicated mutant strains. Citrate concentration was determined as described in Section 2. The results are the average of two independent experiments.

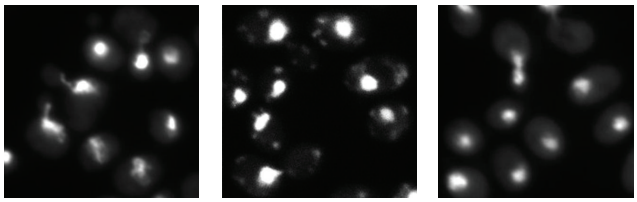

Figure 6: A mutation in *SOD1*, but not *SOD2*, suppresses mtDNA loss due to *aco1*Δ. Cells grown in YPD medium to mid-logarithmic phase were stained with DAPI and examined using fluorescence microscopy. *aco1*Δ, ZLY2630; *sod1*Δ *aco1*Δ, TPY1507; *sod2*Δ *aco1*Δ, ZLY3973.

due to the ionized form of this metabolite rather than to the formation of a citrate/iron chelate that could produce oxidative damage to mtDNA. These observations seem to contradict our conclusion. However, iron homeostasis is a highly complicated process [44]. It was not established that exogenous iron actually increased iron levels in the mitochondria in Lin et al.'s study. It is also possible that growth conditions (YPD in this study versus YPGalactose in Lin et al.'s study) and/or strain backgrounds (BY4741 versus W303-1B) may affect mtDNA loss associated with *aco1*Δ mutations.

3.5. Iron Citrate Toxicity Correlates with mtDNA Loss in aco1Δ Mutant Cells. To affirm our hypothesis that iron citrate toxicity contributes to mtDNA loss in *aco1*Δ mutant cells, we determined citrate levels in wild-type and various mutant strains and found that *aco1*Δ increased the citrate level by 10.5-fold (Figure 5), which is consistent with an 11.9-fold increase reported by Lin et al. [17]. This increase is not due to that *aco1*Δ mutants are rho^0 cells since the citrate level in wild-type rho^0 cells was only 16% higher than that of wild-type rho$^+$ cells. Mutations in *RTG1*, *RTG2*, and *RTG3* reduced citrate levels in *aco1*Δ background cells by 59–85%. Similarly, *cit1*Δ reduced citrate concentration by 62% in *aco1*Δ background cells, which is comparable to an 89% decrease reported by Lin et al. A double mutation in *CIT1* and *CIT2* reduced citrate concentration by 98% in *aco1*Δ background cells, and an additional mutation in *CIT3* did not significantly further reduce citrate levels. Clearly, there is strong correlation between the suppression of mtDNA loss phenotype and lower citrate levels in *aco1*Δ background strains. We also determined the effect of an *mrs3*Δ *mrs4*Δ double mutation on citrate levels. In comparison to a wild-type rho$^+$ strain, citrate concentration in an *mrs3*Δ *mrs4*Δ double mutant was 53% lower. In contrast, citrate concentration in an *mrs3*Δ *mrs4*Δ *aco1*Δ triple mutant is 24% higher than that of an *aco1*Δ mutant. Since *mrs3*Δ *mrs4*Δ *aco1*Δ mutant cells maintained mtDNA, we propose that high levels of citrate per se are not sufficient to lead to mtDNA loss and that citrate toxicity requires certain levels of iron in the mitochondria. Together with our genetic data, these biochemical results suggest that iron citrate toxicity accounts for mtDNA loss in *aco1*Δ mutant cells.

*3.6. A Mutation in SOD1, but Not SOD2, Prevents mtDNA Loss due to aco1*Δ. Our data suggest that high levels of citrate cause mtDNA instability in *aco1*Δ mutant cells likely due to iron citrate toxicity. Iron reacts with hydrogen peroxide in the Fenton reaction to produce highly active, potent hydroxyl radicals, which cause oxidative damage to mitochondria. Hydrogen peroxide is partly produced by the superoxide dismutases, Sod1 in the cytoplasm and Sod2 in the mitochondrial matrix [12]. We hypothesized that a reduced production of hydrogen peroxide due to mutations in *SOD1* or *SOD2* might suppress mtDNA loss in *aco1*Δ mutant cells by lowering the amount of hydroxyl radicals produced via the Fenton reaction. Therefore, we generated *sod1*Δ *aco1*Δ and *sod2*Δ *aco1*Δ double mutants by crossing respective haploid mutant strains followed by meiotic segregation analysis. The resultant double mutant strains were analyzed for mtDNA presence by DAPI staining and fluorescence microscopy. 33 out of 34 *sod1*Δ *aco1*Δ double mutant strains generated maintained mtDNA while 6 out of 6 *sod2*Δ *aco1*Δ double mutants lost mtDNA (Figure 6 and data not shown). These data suggest that hydrogen peroxide generated from reactions catalyzed by Sod1 contributes to mtDNA loss in *aco1*Δ mutant cells. Mutations in *SOD1* also cause oxidative damage due to accumulation of superoxide radicals [15, 16]. However, since an *sod1*Δ mutation suppressed mtDNA loss in *aco1*Δ mutant cells, we propose that hydroxyl radicals are more damaging to mtDNA than superoxide radicals. How would mutations in the cytosolic isoform of superoxide dismutase rescue a mitochondrial defect? It has been shown that a small fraction of Sod1 is localized in the intermembrane space of mitochondria, which protects cells from mitochondrial

oxidative damage [45–47]. Why does not *sod2*Δ suppress mtDNA loss associated with *aco1*Δ? It is possible that loss of Sod2 leads to increased levels of superoxide radicals in the mitochondria, which in the presence of ferrous ions would cause any hydrogen peroxide produced in the mitochondria to be converted to the hydroxyl radicals via the Fenton/Haber Weiss reactions that damage mtDNA.

3.7. Loss of mtDNA in aco1Δ Mutant Cells Is Growth Medium Dependent. It has been proposed that mtDNA loss in *aco1*Δ mutant cells is due to lack of physical protection of mtDNA by Aco1 [20]. One key piece of evidence that supports this hypothesis is the observation that the expression of two catalytically inactive Aco1 mutants, $Aco1^{C382S}$ and $Aco1^{C445S}$, under the control of the *ADH1* promoter from the pRS416 centromeric plasmid, prevented mtDNA loss in *aco1*Δ mutant cells. To maintain the plasmids, transformants were grown in YNBcasD medium. In light of discovery that iron citrate toxicity contributes to mtDNA loss, one alternative explanation for mtDNA retention in cells expressing $ACO1^{C382S}$ and $ACO1^{C445S}$ mutant alleles is due to differences in growth medium, YNBcasD versus YPD. Accordingly, we transformed *aco1*Δ*/ACO1* heterozygous diploid mutant cells with empty pRS416 vector and transformants were sporulated and dissected on YPD or YNBcasD medium. Eleven *aco1*Δ haploid mutants from a YPD dissection plate were obtained and grown in YPD liquid medium and mtDNA was observed by DAPI staining. We found that all of the eleven *aco1*Δ segregants lost mitochondrial DNA (Figure 7 and data not shown). In contrast, among nine *aco1*Δ mutant segregants carrying the empty pRS416 vector from a YNBcasD dissection plate that were grown in YNBcasD liquid medium, seven maintained mtDNA (Figure 7 and data not shown). When these seven *aco1*Δ mutants containing mtDNA were passed onto YPD plate medium twice and then grown in YPD liquid medium, all lost mtDNA (data not shown). Together, these data suggest that mtDNA loss in *aco1*Δ mutant cells is growth medium dependent.

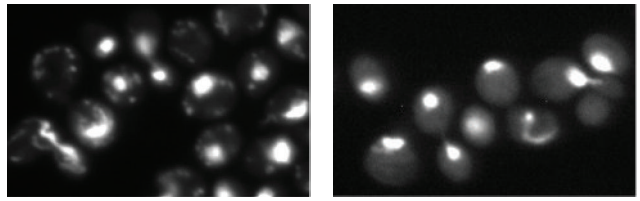

*aco1*Δ (YNBCasD) *aco1*Δ (YPD)

Figure 7: mtDNA loss due to *aco1*Δ is growth medium dependent. *aco1*Δ mutant cells (ZLY2630) carrying empty pRS416 vector were grown in YNBcasD or YPD medium to mid-logarithmic phase, stained with DAPI, and examined using fluorescence microscopy.

4. Conclusions

It has been proposed that yeast aconitase (Aco1) physically binds to mtDNA and promotes its maintenance [20, 21]. Our results in this study suggest a different, but not necessarily mutually exclusive, mechanism. We propose that *aco1*Δ activates the RTG pathway, resulting in increased citrate production through upregulation of genes encoding citrate synthase. Increased levels of citrate lead to iron overload in the mitochondria. Iron then reacts with hydrogen peroxide to generate hydroxyl radicals, which cause oxidative damage to mitochondrial DNA and consequently its instability. Mutations of yeast frataxin (Yfh1) lead to loss of activity of aconitase [48]. Suppression of mtDNA instability due to mutations in both *YFH1* and *ACO1* by reduced iron citrate levels raises the possibility that mtDNA loss in *yfh1* mutant cells may be an indirect consequence of aconitase inactivation. Our data also suggest that the cytosolic superoxide dismutase, Sod1, but not the mitochondrial superoxide dismutase, Sod2, contributes to mtDNA loss in *aco1*Δ mutant cells.

Conflict of Interests

The authors declare no conflict of interests.

Acknowledgments

The authors would like to thank Dr. Jerry Kaplan at The University of Utah for yeast strains, W. M. Keck Foundation for the Keck Facility, and Robin Rowe for sequencing. This work was supported by grant 1R15GM094772-01A1 (to Z. Liu) from the National Institutes of Health.

References

[1] F. Foury, T. Roganti, N. Lecrenier, and B. Purnelle, "The complete sequence of the mitochondrial genome of *Saccharomyces cerevisiae*," *FEBS Letters*, vol. 440, no. 3, pp. 325–331, 1998.

[2] B. F. Lang, M. W. Gray, and G. Burger, "Mitochondrial genome evolution and the origin of eukaryotes," *Annual Review of Genetics*, vol. 33, pp. 351–397, 1999.

[3] R. W. Taylor and D. M. Turnbull, "Mitochondrial DNA mutations in human disease," *Nature Reviews Genetics*, vol. 6, no. 5, pp. 389–402, 2005.

[4] L. C. Greaves, A. K. Reeve, R. W. Taylor, and D. M. Turnbull, "Mitochondrial DNA and disease," *Journal of Pathology*, vol. 226, no. 2, pp. 274–286, 2012.

[5] A. Siddiqui, S. Rivera-Sanchez, R. Castro Mdel et al., "Mitochondrial DNA damage is associated with reduced mitochondrial bioenergetics in Huntington's disease," *Free Radical Biology & Medicine*, vol. 53, no. 7, pp. 1478–1488, 2012.

[6] K. A. Lipinski, A. Kaniak-Golik, and P. Golik, "Maintenance and expression of the S. Cerevisiae mitochondrial genome-From genetics to evolution and systems biology," *Biochimica et Biophysica Acta*, vol. 1797, no. 6-7, pp. 1086–1098, 2010.

[7] V. Contamine and M. Picard, "Maintenance and integrity of the mitochondrial genome: a plethora of nuclear genes in the budding yeast," *Microbiology and Molecular Biology Reviews*, vol. 64, no. 2, pp. 281–315, 2000.

[8] M. Babcock, D. De Silva, R. Oaks et al., "Regulation of mitochondrial iron accumulation by Yfh1p, a putative homolog of frataxin," *Science*, vol. 276, no. 5319, pp. 1709–1712, 1997.

[9] H. Koutnikova, V. Campuzano, F. Foury, P. Dollé, O. Cazzalini, and M. Koenig, "Studies of human, mouse and yeast homologues indicate a mitochondrial function for frataxin," *Nature Genetics*, vol. 16, no. 4, pp. 345–351, 1997.

[10] R. B. Wilson and D. M. Roof, "Respiratory deficiency due to loss of mitochondrial dna in yeast lacking the frataxin homologue," *Nature Genetics*, vol. 16, no. 4, pp. 352–357, 1997.

[11] F. Foury and T. Roganti, "Deletion of the mitochondrial carrier genes MRS3 and MRS4 suppresses mitochondrial iron accumulation in a yeast frataxin-deficient strain," *Journal of Biological Chemistry*, vol. 277, no. 27, pp. 24475–24483, 2002.

[12] O. S. Chen, S. Hemenway, and J. Kaplan, "Genetic analysis of iron citrate toxicity in yeast: implications for mammalian iron homeostasis," *Proceedings of the National Academy of Sciences of the United States of America*, vol. 99, no. 26, pp. 16922–16927, 2002.

[13] V. C. Culotta, "Superoxide dismutase, oxidative stress, and cell metabolism," *Current Topics in Cellular Regulation C*, vol. 36, pp. 117–132, 2001.

[14] C. M. Grant, G. Perrone, and I. W. Dawes, "Glutathione and catalase provide overlapping defenses for protection against hydrogen peroxide in the yeast *Saccharomyces cerevisiae*," *Biochemical and Biophysical Research Communications*, vol. 253, no. 3, pp. 893–898, 1998.

[15] O. Bermingham-McDonogh, E. B. Gralla, and J. S. Valentine, "The copper, zinc-superoxide dismutase gene of *Saccharomyces cerevisiae*: cloning, sequencing, and biological activity," *Proceedings of the National Academy of Sciences of the United States of America*, vol. 85, no. 13, pp. 4789–4793, 1988.

[16] X. F. Liu, I. Elashvili, E. B. Gralla, J. S. Valentine, P. Lapinskas, and V. C. Culotta, "Yeast lacking superoxide dismutase. Isolation of genetic suppressors," *Journal of Biological Chemistry*, vol. 267, no. 26, pp. 18298–18302, 1992.

[17] A. Lin, K. W. Hakala, S. T. Weintraub, and L. McAlister-Henn, "Suppression of metabolic defects of yeast isocitrate dehydrogenase and aconitase mutants by loss of citrate synthase," *Archives of Biochemistry and Biophysics*, vol. 474, no. 1, pp. 205–212, 2008.

[18] M. T. McCammon, C. B. Epstein, B. Przybyla-Zawislak, L. McAlister-Henn, and R. A. Butow, "Global transcription analysis of Krebs tricarboxylic acid cycle mutants reveals an alternating pattern of gene expression and effects on hypoxic and oxidative genes," *Molecular Biology of the Cell*, vol. 14, no. 3, pp. 958–972, 2003.

[19] M. Merkel and J. Kretowicz, "Sensitivity to natamycin in vitro evaluation of Candida spp. and Torulopsis glabrata isolated from vagina," *Polski Tygodnik Lekarski*, vol. 40, no. 9, pp. 257–258, 1985.

[20] X. J. Chen, X. Wang, and R. A. Butow, "Yeast aconitase binds and provides metabolically coupled protection to mitochondrial DNA," *Proceedings of the National Academy of Sciences of the United States of America*, vol. 104, no. 34, pp. 13738–13743, 2007.

[21] X. J. Chen, X. Wang, B. A. Kaufman, and R. A. Butow, "Aconitase couples metabolic regulation to mitochondrial DNA maintenance," *Science*, vol. 307, no. 5710, pp. 714–717, 2005.

[22] Z. Liu and R. A. Butow, "A transcriptional switch in the expression of yeast tricarboxylic acid cycle genes in response to a reduction or loss of respiratory function," *Molecular and Cellular Biology*, vol. 19, no. 10, pp. 6720–6728, 1999.

[23] Z. Liu and R. A. Butow, "Mitochondrial retrograde signaling," *Annual Review of Genetics*, vol. 40, pp. 159–185, 2006.

[24] Z. Liu, T. Sekito, M. Špírek, J. Thornton, and R. A. Butow, "Retrograde signaling is regulated by the dynamic interaction between *Rtg2*p and Mks1p," *Molecular Cell*, vol. 12, no. 2, pp. 401–411, 2003.

[25] S. P. Gangloff, D. Marguet, and G. J.-M. Lauquin, "Molecular cloning of the yeast mitochondrial aconitase gene (*ACO1*) and evidence of a synergistic regulation of expression by glucose plus glutamate," *Molecular and Cellular Biology*, vol. 10, no. 7, pp. 3551–3561, 1990.

[26] M. T. McCammon, "Mutants of *Saccharomyces cerevisiae* with defects in acetate metabolism: isolation and characterization of Acn- mutants," *Genetics*, vol. 144, no. 1, pp. 57–69, 1996.

[27] C. Vélot, P. Haviernik, and G. J.-M. Lauquin, "The *Saccharomyces cerevisiae RTG2* gene is a regulator of aconitase expression under catabolite repression conditions," *Genetics*, vol. 144, no. 3, pp. 893–903, 1996.

[28] D. C. Amberg, D. J. Burke, and J. N. Strathern, *Methods in Yeast Genetics: A Cold Spring Harbor Laboratory Course Manual*, Cold Spring Harbor Laboratory, Cold Spring Harbor, NY, USA, 2005.

[29] L. Li and J. Kaplan, "A mitochondrial-vacuolar signaling pathway in yeast that affects iron and copper metabolism," *Journal of Biological Chemistry*, vol. 279, no. 32, pp. 33653–33661, 2004.

[30] R. S. Sikorski and P. Hieter, "A system of shuttle vectors and yeast host strains designed for efficient manipulation of DNA in *Saccharomyces cerevisiae*," *Genetics*, vol. 122, no. 1, pp. 19–27, 1989.

[31] B. A. Rothermel, A. W. Shyjan, J. L. Etheredge, and R. A. Butow, "Transactivation by *Rtg1*p, a basic helix-loop-helix protein that functions in communication between mitochondria and the nucleus in yeast," *Journal of Biological Chemistry*, vol. 270, no. 49, pp. 29476–29482, 1995.

[32] Y. Jia, B. Rothermel, J. Thornton, and R. A. Butow, "A basic helix-loop-helix-leucine zipper transcription complex in yeast functions in a signaling pathway from mitochondria to the nucleus," *Molecular and Cellular Biology*, vol. 17, no. 3, pp. 1110–1117, 1997.

[33] A. Chelstowska, Z. Liu, Y. Jia, D. Amberg, and R. A. Butow, "Signalling between mitochondria and the nucleus regulates the expression of a new D-lactate dehydrogenase activity in yeast," *Yeast*, vol. 15, no. 13, pp. 1377–1391, 1999.

[34] Z. Liu, T. Sekito, C. B. Epstein, and R. A. Butow, "RTG-dependent mitochondria to nucleus signaling is negatively regulated by the seven WD-repeat protein Lst8p," *EMBO Journal*, vol. 20, no. 24, pp. 7209–7219, 2002.

[35] T. Sekito, Z. Liu, J. Thornton, and R. A. Butow, "RTG-dependent mitochondria-to-nucleus signaling is regulated by MKS1 and is linked to formation of yeast prion [URE3]," *Molecular Biology of the Cell*, vol. 13, no. 3, pp. 795–804, 2002.

[36] X. Liao, W. C. Small, P. A. Srere, and R. A. Butow, "Intramitochondrial functions regulate nonmitochondrial citrate synthase (CIT2) expression in *Saccharomyces cerevisiae*," *Molecular and Cellular Biology*, vol. 11, no. 1, pp. 38–46, 1991.

[37] P. A. Kirchman, S. Kim, C. Lai, and S. Michal Jazwinski, "Interorganelle signaling is a determinant of longevity in *Saccharomyces cerevisiae*," *Genetics*, vol. 152, no. 1, pp. 179–190, 1999.

[38] D. H. Williamson and D. J. Fennell, "Visualization of yeast mitochondrial dna with the fluorescent stain 'DAPI'," *Methods in Enzymology C*, vol. 56, pp. 728–733, 1979.

[39] Y.-K. Jia, A.-M. Bécam, and C. J. Herbert, "The CIT3 gene of *Saccharomyces cerevisiae* encodes a second mitochondrial isoform of citrate synthase," *Molecular Microbiology*, vol. 24, no. 1, pp. 53–59, 1997.

[40] K. S. Kim, M. S. Rosenkrantz, and L. Guarente, "*Saccharomyces cerevisiae* contains two functional citrate synthase genes," *Molecular and Cellular Biology*, vol. 6, no. 6, pp. 1936–1942, 1986.

[41] A. S. Lewin, V. Hines, and G. M. Small, "Citrate synthase encoded by the CIT2 gene of *Saccharomyces cerevisiae* is peroxisomal," *Molecular and Cellular Biology*, vol. 10, no. 4, pp. 1399–1405, 1990.

[42] U. Mühlenhoff, J. A. Stadler, N. Richhardt et al., "A specific role of the yeast mitochondrial carriers Mrs3/4p in mitochondrial iron acquisition under iron-limiting conditions," *Journal of Biological Chemistry*, vol. 278, no. 42, pp. 40612–40620, 2003.

[43] E. M. Froschauer, R. J. Schweyen, and G. Wiesenberger, "The yeast mitochondrial carrier proteins Mrs3p/Mrs4p mediate iron transport across the inner mitochondrial membrane," *Biochimica et Biophysica Acta*, vol. 1788, no. 5, pp. 1044–1050, 2009.

[44] J. C. Rutherford and A. J. Bird, "Metal-responsive transcription factors that regulate iron, zinc, and copper homeostasis in eukaryotic cells," *Eukaryotic Cell*, vol. 3, no. 1, pp. 1–13, 2004.

[45] H. Kawamata and G. Manfredi, "Import, maturation, and function of SOD1 and its copper chaperone CCS in the mitochondrial intermembrane space," *Antioxidants and Redox Signaling*, vol. 13, no. 9, pp. 1375–1384, 2010.

[46] C. Klöppel, C. Michels, J. Zimmer, J. M. Herrmann, and J. Riemer, "In yeast redistribution of Sod1 to the mitochondrial intermembrane space provides protection against respiration derived oxidative stress," *Biochemical and Biophysical Research Communications*, vol. 403, no. 1, pp. 114–119, 2010.

[47] L. A. Sturtz, K. Diekert, L. T. Jensen, R. Lill, and V. C. Culotta, "A fraction of yeast Cu,Zn-superoxide dismutase and its metallochaperone, CCS, localize to the intermembrane space of mitochondria. A physiological role for SOD1 in guarding against mitochondrial oxidative damage," *Journal of Biological Chemistry*, vol. 276, no. 41, pp. 38084–38089, 2001.

[48] F. Foury, "Low iron concentration and aconitase deficiency in a yeast frataxin homologue deficient strain," *FEBS Letters*, vol. 456, no. 2, pp. 281–284, 1999.

Hindawi Publishing Corporation
Oxidative Medicine and Cellular Longevity
Volume 2013, Article ID 161986, 10 pages
http://dx.doi.org/10.1155/2013/161986

Research Article

Ammonium-Dependent Shortening of CLS in Yeast Cells Starved for Essential Amino Acids Is Determined by the Specific Amino Acid Deprived, through Different Signaling Pathways

Júlia Santos,[1,2] Cecília Leão,[1,2] and Maria João Sousa[3]

[1] *Life and Health Sciences Research Institute (ICVS), School of Health Sciences, University of Minho, 4710-057 Braga, Portugal*
[2] *ICVS/3B's-PT Government Associate Laboratory, Braga/Guimarães, Portugal*
[3] *Molecular and Environmental Biology Centre (CBMA), Department of Biology, University of Minho, 4710-057 Braga, Portugal*

Correspondence should be addressed to Maria João Sousa; mjsousa@bio.uminho.pt

Received 16 May 2013; Revised 9 July 2013; Accepted 16 July 2013

Academic Editor: Sergio Giannattasio

Ammonium (NH_4^+) leads to chronological life span (CLS) shortening in *Saccharomyces cerevisiae* BY4742 cells, particularly evident in cells starved for auxotrophy-complementing amino acids (leucine, lysine, and histidine) simultaneously. Here, we report that the effect of NH_4^+ on aging yeast depends on the specific amino acid they are deprived of. Compared with no amino acid starvation, starvation for leucine alone or in combination with histidine resulted in the most pronounced NH_4^+-induced CLS shortening, whereas starvation for lysine, alone or in combination with histidine resulted in the least sensitivity to NH_4^+. We also show that NH_4^+-induced CLS shortening is mainly mediated by Tor1p in cells starved for leucine or histidine but by Ras2p in cells starved for lysine, and in nonstarved cells. Sch9p protected cells from the effect of NH_4^+ under all conditions tested (starved or nonstarved cells), which was associated with Sch9p-dependent Hog1p phosphorylation. Our data show that NH_4^+ toxicity can be modulated through manipulation of the specific essential amino acid supplied to cells and of the conserved Ras2p, Tor1p, and Sch9p regulators, thus providing new clues to the development of environmental interventions for CLS extension and to the identification of new therapeutic targets for diseases associated with hyperammonemia.

1. Introduction

In all living organisms, cell survival is mediated by metabolic regulation in response to environmental conditions. This regulation is conserved from yeasts to mammals and is mediated by complex nutrient signaling pathways that control the necessary metabolic changes that take place when environmental conditions change [1]. In yeast, when nutrients are depleted, cells undergo a growth arrest phase characterized by downregulation of growth signaling pathways and upregulation of several processes, such as accumulation of carbohydrates, autophagy, and stress resistance [2, 3]. The length of time these nondividing yeast cells remain viable for is defined as the chronological life span (CLS) of the population [4]. The composition of the culture medium can modulate CLS, and therefore, culturing cells in different media leads to differences in CLS [5]. Manipulation of several single components of the culture medium is known to extend CLS, such as reducing glucose concentration (known as caloric restriction-CR) or manipulating the supply of amino acids [5–9]. Several studies in the literature report different effects of amino acids on life span regulation, depending on which amino acid is deprived [6–10]. In this context, it is known that starvation for nonessential amino acids (strains without auxotrophies) used as preferred nitrogen sources can extend CLS [11–13], while starvation for auxotrophy-complementing amino acids (essential amino acids) reduces CLS [7, 10]. However, not all essential amino acids contribute equally to the effects on CLS. In fact, it has been described that leucine plays a more important role in CLS extension in auxotrophic strains [6, 10] and that extra supplementation of leucine promotes CLS extension in standard 2% glucose medium [6]. Recently, it has also been shown that leucine influences autophagy and extension of CLS during CR [14].

The target of rapamycin complex 1 (TORC1) controls cell growth in response to the availability of nutrients, including amino acids [15, 16]. The TOR pathway responds to nitrogen by regulating processes such as the transcription of genes involved in nitrogen metabolism: nitrogen catabolite repression (NCR) sensitive genes, amino acid biosynthesis genes (general amino acid control pathway-GAAC), retrograde response genes (RTG-Pathway), and genes involved in the stability of amino acid permeases and autophagy [17, 18]. In mammalian cells, amino acids, predominantly leucine, regulate mTOR by controlling the ability of the positive regulator Rheb-GTP to activate mTORC1. The fundamental role of leucine in TORC1 regulation has been demonstrated through the observation that withdrawal of leucine alone is almost as effective in downregulating TORC1 as withdrawal of all amino acids combined [19]. In yeast, the EGO complex is an upstream regulator of TORC1, thought to be responsible for amino acid signaling to TORC1. During leucine starvation, TORC1 activation by this complex is disrupted, which results in a reduction in Sch9p phosphorylation and slow growth [20, 21].

The protein kinase A (PKA) pathway is involved in the regulation of metabolism, stress response, and proliferation, responding to the presence of a rapidly fermentable sugar and other essential nutrients sustaining growth, such as amino acids and phosphate [16, 22]. Readdition of nitrogen (amino acids or ammonium) to cells starved for nitrogen activates the PKA pathway through plasma membrane sensors known as transceptors. Sch9p is a protein kinase that shares many targets with PKA and TORC1, and different interactions between these pathways, either cooperating or antagonizing their effects, have been described [23]. It was shown that Sch9p mediates PKA activation in the fermentable growth medium induced (FGM) pathway, in response to amino acid and ammonium, but not in phosphate-induced activation [24].

We have previously shown that decreasing the ammonium (NH_4^+) concentration in the culture medium extends the CLS of *Saccharomyces cerevisiae* BY4742 cells [25]. NH_4^+ reduced the CLS of cells cultured to stationary phase under both standard amino acid supplementation and amino acid restriction conditions in a concentration-dependent manner, and a significant increase in cell survival was observed when the starting NH_4^+ concentration in the medium was decreased. We also showed that when stationary phase cells were transferred to water, the CLS was also significantly shortened by addition of NH_4^+, indicating that NH_4^+ alone could induce the loss of cell viability observed in culture media. The negative effects of NH_4^+ were particularly evident in cells cultured or incubated under restriction of auxotrophy-complementing amino acid markers (leucine, lysine, and histidine). These negative effects of NH_4^+ do not appear to require its metabolization. The PKA and TOR pathways were involved in NH_4^+-induced CLS shortening, but deleting *SCH9* did not revert the decrease in cell viability despite abolishing PKA activation in response to NH_4^+, suggesting Sch9p plays an independent role in cell survival [25].

Here, we show that NH_4^+ toxicity during yeast aging in water depends on the specific starved auxotrophy-complementing amino acid. Sch9p, contrary to Tor1p and Ras2p, mediates cell survival in response to NH_4^+ in all starvation conditions through the phosphorylation of Hog1p. Our results provide new insights in the modulation of CLS by NH_4^+, linking NH_4^+ toxicity to amino acid limitation. This scenario of enhanced NH_4^+ toxicity in amino acid starvation conditions is present in hyperammonemic patients, who are often on dietary protein restriction [26]. The use of a simpler model like yeast can help elucidate the underlying mechanism involved in the modulation of conserved signaling pathways, in response to NH_4^+.

2. Materials and Methods

2.1. Strains and Growth Conditions. *Saccharomyces cerevisiae* strain BY4742 (*MAT*a *his3*Δ1 *leu2*Δ0 *lys2*Δ0 *ura3*Δ0) (EUROSCARF, Frankfurt, Germany) and the respective knockouts in *HOG1*, *RAS2*, *SCH9,* and *TOR1* genes were used. For experiments with nonstarved and amino-acid-starved cells, the strains were first cultured at 26°C, 150 rpm, in defined minimal medium (SC medium) containing 0.17% yeast nitrogen base without amino acids and without ammonium sulphate (Difco, BD), supplemented with 0.5% $(NH_4)_2SO_4$, with appropriate amino acids and nucleotide base (50 mg/L histidine, 50 mg/L lysine, 300 mg/L leucine, and 100 mg/L uracil) and 2% D-glucose, to exponential phase (OD_{600} = 1.0–1.5). These cells were harvested and resuspended in (A) SC medium containing 4% glucose (nonstarved cells) or in (B) SC medium containing 4% glucose and lacking (1) amino acids (aa-starved cells); (2) leucine (Leu-starved cells); (3) histidine (His-starved cells); (4) lysine (Lys-starved cells); (5) histidine and lysine (His-Lys-starved cells); (6) leucine and lysine (Leu-Lys-starved cells), and (7) leucine and histidine (Leu-His-starved cells). After 24 hours, cells were collected by centrifugation, washed three times with water, and resuspended at a cell density of about 3.8×10^7 cells/mL in water (pH 7.0), or water with $(NH_4)_2SO_4$ (0.5%, pH 7.0). Viability of 24-hour-starved cultures was considered to be 100% of survival, and this was considered day 0 of the experiment. pH 7.0 was maintained throughout the experiment in cultures with adjusted pH. Cell viability of culture aliquots was assessed by CFU at day 0 (100% viability) and in subsequent days, as indicated. For CFU determination, diluted samples were incubated for 2 days at 30°C on YEPD agar plates.

2.2. Trehalase Activity. Trehalase activity was determined according to [27]. Briefly, crude enzyme extracts were obtained by resuspending the cell pellet in ice-cold 50 mM MES/KOH buffer (pH 7.0) containing 50 μM $CaCl_2$ and adding a roughly equal volume of 0.5 mm diameter glass beads, followed by vigorous mixing during 1 minute intervals interspersed with periods of cooling on ice. The extracts were then dialyzed overnight at 4°C in a dialysis cellulose membrane (Cellu Sep H1, Orange). The dialyzed extract was then used to assess trehalase activity by measuring the released glucose using a glucose oxidase assay (GOD, Roche).

Protein concentration was determined using the Bradford assay (Bio-Rad, Germany) according to the manufacturer's instructions.

2.3. Western Blot Analysis. Western blot analysis was performed according to [28]. Briefly, protein lysates were separated on 12.5% SDS-PAGE gels and transferred to polyvinylidene fluoride membranes (Hybond-P; Amersham). The membranes were blocked with 5% bovine serum albumin (BSA) in Tris-buffered saline (TBS, 50 mM Tris, 150 mM NaCl, and pH 7.6) containing 0.05% Tween 20 for 1 h at room temperature. Membranes were then incubated overnight at 4°C with primary antibodies directed against Hog1p (rabbit anti-Hog1p MAPK; Santa Cruz Biotechnology, Inc., USA) at a 1 : 1000 dilution or rabbit anti-phospho-p38 MAPK (Cell Signaling Technology, Beverly, MA, USA) at a 1 : 50000 dilution and against Pgk1p (mouse monoclonal anti-PGK1; Molecular Probes) at a 1 : 5000 dilution. This was followed by a one-hour incubation at room temperature with secondary antibody Peroxidase-AffiniPure Goat AntiRabbit IgG (1 : 10000; Jackson ImmunoResearch) or Peroxidase-AffiniPure Goat AntiMouse IgG (1 : 10000; Jackson ImmunoResearch).

3. Results and Discussion

3.1. NH_4^+-Induced Cell Death during Yeast Aging in Water Depends on the Specific Auxotrophy-Complementing Amino Acid Deprived from the Starvation Medium. In *Saccharomyces cerevisiae* BY4742, NH_4^+ leads to chronological life span (CLS) shortening, particularly relevant in cells starved for the auxotrophy-complementing amino acids simultaneously. The effect of NH_4^+ has been observed both in cells aged in spent culture medium limited for the essential amino acids and in cells aged in water after a 24-hour incubation in amino-acid-deprived medium [25]. We now sought to evaluate how the absence of specific auxotrophy-complementing amino acids affects NH_4^+ toxicity during yeast CLS. For this purpose, cells were first grown to exponential phase in SC medium and then starved for each of the three essential amino acids of the BY4742 strain (leucine, lysine, and histidine) alone or in combinations of two, as well as in their absence (aa-starved cells). As a control, we used the same medium, but without amino acid deprivation, therefore adding the three auxotrophy-complementing amino acids (nonstarved cells). Cells were then transferred to water with and without NH_4^+, and cell viability was evaluated over time. The protocol followed is systematized in Figure S1 in Supplementary material available online at http://dx.doi.org/10.1155/2013/161986.

The results presented in Figure 1(a) revealed that aa-, lysine- (Lys-), or nonstarved cells displayed a longer CLS in water without NH_4^+ than leucine- (Leu-) or histidine-(His-) starved cells. Furthermore, absence of any of the three amino acids in the medium, individually or at the same time, decreased CLS upon transfer of cells to water with NH_4^+, in comparison with the CLS of cells incubaed without amino acid restriction, though this effect was much less accentuated when only lysine was removed (Figure 1(b)). Two of the amino acids were then removed at the same time in different combinations (Figures 1(c) and 1(d)). Simultaneous absence of lysine and histidine (Lys-His-starved cells) had the least effect on NH_4^+-induced CLS shortening (Figure 1(d)), whereas NH_4^+ was most toxic to cells starved both for leucine and histidine (Leu-His starved cells). Comparing these results with those from Figure 1(b) (removal of one amino acid at a time from the medium), it can be observed that survival of Leu- or His-starved cells in water with NH_4^+ was much lower than that of cells that were also starved for lysine (Leu-Lys- or His-Lys-starved cells). On the other hand, the opposite effect was observed if Lys- or His-starved cells were simultaneously starved for leucine (Lys-Leu- or His-Leu-starved cells), where NH_4^+-induced CLS shortening was more severe. Additionally, histidine starvation in combination with one of the other two amino acids does not appear to have a major role in regulating CLS in response to NH_4^+, since the cell death profiles under those conditions were similar to those exhibited by Lys- or Leu-starved cells.

Taken together, the results suggest that from the three auxotrophy-complementing amino acids tested, starvation for leucine alone or in combination with histidine resulted in the most severe effects on NH_4^+-induced CLS shortening, while starvation for lysine, alone or in combination with histidine, resulted in the less sensitive NH_4^+ phenotype.

3.2. Ras2p, Tor1p, and Sch9p Differently Mediate NH_4^+-Induced Cell Death during Yeast Aging in Water. The toxic effects of NH_4^+ in aa-starved BY4742 cells are the result of activation of the PKA and TOR pathways and are negatively regulated by Sch9p [25]. In addition, the results shown in the previous section demonstrated that ammonium affects CLS shortening depending on the specific essential amino acid deprived from the medium. We therefore sought to elucidate the role of Ras2/PKA, Tor1p, and Sch9p signaling pathways in CLS shortening induced by NH_4^+ under the different starvation conditions. For this, we first tested the effect of starving *tor*1Δ, *ras*2Δ, and *sch*9Δ cells for each of the three auxotrophy-complementing amino acids individually. As a control, we used the same medium in the absence or presence of all three essential amino acids. Similarly to what we described above, cells were first grown to exponential phase in SC medium, then incubated in the different starvation media, and next transferred to water with or without NH_4^+ (For schematic representation of the protocol please see Figure S1).

The *tor*1Δ strain displayed a lower NH_4^+-induced cell death than the wild-type strain in all starvation conditions tested (Figures 1(b) and 2(b)). Furthermore, Lys-starved cells displayed almost the same loss of cell viability as nonstarved cells in the presence of NH_4^+, showing that starvation for this amino acid does not induce sensitivity to NH_4^+ in the absence of *TOR1*. For nonstarved cells, there was no difference in the effect of NH_4^+ between wild-type and *tor*1Δ strains. On the other hand, deletion of *TOR1* also rescued the CLS of His-starved cells in water without NH_4^+ (Figures 1(a) and 2(a)).

In the *ras*2Δ strain, the loss of cell viability induced by NH_4^+ in nonstarved cells or Lys-starved cells was significantly reduced when compared with the wild-type

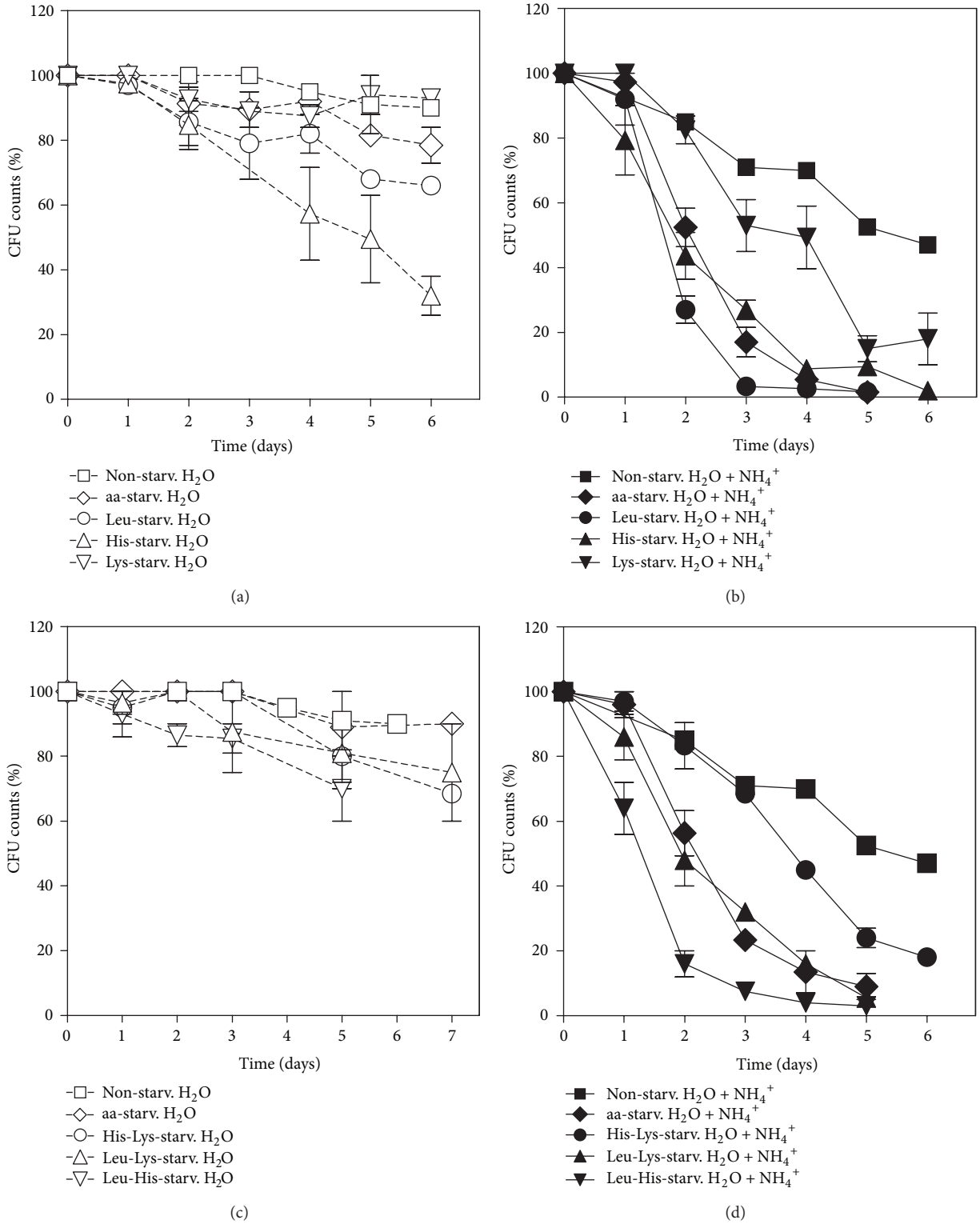

Figure 1: Ammonium-induced cell death during yeast aging in water is dependent on the specific auxotrophy-complementing amino acid deprived from the starvation medium. Survival of wild-type *S. cerevisiae* (BY4742) cells, nonstarved or starved for leucine, histidine, or lysine, in different combinations upon ((a) and (c)) transfer to water (open symbol) or ((b) and (d)) water with $(NH_4)_2SO_4$, 0.5% (dark symbol). In all the cultures, starting cell density was about 3.8×10^7 cells/mL, and the initial pH was adjusted to 7.0. Values are means ± SEM ($n = 3$). (b) $^{**}P < 0.01$ (aa-starved $H_2O + NH_4^+$ versus Lys-starved $H_2O + NH_4^+$), $^{**}P < 0.01$ (aa-starved $H_2O + NH_4^+$ versus Leu-starved $H_2O + NH_4^+$), and $^{***}P < 0.001$ (nonstarved $H_2O + NH_4^+$ versus Lys-starved $H_2O + NH_4^+$); (d) $^{*}P < 0.01$ (nonstarved $H_2O + NH_4^+$ versus His-Lys-starved $H_2O + NH_4^+$), $^{**}P < 0.01$ (aa-starved $H_2O + NH_4^+$ versus Leu-His-starved $H_2O + NH_4^+$), and $^{***}P < 0.001$ (aa-starved $H_2O + NH_4^+$ versus His-Lys-starved $H_2O + NH_4^+$). Statistical analysis was performed by two-way ANOVA. All time points have error bars; however, for time points with reduced standard error, they are not visible.

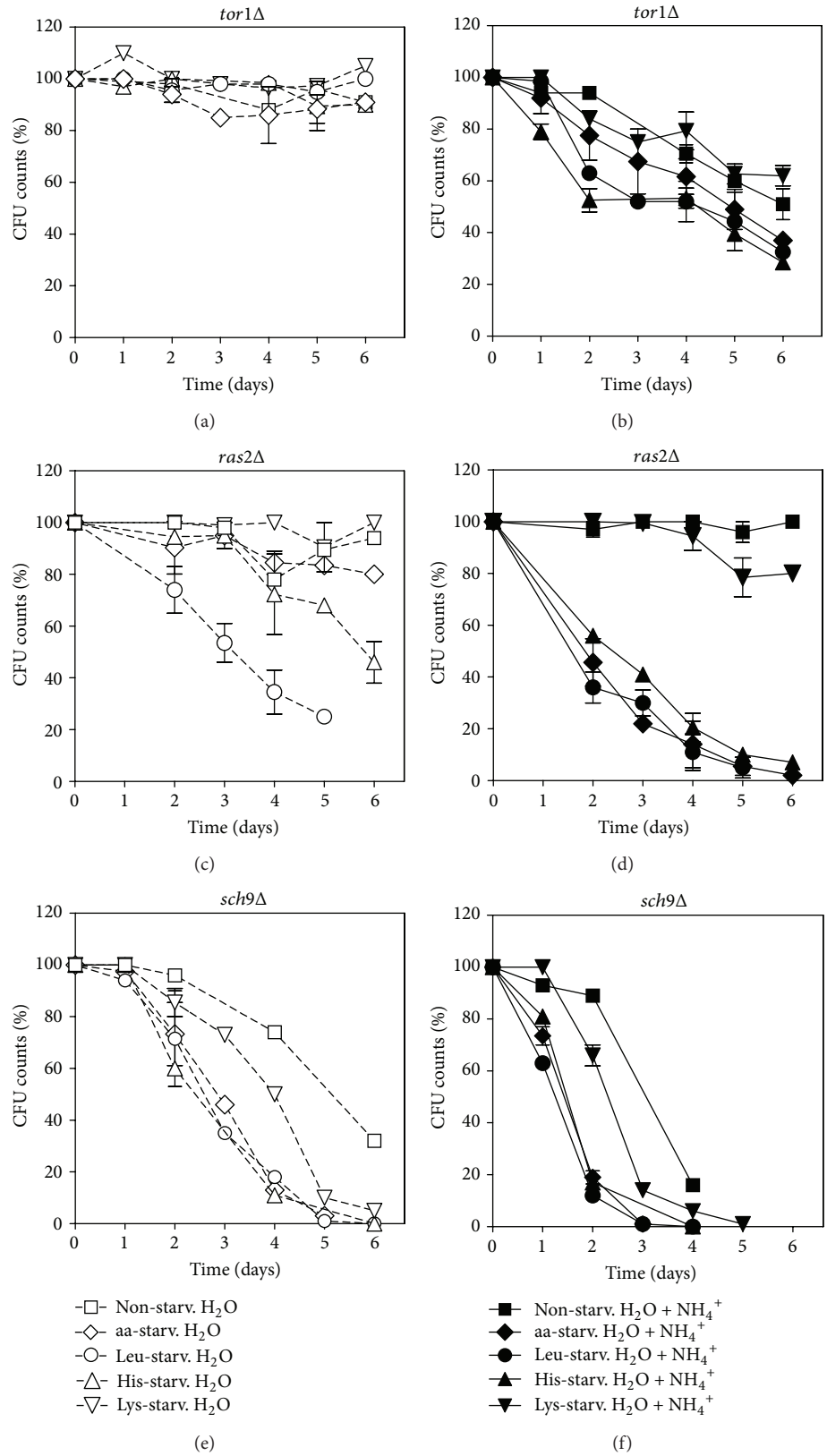

Figure 2: Tor1p regulates ammonium CLS shortening in response to amino acid starvation. Survival of ((a) and (b)) *tor1*Δ, ((c) and (d)) *ras2*Δ, and ((e) and (f)) *sch9*Δ cells, nonstarved or starved for leucine, histidine, or lysine, individually or all at the same time, upon transfer to water (open symbol) or water with $(NH_4)_2SO_4$, 0.5% (dark symbols). In all the cultures, starting cell density was about 3.8×10^7 cells/mL, and the initial pH was adjusted to 7.0. Values are means ± SEM ($n = 3$). All time points have error bars; however, for time points with reduced standard error, they are not visible.

strain. In contrast, deletion of *RAS2* had only a slight effect on the sensitivity of His- or Leu-starved cells to NH_4^+, as well as of cells starved for all three amino acids (aa-starved cells). Furthermore, for the last two starvation conditions, deletion of *RAS2* induced a strong shortening of CLS in water without NH_4^+, indicating that Ras2p is important to ensure longevity under these conditions (Figures 1(a) and 2(c)).

Absence of Sch9p reduced survival after cells were transferred to water with or without NH_4^+ for all conditions tested (starved or nonstarved). Data from Figures 2(e) and 2(f) show that Leu- or His-starved cells of the *sch*9Δ strain behaved as aa-starved cells when transferred to water with or without NH_4^+. In non- or Lys-starved cells, the loss of cell viability in water, with or without NH_4^+, was much less pronounced than in the other starvation conditions, as observed for wild-type cells.

3.3. Ras2p, Tor1p, and Sch9p Mediate PKA Activation in Response to NH_4^+ during Yeast Aging in Water. To further evaluate the role of PKA in NH_4^+-induced CLS shortening and the potential effects of Tor1p, Ras2p, and Sch9p as PKA upstream regulators, we assessed PKA activation in BY4742 (wild-type), *tor*1Δ, *ras*2Δ, and *sch*9Δ strains starved for each of the three essential amino acids, individually or in combination. Trehalase is a target of PKA regulation, and its activity has been extensively used to monitor PKA activation [22, 29]. In order to evaluate PKA activation, we therefore measured trehalase activity in cells grown and incubated as described above in material and methods section. (For schematic representation of the protocol please see Figure S1). We observed that in wild-type cells, leucine starvation resulted in the highest trehalase activity after 2 h of incubation with NH_4^+, whereas its presence alone led to the lowest trehalase activity. In contrast, and under the same conditions, starvation for lysine or histidine alone gave rise to the lowest trehalase activity, whereas their presence alone led to the highest trehalase activity (Figure 3(a)). The results also showed that in the presence of NH_4^+, aa-starved cells exhibited a PKA activation pattern similar to nonstarved cells, with values that are between those obtained for Leu- and His- or Lys-starved cells. This suggests that in aa-starved cells, the higher contribution expected from PKA activation due to the absence of leucine is probably balanced by the decrease of PKA activity induced by the absence of histidine and lysine. PKA activation by NH_4^+ was decreased in *tor*1Δ, *ras*2Δ, and *sch*9Δ mutants in comparison with the wild-type strain, both for nonstarved cells and under all amino acid starvation conditions (Figures 3(b), 3(c), and 3(d)). The observed reduction in PKA activation correlates with the decrease in NH_4^+-induced CLS shortening in the *tor*1Δ strain under all the conditions tested. In addition, the decrease in PKA activation induced by NH_4^+ in the *ras2*Δ strain was accompanied by an increase in cell survival for non- or lysine-starved cells, but not for cells under the remaining starvation conditions (Leu-, His-, or aa-starved cells). Conversely, for nonstarved cells and for cells starved in the presence of leucine (His-starved and Lys-starved cells) before transfer to water (T0), there was a significant increase in PKA activation in the *ras*2Δ strain, indicating that Ras2p seems to downregulate PKA activity in the presence of leucine. On the other hand, the decrease in PKA activation induced by NH_4^+ in the *sch9*Δ strain was not associated with an extended CLS in water with NH_4^+ in nonstarved cells or under any of the starvation conditions tested, which is in accordance with previous results described for aa-starved cells [25]. Together, the results suggest that NH_4^+ induces PKA activation through Tor1p, Ras2p, and Sch9p. However, absence of Ras2p, although able to decrease PKA activation, did not revert NH_4^+-induced CLS shortening in Leu-, His-, and aa-starved cells, indicating that in the absence of this protein, other pathways, independent of PKA and possibly mediated by Tor1p, are still activated and can induce cell death. Furthermore, Ras2p, at least under some conditions, appears to also activate other pathways relevant to cell survival, since its absence leads to a shorter CLS in water. A prosurvival role was also observed for Sch9p under all conditions, either in the absence or presence of NH_4^+.

3.4. Sch9p Protects Cells from NH_4^+-Induced Cell Death through Hog1p Activation. Hog1p is a kinase that regulates and is regulated by Sch9p and mediates stress response independently of the PKA and TOR pathways [30]. It was previously shown that Hog1p is involved in the resistance of aa-starved cells to the toxic effects of NH_4^+ during CLS in water [25]. In order to access if the protective role of Sch9p in response to NH_4^+ under the different amino acid starvation conditions described in the previous sections could be mediated through a Sch9p-dependent Hog1p activation, we examined Hog1p phosphorylation during CLS in water with and without NH_4^+ in BY4742 (wild-type) and *sch*9Δ cells. As shown in Figure 4, Hog1p phosphorylation in wild-type cells increased in the presence of NH_4^+ in all starvation conditions tested (aa-, Leu-, His-, and Lys-starved cells), being higher in His- and Lys-starved cells. Deletion of *SCH9* almost abolished Hog1p phosphorylation in aa-, Leu-, and His-starved cells, whereas some residual phosphorylation was still detected in Lys-starved cells. The lower Hop1p phosphorylation observed for cells starved for aa- and Leu-starved cells is in agreement with previous results, showing that the presence of leucine is required for Sch9p phosphorylation via TORC1 [21]. Also, Hog1p phosphorylation in Lys-starved *sch*9Δ cells is in agreement with the activation of pathways other than the PKA in the absence of Ras2p, suggested by the rescue of the loss of viability found for Lys-starved *ras*2Δ cells (Figure 2(d)).

Taken together, results show that Sch9p is involved in Hog1p activation in response to NH_4^+ under all starvation conditions, indicating that the increased resistance afforded by Sch9p could, actually, be mediated through Hog1p activation.

4. Conclusions

It has been previously shown that the CLS of stationary phase cells of *Saccharomyces cerevisiae* BY4742 transferred to water was significantly shortened by the addition of NH_4^+ and that the negative effects of NH_4^+ were particularly evident for cells under restriction of auxotrophy-complementing amino acid markers (leucine, lysine, and histidine) [25]. The

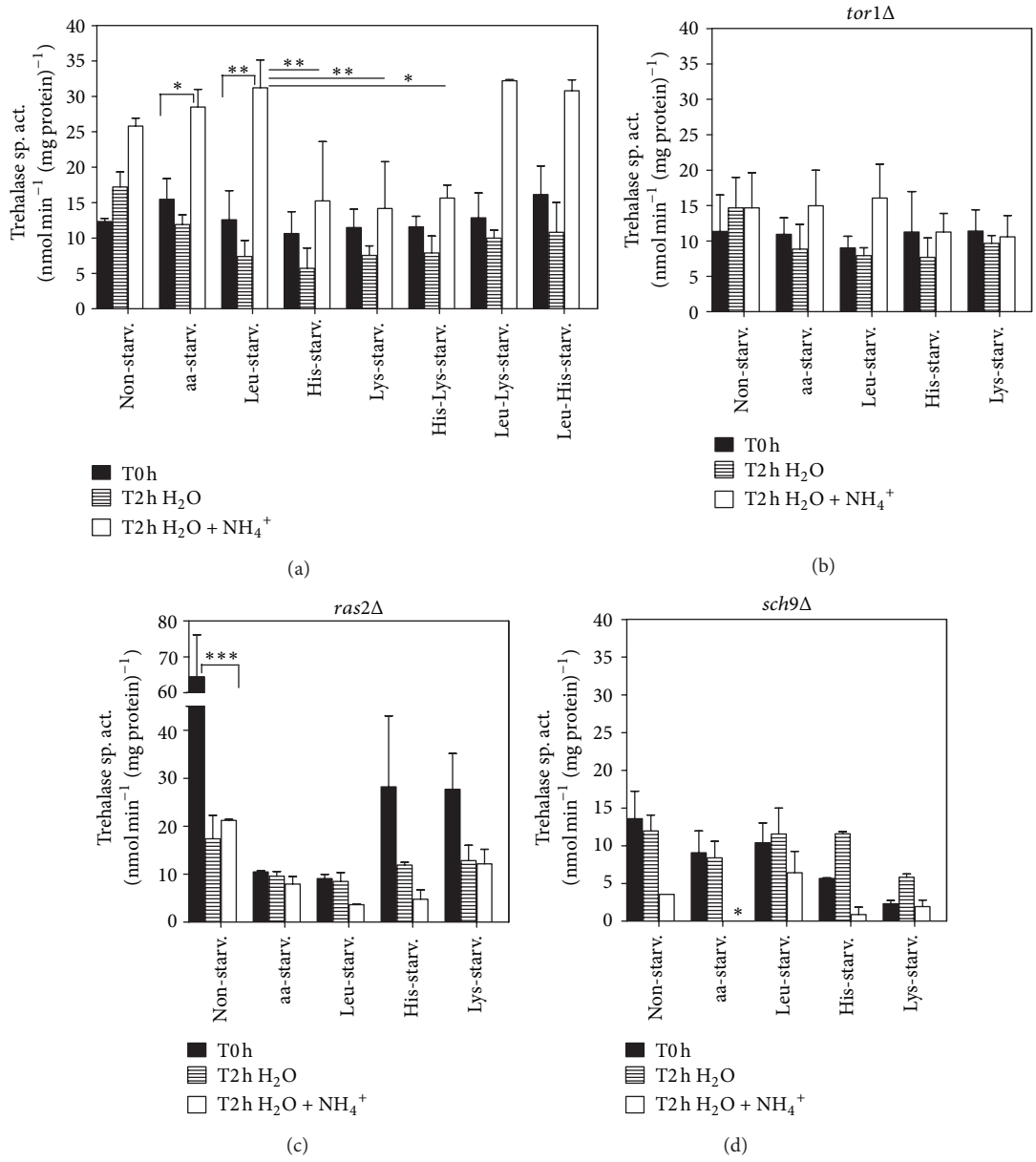

Figure 3: Ammonium induction of PKA activity depends on Tor1p, Ras2p and Sch9p regulation. Trehalase activity of cells nonstarved or starved for leucine, histidine, or lysine, individually or in different combinations, of (a) wild-type *S. cerevisiae* (BY4742) and of mutant deleted strains (b) *tor1*Δ, (c) *ras2*Δ, and (d) *sch9*Δ; before being, transferred to water (T0h) and after 2 hours in water (T2h H_2O) or water with $(NH_4)_2SO_4$, 0.5% (T2h H_2O + NH_4^+). In all the cultures, starting cell density was about 3.8×10^7 cells/mL, and the initial pH was adjusted to 7.0. Values are means ± SEM (n = 3–4). (a) $^*P < 0.05$ (aa-starved T0h versus aa-starved T2h H_2O + NH_4^+), $^{**}P < 0.01$ (Leu-starved T0h versus Leu-starved T2h H_2O + NH_4^+), $^{**}P < 0.01$ (Leu-starved T2h H_2O + NH_4^+ versus His-starved T2h H_2O + NH_4^+), $^{**}P < 0.01$ (Leu-starved T2h H_2O + NH_4^+ versus Lys-starved T2h H_2O + NH_4^+), $^*P < 0.05$ (Leu-starved T2h H_2O + NH_4^+ versus His-Lys-starved T2h H_2O + NH_4^+); (c) $^{***}P < 0.001$ (nonstarved T0h versus nonstarved H_2O + NH_4^+); (d) $^*P < 0.05$ (aa-starved T0h versus aa-starved T2h H_2O + NH_4^+). Statistical analysis was performed by two-way and one-way ANOVA.

results presented herewith demonstrate that NH_4^+-induced cell death during aging in water depends on the specific auxotrophy-complementing amino acid deprived from the starvation medium. While Lys-starved cells were only slightly more sensitive to NH_4^+-induced CLS shortening than non-starved cells, Leu- and His-starved cells displayed a much stronger sensitivity to NH_4^+ during CLS, which was comparable to that previously described for cells simultaneously starved for all three essential amino acids (aa-starved cells). When we compare cells starved for one amino acid at a time with nonstarved cells, absence of any of the three auxotrophy-complementing amino acids from the medium has a detrimental effect leading to a faster loss of cell survival in response to ammonium. However, when cells are starved for at least one amino acid, the presence of lysine in the medium is detrimental, histidine does not seem to have an effect, and

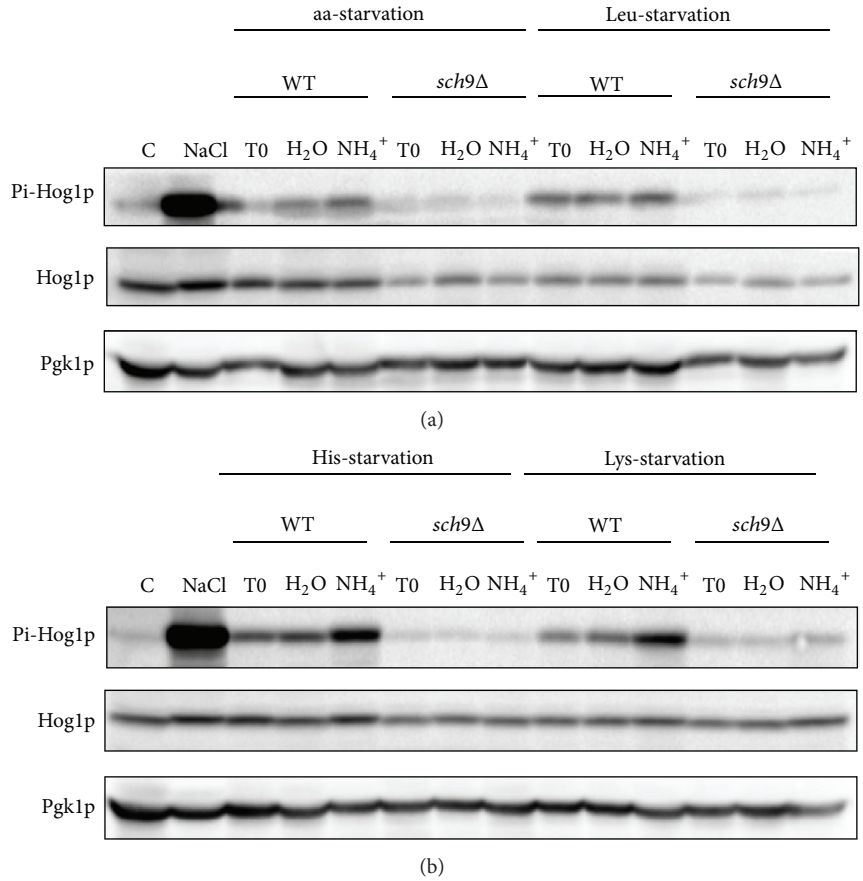

Figure 4: Ammonium induces Sch9p-dependent Hog1p phosphorylation in starvation conditions. Westernblot analysis of Pi-Hog1p levels present in *S. cerevisiae* (BY4742) wild-type (WT) and *sch9*Δ cells starved for (a) all three amino acids or leucine and (b) starved for histidine or lysine, before (T0) and after 20 minutes upon transfer to water (H_2O) or water with $(NH_4)_2SO_4$, 0.5% (NH_4^+). In all the cultures, starting cell density was about 3.8×10^7 cells/mL, and the initial pH was adjusted to 7.0. Control cells were grown on YPD medium (Control-C) and incubated for 5 minutes in YPD medium supplemented with 1 M NaCl.

leucine has a protective effect on ammonium-induced CLS shortening. The results regarding leucine are in accordance with the literature since it has been described that leucine plays a more important role in CLS extension in auxotrophic strains [6, 10]. In a recent study, supplementation of extra leucine to SC medium or transformation of auxotrophic leucine strain into a prototrophic leucine strain resulted in CLS extension. The importance of leucine was attributed to the regulation of the branched side chain amino acids synthesis that appears to be misregulated in a *leu2*Δ strain. In agreement, supplemental levels of the branch side amino acids isoleucine, threonine, and valine also extended CLS in a *leu2*Δ strain [6]. The negative effect observed for lysine in cell survival during ammonium-induced cell death can possibly be due to the fact that autophagy is inhibited in the presence of ammonium [25], and the lack of autophagy might be responsible for this effect since lysine seems to act in an autophagy-dependent manner on the regulation of CLS. Autophagy-deficient strains showed no improvement in CLS extension after regaining LYS prototrophy in contrast to wild-type autophagy competent cells that increased CLS extension with LYS prototrophy [6].

Both Ras2p and Tor1p are involved in NH_4^+-induced CLS shortening in aa-starved cells [25]. We now further established that Ras2p involvement on NH_4^+-induced CLS shortening was present under all conditions tested, and did not depend on starvation. In turn, Tor1p function in the decrease of CLS by NH_4^+ was relevant only under amino acid starvation, being differently modulated by the specific amino acid deprived from the medium. Starvation for leucine and histidine, which induced a strong shortening of CLS in the presence of NH_4^+, had a high impact in the regulation of Tor1p function, whereas starvation for lysine, which was associated with only a small NH_4^+-induced CLS shortening, had a considerably less significant impact on Tor1p regulation. These results are in agreement with previous results showing that leucine has an important impact in the regulation of TORC1 [20, 21]. Our results suggest that the presence of NH_4^+ in the medium (commonly present as the nitrogen source) may be at least partly responsible for the reported decrease in CLS in leucine-starved cells [6, 14].

PKA activation has been described to be associated with the NH_4^+-induced CLS shortening of aa-starved cells in water [25]. From the results now obtained, and when we compare values from nonstarved and starved wild-type cells, it appears that leucine starvation (alone or in combination with starvation for another amino acid) is the main factor responsible for PKA activation in response to

NH_4^+, correlating with its stronger effect on CLS shortening. This activation is dependent on Ras2p, Tor1p, and Sch9p, as deficiency in any of these proteins leads to its decrease. However, since the decrease in PKA activation resulted in distinct cell fate outcomes in the different mutants, the results suggest that these proteins activate PKA by independent pathways and/or also regulate other pathways that they do not share and that have different impacts on NH_4^+-induced CLS shortening. Also, we cannot exclude the possibility that the observed effects on trehalase activity may result from a potential effect of Sch9p, Ras2p, or Tor1p on the activity of other proteins also involved in trehalase regulation such as Bmh1/2p or Dcs1p [29].

Opposite to our results, Sch9p has been described to inhibit PKA activity when glucose is added to glycerol-grown cells. However, these authors observed that the inhibition was mediated through the regulation of Tpk2p localization [31], an isoform that does not seem to have a relevant role in response to ammonium under our conditions. In fact, we have previously observed that Tpk1p is the main PKA isoform involved in ammonium effects [25]. In addition to its involvement in PKA activation, Sch9p also increases Hog1p phosphorylation, extending CLS in water with or without NH_4^+.

In summary, herewith we show that the toxic effects of NH_4^+ on CLS shortening are regulated by a starvation-dependent and a starvation-independent component and are mediated essentially by Tor1p in the first case and by Ras2p in the second. We also provide evidence that when cells are starved for amino acids, the presence of leucine can ameliorate NH_4^+-induced CLS shortening, while lysine has the opposite effect, and the presence of histidine has no effect. Together, our data add new knowledge on CLS regulation, indicating that the modulation of nitrogen sources supplied to cells can drastically modulate CLS and providing new clues for the development of environmental interventions for chronological life span extension. Additionally, and since NH_4^+-induced cell death is involved in different human disorders that are accompanied by hyperammonemia [32], our results, showing that NH_4^+ toxicity can be modulated by amino acids through different pathways, may also afford new insights into the understanding of the cell molecular bases triggering cell death in such pathologies.

Authors' Contribution

Maria João Sousa and Cecília Leão contributed equally to this work.

Acknowledgment

This work was supported by FCT, Portugal, Grant PTDC/AGR-ALI/102608/2008.

References

[1] J. Santos, C. Leao, and M. J. Sousa, "Growth culture conditions and nutrient signaling modulating yeast chronological longevity," *Oxidative Medicine and Cellular Longevity*, vol. 2012, Article ID 680304, 10 pages, 2012.

[2] J. V. Gray, G. A. Petsko, G. C. Johnston, D. Ringe, R. A. Singer, and M. Werner-Washburne, "Sleeping beauty': quiescence in *Saccharomyces cerevisiae*," *Microbiology and Molecular Biology Reviews*, vol. 68, no. 2, pp. 187–206, 2004.

[3] M. Rubio-Texeira, G. Van Zeebroeck, K. Voordeckers, and J. M. Thevelein, "*Saccharomyces cerevisiae* plasma membrane nutrient sensors and their role in PKA signaling," *FEMS Yeast Research*, vol. 10, no. 2, pp. 134–149, 2010.

[4] V. D. Longo, E. B. Gralla, and J. S. Valentine, "Superoxide dismutase activity is essential for stationary phase survival in *Saccharomyces cerevisiae*: mitochondrial production of toxic oxygen species *in vivo*," *Journal of Biological Chemistry*, vol. 271, no. 21, pp. 12275–12280, 1996.

[5] P. Fabrizio and V. D. Longo, "The chronological life span of *Saccharomyces cerevisiae*," *Aging Cell*, vol. 2, no. 2, pp. 73–81, 2003.

[6] A. L. Alvers, L. K. Fishwick, M. S. Wood et al., "Autophagy and amino acid homeostasis are required for chronological longevity in *Saccharomyces cerevisiae*," *Aging Cell*, vol. 8, no. 4, pp. 353–369, 2009.

[7] P. Gomes, B. Sampaio-Marques, P. Ludovico, F. Rodrigues, and C. Leão, "Low auxotrophy-complementing amino acid concentrations reduce yeast chronological life span," *Mechanisms of Ageing and Development*, vol. 128, no. 5-6, pp. 383–391, 2007.

[8] C. J. Murakami, C. R. Burtner, B. K. Kennedy, and M. Kaeberlein, "A method for high-throughput quantitative analysis of yeast chronological life span," *Journals of Gerontology A*, vol. 63, no. 2, pp. 113–121, 2008.

[9] D. L. Smith Jr., J. M. McClure, M. Matecic, and J. S. Smith, "Calorie restriction extends the chronological lifespan of *Saccharomyces cerevisiae* independently of the Sirtuins," *Aging Cell*, vol. 6, no. 5, pp. 649–662, 2007.

[10] V. M. Boer, S. Amini, and D. Botstein, "Influence of genotype and nutrition on survival and metabolism of starving yeast," *Proceedings of the National Academy of Sciences of the United States of America*, vol. 105, no. 19, pp. 6930–6935, 2008.

[11] J. C. Jiang, E. Jaruga, M. V. Repnevskaya, and S. M. Jazwinski, "An intervention resembling caloric restriction prolongs life span and retards aging in yeast," *FASEB Journal*, vol. 14, no. 14, pp. 2135–2137, 2000.

[12] S.-J. Lin, P.-A. Defossez, and L. Guarente, "Requirement of NAD and SIR2 for life-span extension by calorie restriction in *Saccharomyces cerevisiae*," *Science*, vol. 289, no. 5487, pp. 2126–2128, 2000.

[13] R. W. Powers III, M. Kaeberlein, S. D. Caldwell, B. K. Kennedy, and S. Fields, "Extension of chronological life span in yeast by decreased TOR pathway signaling," *Genes and Development*, vol. 20, no. 2, pp. 174–184, 2006.

[14] J. P. Aris, A. L. Alvers, R. A. Ferraiuolo et al., "Autophagy and leucine promote chronological longevity and respiration proficiency during calorie restriction in yeast," *Experimental Gerontology*, 2013.

[15] R. Loewith and M. N. Hall, "Target of rapamycin (TOR) in nutrient signaling and growth control," *Genetics*, vol. 189, no. 4, pp. 1177–1201, 2011.

[16] B. Smets, R. Ghillebert, P. De Snijder et al., "Life in the midst of scarcity: adaptations to nutrient availability in *Saccharomyces cerevisiae*," *Current Genetics*, vol. 56, no. 1, pp. 1–32, 2010.

[17] J. L. Crespo and M. N. Hall, "Elucidating TOR signaling and rapamycin action: lessons from *Saccharomyces cerevisiae*," *Microbiology and Molecular Biology Reviews*, vol. 66, no. 4, pp. 579–591, 2002.

[18] C. De Virgilio and R. Loewith, "The TOR signalling network from yeast to man," *International Journal of Biochemistry and Cell Biology*, vol. 38, no. 9, pp. 1476–1481, 2006.

[19] J. Avruch, X. Long, S. Ortiz-Vega, J. Rapley, A. Papageorgiou, and N. Dai, "Amino acid regulation of TOR complex 1," *American Journal of Physiology. Endocrinology and Metabolism*, vol. 296, no. 4, pp. E592–E602, 2009.

[20] M. Binda, M.-P. Péli-Gulli, G. Bonfils et al., "The Vam6 GEF controls TORC1 by activating the EGO complex," *Molecular Cell*, vol. 35, no. 5, pp. 563–573, 2009.

[21] G. Bonfils, M. Jaquenoud, S. Bontron, C. Ostrowicz, C. Ungermann, and C. De Virgilio, "Leucyl-tRNA synthetase controls TORC1 via the EGO complex," *Molecular Cell*, vol. 46, no. 1, pp. 105–110, 2012.

[22] J. M. Thevelein, L. Cauwenberg, S. Colombo et al., "Nutrient-induced signal transduction through the protein kinase A pathway and its role in the control of metabolism, stress resistance, and growth in yeast," *Enzyme and Microbial Technology*, vol. 26, no. 9-10, pp. 819–825, 2000.

[23] B. Smets, P. De Snijder, K. Engelen et al., "Genome-wide expression analysis reveals TORC1-dependent and -independent functions of Sch9," *FEMS Yeast Research*, vol. 8, no. 8, pp. 1276–1288, 2008.

[24] M. Crauwels, M. C. V. Donaton, M. B. Pernambuco, J. Winderickx, J. H. De Winde, and J. M. Thevelein, "The Sch9 protein kinase in the yeast *Saccharomyces cerevisiae* controls cAPK activity and is required for nitrogen activation of the fermentable-growth-medium-induced (FGM) pathway," *Microbiology*, vol. 143, no. 8, pp. 2627–2637, 1997.

[25] J. Santos, M. J. Sousa, and C. Leao, "Ammonium is toxic for aging yeast cells, inducing death and shortening of the chronological lifespan," *PLoS One*, vol. 7, Article ID e37090, 2012.

[26] O. Braissant, "Current concepts in the pathogenesis of urea cycle disorders," *Molecular Genetics and Metabolism*, vol. 100, supplement 1, pp. S3–S12, 2010.

[27] M. B. Pernambuco, J. Winderickx, M. Crauwels, G. Griffioen, W. H. Mager, and J. M. Thevelein, "Glucose-triggered signalling in *Saccharomyces cerevisiae*: different requirements for sugar phosphorylation between cells grown on glucose and those grown on non-fermentable carbon sources," *Microbiology*, vol. 142, part 7, pp. 1775–1782, 1996.

[28] N. Camougrand, I. Kissová, B. Salin, and R. J. Devenish, "Monitoring mitophagy in yeast," *Methods in enzymology*, vol. 451, pp. 89–107, 2008.

[29] W. Schepers, G. Van Zeebroeck, M. Pinkse, P. Verhaert, and J. M. Thevelein, "*In vivo* phosphorylation of Ser21 and Ser83 during nutrient-induced activation of the yeast protein kinase A, (PKA) target trehalase," *The Journal of Biological Chemistry*, vol. 287, pp. 44130–44142, 2012.

[30] A. Pascual-Ahuir and M. Proft, "The Sch9 kinase is a chromatin-associated transcriptional activator of osmostress-responsive genes," *EMBO Journal*, vol. 26, no. 13, pp. 3098–3108, 2007.

[31] A. Zhang, Y. Shen, W. Gao, and J. Dong, "Role of Sch9 in regulating Ras-cAMP signal pathway in *Saccharomyces cerevisiae*," *FEBS Letters*, vol. 585, no. 19, pp. 3026–3032, 2011.

[32] M. D. Norenberg, K. V. R. Rao, and A. R. Jayakumar, "Signaling factors in the mechanism of ammonia neurotoxicity," *Metabolic Brain Disease*, vol. 24, no. 1, pp. 103–117, 2009.

Hindawi Publishing Corporation
Oxidative Medicine and Cellular Longevity
Volume 2013, Article ID 802870, 10 pages
http://dx.doi.org/10.1155/2013/802870

Research Article

Ethanol and Acetate Acting as Carbon/Energy Sources Negatively Affect Yeast Chronological Aging

Ivan Orlandi,[1,2] Rossella Ronzulli,[2] Nadia Casatta,[2] and Marina Vai[1,2]

[1] *SYSBIO Centre for Systems Biology Milano, Università di Milano-Bicocca, Piazza della Scienza 2, 20126 Milano, Italy*
[2] *Dipartimento di Biotecnologie e Bioscienze, Università di Milano-Bicocca, Piazza della Scienza 2, 20126 Milano, Italy*

Correspondence should be addressed to Marina Vai; marina.vai@unimib.it

Received 13 June 2013; Accepted 9 July 2013

Academic Editor: Joris Winderickx

In *Saccharomyces cerevisiae*, the chronological lifespan (CLS) is defined as the length of time that a population of nondividing cells can survive in stationary phase. In this phase, cells remain metabolically active, albeit at reduced levels, and responsive to environmental signals, thus simulating the postmitotic quiescent state of mammalian cells. Many studies on the main nutrient signaling pathways have uncovered the strong influence of growth conditions, including the composition of culture media, on CLS. In this context, two byproducts of yeast glucose fermentation, ethanol and acetic acid, have been proposed as extrinsic proaging factors. Here, we report that ethanol and acetic acid, at physiological levels released in the exhausted medium, both contribute to chronological aging. Moreover, this combined proaging effect is not due to a toxic environment created by their presence but is mainly mediated by the metabolic pathways required for their utilization as carbon/energy sources. In addition, measurements of key enzymatic activities of the glyoxylate cycle and gluconeogenesis, together with respiration assays performed in extreme calorie restriction, point to a long-term quiescent program favoured by glyoxylate/gluconeogenesis flux contrary to a proaging one based on the oxidative metabolism of ethanol/acetate via TCA and mitochondrial respiration.

1. Introduction

Human aging is associated with a host of time-dependent changes which are the clear manifestation of the progressive decline in cognitive and physical functions of an organism. Albeit extremely complex, aging has turned out to be influenced by mechanisms and nutrient/energy sensing signaling pathways that show strong evolutionary conservation. In this context, the single-celled yeast *Saccharomyces cerevisiae*, exploited as a model system, has provided valuable insight by making it possible to adopt experimental approaches that are not always feasible in higher eukaryotic systems. For example, the nutritional and metabolic status of yeast cells can be diversely coordinated by the simple choice of cultural conditions. Glucose is the preferred carbon and energy source, but in its absence other substrates such as glycerol, ethanol, acetate, or even fatty acids can be used [1]. Thus, the yeast life cycle can integrate metabolic characteristics that are typical for rapid growing cells, storage cells, or highly metabolizing cells depending on nutrient supply.

In the field of aging-related research, replicative and chronological lifespan models have been described which offer the opportunity to study the aging process of both proliferating and postmitotic quiescent mammalian cells, respectively [2–4]. The chronological lifespan (CLS) is defined as the length of time that a population of nondividing cells survives in stationary phase. Viability over time is measured as the ability to resume mitotic growth upon return to rich fresh medium [5]. In a standard CLS experiment, yeast cells are usually grown in synthetic defined media containing 2% glucose [6] where the metabolism is characterized by a high glycolytic flux, glucose fermentation, and a negligible aerobic respiration. Upon glucose depletion, the diauxic shift occurs which results in a shift from fermentation to respiration of the C2 compounds previously produced. This shift involves a massive reprogramming of gene expression including genes which encode enzymes involved in gluconeogenesis, the glyoxylate and TCA cycles. Moreover, overall growth rate is dramatically reduced. Finally, when nutrients are fully exhausted, cell division stops, and the yeast culture enters

a quiescent stationary phase [7, 8]. In the stationary phase, yeast cells display a survival-based metabolism characterized by low metabolic rates and upregulation of stress resistance resulting from the integrated responses of different signaling pathways [9].

CLS can be increased by calorie restriction (CR) which, in yeast, is generally imposed by reducing the glucose concentration in the initial growth medium [10–12] or by transferring postdiauxic cells to water (extreme CR) [5]. Moreover, inhibition/reduction activity of two pathways which sense nutrient availability, namely, TORC1-Sch9 and Ras-PKA ones, also extends CLS [13–16]. These signaling pathways lead in part to common downstream targets which include the protein kinase Rim15 and the transcriptional factors Msn2/4 and Gis1 [17–19]. These factors, besides regulating directly or indirectly stress defence mechanisms, control the accumulation/utilization of intracellular and extracellular carbon sources [20–23]. In particular, Gis1 regulates the accumulation of acetate, a metabolite involved in chronological aging [24]. Interestingly, lack of the NAD^+-dependent deacetylase Sir2, the founding member of Sirtuins, further extends the CLS of long-lived mutants such as *sch9*Δ, as well as the CLS in water indicating that the sole presence of Sir2 can serve as a "blocker" of extreme longevity extension [25]. In addition, *SIR2* inactivation induces stress resistance and affects positively the metabolism of extracellular carbon sources such as ethanol and acetate [25, 26]. These two by-products of glucose fermentation which are metabolised by yeast cells during the post-diauxic phase have been proposed as extrinsic factors promoting chronological aging [25, 27]. In fact, in some long-lived mutants, as well as in short-lived ones, an inverse correlation between the amount of extracellular ethanol or acidic acid and their CLS has been found [25, 26, 28–30]. In line with this, genetic or metabolic (CR) interventions which drive yeast metabolism away from acetic acid production increase CLS [27, 31]. Furthermore, although some connections have been established between nutrient-sensing pathways and the proaging effect of acetic acid involving superoxide anion accumulation which inhibits quiescence [32], the mechanisms by which this compound (and also ethanol) reduces the CLS are still controversial [33].

Here we present results showing that both ethanol and acetic acid contribute to chronological aging. In this context, these compounds are not simply extrinsic toxic factors, but it is their metabolic utilization as carbon/energy sources which results in proaging effects. In particular, in extreme CR, their oxidative metabolism increasing respiration impairs mitochondrial functionality and negatively affects long-term cell survival.

2. Materials and Methods

2.1. Yeast Strains and Growth Conditions. All yeast strains with null mutations were generated by PCR-based methods in a W303-1A background (*MAT*a *ade2-1 his3-11,15 leu2-3,112 trp1-1 ura3-1 can1-100*): *fps1*Δ (*fps1*Δ::*KlLEU2*), *sir2*Δ (*sir2*Δ::*URA3*) [34], *icl1*Δ (*icl1*Δ::*KlLEU2*), and *pck1*Δ (*pck1*Δ::*KlLEU2*) [26]. Yeast cells were grown in batches at 30°C in minimal medium (Difco Yeast Nitrogen Base without amino acids, 6.7 g/L), supplemented with 2% w/v glucose. Auxotrophies were compensated for with a fourfold excess of supplements [25]. All strains were inoculated at the same cellular density (culture volume no more than 20% of the flask volume). Growth was monitored by determining cell number using a Coulter Counter-Particle Count and Size Analyser, as described [35]. Doubling time (Td) was obtained by linear regression of the cell number increase over time on a semilogarithmic plot. For pH measurements, small aliquots of expired media were removed from the culture, and pH was determined using a pH meter.

2.2. Metabolite Measurements and Enzymatic Assays. At designated time-points, aliquots of the yeast cultures were centrifuged, and both pellets (washed twice) and supernatants were frozen at −20°C until used. Glucose, ethanol, and acetate concentrations in the growth medium were determined using enzymatic assays (K-HKGLU, K-ETOH, and K-ACET kits from Megazyme).

Immediately after preparation of cell-free extracts, Pck1 and Icl1 activities were determined as previously described [26]. Total protein concentration was estimated using the BCA Protein Assay Kit (Pierce).

Final values represent the average of three independent experiments. Differences in measurements were assessed by Student's t-test. The level of statistical significance was set at a P value of ≤ 0.05.

2.3. CLS Determination. Survival experiments in expired medium were performed on cells grown in minimal medium (with a fourfold excess of supplements) of 2% glucose as described by [25]. During growth, cell number and extracellular glucose, ethanol, and acetic acid were measured in order to define the growth profile (exponential phase, diauxic shift, post-diauxic phase, and stationary phase) of the culture. Cell survival was monitored by harvesting aliquots of cells starting 72 h (Day 3, first age-point) after the diauxic shift (Day 0). CLS was measured according to [25] by counting colony-forming units (CFUs) every 2-3 days. The number of CFUs on Day 3 was considered the initial survival (100%). Survival was also monitored in the presence of 50 mM pyrazole (Sigma) which was added in the expired medium at Day 1 after the diauxic shift.

For survival experiments in water, at Day 1 cells were harvested, washed with sterile distilled water, and resuspended in a volume of water equal to the initial culture volume. Every 48 h, cells were washed with water and resuspended in fresh water to remove nutrients released by dead cells [5]. The pH of the water was adjusted to 3.2 since it was the pH value measured in the expired medium or to 5.6. Survival experiments in water containing ethanol, acetic acid, or both were performed essentially as described [25, 26, 29]. Treatments are outlined in the text.

For CLS determination in media-swap experiments, cells were grown in minimal medium of 2% glucose (with a fourfold excess of supplements) and at Day 1 after the diauxic shift, harvested by centrifugation. Cell pellets were washed

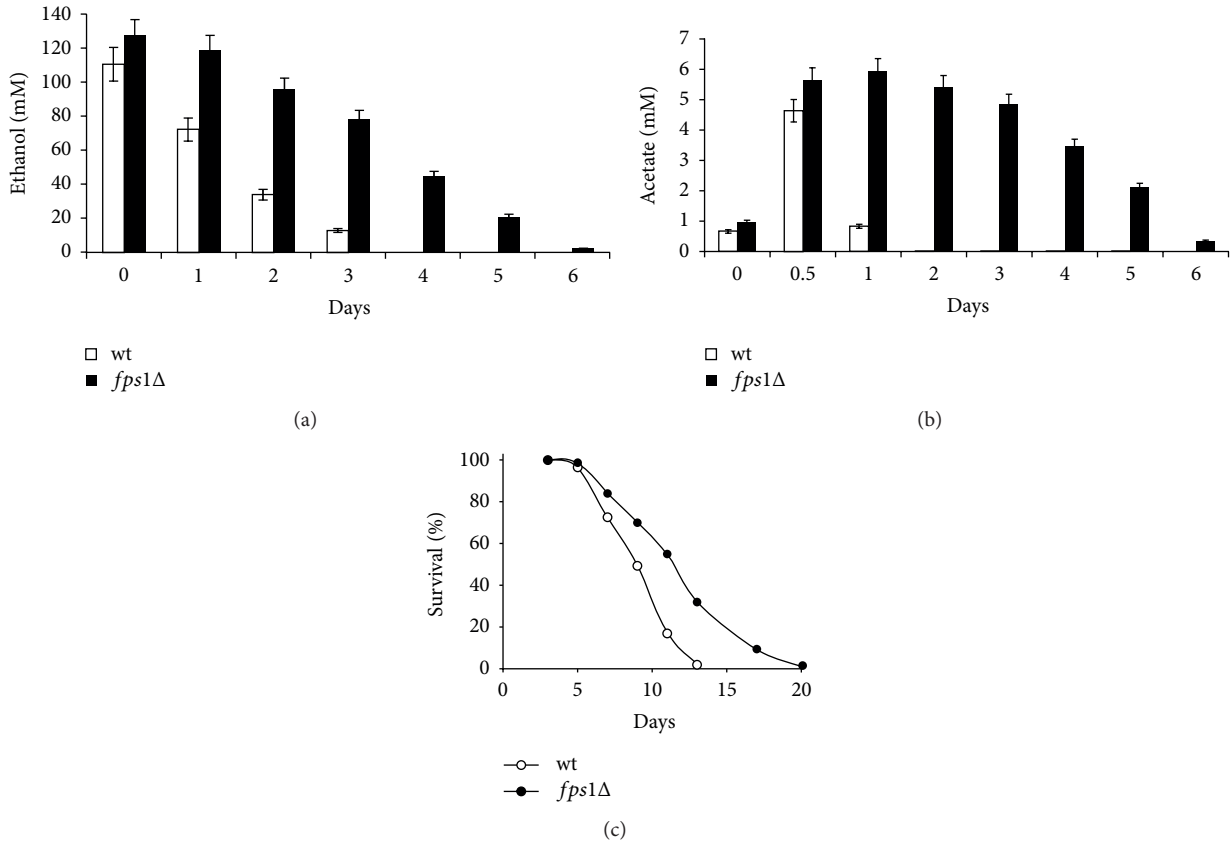

Figure 1: *FPS1* inactivation increases CLS in concert with a decreased uptake of ethanol and acetate. Bar charts of extracellular ethanol (a) and acetate (b) concentrations measured at the indicated time-points in wild type (wt) and *fps1*Δ mutant cultures during chronological aging. Day 0, diauxic shift. Data were obtained from mean values determined in three independent experiments. Standard deviations are indicated. (c) CLS of wt and *fps1*Δ mutant cells. At every time-point, viability was determined by counting CFUs on YEPD plates. 72 h after the diauxic shift (Day 3) was considered the first age-point (see Section 2). One representative experiment is shown.

and then resuspended in the filtered original medium or equivalently conditioned one of the indicated strain. Resuspension in media collected at Day 1 was also performed in the presence of 50 mM pyrazole. Viability was measured as previously described.

2.4. Respiration Assays. The oxygen consumption of intact cells was measured at 30°C using a "Clark-type" oxygen electrode in a thermostatically controlled chamber (Oxygraph System, Hansatech Instruments, Norfolk, UK). For all respiration assays, 2 mL of cell suspension at a concentration of 5×10^6/mL were quickly transferred from the flask to the oxygraph chamber, and routine respiration was recorded. Data were recorded at sampling intervals of 1 s (Oxygraph Plus software, Hansatech Instruments, Norfolk, UK). Respiratory rates were determined from the slope of a plot of O_2 concentration against time, divided by the cellular concentration. All assays were conducted in biological triplicate.

Index of respiratory competence (IRC) was also measured according to [36] by plating identical samples on YEPD plates and on rich medium of 3% glycerol (YEPG) plates. IRC was calculated as colonies on YEPG divided by colonies on YEPD times 100%.

3. Results and Discussion

3.1. Lack of Fps1 Channel Increases CLS. Ethanol and acetic acid are two normal by-products of glucose fermentation, transiently accumulated in the yeast culture medium, which restrict CLS [25, 27]. Moreover, given the low concentration reached by acetic acid in the medium of chronologically aging cells and its faster exhaustion compared to that of ethanol, its physiological relevance as an extracellular factor promoting chronological aging is a matter of debate [33]. In this context, as a first step, we examined the effects on CLS of abolishing the major route of entry into the cell of the undissociated acetic acid such as the Fps1 channel. Uptake of acetate is linked to an active transport for the dissociated form of the acid through the Jen1 and Ady2 transporters accompanied by passive/facilitated diffusion of the undissociated acid through the Fps1 aquaglyceroporin [37, 38]. The former is inducible and subjected to glucose repression [39, 40] while the passive transmembrane flux is strongly influenced by the pH of the medium. In fact, the acetic/acetate couple forms a buffer system in a dynamic equilibrium: at low pH the equilibrium increasingly favours the protonated form while at pH above the pKa of acetic acid (4.75) charged acetate anions prevail. As shown in Figures 1(a)

Table 1: pH values of exhausted media.

Days	wt	*fps1*Δ	*icl1*Δ	wt + pyrazole	*icl1*Δ + pyrazole
0	3.21 ± 0.07	3.20 ± 0.06	3.11 ± 0.06		
1	3.18 ± 0.04	3.16 ± 0.03	3.08 ± 0.05	3.18 ± 0.05	3.08 ± 0.07
2	3.13 ± 0.06	3.08 ± 0.04	2.98 ± 0.05	3.11 ± 0.04	2.89 ± 0.04
3	2.97 ± 0.05	2.90 ± 0.04	2.86 ± 0.06	2.93 ± 0.06	2.75 ± 0.07
4	2.81 ± 0.03	2.68 ± 0.06	2.68 ± 0.04	2.76 ± 0.07	2.63 ± 0.06
5	2.72 ± 0.06	2.56 ± 0.06	2.53 ± 0.06	2.65 ± 0.04	2.48 ± 0.07
6	2.70 ± 0.06	2.55 ± 0.05	2.49 ± 0.07	2.63 ± 0.07	2.43 ± 0.07

pH of the exhausted media was measured starting from diauxic shift, Day 0. Data presented are the mean values of three biological replicates. Standard deviations are indicated.

and 1(b), measurements of extracellular ethanol and acetate revealed that, at the diauxic shift, in the *fps1*Δ culture the amount of these C2 compounds was slightly higher than that in the wild type (wt) culture, in line with exometabolome data obtained during glucose fermentation [41]. However, after the diauxic shift (respiratory metabolism) a significant effect was observed on the depletion of both ethanol and acetic acid which was reduced in the mutant. In particular, as opposed to the expected fast exhaustion of acetic acid in the wt medium (Figure 1(b) and [29]), in the *fps1*Δ mutant this compound decreased very slowly, and it was still present 6 days following the entry in the post-diauxic phase (Figure 1(b)), which is in agreement with the role for Fps1 in facilitating the diffusion of the undissociated acid. In fact, during this phase in which the pH of the medium dropped to values of 2.70 for the wt and 2.55 for the *fps1*Δ mutant at Day 6 (Table 1), acetic acid is substantially undissociated, and the diffusional entry into the cells is elevated. Upon *FPS1* deletion, mutant cells can only rely on the uptake of the low fraction of acetate anions by the active transporters. Interestingly, chronologically aging *fps1*Δ cells lived longer than wt (Figure 1(c)) despite a prolonged exposure to acetic acid and ethanol.

3.2. Inhibition of Ethanol Metabolism Increases CLS. During chronological aging, after the diauxic shift, ethanol which is the main by-product of glucose fermentation, is metabolised by virtually the same pathway as acetate. In fact, after its oxidation to acetaldehyde by alcohol dehydrogenase 2 (Adh2), it is converted to acetate. Subsequently, acetate is activated into acetyl-CoA which is used to fuel the glyoxylate and TCA cycles (Figure 2(a)) [42, 43]. Consequently, we wondered whether blocking the main pathway for acetate production might influence the chronological survival of wt cells in their exhausted medium. To this end, after the diauxic shift when cells began to utilize the excreted ethanol, pyrazole which is an irreversible inhibitor of Adh2 [44] was added to the culture medium and CLS monitored. As depicted in Figure 2(b), pyrazole treatment led to CLS extension. A similar salutary effect took place also when pyrazole was added to the culture medium of postdiauxic *icl1*Δ cells (Figure 2(c)). *ICL1* encodes isocitrate lyase (Icl1), which is one of the unique enzymes of the glyoxylate cycle. During growth on C2 compounds, this cycle plays an essential role for anaplerosis of oxaloacetate which is the substrate of the key gluconeogenic enzyme phosphoenolpyruvate carboxykinase (Pck1) (Figure 2(a)) [43]. In the context of a CLS standard experiment, *ICL1* deletion results in a short-lived phenotype and impairment in acetate utilization [26]. Furthermore, pyrazole treatments led to a very slight acidification in the expired media of the wt and *icl1*Δ cultures (Table 1) indicating that the extracellular acidic pH alone is not sufficient to chronologically age yeast cells. Since we had already observed that pyrazole was able to abrogate the shortening effect of ethanol on CLS extension following extreme CR such as incubation in water [26], this confirms that some aspects of ethanol metabolism and not its mere presence (it enters the cells by passive diffusion) negatively affect CLS. We next performed some media-swap experiments between wt and *icl1*Δ cultures. Both strains were grown in minimal medium, and, at Day 1 after the diauxic shift, cultures were centrifuged and media were exchanged. The *icl1*Δ preconditioned medium, which contained more ethanol and acetic acid compared with the wt preconditioned one (Figures 2(d) and 2(e)) shortened the CLS of wt cells (Figure 2(b)). This detrimental effect on wt viability was abolished upon pyrazole addition, and CLS increased to the same extent as that of chronologically aging wt cells in their original medium in the presence of pyrazole (Figure 2(b)). Moreover, the wt preconditioned medium extended the CLS of the short-lived *icl1*Δ mutant (Figure 2(c)). Inhibition of ethanol oxidation by pyrazole further extended the CLS of the mutant which resulted, also in this case, similar to that of the chronologically aging mutant in its original medium supplemented with the Adh2 inhibitor (Figure 2(c)). Together these findings may point to proaging signaling effects of the metabolic pathways involved in the utilization of ethanol/acetate as carbon and energy source(s) by chronologically aging cells. This is consistent with the proposed role for acetic acid as a physiological trigger of growth signaling pathways which by promoting entry into S phase in unfavorable conditions would lead, among other effects, to replication stress in chronologically aging cells [45]. A DNA replication stress would negatively affect CLS [32, 46], and in this context experimental manipulations inducing such a stress have been recently shown to determine the loss of the reproductive capacity of chronologically aging cells [47]. Moreover, replication stress promotes apoptosis [48, 49]: a highly regulated cellular "suicide" program which is also activated during chronological aging [50]. In addition, acetic acid represents a compound which triggers apoptosis in the presence of glucose [51–53] and in glucose-derepressed *ach1*Δ

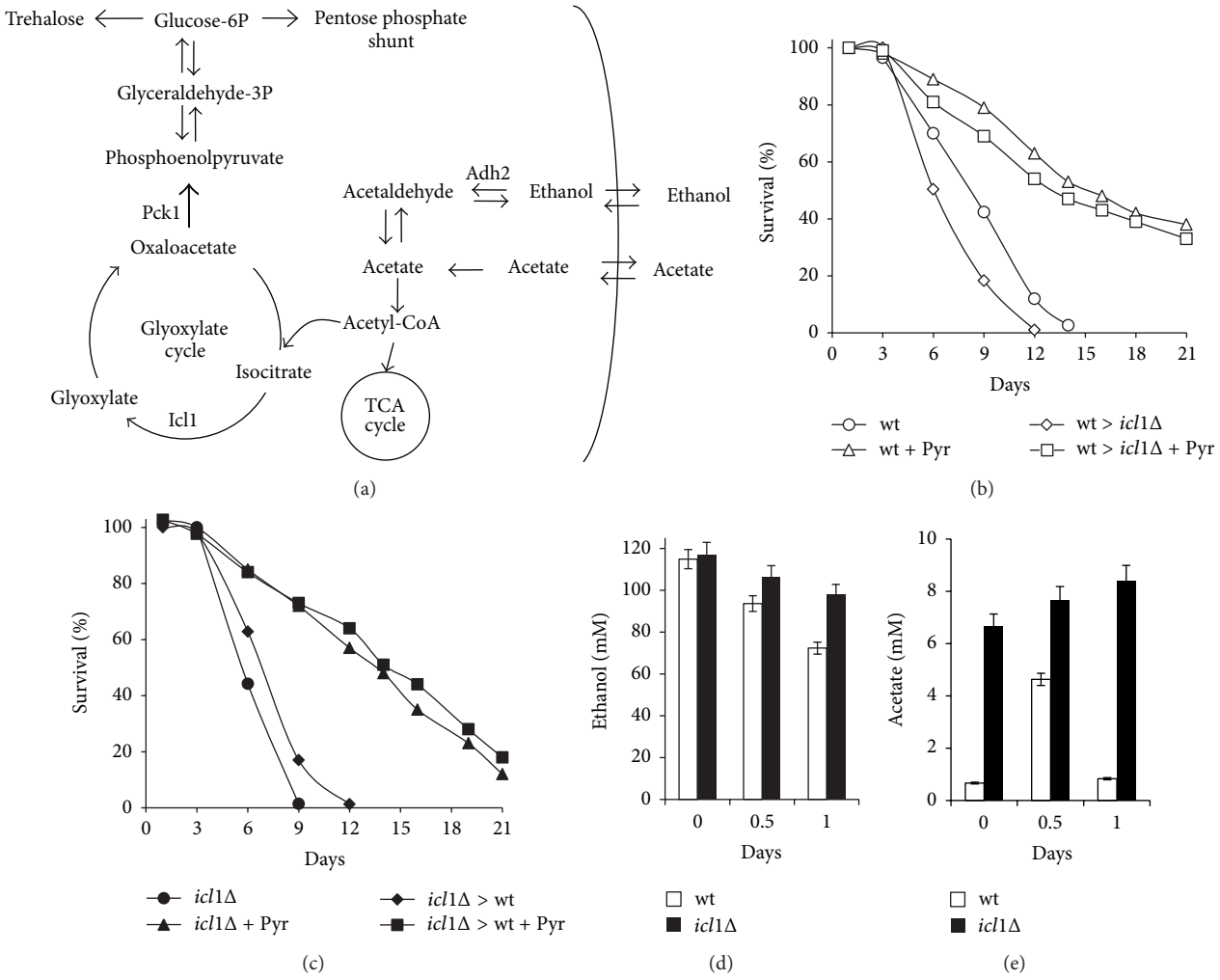

Figure 2: Pyrazole prevents the CLS shortening effect of ethanol. (a) Scheme of metabolic pathways allowing ethanol and acetate utilization. Only relevant reactions are shown. Adh2: alcohol dehydrogenase 2, Icl1: isocitrate lyase 1, Pck1: phosphoenolpyruvate carboxykinase 1. At Day 1 after the diauxic shift, pyrazole (50 mM) was added to the expired media of wt (b) and *icl1*Δ mutant (c) cells. In parallel, aliquots of cells were harvested and subjected to cell-free media swap with or without pyrazole. At every time-point, viability was measured as in Figure 1(c). One representative experiment is shown. Extracellular ethanol (d) and acetate (e) concentrations determined in the wt and *icl1*Δ cultures at Day 1. Day 0, diauxic shift. Standard deviations are indicated.

cells [29]. Ach1 is an enzyme involved in acetate metabolism, and its lack decreases CLS [29, 54]. Consequently, stimulation of growth induced by acetic acid after the diauxic shift in the lack of favorable conditions required for cell cycle progression would ultimately cause apoptosis.

3.3. Physiological Amount of Acetic Acid Reduces CLS. Next, we evaluated whether the physiological amount of acetic acid accumulated as a by-product of glucose fermentation could influence the chronological survival of yeast cells associated with their transfer to water, which is the extreme condition of CR known to extend CLS [25]. Therefore, we monitored the CLS of wt cells that, after the diauxic shift, were switched from expired medium to water supplemented with the amount of acetic acid (5 mM) we had detected in the expired medium (Figure 1(b) and [26, 29]). Treatments were performed in water whose pH was adjusted to 3.2 (the pH of the expired medium we measured) and in water buffered to pH 5.6. In the former condition the uptake of acetate is facilitated compared with that at pH 5.6 where the amount of the acetate anion considerably increases. As shown in Figure 3(a), the addition of 5 mM acetic acid to low pH water reduced CLS, but to a lesser extent than that elicited by ethanol [25, 26] which also in this case was supplied in amount comparable with that found in the expired medium. It is noteworthy that the addition of these C2 compounds together prevented CLS extension associated with transfer to low pH water resulting in a CLS similar to that of chronologically aging cells in their exhausted medium (Figure 3(a)). This suggests that it is a combined proaging effect of both metabolites which influences the CLS. Buffering water to pH 5.6 did not result in a CLS substantially different from that observed at pH 3.2 while the negative effect on chronological survival linked to the presence of acetic acid, ethanol, or both

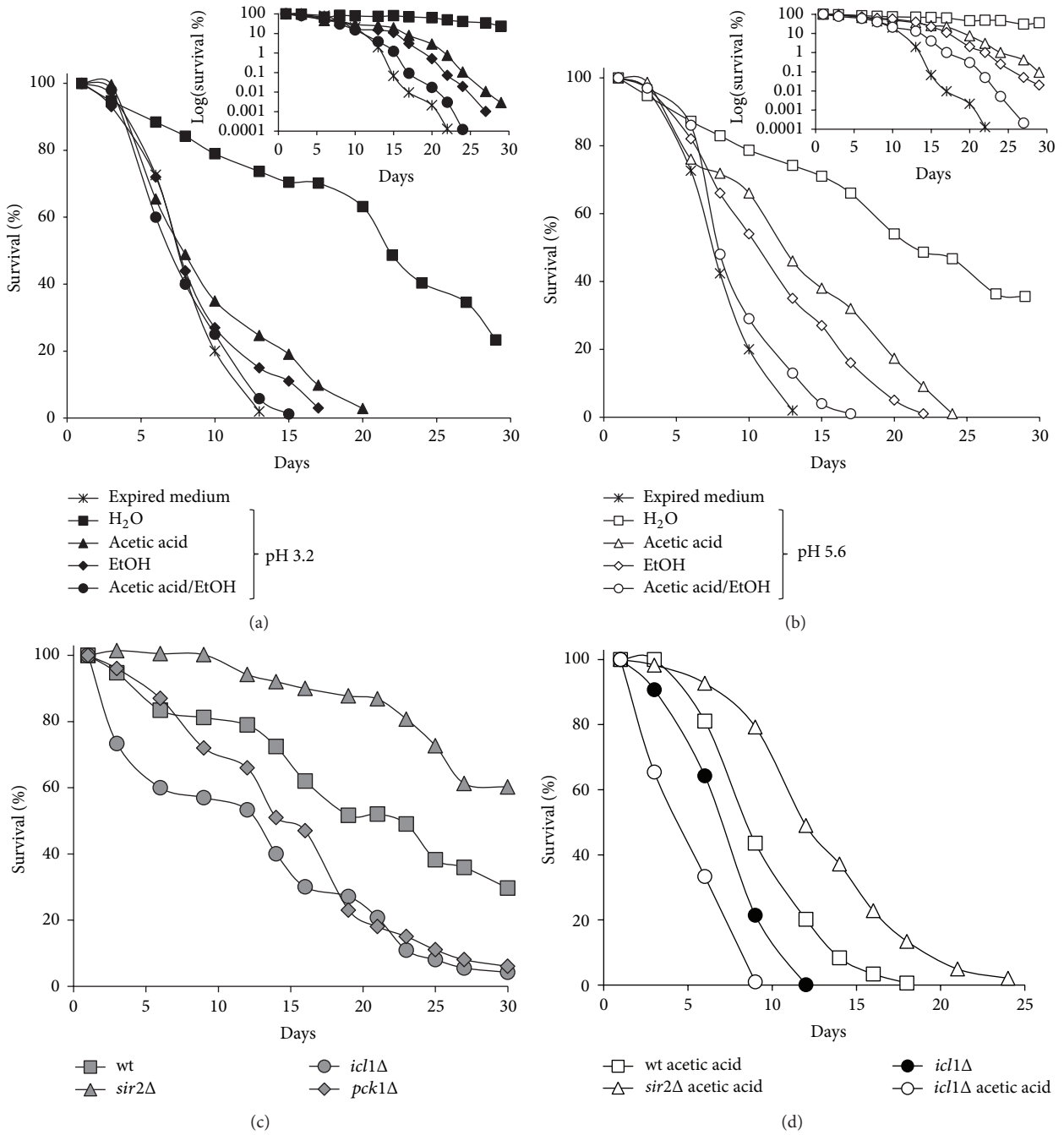

Figure 3: The glyoxylate-requiring gluconeogenesis plays a positive role in extreme life-span extension. At Day 1 after the diauxic shift, wt cells were switched to water adjusted to pH 3.2 (a) and to pH 5.6 (b) and challenged with ethanol (6 g/L), acetic acid (5 mM), or both. Every 48 h, cultures were resuspended in fresh water, and each time ethanol and acetic acid were added when indicated. At every time-point, viability was measured. Survival of cells in their expired medium was also monitored as control. Insets: CLS plotted on a log scale. One representative experiment is shown. (c) CLS of wt, *icl1*Δ, *pck1*Δ, and *sir2*Δ cells switched to pH 3.2 water at Day 1 after the diauxic shift. (d) In parallel, the indicated cultures were challenged with 5 mM acetic acid as in (a). Survival of *icl1*Δ cells in their exhausted medium was also monitored. One representative experiment is shown.

these compounds together was reduced (Figure 3(b)). Thus, buffering the extracellular medium alone is not sufficient to induce the fully extension of CLS observed in water, in line with data showing that an acidic environment alone is not sufficient to suppress the CLS extension associated with a CR regimen of growth which reduces acetic acid production [27, 29]. This further confirms that acidification accelerates chronological aging by influencing acetic/acetate equilibrium and consequently acetate uptake.

In the chronological aging paradigm, a proaging role is played by Sir2 which has as nonchromatin substrate the Pck1 enzyme. *SIR2* inactivation increases acetylated Pck1 in

concert with increased enzymatic activity [26, 28]. Since this correlates with an enhanced glyoxylate/gluconeogenic flux and with a more efficient acetate utilization [26], we analyzed whether the addition of 5 mM acetic acid could influence the CLS of *sir2*Δ cells that, after the diauxic shift, were incubated in low pH water. In parallel, the same analysis was performed for the *icl1*Δ mutant. As shown in Figure 3(c), the effect produced by the single *SIR2* and *ICL1* deletions on the CLS in water was the opposite. In fact, lack of Sir2 significantly extended the CLS compared with that of wt cells in agreement with [25–28] while lack of Icl1 reduced it. Interestingly, a similar decrease in cell survival has been observed following *PCK1* deletion ([28] and Figure 3(c)). Moreover, acetic acid-back *sir2*Δ cultures lived longer than acetic acid-back wt ones (Figure 3(d)). On the contrary, chronological survival of *icl1*Δ cells was affected dramatically by the same amount of acetic acid (Figure 3(d)), indicating that acetic acid, at this concentration, becomes extremely toxic for cells with an impaired glyoxylate cycle activity. Taken together these data suggest that the glyoxylate-requiring gluconeogenesis and the cell ability to metabolize acetate play positive roles in the CLS extension linked to extreme CR.

3.4. Ethanol Reduces Glyoxylate/Gluconeogenesis and Enhances Respiration of Cells in Extreme CR. Starting from the aforementioned results, for the purpose of investigating the connection between the glyoxylate-requiring gluconeogenesis and chronological longevity we measured the enzymatic activity of Pck1 and Icl1 in chronologically aging wt cells in their expired medium or transferred to water. In parallel, we also examined cellular respiration. In fact, it is well known that in the former experimental condition, when glucose is depleted, cells consume the earlier produced ethanol/acetate via gluconeogenesis (Figures 4(a) and 4(b)), and concomitantly they increase their respiration (Figure 4(c)). In the extreme condition of CR, once cells were switched to water, the levels of Icl1 and Pck1 enzymatic activities increased and remained higher than those detected during aging in the expired medium (Figures 4(a) and 4(b)). In addition, they barely respired (Figure 4(c)). It is noteworthy that when these cells were challenged with ethanol, Icl1 and Pck1 enzymatic activities were reduced (Figures 4(a) and 4(b)), and the cellular respiration increased (Figure 4(c)). Similar results (with reduction and increase to a lesser extent) were obtained when acetate substituted for ethanol (data not shown) indicating that both C2 compounds are metabolised by the CR cells. Since the ability to respire relies on functional mitochondria and a direct correlation between reduced CLS and dysfunctional mitochondria has been reported [6, 55], we decided to analyze the index of respiratory competence (IRC). This index measures the percentage of viable cells which are competent to respire [36]. At Day 1, the IRC was about 100% for chronologically aging cells in the exhausted medium, in water, and in water/ethanol (Figure 4(d)) indicating that all the cells are respiration competent. Starting from Day 12, this value began to decrease progressively for the cells in the exhausted medium and for those in water/ethanol reaching about 20% and 50%, respectively by Day 21 which is indicative of a time-dependent loss of mitochondrial functionality. On the contrary, in the extreme CR condition the IRC was still about 80% (Figure 4(d)) indicating, on the one hand, that the low level of respiration is not due to impairment in mitochondrial functionality and, on the other hand, that resuspension in water exerts a protective role on mitochondria which become more prone to damage following ethanol addition.

To this effect, a causative role in inducing mitochondrial dysfunction is played by reactive oxygen species (ROS), and, at the same time, mitochondrial dysfunction leads to increased ROS formation [56]. Moreover, mitochondria are the major intracellular source of potentially harmful ROS such as the superoxide anion. This radical can directly induce oxidative damage or can be converted to other ROS which, in turn, induce aging-associated damage [57]. Chronological aging in the absence of any extracellular nutrient, namely, water, which correlates with an increased CLS, implies that cells have to establish a survival-based metabolism where energy is conserved by shutting down expensive growth-promoting pathways and concomitantly stress resistance and access to alternate energy stores are provided. In addition, cells have to limit damage to cellular components. In this context, reducing respiration may be beneficial since, although highly efficient in producing ATP, the oxidative metabolism produces the superoxide anion which is generated in the electron transport chain.

The other feature of cells in extreme CR discovered was an increase in the enzymatic activities of Pck1 (the main flux-controlling step of gluconeogenesis) and Icl1. This feature, combined with the fact that loss of their function blocks CLS extension, further supports the notion of a positive crucial role of glyoxylate/gluconeogenesis in the control of this form of longevity [28]. Increasing glyoxylate/gluconeogenesis may be advantageous to improve survivability during chronological aging in water since gluconeogenesis switches the direction of metabolite flow towards the biosynthetic precursor, glucose-6-phosphate, which is also needed for glucose stores (Figure 2(a)). In particular, trehalose has been proposed as the carbohydrate of choice for surviving starvation and upon cell cycle reentry from quiescence [58]. Moreover, hexoses generated from gluconeogenesis can be used via the pentose phosphate pathway generating additional NADPH which is essential for the activity of antioxidant defenses [59]. On the other hand, with regard to the glyoxylate pathway, it is important to recall that it does not only have the function of fueling gluconeogenesis but can contribute to NADH production [60].

This metabolic scenario may give some explanation why the CLS extension in water is intensified following *SIR2* inactivation [25]. In fact, the increase in the acetylated active form of Pck1 due to the lack of the Sir2-targeted deacetylation enhancing the glyoxylate/gluconeogenic flux [26] might further favour the establishment of a long-term quiescent program. On the contrary, the oxidative metabolism of ethanol/acetate via the TCA and mitochondrial electron transport chain increasing respiration may generate harmful ROS which impair mitochondrial functionality. This, in

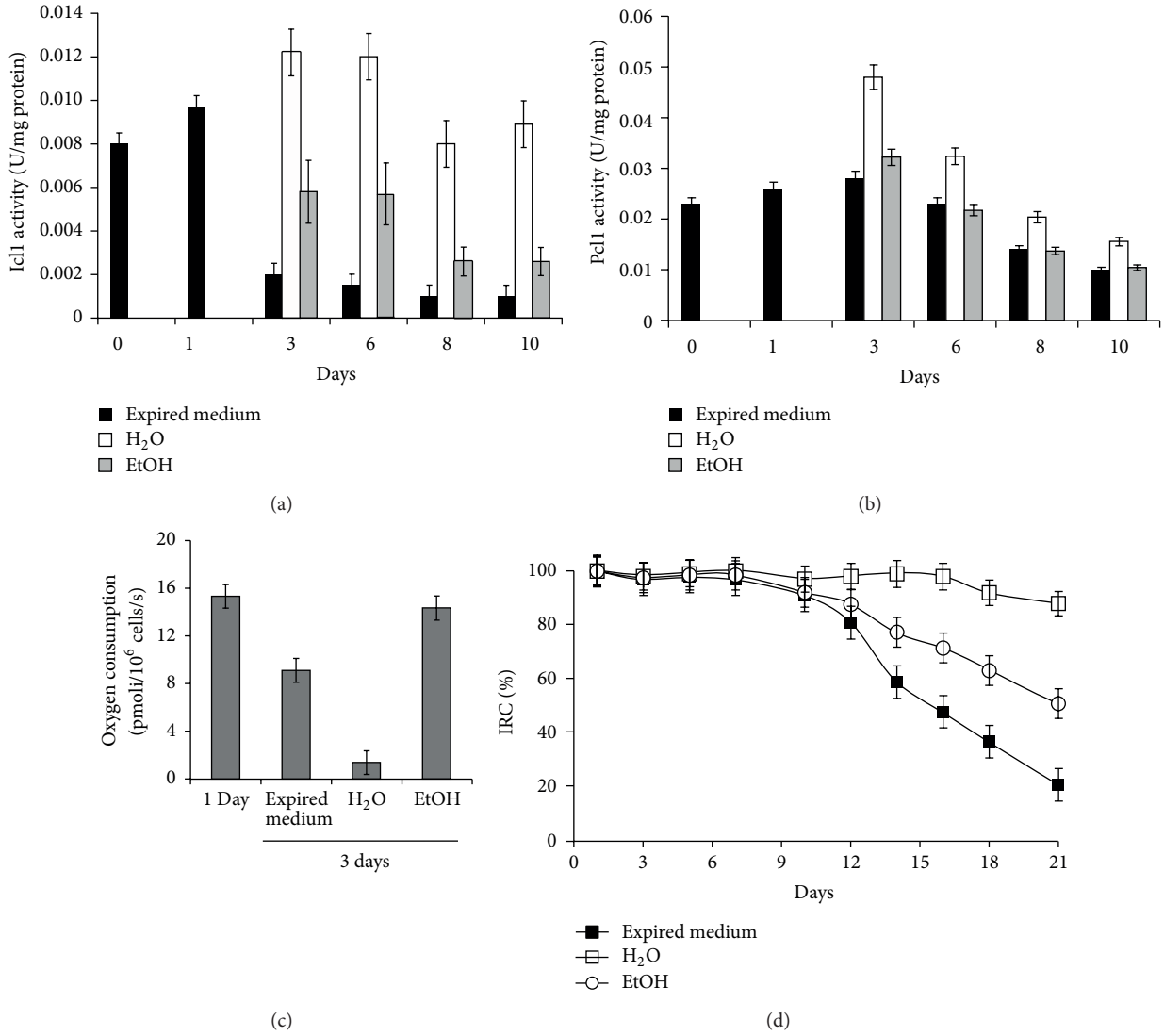

Figure 4: Ethanol affects the glyoxylate-requiring gluconeogenesis and the respiration of cells in extreme CR. At the indicated time-points, Icl1 (a) and Pckl (b) enzymatic activities were measured in wt cells during chronological aging in their expired medium and after the switch to water or water/ethanol as in Figure 3. Day 0, diauxic shift. (c) Cellular respiration of the same cells in the indicated experimental conditions. Error bars are the standard deviation of three replicates. (d) Chronologically aging wt cultures at the indicated time-points were serially diluted, plated onto YEPD and YEPG plates, and the index of respiratory competence (IRC) was determined. Standard deviations of three independent experiments are indicated.

concert with induced growth signals in the lack of favorable conditions required for cell cycle progression [32], most likely negatively affects cell survival. Bearing in mind that the relationship between respiration, ROS, and CLS is very complex, how can the proaging effect induced by ethanol in nutrient starvation conditions fit with the ability of pregrowth on the same respiratory carbon/energy source to extend CLS [61, 62]? In fact, in addition to the role played by a mitochondrial respiratory threshold in regulating CLS [63], mitochondrial respiration affects chronological survival through ROS generation. They can be either deleterious or beneficial depending on the biological context/phases of the yeast cell cycle in which they are produced [57]. Although mitochondrial ROS have been associated with damaging effects which promote and/or accelerate chronological aging [64], they also function as signaling molecules with hormetic effects on longevity [65, 66]. In particular, elevating mitochondrial ROS during yeast exponential growth elicits an adaptive response which promotes CLS extension [67]. Similarly, the effects on CLS observed following growth on ethanol [61, 62] are also in line with an adaptive mitochondrial longevity signal generated during active growth which contributes to establishment of a better quiescent program.

Acknowledgments

The authors are grateful to Neil Campbell for English editing. They thank Nico Mitro and Matteo Audano for assistance in respiration assays. They acknowledge funding of the project SysBioNet, Italian Roadmap Research Infrastructures 2012.

References

[1] B. Turcotte, X. B. Liang, F. Robert, and N. Soontorngun, "Transcriptional regulation of nonfermentable carbon utilization in budding yeast," *FEMS Yeast Research*, vol. 10, no. 1, pp. 2–13, 2010.

[2] V. D. Longo and B. K. Kennedy, "Sirtuins in aging and age-related disease," *Cell*, vol. 126, no. 2, pp. 257–268, 2006.

[3] M. MacLean, N. Harris, and P. W. Piper, "Chronological lifespan of stationary phase yeast cells; a model for investigating the factors that might influence the ageing of postmitotic tissues in higher organisms," *Yeast*, vol. 18, no. 6, pp. 499–509, 2001.

[4] K. A. Steinkraus, M. Kaeberlein, and B. K. Kennedy, "Replicative aging in yeast: the means to the end," *Annual Review of Cell and Developmental Biology*, vol. 24, pp. 29–54, 2008.

[5] P. Fabrizio and V. D. Longo, "The chronological life span of *Saccharomyces cerevisiae*," *Aging Cell*, vol. 2, no. 2, pp. 73–81, 2003.

[6] P. Fabrizio and V. D. Longo, "The chronological life span of *Saccharomyces cerevisiae*," *Methods in Molecular Biology*, vol. 371, pp. 89–95, 2007.

[7] L. Galdieri, S. Mehrotra, S. Yu, and A. Vancura, "Transcriptional regulation in yeast during diauxic shift and stationary phase," *OMICS*, vol. 14, no. 6, pp. 629–638, 2010.

[8] J. V. Gray, G. A. Petsko, G. C. Johnston, D. Ringe, R. A. Singer, and M. Werner-Washburne, "'Sleeping beauty': quiescence in *Saccharomyces cerevisiae*," *Microbiology and Molecular Biology Reviews*, vol. 68, no. 2, pp. 187–206, 2004.

[9] B. Smets, R. Ghillebert, P. de Snijder et al., "Life in the midst of scarcity: adaptations to nutrient availability in *Saccharomyces cerevisiae*," *Current Genetics*, vol. 56, no. 1, pp. 1–32, 2010.

[10] L. Fontana, L. Partridge, and V. D. Longo, "Extending healthy life span-from yeast to humans," *Science*, vol. 328, no. 5976, pp. 321–326, 2010.

[11] M. Kaeberlein, "Lessons on longevity from budding yeast," *Nature*, vol. 464, no. 7288, pp. 513–519, 2010.

[12] W. Mair and A. Dillin, "Aging and survival: the genetics of life span extension by dietary restriction," *Annual Review of Biochemistry*, vol. 77, pp. 727–754, 2008.

[13] R. W. Powers III, M. Kaeberlein, S. D. Caldwell, B. K. Kennedy, and S. Fields, "Extension of chronological life span in yeast by decreased TOR pathway signaling," *Genes and Development*, vol. 20, no. 2, pp. 174–184, 2006.

[14] P. Fabrizio, F. Pozza, S. D. Pletcher, C. M. Gendron, and V. D. Longo, "Regulation of longevity and stress resistance by Sch9 in yeast," *Science*, vol. 292, no. 5515, pp. 288–290, 2001.

[15] P. Fabrizio, L.-L. Liou, V. N. Moy et al., "SOD2 functions downstream of Sch9 to extend longevity in yeast," *Genetics*, vol. 163, no. 1, pp. 35–46, 2003.

[16] M. Wei, P. Fabrizio, J. Hu et al., "Life span extension by calorie restriction depends on Rim15 and transcription factors downstream of Ras/PKA, Tor, and Sch9," *PLoS Genetics*, vol. 4, no. 1, article e13, 2008.

[17] E. Cameroni, N. Hulo, J. Roosen, J. Winderickx, and C. de Virgilio, "The novel yeast PAS kinase Rim15 orchestrates G_0-associated antioxidant defense mechanisms," *Cell Cycle*, vol. 3, no. 4, pp. 462–468, 2004.

[18] P. Fabrizio, S. D. Pletcher, N. Minois, J. W. Vaupel, and V. D. Longo, "Chronological aging-independent replicative life span regulation by Msn2/Msn4 and Sod2 in *Saccharomyces cerevisiae*," *FEBS Letters*, vol. 557, no. 1–3, pp. 136–142, 2004.

[19] I. Pedruzzi, F. Dubouloz, E. Cameroni et al., "TOR and PKA signaling pathways converge on the protein kinase Rim15 to control entry into G_0," *Molecular Cell*, vol. 12, no. 6, pp. 1607–1613, 2003.

[20] N. D. Bonawitz, M. Chatenay-Lapointe, Y. Pan, and G. S. Shadel, "Reduced TOR signaling extends chronological life span via increased respiration and upregulation of mitochondrial gene expression," *Cell Metabolism*, vol. 5, no. 4, pp. 265–277, 2007.

[21] M. Wei, P. Fabrizio, F. Madia et al., "Tor1/Sch9-regulated carbon source substitution is as effective as calorie restriction in life span extension," *PLoS Genetics*, vol. 5, no. 5, Article ID e1000467, 2009.

[22] I. Pedruzzi, N. Bürckert, P. Egger, and C. de Virgilio, "*Saccharomyces cerevisiae* Ras/cAMP pathway controls post-diauxic shift element-dependent transcription through the zinc finger protein Gis1," *The EMBO Journal*, vol. 19, no. 11, pp. 2569–2579, 2000.

[23] J. L. DeRisi, V. R. Iyer, and P. O. Brown, "Exploring the metabolic and genetic control of gene expression on a genomic scale," *Science*, vol. 278, no. 5338, pp. 680–686, 1997.

[24] J. O. Westholm, S. Tronnersjö, N. Nordberg, I. Olsson, J. Komorowski, and H. Ronne, "Gis1 and Rph1 regulate glycerol and acetate metabolism in glucose depleted yeast cells," *PLoS ONE*, vol. 7, no. 2, Article ID e31577, 2012.

[25] P. Fabrizio, C. Gattazzo, L. Battistella et al., "Sir2 blocks extreme life-span extension," *Cell*, vol. 123, no. 4, pp. 655–667, 2005.

[26] N. Casatta, A. Porro, I. Orlandi, L. Brambilla, and M. Vai, "Lack of Sir2 increases acetate consumption and decreases extracellular pro-aging factors," *Biochimica et Biophysica Acta*, vol. 1833, no. 3, pp. 593–601, 2013.

[27] C. R. Burtner, C. J. Murakami, B. K. Kennedy, and M. Kaeberlein, "A molecular mechanism of chronological aging in yeast," *Cell Cycle*, vol. 8, no. 8, pp. 1256–1270, 2009.

[28] Y.-Y. Lin, J.-Y. Lu, J. Zhang et al., "Protein acetylation microarray reveals that NuA4 controls key metabolic target regulating gluconeogenesis," *Cell*, vol. 136, no. 6, pp. 1073–1084, 2009.

[29] I. Orlandi, N. Casatta, and M. Vai, "Lack of Ach1 CoA-transferase triggers apoptosis and decreases chronological lifespan in yeast," *Frontiers in Oncology*, vol. 2, article 67, 2012.

[30] M. Matecic, D. L. Smith Jr., X. Pan et al., "A microarray-based genetic screen for yeast chronological aging factors," *PLoS Genetics*, vol. 6, no. 4, Article ID e1000921, 2010.

[31] C. J. Kenyon, "The genetics of ageing," *Nature*, vol. 464, no. 7288, pp. 504–512, 2010.

[32] M. Weinberger, A. Mesquita, T. Caroll et al., "Growth signaling promotes chronological aging in budding yeast by inducing superoxide anions that inhibit quiescence," *Aging*, vol. 2, no. 10, pp. 709–726, 2010.

[33] V. D. Longo, G. S. Shadel, M. Kaeberlein, and B. Kennedy, "Replicative and chronological aging in *Saccharomyces cerevisiae*," *Cell Metabolism*, vol. 16, no. 1, pp. 18–31, 2012.

[34] L. Calzari, I. Orlandi, L. Alberghina, and M. Vai, "The histone deubiquitinating enzyme Ubp10 is involved in rDNA locus control in *Saccharomyces cerevisiae* by affecting Sir2p association," *Genetics*, vol. 174, no. 4, pp. 2249–2254, 2006.

[35] M. Vanoni, M. Vai, L. Popolo, and L. Alberghina, "Structural heterogeneity in populations of the budding yeast *Saccharomyces cerevisiae*," *Journal of Bacteriology*, vol. 156, no. 3, pp. 1282–1291, 1983.

[36] E. Parrella and V. D. Longo, "The chronological life span of *Saccharomyces cerevisiae* to study mitochondrial dysfunction and disease," *Methods*, vol. 46, no. 4, pp. 256–262, 2008.

[37] M. Casal, S. Paiva, O. Queirós, and I. Soares-Silva, "Transport of carboxylic acids in yeasts," *FEMS Microbiology Reviews*, vol. 32, no. 6, pp. 974–994, 2008.

[38] M. Mollapour and P. W. Piper, "Hog1 mitogen-activated protein kinase phosphorylation targets the yeast Fps1 aquaglyceroporin for endocytosis, thereby rendering cells resistant to acetic acid," *Molecular and Cellular Biology*, vol. 27, no. 18, pp. 6446–6456, 2007.

[39] S. Paiva, F. Devaux, S. Barbosa, C. Jacq, and M. Casal, "Ady2p is essential for the acetate permease activity in the yeast *Saccharomyces cerevisiae*," *Yeast*, vol. 21, no. 3, pp. 201–210, 2004.

[40] R. P. Andrade, P. Kötter, K.-D. Entian, and M. Casal, "Multiple transcripts regulate glucose-triggered mRNA decay of the lactate transporter *JEN1* from *Saccharomyces cerevisiae*," *Biochemical and Biophysical Research Communications*, vol. 332, no. 1, pp. 254–262, 2005.

[41] A. B. Lourenco, F. C. Roque, M. C. Teixeira, J. R. Ascenso, and I. Sa-Correia, "Quantitative ^{1}H-NMR-metabolomics reveals extensive metabolic reprogramming and the effect of the aquaglyceroporin *FPS1* in ethanol-stressed yeast cells," *PLoS ONE*, vol. 8, no. 2, Article ID e55439, 2013.

[42] M. A. van den Berg, P. de Jong-Gubbels, C. J. Kortland, J. P. van Dijken, J. T. Pronk, and H. Y. Steensma, "The two acetyl-coenzyme A synthetases of *Saccharomyces cerevisiae* differ with respect to kinetic properties and transcriptional regulation," *The Journal of Biological Chemistry*, vol. 271, no. 46, pp. 28953–28959, 1996.

[43] M. M. dos Santos, A. K. Gombert, B. Christensen, L. Olsson, and J. Nielsen, "Identification of in vivo enzyme activities in the cometabolism of glucose and acetate by *Saccharomyces cerevisiae* by using ^{13}C-labeled substrates," *Eukaryotic Cell*, vol. 2, no. 3, pp. 599–608, 2003.

[44] C. Wills and D. Hom, "An efficient selection producing structural gene mutants of yeast alcohol dehydrogenase resistant to pyrazole," *Genetics*, vol. 119, no. 4, pp. 791–795, 1988.

[45] W. C. Burhans and M. Weinberger, "Acetic acid effects on aging in budding yeast: are they relevant to aging in higher eukaryotes?" *Cell Cycle*, vol. 8, no. 14, pp. 2300–2302, 2009.

[46] M. Weinberger, L. Feng, A. Paul et al., "DNA replication stress is a determinant of chronological lifespan in budding yeast," *PloS ONE*, vol. 2, no. 8, article e748, 2007.

[47] M. Weinberger, B. Sampaio-Marques, P. Ludovico, and W. C. Burhans, "DNA replication stress-induced loss of reproductive capacity in *S. cerevisiae* and its inhibition by caloric restriction," *Cell Cycle*, vol. 12, no. 8, pp. 1189–1200, 2013.

[48] M. Weinberger, L. Ramachandran, L. Feng et al., "Apoptosis in budding yeast caused by defects in initiation of DNA replication," *Journal of Cell Science*, vol. 118, no. 15, pp. 3543–3553, 2005.

[49] D. Carmona-Gutierrez, T. Eisenberg, S. Büttner, C. Meisinger, G. Kroemer, and F. Madeo, "Apoptosis in yeast: triggers, pathways, subroutines," *Cell Death and Differentiation*, vol. 17, no. 5, pp. 763–773, 2010.

[50] E. Herker, H. Jungwirth, K. A. Lehmann et al., "Chronological aging leads to apoptosis in yeast," *The Journal of Cell Biology*, vol. 164, no. 4, pp. 501–507, 2004.

[51] P. Ludovico, F. Rodrigues, A. Almeida, M. T. Silva, A. Barrientos, and M. Côrte-Real, "Cytochrome *c* release and mitochondria involvement in programmed cell death induced by acetic acid in *Saccharomyces cerevisiae*," *Molecular Biology of the Cell*, vol. 13, no. 8, pp. 2598–2606, 2002.

[52] P. Ludovico, M. J. Sousa, M. T. Silva, C. Leão, and M. Côrte-Real, "*Saccharomyces cerevisiae* commits to a programmed cell death process in response to acetic acid," *Microbiology*, vol. 147, no. 9, pp. 2409–2415, 2001.

[53] S. Giannattasio, N. Guaragnella, M. Côrte-Real, S. Passarella, and E. Marra, "Acid stress adaptation protects *Saccharomyces cerevisiae* from acetic acid-induced programmed cell death," *Gene*, vol. 354, no. 1-2, pp. 93–98, 2005.

[54] C. B. Fleck and M. Brock, "Re-characterisation of *Saccharomyces cerevisiae* Ach1p: fungal CoA-transferases are involved in acetic acid detoxification," *Fungal Genetics and Biology*, vol. 46, no. 6-7, pp. 473–485, 2009.

[55] N. D. Bonawitz, M. S. Rodeheffer, and G. S. Shadel, "Defective mitochondrial gene expression results in reactive oxygen species-mediated inhibition of respiration and reduction of yeast life span," *Molecular and Cellular Biology*, vol. 26, no. 13, pp. 4818–4829, 2006.

[56] G. Farrugia and R. Balzan, "Oxidative stress and programmed cell death in yeast," *Frontiers in Oncology*, vol. 2, article 64, 2012.

[57] Y. Pan, "Mitochondria, reactive oxygen species, and chronological aging: a message from yeast," *Experimental Gerontology*, vol. 46, no. 11, pp. 847–852, 2011.

[58] L. Shi, B. M. Sutter, X. Ye, and B. P. Tu, "Trehalose is a key determinant of the quiescent metabolic state that fuels cell cycle progression upon return to growth," *Molecular Biology of the Cell*, vol. 21, no. 12, pp. 1982–1990, 2010.

[59] N. Pollak, C. Dölle, and M. Ziegler, "The power to reduce: pyridine nucleotides—small molecules with a multitude of functions," *The Biochemical Journal*, vol. 402, no. 2, pp. 205–218, 2007.

[60] G. G. Zampar, A. Kummel, J. Ewald et al., "Temporal system-level organization of the switch from glycolytic to gluconeogenic operation in yeast," *Molecular Systems Biology*, vol. 9, article 651, 2013.

[61] P. W. Piper, N. L. Harris, and M. MacLean, "Preadaptation to efficient respiratory maintenance is essential both for maximal longevity and the retention of replicative potential in chronologically ageing yeast," *Mechanisms of Ageing and Development*, vol. 127, no. 9, pp. 733–740, 2006.

[62] C. J. Murakami, V. Wall, N. Basisty, and M. Kaeberlein, "Composition and acidification of the culture medium influences chronological aging similarly in vineyard and laboratory yeast," *PLoS ONE*, vol. 6, no. 9, Article ID e24530, 2011.

[63] A. Ocampo, J. Liu, E. A. Schroeder, G. S. Shadel, and A. Barrientos, "Mitochondrial respiratory thresholds regulate yeast chronological life span and its extension by caloric restriction," *Cell Metabolism*, vol. 16, no. 1, pp. 55–67, 2012.

[64] M. H. Barros, F. M. da Cunha, G. A. Oliveira, E. B. Tahara, and A. J. Kowaltowski, "Yeast as a model to study mitochondrial mechanisms in ageing," *Mechanisms of Ageing and Development*, vol. 131, no. 7-8, pp. 494–502, 2010.

[65] M. Ristow and S. Schmeisser, "Extending life span by increasing oxidative stress," *Free Radical Biology and Medicine*, vol. 51, no. 2, pp. 327–336, 2011.

[66] D. Gems and L. Partridge, "Stress-response hormesis and aging: 'that which does not kill us makes us stronger'," *Cell Metabolism*, vol. 7, no. 3, pp. 200–203, 2008.

[67] Y. Pan, E. A. Schroeder, A. Ocampo, A. Barrientos, and G. S. Shadel, "Regulation of yeast chronological life span by TORC1 via adaptive mitochondrial ROS signaling," *Cell Metabolism*, vol. 13, no. 6, pp. 668–678, 2011.

Hindawi Publishing Corporation
Oxidative Medicine and Cellular Longevity
Volume 2013, Article ID 437146, 9 pages
http://dx.doi.org/10.1155/2013/437146

Research Article

Saccharomyces cerevisiae Linker Histone—Hho1p Maintains Chromatin Loop Organization during Ageing

Katya Uzunova, Milena Georgieva, and George Miloshev

Laboratory of Yeast Molecular Genetics, "Acad. Roumen Tsanev" Institute of Molecular Biology, Bulgarian Academy of Sciences, "Acad. G. Bonchev" Street, Building 21, 1113 Sofia, Bulgaria

Correspondence should be addressed to George Miloshev; miloshev@bio21.bas.bg

Received 10 May 2013; Revised 5 July 2013; Accepted 8 July 2013

Academic Editor: Cristina Mazzoni

Intricate, dynamic, and absolutely unavoidable ageing affects cells and organisms through their entire lifetime. Driven by diverse mechanisms all leading to compromised cellular functions and finally to death, this process is a challenge for researchers. The molecular mechanisms, the general rules that it follows, and the complex interplay at a molecular and cellular level are yet little understood. Here, we present our results showing a connection between the linker histones, the higher-order chromatin structures, and the process of chronological lifespan of yeast cells. By deleting the gene for the linker histone in *Saccharomyces cerevisiae* we have created a model for studying the role of chromatin structures mainly at its most elusive and so far barely understood higher-order levels of compaction in the processes of yeast chronological lifespan. The mutant cells demonstrated controversial features showing slower growth than the wild type combined with better survival during the whole process. The analysis of the global chromatin organization during different time points demonstrated certain loss of the upper levels of chromatin compaction in the cells without linker histone. The results underlay the importance of this histone for the maintenance of the chromatin loop structures during ageing.

1. Introduction

Ageing consists of natural alterations in the cells which are implemented by molecular programs written in the genome and in the epigenome at the same time. The organization of DNA in chromatin enables the epigenetic information transfer to nuclear processes. The first level of chromatin organization, the nucleosome arrays, consisting of DNA wrapped around nucleosomes is relatively well known [1]. Several lines of evidence have shown that the basic epigenetic role of chromatin in ageing is accomplished at this particular level of chromatin organization [2–5]. The upper levels above the nucleosome arrays, known as 30 nm chromatin fibers, chromatin loops, chromosome territories, and so forth, are yet far from being comprehensibly described [4, 6]. Their part in the epigenetic inheritance is barely known though it was proved that the main participants in the building and preservation of these structures are members of the family of linker histones—H1 [7–9].

Although data about the epigenetic transformations of chromatin during cellular ageing has been accumulated extensively in the recent years, information about age-related higher-order chromatin alterations is practically nonexistent. A good exception is the study showing that loss of two proteins, PBBP4 and PBBP7, subunits of the NURD chromatin remodeling complex, compromises the establishment and maintenance of the higher-order chromatin structure, thus possibly making chromatin more susceptible to DNA damage [10].

A brilliant model for ageing research is the yeast *Saccharomyces cerevisiae* [11]. Many stages and molecular signatures of ageing such as accumulation of oxidative damaging, involvement of mitochondria in the process, and connection with the nutrient response pathways have been revealed in this unicellular eukaryote [12–16]. At the same time the yeast cells are good models for chromatin research, mainly for studying the roles of linker histones. In contrast to the multiple linker histone subtypes in the higher eukaryotic

cells there is only one-copy gene (*HHO1*) for linker histone, Hho1p in *S. cerevisiae* [17]. Interestingly, though the gene is non-essential, its disruption leads to severe alterations in the higher-order chromatin structures during somatic growth, thus stating the need for further analyses of the exact roles and functions of linker histones during different molecular processes [18].

In the current study we searched for the roles which *S. cerevisiae* linker histone—Hho1p, could play in the propagation of the ageing process. The gene for this histone in yeast cells has been knocked-out and thus, linker histone-free strains were developed as suitable models for chromatin studies during cellular ageing. Our results show that the yeast cell cultures devoid of linker histones had slower growth in minimal media accompanied by well-demonstrated delay during their logarithmic growth. Moreover, the cells showed an increased survival rate during the whole period of cultivation. Studies on the overall chromatin organization of these mutant cells uncovered the existence of longer chromatin loop sizes and distorted higher-order chromatin organization accompanying the ageing process. Taken together our results underlay the importance of the linker histones and the higher-order chromatin structures in cellular ageing.

2. Materials and Methods

2.1. Yeast Strains and Growth Media. *Saccharomyces cerevisiae* strains used in the current study were derived from two genetic backgrounds DY2864 and FY1679-08a. The deletions of the gene for the linker histone *HHO1* were done according to the technique of [19]. The disruption cassette *hho1Δ::KlURA3* bore *URA3* gene from *Kluyveromyces lactis* flanked by two long sequences homologous to the outer ends of the chromosomal copy of *HHO1* gene [18]. The genotypes of both the wild type and *hho1delta* strains are listed below.

2.1.1. DY2864

DY2864 (wt): MATa his4-912δ-ADE2 his4-912δ lys2-128δ can1 trp1 ura3 ACT3.

DY2864 (hho1delta): MATa his4-912δ-ADE2 his4-912δ lys2-128δ can1 trp1 ura3 ACT3 ypl127C::K.L.URA3.

2.1.2. FY1679-08a

FY1679-08a (wt): MATa ura3-52/ura3-52 trp1Δ63/TRP1 leu2Δ1/LEU2 his3Δ200/HIS3 GAL2/GAL.

FY1679-08a (hho1delta): MATa ura3-52/ura3-52 trp1Δ63/TRP1 leu2Δ1/LEU2 his3Δ200/HIS3 GAL2/GAL ypl127C::K.L.URA3.

Chronological ageing assays were performed in SD media (1.7% yeast nitrogen base without amino acids and 2% glucose), supplemented with 20 μg/mL of the appropriate nutritional requirements according to the genotype of the strains. Cultivation was at 30°C in a water bath shaker for a period of twenty days. Additionally, monitoring of CLS of the studied yeast strains was done in rich media YPD, containing 1% Yeast extract, 2% Peptone and 2% Dextrose at 30°C.

2.2. Chronological Lifespan Assays. Assessment of cell growth in SD media was done by taking aliquots from the yeast cultures at eight different time points, indicated as 0th (assigned as initial), 1st, 3rd, 6th, 9th, 12th, 14th, and 19th days for subsequent spectrophotometric measurement of OD_{600} (Optical Density at 600 nm wavelength) together with counting the number of cells in a Nuebauer counting chamber. Quantitative measurements of colony forming units (CFUs) were also performed. 20 μL aliquots of the cultures were removed at 1st, 3rd, 5th, 9th, 12th, 14th, and 19th days diluted in sterile water, spread onto YPD plates (100 colonies per plate), and allowed to grow into colonies for 2 days at 30°C. The colonies were then counted and the number of CFUs per plate calculated. Percentage viability was calculated as in [20].

Three independent repetitions of all experiments were performed and the results were statistically analyzed by Students t-test at Microsoft Excel 2010 software.

2.3. Chromatin Structure Studies by Chromatin Comet Assay (ChCA). Chromatin loop organization was studied by the method of Chromatin Comet Assay (ChCA) [18, 21]. 300 μL from the chronologically ageing yeast cultures was gathered by centrifugation at 10 000 g for 1 min (Eppendorf microfuge). After washing in S-buffer (1 M Sorbitol, 25 mM NaH_2PO_4; pH 6.5) the cells were diluted to 10^5 cells/mL with the same buffer supplemented with appropriate concentration of the spheroplasting enzyme Zymolyase (Saikagaku Corp.). The cells were immediately mixed with 1.4% of low-gelling agarose (Sigma type II) and spread like microgels onto microscopic slides by the means of coverslips. Five min incubation at 10°C followed for solidification of the agarose-cell-gel suspensions and after removing the coverslips, the slides containing the microgels were processed for spheroplasting at 37°C for 15 min. All subsequent procedures were performed in neutral conditions as follows: after solidifying microgels and subsequent *in situ* nuclease digestion of spheroplasts slides were submerged in neutral lysis solution (146 mM NaCl; 30 mM EDTA; 10 mM Tris-HCl and 0.1% N-lauroylsarcozine, pH 7.5) for 20 min in a cold room at 10°C. Afterwards slides were washed for 15 min in 0.5 x TBE buffer (89 mM Tris; 89 mM Boric-acid; 5 mM EDTA, pH 8) and subjected to electrophoresis for 10 min at 0.45 V/cm in the same TBE buffer. After successive dehydration in 75% and 100% ethanol for 5 min each, the slides were left to air-dry.

Comets were observed under a Leitz epi-fluorescence microscope (Orthoplan, VARIO ORTHOMAT 2) using 450–490 nm band-pass filter following the staining of DNA with SYBR green I (Molecular Probes Inc, Eugene, OR, USA). Pictures were taken with a digital camera, Olympus μ800, at a resolution of 3 mpx. Images were bright-contrast processed using Adobe Photoshop CS 5.1. software.

The obtained results were quantified by measuring the parameter Comet length on Adobe Photoshop CS 5.1 and then calculated in kilobases as was published elsewhere [18].

Two independent repetitions of the ChCA experiments were done and results were analyzed statistically by GraphPad Prism 3.0 software.

3. Results and Discussion

3.1. The Lack of Saccharomyces cerevisiae Linker Histone Leads to Slower Growth Rate during CLS and at the Same Time to Increased Survival. Chronological lifespan of *S. cerevisiae* wild type and *hho1delta* strains were studied in SD media, recommended as an appropriate media for monitoring CLS of yeast cultures [20, 22] for a period of 20 days at 30°C. CLS assays were performed as cultures' optical densities were followed by spectrophotometric measurements at 600 nm wavelength (OD_{600}) and by counting the number of cells at certain time points during the whole period of cultivation. The obtained results were plotted as combined chart type graphs representing at one time the cultures' OD_{600} (lines) and the absolute number of cells counted in a Nuebauer counting chamber (bars) (Figure 1(a)). The time points selected for monitoring of the growth rate of the cultures were day 0 (assigned as initial or a dilution day), 1st day as a day representing the logarithmic phase of the cultural growth, 3rd day as a day marking the post diauxic phase, 6th day as the beginning of the stationary phase, 9th, 12th, 14th and 19th day as these four days strongly represent the stationary phase of our cultures. These particular time points were picked up according to other authors' data depicting the different stages of yeast CLS summarized in [20]. As seen in Figure 1(a) the mean OD_{600} for the wild type was 4 and for *hho1delta* cultures only 2.6; thus, *hho1delta* cells demonstrated 35% slower mean growth than the wild type. Moreover, *hho1delta* cells demonstrated an inability to reach the highest optical density of the wild type cultures but rather reached only 73% of the highest value of wild type OD_{600} at 3rd day (5.08). The number of cells (cells/mL) counted separately for each time point ascertained these results. Furthermore, they allowed quantification of the growth rate of the yeast cell cultures. Obviously, both the wild type and the mutant reached the highest OD_{600} at 3rd day; however, the mutant had fewer cells. These differences were statistically significant and highlighted the importance of the linker histone during yeast CLS in SD media. Moreover, the mutant cells had an expressed lag phase during its logarithmic growth seen on 1st day with the estimated mean $OD_{600} = 1.5$ for the mutant and mean $OD_{600} = 4.6$ for the wild type. Note that these differences appear regardless that both, the wild type and the mutant, had the same starting cell number (10^6 cell/mL) at the initial day. The dividing potential of *hho1delta* cells seemed somehow impeded in comparison to the normally growing wild type cultures. These data prompted a role of the yeast linker histone in the chronological lifespan and are in unison with the results of Downs et al. [23] demonstrating that cells lacking Hho1p have reduced replicative lifespan. Besides, for quite a long time in contrast to core histones the roles of linker histones in chromatin biology, ageing, and metabolism studies were merely neglected. Our results showing that Hho1p is required for the normal cellular growth in synthetic defined media together with recent data demonstrating Hho1p roles in chromatin compaction during stationary phase and moreover during overall somatic growth [18, 24] start adding new hues on the roles of this linker histone and probably other linker histones in the processes of ageing and longevity.

The CLS studies on the yeast cells lacking the gene for the linker histone continued with probing the cellular viability of these cells during the chronological lifespan. At every second day aliquots were taken from the growing cultures and 10^2 cells were plated on YPD plates, which were further incubated at 30°C for two days. CFUs were counted and percentage survival was assessed for each strain independently. Results are plotted as combined chart type graphs simultaneously representing the percentage of survival (lines) and the absolute number of colonies (bars) (Figure 1(b)). Surprisingly, *hho1delta* mutants exhibited better survival rates than the wild type. Notably, this better survival of the mutant was accompanied by higher heterogeneity in the obtained values suggesting higher diversity in the mutant cellular populations. We assume that this diversity probably can lead to different modes of cellular response toward environmental stress conditions during the chronological lifespan. Such stress conditions can be induced by ROS and acetic acid appearing during the processes of culturing [25]. This line of thoughts necessitates further studies in the field. Up until now our results show complicated and yet not so well-understood functions of the yeast linker histone in the chronological ageing. On one hand, the mutant grows more slowly, but at the same time some of its cells survive better than the wild type. These results prompt a complex way of survival of the cells without the linker histone, probably due to one of the main functions of Hho1p, namely, its participation in the maintenance of the genomic stability [23].

Well known in the field of the yeast ageing research is the fact that the switch between fermentation and respiration is accompanied by total rearrangement of the overall cellular and genomic programme of the yeast cells [26, 27]. Therefore, noting the differences between the wild type and the mutant during cellular growth in minimal media and the diverse modes of cellular survival in the mutant background we speculate that Hho1p is an epigenetic player in gene expression, participating in the switching on and off of specific genes during stationary phase. This hypothesis is quite logic but is not yet proved and needs more experiments in the future. High-throughput microarray analyses of *hho1delta* mutants revealed that the expression pattern of only 27 of all 6000 yeast genes has been slightly changed because of the mutation. However, important is the fact that these studies have been done in rich YPD media and thus do not correlate with cellular longevity studies of yeast in minimal media [28]. Moreover, even the authors of the above study have suggested a continuation of their work with the culturing of yeast *hho1delta* mutants under different conditions and

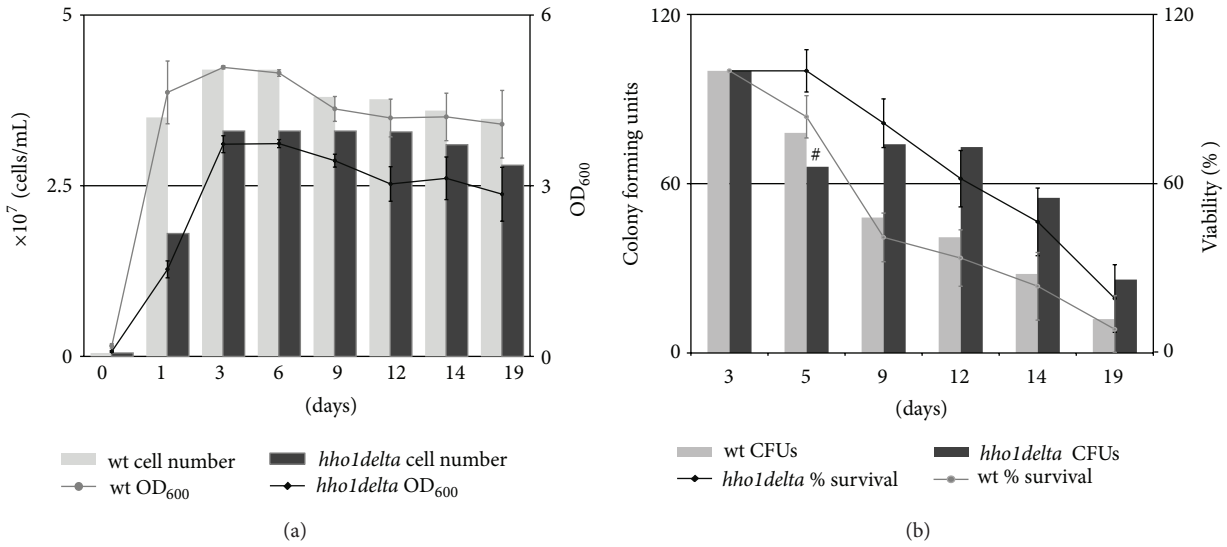

Figure 1: The lack of *S. cerevisiae* linker histone leads to slower growth rate during CLS and increased survival. (a) Yeast wild type and *hho1delta* cells were cultured in SD media for a period of 20 days. At certain time points aliquots were taken for spectrophotometric OD_{600} measurements and for counting the number of cells in a Nuebauer counting chamber. Results are presented as combined graphs comparing at one time the growth rate (lines) and the absolute number of cells at each time point (bars). Every time point stands for three independent repetitions of the experiments with STDVs (±). The difference between the wild type and *hho1delta* culture growth were statistically significant ($P < 0.01$). (b) The survival rate of *hho1delta* mutant cells and their progenitor wild type strains was assessed by plating 10^2 cells on YPD plates at every two days during the CLS 30°C for two days allowing cells to divide. CFUs were then counted and percentage survival was calculated by assuming the number of CFUs for each strain at 3rd day for 100% (lines). Additionally, the number of colonies was included in the graph (bars) thus allowing easy and comprehensible comparison between the CLS of wild type and *hho1delta* cells. $^{\#}P > 0.01$ was statistically insignificant only for CFUs at 5th day. At all other time points the differences between the wild type and *hho1delta* cultures were significant $P < 0.01$ and for the simplicity of the graph presentation are not marked on the figure.

then following changes in the overall gene expression programme.

In order to check whether the lack of the yeast linker histone leads to abnormalities in the ageing process in rich media, we incubated the studied yeast strains in YPD. The results are shown in Figures 1S and 2S (see Supplementary Materials available online at: http://dx.doi.org/10.1155/2013/437146) representing that there is no significant difference between the wild type and the deletion mutants. Growth rates (Figure 1S) and percentage survival (Figure 2S) demonstrated almost the same CLS of the studied cells in YPD which is in unison with the results of other authors presenting slightly changed gene expression patterns in *hho1delta* cells in the same media [28].

Regarding our data showing slower cellular growth and increased percentage survival of the knocked-out yeast cells in SD media in a time course of almost 20 days we decided to check whether Hho1p takes part in the building and maintaining of the higher-order chromatin structures during CLS. As chromatin is the platform on which all processes on the molecule of DNA take place, it is easy to make the assumption that higher-order chromatin structures participate in the processes of ageing. Therefore, we followed the way by which chromatin structure was changing during chronological lifespan.

3.2. Chromatin Comet Assay (ChCA) as a Powerful Tool for Monitoring Higher-Order Chromatin Organization during Ageing. As the method of Chromatin Comet Assay is not very common in ageing research, here we feel that some detailed explanations of how it is performed and what it studies are needed. The method has been developed with several modifications of the standard Comet Assay [29, 30]. The crucial point was to determine the optimal conditions for sensitive and correct visualization of the electrophoretic extension of chromatin loops from the nucleus after mild nuclease digestion (Figure 2(a)). The nucleases that we use in performing the method are MNase (micrococcal nuclease) and DNase I (deoxyribonuclease I), but any kind of DNA cutting enzyme can give reproducible results although with different meaning. Briefly, yeast cells are mixed with a spheroplasting enzyme, in our case Zymolyase, then with low-gelling agarose and are spread as microgels on microscopic slides. After 15 min of spheroplasting at 37°C the microgels are digested *in situ* with the nucleases and again are incubated for 1 min at 37°C. This step allows mild cuttings of chromatin which is dependent on the way chromatin is organized and compacted in the nucleus. A schematic drawing of the ChCA is shown in Figure 2(a) and allows easy following of the main steps of the methodology. The *in situ* nuclease digestion is followed by lysis of cell membranes, resulting in the turning of spheroplasts into nucleoids. During the next step, the

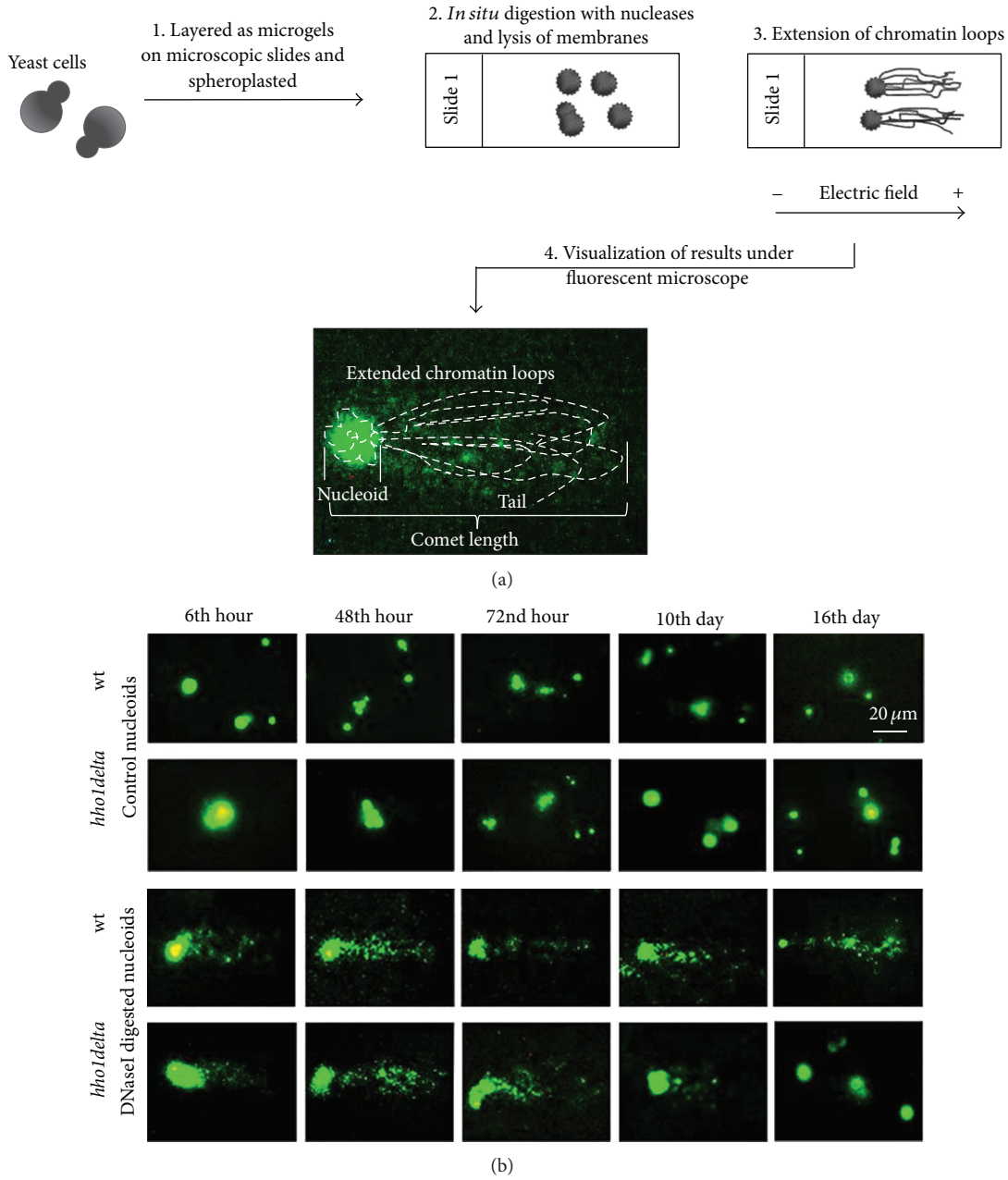

FIGURE 2: Chromatin Comet Assay (ChCA) performance and the logic behind its results. (a) A scheme of the method of (ChCA) is presented with subsequent crucial steps marked with numbers. The method is a modification of the conventional Comet Assay technique and allows easy and fast visualization of higher-order chromatin structures at a single cell level. (b) Representative images of wild type and *hho1delta* mutant comets. The white bar stands for 20 μm.

electrophoresis, under the electric field chromatin loops from the nucleoids protrude toward the anode and thus form a comet-like image (Figure 2(a)). Note that because of the mild nuclease digestion the comet tail consists of chromatin loops, that is, chromatin structures with high molecular weight, around 200–300 kb in size [18, 21], which is far bigger than the DNA fragments obtained in experiments for assessing nuclease sensitivity reaching to nucleosome ladders. This is the reason for accepting ChCA as a method for higher-order chromatin structure studies, more precisely for chromatin loop structure monitoring at a single-cell level. The cellular comets contain a head which stands for the DNA with an intact structure and a tail extended toward the anode. In the tail are the chromatin loops which are relaxed due to several cuts in DNA. Different ways of Comet Assay data quantification exist including measurement of the length of the comet, the length of the comet tail, the intensity of DNA in the tail, and/or the intensity of DNA in the head. When ChCA

is performed these parameters are used for quantitative data analyses, but more often the length of the tail and the length of the comet are measured on image processing software programmes and after that are calculated in kilobases in order to estimate the chromatin loops length [21].

3.3. The Yeast Linker Histone Maintains Chromatin Loop Structures during Chronological Lifespan. The above experiments on wild type and *hho1delta* yeast cells demonstrating the way the mutant and its progenitor wild type strain grow and survive through their CLS allowed us to choose time points for further analyses by Chromatin Comet Assay. We have chosen five time points: the 6th hour, the 48th, the 72nd hour, and 10th and 16th days. Yeast cells taken at these time points were further used for the ChCA and aimed to reveal chromatin loop structure reorganization during ageing. The nuclease used during these particular ChCA experiments was DNase I. Generally, it makes single-stranded DNA cuts with a preference to active chromatin domains [1] and thus allows relaxation of chromatin loops and probing spatial chromatin organization. Representative images of ChCA for each strain are given in Figure 2(b). Control nucleoids for both strains at the studied time points are presented together with chromatin comet images. The wild type nucleoids had a mean diameter around 20 μm while the mutant nucleoids appeared 1.6 times more swollen than the wild type (33 μm mean diameters for *hho1delta* controls). The performed analysis of Variance (GraphPad Prizm software) proved that this increase in the mean diameters of the mutant nucleoids is significant ($P < 0.01$), thus arguing for more relaxed chromatin organization in the yeast nuclei lacking the linker histone. Furthermore, the wild type increased their nuclear diameters with ageing to 40% larger diameter in comparison with the beginning of their CLS (from 1st day—mean diameters 19 μm till 16th day—mean diameters 30 μm). On the contrary the mutant cells rearranged their nucleoid size in a reverse order (Figure 2(b), *hho1delta* controls). Their diameters shrank slightly from 36 μm at 1st day to 25–29 μm at 16th day and got closer to the diameters of the wild type nuclei at the last days of ChCA studies 16th. This is arguing for loss of normal nuclear structure along the ageing process. Moreover, in the mutant cells at 3rd day (72nd hour) we had a sharp drop in the diameters of the nucleoids (down to 10 μm) which strengthens our hypothesis that this particular time point is crucial for the mutant cells and marks total rearrangement in the genome and the expression of specific genes for adaptation of these cells to the switch between the postdiauxic phase and the stationary phase. Further studies are required to clarify these changes in order to explain the role of linker histone in the yeast chronological ageing.

Chromatin loop structures were further analysed by digestion of the nucleoids with DNase I. With the time of cultivation up until the 3rd day both the wild type and *hho1delta* chromatins demonstrated an increase in the length and the intensity of the comets. Markedly, the dynamics of chromatin loop structures, that is, the appearance and the length of the obtained comets, for the two strains demonstrated some differences, though from the 6th till the 48th hours the wild type chromatins exhibited looser and more susceptible to the action of DNase I chromatin. This is expected having in mind that with the time of the ageing process chromatin starts losing its normal characteristics and becomes more relaxed (Figure 2(b), WT DNase I), and the logarithmically growing mutant cells (6th and 48th hour) produced longer comets than the wild type Figure 2(b). This proved that more chromatin loops were relaxed and extended form the mutant nucleoids than in the wild type, which is in good correlation with other data showing that the yeast linker histone is necessary for chromatin compaction during the overall growth of these cells and its lack leads to total rearrangement of chromatin loop structures making them less compacted and more susceptible to the action of nucleases [18, 31]. Surprisingly, though, after the 72nd hour (3rd day) till the last 16th day the mutant comets started to decrease in size till 16th day when empty and faintly visible nuclear "shades" appeared. This suggests total loss of chromatin structure. On the other hand, the decrease in the comet lengths in the wild type at these particular time points was stable and did not lead to total disappearance of the comet images, nor to observation of nuclear "shades."

ChCA data quantification was done by measuring the length of the whole comet and sizing of chromatin loops as published in [18]. Results are shown in Figure 3(a) and demonstrate 12% increase in wild type comet lengths till the 48th hour when cells were already in postdiauxic phase. Then during stationary phase the wild type chromatin became more disordered resulting in more compacted and less susceptible to DNase I chromatin organization. ChCA calculations showed that the chromatin of logarithmically growing wild type cells was organized in loops with approximate length of 200 kb which slightly increased during the postdiauxic phase extending to 225 kb, then decreased to 100–130 kb at the 72nd hour and the 10th day, probably as a result of the adaptation of cells to stationary phase. This adaptation requires activation of specific genes necessary for proper adaptation of cells from fermentation to respiration when cultured in minimal media [32]. At the 16th day we observed higher heterogeneity but the size of the chromatin loops was around 170–200 kb.

Cells without the linker histone demonstrated much more disordered chromatin organization on the first day. At the time when cells set off their logarithmic growth the comet length, that is, the size of the extended chromatin loops was around 230 kb slightly bigger than the wild type (Figures 3(a) and 3(b)). This slight 10% increase in the comet length suggests a more relaxed, less compacted chromatin in the lack of the linker histone. Previous chromatin studies of logarithmically growing *hho1delta* cells are correspondingly consistent with these observations [18]. With the entry of cells in postdiauxic phase, that is, at the 48th hour of cultivation, the difference in chromatin loop organization between *hho1delta* mutant and the wild type increased to 25%. This shows that with the ageing mutant cells reorganized their chromatin structures in a more relaxed manner allowing extension of longer chromatin loops (290 kb in length). The switch between the post-diauxic phase and the stationary phase (72nd hour and 10th day) demonstrated a drop in

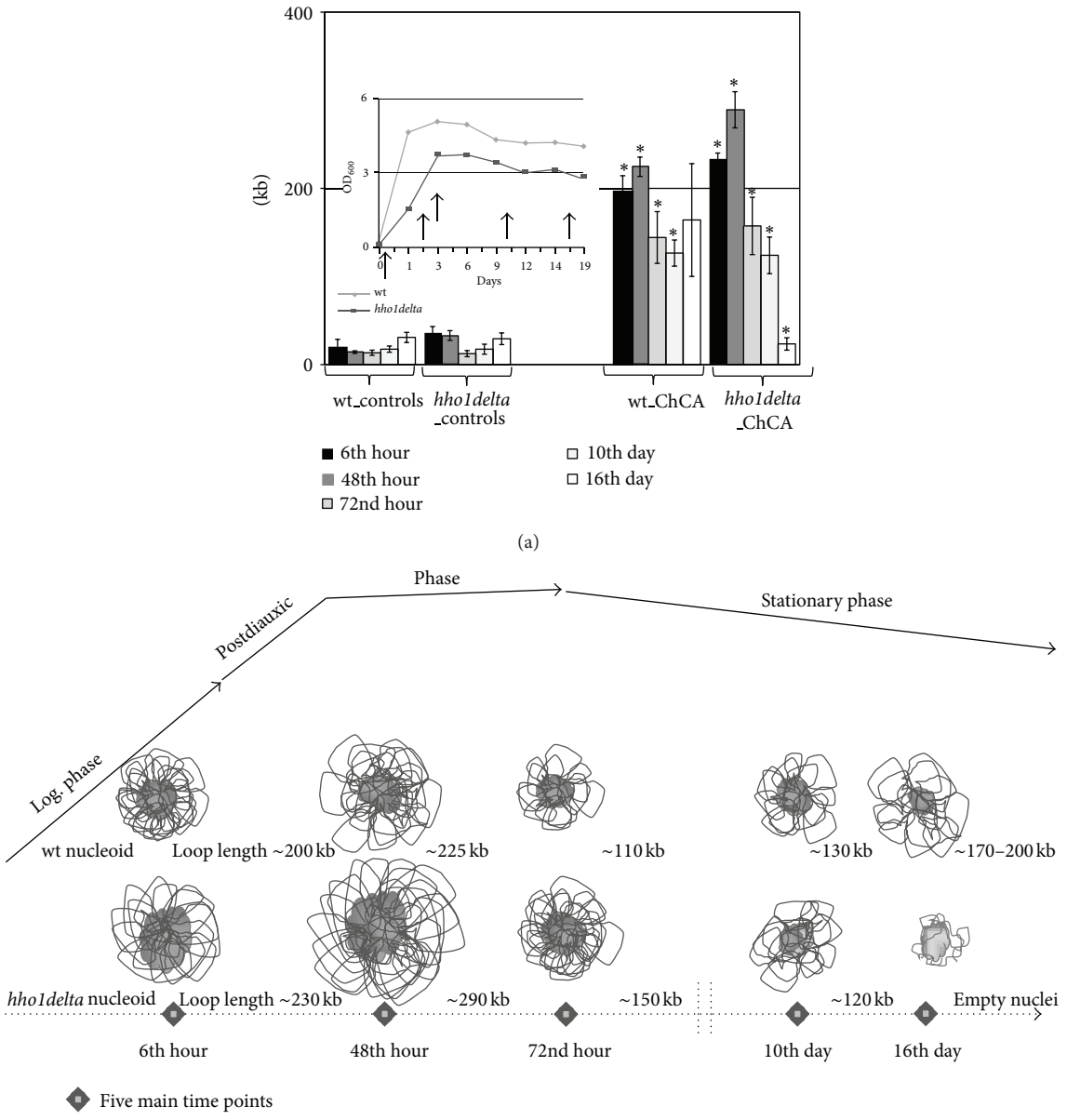

Figure 3: Yeast linker histone maintains and preserves the higher-order chromatin structure organization during chronological ageing. Yeast mutants lacking the linker histone were subjected to ChCA and were compared to the wild type. Chromatin structure was studied at five time points designated as main during the CLS of yeast cells in SD media. (a) ChCA results quantification-measurement of comet length and calculation of chromatin loop lengths in kilobases. The five studied time points are marked on the growth curve built in the figure. The results are presented as bars showing the mean comet length values ± STDVs. The statistical analyses proved these results as significant $^{*}P < 0.01$. (b) A model describing changes in the higher-order chromatin organization during chronological ageing. On the time course of the chronological lifespan of yeast cells in minimal media are marked five main time points (diamond shape) and their reference to the CLS phases. Wild type and *hho1delta* nucleoids are drawn with the hypothetical chromatin loop organization changes during ageing. The lack of the linker histone totally abolishes normal chromatin ageing and thus influences overall cellular behaviour during the process.

the comet length to 150–120 kb. This tendency kept on going leading to empty nuclei and nuclear "shades" at the end of the culture.

Chromatin is the background and the driving force for activation and deactivation of genetic information and definitely should be part of the ageing process [33, 34]. Little is known about the higher-order chromatin organization and dynamics during ageing which makes our results informative for the dynamics in these chromatin structures during this process. The presumptive model drawn on Figure 3(b) gives a comprehensible picture of general chromatin loop organization during ageing. This model allows explanation of the differences which were found between the wild type and the cells without linker histone. Some authors [35] have

demonstrated roles of linker histones during senescence by showing that they are lost with the time of the ageing of cells. With our ChCA results of chronologically ageing yeast cells with and without the linker histone we were able to follow the nuclear and chromatin dynamics along the ageing process.

4. Conclusions

Our study has unveiled the role of the yeast linker histone Hho1p in the preservation and maintenance of the higher-order chromatin structures during ageing. Therefore, we think that Hho1p participates in the regulation and governing of the CLS of yeast and can be an active epigenetic player in cellular adaptation during this process. It is involved in the switch between logarithmic growth and the postdiauxic phase and assures the preservation of the genomic stability. These results highlight the epigenetic significance of the linker histones in holding the genomic resilience against stress and in preserving the normal nuclear morphology. Moreover, this study marks the potential of linker histones as compensatory epigenetic players in genetic disorders including syndromes of premature ageing like Hutchinson Gilford Progeria.

Authors' Contribution

K. Uzunova and M. Georgieva have equally contributed to this work.

Acknowledgments

This work was supported by the Bulgarian Science Fund: DMU 02/8 to Milena Georgieva and Katya Uzunova and DID 02/35 to Milena Georgieva and George Miloshev.

References

[1] A. Wolffe, *Chromatin Structure and Function*, Oxford Press, London, UK, 2nd edition, 1995.

[2] T. Kouzarides and S. Berger, "Chromatin modifications and their mechanism of action," in *Epigenetics*, D. Allis, T. Jenuwein, and D. Reinberg, Eds., pp. 191–209, Cold Spring Harbor Lab Press Press, Cold Spring Harbor, NY, USA, 2007.

[3] J. T. Bell, P. Tsai, T. Yang et al., "Epigenome-wide scans identify differentially methylated regions for age and age-related phenotypes in a healthy ageing population," *PLoS Genetics*, vol. 8, no. 4, Article ID e1002629, 2012.

[4] R. Burgess, T. Misteli, and P. Oberdoerffer, "DNA damage, chromatin, and transcription: the trinity of aging," *Current Opinion in Cell Biology*, vol. 24, pp. 724–730, 2012.

[5] S. Han and A. Brunet, "Histone methylation makes its mark on longevity," *Trends in Cell Biology*, vol. 22, no. 1, pp. 42–49, 2012.

[6] G. Trencsenyi, G. Nagy, F. Bako, P. Kertai, and G. Banfalvi, "Incomplete chromatin condensation in enlarged rat myelocytic leukemia cells," *DNA and Cell Biology*, vol. 31, no. 4, pp. 470–478, 2012.

[7] T. J. Maresca and R. Heald, "The long and the short of it: linker histone H1 is required for metaphase chromosome compaction," *Cell Cycle*, vol. 5, no. 6, pp. 589–591, 2006.

[8] K. Hizume, S. H. Yoshimura, and K. Takeyasu, "Linker histone H1 per se can induce three-dimensional folding of chromatin fiber," *Biochemistry*, vol. 44, no. 39, pp. 12978–12989, 2005.

[9] V. A. T. Huynh, P. J. J. Robinson, and D. Rhodes, "A method for the in vitro reconstitution of a defined "30 nm" chromatin fibre containing stoichiometric amounts of the linker histone," *Journal of Molecular Biology*, vol. 345, no. 5, pp. 957–968, 2005.

[10] G. Pegoraro, N. Kubben, U. Wickert, H. Göhler, K. Hoffmann, and T. Misteli, "Ageing-related chromatin defects through loss of the NURD complex," *Nature Cell Biology*, vol. 11, no. 10, pp. 1261–1269, 2009.

[11] L. Váchová, M. Čáp, and Z. Palková, "Yeast colonies: a model for studies of aging, environmental adaptation, and longevity," *Oxidative Medicine and Cellular Longevity*, vol. 2012, Article ID 601836, 8 pages, 2012.

[12] A. Grzelak, E. Macierzyńska, and G. Bartosz, "Accumulation of oxidative damage during replicative aging of the yeast *Saccharomyces cerevisiae*," *Experimental Gerontology*, vol. 41, no. 9, pp. 813–818, 2006.

[13] V. Palermo, C. Falcone, and C. Mazzoni, "Apoptosis and aging in mitochondrial morphology mutants of *S. cerevisiae*," *Folia Microbiologica*, vol. 52, no. 5, pp. 479–483, 2007.

[14] C. Mazzoni, E. Mangiapelo, V. Palermo, and C. Falcone, "Hypothesis: is yeast a clock model to study the onset of humans aging phenotypes?" *Frontiers in Oncology*, vol. 2, article 203, 2012.

[15] M. Ždralević, N. Guaragnella, L. Antonacci, E. Marra, and S. Giannattasio, "Yeast as a tool to study signaling pathways in mitochondrial stress response and cytoprotection," *The Scientific World Journal*, vol. 2012, Article ID 912147, 10 pages, 2012.

[16] S. Johnson, P. Rabinovitch, and M. Kaeberlein, "mTOR is a key modulator of ageing and age-related disease," *Nature*, vol. 493, no. 338, pp. 338–345, 2013.

[17] G. Miloshev and M. Georgieva, "The linker histone and chromatin of yeast *Saccharomyces cerevisiae*," in *Histones Class, Structure and Function*, C. H. Shen, Ed., pp. 59–75, Nova, New York, NY, USA, 2012.

[18] M. Georgieva, A. Roguev, K. Balashev, J. Zlatanova, and G. Miloshev, "Hho1p, the linker histone of *Saccharomyces cerevisiae*, is important for the proper chromatin organization *in vivo*," *Biochimica et Biophysica Acta*, vol. 1819, no. 5, pp. 366–374, 2012.

[19] A. Wach, A. Brachat, C. Rebischung et al., "5 PCR-based gene targeting in *Saccharomyces cerevisiae*," *Methods in Microbiology*, vol. 26, pp. 67–83, 1998.

[20] P. Fabrizio and V. D. Longo, "The chronological life span of *Saccharomyces cerevisiae*," *Aging Cell*, vol. 2, no. 2, pp. 73–81, 2003.

[21] M. Georgieva, M. Harata, and G. Miloshev, "The nuclear actin-related protein Act3p/Arp4 influences yeast cell shape and bulk chromatin organization," *Journal of Cellular Biochemistry*, vol. 104, no. 1, pp. 59–67, 2008.

[22] D. L. Smith Jr., J. M. McClure, M. Matecic, and J. S. Smith, "Calorie restriction extends the chronological lifespan of *Saccharomyces cerevisiae* independently of the Sirtuins," *Aging Cell*, vol. 6, no. 5, pp. 649–662, 2007.

[23] J. A. Downs, E. Kosmidou, A. Morgan, and S. P. Jackson, "Suppression of homologous recombination by the *Saccharomyces cerevisiae* linker histone," *Molecular Cell*, vol. 11, no. 6, pp. 1685–1692, 2003.

[24] G. Schäfer, C. R. E. McEvoy, and H. Patterton, "The *Saccharomyces cerevisiae* linker histone Hho1p is essential for chromatin compaction in stationary phase and is displaced by transcription," *Proceedings of the National Academy of Sciences of the United States of America*, vol. 105, no. 39, pp. 14838–14843, 2008.

[25] M. Breitenbach, M. Jazwinski, and P. Laun, *Aging Research in Yeast*, vol. 57 of *Subcellular Biochemistry*, Springer, Berlin, Germany, 2012.

[26] A. P. Gasch, P. T. Spellman, C. M. Kao et al., "Genomic expression programs in the response of yeast cells to environmental changes," *Molecular Biology of the Cell*, vol. 11, no. 12, pp. 4241–4257, 2000.

[27] P. A. Padilla, E. K. Fuge, M. E. Crawford, A. Errett, and M. Werner-Washburne, "The highly conserved, coregulated *SNO* and *SNZ* gene families in *Saccharomyces cerevisiae* respond to nutrient limitation," *Journal of Bacteriology*, vol. 180, pp. 5718–5726, 1998.

[28] K. Hellauer, E. Sirard, and B. Turcotte, "Decreased expression of specific genes in yeast cells lacking histone H1," *The Journal of Biological Chemistry*, vol. 276, no. 17, pp. 13587–13592, 2001.

[29] P. L. Olive, J. P. Banat, and R. E. Durand, "Heterogeneity in radiation induced DNA damage and repair in tumor and normal cells using the "Comet" assay," *Radiation Research*, vol. 122, pp. 86–89, 1990.

[30] A. Hartmann, E. Agurell, C. Beevers et al., "Recommendations for conducting the *in vivo* alkaline Comet assay," *Mutagenesis*, vol. 18, no. 1, pp. 45–51, 2003.

[31] J. M. Bryant, J. Govin, L. Zhang, G. Donahue, B. F. Pugh, and S. L. Berger, "The linker histone plays a dual role during gametogenesis in *Saccharomyces cerevisiae*," *Molecular and Cellular Biology*, vol. 32, no. 14, pp. 2771–2783, 2012.

[32] M. Werner-Washburne, E. L. Braun, M. E. Crawford, and V. M. Peck, "Stationary phase in *Saccharomyces cerevisiae*," *Molecular Microbiology*, vol. 19, no. 6, pp. 1159–1166, 1996.

[33] R. Zhang and P. D. Adams, "Heterochromatin and its relationship to cell senescence and cancer therapy," *Cell Cycle*, vol. 6, no. 7, pp. 784–789, 2007.

[34] X. Ye, B. Zerlanko, R. Zhang et al., "Definition of pRB- and p53-dependent and -independent steps in HIRA/ASF1a-mediated formation of senescence-associated heterochromatin foci," *Molecular and Cellular Biology*, vol. 27, no. 7, pp. 2452–2465, 2007.

[35] R. Funayama, M. Saito, H. Tanobe, and F. Ishikawa, "Loss of linker histone H1 in cellular senescence," *Journal of Cell Biology*, vol. 175, no. 6, pp. 869–880, 2006.

Hindawi Publishing Corporation
Oxidative Medicine and Cellular Longevity
Volume 2013, Article ID 504230, 17 pages
http://dx.doi.org/10.1155/2013/504230

Review Article

The Proapoptotic Effect of Traditional and Novel Nonsteroidal Anti-Inflammatory Drugs in Mammalian and Yeast Cells

Gianluca Farrugia and Rena Balzan

Department of Physiology and Biochemistry, Faculty of Medicine and Surgery, University of Malta, Msida MSD 2080, Malta

Correspondence should be addressed to Gianluca Farrugia; gianluca.farrugia@gmail.com

Received 14 May 2013; Accepted 8 July 2013

Academic Editor: Paula Ludovico

Nonsteroidal anti-inflammatory drugs (NSAIDs) have long been used to treat pain, fever, and inflammation. However, mounting evidence shows that NSAIDs, such as aspirin, have very promising antineoplastic properties. The chemopreventive, antiproliferative behaviour of NSAIDs has been associated with both their inactivation of cyclooxygenases (COX) and their ability to induce apoptosis *via* pathways that are largely COX-independent. In this review, the various proapoptotic pathways induced by traditional and novel NSAIDs such as phospho-NSAIDs, hydrogen sulfide-releasing NSAIDs and nitric oxide-releasing NSAIDs in mammalian cell lines are discussed, as well as the proapoptotic effects of NSAIDs on budding yeast which retains the hallmarks of mammalian apoptosis. The significance of these mechanisms in terms of the role of NSAIDs in effective cancer prevention is considered.

1. Introduction

In recent years, there has been a growing interest in aspirin and other nonsteroidal anti-inflammatory drugs (NSAIDs) because of their promising antineoplastic properties. Epidemiological, clinical, and experimental evidence strongly indicates that NSAIDs exert a significant chemopreventive, antiproliferative effect on several types of cancer cells (see Table 1). Much of the research concerning the antineoplastic effects of NSAIDs has focused on the effect of aspirin in large bowel cancers, with comparatively fewer studies carried out on the chemopreventive effects of other NSAIDs [1]. In fact, aspirin stands as the most widely studied pharmacological agent for the chemoprevention of colorectal malignancies, with numerous clinical trials being carried out to examine its role in the prevention of adenomas, colorectal carcinomas, and inherited colorectal neoplasias such as the Lynch syndrome and familial adenomatous polyposis (FAP) [2]. Such focus on aspirin may be due, in large part, to the increasingly high prevalence and social impact of human colorectal cancer in recent years [2]. It is also due to the simple fact that long-term aspirin use is already widely practised among patients for the prevention of cardiovascular events such as thrombosis and neurovascular events such as stroke, thus providing a convenient opportunity for researchers to study its other long-term chemopreventive effects. In fact, major findings of aspirin's anticancer effects in humans are also derived from clinical trial data originally compiled for the study of its antithrombotic effects [3, 4]. Aspirin's affordability and ease of access, together with its relatively reduced side effects with respect to other traditional NSAIDs [5], have also helped to increase its appeal as a potential chemopreventive agent and target in anticancer studies.

Nevertheless, a considerable number of investigations have shown that other NSAIDs including sulindac [6–8], indomethacin [9, 10], ibuprofen [11, 12], naproxen [13], and diclofenac [14–16] also exhibit significant antineoplastic behaviour in mammalian cancer cells. Additionally, recent studies have increasingly focused on the chemopreventive properties of a new NSAID class referred to as modified NSAIDs. These are essentially traditional NSAIDs which can either have nitric oxide- (NO-) donating moieties, hydrogen sulphide- (H_2S-) donating moieties, or phosphate moieties covalently attached to the –COOH site *via* aromatic or

aliphatic spacer molecules, as shown in Figure 1. The resulting modified NSAID classes, known as NO-donating NSAIDs (NO-NSAIDs), H_2S-donating NSAIDs (HS-NSAIDs), and phospho-NSAIDs, respectively, have all been shown to be far less toxic than their NSAID precursors and several times more potent in terms of antineoplastic efficacy [17–22]. The exceedingly potent anti-neoplastic properties of novel NSAID chimeras, which are characterized by their possession of both NO- and H_2S-donating moieties (see Figure 1), have also begun to attract significant attention [23, 24].

The mechanistic pathways which mediate the anti-neoplastic effects of traditional and modified NSAIDs are still not fully understood. It has been postulated that the antiproliferative effect of NSAIDs on malignant cells involves the inhibition of proinflammatory COX activity [25] and prostaglandin formation [26]. However, additional evidence shows that NSAIDs can induce apoptotic cell death in tumour cells [27] *via* pathways that are largely independent of COX [6, 28, 29]. The elucidation of apoptotic mechanisms underlying the chemopreventive effect of NSAIDs has long been the focus of intense research using a broad range of experimental models, including whole mammalian specimens, human cancer cell lines, and *Saccharomyces cerevisiae* cells.

1.1. Yeast Cells as a Model for the Study of the Proapoptotic Effects of NSAIDs. Yeast cell species, such as *Saccharomyces cerevisiae*, are among the preferred and extensively used experimental models for the study of programmed cell death associated with ageing, disease, and cancers in living organisms. This is partly because yeast cells retain many core elements of mammalian cell processes such as apoptosis [30]. Additionally, these primitive eukaryotes have a number of important advantages over complex mammalian cell models. Yeast cells are relatively inexpensive and easy to handle, with a relatively brief lifespan that permits rapid generation of experimental results in a shorter span of time. Moreover, the yeast cell genome is very well characterised and relatively easy to manipulate, allowing for the ready availability of yeast mutant strains for experimental studies. Overall, these features collectively account for the successful use of budding yeast as a model organism for the study of molecular pathways underlying mammalian pathologies such as cancer.

These same advantages of the yeast cell experimental model also account for its wide use in the study of proapoptotic pathways underlying the anti-neoplastic behaviour of antitumour drugs such as paclitaxel, bleomycin, valproate, and arsenic [31]. These compounds have been studied extensively in yeast cells in an effort to improve anticancer strategies in human patients. Likewise, *S. cerevisiae* budding yeast cells have also been used to study the growth inhibitory, proapoptotic effects of NSAIDs such as aspirin [32] and diclofenac [33].

The study of the proapoptotic effects of NSAIDs in yeast models is still a relatively new concept, with far fewer studies having been carried out in yeast with respect to mammalian cells. Regardless, evidence acquired thus far from yeast studies of NSAIDs such as aspirin has already yielded valuable insights into their proapoptotic behaviour, highlighting factors which play key roles in NSAID-induced death (such as reactive oxygen species (ROS) and mitochondrial dysfunction). In fact, compelling evidence has shown that *S. cerevisiae* cells constitute a powerful model for the screening and development of NSAIDs and other proapoptotic drugs designed for use in human cancer patients, overcoming the problem of cell specificity in the design of antitumour compounds [31], whilst also serving as an inexpensive model to initially test the effect of antitumour drugs before assaying them in more relevant mammalian systems. Therefore, yeast cells clearly serve an important role as a complementary experimental model to mammalian cells in the study and elucidation of NSAID-induced mechanisms of apoptosis.

In this review, important biomolecular pathways triggered by traditional and novel NSAIDs which lead to the induction of apoptosis in mammalian cell lines and in *S. cerevisiae* yeast cells will be discussed. The significance of these proapoptotic mechanisms, in the context of the role NSAIDs may play in the design of more effective cancer prevention strategies, is also considered.

Table 1: Human cancer cell targets of the proapoptotic effects of prominent traditional and modified NSAIDs.

NSAID type	Target cell type [references]
Traditional NSAIDs	
Aspirin	Colon cancer cells [34–36], leukaemia cells [37, 38], cervical cancer cells [39, 40], gastric cancer cells [41–44], hepatocellular carcinoma cells [45, 46], endometrial cancer cells [29], neuroblastoma cells [47]
Indomethacin	Colon cancer cells [7, 35], Gastric cancer cells [44], Endometrial cancer cells [29]
Sulindac	Colon cancer cells [6, 7, 48, 49], prostate cancer cells [48], hepatocellular carcinoma cells [8], lung cancer cells [50]
Ibuprofen	Colon cancer cells [51]
Diclofenac	Neuroblastoma cells [15], melanoma cells [16]
Tolfenamic Acid	Prostate cancer cells [52]
Modified NSAIDs	
NO-Aspirin	Pancreatic cancer cells [53], colon cancer cells [17, 54–58]
NO-sulindac	Colon cancer cells [17], melanoma cells [59]
NO-ibuprofen	Colon cancer cells [17]
NOSH-aspirin	Colon cancer cells [24]
Phosphoaspirin	Colon [19, 21, 56], pancreatic [21], and breast [21] cancer cells
Phosphosulindac	Colon, pancreatic, and breast cancer cells [21]
HS-aspirin	Colon cancer cells [22], breast cancer cells [60]
HS-ibuprofen	Colon cancer cells [22]
HS-naproxen	Colon cancer cells [22]
HS-sulindac	Colon cancer cells [22]

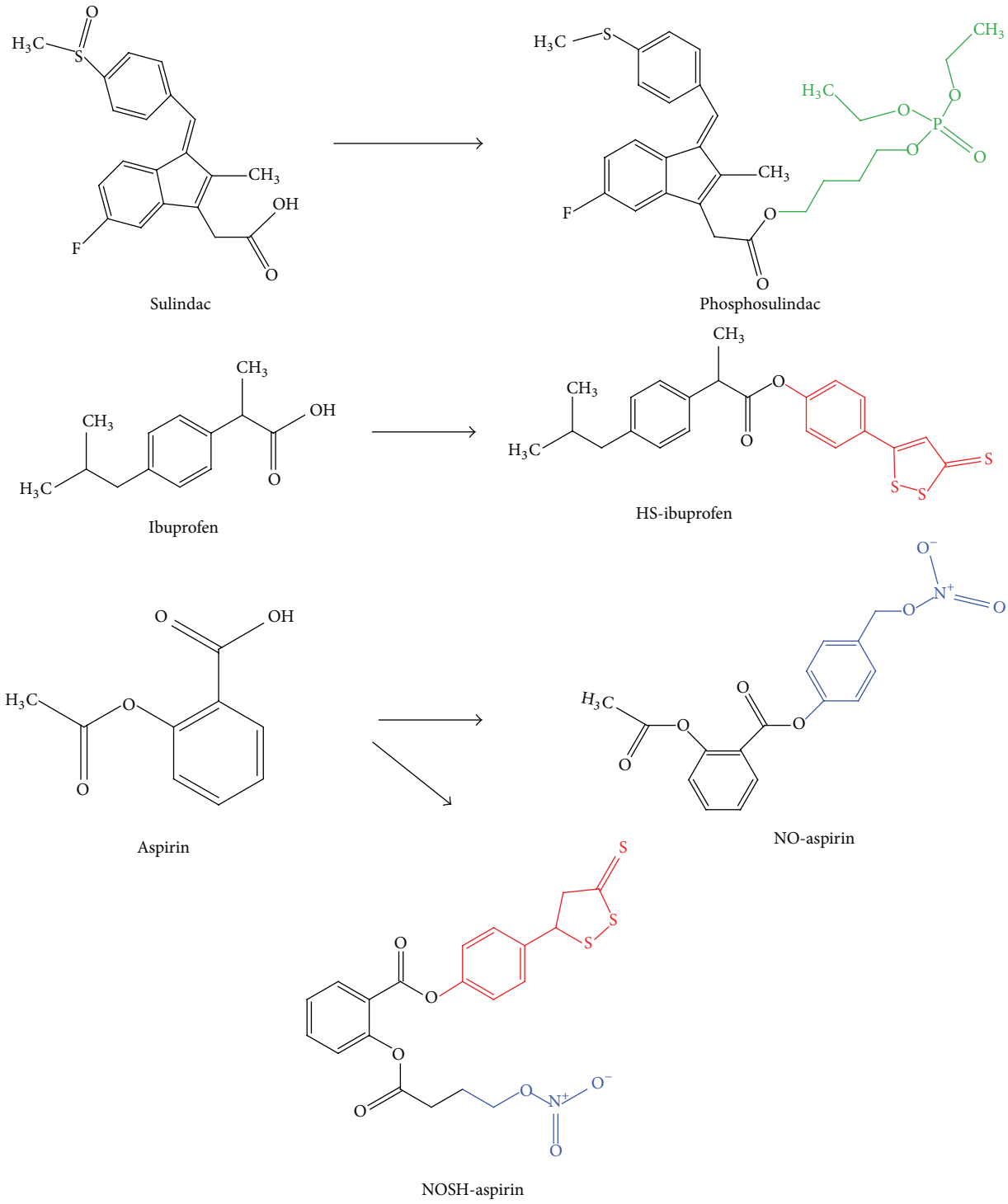

Figure 1: Chemical structures of modified NSAIDs and their traditional NSAID precursors. Phosphosulindac, which exemplifies phospho-NSAIDs, consists of the sulindac molecule linked at the –COOH site to a phosphate group *via* an aliphatic spacer molecule (both shown in green). In the HS-NSAID known as HS-ibuprofen, an aromatic spacer molecule links an H_2S-releasing dithiolethione group (both shown in red) to the ibuprofen structure. Similarly, the NO-NSAID NO-aspirin is composed of an NO-releasing-NO_2 group and an aromatic spacer molecule (both shown in blue) which is linked to the –COOH group of aspirin. Finally, the modified NSAID chimera known as NOSH-aspirin is characterized by the aspirin structure linked *via* two separate spacer molecules to both a H_2S-releasing moiety (shown in red) and an NO-releasing moiety (shown in blue).

2. NSAID-Induced COX Inhibition and Apoptotic Cell Death

The cyclooxygenase isoforms COX-1 and COX-2, both of which are key requirements for the synthesis of prostaglandins in mammalian cells, constitute the best defined pharmacological targets of NSAIDs such as aspirin [61, 62]. Thus, it has long been postulated that the chemopreventive effect of NSAIDs is mediated by their ability to inactivate COX-enzymes, causing inhibition of prostaglandin synthesis and consequent suppression of both tissue inflammation and cell proliferation, two conditions heavily associated with tumour formation [25]. In fact, both prostaglandins and COX enzymes, particularly COX-2, are implicated in tumorigenesis [1, 2, 63, 64] and have been observed in high quantities in several types of human tumours, including colorectal carcinomas [65–69]. Moreover, prostaglandins such as PGE_2 are known to promote angiogenesis, alter cellular immunity, increase both proliferation and invasiveness of cells, and enhance cellular resistance to apoptosis [2, 68, 70].

It has been shown that deletion of receptors for PGE_2 confers resistance to both polyp and cancer formation [71]. Similarly, disruption of COX-2 activity was found to reduce the incidence of polyp [72, 73] and aberrant crypt foci formation [74] in the intestines of rodent models. Inhibition of COX-2 has also been shown to be effective in preventing the formation of human colorectal adenomas [75, 76] and oesophageal squamous cell carcinoma [64]. Thus, inhibition of COX-2-dependent prostaglandin synthesis is thought to mediate, at least in part, the tumour-suppressive, antiproliferative effects of NSAIDs such as the suppression of angiogenesis and the induced lowering of resistance to apoptosis. In fact, inhibition of invasive tumour formation in NSAID-treated mouse models has been associated with decreased cellular levels of PGE_2 [26].

The anti-neoplastic behaviour of NSAIDs is also associated with their ability to actively induce apoptosis in malignant cells. However, the means by which COX-2 inhibition could possibly mediate NSAID-induced cancer cell apoptosis has long been the subject of debate [77, 78]. As such, there is no clear evidence implicating direct involvement of prostaglandins in NSAID-induced apoptosis, which suggests that prostaglandins do not directly mediate NSAID-induced death [77–79]. In fact, studies have indicated that aspirin-induced apoptosis in mouse [80] and human [81] cancer cells can occur independently of prostaglandin inhibition. Similarly, Chan and coworkers [7] demonstrated that apoptosis induced by sulindac and indomethacin in mammalian HCT116 and SW480 colon cancer cell lines did not depend on prostaglandin depletion since supplementation of these same cells with prostaglandins failed to protect them from apoptosis. However, this same study did present evidence of COX-2-dependent apoptosis induced by these NSAIDs. The authors suggested that cellular accumulation of the prostaglandin precursor arachidonic acid, brought about by the NSAID-induced inhibition of COX-2, caused cancer cell apoptosis by stimulating sphingomyelinase-mediated synthesis of ceramide [7], which is a proapoptotic molecule [82]. Arachidonic acid accumulation in cancer cells also induces ROS accumulation [83], mitochondrial permeability transition, and cytochrome *c* release [84], all of which lead to apoptotic cell death.

3. COX-Independent NSAID-Induced Apoptotic Cell Death

The proapoptotic effects underlying the chemopreventive potential of NSAIDs cannot be accounted for by COX inhibition alone. Firstly, NSAIDs have been shown to inhibit proliferation and induce apoptosis in malignant cell lines which do not express either COX-1 or COX-2, as observed in cyclooxygenase-null mouse embryo fibroblasts [85] and human colon cancer cells [28, 81, 86]. Furthermore, NSAID compounds which cannot inactivate COX-2, such as sulindac sulfone, a metabolite of sulindac [87], have been shown to induce apoptosis of gastric tumour cells [88] and inhibit colon tumour formation in rodents [89, 90]. Additionally, NSAID concentrations required to induce apoptosis in cancer cells have often been found to be significantly higher than that required to inhibit COX-2, suggesting the presence of alternative cellular targets of NSAIDs [27, 37, 77, 91]. Indeed, numerous studies have shown that NSAID-induced apoptosis in mammalian tumour cells can be mediated by several largely COX-independent metabolic pathways, the most prominent of which are presented in the following discussion.

3.1. Activation of Caspases and Modulation of Bcl-2 Proteins. NSAIDs can mediate apoptosis by inducing the activation of caspases, a family of proapoptotic cysteine proteinase enzymes which typically exist as latent zymogens in cells. Activation of these proteins by proapoptotic signals initiates a caspase cascade whereby initiator caspases specifically activate other executioner-type caspases. The latter then degrade multiple cellular components so that cells begin to acquire the morphological and biochemical features of apoptosis [92]. Bellosillo and coworkers [37] were among the first to present evidence of NSAID-induced caspase activation. They showed that B-chronic lymphocytic leukemia (B-CLL) cells treated with high doses of aspirin underwent apoptosis characterised by DNA fragmentation and degradation of poly (ADP-ribose) polymerase (PARP), which is a caspase substrate. The apoptotic phenotype was inhibited by application of the pan-caspase inhibitor Z-VAD-FMK, thus confirming the involvement of caspases in aspirin-induced B-cell apoptosis. Similarly, Castaño and coworkers [34] affirmed caspase involvement in aspirin-induced apoptosis of HT-29 human colon adenocarcinoma cells. However, contrary to its effect in B cells, aspirin did not induce PARP degradation in HT-29 cells. This observation is probably one of the earliest to suggest that NSAID-induced activation of caspases can occur *via* different pathways.

Indeed, it has since been shown that NSAIDs activate caspases both *via* the mitochondrial-mediated (intrinsic) pathway, which involves mitochondrial cytochrome *c* release and subsequent activation of caspase 9, and *via* the death-receptor mediated (extrinsic) pathway, which involves the activation of caspase 8 [41]. Proapoptotic NSAID-induced activation

of caspases, mediated by the early release of mitochondrial cytochrome *c* in mammalian cancer cells, has clearly been demonstrated by studies such as that of Piqué et al. [38]. The authors reported that cytochrome *c* release preceded both the disruption of the mitochondrial membrane potential ($\Delta\Psi m$) and the activation of caspases. The latter observation was confirmed by Zimmermann and coworkers [39] who in turn showed that, in aspirin-induced apoptosis of human cancer cells, the release of mitochondrial cytochrome *c* was itself triggered by translocation of proapoptotic Bax protein to the mitochondria. Conversely, overexpression of antiapoptotic Bcl-2 protein inhibited both cytochrome *c* release and apoptosis of aspirin-treated cancer cells. Furthermore, deletion of apoptotic protease-activating factor-1 (APAF-1), a cytosolic molecule which mediates caspase 9 activation after binding to mitochondrial cytochrome *c*, rendered cells resistant to aspirin-induced apoptosis. These observations indicate that cytochrome *c* release is a critical mediatory mechanism of apoptotic cell death induced by NSAIDs [39]. In fact, it has also been shown that aspirin-induced apoptosis of *S. cerevisiae* cells deficient in manganese superoxide dismutase (MnSOD) and cultivated in nonfermentable ethanol medium is preceded by the early release of cytochrome *c*, followed by a drastic fall in $\Delta\Psi m$ [93].

Extrinsic activation of caspase 8 is also an important mediator of NSAID-induced cancer cell apoptosis [42, 48]. Activated caspase 8 can initiate apoptosis by activating downstream caspases or by cleaving the BH3-domain only protein Bid. Truncated Bid (tBid) can translocate to the mitochondria to trigger cytochrome *c* release [94, 95] and can also activate Bax [96]. Indeed, aspirin-induced apoptosis of AGS gastric cancer cells was marked by activation of caspase 8 and Bid cleavage, along with the mitochondrial translocation of Bax, activation of downstream caspases, and cleavage of PARP. Specific inhibition of caspase 8 abrogated cleavage of both Bid and PARP and prevented aspirin-induced AGS cell apoptosis, thus implicating extrinsic caspase activation in the initiation of aspirin-induced apoptosis [42]. However, in this same study, the release of cytochrome *c* and activation of caspase 9 were also observed, thus suggesting the involvement even of mitochondrial-mediated caspase activation. In fact several other studies have since shown that the chemopreventive apoptotic effect of aspirin [41, 43, 45, 46] and modified NSAIDs such as NO-aspirin [97] and phosphosulindac [20] on mammalian cancer cells may involve the initiation of both intrinsic and extrinsic caspase activation pathways, which operate in parallel to one another.

The ability of NSAIDs to activate caspases largely explains the profound influence they have on Bcl-2 proteins such as Bax, Bid, and Bcl-2 [42, 43], the expression and cellular distribution of which can be greatly altered by NSAIDs to mediate apoptosis in cancer cells. NSAIDs such as aspirin and indomethacin have long been shown to induce cancer cell apoptosis by upregulating the expression of proapoptotic Bcl-2 proteins, such as Bax and Bak, and by downregulating expression of anti-apoptotic Bcl-2 proteins such as Bcl-2 and Bcl-X_L [29, 44]. More recent work has shown that NSAID-induced downregulation of Bcl-X_L can be induced in part by proteasome-mediated protein degradation [98].

NSAID-induced intrinsic and extrinsic activation of caspases, along with modulation of Bcl-2 protein expression, all seem to converge at the mitochondria. Here, these pathways induce events such as the release of cytochrome *c* and other proapoptotic molecules, including SMAC/Diablo, from the mitochondria [43], which irreversibly commit cells to the full apoptotic phenotype. Thus mitochondria clearly constitute a very important target of NSAID-induced apoptosis, as indicated by the many studies associating NSAID-induced apoptosis of mammalian cells with mitochondrial dysfunction, such as uncoupling of oxidative phosphorylation [99], induced mitochondrial permeability transition [100, 101], and inactivation of mitochondrial enzymes such as aconitase and respiratory chain proteins [45].

Likewise, it has been shown that the mitochondria of *S. cerevisiae* cells constitute a critical target of NSAIDs such as aspirin [32], the proapoptotic effects of which were shown to be associated with inhibition of the electron transport chain [93]. Similarly, Van Leeuwen and coworkers [33] observed that growth inhibition and apoptosis of *S. cerevisiae* cells caused by treatment with the NSAID diclofenac were due to mitochondrial dysfunctional events involving the inhibition of the electron transport chain. The fact that yeast cells, which are primitive eukaryotes, share a common mitochondrial target of NSAIDs with mammalian cells is highly significant, because it suggests that mitochondria constitute a unifying, dominant target of NSAID-induced apoptosis in all mammalian cancer cell types. This may certainly help inform the design of more effective NSAIDs for chemopreventive purposes and illustrates the important contribution of yeast cells as a complementary experimental model for the study of NSAID-induced apoptotic mechanisms.

3.2. Depletion of Polyamines. Polyamines such as spermine, spermidine, and putrescine are abundant polycations found in all eukaryotic cells and play an essential role in cellular development and proliferation [102]. High polyamine levels are in fact associated with the induction of cell proliferation [103, 104], whilst lowered polyamine levels have been found to promote cell growth inhibition [105] and apoptosis [106]. Hence, it is no surprise that the polyamine content of cancer cells tends to be significantly higher than that of normal cells [102], thus representing a potential target of anti-neoplastic agents such as NSAIDs, a number of which have been shown to mediate their chemopreventive effect by promoting the catabolic degradation of polyamines in cancer cells [35, 49, 107]. This takes place by virtue of the general ability of NSAIDs to modulate cellular polyamine metabolism, which is regulated by the biosynthetic enzyme ornithine decarboxylase (ODC) and the catabolic polyamine-acetylating enzyme spermidine/spermine N^1-acetyltransferase (SSAT) [49, 107]. For instance, indomethacin-induced growth inhibition of human colon cancer cells has been shown to be associated with downregulation of ODC activity and upregulation of SSAT activity, which concurrently impair the synthesis of polyamines and increase the rate at which they are degraded. The consequent depletion of cellular polyamines was accompanied by apoptotic cell death [35]. Other traditional NSAIDs

such as aspirin [108], sulindac sulfone [49], and ibuprofen [107] mainly induce the enhanced degradation and export of polyamines by upregulating gene expression of SSAT in cancer cells, resulting in reduced proliferation and increased apoptosis. This is also true of modified NSAIDs such as phosphosulindac [20], the antiproliferative proapoptotic effect of which can, like its NSAID precursor sulindac [109], be enhanced even further by concurrent treatment of cells with ODC inhibitors such as difluoromethylornithine (DFMO) [20, 110, 111]. Both DFMO and phosphosulindac act synergistically to enhance the depletion of polyamines in colon cancer cells, strongly inhibiting their proliferation and greatly enhancing apoptosis [20].

3.3. Modulation of NF-κB Activity. Nuclear factor kappa B (NF-κB) is a ubiquitous cellular transcription factor which regulates the expression of genes associated with inflammation, immune responses, cell growth, differentiation, and apoptosis. Composed of p65 (RelA) and p50 polypeptides, this complex transcription factor is sequestered in an inactive, heterodimeric form within the cell cytoplasm by I kappa B alpha (IκBα) or beta (IκBβ) inhibitor proteins [112, 113]. Stimulation by appropriate signals (such as proinflammatory cytokines including tumour necrosis factor (TNF)) triggers the IKα or IKβ kinase- (IKK-) mediated phosphorylation of IκB proteins, which consequently undergo ubiquitin-dependent proteasomal degradation. This permits translocation of NF-κB molecules to the nucleus, where they then bind to and promote the transcription of numerous target genes bearing a κB-binding motif [79, 113, 114].

The constitutive activation of NF-κB is a hallmark of several types of cancers [115–117] and is heavily associated with cancer cell resistance to cytotoxic agents, due in part to its induced upregulation of anti-apoptotic proteins [118]. Thus, NF-κB constitutes yet another potential target of chemotherapeutic agents such as NSAIDs, which can modulate NF-κB signalling in cancer cells to promote the onset of apoptosis [36, 54, 60, 107, 111, 114, 119].

Traditional NSAIDs such as aspirin have been reported to inhibit NF-κB activation by preventing the degradation of IκB [119]. Aspirin can inhibit TNF-induced IκBα degradation [120] by modulation of p38 mitogen-activated protein (MAP) kinase pathways [121] and by disrupting the ubiquitin-dependent proteasomal pathway, of which IκBα is a substrate [47]. Aspirin can also block IκBβ degradation through competitive inhibition of IKKβ-ATP molecular binding, thus facilitating selective inhibition of IKK kinase (IKKβ) [114]. All these mechanisms prevent NF-κB activation and subsequent transcription of anti-apoptotic proteins. It has also been shown that the NSAID sulindac specifically inhibits IKKβ activity and NF-κB activation in cancer cells, thus promoting apoptosis [122]. Likewise, the growth inhibitory effect of NSAIDs such as ibuprofen [51], indomethacin, and etoricoxib, a recently developed COX-2 inhibitor [117], is associated with their inhibition of NF-κB signalling in cancer cells.

The growth inhibitory effect mediated by modified NSAIDs such as NO-NSAIDs, on various cancer cell lines, also involves the modulation of NF-κB signalling [54, 55]. The growth inhibitory effect of NO-aspirin, associated with its ability to reduce proliferation and enhance apoptosis of cancer cells, was shown to be significantly correlated to its profound inhibition of the NF-κB signalling pathway, the occurrence of which was suggested to be due to inhibition of NF-κB binding to DNA in the nucleus [55]. Sun and Rigas [56] went on to demonstrate that proapoptotic inhibition of NF-κB signalling in human colon cancer cell lines, treated with NO-aspirin, stemmed from the latter's induced generation of reactive oxygen and nitrogen species (RONS), which may have interacted directly or indirectly (*via* the redox-sensitive thioredoxin (TRX) system) with NF-κB, impairing its ability to bind to recognition DNA sequences in the nucleus. This is highly conceivable given that NF-κB transcriptional activity is sensitive to redox changes [123]. In fact, it has since been shown that structurally diverse NO-NSAIDs such as NO-aspirin and NO-naproxen can suppress NF-κB signalling in cells *via* S-nitrosylation of the NF-κB transcription factor. This redox-signalling mechanism is mediated by the released NO group which, on binding to the p65 monomer of NF-κB, impairs the transcription factor's ability to bind to DNA [57]. The redox-induced inhibition of NF-κB signalling is thought also to partly mediate the growth inhibitory effect (including apoptosis, cell cycle arrest, and inhibition of proliferation) of phospho-NSAIDs [19, 21, 111] and HS-NSAIDs in cancer cells [60].

Intriguingly, the effect of NSAIDs on NF-κB activity seems to be cell-type specific, since aspirin-induced apoptosis of HCT 116 colon cancer cells was shown to be mediated by the activation of NF-κB signalling, rather than its inhibition [36]. Additionally, Din and coworkers [124] observed that aspirin-induced IκBα degradation, activation of NF-κB signalling, and apoptosis took place in colorectal cancer cells but not in other malignant cell types. Loss of cellular IκBα, which is indicative of NF-κB activation, has also been reported in aspirin-induced apoptosis of both immortalised human endothelial cells [125] and animal models of human colorectal cancer [126]. Likewise, Babbar and coworkers [107] observed that aspirin caused the activation of NF-κB signalling in Caco-2 colon cancer cells, suggesting even that this event was responsible for the upregulation of SSAT expression and polyamine depletion which led to apoptosis. Besides aspirin, other traditional NSAIDs such as diclofenac have also been reported to induce activation of NF-κB signalling as a means to attenuate cancer cell proliferation and promote apoptosis [127]. It has been argued that the varying effects of NF-κB may be due to the specificity by which this transcription factor binds to DNA and activates target genes. Such specificity is in turn dependent on the dimeric composition of the NF-κB complex and on the transcriptional cofactors that it has recruited, both of which can vary depending on the kinetics of induction [128]. Therefore, different stimuli or even the same stimulus exerted under different conditions can induce different NF-κB complexes and different downstream responses [36, 107].

3.4. Modulation of MAP-Kinase Activity. Mitogen activated protein (MAP) kinases are serine/threonine-specific proteins which respond to extracellular stimuli and regulate various

cellular pathways including mitosis, cell proliferation, survival and death [129]. The three principal MAP kinase subgroups include the extracellular signal-regulated kinases ERK1/2 (p42/p44), c-Jun N-terminal kinases/stress-activated protein kinases (JNKs/SAPKs), and the p38 MAP kinases [121]. NSAIDs such as aspirin and its metabolite salicylate have long been shown to modulate MAP kinase signalling in mammalian cells [130, 131]. This is exemplified by the salicylate-induced activation of p38 MAP kinase signalling in FS-4 fibroblasts, which induced apoptosis [130] *via* a pathway involving the NSAID-induced inhibition of IκBα degradation and NF-κB signalling [121]. Based on these observations, the authors concluded that apoptotic cell death induced by p38 MAP kinase activation played an important role in mediating the anti-neoplastic effects of NSAIDs. The important mediatory role of MAP kinase modulation in the context of the anti-neoplastic effects of NSAIDs was further highlighted by Jones and coworkers [132], who demonstrated that NSAID-induced inhibition of angiogenesis involved the disruption of ERK1/2 kinase signalling, a typically prosurvival pathway [133]. Additionally, inhibition of ERK1/2 signalling was shown to be the mechanism by which aspirin sensitises human cervical cancer cells to apoptosis induced by tumour necrosis factor-related apoptosis-inducing ligand (TRAIL) [40]. Modulation of MAP kinases has also been implicated in the suppressive effect of certain NSAIDs such as aspirin upon the factor activator protein (AP-1), a downstream target of MAP kinases which is critical for inducing neoplasia and activation of genes associated with inflammation and infection [134].

The modulation of MAP kinases has been shown to be critical for the growth inhibitory effect of modified NSAIDs such as NO-aspirin [135]. Aside from its propensity to inhibit NF-κB signalling, NO-aspirin was shown to induce the activation (marked by increased phosphorylation) of all three main MAP kinases in a concentration-dependent manner, in colon cancer cells. This was caused by the NO-aspirin-induced generation of RONS and subsequent oxidation of cellular thioredoxin-1 protein (Trx1p), which facilitated the proapoptotic autophosphorylation and activation of ASK1, a protein involved in the MAP kinase cascade and only kept inactive when attached to reduced Trx1p [56]. The same authors implicated ASK1-Trx1p cleavage in the activation of MAP kinase signalling, which in turn partly mediated the growth inhibitory effect of NO-aspirin, an effect marked by increased apoptosis and inhibition of cell proliferation. Likewise, NO-aspirin-induced cell cycle arrest and apoptosis of pancreatic cancer cells has been shown to occur *via* ROS-mediated modulation of all three MAP kinase signalling pathways and their downstream effector molecules such as p21 and cyclin D1 [53]. The rapid response of MAP kinases to the presence of RONS is not surprising given their well-established redox sensitivity [136]. The modulation of MAP kinase pathways was also implicated in the chemopreventive effect of NO-sulindac on UVB-induced melanoma cells [59] and in phospho-NSAID-mediated, redox-dependent apoptosis of colon cancer cells [19, 111].

3.5. Inhibition of Wnt/β-Catenin Signalling. The Wnt signalling pathway regulates the biosynthesis of β-catenin, a protein which is required for cell-to-cell adhesion and involved in the expression of genes associated with cancer [137]. Constitutive activation of Wnt/β-catenin signalling has been implicated in the development of numerous human malignancies [138–143]. Aberrant Wnt/β-catenin signalling is associated with the nuclear accumulation of β-catenin and the subsequent activation of the transcription factor known as T-cell factor (TCF). The resulting β-catenin/TCF complex promotes the transcriptional activation of target genes associated with proliferation, such as *cyclin D1* [144, 145], hence the implicated role of Wnt/β-catenin signalling in human carcinogenesis.

The NSAIDs aspirin and indomethacin have been shown to attenuate Wnt/β-catenin signalling in colorectal cancer cells, in a dose-dependent manner, by inhibiting the transcription of β-catenin/TCF-responsive genes. This NSAID-induced inhibition did not involve cleavage of the β-catenin/TCF complex but rather the hyperphosphorylation and consequent stabilization of β-catenin, presumably caused by the inactivation of a phosphatase enzyme [146, 147]. Further studies have since shown that aspirin-mediated downregulation of Wnt/β-catenin/TCF signalling can indeed be mediated by its induced inactivation of protein phosphatase 2A [148] but also, in part, by the downregulation of upstream specificity protein (Sp) transcription factors [149]. Other NSAIDs, such as sulindac, can also mediate the antiproliferative degradation of β-catenin in cancer cells partly by proteasomal degradation and partly by caspase-mediated cleavage [150], whilst others such as diclofenac have been shown to suppress Wnt/β-catenin/TCF signalling *via* the activation of NF-κB [127].

The downregulation of Wnt/β-catenin/TCF signalling induced by NSAIDs has been associated with the profound growth inhibition of various cancer cell types, in a manner that seems in large part to be due to inhibition of cell proliferation rather than by direct induction of apoptosis [127, 142, 146, 150, 151]. However, the proapoptotic effect of NSAIDs such as sulindac [152] in colorectal cancer cell lines has been shown to involve downregulation of Wnt/β-catenin/TCF signalling. Furthermore, Wnt/β-catenin signalling was observed to play a key role in directly mediating the proapoptotic effect of aspirin in human mesenchymal stem cells [153]. Regardless, the high prevalence of β-catenin downregulation reported in studies of NSAID-induced growth inhibition of cancer cells underlines the importance of this pathway as a chemopreventive target of NSAIDs.

This is certainly true for modified NSAIDs such as NO-aspirin, the growth inhibitory effect of which is strongly associated with a number of induced cellular events including the profound concentration-dependent inhibition of β-catenin signalling in colon cancer cells [54, 58, 145, 154]. In this regard, NO-aspirin is far more effective than aspirin in that, at concentrations far below those required for the inhibition of cell proliferation, it actually prevented formation of the β-catenin/TCF complex, whereas aspirin did not [145]. Moreover, at higher concentrations, NO-aspirin can induce caspase-3-mediated cleavage of β-catenin itself, leading to

a significant decline of cellular β-catenin levels and loss of cell-to-cell adhesion amongst colon cancer cells [58]. The significant downregulation of Wnt/β-catenin signalling, mediated at least in part by caspase-mediated β-catenin degradation, has also been implicated in the growth inhibitory effect of NO-aspirin on leukaemia [97] and breast cancer cell lines [155]. The same applies for phospho-NSAIDs such as phosphosulindac, the growth inhibitory effect of which was shown to involve β-catenin degradation in breast cancer stem cells [156].

3.6. Oxidative Stress and Disruption of Redox Balance. NSAIDs can mediate apoptosis in both malignant cell lines and budding yeast cells by upregulating the generation of ROS and by inducing oxidative stress. Indeed, it has been argued that ROS generation may constitute a central unifying mechanism by which the anti-neoplastic effects of NSAIDs are mediated, given that oxidative stress is coupled with many proapoptotic signals such as NF-κB inhibition and MAP kinase activation [157, 158]. The fact that ROS accumulation also mediates NSAID-induced apoptosis in primitive eukaryotes such as yeast [33] further corroborates this argument. However, the cellular prooxidant behaviour of NSAIDs has often been the subject of controversy due to conflicting reports that NSAIDs such as indomethacin and sulindac [159, 160] scavenge ROS and exert a cytoprotective antioxidant effect in cells. Likewise, there are numerous reports derived from *in vivo* studies of rats showing that NSAIDs such as aspirin can exert a cytoprotective antioxidant effect associated with the attenuation of ROS [161, 162] and of lipid peroxidation [163, 164], along with the upregulation of antioxidants such as reduced glutathione (GSH) [165] and superoxide dismutases (SODs) [166]. It has also been shown that low doses of aspirin can confer long-term cytoprotective resistance against H_2O_2-induced oxidative stress in *S. cerevisiae* cells [167].

Nevertheless, other investigations have clearly shown that NSAIDs can induce the proapoptotic accumulation of ROS in both yeast [33] and mammalian cells [157]. For instance, apoptotic cell death of respiring *S. cerevisiae* cells cultivated in the presence of diclofenac was clearly linked to a significant increase in cellular ROS, as measured by the ROS-sensitive fluorescent probe 2′,7′-dichlorodihydrofluorescein diacetate (DCDHF-DA) [33]. Similarly, indomethacin-induced apoptosis of gastric epithelial cells, which was abrogated after treatment with antioxidants such as N-acetylcysteine (NAC), was shown to require the generation of ROS [168], an event likewise implicated in the proapoptotic depletion of polyamines induced by indomethacin in colorectal cancer cells [35]. Additionally, Chan and coworkers [7] showed that human colorectal cancer cell apoptosis induced by both indomethacin and sulindac was marked by the accumulation of arachidonic acid, an event which is itself heavily associated with the accumulation of cellular ROS [83, 169]. The accumulation of ROS was also shown to be a critical inducer of mitochondrial cytochrome *c* release, disruption of $\Delta\Psi_m$, caspase activation, and apoptosis in salicylate-treated mammalian tumour cells [170]. Additionally, the NSAID sulindac and its metabolites have been shown to enhance the antitumour effect of the proteasome-inhibitor bortezomib, primarily through the synergistic generation of ROS [171]. It has been suggested that conflicting reports of NSAID redox behaviour in eukaryotic cells might simply be due to differences in the timing of measurements of ROS and antioxidant changes in experimental setups, given that cellular antioxidant levels are naturally expected to increase in subsequent response to elevated ROS [157].

The molecular mechanisms underlying NSAID-induced proapoptotic generation of ROS in mammalian and yeast cells have not yet been fully elucidated. However, it is well known that mitochondria, a major source of cellular ROS [172] and a central component of the apoptotic machinery, are profoundly affected by NSAIDs in both yeast [33, 93] and mammalian cells [99, 101]. For example, the aspirin metabolite salicylate has been shown to inhibit the mitochondrial electron transport chain in mammalian cells by interacting with an Fe-S cluster of Complex I, through its o-hydroxyl group. This was found to induce ROS accumulation and oxidative stress, which in turn caused proapoptotic events such as mitochondrial permeability transition and cytochrome *c* release [173]. Likewise, aspirin-induced cell cycle arrest and apoptosis of HepG2 hepatoma cells were shown to be induced by ROS accumulation and increased oxidative stress, accompanied by severe mitochondrial dysfunction such as the inactivation of electron transport chain proteins and aconitase [45]. Van Leeuwen et al. [33] observed that reduced cell growth and viability of *S. cerevisiae* yeast cells treated with diclofenac are due to mitochondrial dysfunction associated with the inhibition of electron transport chain subunit proteins Rip1p (of Complex III) and Cox9p (of Complex IV). This caused inhibition of cell respiration and subsequent ROS production, resulting in cell death. Inhibition of cellular respiration induced by aspirin was also observed in MnSOD-deficient yeast cells cultivated in ethanol medium [93], and recent studies in our laboratory have established the aspirin-induced proapoptotic generation of mitochondrial superoxide radicals in these cells (unpublished work).

It has been shown that the proapoptotic induction of oxidative stress induced by NSAIDs such as aspirin is strongly associated with the modulation of cellular redox homeostasis. This is exemplified by the observed increase of aspirin-induced apoptosis in HepG2 cells with GSH depletion and compromised redox balance [174]. In addition to this, studies in *S. cerevisiae* yeast cells have shown that aspirin-treated MnSOD-deficient yeast cells grown in ethanol medium experienced a very significant decrease in cellular reducing power with respect to wildtype cells, as measured by the $NADPH/NADP^+$ concentration ratio. This was accompanied by a significant decrease of the GSH/GSSG concentration ratio, owing to a buildup of GSSG, prior to cell death [175].

The induction of oxidative stress mediated by disruption of cellular redox balance is also central to the apoptotic effect of modified NSAIDs in cancer cells [53, 56, 58, 158]. For instance, oxidative stress induced by NO-aspirin in colon cancer cells was shown to be mediated by the depletion of cellular GSH, caused by the latter's association with the spacer

component of NO-aspirin and subsequent formation of a GSH conjugate. The resulting redox imbalance then initiated a number of downstream proapoptotic pathways such as β-catenin cleavage, inhibition of Wnt signaling, and mitochondrial-mediated activation of caspases [58]. Sun and Rigas [56] further demonstrated that redox-induced apoptosis of colorectal cancer cells treated with NO-aspirin involved the generation of RONS, the growth inhibitory effect of which was mediated by oxidative alteration and impairment of the thioredoxin redox system. Oxidised thioredoxin-1 induced MAP kinase activation and NF-κB inhibition, both of which are critical mediatory pathways of NO-aspirin-induced apoptosis [55, 135].

Oxidative stress, marked by RONS accumulation and redox imbalance associated with the suppression of GSH and increased oxidation of Trx-1, also plays a central role in apoptosis induced by phospho-NSAIDs [19–21, 56, 110, 111]. Like NO-NSAIDs, the strong prooxidant effect exerted by phospho-NSAIDs is reported to set in motion a pleiotropic cascade of redox-sensitive signalling events including activation of MAP kinases and inhibition of NF-κB signalling [19, 21, 56] along with the depletion of cellular polyamines, at least in the case of phosphosulindac [20, 110, 111]. The collective initiation of all these antiproliferative, proapoptotic pathways accounts for the very potent growth-inhibitory effects of phospho-NSAIDs, with respect to their traditional NSAID precursors [111]. Likewise, recent studies have shown that both apoptosis and cell cycle arrest of cancer cells treated with HS-NSAIDs, such as HS-aspirin, are induced as a result of oxidative stress and redox imbalance [60].

3.7. Other NSAID-Induced Proapoptotic Pathways. Further mechanisms by which NSAIDs can promote apoptosis in malignant cells include the induced depletion of survivin, an inhibitor of apoptosis protein which regulates the cell cycle and apoptosis in eukaryotic cells. Survivin expression in cancers tends to be very high and is in fact associated with tumour cell chemoresistance, making it an attractive target of antineoplastic treatments [176], including NSAIDs. Lu and coworkers [177] showed that aspirin caused significant and targeted depletion of survivin in breast cancer cells by upregulating its proteasomal degradation, consequently sensitizing the tumour cells to TRAIL-induced apoptosis. Moreover, aspirin acted synergistically with TRAIL to promote apoptosis of the breast tumour cells. Similarly it has been shown that cell cycle arrest and apoptotic cell death induced by the NSAIDs ibuprofen [51] and tolfenamic acid [52] in human colon and prostate cancer cells, respectively, are accompanied by significant depletion of survivin levels.

Another COX-independent proapoptotic pathway induced by NSAIDs is the impairment of proteasome function, as demonstrated by Dikshit and co-workers [47], who observed a time- and dose-dependent decline of proteasomal activity in neuroblastoma cells treated with aspirin. Accompanied by the accumulation of ubiquitylated proteins and profound mitochondrial abnormalities, the aspirin-induced impairment of proteasomal function was shown to activate the intrinsic apoptotic pathway, marked by a release of cytochrome *c* and the activation of caspase 9.

Finally, NSAIDs such as sulindac have been reported to induce sensitization of cancer cells to *mda7/IL24*-mediated apoptosis. The *mda7* gene, also known as *IL24*, is of the interleukin (IL) 10 family of cytokines [178, 179]. Ectopic expression of *mda7* is known to exert a potent tumour-suppressive effect against a variety of human cancer cells, with little to no effect on normal cells [180–182]. Furthermore, intratumoural administration of adenoviral vectors which express *mda7* (Ad-mda7) has been shown to exhibit antitumour and antiangiogenic activity in human lung tumour xenografts [183]. Also, Oida and coworkers [50] demonstrated that Ad-mda7-mediated growth inhibition and apoptosis of human lung cancer cells was greatly enhanced by concurrent administration of sulindac, which increased the half-life of MDA7 protein in the cells. This resulted in the increased expression of MDA7 protein and of its proapoptotic downstream effector proteins including p38MAPK, caspase-9, and caspase-3, consequently sensitizing the lung cancer cells to apoptosis. Therefore, sulindac essentially altered MDA7 protein turnover in lung cancer cells in such a way as to promote apoptotic cell death [50].

4. Concluding Remarks

Ongoing investigations of proapoptotic mechanisms underlying the promising anti-neoplastic properties of NSAIDs such as aspirin remain a top research priority, since an improved understanding of such pathways will help to enhance current anticancer drug treatments [2]. What is certain thus far is that NSAIDs generally exert a dose-dependent pleiotropic effect on cancer cells (see Figure 2), initiating a very complex cascade of signalling events which collectively induce apoptosis. Although much more remains to be elucidated, there is also mounting evidence which suggests that NSAID-induced signalling events associated with the induction of oxidative stress, such as mitochondrial dysfunction and altered redox signalling, may be the dominant pathways underlying all other proapoptotic effects induced by NSAIDs in cancer cells [184].

Consistent with the growing number of mammalian cell studies implicating oxidative stress as the dominant pathway of NSAID-induced growth inhibition [185], the proapoptotic effects of NSAIDs in yeast cells are likewise associated mainly with mitochondrial dysfunction, ROS generation, and redox imbalance. In particular, yeast cell studies have highlighted the pivotal importance of mitochondrial MnSOD as a cytoprotective defence against NSAIDs such as aspirin [32]. This implies that specific, targeted modulation of mitochondrial MnSOD can be exploited to enhance NSAID-induced oxidative stress and apoptosis in malignant mammalian cells.

It is currently hypothesised that cancer cells constantly experience much higher levels of oxidative stress with respect to normal cells, due to their increased metabolic rate [186]. Because of this, cancer cells are more reliant on antioxidant enzymes such as MnSOD and are thus believed to be far more sensitive to perturbations in redox balance compared to normal cells [16]. In fact, it has been shown that silencing of MnSOD, using anti-sense MnSOD antibodies, amplifies ROS

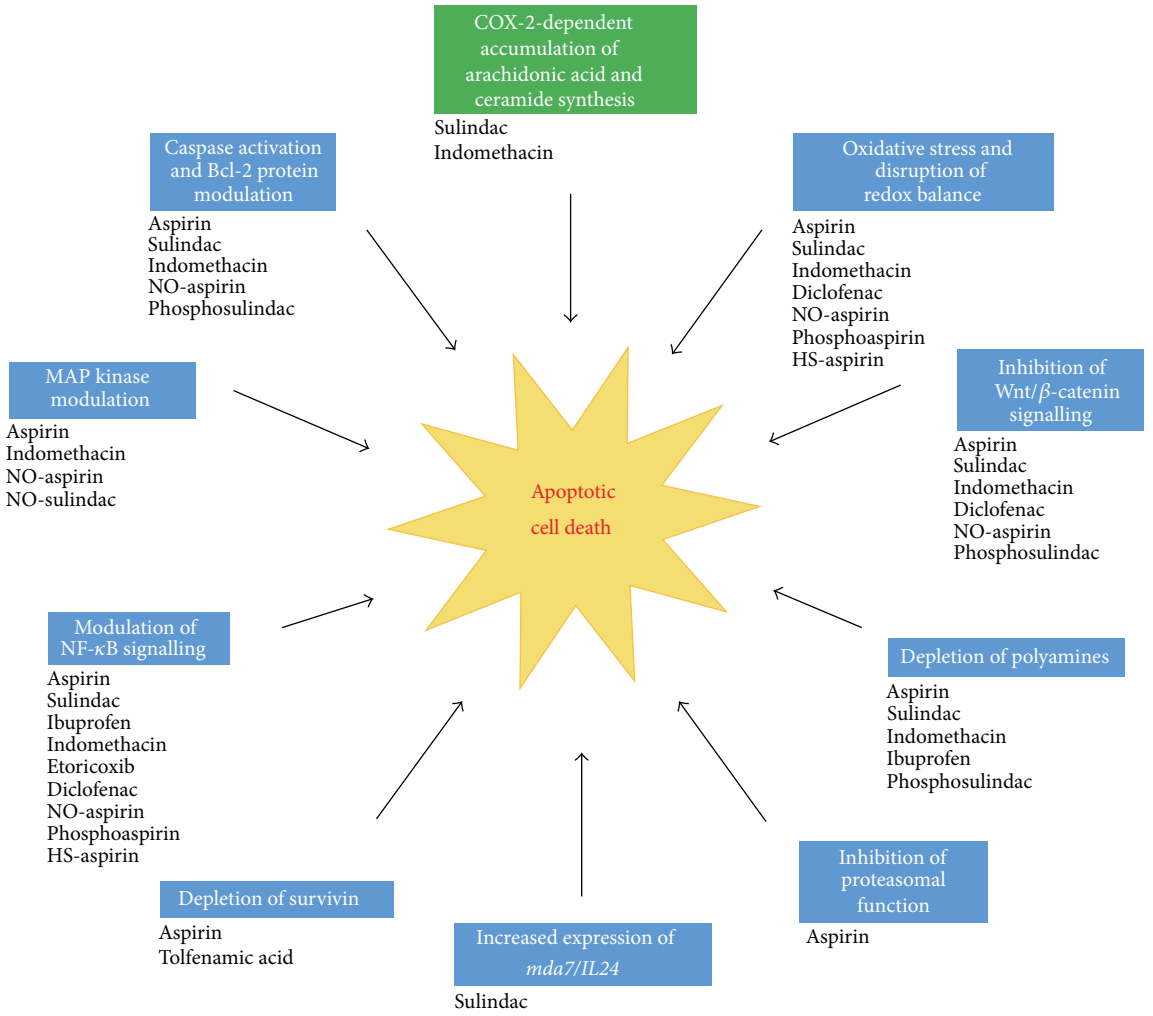

Figure 2: The major proapoptotic pathways induced by NSAIDs. Both traditional and modified NSAIDs have been shown to induce apoptosis in eukaryotic cells by initiating mechanisms which are largely independent of COX inhibition (shown in blue), with the exception being the COX-2-dependent accumulation of arachidonic acid and subsequent synthesis of ceramide induced by sulindac and indomethacin (shown in green). Important COX-independent proapoptotic pathways induced by NSAIDs include caspase activation and modulation of Bcl-2 proteins, depletion of polyamines, modulation of NF-κB signalling and of MAP kinase activity, inhibition of Wnt/β-catenin signalling, inhibition of proteasomal function, depletion of survivin, increased expression of *mda7/IL24* and also oxidative stress associated with mitochondrial dysfunction, ROS accumulation and the disruption of cellular redox balance.

accumulation and apoptosis in squamous cell carcinomas exposed to gamma radiation and anticancer drugs [187]. Moreover, it has recently been shown that silencing of MnSOD messenger RNA, using small interfering RNA (siRNA), amplified apoptosis of melanoma cells induced by the NSAID diclofenac [16]. This same study also demonstrated that diclofenac-induced accumulation of ROS, depletion of MnSOD expression and activity, and apoptosis were specific to melanoma cells.

In light of all these lines of evidence compiled through complementary study of both mammalian and yeast cell models, the induction of oxidative stress and redox imbalance induced by NSAIDs, together with the targeted modulation of mitochondrial MnSOD, merits serious consideration for future investigations.

Acknowledgments

Work in the authors' laboratory is partly funded by the Malta Government Scholarship Scheme (MGSS) Award, fund no. ME 367/07/8, to Gianluca Farrugia and partly by the Research Fund grants to Rena Balzan from the University of Malta.

References

[1] J. A. Baron and R. S. Sandler, "Nonsteroidal. anti-inflammatory drugs and cancer prevention," *Annual Review of Medicine*, vol. 51, pp. 511–523, 2000.

[2] A. T. Chan, N. Arber, J. Burn et al., "Aspirin in the chemoprevention of colorectal neoplasia: an overview," *Cancer Prevention Research*, vol. 5, no. 2, pp. 164–178, 2012.

[3] P. M. Rothwell, M. Wilson, C.-E. Elwin et al., "Long-term effect of aspirin on colorectal cancer incidence and mortality: 20-year follow-up of five randomised trials," *The Lancet*, vol. 376, no. 9754, pp. 1741–1750, 2010.

[4] P. M. Rothwell, F. G. R. Fowkes, J. F. Belch, H. Ogawa, C. P. Warlow, and T. W. Meade, "Effect of daily aspirin on long-term risk of death due to cancer: analysis of individual patient data from randomised trials," *The Lancet*, vol. 377, no. 9759, pp. 31–41, 2011.

[5] M. A. Trujillo, H. S. Garewal, and R. E. Sampliner, "Nonsteroidal antiinflammatory agents in chemoprevention of colorectal cancer: at what cost?" *Digestive Diseases and Sciences*, vol. 39, no. 10, pp. 2260–2266, 1994.

[6] S. J. Shiff, L. Qiao, L.-L. Tsai, and B. Rigas, "Sulindac sulfide, an aspirin-like compound, inhibits proliferation, causes cell cycle quiescence, and induces apoptosis in HT-29 colon adenocarcinoma cells," *Journal of Clinical Investigation*, vol. 96, no. 1, pp. 491–503, 1995.

[7] T. A. Chan, P. J. Morin, B. Vogelstein, and K. W. Kinzler, "Mechanisms underlying nonsteroidal antiinflammatory drug-mediated apoptosis," *Proceedings of the National Academy of Sciences of the United States of America*, vol. 95, no. 2, pp. 681–686, 1998.

[8] M. A. Rahman, D. K. Dhar, R. Masunaga, A. Yamanoi, H. Kohno, and N. Nagasue, "Sulindac and exisulind exhibit a significant antiproliferative effect and induce apoptosis in human hepatocellular carcinoma cell lines," *Cancer Research*, vol. 60, no. 8, pp. 2085–2089, 2000.

[9] M. Pollard and P. H. Luckert, "Prolonged antitumor effect of indomethacin on autochthonous intestinal tumors in rats," *Journal of the National Cancer Institute*, vol. 70, no. 6, pp. 1103–1105, 1983.

[10] C. H. Chiu, M. F. McEntee, and J. Whelan, "Discordant effect of aspirin and indomethacin on intestinal tumor burden in Apc(Min/+) mice," *Prostaglandins Leukotrienes and Essential Fatty Acids*, vol. 62, no. 5, pp. 269–275, 2000.

[11] J. Andrews, D. Djakiew, S. Krygier, and P. Andrews, "Superior effectiveness of ibuprofen compared with other NSAIDs for reducing the survival of human prostate cancer cells," *Cancer Chemotherapy and Pharmacology*, vol. 50, no. 4, pp. 277–284, 2002.

[12] Y.-S. Zhao, S. Zhu, X.-W. Li et al., "Association between NSAIDs use and breast cancer risk: a systematic review and meta-analysis," *Breast Cancer Research and Treatment*, vol. 117, no. 1, pp. 141–150, 2009.

[13] T. M. Motawi, Y. Bustanji, S. El-Maraghy, M. O. Taha, and M. A. Al-Ghussein, "Evaluation of naproxen and cromolyn activities against cancer cells viability, proliferation, apoptosis, p53 and gene expression of survivin and caspase-3," *Journal of Enzyme Inhibition and Medicinal Chemistry*, 2013.

[14] J. I. Johnsen, M. Lindskog, F. Ponthan et al., "Cyclooxygenase-2 is expressed in neuroblastoma, and nonsteroidal anti-inflammatory drugs induce apoptosis and inhibit tumor growth in vivo," *Cancer Research*, vol. 64, no. 20, pp. 7210–7215, 2004.

[15] F. Cecere, A. Iuliano, F. Albano et al., "Diclofenac-induced apoptosis in the neuroblastoma cell line SH-SY5Y: possible involvement of the mitochondrial superoxide dismutase," *Journal of Biomedicine and Biotechnology*, vol. 2010, Article ID 801726, 11 pages, 2010.

[16] F. Albano, A. Arcucci, G. Granato et al., "Markers of mitochondrial dysfunction during the diclofenac-induced apoptosis in melanoma cell lines," *Biochimie*, vol. 95, pp. 934–945, 2013.

[17] J. L. Williams, S. Borgo, I. Hasan, E. Castillo, F. Traganos, and B. Rigas, "Nitric oxide-releasing nonsteroidal anti-inflammatory drugs (NSAIDs) alter the kinetics of human colon cancer cell lines more effectively than traditional NSAIDs: implications for colon cancer chemoprevention," *Cancer Research*, vol. 61, no. 8, pp. 3285–3289, 2001.

[18] K. Kashfi, Y. Ryann, L. L. Qiao et al., "Nitric oxide-donating nonsteroidal anti-inflammatory drugs inhibit the growth of various cultured human cancer cells: evidence of a tissue type-independent effect," *Journal of Pharmacology and Experimental Therapeutics*, vol. 303, no. 3, pp. 1273–1282, 2002.

[19] W. Zhao, G. G. Mackenzie, O. T. Murray, Z. Zhang, and B. Rigas, "Phosphoaspirin (MDC-43), a novel benzyl ester of aspirin, inhibits the growth of human cancer cell lines more potently than aspirin: a redox-dependent effect," *Carcinogenesis*, vol. 30, no. 3, pp. 512–519, 2009.

[20] L. Huang, C. Zhu, Y. Sun et al., "Phospho-sulindac (OXT-922) inhibits the growth of human colon cancer cell lines: a redox/polyamine-dependent effect," *Carcinogenesis*, vol. 31, no. 11, pp. 1982–1990, 2010.

[21] L. Huang, G. G. Mackenzie, Y. Sun et al., "Chemotherapeutic properties of phospho-nonsteroidal anti-inflammatory drugs, a new class of anticancer compounds," *Cancer Research*, vol. 71, no. 24, pp. 7617–7627, 2011.

[22] M. Chattopadhyay, R. Kodela, N. Nath et al., "Hydrogen sulfide-releasing NSAIDs inhibit the growth of human cancer cells: a general property and evidence of a tissue type-independent effect," *Biochemical Pharmacology*, vol. 83, no. 6, pp. 715–722, 2012.

[23] R. Kodela, M. Chattopadhyay, and K. Kashfi, "NOSH-aspirin: a novel nitric oxide-hydrogen sulfide-releasing hybrid: a new class of anti-inflammatory pharmaceuticals," *ACS Medicinal Chemistry Letters*, vol. 3, no. 3, pp. 257–262, 2012.

[24] M. Chattopadhyay, R. Kodela, K. R. Olson, and K. Kashfi, "NOSH-aspirin (NBS-1120), a novel nitric oxide- and hydrogen sulfide-releasing hybrid is a potent inhibitor of colon cancer cell growth in vitro and in a xenograft mouse model," *Biochemical and Biophysical Research Communications*, vol. 419, no. 3, pp. 523–528, 2012.

[25] L. M. Coussens and Z. Werb, "Inflammation and cancer," *Nature*, vol. 420, no. 6917, pp. 860–867, 2002.

[26] B. S. Reddy, C. V. Rao, A. Rivenson, and G. Kelloff, "Inhibitory effect of aspirin on azoxymethane-induced colon carcinogenesis in F344 rats," *Carcinogenesis*, vol. 14, no. 8, pp. 1493–1497, 1993.

[27] L. Qiao, R. Hanif, E. Sphicas, S. J. Shiff, and B. Rigas, "Effect of aspirin on induction of apoptosis in HT-29 human colon adenocarcinoma cells," *Biochemical Pharmacology*, vol. 55, no. 1, pp. 53–64, 1998.

[28] H.-G. Yu, J.-A. Huang, Y.-N. Yang et al., "The effects of acetylsalicylic acid on proliferation, apoptosis, and invasion of cyclooxygenase-2 negative colon cancer cells," *European Journal of Clinical Investigation*, vol. 32, no. 11, pp. 838–846, 2002.

[29] J. Gao, K. Niwa, W. Sun et al., "Non-steroidal anti-inflammatory drugs inhibit cellular proliferation and upregulate cyclooxygenase-2 protein expression in endometrial cancer cells," *Cancer Science*, vol. 95, no. 11, pp. 901–907, 2004.

[30] D. Carmona-Gutierrez, T. Eisenberg, S. Büttner, C. Meisinger, G. Kroemer, and F. Madeo, "Apoptosis in yeast: triggers, pathways, subroutines," *Cell Death and Differentiation*, vol. 17, no. 5, pp. 763–773, 2010.

[31] B. Almeida, A. Silva, A. Mesquita, B. Sampaio-Marques, F. Rodrigues, and P. Ludovico, "Drug-induced apoptosis in yeast," *Biochimica et Biophysica Acta*, vol. 1783, no. 7, pp. 1436–1448, 2008.

[32] R. Balzan, K. Sapienza, D. R. Galea, N. Vassallo, H. Frey, and W. H. Bannister, "Aspirin commits yeast cells to apoptosis depending on carbon source," *Microbiology*, vol. 150, no. 1, pp. 109–115, 2004.

[33] J. S. Van Leeuwen, R. Orij, M. A. H. Luttik, G. J. Smits, N. P. E. Vermeulen, and J. C. Vos, "Subunits Rip1p and Cox9p of the respiratory chain contribute to diclofenac-induced mitochondrial dysfunction," *Microbiology*, vol. 157, no. 3, pp. 685–694, 2011.

[34] E. Castaño, M. Dalmau, M. Barragán, G. Pueyo, R. Bartrons, and J. Gil, "Aspirin induces cell death and caspase-dependent phosphatidylserine externalization in HT-29 human colon adenocarcinoma cells," *British Journal of Cancer*, vol. 81, no. 2, pp. 294–299, 1999.

[35] L. Turchanowa, N. Dauletbaev, V. Milovic, and J. Stein, "Non-steroidal anti-inflammatory drugs stimulate spermidine/spermine acetyltransferase and deplete polyamine content in colon cancer cells," *European Journal of Clinical Investigation*, vol. 31, no. 10, pp. 887–893, 2001.

[36] L. A. Stark, F. V. Din, R. M. Zwacka, and M. G. Dunlop, "Aspirin-induced activation of the NF-kappaB signaling pathway: a novel mechanism for aspirin-mediated apoptosis in colon cancer cells," *The FASEB Journal*, vol. 15, no. 7, pp. 1273–1275, 2001.

[37] B. Bellosillo, M. Piqué, M. Barragán et al., "Aspirin and salicylate induce apoptosis and activation of caspases in B-cell chronic lymphocytic leukemia cells," *Blood*, vol. 92, no. 4, pp. 1406–1414, 1998.

[38] M. Piqué, M. Barragán, M. Dalmau, B. Bellosillo, G. Pons, and J. Gil, "Aspirin induces apoptosis through mitochondrial cytochrome c release," *FEBS Letters*, vol. 480, no. 2-3, pp. 193–196, 2000.

[39] K. C. Zimmermann, N. J. Waterhouse, J. C. Goldstein, M. Schuler, and D. R. Green, "Aspirin induces apoptosis through release of cytochrome c from mitochondria," *Neoplasia*, vol. 2, no. 6, pp. 505–513, 2000.

[40] R. Im and Y. J. Jang, "Aspirin enhances TRAIL-induced apoptosis via regulation of ERK1/2 activation in human cervical cancer cells," *Biochemical and Biophysical Research Communications*, vol. 424, pp. 65–70, 2012.

[41] J. J. Power, M. S. Dennis, M. J. Redlak, and T. A. Miller, "Aspirin-induced mucosal cell death in human gastric cells: evidence supporting an apoptotic mechanism," *Digestive Diseases and Sciences*, vol. 49, no. 9, pp. 1518–1525, 2004.

[42] Q. Gu, J. De Wang, H. H. X. Xia et al., "Activation of the caspase-8/Bid and Bax pathways in aspirin-induced apoptosis in gastric cancer," *Carcinogenesis*, vol. 26, no. 3, pp. 541–546, 2005.

[43] M. J. Redlak, J. J. Power, and T. A. Miller, "Role of mitochondria in aspirin-induced apoptosis in human gastric epithelial cells," *American Journal of Physiology*, vol. 289, no. 4, pp. G731–G738, 2005.

[44] X. M. Zhou, B. C. Y. Wong, X. M. Fan et al., "Non-steroidal anti-inflammatory drugs induce apoptosis in gastric cancer cells through up-regulation of bax and bak," *Carcinogenesis*, vol. 22, no. 9, pp. 1393–1397, 2001.

[45] H. Raza, A. John, and S. Benedict, "Acetylsalicylic acid-induced oxidative stress, cell cycle arrest, apoptosis and mitochondrial dysfunction in human hepatoma HepG2 cells," *European Journal of Pharmacology*, vol. 668, no. 1-2, pp. 15–24, 2011.

[46] M. A. Hossain, D. H. Kim, J. Y. Jang et al., "Aspirin induces apoptosis in vitro and inhibits tumor growth of human hepatocellular carcinoma cells in a nude mouse xenograft model," *International Journal of Oncology*, vol. 40, no. 4, pp. 1298–1304, 2012.

[47] P. Dikshit, M. Chatterjee, A. Goswami, A. Mishra, and N. R. Jana, "Aspirin induces apoptosis through the inhibition of proteasome function," *Journal of Biological Chemistry*, vol. 281, no. 39, pp. 29228–29235, 2006.

[48] Y. Huang, Q. He, M. J. Hillman, R. Rong, and M. S. Sheikh, "Sulindac sulfide-induced apoptosis involves death receptor 5 and the caspase 8-dependent pathway in human colon and prostate cancer cells," *Cancer Research*, vol. 61, no. 18, pp. 6918–6924, 2001.

[49] N. Babbar, N. A. Ignatenko, R. A. Casero Jr., and E. W. Gerner, "Cyclooxygenase-independent induction of apoptosis by sulindac sulfone is mediated by polyamines in colon cancer," *Journal of Biological Chemistry*, vol. 278, no. 48, pp. 47762–47775, 2003.

[50] Y. Oida, B. Gopalan, R. Miyahara et al., "Sulindac enhances adenoviral vector expressing mda-7/IL-24-mediated apoptosis in human lung cancer," *Molecular Cancer Therapeutics*, vol. 4, no. 2, pp. 291–304, 2005.

[51] E. J. Greenspan, J. P. Madigan, L. A. Boardman, and D. W. Rosenberg, "Ibuprofen inhibits activation of nuclear β-catenin in human colon adenomas and induces the phosphorylation of GSK-3β," *Cancer Prevention Research*, vol. 4, no. 1, pp. 161–171, 2011.

[52] U. T. Sankpal, M. Abdelrahim, S. F. Connelly et al., "Small molecule tolfenamic acid inhibits PC-3 cell proliferation and invasion in vitro, and tumor growth in orthotopic mouse model for prostate cancer," *Prostate*, vol. 72, pp. 1648–1658, 2012.

[53] H. Zhou, L. Huang, Y. Sun, and B. Rigas, "Nitric oxide-donating aspirin inhibits the growth of pancreatic cancer cells through redox-dependent signaling," *Cancer Letters*, vol. 273, no. 2, pp. 292–299, 2009.

[54] J. L. Williams, N. Nath, J. Chen et al., "Growth inhibition of human colon cancer cells by nitric oxide (NO)-donating aspirin is associated with cyclooxygenase-2 induction and beta-catenin/T-cell factor signaling, nuclear factor-kappaB, and NO synthase 2 inhibition: Implications for chemoprevention," *Cancer Research*, vol. 63, no. 22, pp. 7613–7618, 2003.

[55] J. I. Williams, P. Ji, N. Ouyang, X. Liu, and B. Rigas, "NO-donating aspirin inhibits the activation of NF-κB in human cancer cell lines and Min mice," *Carcinogenesis*, vol. 29, no. 2, pp. 390–397, 2008.

[56] Y. Sun and B. Rigas, "The thioredoxin system mediates redox-induced cell death in human colon cancer cells: implications for the mechanism of action of anticancer agents," *Cancer Research*, vol. 68, no. 20, pp. 8269–8277, 2008.

[57] M. Chattopadhyay, S. Goswami, D. B. Rodes et al., "NO-releasing NSAIDs suppress NF-κB signaling in vitro and in vivo through S-nitrosylation," *Cancer Letters*, vol. 298, no. 2, pp. 204–211, 2010.

[58] J. Gao, X. Liu, and B. Rigas, "Nitric oxide-donating aspirin induces apoptosis in human colon cancer cells through induction of oxidative stress," *Proceedings of the National Academy of Sciences of the United States of America*, vol. 102, no. 47, pp. 17207–17212, 2005.

[59] C. Chaudhary, T. Singh, P. Kapur et al., "Nitric oxide-releasing sulindac is a novel skin cancer chemopreventive agent for

UVB-induced photocarcinogenesis," *Toxicology and Applied Pharmacology*, vol. 268, pp. 249–255, 2013.

[60] M. Chattopadhyay, R. Kodela, N. Nath, A. Barsegian, D. Boring, and K. Kashfi, "Hydrogen sulfide-releasing aspirin suppresses NF-κB signaling in estrogen receptor negative breast cancer cells in vitro and in vivo," *Biochemical Pharmacology*, vol. 83, no. 6, pp. 723–732, 2012.

[61] J. R. Vane, "Inhibition of prostaglandin synthesis as a mechanism of action for aspirin-like drugs," *Nature: New biology*, vol. 231, no. 25, pp. 232–235, 1971.

[62] J. R. Vane, J. A. Mitchell, I. Appleton et al., "Inducible isoforms of cyclooxygenase and nitric-oxide synthase in inflammation," *Proceedings of the National Academy of Sciences of the United States of America*, vol. 91, no. 6, pp. 2046–2050, 1994.

[63] K. Uefuji, T. Ichikura, and H. Mochizuki, "Cyclooxygenase-2 expression is related to prostaglandin biosynthesis and angiogenesis in human gastric cancer," *Clinical Cancer Research*, vol. 6, no. 1, pp. 135–138, 2000.

[64] L. Zhang, Y.-D. Wu, P. Li et al., "Effects of cyclooxygenase-2 on human esophageal squamous cell carcinoma," *World Journal of Gastroenterology*, vol. 17, no. 41, pp. 4572–4580, 2011.

[65] C. E. Eberhart, R. J. Coffey, A. Radhika, F. M. Giardiello, S. Ferrenbach, and R. N. Dubois, "Up-regulation of cyclooxygenase 2 gene expression in human colorectal adenomas and adenocarcinomas," *Gastroenterology*, vol. 107, no. 4, pp. 1183–1188, 1994.

[66] H. Sano, Y. Kawahito, R. L. Wilder et al., "Expression of cyclooxygenase-1 and -2 in human colorectal cancer," *Cancer Research*, vol. 55, no. 17, pp. 3785–3789, 1995.

[67] W. Kutchera, D. A. Jones, N. Matsunami et al., "Prostaglandin H synthase 2 is expressed abnormally in human colon cancer: evidence for a transcriptional effect," *Proceedings of the National Academy of Sciences of the United States of America*, vol. 93, no. 10, pp. 4816–4820, 1996.

[68] A. Lupulescu, "Prostaglandins, their inhibitors and cancer," *Prostaglandins Leukotrienes and Essential Fatty Acids*, vol. 54, no. 2, pp. 83–94, 1996.

[69] G. N. Levy, "Prostaglandin H synthases, nonsteroidal anti-inflammatory drugs, and colon cancer," *FASEB Journal*, vol. 11, no. 4, pp. 234–247, 1997.

[70] S. J. Shiff and B. Rigas, "Nonsteroidal anti-inflammatory drugs and colorectal cancer: evolving concepts of their chemopreventive actions," *Gastroenterology*, vol. 113, no. 6, pp. 1992–1998, 1997.

[71] D. Wang and R. N. Dubois, "Prostaglandins and cancer," *Gut*, vol. 55, no. 1, pp. 115–122, 2006.

[72] M. Oshima, J. E. Dinchuk, S. L. Kargman et al., "Suppression of intestinal polyposis in Apc(Δ716) knockout mice by inhibition of cyclooxygenase 2 (COX-2)," *Cell*, vol. 87, no. 5, pp. 803–809, 1996.

[73] P. C. Chulada, M. B. Thompson, J. F. Mahler et al., "Genetic disruption of Ptgs-1, as well as of Ptgs-2, reduces intestinal tumorigenesis in Min mice," *Cancer Research*, vol. 60, no. 17, pp. 4705–4708, 2000.

[74] B. S. Reddy, C. V. Rao, and K. Seibert, "Evaluation of cyclooxygenase-2 inhibitor for potential chemopreventive properties in colon carcinogenesis," *Cancer Research*, vol. 56, no. 20, pp. 4566–4569, 1996.

[75] N. Arber, C. J. Eagle, J. Spicak et al., "Celecoxib for the prevention of colorectal adenomatous polyps," *New England Journal of Medicine*, vol. 355, no. 9, pp. 885–895, 2006.

[76] J. A. Baron, R. S. Sandler, R. S. Bresalier et al., "A randomized trial of rofecoxib for the chemoprevention of colorectal adenomas," *Gastroenterology*, vol. 131, no. 6, pp. 1674–1682, 2006.

[77] Y. Dai and W.-H. Wang, "Non-steroidal anti-inflammatory drugs in prevention gastric cancer," *World Journal of Gastroenterology*, vol. 12, no. 19, pp. 2884–2889, 2006.

[78] N. R. Jana, "NSAIDs and apoptosis," *Cellular and Molecular Life Sciences*, vol. 65, no. 9, pp. 1295–1301, 2008.

[79] K. Sapienza and R. Balzan, "Aspirin and apoptosis," in *New Research on Aspirin and Health*, C. L. Millwood, Ed., Nova Science Publishers, New York, NY, USA, 2007.

[80] C.-H. Chiu, M. F. McEntee, and J. Whelan, "Sulindac causes rapid regression of preexisting tumors in Min/+ mice independent of prostaglandin biosynthesis," *Cancer Research*, vol. 57, no. 19, pp. 4267–4273, 1997.

[81] R. Hanif, A. Pittas, Y. Feng et al., "Effects of nonsteroidal anti-inflammatory drugs on proliferation and on induction of apoptosis in colon cancer cells by a prostaglandin-independent pathway," *Biochemical Pharmacology*, vol. 52, no. 2, pp. 237–245, 1996.

[82] Y. A. Hannun, "Functions of ceramide in coordinating cellular responses to stress," *Science*, vol. 274, no. 5294, pp. 1855–1859, 1996.

[83] Y. Cao, A. T. Pearman, G. A. Zimmerman, T. M. McIntyre, and S. M. Prescott, "Intracellular unesterified arachidonic acid signals apoptosis," *Proceedings of the National Academy of Sciences of the United States of America*, vol. 97, no. 21, pp. 11280–11285, 2000.

[84] L. Scorrano, D. Penzo, V. Petronilli, F. Pagano, and P. Bernardi, "Arachidonic acid causes cell death through the mitochondrial permeability transition. Implications for tumor necrosis factor-α apoptotic signaling," *Journal of Biological Chemistry*, vol. 276, no. 15, pp. 12035–12040, 2001.

[85] X. Zhang, S. G. Morham, R. Langenbach, and D. A. Young, "Malignant transformation and antineoplastic actions of nonsteroidal antiinflammatory drugs (NSAIDs) on cyclooxygenase-null embryo fibroblasts," *Journal of Experimental Medicine*, vol. 190, no. 4, pp. 451–459, 1999.

[86] D. J. E. Elder, D. E. Halton, A. Hague, and C. Paraskeva, "Induction of apoptotic cell death in human colorectal carcinoma cell lines by a cyclooxygenase-2 (COX-2)-selective nonsteroidal anti-inflammatory drug: independence from COX-2 protein expression," *Clinical Cancer Research*, vol. 3, no. 10, pp. 1679–1683, 1997.

[87] H. J. Thompson, S. Briggs, N. S. Paranka et al., "Inhibition of mammary carcinogenesis in rats by sulfone metabolite of sulindac," *Journal of the National Cancer Institute*, vol. 87, no. 16, pp. 1259–1260, 1995.

[88] G. A. Piazza, A. L. K. Rahm, M. Krutzsch et al., "Antineoplastic drugs sulindac sulfide and sulfone inhibit cell growth by inducing apoptosis," *Cancer Research*, vol. 55, no. 14, pp. 3110–3116, 1995.

[89] D. Charalambous and P. E. O'Brien, "Inhibition of colon cancer precursors in the rat by sulindac sulphone is not dependent on inhibition of prostaglandin synthesis," *Journal of Gastroenterology and Hepatology*, vol. 11, no. 4, pp. 307–310, 1996.

[90] G. A. Piazza, D. S. Alberts, L. J. Hixson et al., "Sulindac sulfone inhibits azoxymethane-induced colon carcinogenesis in rats without reducing prostaglandin levels," *Cancer Research*, vol. 57, no. 14, pp. 2909–2915, 1997.

[91] R. Yamazaki, N. Kusunoki, T. Matsuzaki, S. Hashimoto, and S. Kawai, "Aspirin and sodium salicylate inhibit proliferation

and induce apoptosis in rheumatoid synovial cells," *Journal of Pharmacy and Pharmacology*, vol. 54, no. 12, pp. 1675–1679, 2002.

[92] B. B. Wolf and D. R. Green, "Suicidal tendencies: apoptotic cell death by caspase family proteinases," *Journal of Biological Chemistry*, vol. 274, no. 29, pp. 20049–20052, 1999.

[93] K. Sapienza, W. Bannister, and R. Balzan, "Mitochondrial involvement in aspirin-induced apoptosis in yeast," *Microbiology*, vol. 154, no. 9, pp. 2740–2747, 2008.

[94] H. Li, H. Zhu, C.-J. Xu, and J. Yuan, "Cleavage of BID by caspase 8 mediates the mitochondrial damage in the Fas pathway of apoptosis," *Cell*, vol. 94, no. 4, pp. 491–501, 1998.

[95] M. Kruidering and G. I. Evan, "Caspase-8 in apoptosis: the beginning of "the end"?" *IUBMB Life*, vol. 50, no. 2, pp. 85–90, 2000.

[96] X. Roucou, S. Montessuit, B. Antonsson, and J.-C. Martinou, "Bax oligomerization in mitochondrial membranes requires tBid (caspase-8-cleaved Bid) and a mitochondrial protein," *Biochemical Journal*, vol. 368, no. 3, pp. 915–921, 2002.

[97] N. Nath, G. Labaze, B. Rigas, and K. Kashfi, "NO-donating aspirin inhibits the growth of leukemic Jurkat cells and modulates β-catenin expression," *Biochemical and Biophysical Research Communications*, vol. 326, no. 1, pp. 93–99, 2005.

[98] A. Bank, J. Yu, and L. Zhang, "NSAIDs downregulate Bcl-XL and dissociate BAX and Bcl-X L to induce apoptosis in colon cancer cells," *Nutrition and Cancer*, vol. 60, no. 1, pp. 98–103, 2008.

[99] I. Petrescu and C. Tarba, "Uncoupling effects of diclofenac and aspirin in the perfused liver and isolated hepatic mitochondria of rat," *Biochimica et Biophysica Acta-Bioenergetics*, vol. 1318, no. 3, pp. 385–394, 1997.

[100] S. A. Uyemura, A. C. Santos, F. E. Mingatto, M. C. Jordani, and C. Curti, "Diclofenac sodium and mefenamic acid: potent inducers of the membrane permeability transition in renal cortex mitochondria," *Archives of Biochemistry and Biophysics*, vol. 342, no. 2, pp. 231–235, 1997.

[101] K.-W. Oh, T. Qian, D. A. Brenner, and J. J. Lemasters, "Salicylate enhances necrosis and apoptosis mediated by the mitochondrial permeability transition," *Toxicological Sciences*, vol. 73, no. 1, pp. 44–52, 2003.

[102] A. E. Pegg, "Polyamine metabolism and its importance in neoplastic growth and as a target for chemotherapy," *Cancer Research*, vol. 48, no. 4, pp. 759–774, 1988.

[103] D. Russell and S. H. Snyder, "Amine synthesis in rapidly growing tissues: ornithine decarboxylase activity in regenerating rat liver, chick embryo, and various tumors," *Proceedings of the National Academy of Sciences of the United States of America*, vol. 60, no. 4, pp. 1420–1427, 1968.

[104] F. L. Meyskens Jr. and E. W. Gerner, "Development of difluoromethylornithine as a chemoprevention agent for the management of colon cancer," *Journal of Cellular Biochemistry*, vol. 58, no. 22, pp. 126–131, 1995.

[105] F. Scorcioni, A. Corti, P. Davalli, S. Astancolle, and S. Bettuzzi, "Manipulation of the expression of regulatory genes of polyamine metabolism results in specific alterations of the cell-cycle progression," *Biochemical Journal*, vol. 354, no. 1, pp. 217–223, 2001.

[106] L. Li, J. N. Rao, B. L. Bass, and J.-Y. Wang, "NF-κB activation and susceptibility to apoptosis after polyamine depletion in intestinal epithelial cells," *American Journal of Physiology*, vol. 280, no. 5, pp. G992–G1004, 2001.

[107] N. Babbar, E. W. Gerner, and R. A. Casero Jr., "Induction of spermidine/spermine N1-acetyltransferase (SSAT) by aspirin in Caco-2 colon cancer cells," *Biochemical Journal*, vol. 394, no. 1, pp. 317–324, 2006.

[108] M. E. Martínez, T. G. O'Brien, K. E. Fultz et al., "Pronounced reduction in adenoma recurrence associated with aspirin use and a polymorphism in the ornithine decarboxylase gene," *Proceedings of the National Academy of Sciences of the United States of America*, vol. 100, no. 13, pp. 7859–7864, 2003.

[109] F. L. Meyskens Jr., C. E. McLaren, D. Pelot et al., "Difluoromethylornithine plus sulindac for the prevention of sporadic colorectal adenomas: a randomized placebo-controlled, double-blind trial," *Cancer Prevention Research*, vol. 1, no. 1, pp. 32–38, 2008.

[110] G. G. Mackenzie, N. Ouyang, G. Xie et al., "Phospho-sulindac (OXT-328) combined with difluoromethylornithine prevents colon cancer in mice," *Cancer Prevention Research*, vol. 4, no. 7, pp. 1052–1060, 2011.

[111] G. G. MacKenzie, Y. Sun, L. Huang et al., "Phospho-sulindac (OXT-328), a novel sulindac derivative, is safe and effective in colon cancer prevention in mice," *Gastroenterology*, vol. 139, no. 4, pp. 1320–1332, 2010.

[112] P. A. Baeuerle and D. Baltimore, "Nf-κB: ten years after," *Cell*, vol. 87, no. 1, pp. 13–20, 1996.

[113] M. Karin, "The beginning of the end: IκB kinase (IKK) and NF-κB activation," *Journal of Biological Chemistry*, vol. 274, no. 39, pp. 27339–27342, 1999.

[114] M.-J. Yin, Y. Yamamoto, and R. B. Gaynor, "The anti-inflammatory agents aspirin and salicylate inhibit the activity of IκB kinase-β," *Nature*, vol. 396, no. 6706, pp. 77–80, 1998.

[115] H. Algül, G. Adler, and R. M. Schmid, "NF-kappaB/Rel transcriptional pathway: implications in pancreatic cancer," *International Journal of Gastrointestinal Cancer*, vol. 31, pp. 71–78, 2002.

[116] K. M. Ahmed, N. Cao, and J. J. Li, "HER-2 and NF-κB as the targets for therapy-resistant breast cancer," *Anticancer Research*, vol. 26, no. 6 B, pp. 4235–4243, 2006.

[117] S. Setia and S. N. Sanyal, "Downregulation of NF-kappaB and PCNA in the regulatory pathways of apoptosis by cyclooxygenase-2 inhibitors in experimental lung cancer," *Molecular and Cellular Biochemistry*, vol. 369, pp. 75–86, 2012.

[118] D. J. A. de Groot, E. G. E. de Vries, H. J. M. Groen, and S. de Jong, "Non-steroidal anti-inflammatory drugs to potentiate chemotherapy effects: from lab to clinic," *Critical Reviews in Oncology/Hematology*, vol. 61, no. 1, pp. 52–69, 2007.

[119] E. Kopp and S. Ghosh, "Inhibition of NF-κB by sodium salicylate and aspirin," *Science*, vol. 265, no. 5174, pp. 956–959, 1994.

[120] J. W. Pierce, M. A. Read, H. Ding, F. W. Luscinskas, and T. Collins, "Salicylates inhibit IκB-α phosphorylation, endothelial-leukocyte adhesion molecule expression, and neutrophil transmigration," *Journal of Immunology*, vol. 156, no. 10, pp. 3961–3969, 1996.

[121] P. Schwenger, D. Alpert, E. Y. Skolnik, and J. Vilček, "Activation of p38 mitogen-activated protein kinase by sodium salicylate leads to inhibition of tumor necrosis factor-induced IκBα phosphorylation and degradation," *Molecular and Cellular Biology*, vol. 18, no. 1, pp. 78–84, 1998.

[122] Y. Yamamoto, M.-J. Yin, K.-M. Lin, and R. B. Gaynor, "Sulindac inhibits activation of the NF-κB pathway," *Journal of Biological Chemistry*, vol. 274, no. 38, pp. 27307–27314, 1999.

[123] J. R. Matthews, N. Wakasugi, J.-L. Virelizier, J. Yodoi, and R. T. Hay, "Thioredoxin regulates the DNA binding activity of N F-κB by reduction of a disulphide bond involving cysteine 62," *Nucleic Acids Research*, vol. 20, no. 15, pp. 3821–3830, 1992.

[124] F. V. N. Din, M. G. Dunlop, and L. A. Stark, "Evidence for colorectal cancer cell specificity of aspirin effects on NFκB signalling and apoptosis," *British Journal of Cancer*, vol. 91, no. 2, pp. 381–388, 2004.

[125] G. M. Borthwick, A. S. Johnson, M. Partington, J. Burn, R. Wilson, and H. M. Arthur, "Therapeutic levels of aspirin and salicylate directly inhibit a model of angiogenesis through a Cox-independent mechanism," *FASEB Journal*, vol. 20, no. 12, pp. 2009–2016, 2006.

[126] L. A. Stark, K. Reid, O. J. Sansom et al., "Aspirin activates the NF-κB signalling pathway and induces apoptosis in intestinal neoplasia in two in vivo models of human colorectal cancer," *Carcinogenesis*, vol. 28, no. 5, pp. 968–976, 2007.

[127] M. Cho, J. Gwak, S. Park et al., "Diclofenac attenuates Wnt/β-catenin signaling in colon cancer cells by activation of NF-κB," *FEBS Letters*, vol. 579, no. 20, pp. 4213–4218, 2005.

[128] K.-A. Sheppard, D. W. Rose, Z. K. Haque et al., "Transcriptional activation by NF-κB requires multiple coactivators," *Molecular and Cellular Biology*, vol. 19, no. 9, pp. 6367–6378, 1999.

[129] M. H. Cobb and E. J. Goldsmith, "How MAP kinases are regulated," *Journal of Biological Chemistry*, vol. 270, no. 25, pp. 14843–14846, 1995.

[130] P. Schwenger, P. Bellosta, I. Vietor, C. Basilico, E. Y. Skolnik, and J. Vilček, "Sodium salicylate induces apoptosis via p38 mitogen-activated protein kinase but inhibits tumor necrosis factor-induced c-Jun N-terminal kinase/stress-activated protein kinase activation," *Proceedings of the National Academy of Sciences of the United States of America*, vol. 94, no. 7, pp. 2869–2873, 1997.

[131] P. Schwenger, E. Y. Skolnik, and J. Vilček, "Inhibition of tumor necrosis factor-induced p42/p44 mitogen-activated protein kinase activation by sodium salicylate," *Journal of Biological Chemistry*, vol. 271, no. 14, pp. 8089–8094, 1996.

[132] M. K. Jones, H. Wang, B. M. Peskar et al., "Inhibition of angiogenesis by nonsteroidal anti-inflammatory drugs: insight into mechanisms and implications for cancer growth and ulcer healing," *Nature Medicine*, vol. 5, no. 12, pp. 1418–1423, 1999.

[133] Z. Xia, M. Dickens, J. Raingeaud, R. J. Davis, and M. E. Greenberg, "Opposing effects of ERK and JNK-p38 MAP kinases on apoptosis," *Science*, vol. 270, no. 5240, pp. 1326–1331, 1995.

[134] Z. Dong, C. Huang, R. E. Brown, and W.-Y. Ma, "Inhibition of activator protein 1 activity and neoplastic transformation by aspirin," *Journal of Biological Chemistry*, vol. 272, no. 15, pp. 9962–9970, 1997.

[135] T. R. Hundley and B. Rigas, "Nitric oxide-donating aspirin inhibits colon cancer cell growth via mitogen-activated protein kinase activation," *Journal of Pharmacology and Experimental Therapeutics*, vol. 316, no. 1, pp. 25–34, 2006.

[136] M. Benhar, D. Engelberg, and A. Levitzki, "ROS, stress-activated kinases and stress signaling in cancer," *EMBO Reports*, vol. 3, no. 5, pp. 420–425, 2002.

[137] R. T. Moon, B. Bowerman, M. Boutros, and N. Perrimon, "The promise and perils of Wnt signaling through β-catenin," *Science*, vol. 296, no. 5573, pp. 1644–1646, 2002.

[138] X. P. Hao, T. G. Pretlow, J. S. Rao, and T. P. Pretlow, "β-catenin expression is altered in human colonic aberrant crypt foci," *Cancer Research*, vol. 61, no. 22, pp. 8085–8088, 2001.

[139] J. M. Chiang, Y. H. Wu Chou, T. C. Chen, K. F. Ng, and J. L. Lin, "Nuclear β-catenin expression is closely related to ulcerative growth of colorectal carcinoma," *British Journal of Cancer*, vol. 86, no. 7, pp. 1124–1129, 2002.

[140] E. J. Chung, S.-G. Hwang, P. Nguyen et al., "Regulation of leukemic cell adhesion, proliferation, and survival by β-catenin," *Blood*, vol. 100, no. 3, pp. 982–990, 2002.

[141] D. Lu, Y. Zhao, R. Tawatao et al., "Activation of the Wnt signaling pathway in chronic lymphocytic leukemia," *Proceedings of the National Academy of Sciences of the United States of America*, vol. 101, no. 9, pp. 3118–3123, 2004.

[142] W. Lu, H. N. Tinsley, A. Keeton, Z. Qu, G. A. Piazza, and Y. Li, "Suppression of Wnt/β-catenin signaling inhibits prostate cancer cell proliferation," *European Journal of Pharmacology*, vol. 602, no. 1, pp. 8–14, 2009.

[143] P. Cowin, T. M. Rowlands, and S. J. Hatsell, "Cadherins and catenins in breast cancer," *Current Opinion in Cell Biology*, vol. 17, no. 5, pp. 499–508, 2005.

[144] M. Shtutman, J. Zhurinsky, I. Simcha et al., "The cyclin D1 gene is a target of the β-catenin/LEF-1 pathway," *Proceedings of the National Academy of Sciences of the United States of America*, vol. 96, no. 10, pp. 5522–5527, 1999.

[145] N. Nath, K. Kashfi, J. Chen, and B. Rigas, "Nitric oxide-donating aspirin inhibits β-catenin/T cell factor (TCF) signaling in SW480 colon cancer cells by disrupting the nuclear β-catenin-TCF association," *Proceedings of the National Academy of Sciences of the United States of America*, vol. 100, no. 22, pp. 12584–12589, 2003.

[146] S. Dihlmann, A. Siermann, and M. Von Knebel Doeberitz, "The nonsteroidal anti-inflammatory drugs aspirin and indomethacin attenuate β-catenin/TCF-4 signaling," *Oncogene*, vol. 20, no. 5, pp. 645–653, 2001.

[147] S. Dihlmann, S. Klein, and M. V. K. Doeberitz Mv, "Reduction of beta-catenin/T-cell transcription factor signaling by aspirin and indomethacin is caused by an increased stabilization of phosphorylated beta-catenin," *Molecular cancer therapeutics*, vol. 2, no. 6, pp. 509–516, 2003.

[148] C. L. Bos, L. L. Kodach, G. R. Van Den Brink et al., "Effect of aspirin on the Wnt/β-catenin pathway is mediated via protein phosphatase 2A," *Oncogene*, vol. 25, no. 49, pp. 6447–6456, 2006.

[149] S. Pathi, I. Jutooru, G. Chadalapaka, V. Nair, S. O. Lee, and S. Safe, "Aspirin inhibits colon cancer cell and tumor growth and downregulates specificity protein (sp) transcription factors," *PLoS ONE*, vol. 7, Article ID e48208, 2012.

[150] P. L. Rice, J. Kelloff, H. Sullivan et al., "Sulindac metabolites induce caspase- and proteasome-dependent degradation of beta-catenin protein in human colon cancer cells," *Molecular cancer therapeutics*, vol. 2, no. 9, pp. 885–892, 2003.

[151] Y. Wang, X. Chen, W. Zhu, H. Zhang, S. Hu, and X. Cong, "Growth inhibition of mesenchymal stem cells by aspirin: involvement of the wnt/β-catenin signal pathway," *Clinical and Experimental Pharmacology and Physiology*, vol. 33, no. 8, pp. 696–701, 2006.

[152] H. Li, L. Liu, M. L. David et al., "Pro-apoptotic actions of exisulind and CP461 in SW480 colon tumor cells involve β-catenin and cyclin D1 down-regulation," *Biochemical Pharmacology*, vol. 64, no. 9, pp. 1325–1336, 2002.

[153] L. Deng, S. Hu, A. R. Baydoun, J. Chen, X. Chen, and X. Cong, "Aspirin induces apoptosis in mesenchymal stem cells requiring Wnt/β-catenin pathway," *Cell Proliferation*, vol. 42, no. 6, pp. 721–730, 2009.

[154] C. V. Rao, B. S. Reddy, V. E. Steele et al., "Nitric oxide-releasing aspirin and indomethacin are potent inhibitors against colon cancer in azoxymethane-treated rats: effects on molecular targets," *Molecular Cancer Therapeutics*, vol. 5, no. 6, pp. 1530–1538, 2006.

[155] N. Nath, R. Vassell, M. Chattopadhyay, M. Kogan, and K. Kashfi, "Nitro-aspirin inhibits MCF-7 breast cancer cell growth: effects on COX-2 expression and Wnt/β-catenin/TCF-4 signaling," *Biochemical Pharmacology*, vol. 78, no. 10, pp. 1298–1304, 2009.

[156] C. Zhu, K. W. Cheng, N. Ouyang et al., "Phosphosulindac (OXT-328) selectively targets breast cancer stem cells in vitro and in human breast cancer xenografts," *Stem Cells*, vol. 30, pp. 2065–2075, 2012.

[157] M. Adachi, H. Sakamoto, R. Kawamura, W. Wang, K. Imai, and Y. Shinomura, "Nonsteroidal anti-inflammatory drugs and oxidative stress in cancer cells," *Histology and Histopathology*, vol. 22, no. 4–6, pp. 437–442, 2007.

[158] B. Rigas, "Novel agents for cancer prevention based on nitric oxide," *Biochemical Society Transactions*, vol. 35, no. 5, pp. 1364–1368, 2007.

[159] E. Fernandes, S. A. Toste, J. L. F. C. Lima, and S. Reis, "The metabolism of sulindac enhances its scavenging activity against reactive oxygen and nitrogen species," *Free Radical Biology and Medicine*, vol. 35, no. 9, pp. 1008–1017, 2003.

[160] D. Costa, A. Gomes, S. Reis, J. L. F. C. Lima, and E. Fernandes, "Hydrogen peroxide scavenging activity by non-steroidal anti-inflammatory drugs," *Life Sciences*, vol. 76, no. 24, pp. 2841–2848, 2005.

[161] A. El Midaoui, R. Wu, and J. De Champlain, "Prevention of hypertension, hyperglycemia and vascular oxidative stress by aspirin treatment in chronically glucose-fed rats," *Journal of Hypertension*, vol. 20, no. 7, pp. 1407–1412, 2002.

[162] T. Ishizuka, A. Niwa, M. Tabuchi, K. Ooshima, and H. Higashino, "Acetylsalicylic acid provides cerebrovascular protection from oxidant damage in salt-loaded stroke-prone rats," *Life Sciences*, vol. 82, no. 13-14, pp. 806–815, 2008.

[163] S. S. Kumari, A. Varghese, D. Muraleedharan, and V. P. Menon, "Protective action of aspirin in experimental myocardial infarction induced by isoproterenol in rats and its effect on lipid peroxidation," *Indian Journal of Experimental Biology*, vol. 28, no. 5, pp. 480–485, 1990.

[164] L.-Y. Qiu, J. Yu, Y. Zhou, and C.-H. Chen, "Protective effects and mechanism of action of aspirin on focal cerebral ischemia-reperfusion in rats," *Yaoxue Xuebao*, vol. 38, no. 8, pp. 561–564, 2003.

[165] M. Tauseef, K. K. Sharma, and M. Fahim, "Aspirin restores normal baroreflex function in hypercholesterolemic rats by its antioxidative action," *European Journal of Pharmacology*, vol. 556, no. 1–3, pp. 136–143, 2007.

[166] S. S. Kanwar, K. Vaiphei, B. Nehru, and S. N. Sanyal, "Antioxidative effects of nonsteroidal anti-inflammatory drugs during the initiation stages of experimental colon carcinogenesis in rats," *Journal of Environmental Pathology, Toxicology and Oncology*, vol. 27, no. 2, pp. 89–100, 2008.

[167] E. C. Yiannakopoulou and E. Tiligada, "Protective effect of salicylates against hydrogen peroxide stress in yeast," *Journal of Applied Microbiology*, vol. 106, no. 3, pp. 903–908, 2009.

[168] H. Kusuhara, H. Komatsu, H. Sumichika, and K. Sugahara, "Reactive oxygen species are involved in the apoptosis induced by nonsteroidal anti-inflammatory drugs in cultured gastric cells," *European Journal of Pharmacology*, vol. 383, no. 3, pp. 331–337, 1999.

[169] C. Giardina and M. S. Inan, "Nonsteroidal anti-inflammatory drugs, short-chain fatty acids, and reactive oxygen metabolism in human colorectal cancer cells," *Biochimica et Biophysica Acta*, vol. 1401, no. 3, pp. 277–288, 1998.

[170] Y. M. Chung, Y. S. Bae, and S. Y. Lee, "Molecular ordering of ROS production, mitochondrial changes, and caspase activation during sodium salicylate-induced apoptosis," *Free Radical Biology and Medicine*, vol. 34, no. 4, pp. 434–442, 2003.

[171] T. Minami, M. Adachi, R. Kawamura, Y. Zhang, Y. Shinomura, and K. Imai, "Sulindac enhances the proteasome inhibitor bortezomib-mediated oxidative stress and anticancer activity," *Clinical Cancer Research*, vol. 11, no. 14, pp. 5248–5256, 2005.

[172] E. Herrero, J. Ros, G. Bellí, and E. Cabiscol, "Redox control and oxidative stress in yeast cells," *Biochimica et Biophysica Acta*, vol. 1780, no. 11, pp. 1217–1235, 2008.

[173] V. Battaglia, M. Salvi, and A. Toninello, "Oxidative stress is responsible for mitochondrial permeability transition induction by salicylate in liver mitochondria," *Journal of Biological Chemistry*, vol. 280, no. 40, pp. 33864–33872, 2005.

[174] H. Raza and A. John, "Implications of altered glutathione metabolism in aspirin-induced oxidative stress and mitochondrial dysfunction in HepG2 cells," *PLoS ONE*, vol. 7, no. 4, Article ID e36325, 2012.

[175] K. Sapienza and R. Balzan, "Metabolic aspects of aspirin-induced apoptosis in yeast," *FEMS Yeast Research*, vol. 5, no. 12, pp. 1207–1213, 2005.

[176] S. Fukuda and L. M. Pelus, "Survivin, a cancer target with an emerging role in normal adult tissues," *Molecular Cancer Therapeutics*, vol. 5, no. 5, pp. 1087–1098, 2006.

[177] M. Lu, A. Strohecker, F. Chen et al., "Aspirin sensitizes cancer cells to TRAIL-induced apoptosis by reducing survivin levels," *Clinical Cancer Research*, vol. 14, no. 10, pp. 3168–3176, 2008.

[178] M. Wang, Z. Tan, R. Zhang, S. V. Kotenko, and P. Liang, "Interleukin 24 (MDA-7/MOB-5) signals through two heterodimeric receptors, IL-22R1/IL-20R2 and IL-20R1/IL-20R2," *Journal of Biological Chemistry*, vol. 277, no. 9, pp. 7341–7347, 2002.

[179] S. Chada, R. B. Sutton, S. Ekmekcioglu et al., "MDA-7/IL-24 is a unique cytokine-tumor suppressor in the IL-10 Family," *International Immunopharmacology*, vol. 4, no. 5, pp. 649–667, 2004.

[180] Z.-Z. Su, M. T. Madireddi, J. J. Lin et al., "The cancer growth suppressor gene mda-7 selectively induces apoptosis in human breast cancer cells and inhibits tumor growth in nude mice," *Proceedings of the National Academy of Sciences of the United States of America*, vol. 95, no. 24, pp. 14400–14405, 1998.

[181] H. Jiang, Z.-Z. Su, J. J. L. Jiao Jiao Lin, N. I. Goldstein, C. S. H. Young, and P. B. Fisher, "The melanoma differentiation associated gene mda-7 suppresses cancer cell growth," *Proceedings of the National Academy of Sciences of the United States of America*, vol. 93, no. 17, pp. 9160–9165, 1996.

[182] Y. Saito, R. Miyahara, B. Gopalan et al., "Selective induction of cell cycle arrest and apoptosis in human prostate cancer cells through adenoviral transfer of the melanoma differentiation-associated-7 (mda-7)/interleukin-24 (IL-24) gene," *Cancer Gene Therapy*, vol. 12, no. 3, pp. 238–247, 2005.

[183] T. Saeki, A. Mhashilkar, X. Swanson et al., "Inhibition of human lung cancer growth following adenovirus-mediated mda-7 gene expression in vivo," *Oncogene*, vol. 21, no. 29, pp. 4558–4566, 2002.

[184] Y. Sun, J. Chen, and B. Rigas, "Chemopreventive agents induce oxidative stress in cancer cells leading to COX-2 overexpression and COX-2-independent cell death," *Carcinogenesis*, vol. 30, no. 1, pp. 93–100, 2009.

[185] B. Rigas and Y. Sun, "Induction of oxidative stress as a mechanism of action of chemopreventive agents against cancer," *British Journal of Cancer*, vol. 98, no. 7, pp. 1157–1160, 2008.

[186] Y. Qin, W. Dai, Y. Wang, X. G. Gong, and M. Lu, "Fe-SOD cooperates with Nutlin3 to selectively inhibit cancer cells in vitro and in vivo," *Biochemical and Biophysical Research Communications*, vol. 431, pp. 169–175, 2013.

[187] E. Ueta, K. Yoneda, T. Kimura et al., "Mn-SOD antisense upregulates in vivo apoptosis of squamous cell carcinoma cells by anticancer drugs and γ-rays regulating expression of the BcL-2 family proteins, COX-2 and p21," *International Journal of Cancer*, vol. 94, no. 4, pp. 545–550, 2001.

Hindawi Publishing Corporation
Oxidative Medicine and Cellular Longevity
Volume 2013, Article ID 102485, 9 pages
http://dx.doi.org/10.1155/2013/102485

Research Article

Rapidly Developing Yeast Microcolonies Differentiate in a Similar Way to Aging Giant Colonies

Libuše Váchová,[1] Ladislava Hatáková,[2] Michal Čáp,[2] Michaela Pokorná,[2] and Zdena Palková[2]

[1] *Institute of Microbiology of the ASCR, v.v.i., 142 20 Prague 4, Czech Republic*
[2] *Department of Genetics and Microbiology, Faculty of Science, Charles University in Prague, 128 44 Prague 2, Czech Republic*

Correspondence should be addressed to Zdena Palková; zdenap@natur.cuni.cz

Received 10 May 2013; Accepted 25 June 2013

Academic Editor: Joris Winderickx

During their development and aging on solid substrates, yeast giant colonies produce ammonia, which acts as a quorum sensing molecule. Ammonia production is connected with alkalization of the surrounding medium and with extensive reprogramming of cell metabolism. In addition, ammonia signaling is important for both horizontal (colony centre versus colony margin) and vertical (upper versus lower cell layers) colony differentiations. The centre of an aging differentiated giant colony is thus composed of two major cell subpopulations, the subpopulation of long-living, metabolically active and stress-resistant cells that form the upper layers of the colony and the subpopulation of stress-sensitive starving cells in the colony interior. Here, we show that microcolonies originating from one cell pass through similar developmental phases as giant colonies. Microcolony differentiation is linked to ammonia signaling, and cells similar to the upper and lower cells of aged giant colonies are formed even in relatively young microcolonies. A comparison of the properties of these cells revealed a number of features that are similar in microcolonies and giant colonies as well as a few that are only typical of chronologically aged giant colonies. These findings show that colony age *per se* is not crucial for colony differentiation.

1. Introduction

When developing on solid media or in nonshaken liquid environments, yeast cells can organize into structured and differentiated multicellular communities where individual cells gain specific properties and can fulfill specific roles. Colonies, stalks, biofilms, and flors on liquid surfaces are examples of such organized communities [1–11]. Colonies growing on solid agar medium usually originate either from individual cells (microcolonies) or from a cell suspension spotted onto the agar (giant colonies) [12–14]. The morphology and internal architecture of both microcolonies and giant colonies are dependent on the yeast species or even the strain that forms the colony, the cultivation conditions (e.g., nutrient sources), and developmental phase (i.e., the age of the colony). Thus, for example, natural strains of *Saccharomyces cerevisiae* form structured biofilm colonies [15, 16] that to some extent resemble the colonies formed by pathogenic yeasts of the *Candida* or *Cryptococcus* species [7]. These structured colonies exhibit features (such as the presence of multidrug resistance transporters and an extracellular matrix) that are important for the formation, development, and survival of natural yeast biofilms [17]. The internal architecture of these structured colonies differs strikingly from the architecture of smooth colonies that are formed by laboratory strains of *S. cerevisiae*.

As we have shown previously, giant colonies of *S. cerevisiae* laboratory strains grown on solid complex respiratory medium pass through distinct developmental phases that can be detected by monitoring the pH changes of the medium, changing from the acidic to near alkali and vice versa [13]. The alkali phase of colony development is accompanied by the production of volatile ammonia that functions as a signal important for colony metabolic reprogramming and long-term survival [13, 18–20]. Such metabolic reprogramming appears to be more important for colony survival than some

mechanisms eliminating stress factors, such as stress defense enzymes [21]. We have demonstrated that ammonia-related changes are important for diversification between the cells in the center and margin of a colony [20–22]. We have also recently shown that ammonia signaling and related metabolic reprogramming are involved in the diversification of the cells of the colony and the formation of cells with specialized functions precisely localized within the colony [23, 24]. Thus, during the switch of giant colonies to the alkali phase, both horizontal and vertical differentiations occur, where central and margin cells behave differently, as do cells located in the upper and lower regions of the colony center. Detailed analysis of the central colony region revealed two major cell subpopulations located in the upper (U cells) and lower (L cells) colony areas that differ in their morphology, physiology, and gene expression. U cells are large stress-resistant cells with a longevity phenotype, while L cells are smaller, more sensitive to various stresses (such as heat shock and ethanol treatment), and lose viability over the time. Both cell types significantly differ in their gene expression, as shown by a transcriptomic comparison of U and L cells isolated from 15- and 20-day-old colonies [23]. According to these transcriptomic data, U cells seem to be metabolically active cells with induced amino acid metabolism, glycolysis, and some other pathways such as the pentose-phosphate shunt. U cells also express a large group of genes coding for ribosomal and some other proteins of the translational machinery. These genes are usually controlled by the TOR pathway under nutrient-rich conditions. Some other expression characteristics of U cells, however, indicate that some pathways usually active under conditions of nutrient limitation are also induced in U cells and affect their physiology [23]. For example, a large group of amino acid biosynthetic genes is controlled by the transcription factor Gcn4p [25]. In contrast to U cells, L cells behave like stressed cells—they have low metabolic activity and seem to activate some degradative mechanisms that can contribute to the release of compounds that can be exploited by U cells.

An important question is to what extent chronological aging of the whole colony population on one side and active signaling (which includes the action of ammonia and related metabolic reprogramming as well as other not yet identified signaling and regulatory processes) on the other side contribute to *S. cerevisiae* colony development, differentiation, and long-term survival. As was mentioned above, giant colonies activate ammonia signaling and form U and L cells between days 7 and 10 of colony development when most of the colonial cells are in the stationary (or slow growth) phase. That is, cells differentiating into U and L cells are relatively old and most of them have already persisted in nondividing form for several days. Both of the above-mentioned processes (chronological aging and signal-related metabolic reprogramming) are therefore running in parallel in giant colonies and thus both could contribute to colony differentiation and U and L cell properties. In contrast to giant colonies, switch to the alkali phase and ammonia signaling among microcolonies usually starts much earlier than in giant colonies and central differentiated cells are therefore much younger (i.e., less chronologically aged) in microcolonies than in giant colonies. However, the major expression changes that accompany medium alkalization and ammonia production in microcolonies resemble those changes identified in giant colonies [18]. Similarly, Ato1p, a putative ammonia exporter, is produced in the margin and upper central cell layer in both giant colonies and microcolonies when they begin to alkalize the medium [22, 24]. Here, we examined the main features of the central parts of differentiated microcolonies and compared these features to those described in giant colonies. Through this analysis, we showed that prominent characteristics of central upper cells of yeast colonies are not related to colony aging but dependent on active colony reprogramming. On the other hand, some other features such as in particular the stress resistance of cells in the colony interior (L cells) significantly differ in younger microcolonies compared to giant colonies, being related to colony aging.

2. Results and Discussion

2.1. Microcolonies Pass through the Same Developmental Phases as Giant Colonies. Similarly to giant colonies, microcolonies of BY4742 growing on GMA solid plates pass through the developmental phases characterized by changes in external pH and ammonia production [24, 26]. Microcolonies, thus, pass through the first acidic, alkali and second acidic developmental phases (Figure 1(a)), where the alkali phase is accompanied by ammonia production. In contrast to giant colonies, in which the timing of the transition to the ammonia-producing period is typically standardized by the inoculation of six giant colonies on the plate [18], the timing of the acid-to-alkali microcolony transition is dependent on the density of the plated microcolonies. More densely plated microcolonies switch to the ammonia-producing period earlier than microcolonies growing at a lower density on the plate. Like giant colonies that synchronize ammonia production and developmental phases [27], microcolonies on the same plate also synchronize themselves via the ammonia that starts to be produced by the most densely plated microcolonies. For the experiments described in the following sections, we used a standard plating of approximately 5000 microcolonies per plate, that is the density of microcolonies that results in microcolony transition to the alkali phase between days 3 and 4 of colony growth.

2.2. Switch to Ammonia Production Is Accompanied by Differentiation of Microcolonies and Formation of U_m and L_m Cells. As with giant colonies [23], the transition of microcolonies to the alkali phase is accompanied by a diversification of the relatively homogeneous cell population of the 1st acidic phase microcolonies to two major cell types that are localized in the upper and lower layers of alkali phase microcolonies. Figure 1 shows that these upper and lower cells morphologically resemble the U and L cells of giant colonies, respectively. Cells in the lower parts of a microcolony (L_m cells) are smaller and usually contain one large vacuole, while cells in the upper parts (U_m cells) are larger with no visible vacuoles. The staining of microcolony sections by Nile red (Figure 2) as well

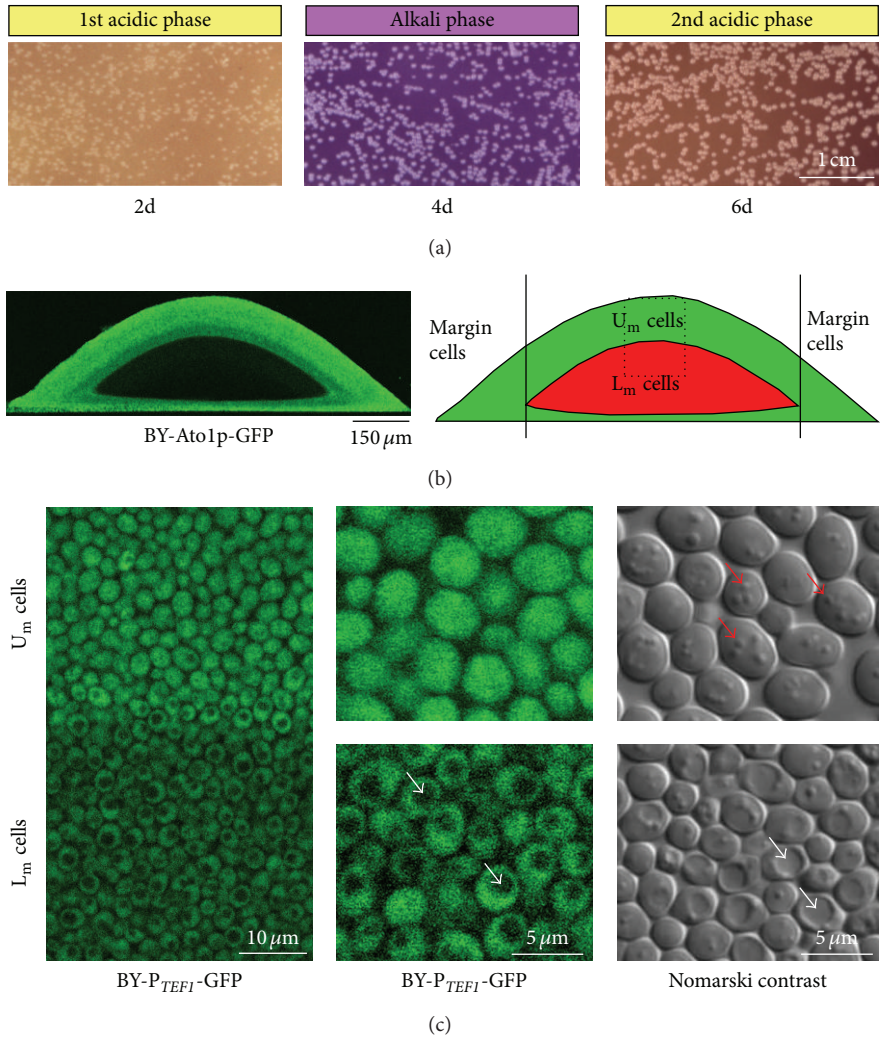

FIGURE 1: Developmental phases and vertical differentiation of yeast microcolonies. (a) Microcolonies develop on GMA-BKP. BKP functions as pH dye indicator with pKa of 6.3, the color of which changes from yellow at acidic pH to purple in more alkali pH. Microcolonies were in the 1st acidic (2 d), alkali (4 d), and beginning of the 2nd acidic (6 d) phases. Bird views of microcolonies are shown. (b) Vertical transversal cross-section viewed by 2PE-CM of akali-phase microcolony formed by the strain producing Ato1p-GFP (left) and scheme of the localization of three cell subpopulations within the microcolony (right). (c) Boundary between U_m and L_m cells (left) and morphology of U_m and L_m cells (center) of BY-P_{TEF1}-GFP strain at vertical cross-sections of 4-day-old microcolonies analyzed by 2PE-CM. Cytosolic expression of GFP is used for *in situ* visualization of U_m and L_m cells by 2PE-CM since it enables the visualization of large vacuoles in L_m cells (from which the fluorescence is excluded) and the size of U_m and L_m cells. Morphology of U_m and L_m cells from 4-day-old BY4742 microcolonies separated by gradient centrifugation and visualized by Nomarski contrast (right). White arrows show large vacuoles in L_m cells; red arrows show lipid droplets in U_m cells.

as Nomarski contrast visualization (Figure 1(c)) confirmed that similarly to giant colonies, U_m cells contain several large lipid droplets, while L_m cells usually contain one small lipid droplet.

In addition to their morphology similarities, we found similar profiles of proteins produced by the U_m cells from 4-day-old microcolonies and by the U cells of 15-day-old giant colonies [23]. Hence, all three Ato proteins (Ato1p, Ato2p, and Ato3p) started to be produced exclusively in U_m cells but not in L_m cells (as shown for Ato3p-GFP in Figure 3) after the microcolonies had entered the alkali phase. Similarly, Pox1p-GFP and Icl2p-GFP are preferentially produced in U_m cells (Figure 3) as well as in the U cells of giant colonies [23]. In addition, the production profile of Ole1p-GFP is also similar in microcolonies and giant colonies. Ole1p-GFP is produced and properly localized to the endoplasmatic reticulum (ER) in L and L_m cells, respectively, while it is degraded within vacuoles in U and U_m cells, respectively, (Figure 3).

Another typical feature of differentiated giant colonies is an increased activity of TORC1 in U cells and its inactivation in L cells, as shown by the different localization of Gat1p-GFP in the two cell types [23]. The GATA transcription factor Gat1p was shown to be phosphorylated by TORC1, which results in Gat1p cytosolic localization and thus functional

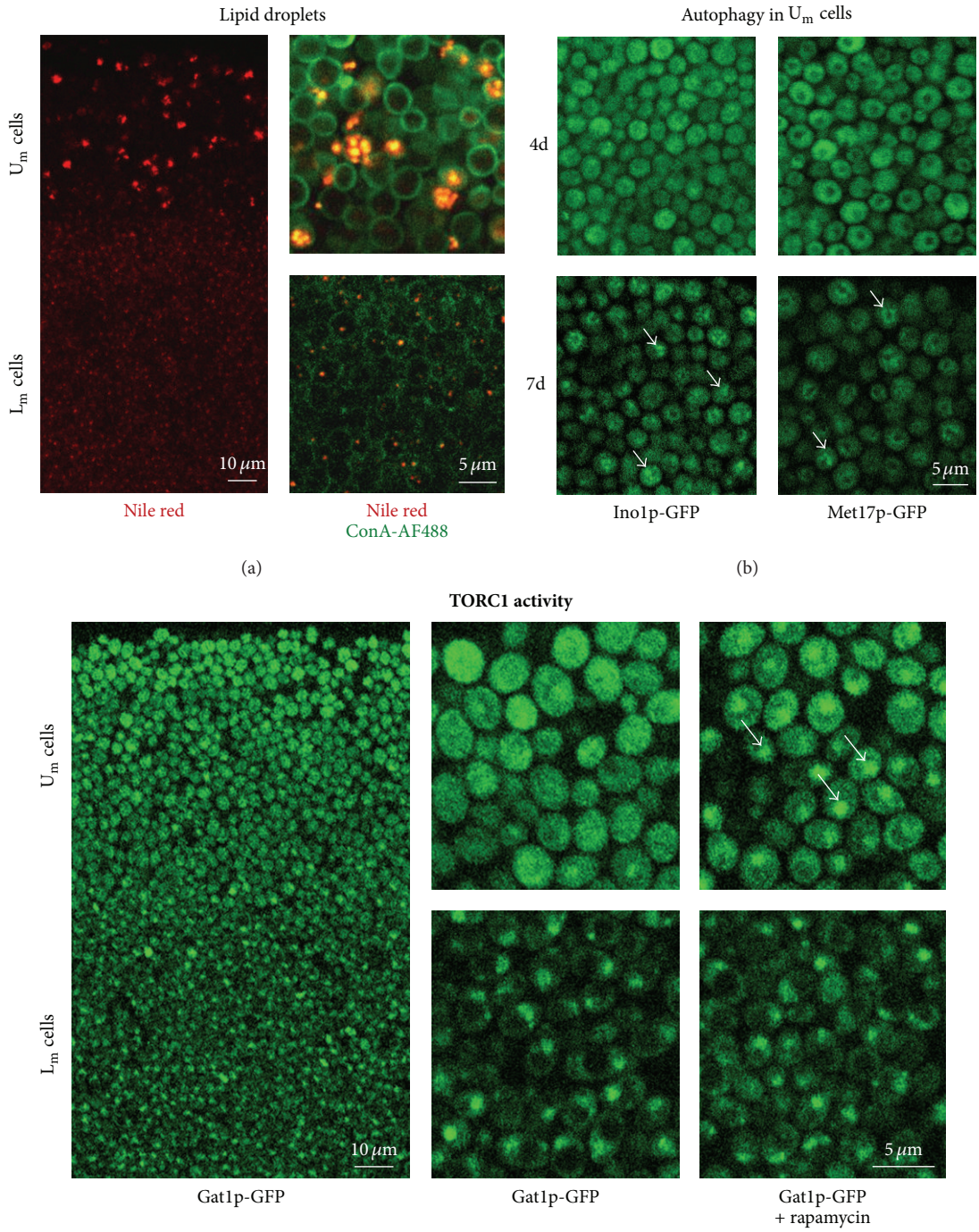

Figure 2: Localization of cells containing storage compounds (lipid droplets) and cells with active autophagy and TORC1 signaling pathway. (a) Vertical transversal cross-sections of 4-day-old BY4742 microcolonies. Left, boundary between U_m and L_m cells, lipid droplets are stained with Nile red. Right, lipid droplets of U_m and L_m cells stained with Nile red (red) and cell walls with concanavalin A conjugated with Alexa Fluor 488 (green). (b) Vertical cross-sections of 4- and 7-day-old microcolonies of strains producing cytosolic proteins Ino1p-GFP or Met17p-GFP. U_m cells are shown; arrows indicate GFP in vacuoles of 7-day-old U_m cells where cytosolic proteins were delivered to vacuoles via autophagy. (c) Vertical cross-sections of 4-day-old microcolonies formed by Gat1p-GFP strain showing localization of Gat1p-GFP protein in U_m and L_m cells. Arrows indicate relocalization of Gat1p-GFP from the cytosol to the nuclei of U_m cells after treating the cut edge of the colony section with 250 ng/mL rapamycin, an inhibitor of TORC1.

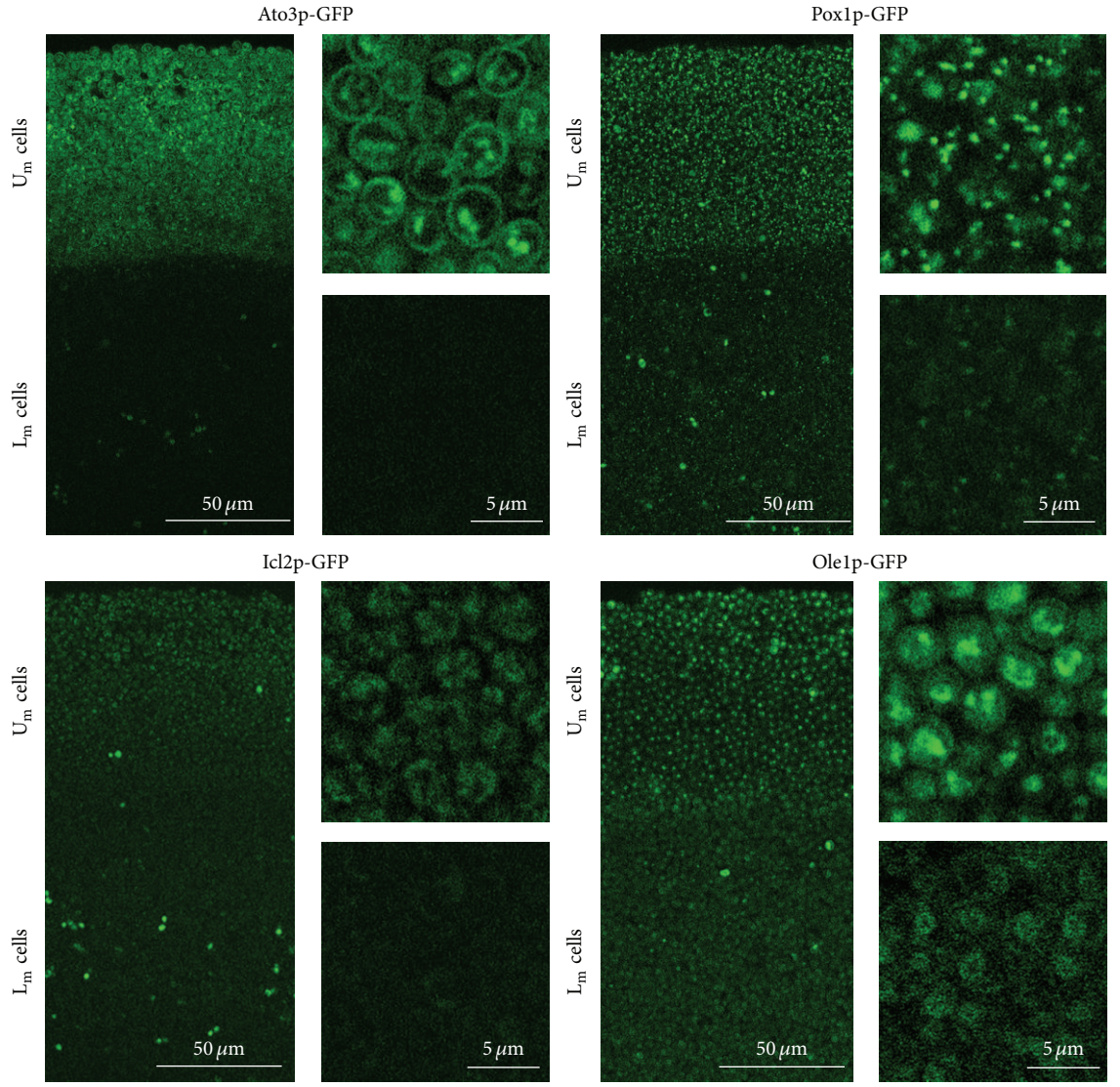

Figure 3: Profile of selected, GFP-labeled proteins in alkali phase microcolonies. 2PE-CM of vertical transversal cross-sections of alkali phase (4-day-old) microcolonies formed by strains producing particular labeled proteins.

inhibition [28]. Confocal microscopy of microcolony cross-sections clearly showed that Gat1p-GFP is localized to the nuclei of L_m cells, which indicates that TORC1 is inactive in L_m cells (Figure 2(c)). In U_m cells, TORC1 is apparently active, as Gat1p-GFP is predominantly in the cytosol (i.e., phosphorylated) and it only moves to the nucleus when a TORC1 inhibitor rapamycin is added to the colony sections.

In summary, these data show that several typical features of the U cells of giant colonies are found in the U_m cells of microcolonies that switch to the alkali phase of ammonia production, even though U_m cells are far younger chronologically than the U cells of giant colonies. The typical features of U cells, such as the accumulation of lipid droplets, production of typical marker proteins, and active TORC1, are found in U_m cells soon after the upper and lower layers have formed in microcolonies entering the alkali phase. These data therefore indicate that ammonia-related signaling events are more significant than chronological age in the formation of these typical features of upper cells. This is in agreement with the previous finding that in giant colonies, the formation of cells morphologically resembling U cells can also be prematurely induced by ammonia from an artificial source [23].

2.3. Autophagy Appears Later in U_m Cells. Another typical feature of the U cells of giant colonies is active autophagy [23]. Monitoring the cellular localization of GFP in the microcolonies of strains producing cytosolic Ino1p and Met17p labeled with GFP showed a significant vacuolar GFP signal in the U_m cells of 7-day-old microcolonies (Figure 2). However, no vacuolar localization of GFP was visible in 4-day-old colonies. As in the L cells of giant colonies, no vacuolar GFP was detected in L_m cells of any age. These data showed that U_m cells activate autophagy like the U cells of giant

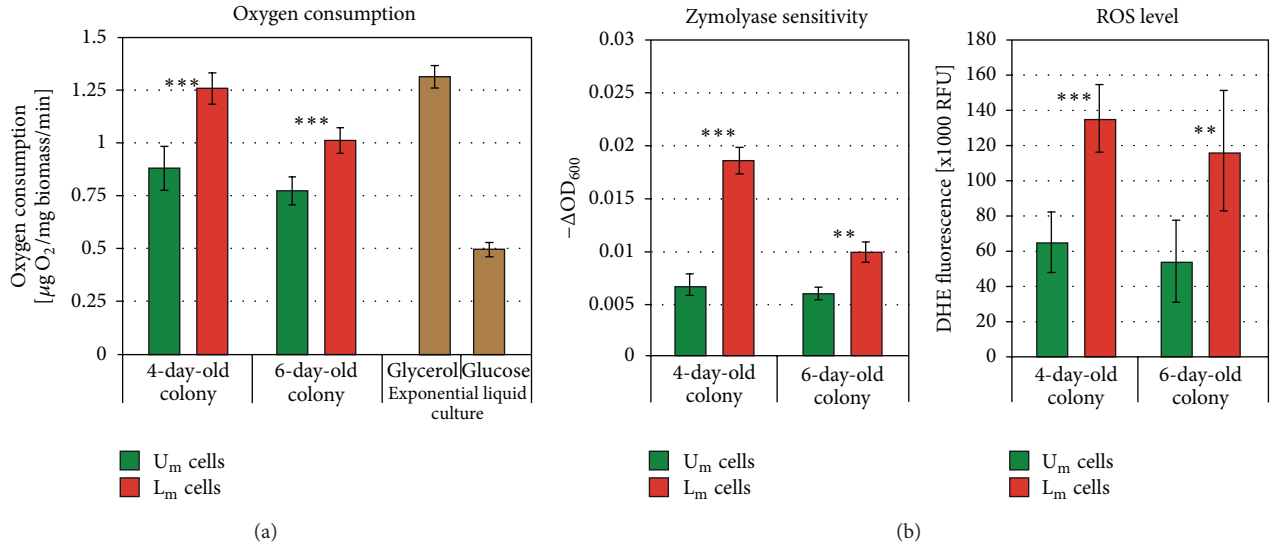

FIGURE 4: Physiological differences between U_m and L_m cells from 4- and 6-day-old colonies. (a) Oxygen consumption as a measure of respiratory capacity of U_m and L_m cells isolated from 4- and 6-day-old microcolonies. Respiration of glucose- and glycerol-grown cells from exponential liquid shaken cultures is shown for comparison. (b) Stress-related features of U_m and L_m. Sensitivity to zymolyase is shown as a decrease in optical density of cell suspensions (left). Production of ROS measured as fluorescence of DHE (right). All data represent averages of at least three experiments ±SD. **—t-test P value < 0.01; ***—t-test P value < 0.001.

colonies. However, the autophagy is initiated later than other typical processes of U_m cells and seems, therefore, to be more dependent on the chronological aging of U_m cells.

2.4. U_m and L_m Cells Differ in Their Respiratory Capacity. An important and unexpected difference between the U and L cells of giant colonies is in the capacity of these cells to consume oxygen [23]. Although localized close to the air, U cells exhibit significantly decreased ability to consume oxygen as compared with L cells, and, accordingly, U cells contain large swollen mitochondria with few cristae. On the other hand, L cells maintain their capacity to consume oxygen quite effectively and contain normal-looking cristated mitochondria. To compare the respiration of U_m and L_m cells, we separated these cells from 4- to 6-day-old microcolonies by gradient centrifugation and measured their respiratory capacity. As shown in Figure 4(a), the U_m cells of 4-day-old microcolonies already consume less oxygen than L_m cells of the same age. This difference persisted in older colonies. These data show that as with the other features described above, the decreased respiratory capacity of U cells identified in 15-day-old giant colonies and in 4-day-old alkali phase microcolonies is a characteristic that is also most likely predominantly induced by a signaling event and not by the aging of colony.

2.5. L_m Cells Differ from L Cells of Giant Colonies in Some of Their Features. Other physiological differences between the U and L cells of giant colonies are in terms of reactive oxygen species (ROS) production, resistance to the cell wall degrading enzyme zymolyase, and sensitivity to various stresses, such as heat shock and ethanol treatment [23]. Measurement of the ROS level in U_m and L_m cells separated from microcolonies and stained with dihydroethidium (DHE) showed that L_m cells produce significantly higher amount of ROS than U_m cells. This difference was significant in 4-day-old microcolonies and persisted in older microcolonies (Figure 4(b)). L_m cells are also more sensitive to zymolyase treatment than U_m cells, thus, indicating a weaker cell wall of L_m cells. Thus, the differences in both ROS production and zymolyase resistance between U_m and L_m cells were similar to those observed between the U and L cells of giant colonies.

On the other hand, an analysis of U_m and L_m cells from 4- to 6-day-old microcolonies did not reveal significant differences in the sensitivity of the two cell types to heat shock and ethanol treatment (not shown). In general, both U_m and L_m cells were slightly more resistant to heat shock than U cells from 15-day-old giant colonies and significantly more resistant than L cells from such colonies (i.e., than cells that exhibit a strong decrease in viability after heat shock and ethanol treatment) [23]. In other words, L_m cells from 6-day-old colonies have not yet decreased their resistance to these stresses.

Another difference between microcolonies and giant colonies was in their levels of certain amino acids in the upper and lower cells. While the level of intracellular glutamine was significantly higher in U than in the L cells of giant colonies, only a negligible difference was observed between the U_m and L_m cells of 6-day-old microcolonies (and no difference in 4-day-old microcolonies). On the other hand, differences in amino acids such as lysine, alanine, and GABA that are present in higher concentrations in L cells than in the U cells of giant colonies are already detectable in 6-day-old microcolonies. Lysine, alanine, and GABA are present in 2.3, 1.6, and 4.9 times higher concentrations in L_m cells than in U_m cells, respectively. These values are comparable with L/U ratio

of 1.6, 2.2, and 3.6, respectively, for 15-day-old giant colonies [23]. These data indicate that particularly a drop in glutamine in L cells is also connected with the chronological aging or prolonged starvation of colonies.

In summary, the data indicate that L_m cells from 4- to 6-day-old microcolonies are in a better physiological condition than the L cells of 15- to 20-day-old giant colonies. The observed decrease in the resistance and viability of the L cells of giant colonies as well as the drop in their glutamine content thus seems to appear later during colony chronological aging and is probably not directly related to the changes induced by ammonia signaling and/or related metabolic reprogramming. This conclusion is also supported by the observation that some of the proteins that started to be produced in the L cells of 15-day-old giant colonies and the production which increases later in 20-day-old giant colonies (such as Ino1p and Met17p) are not yet produced in the L_m cells of 4- to 6-day-old microcolonies (not shown).

3. Conclusions

The presented data show that various features typical of the U cells of giant colonies growing on complex respiratory medium and undergoing differentiation during their transition to the ammonia-producing alkali phase (10- to 15-day-old colonies) [23] are also found in U_m cells located in the upper layers of alkali phase microcolonies that are only 3 to 4 days old. These features include the production of specific proteins, accumulation of storage material such as lipid droplets, activity of specific regulators such as TORC1, decreased function of mitochondria, low level of ROS, and high resistance to zymolyase, indicating a strengthening of the cell wall. Thus, all of these features of U cells seem to be predominantly related to signaling events and the metabolic reprogramming that accompanies the colony transition from the acidic to the alkali developmental phase [18, 22], rather than to the cell chronological aging. Such signaling processes leading to colony reprogramming could be initiated (by not yet identified mechanism(s)), for example, in the first microcolony that senses a nutrient shortage, that is, in a microcolony that is located in the densest area of plated microcolonies. Ammonia is then the signal that spreads the information about "the need for reprogramming" to the other microcolonies over the whole plate. The ability of ammonia to prematurely induce colonies to ammonia production independently of their current developmental phase [27] guarantees that even the sparsely plated microcolonies become induced and initiate the reprogramming and differentiation while still experiencing nutrient abundance. U_m cells gain the major properties of the U cells of giant colonies, although they have spent a much shorter time in the stationary or slow growing phase than U cells.

A comparison of the transcriptomes of "outside" and "inside" cells separated by FACS from 4-day-old microcolonies growing on complex glucose medium [29] showed that some expression characteristics of U cells from giant colonies grown on complex respiratory medium [23] are also found in "outside" cells. These characteristics include the expression of genes coding for ribosomal proteins and proteins of the translational machinery, genes for glycolytic enzymes, genes involved in amino acid metabolism, and some others [29]. Similarly, we observed the production of carbonic anhydrase Nce103p in the upper cell layers of microcolonies growing both on complex glucose [30] and complex glycerol (unpublished data) agar media. These data indicate that the expression of particular genes and activation of specific metabolic pathways could be profitable for cells in the upper layers of yeast colonies.

In contrast to U_m cells, only some features of L cells are preserved in L_m cells of 4- to 6-day-old microcolonies compared to 15- to 20-day-old giant colonies. These include a higher respiratory capacity, higher production of ROS, higher sensitivity to zymolyase, and the production of some proteins (such as Ole1p). Traven et al. [29] also demonstrated an increased expression of genes required for the activity of the mitochondrial respiratory chain genes in the "inside" cells of 4-day-old microcolonies (cells at a similar position within the colony to L cells) grown on glucose complex medium. All of these features are also typical of the L cells of 15- to 20-day-old giant colonies grown on complex respiratory medium [23]. On the other hand, other features of the L cells of giant colonies are not yet present in the L_m cells of 4- to 6-day-old microcolonies. In particular, L_m cells do not exhibit an enhanced sensitivity to some stresses such as heat shock and ethanol treatment, which indicates that these cells are in a better physiological condition than much older L cells from giant colonies. These stress-related features seem to be therefore more dependent on the chronological age of L cells and could be also related to the duration of the coexistence of U and L cells. Previous findings suggested that U cells are fed at the expense of L cells [23] which could then lead to a deepening of starvation of L cells over the time and to a consequent decrease in their overall viability in older giant colonies. Similarly, autophagy, which seems to be important for the longevity of U cells [23], is only activated later in U_m of 6- to 7-day-old microcolonies. This finding suggests that the regulation of autophagy is partially dependent on signaling events guiding the development of U cells (autophagy is only activated in U cells) but that it is also dependent on the aging and nutrition status of U cells.

4. Material and Methods

4.1. Strains and Media. *S. cerevisiae* strain BY4742 (MATα, *his3*Δ, *leu2*Δ, *lys2*Δ, *ura3*Δ) was from the EUROSCARF collection. BY4742-derived strains containing proteins (Ato1p, Ato3p, Pox1p, Icl2p, Ole1p, Ino1p, Met17p, and Gat1p) fused with GFP at their C-terminus were constructed as described previously [23, 24]. BY-P_{TEF1}-GFP strain expressing GFP under the control of constitutive promoter of *TEF1* gene (P_{TEF1}) was constructed by integration of P_{TEF1}-GFP-natNT2 cassette amplified from pYM-N21 plasmid [31] into *HIS3* locus of BY4742 strain. Yeast microcolonies were grown at 28°C either on GMA (1% yeast extract, 3% glycerol, 1% ethanol, 2% agar, 10 mM $CaCl_2$) or on GMA-BKP (GMA,

0.01% bromocresol purple). For standard experiments, cells were plated at an approximate density of 5×10^3 per plate.

4.2. Two-Photon Excitation Confocal Microscopy (2PE-CM). The microcolony sample preparation and 2PE-CM of transversal vertical cross-section of microcolonies were performed according to [24]. When required, the microcolony cross-sections were stained with Nile red (2.5 μg/mL) and concanavalin A labeled with Alexa Fluor 488 (ConA-AF, 30 μg/mL) as described in [17]. Alternatively, GFP fluorescence was monitored. An SP2 AOBS MP confocal scanner microscope (Leica) fitted with a Ti:Sapphire Chameleon Ultra laser (Coherent Inc.) and 63×/1.20 water immersion plan apochromat objective were used. Excitation wavelength was 920 nm, and emission bandwidths were 470–540 nm for ConA, 580–750 nm for NR, and 480–595 nm for GFP.

4.3. Colony Images. Colony images were captured in transmitted light with a Navitar objective and a complementary metal-oxide semiconductor camera (ProgRes CT3; Jenoptik).

4.4. Sorbitol Gradient Cell Fractionation. Cells from microcolonies were fractionated into subpopulations by centrifugation as described in [23] with the following modification: instead of sucrose, a 10–35% sorbitol gradient was used to avoid changes that could be induced by sucrose in the relatively young cells of microcolonies.

4.5. U and L Cell Resistance to Stresses. Cell resistance was assayed using 10-fold serial dilutions of cell suspensions ($OD_{600} = 10$) that were incubated at 52°C for 45 or 90 min or in 20% ethanol for 60 min and compared to untreated controls. Zymolyase resistance was determined as the decrease in the OD_{600} of a cell suspension (starting $OD_{600} = 0.5$) in 50 mM potassium phosphate buffer, pH 7.5 with 2 mM dithiothreitol, and 5 U/mL zymolyase (MP Biomedicals).

4.6. Respiration Rate and ROS Quantification. The oxygen consumption of 5 mg of freshly isolated U_m or L_m wet cell biomass was determined at 30°C in 1 mL of water using a 782 oxygen meter with a 1-mL MT-200A cell (Strathkelvin Instruments). ROS was quantified using DHE staining according to Čáp et al. [21] with minor modifications. Briefly, isolated U_m and L_m cells were resuspended in water to a final concentration of 100 mg/mL. 7.5 μL of this suspension was incubated with 42.5 μL of water and 5 μL of 25 μg/mL DHE solution (freshly prepared from 1 mg/mL stock solution in DMSO). Cells were stained for 25 min in the dark and diluted with 1.95 mL of water, and the DHE fluorescence was measured using a FluoroMax 3 spectrofluorometer (Jobin Yvon) with excitation/emission wavelengths of 480/604 nm.

4.7. Amino Acid Concentration. Total intracellular amino acids were extracted from cell suspensions in water by boiling for 5 min, and the concentration was determined by HPLC with precolumn derivatization by OPA [23, 32] with a ZORBAX Eclipse AAA, 3.5 mm, 4.6 × 75 mm reverse phase column (Agilent), and fluorescence detection.

Authors' Contribution

L. Hatáková and M. Čáp contributed equally to the work.

Acknowledgments

The authors thank Hana Žďárská for her assistance, technical support, and construction of the BY-P_{TEF1}-GFP strain. This work was supported by the Grant Agency of the Czech Republic (13-08605S), Charles University in Prague (UNCE 204013), and the Ministry of Education (MSM0021620858), RVO 61388971 and cofinanced by the European Social Fund and the state budget of the Czech Republic (CZ.1.07/2.3.00/30.0061).

References

[1] J. Bonhomme and C. d'Enfert, "*Candida albicans* biofilms: building a heterogeneous, drug-tolerant environment," *Current Opinion in Microbiology*, 2013.

[2] C. Cantarelli and A. Martini, "On the pellicle formation by "flor" yeasts," *Antonie van Leeuwenhoek*, vol. 35, pp. F35–F36, 1969.

[3] D. Engelberg, A. Mimran, H. Martinetto et al., "Multicellular stalk-like structures in *Saccharomyces cerevisiae*," *Journal of Bacteriology*, vol. 180, no. 15, pp. 3992–3996, 1998.

[4] S. P. Hawser and L. J. Douglas, "Biofilm formation by *Candida* species on the surface of catheter materials *in vitro*," *Infection and Immunity*, vol. 62, no. 3, pp. 915–921, 1994.

[5] C. C. Lindegren and E. Hamilton, "Autolysis and sporulation in the yeast colony," *Botanical Gazette*, vol. 105, pp. 316–321, 1944.

[6] Z. Palkova, "Multicellular microorganisms: laboratory versus nature," *EMBO Reports*, vol. 5, no. 5, pp. 470–476, 2004.

[7] Z. Palková and L. Váchová, "Life within a community: benefit to yeast long-term survival," *FEMS Microbiology Reviews*, vol. 30, no. 5, pp. 806–824, 2006.

[8] S. Piccirillo, M. G. White, J. C. Murphy, D. J. Law, and S. M. Honigberg, "The Rim101p/PacC pathway and alkaline pH regulate pattern formation in yeast colonies," *Genetics*, vol. 184, no. 3, pp. 707–716, 2010.

[9] T. B. Reynolds and G. R. Fink, "Bakers' yeast, a model for fungal biofilm formation," *Science*, vol. 291, no. 5505, pp. 878–881, 2001.

[10] G. Zara, S. Zara, C. Pinna, S. Marceddu, and M. Budroni, " *FLO11* gene length and transcriptional level affect biofilm-forming ability of wild flor strains of *Saccharomyces cerevisiae*," *Microbiology*, vol. 155, no. 12, pp. 3838–3846, 2009.

[11] S. Zara, M. K. Gross, G. Zara, M. Budroni, and A. T. Bakalinsky, "Ethanol-independent biofilm formation by a flor wine yeast strain of *Saccharomyces cerevisiae*," *Applied and Environmental Microbiology*, vol. 76, no. 12, pp. 4089–4091, 2010.

[12] A. Kockova-Kratochvilova, *Yeasts and Yeast-Like Organisms*, VCH, Weinheim, Germany, 1990.

[13] Z. Palkova, B. Janderova, J. Gabriel, B. Zikanova, M. Pospisek, and J. Forstova, "Ammonia mediates communication between yeast colonies," *Nature*, vol. 390, no. 6659, pp. 532–536, 1997.

[14] M. Richards, "The use of giant-colony morphology for the differentiation of brewing yeast," *Journal of the Institute of Brewing*, vol. 73, pp. 162–166, 1966.

[15] J. A. Granek and P. M. Magwene, "Environmental and genetic determinants of colony morphology in yeast," *PLoS Genetics*, vol. 6, no. 1, Article ID e1000823, 2010.

[16] M. Kuthan, F. Devaux, B. Janderová, I. Slaninová, C. Jacq, and Z. Palková, "Domestication of wild *Saccharomyces cerevisiae* is accompanied by changes in gene expression and colony morphology," *Molecular Microbiology*, vol. 47, no. 3, pp. 745–754, 2003.

[17] L. Váchová, V. Štovíček, O. Hlaváček et al., "Flo11p, drug efflux pumps, and the extracellular matrix cooperate to form biofilm yeast colonies," *Journal of Cell Biology*, vol. 194, no. 5, pp. 679–687, 2011.

[18] Z. Palková, F. Devaux, M. Řičicová, L. Mináriková, S. Le Crom, and C. Jacq, "Ammonia pulses and metabolic oscillations guide yeast colony development," *Molecular Biology of the Cell*, vol. 13, no. 11, pp. 3901–3914, 2002.

[19] L. Váchová, F. Devaux, H. Kučerová, M. Řičicová, C. Jacq, and Z. Palková, "Sok2p transcription factor is involved in adaptive program relevant for long term survival of *Saccharomyces cerevisiae* colonies," *Journal of Biological Chemistry*, vol. 279, no. 36, pp. 37973–37981, 2004.

[20] L. Váchová and Z. Palková, "Physiological regulation of yeast cell death in multicellular colonies is triggered by ammonia," *Journal of Cell Biology*, vol. 169, no. 5, pp. 711–717, 2005.

[21] M. Čáp, L. Váchová, and Z. Palková, "Yeast colony survival depends on metabolic adaptation and cell differentiation rather than on stress defense," *Journal of Biological Chemistry*, vol. 284, no. 47, pp. 32572–32581, 2009.

[22] L. Vachova, H. Kucerova, F. Devaux, M. Ulehlova, and Z. Palkova, "Metabolic diversification of cells during the development of yeast colonies," *Environmental Microbiology*, vol. 11, pp. 494–504, 2009.

[23] M. Cap, L. Stepanek, K. Harant, L. Vachova, and Z. Palkova, "Cell differentiation within a yeast colony: metabolic and regulatory parallels with a tumor-affected organism," *Molecular Cell*, vol. 46, pp. 436–448, 2012.

[24] L. Váchová, O. Chernyavskiy, D. Strachotová et al., "Architecture of developing multicellular yeast colony: spatio-temporal expression of Ato1p ammonium exporter," *Environmental Microbiology*, vol. 11, no. 7, pp. 1866–1877, 2009.

[25] K. Natarajan, M. R. Meyer, B. M. Jackson et al., "Transcriptional profiling shows that Gcn4p is a master regulator of gene expression during amino acid starvation in yeast," *Molecular and Cellular Biology*, vol. 21, no. 13, pp. 4347–4368, 2001.

[26] L. Váchová and Z. Palková, "Aging and longevity of yeast colony populations: metabolic adaptation and differentiation," *Biochemical Society Transactions*, vol. 39, no. 5, pp. 1471–1475, 2011.

[27] Z. Palková and J. Forstová, "Yeast colonies synchronise their growth and development," *Journal of Cell Science*, vol. 113, no. 11, pp. 1923–1928, 2000.

[28] T. S. Cunningham, R. Andhare, and T. G. Cooper, "Nitrogen catabolite repression of *DAL80* expression depends on the relative levels of Gat1p and Ure2p production in *Saccharomyces cerevisiae*," *Journal of Biological Chemistry*, vol. 275, no. 19, pp. 14408–14414, 2000.

[29] A. Traven, A. Janicke, P. Harrison, A. Swaminathan, T. Seemann, and T. H. Beilharz, "Transcriptional profiling of a yeast colony provides new insight into the heterogeneity of multicellular fungal communities," *PLoS ONE*, vol. 7, Article ID e46243, 2012.

[30] F. Cottier, M. Raymond, O. Kurzai et al., "The bZIP transcription factor Rca1p is a central regulator of a novel CO_2 sensing pathway in yeast," *PLoS Pathogens*, vol. 8, no. 1, Article ID e1002485, 2012.

[31] C. Janke, M. M. Magiera, N. Rathfelder et al., "A versatile toolbox for PCR-based tagging of yeast genes: new fluorescent proteins, more markers and promoter substitution cassettes," *Yeast*, vol. 21, no. 11, pp. 947–962, 2004.

[32] P. Lindroth and K. Mopper, "High performance liquid chromatographic determination of subpicomole amounts of amino acids by precolumn fluorescence derivatization with o-phthaldialdehyde," *Analytical Chemistry*, vol. 51, no. 11, pp. 1667–1674, 1979.

Hindawi Publishing Corporation
Oxidative Medicine and Cellular Longevity
Volume 2013, Article ID 146860, 10 pages
http://dx.doi.org/10.1155/2013/146860

Review Article

Adenine Nucleotide Translocase, Mitochondrial Stress, and Degenerative Cell Death

Yaxin Liu and Xin Jie Chen

Department of Biochemistry and Molecular Biology, State University of New York Upstate Medical University, Syracuse, NY 13210, USA

Correspondence should be addressed to Xin Jie Chen; chenx@upstate.edu

Received 10 May 2013; Revised 14 June 2013; Accepted 24 June 2013

Academic Editor: Sergio Giannattasio

Mitochondria are intracellular organelles involved in ATP synthesis, apoptosis, calcium signaling, metabolism, and the synthesis of critical metabolic cofactors. Mitochondrial dysfunction is associated with age-related degenerative diseases. How mitochondrial dysfunction causes cell degeneration is not well understood. Recent studies have shown that mutations in the adenine nucleotide translocase (Ant) cause aging-dependent degenerative cell death (DCD) in yeast, which is sequentially manifested by inner membrane stress, mitochondrial DNA (mtDNA) loss, and progressive loss of cell viability. Ant is an abundant protein primarily involved in ADP/ATP exchange across the mitochondrial inner membrane. It also mediates basal proton leak and regulates the mitochondrial permeability transition pore. Missense mutations in the human Ant1 cause several degenerative diseases which are commonly manifested by fractional mtDNA deletions. Multiple models have been proposed to explain the Ant1-induced pathogenesis. Studies from yeast have suggested that in addition to altered nucleotide transport properties, the mutant proteins cause a global stress on the inner membrane. The mutant proteins likely interfere with general mitochondrial biogenesis in a dominant-negative manner, which secondarily destabilizes mtDNA. More recent work revealed that the Ant-induced DCD is suppressed by reduced cytosolic protein synthesis. This finding suggests a proteostatic crosstalk between mitochondria and the cytosol, which may play an important role for cell survival during aging.

1. Introduction

Mitochondria are essential organelles as they produce most of ATP to support cellular activities, synthesize critical metabolic factors such as heme and iron-sulfur clusters, and are involved in lipid and phospholipid metabolism as well as calcium signalling [1]. Mitochondria also play an important role in determining the fate of cell via their involvement in cell death. Cell death can be classified into different categories. According to the morphological appearance, for instance, cells undergo death via necrosis (accidental cell death or programmed necrosis), apoptosis, or aberrant autophagy, all with significant involvement of mitochondria. In yeast, mitochondria-mediated apoptosis is believed to execute with some steps common to the mammalian cells. Oxidative burst, mitochondrial fragmentation, the collapse of mitochondrial membrane potential, and the release of cytochrome *c* are commonly observed in apoptotic yeast cells [2, 3].

In addition to the relatively acute forms of cell death aforementioned, mitochondrial function also progressively deteriorates during aging, which leads to cellular senescence. It is conventionally thought that mitochondria contribute to aging mainly through the overproduction of reactive oxygen species (ROS) and underproduction of ATP in aged cells. Interestingly, recent studies have suggested that mitochondria may overcome these stresses and promote cell survival by altered cellular signalling [4–7]. In this review, we will present a novel form of mitochondria-induced cell death in yeast cells, tentatively referred as degenerative cell death (DCD). DCD is characterized by mitochondrial inner membrane stress, mtDNA damage, and progressive loss of cell viability. The key feature of DCD, which is distinct from the currently known forms of cell death in yeast (e.g., apoptosis and necrosis), is the loss of mtDNA which cannot be tolerated by cells with compromised inner membrane integrity. This was revealed by studying some mutant forms of adenine nucleotide translocase, which causes aging-dependent cellular degeneration. These studies may provide new perspectives for the mechanism of mitochondrial degeneration, in

addition to the well-established roles of oxidative stress and mitochondrial quality control which contribute to aging.

2. Physiological Roles of Adenine Nucleotide Translocase

Adenine nucleotide translocase (or adenine nucleotide translocator or Ant) is the most abundant protein in mitochondria, accounting for up to 10% of total mitochondrial protein content [8]. It is encoded by the nuclear DNA, synthesized in cytosol, imported into mitochondria, and finally inserted into the inner membrane [9–11]. Ant belongs to the mitochondrial carrier family (MCF) proteins, a class of proteins that plays an important role in the transport of metabolites and cofactors across the mitochondrial inner membrane [12, 13]. The primary function of Ant is to catalyze ADP/ATP exchange across the inner membrane. Under respiring conditions, ATP^{4-} generated by oxidative phosphorylation is exported to the cytosol for use in cellular activities and ADP^{3-} is imported into the mitochondrial matrix for continuous ATP synthesis. Ant is therefore an ADP^{3-}/ATP^{4-} exchanger. During this strict exchange process, one net negative charge is moved from the matrix to the cytosol, resulting in a charge differential that is driven by membrane potential across the mitochondrial inner membrane [14]. Ant binds to its substrates with relatively low affinity, while its high abundance can compensate for the inefficient transport. Ant also has an intrinsic property of mediating proton leakage [8]. In addition to its involvement in a fatty acid-dependent proton leakage pathway, it accounts for 1/2 to 2/3 of the basal proton conductance through an unknown mechanism. Hence, Ant can result in mild uncoupling and decrease efficiency of ATP synthesis.

The Ant protein has multiple isoforms in different species. In humans, there are four isoforms that have distinct tissue-specific expression patterns. Ant1 is predominantly expressed in postdifferentiated tissues such as heart and skeletal muscle [15]. Ant2 is more abundant in certain proliferating tissues [16, 17]. Ant3 is ubiquitously expressed and Ant4 is specifically expressed in the testis [18]. Only three isoforms of Ant have been found in mouse (Ant1, 2, and 4). Mouse Ant1 is a heart/skeletal muscle specific isoform, while mouse Ant2 is highly expressed in all tissues except muscle. Mouse Ant4 is expressed primarily in testis as in humans [15, 18]. Yeast contains three isoforms of ADP/ATP carrier (Aac), which are homologues of Ant in humans. Aac2 is the major ADP/ATP carrier in aerobically grown yeast cells [19].

Like other members in MCF, Ant has three repeats of a ~100 amino acid sequence and each repeat contains two transmembrane domains that form alpha helices [20, 21]. Biochemical characterization of Ant benefited from two specific inhibitors of Ant, bongkrekic acid (BA) and carboxyatractyloside (CATR). Both of the inhibitors bind with the stoichiometry of one inhibitor per two molecules. BA binds the matrix side of Ant and CATR binds on the intermembrane space side [22–24]. The transition between CATR and BA conformations is suggested to be the structural switch involved in ADP/ATP transport [19]. The crystal structure of bovine Ant complexed with CATR revealed the organization of six transmembrane domains with both N- and C-termini extending into the intermembrane space [25] (Figure 1). All the transmembrane domains are α-helices, which are tilted and form a cavity with the opening toward the intermembrane space. Three kinks are introduced by proline residues between two helices on the matrix side of Ant, which may act as hinges to facilitate the opening and closing of the nucleotide translocation channel [25]. Recent study of yeast Aac2 using hydrogen/deuterium exchange-mass spectrometry showed that the BA-bound Aac2 is structurally different from the CATR-bound form. The BA conformation has better solvent accessibility from the matrix side [26, 27]. Ant has the RRRMMM signature sequence, which is absent from other mitochondrial carriers. This motif spans over the thinnest part of the channel and the arginine residues are essential for attracting the negatively charged nucleotides to facilitate transport [25, 28, 29]. In addition to the arginine residues, the methionine triplet also contributes to nucleotide translocation or binding [27].

It has been debated whether Ant functions as a monomer or a dimer. A dimeric structure was first suggested by native gel electrophoresis, ultracentrifugation, neutron scattering, and cross-linking studies [30–35]. In the dimer model, the C terminus of one monomer is predicted to be close to the N terminus of a second monomer [36–38]. However, more recent reports suggested that Ant may be present in a monomeric form. The crystal structure of bovine Ant1 was solved as a monomer [25]. The study using differential tagging showed that the yeast Aac2 is a monomer in mild detergents because tagged Aac2 does not form dimers with untagged Aac2 [39]. Other techniques such as analytical ultracentrifugation, small-angle neutron scattering and electron cryomicroscopy also suggested that Ant more likely functions as monomers (reviewed in [40]).

Ant may also affect the mitochondrial permeability transition pore (mPTP) on the inner membrane, but its exact role in this activity has been highly debated [41–44]. Elevated Ca^{2+} and other factors are involved in the stimulation of mPTP opening followed by increased permeability of solutes across the inner membrane, which results in the dissipation of membrane potential, mitochondrial swelling, and finally cell death through apoptosis or necrosis. It has also been documented that mPTP plays a role in mediating organismal aging [45]. Early studies suggested Ant as a critical component of mPTP, along with voltage-dependent anion channel (VDAC) in the outer membrane and cyclophilin D (CyPD) in the matrix [46, 47]. However, Kokoszka et al. inactivated the two Ant isoforms in mouse and still detected the opening of mPTP triggered by Ca^{2+}, suggesting that Ant is not essential for mPTP [48]. Ant still plays a role in the regulation of mPTP since more Ca^{2+} are required to activate the mPTP and the Ant ligands no longer regulate the mPTP. The very recent studies defined the mPTP as the dimers of the F_oF_1-ATP synthase that is regulated by CyPD [49] and the c subunit of the enzyme appears to be critical for permeability transition [50]. Given that adenine nucleotides are the substrates of the ATP synthase, Ant may contribute to mPTP regulation by affecting

nucleotide levels in the matrix where the F_1-ATPase sector of the ATP synthase is located. It has been reported in yeast that loss of Ant (or Aac) protects cells from acetic acid and diamide-induced mitochondrial outer membrane permeabilization, mitochondrial degradation, and apoptosis [51–53]. Interestingly, this was proposed to involve mPTP probably via an activity independent of nucleotide translocation.

3. Altered Ant Expression and Human Diseases

Given the importance of Ant to mitochondrial physiology, mutations or altered expression of Ant has been found to be associated with a growing list of human diseases (Table 1). In all the four Ant isoforms, Ant1 is so far the only one found to directly cause mitochondrial diseases. Early work has shown that *ANT1*$^{-/-}$ mice presented overproliferation of mitochondria in skeletal and heart muscles, ragged-red fibers (fibers that have a ragged contour and an accumulation of red staining material which is associated with proliferation of abnormal mitochondria), cardiac hypertrophy, exercise intolerance, lactic acidosis, and deficiency in coupled respiration in mitochondria [54]. In humans, deficiency in Ant1 is associated with Senger's syndrome, an autosomal recessive disease characterized by hypertrophic cardiomyopathy, mitochondrial myopathy, lactic acidosis, and congenital cataracts [55]. Although depletion of Ant1 in heart and muscle tissues has been proposed to be the primary cause of the Senger's syndrome, no mutations have been found in *ANT1*. It has been speculated that the transcription, translation, or posttranslational modification of Ant1 may be affected [56]. Recently, two nonsense mutations in the gene encoding the mitochondrial acylglycerol kinase (AGK) were identified from a patient with typical symptoms of Senger's syndrome [57]. AGK is a multisubstrate lipid kinase involved in phospholipid metabolism. The loss of AGK may result in the decrease of Ant by affecting its biogenesis. In addition to Senger's syndrome, loss of Ant1 due to a homozygous null mutation also causes cardiomyopathy, and the severity of the cardiac disease correlates with the mtDNA haplogroup. Patients with the haplogroup U mtDNAs are more affected than those having the haplogroup H [58]. Overall, deficiency in Ant1 expression and biogenesis would be expected to cause not only reduced ATP output but also oxidative damage because of F_oF_1-ATP synthase stalling, increased electron leak, and ROS production.

In contrast to Ant1 deficiency, overexpressed Ant1 may contribute to the pathogenesis of other diseases such as facioscapulohumeral muscular dystrophy (FSHD). FSHD is a highly variable autosomal dominant neuromuscular disorder. Patients with FSHD suffer from cumulative progression of muscle weakness in the face, feet, shoulders, and hips, along with occasionally sensorineural hearing loss [59]. Deletions of the D4Z4 repeated sequences on chromosome IV are commonly found in FSHD patients, which may lead to transcriptional derepression of nearby genes including *ANT1*, *FRG1*, *FRG2*, and *DUX4* [60–63]. Overexpression of *FRG1*, a gene involved in pre-mRNA splicing, and not *ANT1*, was proposed to be responsible for FSHD [64]. Other studies instead proposed that expression of *DUX4* is critical for FSHD pathogenesis [63]. Nevertheless, recent studies have also reported the overexpression of Ant1 and increased oxidative stress in FSHD muscles [65]. These observations suggest that Ant1 may play a role in the pathogenesis of FSHD.

Although the sequence identity between the Ant isoforms is as high as 70%~90% [66], their nucleotide transport properties may differ and altered expression of these isoforms could have different metabolic consequences. For example, *ANT2* is upregulated in hormone-dependent cancers. Brenner et al. showed that *ANT2* mRNA is significantly elevated in primary tissues derived from patients with breast, uterus, ovary, lung, thyroid gland bladder, and testis cancers [67]. Unlike healthy cells, cancer cells intensively employ glycolysis and have reduced oxidative phosphorylation (OXPHOS) to adapt to the intratumoral hypoxic conditions [68]. It has been known in yeast that when cells are severely compromised in mitochondrial function (e.g. ρ^o cells), the mitochondrial membrane potential is maintained through reversed nucleotide transport by the ADP/ATP carrier. ATP is imported into the matrix, where it is recycled back to ADP as long as an active F_1-ATPase is present. ADP is then exported into the cytosol. This reversal ADP/ATP exchange is critical for mitochondrial biogenesis and cell viability under severe mitochondrial damage conditions [69–72]. By analogy, cancer cells are speculated to import glycolytically produced ATP into mitochondrial matrix via Ant2 [73]. The human F_oF_1-ATPase may hydrolyze ATP to ADP that facilitates the electrogenic $ATP^{4-}_{cystol}/ADP^{3-}_{matrix}$ exchange [74]. Given the key role of Ant2 in cancer metabolism, it may be used as a potential target for cancer therapy.

4. Dominant Mutations in Ant1 and Human Diseases

Missense mutations in Ant1 have been found to cause several human diseases. One of them is autosomal dominant Progressive External Ophthalmoplegia (adPEO), which is characterized by late or adult onset muscle weakness (especially in eye muscles), exercise intolerance, sensory ataxia, hypertrophic cardiomyopathy, and myopathy [75–77]. Multiple mtDNA deletions and mild defects in the respiratory complexes were detected in affected tissues. adPEO is also caused by specific missense mutations in the mitochondrial twinkle helicase or in the mtDNA specific polymerase, Polγ [78, 79], which are directly involved in mtDNA replication. Moreover, a total of five Ant1 missense mutations have been reported in one sporadic and four familial cases of adPEO. Most of these mutations occur in highly conserved amino acids: Ala90, Leu98, Asp104, Ala114 and Val289 [75–77, 80]. In addition to adPEO, the A123D missense mutation has been identified in a homozygous patient, which is manifested by slow progressive mitochondrial myopathy and cardiomyopathy, but not opthalmoplegia [81]. All those six mutable amino acids except Val289 locate in the helix 2-loop-helix 3 region (Figure 1), which is suggested to undergo dynamic structural changes during nucleotide transport [82]. A later study has shown that the sporadic V289M mutation is accompanied with a mutation in *POLG1*, the gene encoding the large

Table 1: Ant-associated human diseases.

Disease	Mutation	Pathogenic Mechanism	Characteristics
adPEO	*ant1*^{A90D}, *ant1*^{L98P}, *ant1*^{D104G}, *ant1*^{A114P}, *ant1*^{V289M}	Membrane stress; altered transport properties	Adult/late-onset, mitochondrial myopathy; muscle weakness (especially in the eyes); sensory ataxia; mtDNA deletions
Cancer	Overexpression of Ant2	Reversed ADP/ATP exchange by Ant2	The adaption to intratumoral hypoxia of cancer cells
FSHD	Deletions of subtelomeric repeats on chromosome IV	*DUX4* overexpression; possibly *ANT1* overexpression	Adult-onset disease, muscle weakness in face, shoulders, and hips, oxidative stress
Mitochondrial myopathy and cardiomyopathy	*ANT1* null mutations	Defect in nucleotide transport	Cardiomyopathy, myopathy, exercise intolerance, and lactic acidosis
	ant1^{A123D}	Defect in nucleotide transport; other mechanisms?	
Senger's syndrome	Mutation in AGK affecting Ant biogenesis leads to depletion of Ant1	Defect in nucleotide transport	Cardiac hypertrophy, mitochondrial myopathy, cataracts, lactic acidosis

subunit of Polγ [83]. Thus, the contribution of this particular Ant1 mutant allele to the pathogenesis is uncertain when present at a heterozygous state.

5. Models for Human Diseases Caused by Gain-of-Function Ant1 Mutations

Several model systems have been developed to study the pathogenic mechanism of human diseases caused by the gain-of-function mutations in Ant1 (Figure 2). Kaukonen et al. first introduced the adPEO-type Aac2^{A128P} allele, equivalent to human Ant1^{A114P}, in haploid yeast strains that are disrupted of the *AAC1* and *AAC2* genes [75]. Cells expressing the mutant allele showed a growth defect on nonfermentable carbon sources. The data suggested that the A128P mutation may affect ADP/ATP translocation. This may lead to imbalanced adenine nucleotides, altered intramitochondrial dATP levels in the matrix, and, ultimately, multiple mtDNA deletions.

In a subsequent study, the human *ANT1* gene was expressed in a yeast mutant disrupted of all the three *AAC* genes [84]. The Ant1^{L98P} and Ant1^{V289M} variants were introduced to evaluate their efficiency in promoting respiratory growth. The complementation test showed that in contrast to the wild type *ANT1*, the two mutant alleles failed to restore cell growth on the nonfermentable lactate medium. Interestingly, the mutant proteins were not detected in the mitochondrial fraction of yeast cells by atractyloside binding and immunodecoration assays, whereas the RNA levels of the mutant *ANT1* were comparable with the wild type. This observation led to the speculation that Ant1^{L98P} and Ant1^{V289M} may not be imported into mitochondria in human diseases.

As the primary function of Ant is to promote adenine nucleotide transport, the simplest explanation for Ant1-induced adPEO is that the mutant proteins are defective in the transport activity. The dominant phenotypes can only be explained by assuming that Ant1 operates in a dimeric form or that the heterozygous cells are haploinsufficient for the protein. Fontanesi et al. found that the growth of

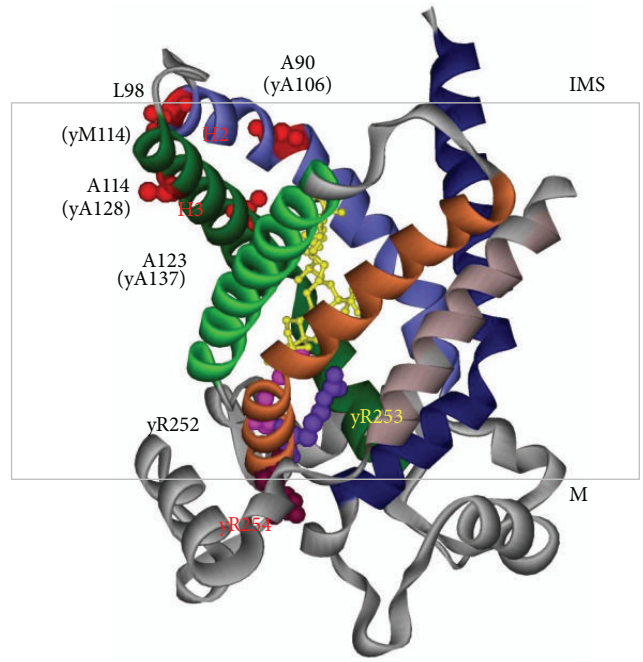

Figure 1: Projected localization of A90, L98, A114, A123, and the arginine triplet on the crystal structure of bovine Ant1 in the cytosolic conformation bound by CATR (yellow) [25]. The corresponding amino acids in yeast Aac2 are also indicated. R252, R253, and R254 in yeast correspond to R234, R235, and R236 in the bovine protein. IMS, intermembrane space; M, matrix.

haploid yeast cells expressing only *aac2*^{A128P}, *aac2*^{M114P}, or *aac2*^{S303M} was severely affected on nonfermentable carbon sources [85]. In addition, cytochrome content, cytochrome *c* oxidase activity, and mitochondrial respiration were all decreased in the mutant cells. In heteroallelic haploid cells, in which the wild type and mutant *aac2* were coexpressed, the level of mitochondrial respiration remained low. This is consistent with the dominant nature of adPEO pathogenesis. The authors also measured the transport properties of

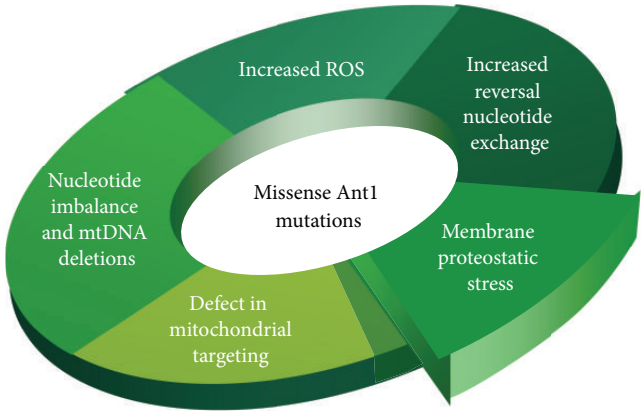

Figure 2: Proposed models for the pathogenic mechanisms of human diseases induced by dominant missense Ant1 mutations. These models predict that the mutant proteins (1) are defective in targeting onto the mitochondrial inner membrane; (2) are defective in nucleotide transport which sequentially causes ATP overaccumulation in the matrix, electron transport chain stalling, membrane hyperpolarization, increased ROS production, and oxidative damage; (3) are engaged in the futile $ATP_{cytosol}/ATP_{matrix}$ exchange which leads to matrix nucleotide imbalance and mtDNA deletions; (4) reverse the $ADP_{cytosol}/ATP_{matrix}$ exchange under normal conditions which also leads to ATP overaccumulation in the matrix; and (5) cause proteostatic stress on the mitochondrial inner membrane.

$Aac2^{A128P}$, $Aac2^{M114P}$, and $Aac2^{S303M}$ by determining ATP homoexchange rate, ADP homoexchange rate, and ADP/ATP heteroexchange rate in reconstituted proteoliposomes *in vitro*. Interestingly, all the three mutant proteins still retain a robust transport activity for ATP and ADP. However, the mutant proteins preferentially import ATP over ADP. The authors proposed that this may lead to a futile ATP/ATP homoexchange instead of the physiologically productive $ATP_{matrix}/ADP_{cytosol}$ heteroexchange mode. This may ultimately result in elevated mitochondrial ATP level. One possible consequence of ATP/ADP imbalance is the increased dATP level, which in turn affects the accuracy of mtDNA replication [85]. However, it is important to note that dATP is likely imported directly from cytosol in yeast rather than converted from ADP or ATP in the mitochondrial matrix. Whether the altered transport properties have physiological implications especially in heterozygous diploid cells needs to be further evaluated.

Another model proposed by Kawamata et al. also involves a possible alteration to the nucleotide transport property of Ant1. These authors evaluated the effect of $Ant1^{A114P}$ and $Ant1^{V289M}$ on mitochondrial function in the mouse C2C12 myotube cells [86]. Exogenous Ant1 mutant proteins were confirmed to be localized on the mitochondrial inner membrane. However, no significant differences on oxygen consumption, ATP synthesis, total cellular ATP level, CATR sensitivity, or mtDNA content were detected between the cells expressing the mutant and wild type Ant1. Of interest, mitochondria of A114P-, but not V289M-, expressing myotubes were found to have a reduced ADP/ATP exchange rate and a slightly smaller ADP-induced depolarization. Reduced ADP-induced depolarization suggests a defect in ADP translocation. In addition, cells expressing the A114P and V289M alleles showed abnormal translocator reversal potential. They were switched to the $ATP_{cytosol}/ADP_{matrix}$ exchange mode at a higher membrane potential. It was speculated that mutant Ant1 is more prone to invert the direction of ADP/ATP exchange even at the membrane potential still in the physiological range for ATP synthesis. This may lead to increased ATP and nucleotide imbalance in the mitochondrial matrix. Importantly, this phenotype is not caused by loss of function, because the ADP/ATP exchange rate in Ant1-silenced myotubes showed different properties.

Whether altered nucleotide transport is the pathogenic mechanism of Ant1-induced diseases is still inconclusive. The study of $Aac2^{A137D}$ in yeast provided some useful information. $Aac2^{A137D}$ is equivalent to the human $Ant1^{A123D}$ mutation, which does not cause ophthalmoplegia in a homozygous patient but share other common symptoms with adPEO patients including hypertrophic cardiomyopathy, mild myopathy, ragged muscle fibers, exercise intolerance, lactic acidosis, and accumulation of mtDNA deletions. Yeast cells expressing only $Aac2^{A137D}$ are respiratory deficient as they do not grow on nonfermentable carbon sources [81]. The *in vitro* reconstitution assay showed that $Aac2^{A137D}$ completely lacks the ability to transport ATP or ADP. This provides strong evidence that mtDNA deletions in the $Ant1^{A123D}$ patient arise independently of nucleotide transport. The yeast $aac2^{A137D}$ cells have a low viability, which is suppressed by ROS scavengers. This supports the idea that the mutant is vulnerable to oxidative stress and anti-ROS treatments may be a potential therapeutic strategy [81].

6. The Proteostatic Stress Model

More recent studies in yeast supported the idea that *aac2* alleles resembling the human pathogenic *ant1* mutations may interfere with general mitochondrial biogenesis in a dominant manner [87, 88]. It was shown that yeast cells coexpressing the mutant *aac2* alleles and the wild type *AAC2* exhibit reduced cellular respiration, suggesting that the electron transport chain is severely damaged. In a yeast strain that overexpresses $aac2^{A128P}$, mitochondria showed dramatic depolarization as well as swelling and disintegration of mitochondria. More importantly, when cells expressing only one chromosomally integrated copy of $aac2^{A128P}$ were incubated at 25°C, cell growth is inhibited on glucose medium. Yeast is well known for its ability to grow on fermentable carbon sources without mitochondrial respiration. The growth inhibition strongly suggests that expression of the mutant Aac2 interferes with general mitochondrial biogenesis. Furthermore, when two copies of $aac2^{A128P}$, $aac2^{M114P}$, $aac2^{A106D}$, or $aac2^{A137D}$ were intergraded into the genome, the frequencies of respiratory-deficient petite colonies on glucose medium are greatly increased. This observation recapitulates the mtDNA instability phenotype in human adPEO. Petite frequencies are further increased when cells are grown on raffinose plus galactose medium

which stimulates respiration. Concomitantly, cell viability is dramatically reduced.

Additional phenotypes supported the model that expression of the mutant Aac2 causes general mitochondrial damage [88]. Firstly, the expression of mtDNA-encoded protein, Cox2p, is reduced in the *aac2* mutants. Secondly, yeast cells expressing the four *aac2* mutant alleles are intolerant to ρ^o condition. The ρ^o-lethality phenotype is an indication of low membrane potential. Cells lose viability when membrane potential is further reduced by the loss of mtDNA. Thirdly, these *aac2* mutants are also hypersensitive to the chemical uncoupler CCCP, consistent with the low membrane potential model. Fourthly, cells coexpressing the mutant *aac2* and wild type alleles have a diminished respiratory control ratio (RCR), which indicates uncoupled respiration. These data support the model that the mutant Aac2 may cause general stress on the membrane, which leads to defects in respiratory complex biogenesis, membrane uncoupling, loss of ion homeostasis, and the inhibition of cell growth.

Since $aac2^{A137D}$ completely lacks nucleotide transport activity but exhibits similar phenotypes as other mutant *aac2* alleles, these results suggest that mitochondrial damage is independent of ADP/ATP exchange. Further evidence came from the analysis of the double mutants combining $aac2^{A128P}$ with mutations in the Arg252–254 triplet which mitigates adenine transport function [89]. It was found that the arginine mutations barley affects the inhibition of cell growth by the $aac2^{A128P}$ allele. Mitochondrial damage is therefore independent of nucleotide transport. In summary, the data suggested that the mutant Aac2 proteins primarily damage the inner membrane, which consequently affects mitochondrial biogenesis. The loss of mtDNA integrity is likely a consequence of membrane stress.

The global mitochondrial damage model is supported by another study from El-Khoury and Sainsard-Chanet using the filamentous fungi *Podospora anserina* as a model system [90]. The A114P, L98P, and V289M alleles were introduced into the *P. anserina ANT1* ortholog, *PaANT*. The three mutant strains showed a delayed and reduced rate of germination, a slow vegetative growth rate, and other somatic and sexual defects. In *P. anserina*, lifespan is a good indicator of mtDNA integrity. The three mutant strains were suggested to accumulate mtDNA deletions as they showed dramatically reduced lifespan in certain mating type (mat^-). Interestingly, short lifespan caused by A114P and L98P mutations, but not V289M, was suppressed by the *rmp1*-2 allele, which is one of the two naturally occurring alleles of *rmp1*. The *rmp1* gene is associated with the timing of death and linked to the *mat* locus tightly. The results indicated that the lifespan in the A114P and L98P mutants is dependent on whether it has the *rmp1*-1 or the *rmp1*-2 allele, but not the mating type. Further studies suggested that premature cell death is independent of mtDNA instability. Mutant strains also exhibited decreased ROS production and mitochondrial inner membrane potential, which could not be suppressed by the *rmp1*-2 allele.

Another important finding in the yeast model is that the missense *aac2* alleles are all synthetically lethal with the disruption of the *YME1* gene, which encodes a chaperone/protease on the inner membrane for degradation of misfolded proteins. This observation strongly suggests that proteostatic stress on the membrane may be responsible for the global mitochondrial damage and the inhibition of cell growth [88].

7. Ant Mutations Induce Degenerative Cell Death

The Chen group found that mitochondrial damage by the mutant *aac2* alleles causes aging-dependent DCD [89]. When yeast cells heterozygous for $AAC2/aac2^{A128P}$ were individually spotted on complete glucose medium by micromanipulation, a subfraction of cells formed barely visible microcolonies [87, 89]. The microcolonies contain 2,000~4,000 cells that fail to divide and to produce proliferating lineages. It appears that cells can divide for up to 12~13 generations before complete growth arrest. The delayed loss of the ability to proliferate is termed degenerative cell death (DCD). DCD is likely initiated by membrane stress-induced mtDNA loss (Figure 3). As the *aac2* mutants are ρ^o-lethal, mtDNA loss therefore causes cell death. Cells can continue to divide for limited cell generations after mtDNA loss, probably reflecting either progressive accumulation of cellular factors that inhibit cell division or a dilution of mitochondrial factors that are essential for cell viability. This is supported by pedigree analysis showing that in haploid cells coexpressing *AAC2* and $aac2^{A128P}$, the degenerative mother cell consistently produces degenerative daughter cells. The daughter cells likely inherit the permanently damaged mtDNA from the mother cell which causes cell death. Interestingly, DCD caused by $aac2^{A128P}$ is aging dependent. Replicatively aged mother cells have increased DCD. Approximate half of the founding mother cells have their first degenerative daughter cells after 9~11 cell divisions [89], which is a mid-age onset given that the median lifespan of most *Saccharomyces cerevisiae* strains is about 25 generations.

To understand the mechanism of DCD, much effort has been invested to identify pathways that suppress the degenerative process. It was found that genetic manipulations that reduce cytosolic protein synthesis remarkably suppress DCD [89]. For instance, *RPL6B* encodes a component of 60S ribosomal subunit and its disruption is expected to reduce cytosolic protein synthesis. By meiotic analysis, $aac2^{A128P}$-expressing segregants produce small and sectoring colonies indicative of DCD, whereas cells harboring both $aac2^{A128P}$ and *rpl6B*Δ form regular colonies as the wild type. Other genes that suppress in the same manner include *GRP1* (encoding a G-protein-coupled receptor upstream of the protein kinase A pathway), *REI1* (involved in ribosomal biogenesis), *TOR1* and *SCH9* (encoding kinases in the TOR signaling pathway). DCD is also suppressed by cycloheximide, an inhibitor of cytosolic protein synthesis, which further supports the model that reduced cytosolic protein synthesis suppresses mitochondrial degeneration and DCD [89]. In *P. anserina*, premature cell death and mtDNA instability

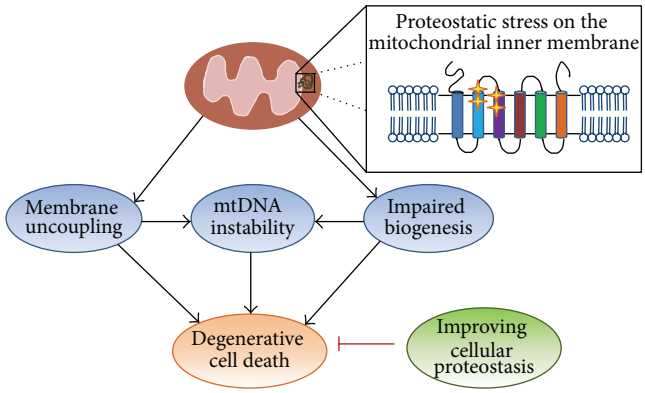

FIGURE 3: Schematic diagram showing the proteostatic stress model for the pathogenic mechanism of Ant1-induced degenerative cell death. This model predicts that the mutant Ant induces proteostatic stress on the mitochondrial inner membrane, which interferes with general mitochondrial biogenesis and the maintenance of membrane potential, followed by mtDNA destabilization. The severe membrane damage and mtDNA destabilization collectively contribute to degenerative cell death. Degenerative cell death is suppressed by reduced cytosolic protein synthesis which improves global proteostasis. Stars indicate the localization of mutations.

induced by *ANT1* mutations are suppressed by a mutation in the *AS1* gene encoding a ribosomal protein [90].

Expression of the $aac2^{A128P}$ allele shortens the replicative lifespan of yeast cells in a dominant-negative manner, and the shortened lifespan is corrected by the disruption of *RPL6B*, *REI1*, and *SCH9* [89]. This observation supports an epistatic interaction between mitochondrial inner membrane stress and cytosolic protein homeostasis in the control of replicative lifespan. A role of mitochondria in aging and lifespan control is well established [91, 92]. It has been extensively documented that adaptive mitochondria-to-nucleus signaling via the retrograde-response pathway increases cell's lifespan (for review, see [93]). It remains unknown whether $aac2^{A128P}$-induced mitochondrial damage triggers an adaptive adjustment of cytosolic protein homeostasis during replicative aging.

8. Conclusions and Prospects

The pathogenic mechanism of Ant1-induced human diseases is not fully settled. Studies using yeast cells have indicated that the mutant Ant1 may gain a novel property to affect global mitochondrial biogenesis in addition to a potential effect on nucleotide homeostasis. The mutant Ant either directly uncouples the respiration or indirectly compromises protein homeostasis on the membrane which subsequently affects mitochondrial biogenesis. The severe inner membrane damage is manifested by DCD. DCD is initiated by inner membrane damage, followed by mtDNA loss and progressive loss of cell viability because of ρ^o-lethality. These characteristics distinguish it from currently described forms of cell death in yeast including apoptosis and necrosis. Ant-induced DCD is suppressed by reduced cytosolic protein synthesis. This finding strongly suggests that proteostatic stress may play a role in cell degeneration (Figure 3). Future studies are required to understand the mechanism of Ant-induced membrane stress and its contribution to aging-dependent cell degeneration.

Abbreviations

Aac:	ADP/ATP carrier
adPEO:	Autosomal dominant Progressive External Ophthalmoplegia
AGK:	Acylglycerol kinase
Ant:	Adenine nucleotide translocase
BA:	Bongkrekic acid
CATR:	Carboxyatractyloside
CCCP:	Carbonyl cyanide *m*-chlorophenyl hydrazone
CyPD:	Cyclophilin D
DCD:	Degenerative cell death
FSHD:	Facioscapulohumeral muscular dystrophy
MCF:	Mitochondrial carrier family
mtDNA:	Mitochondrial DNA
mPTP:	Mitochondrial permeability transition pore
OXPHOS:	Oxidative phosphorylation
ROS:	Reactive oxidative species

Conflict of Interests

The authors declare that they have no financial conflict of interests.

Acknowledgments

This work was supported by the Grant AG023731 from the National Institute on Aging, National Institute of Health.

References

[1] D. C. Wallace, "Why do we still have a maternally inherited mitochondrial DNA? insights from evolutionary medicine," *Annual Review of Biochemistry*, vol. 76, pp. 781–821, 2007.

[2] T. Eisenberg, S. Büttner, G. Kroemer, and F. Madeo, "The mitochondrial pathway in yeast apoptosis," *Apoptosis*, vol. 12, no. 5, pp. 1011–1023, 2007.

[3] N. Guaragnella, L. Antonacci, S. Passarella, E. Marra, and S. Giannattasio, "Hydrogen peroxide and superoxide anion production during acetic acid-induced yeast programmed cell death," *Folia Microbiologica*, vol. 52, no. 3, pp. 237–240, 2007.

[4] A. Caballero, A. Ugidos, B. Liu et al., "Absence of mitochondrial translation control proteins extends life span by activating sirtuin-dependent silencing," *Molecular Cell*, vol. 42, no. 3, pp. 390–400, 2011.

[5] X. J. Chen, "The search for nonconventional mitochondrial determinants of aging," *Molecular Cell*, vol. 42, no. 3, pp. 271–273, 2011.

[6] S. M. Jazwinski, "The retrograde response: when mitochondrial quality control is not enough," *Biochimica et Biophysica Acta*, vol. 1833, no. 2, pp. 400–409, 2013.

[7] J. R. Delaney, U. Ahmed, A. Chou et al., "Stress profiling of longevity mutants identifies Afg3 as a mitochondrial determinant of cytoplasmic mRNA translation and aging," *Aging Cell*, vol. 12, no. 1, pp. 156–166, 2013.

[8] M. D. Brand, J. L. Pakay, A. Ocloo et al., "The basal proton conductance of mitochondria depends on adenine nucleotide translocase content," *Biochemical Journal*, vol. 392, no. 2, pp. 353–362, 2005.

[9] M. Endres, W. Neupert, and M. Brunner, "Transport of the ADP/ATP carrier of mitochondria from the TOM complex to the TIM22.54 complex," *EMBO Journal*, vol. 18, no. 12, pp. 3214–3221, 1999.

[10] N. Pfanner, P. Hoeben, M. Tropschug, and W. Neupert, "The carboxyl-terminal two-thirds of the ADP/ATP carrier polypeptide contains sufficient information to direct translocation into mitochondria," *Journal of Biological Chemistry*, vol. 262, no. 31, pp. 14851–14854, 1987.

[11] M. T. Ryan, H. Müller, and N. Pfanner, "Functional staging of ADP/ATP carrier translocation across the outer mitochondrial membrane," *Journal of Biological Chemistry*, vol. 274, no. 29, pp. 20619–20627, 1999.

[12] F. Palmieri, "The mitochondrial transporter family (SLC25): physiological and pathological implications," *Pflugers Archiv European Journal of Physiology*, vol. 447, no. 5, pp. 689–709, 2004.

[13] H. Wohlrab, "The human mitochondrial transport protein family: identification and protein regions significant for transport function and substrate specificity," *Biochimica et Biophysica Acta*, vol. 1709, no. 2, pp. 157–168, 2005.

[14] J. Duszyński, K. Bogucka, G. Letko, U. Küster, W. Kunz, and L. Wojtczak, "Relationship between the energy cost of ATP transport and ATP synthesis in mitochondria," *Biochimica et Biophysica Acta*, vol. 637, no. 2, pp. 217–223, 1981.

[15] S. E. Levy, Y.-S. Chen, B. H. Graham, and D. C. Wallace, "Expression and sequence analysis of the mouse adenine nucleotide translocase 1 and 2 genes," *Gene*, vol. 254, no. 1-2, pp. 57–66, 2000.

[16] G. Stepien, A. Torroni, A. B. Chung, J. A. Hodge, and D. C. Wallace, "Differential expression of adenine nucleotide translocator isoforms in mammalian tissues and during muscle cell differentiation," *Journal of Biological Chemistry*, vol. 267, no. 21, pp. 14592–14597, 1992.

[17] A. Chevrollier, D. Leiseau, and G. Stepien, "What is the specific role of *ANT2* in cancer cells?" *Medecine/Sciences*, vol. 21, no. 2, pp. 156–161, 2005.

[18] J. V. Brower, N. Rodic, T. Seki et al., "Evolutionarily conserved mammalian adenine nucleotide translocase 4 is essential for spermatogenesis," *Journal of Biological Chemistry*, vol. 282, no. 40, pp. 29658–29666, 2007.

[19] M. Klingenberg, "The ADP and ATP transport in mitochondria and its carrier," *Biochimica et Biophysica Acta*, vol. 1778, no. 10, pp. 1978–2021, 2008.

[20] M. Saraste and J. E. Walker, "Internal sequence repeats and the path of polypeptide in mitochondrial ADP/ATP translocase," *FEBS Letters*, vol. 144, no. 2, pp. 250–254, 1982.

[21] J. E. Walker and M. J. Runswick, "The mitochondrial transport protein superfamily," *Journal of Bioenergetics and Biomembranes*, vol. 25, no. 5, pp. 435–446, 1993.

[22] G. Brandolin, A. le Saux, V. Trezeguet, G. J. M. Lauquin, and P. V. Vignais, "Chemical, immunological, enzymatic, and genetic approaches to studying the arrangement of the peptide chain of the ADP/ATP carrier in the mitochondrial membrane," *Journal of Bioenergetics and Biomembranes*, vol. 25, no. 5, pp. 459–472, 1993.

[23] P. Riccio, H. Aquila, and M. Klingenberg, "Purification of the carboxy atractylate binding protein from mitochondria," *FEBS Letters*, vol. 56, no. 1, pp. 133–138, 1975.

[24] H. Aquila, W. Eiermann, W. Babel, and M. Klingenberg, "Isolation of the ADP/ATP translocator from beef heart mitochondria as the bongkrekate-protein complex," *The European Journal of Biochemistry*, vol. 85, no. 2, pp. 549–560, 1978.

[25] E. Pebay-Peyroula, C. Dahout-Gonzalez, R. Kahn, V. Trézéguet, G. J.-M. Lauquin, and G. Brandolin, "Structure of mitochondrial ADP/ATP carrier in complex with carboxyatractyloside," *Nature*, vol. 426, no. 6962, pp. 39–44, 2003.

[26] M. Rey, P. Man, B. Clémençon et al., "Conformational dynamics of the bovine mitochondrial ADP/ATP carrier isoform 1 revealed by hydrogen/deuterium exchange coupled to mass spectrometry," *Journal of Biological Chemistry*, vol. 285, no. 45, pp. 34981–34990, 2010.

[27] B. Clémençon, M. Rey, V. Trézé, E. Forests, and L. Pelosis, "Yeast ADP/ATP carrier isoform 2: conformational dynamics and role of the RRRMMM signature sequence methionines," *Journal of Biological Chemistry*, vol. 286, no. 41, pp. 36119–36131, 2011.

[28] H. Nury, C. Dahout-Gonzalez, V. Trézéguet, G. J. M. Lauquin, G. Brandolin, and E. Pebay-Peyroula, "Relations between structure and function of the mitochondrial ADP/ATP carrier," *Annual Review of Biochemistry*, vol. 75, pp. 713–741, 2006.

[29] D. Heidkämper, V. Müller, D. R. Nelson, and M. Klingenberg, "Probing the role of positive residues in the ADP/ATP carrier from yeast. The effect of six arginine mutations on transport and the four ATP versus ADP exchange modes," *Biochemistry*, vol. 35, no. 50, pp. 16144–16152, 1996.

[30] S. D. Dyall, S. C. Agius, C. de Marcos Lousa, V. Trézéguet, and K. Tokatlidis, "The dynamic dimerization of the yeast ADP/ATP carrier in the inner mitochondrial membrane is affected by conserved cysteine residues," *Journal of Biological Chemistry*, vol. 278, no. 29, pp. 26757–26764, 2003.

[31] H. Hackenberg and M. Klingenberg, "Molecular weight and hydrodynamic parameters of the adenosine 5′-diphosphate-adenosine 5′-triphosphate carrier in triton X-100," *Biochemistry*, vol. 19, no. 3, pp. 548–555, 1980.

[32] M. R. Block, G. Zaccaï, G. J. M. Lauquin, and P. V. Vignais, "Small angle neutron scattering of the mitochondrial ADP ATP carrier protein in detergent," *Biochemical and Biophysical Research Communications*, vol. 109, no. 2, pp. 471–477, 1982.

[33] M. Hashimoto, E. Majima, S. Goto, Y. Shinohara, and H. Terada, "Fluctuation of the first loop facing the matrix of the mitochondrial ADP/ATP carrier deduced from intermolecular cross-linking of Cys56 residues by bifunctional dimaleimides," *Biochemistry*, vol. 38, no. 3, pp. 1050–1056, 1999.

[34] Y. Kihira, E. Majima, Y. Shinohara, and H. Terada, "Cysteine labeling studies detect conformational changes in region 106-132 of the mitochondrial ADP/ATP carrier of *Saccharomyces cerevisiae*," *Biochemistry*, vol. 44, no. 1, pp. 184–192, 2005.

[35] E. Majima, K. Ikawa, M. Takeda, M. Hashimoto, Y. Shinohara, and H. Terada, "Translocation of loops regulates transport activity of mitochondrial ADP/ATP carrier deduced from formation of a specific intermolecular disulfide bridge catalyzed by copper-o-phenanthroline," *Journal of Biological Chemistry*, vol. 270, no. 49, pp. 29548–29554, 1995.

[36] V. Trézéguet, A. le Saux, C. David et al., "A covalent tandem dimer of the mitochondrial ADP/ATP carrier is functional in vivo," *Biochimica et Biophysica Acta*, vol. 1457, no. 1-2, pp. 81–93, 2000.

[37] T. Hatanaka, M. Hashimoto, E. Majima, Y. Shinohara, and H. Terada, "Functional expression of the tandem-repeated homodimer of the mitochondrial ADP/ATP carrier in *Saccharomyces cerevisiae*," *Biochemical and Biophysical Research Communications*, vol. 262, no. 3, pp. 726–730, 1999.

[38] S.-G. Huang, S. Odoy, and M. Klingenberg, "Chimers of two fused ADP/ATP carrier monomers indicate a single channel for ADP/ATP transport," *Archives of Biochemistry and Biophysics*, vol. 394, no. 1, pp. 67–75, 2001.

[39] L. Bamber, D.-J. Slotboom, and E. R. S. Kunji, "Yeast mitochondrial ADP/ATP carriers are monomeric in detergents as demonstrated by differential affinity purification," *Journal of Molecular Biology*, vol. 371, no. 2, pp. 388–395, 2007.

[40] E. R. S. Kunji and P. G. Crichton, "Mitochondrial carriers function as monomers," *Biochimica et Biophysica Acta*, vol. 1797, no. 6-7, pp. 817–831, 2010.

[41] D. R. Hunter and R. A. Haworth, "The Ca^{2+}-induced membrane transition in mitochondria. The protective mechanisms," *Archives of Biochemistry and Biophysics*, vol. 195, no. 2, pp. 453–459, 1979.

[42] R. A. Haworth and D. R. Hunter, "The Ca^{2+}-induced membrane transition in mitochondria. II. Nature of the Ca^{2+} trigger site," *Archives of Biochemistry and Biophysics*, vol. 195, no. 2, pp. 460–467, 1979.

[43] P. Bernardi, K. M. Broekemeier, and D. R. Pfeiffer, "Recent progress on regulation of the mitochondrial permeability transition pore; a cyclosporin-sensitive pore in the inner mitochondrial membrane," *Journal of Bioenergetics and Biomembranes*, vol. 26, no. 5, pp. 509–517, 1994.

[44] M. Zoratti and I. Szabo, "The mitochondrial permeability transition," *Biochimica et Biophysica Acta*, vol. 1241, no. 2, pp. 139–176, 1995.

[45] D. Brust, B. Daum, C. Breunig, A. Hamann, W. Kühlbrandt, and H. D. Osiewacz, "Cyclophilin D links programmed cell death and organismal aging in Podospora anserina," *Aging Cell*, vol. 9, no. 5, pp. 761–775, 2010.

[46] K. Woodfield, A. Rück, D. Brdiczka, and A. P. Halestrap, "Direct demonstration of a specific interaction between cyclophilin-D and the adenine nucleotide translocase confirms their role in the mitochondrial permeability transition," *Biochemical Journal*, vol. 336, no. 2, pp. 287–290, 1998.

[47] M. Crompton, S. Virji, and J. M. Ward, "Cyclophilin-D binds strongly to complexes of the voltage-dependent anion channel and the adenine nucleotide translocase to form the permeability transition pore," *The European Journal of Biochemistry*, vol. 258, no. 2, pp. 729–735, 1998.

[48] J. E. Kokoszka, K. G. Waymire, S. E. Levy et al., "The ADP/ATP translocator is not essential for the mitochondrial permeability transition pore," *Nature*, vol. 427, no. 6973, pp. 461–465, 2004.

[49] V. Giorgio, S. von Stockum, M. Antoniel et al., "Dimers of mitochondrial ATP synthase form the permeability transition pore," *Proceedings of the National Academy of Sciences*, vol. 110, no. 15, pp. 5887–5892, 2013.

[50] M. Bonora, A. Bononi, E. de Marchi et al., "Role of the c subunit of the F_O ATP synthase in mitochondrial permeability transition," *Cell Cycle*, vol. 12, no. 4, pp. 674–683, 2013.

[51] C. Pereira, N. Camougrand, S. Manon, M. J. Sousa, and M. Côrte-Real, "ADP/ATP carrier is required for mitochondrial outer membrane permeabilization and cytochrome c release in yeast apoptosis," *Molecular Microbiology*, vol. 66, no. 3, pp. 571–582, 2007.

[52] C. Pereira, S. Chaves, S. Alves et al., "Mitochondrial degradation in acetic acid-induced yeast apoptosis: the role of Pep4 and the ADP/ATP carrier," *Molecular Microbiology*, vol. 76, no. 6, pp. 1398–1410, 2010.

[53] H. Pereira, F. Azevedo, A. Rego, M. J. Sousa, S. R. Chaves, and M. Corte-Real, "The protective role of yeast Cathepsin D in acetic acid-induced apoptosis depends on ANT, (Aac2p) but not on the voltage-dependent channel (Por1p)," *FEBS Letters*, vol. 587, no. 2, pp. 200–205, 2013.

[54] B. H. Graham, K. G. Waymire, B. Cottrell, I. A. Trounce, G. R. MacGregor, and D. C. Wallace, "A mouse model for mitochondrial myopathy and cardiomyopathy resulting from a deficiency in the heart/muscle isoform of the adenine nucleotide translocator," *Nature Genetics*, vol. 16, no. 3, pp. 226–234, 1997.

[55] E. Z. Jordens, L. Palmieri, M. Huizing et al., "Adenine nucleotide translocator 1 deficiency associated with Sengers syndrome," *Annals of Neurology*, vol. 52, no. 1, pp. 95–99, 2002.

[56] J. D. Sharer, "The adenine nucleotide translocase type 1 (ANT1): a new factor in mitochondrial disease," *IUBMB Life*, vol. 57, no. 9, pp. 607–614, 2005.

[57] J. A. Mayr, T. B. Haack, E. Graf et al., "Lack of the mitochondrial protein acylglycerol kinase causes sengers syndrome," *The American Journal of Human Genetics*, vol. 90, no. 2, pp. 314–320, 2012.

[58] K. A. Strauss, L. Dubiner, M. Simon et al., "Severity of cardiomyopathy associated with adenine nucleotide translocator-1 deficiency correlates with mtDNA haplogroup," *Proceedings of the National Academy of Sciences of the United States of America*, vol. 110, no. 9, pp. 3453–3458, 2013.

[59] G. W. Padberg, P. W. Lunt, M. Koch, and M. Fardeau, "Diagnostic criteria for facioscapulohumeral muscular dystrophy," *Neuromuscular Disorders*, vol. 1, no. 4, pp. 231–234, 1991.

[60] C. Wijmenga, J. E. Hewitt, L. A. Sandkuijl et al., "Chromosome 4q DNA rearrangements associated with facioscapulohumeral muscular dystrophy," *Nature Genetics*, vol. 2, no. 1, pp. 26–30, 1992.

[61] D. Gabellini, M. R. Green, and R. Tupler, "Inappropriate gene activation in FSHD: a repressor complex binds a chromosomal repeat deleted in dystrophic muscle," *Cell*, vol. 110, no. 3, pp. 339–348, 2002.

[62] S. M. van der Maarel and R. R. Frants, "The D4Z4 repeat-mediated pathogenesis of facioscapulohumeral muscular dystrophy," *The American Journal of Human Genetics*, vol. 76, no. 3, pp. 375–386, 2005.

[63] R. J. L. F. Lemmers, P. J. van der Vliet, R. Klooster et al., "A unifying genetic model for facioscapulohumeral muscular dystrophy," *Science*, vol. 329, no. 5999, pp. 1650–1653, 2010.

[64] D. Gabellini, G. D'Antona, M. Moggio et al., "Facioscapulohumeral muscular dystrophy in mice overexpressing *FRG1*," *Nature*, vol. 439, no. 7079, pp. 973–977, 2006.

[65] D. Laoudj-Chenivesse, G. Carnac, C. Bisbal et al., "Increased levels of adenine nucleotide translocator 1 protein and response to oxidative stress are early events in facioscapulohumeral muscular dystrophy muscle," *Journal of Molecular Medicine*, vol. 83, no. 3, pp. 216–224, 2005.

[66] B. Clemencon, M. Babot, and V. Trezeguet, "The mitochondrial ADP/ATP carrier (SLC25 family): pathological implications of its dysfunction," *Molecular Aspects of Medicine*, vol. 34, no. 2-3, pp. 485–493, 2013.

[67] M. le Bras, A. Borgne-Sanchez, Z. Touat et al., "Chemosensitization by knockdown of adenine nucleotide translocase-2," *Cancer Research*, vol. 66, no. 18, pp. 9143–9152, 2006.

[68] R. Moreno-Sanchez, S. Rodriguez-Enriquez, A. Marin-Hernandez, and E. Saavedra, "Energy metabolism in tumor cells," *FEBS Journal*, vol. 274, no. 6, pp. 1393–1418, 2007.

[69] M.-F. Giraud and J. Velours, "The absence of the mitochondrial ATP synthase δ subunit promotes a slow growth phenotype of rho- yeast cells by a lack of assembly of the catalytic sector F_1," *The European Journal of Biochemistry*, vol. 245, no. 3, pp. 813–818, 1997.

[70] X. J. Chen and G. D. Clark-Walker, "Specific mutations in α and γ-subunits of F1-ATPase affect mitochondrial genome integrity in the petite-negative yeast *Kluyveromyces lactis*," *EMBO Journal*, vol. 14, no. 13, pp. 3277–3286, 1995.

[71] X. J. Chen and G. D. Clark-Walker, "The mitochondrial genome integrity gene, *MGI1*, of Kluyveromyces lactis encodes the β-subunit of F_1-ATPase," *Genetics*, vol. 144, no. 4, pp. 1445–1454, 1996.

[72] X. J. Chen and G. D. Clark-Walker, "The petite mutation in yeasts: 50 years on," *International Review of Cytology*, vol. 194, pp. 197–238, 2000.

[73] A. Chevrollier, D. Loiseau, P. Reynier, and G. Stepien, "Adenine nucleotide translocase 2 is a key mitochondrial protein in cancer metabolism," *Biochimica et Biophysica Acta*, vol. 1807, no. 6, pp. 562–567, 2011.

[74] K. Buchet and C. Godinot, "Functional F_1-ATPase essential in maintaining growth and membrane potential of human mitochondrial DNA-depleted $\rho\circ$ cells," *Journal of Biological Chemistry*, vol. 273, no. 36, pp. 22983–22989, 1998.

[75] J. Kaukonen, J. K. Juselius, V. Tiranti et al., "Role of adenine nucleotide translocator 1 in mtDNA maintenance," *Science*, vol. 289, no. 5480, pp. 782–785, 2000.

[76] L. Napoli, A. Bordoni, M. Zeviani et al., "A novel missense adenine nucleotide translocator-1 gene mutation in a greek adPEO family," *Neurology*, vol. 57, no. 12, pp. 2295–2298, 2001.

[77] H. Komaki, T. Fukazawa, H. Houzen, K. Yoshida, I. Nonaka, and Y. Goto -I, "A novel D104G mutation in the adenine nucleotide translocator 1 gene in autosomal dominant progressive external ophthalmoplegia patients with mitochondrial DNA with multiple deletions.," *Annals of Neurology*, vol. 51, no. 5, pp. 645–648, 2002.

[78] G. van Goethem, B. Dermaut, A. Löfgren, J.-J. Martin, and C. van Broeckhoven, "Mutation of *POLG* is associated with progressive external ophthalmoplegia characterized by mtDNA deletions," *Nature Genetics*, vol. 28, no. 3, pp. 211–212, 2001.

[79] J. N. Spelbrink, F. Y. Li, V. Tiranti et al., "Human mitochondrial DNA deletions associated with mutations in the gene encoding Twinkle, a phage T7 gene 4-like protein localized in mitochondria," *Nature Genetics*, vol. 28, no. 3, pp. 223–231, 2001.

[80] M. Deschauer, G. Hudson, T. Müller, R. W. Taylor, P. F. Chinnery, and S. Zierz, "A novel *ANT*1 gene mutation with probable germline mosaicism in autosomal dominant progressive external ophthalmoplegia," *Neuromuscular Disorders*, vol. 15, no. 4, pp. 311–315, 2005.

[81] L. Palmieri, S. Alberio, I. Pisano et al., "Complete loss-of-function of the heart/muscle-specific adenine nucleotide translocator is associated with mitochondrial myopathy and cardiomyopathy," *Human Molecular Genetics*, vol. 14, no. 20, pp. 3079–3088, 2005.

[82] Y. Kihira, A. Iwahashi, E. Majima, H. Terada, and Y. Shinohara, "Twisting of the second transmembrane α-helix of the mitochondrial ADP/ATP carrier during the transition between two carrier conformational states," *Biochemistry*, vol. 43, no. 48, pp. 15204–15209, 2004.

[83] G. Galassi, E. Lamantea, F. Invernizzi et al., "Additive effects of *POLG1* and *ANT1* mutations in a complex encephalomyopathy," *Neuromuscular Disorders*, vol. 18, no. 6, pp. 465–470, 2008.

[84] C. de Marcos Lousa, V. Trézéguet, A.-C. Dianoux, G. Brandolin, and G. J.-M. Lauquin, "The human mitochondrial ADP/ATP carriers: kinetic properties and biogenesis of wild-type and mutant proteins in the yeast *S. cerevisiae*," *Biochemistry*, vol. 41, no. 48, pp. 14412–14420, 2002.

[85] F. Fontanesi, L. Palmieri, P. Scarcia et al., "Mutation in *AAC2*, equivalent to human adPEO-associated ANT1 mutations, lead to defective oxidative phosphorylation in *Saccharomyces cerevisiae* and affect mitochondrial DNA stability," *Human Molecular Genetics*, vol. 13, no. 9, pp. 923–934, 2004.

[86] H. Kawamata, V. Tiranti, J. Magrané, C. Chinopoulos, and G. Manfredi, "adPEO mutations in ANT1 impair ADP-ATP translocation in muscle mitochondria," *Human Molecular Genetics*, vol. 20, no. 15, Article ID ddr200, pp. 2964–2974, 2011.

[87] X. J. Chen, "Induction of an unregulated channel by mutations in adenine nucleotide translocase suggests an explanation for human ophthalmoplegia," *Human Molecular Genetics*, vol. 11, no. 16, pp. 1835–1843, 2002.

[88] X. Wang, K. Salinas, X. Zuo, B. Kucejova, and X. J. Chen, "Dominant membrane uncoupling by mutant adenine nucleotide translocase in mitochondrial diseases," *Human Molecular Genetics*, vol. 17, no. 24, pp. 4036–4044, 2008.

[89] X. Wang, X. Zuo, B. Kucejova, and X. J. Chen, "Reduced cytosolic protein synthesis suppresses mitochondrial degeneration," *Nature Cell Biology*, vol. 10, no. 9, pp. 1090–1097, 2008.

[90] R. El-Khoury and A. Sainsard-Chanet, "Suppression of mitochondrial DNA instability of autosomal dominant forms of progressive external ophthalmoplegia-associated *ANT1* mutations in *Podospora anserina*," *Genetics*, vol. 183, no. 3, pp. 861–871, 2009.

[91] A. Bratic and N.-G. Larsson, "The role of mitochondria in aging," *Journal of Clinical Investigation*, vol. 123, no. 3, pp. 951–957, 2013.

[92] H. D. Osiewacz and D. Bernhardt, "Mitochondrial quality control: impact on agingand life span—a mini review," *Gerontology*. In press.

[93] M. Breitenbach, S. M. Jazwinski, and P. Laun, "The retrograde response and other pathways of interorganelle communication in yeast replicative aging," in *Aging Research in Yeast*, vol. 57, pp. 79–100, Springer, Amsterdam, The Netherlands, 2012.

Hindawi Publishing Corporation
Oxidative Medicine and Cellular Longevity
Volume 2013, Article ID 932472, 13 pages
http://dx.doi.org/10.1155/2013/932472

Research Article

Thiol Redox Sensitivity of Two Key Enzymes of Heme Biosynthesis and Pentose Phosphate Pathways: Uroporphyrinogen Decarboxylase and Transketolase

Brian McDonagh,[1,2] José Rafael Pedrajas,[3] C. Alicia Padilla,[1] and José Antonio Bárcena[1]

[1] *Department of Biochemistry and Molecular Biology, University of Córdoba and Córdoba Maimónides Institute for Biomedical Research (IMIBIC), 14071 Córdoba, Spain*
[2] *Department of Musculoskeletal Biology, Institute of Ageing and Chronic Disease (IACD), University of Liverpool, Liverpool L69 3GA, UK*
[3] *Molecular Signaling and Antioxidant Systems in Plants, Department of Experimental Biology, University of Jaén, 23071 Jaén, Spain*

Correspondence should be addressed to José Antonio Bárcena; ja.barcena@uco.es

Received 24 April 2013; Revised 10 June 2013; Accepted 19 June 2013

Academic Editor: Paula Ludovico

Uroporphyrinogen decarboxylase (Hem12p) and transketolase (Tkl1p) are key mediators of two critical processes within the cell, heme biosynthesis, and the nonoxidative part of the pentose phosphate pathway (PPP). The redox properties of both Hem12p and Tkl1p from *Saccharomyces cerevisiae* were investigated using proteomic techniques (SRM and label-free quantification) and biochemical assays in cell extracts and *in vitro* with recombinant proteins. The *in vivo* analysis revealed an increase in oxidized Cys-peptides in the absence of Grx2p, and also after treatment with H_2O_2 in the case of Tkl1p, without corresponding changes in total protein, demonstrating a true redox response. Out of three detectable Cys residues in Hem12p, only the conserved residue Cys52 could be modified by glutathione and efficiently deglutathionylated by Grx2p, suggesting a possible redox control mechanism for heme biosynthesis. On the other hand, Tkl1p activity was sensitive to thiol redox modification and although Cys622 could be glutathionylated to a limited extent, it was not a natural substrate of Grx2p. The human orthologues of both enzymes have been involved in certain cancers and possess Cys residues equivalent to those identified as redox sensitive in yeast. The possible implication for redox regulation in the context of tumour progression is put forward.

1. Introduction

During the initiation and progression of any disease state there is a shift in the metabolic programming within the cell. The increasing accuracy and availability of genomic, proteomic and systems biology approaches have allowed researchers to identify and understand how specific metabolic pathways are deregulated as a result of a disease state. The identification and modulation of key proteins, located at crucial junctions that can control metabolic flow, would offer promising therapeutic candidates for a number of disease states [1]. *Saccharomyces cerevisiae*, due to its large number of mammalian homologues and gene similarity together with ease of manipulation, has proved a model organism for basic research into the metabolic functions and regulation of particular proteins [2, 3].

One common basic characteristic to all types of cancers is reprogramming of energy metabolism to generate ATP through intense glycolytic flux with enhancement of lactate production and decreased respiration rate in spite of oxygen availability, a phenomenon known as "the Warburg effect" [3, 4]. Today we know that this metabolic adaptation is not due to mitochondrial damage since under certain circumstances cancer cells can switch back to respiration and grow faster. *S. cerevisiae* experiences the "Crabtree effect," the ability to repress respiration and oxidative phosphorylation in response to glucose and changing to respiratory metabolism when glucose availability decreases, a behavior resembling

that of cancer cells [5]. The prevailing paradigm is that cancer cells achieve a compromised balance between energy production and synthesis of macromolecules from glycolytic precursors [6] and the regulatory mechanisms behind this peculiar behavior are a hot topic in cancer research. *S. cerevisiae* could prove particularly suitable as model organism to study the regulatory key points governing this metabolic remodeling [3].

Iron serves as a cofactor for a wide variety of cellular processes, including oxygen transport, cellular respiration, the tricarboxylic acid (TCA) cycle, lipid metabolism, synthesis of metabolic intermediates, gene regulation, and DNA replication and repair [7]. Complex biosynthetic pathways are used for the assembly of Fe-porphyrin (Heme) and Fe–S clusters, essential cofactors of a large number of important enzymes. Alterations in iron homeostasis underlie many human diseases, including Friedreich's ataxia, hereditary hemochromatosis, aceruloplasminemia, Parkinson's disease, microbial pathogenesis, and cancer, as well as aging [8].

Our understanding of many of the known metabolic disorders concerning iron and its relationship to the mitochondria comes directly from yeast studies [7]. These pathways are tightly regulated due to the potential for the excessive production of reactive oxygen species (ROS) as a result of electron leakage. ROS are necessary for normal cell function and signalling, essentially by reversible redox modifications of specific cysteine residues on key proteins. This offers a quick and effective means for controlling a wide and diverse range of biological functions within the cell, whether by direct modulation of the catalytic sites, facilitating cofactor or substrate binding thus modulating their conformation or regulatory role [9]. The reversible oxidation and reduction of protein thiols by disulfide oxidoreductases with conserved active sites, such as thioredoxins (Trx's) and glutaredoxins (Grx's), can alter the functions of enzymes, receptors, transporters, and transcription factors [10]. The formation of protein mixed disulfides with glutathione (protein-SSG) is a specific form of redox modification called glutathionylation whose reversibility or deglutathionylation is primary catalyzed by Grx's [11]. Aberrant regulation of protein glutathionylation/deglutathionylation reactions due to changes in glutaredoxin activity can disrupt both apoptotic and survival signaling pathways [12].

A recent report demonstrated increases in ROS in human lung cancer cells caused the oxidation of a Cys358 of pyruvate kinase M2. As a consequence, glucose flux was diverted into the PPP to generate reducing power for antioxidant defenses [13]. Using a redox proteomic approach, we had previously identified this conserved cysteine residue in the yeast isoform of pyruvate kinase as redox sensitive in response to oxidative stress (OS) [14]. We confirmed that reversible redox modification of specific Cys residues of key glycolytic proteins allows a redirection of energy metabolites towards the PPP for NADPH production and antioxidant defense, as described earlier for glyceraldehyde-3-phosphate dehydrogenase [15–17]. In a subsequent redox shotgun proteomic screen using wild type (WT) yeast and a strain lacking the oxidoreductase glutaredoxin 2 (Grx2p), uroporphyrinogen decarboxylase (Hem12p) and transketolase (Tkl1p) were detected as containing reversibly oxidized Cys residues only in the strain lacking Grx2p, indicating they are involved in thiol disulfide exchange [18]. In the approach, proteins were tryptic digested and peptides containing reversibly oxidized Cys residues were affinity purified and analysed by MS/MS. The clear differences in the redox state of specific Cys residues of Hem12p and Tkl1p suggest that they may be direct or indirect targets of Grx2p. These proteins were selected for further analysis on the basis of their crucial roles in metabolism within the cell, as described above, and to clarify their redox properties.

In the nonoxidative part of the PPP, transketolase is a key enzyme that is located at the metabolic junction between the glycolytic and the PPP, which makes it an ideal candidate for the regulation of metabolic flux (Figure 1(a)). Its role is widespread across all life kingdoms as it also plays a similar role in the Calvin Cycle in plants. The PPP is essential for the production of NADPH, ribulose 5-phosphate needed for nucleotide biosynthesis, and erythrose 4-phosphate needed for aromatic amino acid biosynthesis. The reactions catalyzed by Tkl1p are essential for the diversion of the glycolytic metabolic flux toward biosynthetic pathways, which are especially active in rapidly proliferating cells. Not surprisingly, transketolase activity is increased in tumour cells [19].

Cancer therapies are increasingly being focused on the biochemistry of cancer cells as opposed to their genetic origins [20], hence understanding of regulatory mechanisms is essential to effectively target these cells [21].

Uroporphyrinogen decarboxylase, Hem12p, is involved in the 5th step of heme biosynthesis in the cytosol, before biosynthesis is completed within mitochondria (Figure 1(b)) [22]. Beside its well-known roles in oxygen transport, electron transfer, and peroxide metabolism, heme is central to oxygen sensing in many living organisms and plays a signaling role in a wide array of biological processes [23]. Altered heme expression and accumulation of heme intermediates, are responsible for a number of diseases generally referred to as porphyrias. Defects in the activity of the human orthologue of Hem12p, UroD, are associated with hepatoerythropoietic porphyria [24]. Overexpression of UroD has been recently demonstrated in tumour biopsies of patients with head and neck cancer [25].

In this study we characterized the redox properties of these enzymes from an *in vivo* experiment in *S. cerevisiae* and after exposure to H_2O_2. Hem12p and Tkl1p contain specific Cys residues that are redox sensitive, but yet they differ in their response to OS. To further investigate their properties *in vitro* we produced recombinant versions of these proteins and characterized their redox properties by traditional biochemical assays in combination with high-resolution proteomics to both identify and quantify the oxidative modifications on specific Cys residues.

2. Material and Methods

2.1. Materials. All reagents and chemicals were obtained from Sigma unless stated and were of analytical grade or above. The buffer used throughout unless stated was 50 mM

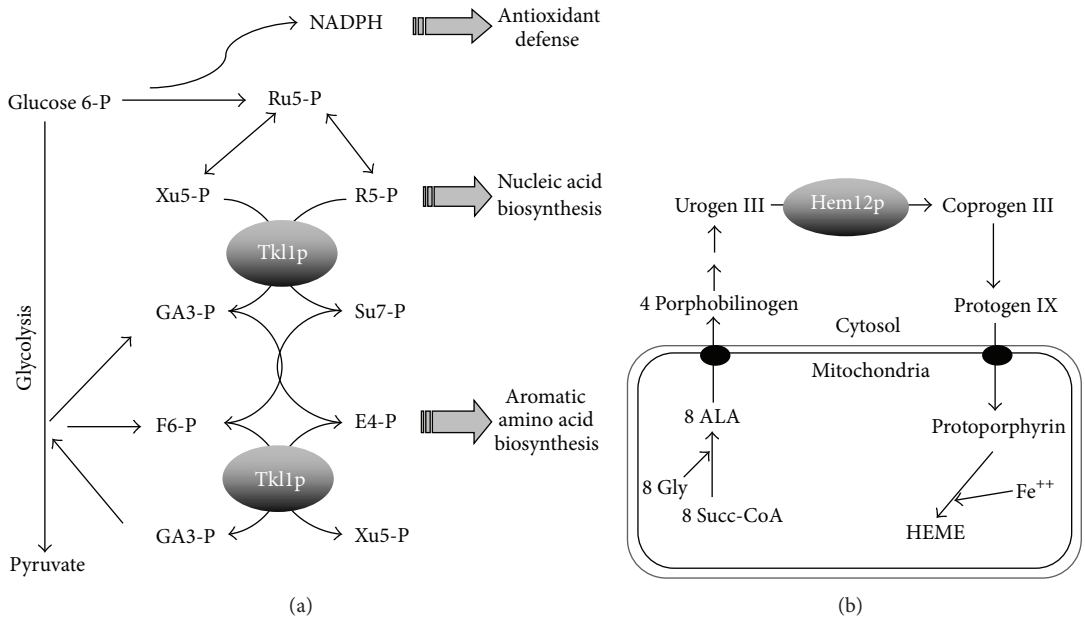

Figure 1: Metabolic positioning of Tkl1p and Hem12p. (a) Transketolase (Tkl1p) catalyses a number of reactions in the PPP, linking energy metabolism, antioxidant response, and biosynthesis of nucleic acids and aromatic amino acids. (b) Uroporphyrinogen decarboxylase (Hem12p) catalyses the 5th step in heme biosynthesis before biosynthesis is completed within mitochondria. Heme biosynthesis is closely linked to oxygen tension and iron homeostasis. ALA, 5-aminolevulinic acid; Urogen, Coprogen, and Protogen stand for uroporphyrinogen, coproporphyrinogen, and protoporphyrinogen, respectively. Other abbreviations are those usually employed for common metabolites.

Tris-Cl, pH 8.0. Recombinant Hem12p and Tkl1p were produced by Abyntek Biopharma S.L. (Spain). Proteins were overexpressed in *E. coli* using synthetic DNA with codon optimization, C-terminal tagged with poly-histidine, and purified by affinity capture on Ni-Sepharose.

2.2. Strain, Growth Conditions, and Analysis of the "Thiol Redox Peptidome". *S. cerevisiae* strains used for redox peptidome analysis were CMML235 (WT), *MATa*, *ura*3-52, *leu2*Δ1, *his3*Δ200, and MML44 (ΔGrx2), CML235 + *grx2*::*LEU2*, a kind gift from Professor E. Herrero, University of Lleida, Spain [27]. Cells were grown on YPD medium at 30°C until exponential phase (optical density of ~1 at 600 nm) and were treated (or not) with 1 mM H_2O_2 for 30 min. Shaking was set at 180 rpm and 1.5 L conical flasks containing 250 mL of media were used. Cells from three independent biological replicates were harvested and the reversibly oxidized Cys containing peptides were isolated and identified as described previously [14, 18]. Briefly, in cell extracts free thiols were initially blocked with N-ethylmaleimide (NEM), and reversibly oxidized thiols were then reduced and subsequently labelled with thiol specific, biotin-HPDP. Proteins were tryptic digested and those peptides containing reversibly oxidized Cys residues were affinity purified on avidin Sepharose and analysed by MS/MS. These peptides were used to identify proteins and to map the reversibly oxidized cysteines.

2.3. Mass Spectrometry Analysis. Initial mass spectrometry analysis was performed as before [18]. Samples containing the affinity purified peptides were subjected to complete evaporation in a Speedvac centrifuge and then suspended in 20 μL of 5% acetonitrile/2% formic acid. 5 μL was used for the analysis in a Surveyor HPLC-LTQ Orbitrap XL (Thermo, USA) instrument equipped with a nanospray source. Peptides were trapped and cleaned in an Agilent 300SB-C18 5 × 0.3 mm trap column (Agilent Technologies, Germany) at a flow rate of 10 μL/min of 5% acetonitrile/0.1% formic acid for 15 min and then resolved in a Biobasic-18 100 × 0.075 mm column (Thermo, USA) at a flow rate of 0.3 μL/min postsplitting for 60 min using an acetonitrile gradient, supplemented with 0.1% formic acid, from 5 to 40%. The spray voltage and the capillary temperature of the MS were set to 2.0 kV and 170°C, respectively. Over the total analysis time, one Full Scan in FT mode at resolution 30000@400 m/z in the range 400–1500 m/z followed by five CID activated MS/MS in dependent mode corresponding to the five most abundant masses, was acquired. Dynamic exclusion was set to on.

For MALDI-TOF/TOF analysis peptides were desalted and concentrated by using μC-18 ZipTip columns (Millipore) and directly loaded onto the MALDI plate using α-cyano hydroxycinnamic acid as the matrix. Mass analysis of peptides of each sample was performed with a MALDI-TOF/TOF (4800, AB Sciex) mass spectrometer using m/z range up to 10,000, with an accelerating voltage of 20 kV. Spectra were internally calibrated with peptides from trypsin autolysis ($M + H^+ = 842.509$, $M + H^+ = 2211.104$). Dynamic modifications included for Cys residues included NEM, glutathionylation, oxidation (–SOH), dioxidation ($-SO_2H$), and trioxidation ($-SO_3H$).

2.4. Label-Free Quantification. The relative quantification of detected Cys containing peptides was performed from affinity purified reversibly oxidized tryptic peptides from cell extracts and separately from recombinant proteins using Progenesis software (Version 3.0, Nonlinear Dynamics, UK), a label-free quantification programme for MS data [28]. The data from 3 independent replicates of the MS scans and MS/MS spectra were transformed to peak lists with Progenesis LC-MS using a proprietary algorithm and then stored in peak lists comprising m/z and relative abundance that show significant differences in the peak areas of parent ions using an ANOVA (P value < 0.05) analysis within the programme. One sample was set as a reference, and the retention times of all other samples within the experiment were aligned to this sample. In the case of the recombinant proteins after different treatments, the relative oxidation state of the Cys residues was calculated by taking the sum of the abundance of the Cys containing peptide with appropriate modification and normalising it against the abundance of the whole protein, that is, the relative abundance of all peptides detected corresponding to that protein. This is explained in more detail in Supplementary Information.

A selective reaction monitoring (SRM) experiment with appropriate proteotypic peptides for Hem12p and Tkl1p was performed to determine if there were significant differences in their concentrations between yeast strains. Initially, the recombinant proteins were diluted, tryptic digested, and analysed in a triple quadrupole mass spectrometer (4000 QTrap, ABI Sciex). The diluted proteins and their peptides were quantified using Progenesis label-free quantification (Figure S1). Five proteotypic peptides and appropriate transitions were selected from http://www.SRMatlas.org/ [29], for each recombinant protein. The major transition for each peptide was used in a SRM analysis for the relative abundance of each protein in WT and ΔGrx2 yeast strains. Two independent biological replicates of the yeast strains were analyzed by positive ion ESI LC-MS^2 on a triple quadrupole mass spectrometer (4000 Qtrap, ABI Sciex). Samples were cleaned on a Zorbax 300SB-C18, 5 mm × 0.3 mm trap column (Agilent Technologies) for 5 min at a flow rate of 10 μL/min and 95% solvent A (solvent A: 0.1% formic acid on water; solvent B: 0.1% formic acid on acetonitrile). Peptides were separated in gradient mode using a flow rate of 300 nL/min over a 75 μm × 150 mm Biobasic C18 column (Thermo). Gradient was as follows: 60 min from 5% to 40% B, 10 min from 40% to 65% B. Eluted peptides were directly electrosprayed into the mass spectrometer at ESI voltage = 2800 V. The instrument was set up to cycle through all SRM transitions, followed by one enhanced resolution scan (ER) of the most prominent mass and one enhanced product ion scan (EPI, with Q0 trapping activated and scan rate of 1000 amu) of the selected mass. For SRM transitions, Q1 resolution was set to high (resolution = 2500, FWHM = 0.4 Da at m/z = 1000) and Q3 resolution was set to unit (resolution = 1700, FWHM = 0.6 Da at m/z = 1000). Dwell time for all MRM transitions was set to 50 ms. Specific instrument settings were as follows: Declustering Potential (DP) = 100, EP = 10, Curtain Gas (CUR) = 10, CAD gas = 12, Interface Heater Temperature (IHT) = 80°C. Peak detection and automatic quantification methods were built using Analyst 1.4.2 software (AB Sciex). To ensure correct peak identification and quantification, peak detection was inspected visually for coelution, similar shape, and for retention order.

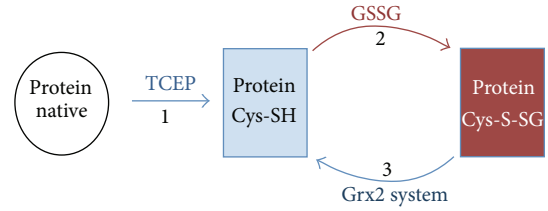

Figure 2: Scheme for recombinant protein redox analysis. (1) Proteins are initially reduced with TCEP and an aliquot is removed and blocked with NEM; (2) the remaining protein is glutathionylated with a high concentration of GSSG, and an aliquot is removed and any remaining free thiols are blocked with NEM; (3) the protein aliquots removed are desalted and incubated with the Grx2p system and newly formed free thiols are blocked with NEM. Aliquots prepared are used for analysis by MS/MS and free thiol determinations using DTNB.

2.5. In Vitro Redox Interconversion. *In vitro* redox conversion of recombinant proteins was performed as described previously [30] and outlined in Figure 2. Briefly, recombinant protein was initially reduced with 50 μM TCEP (*tris*(2-carboxyethyl)phosphine) for 30 min; the mixture was incubated with 20 mM GSSG or dieosinediglutathione (DiEGSSG) or Tris buffer for controls at 37°C for 30 min. After incubation, excess GSSG was removed by Zeba spin Desalting Columns (Thermo). In the case of Tkl1p, thiamine pyrophosphate (TPP) and $MgCl_2$ were maintained in the buffer and subsequently added to the mixture after any desalting procedures. For deglutathionylation, following treatment with GSSG, the proteins were incubated with Grx2p mix containing, 5 nM yeast recombinant Grx2p [31], 0.4 mM NADPH, 0.75 mM GSH, and 80 nM glutathione reductase (GR) (all Sigma). Remaining reduced thiol groups were subsequently blocked with NEM at all stages. Aliquots of the mixture containing 10 μM of protein were subjected to 12% SDS-PAGE electrophoresis under nonreducing conditions. Gels were stained with Coomassie R-250 and duplicate gels were transferred to nitrocellulose membranes and reversibly stained with Ponceau S to ensure complete transfer. Membranes were blocked with 2% BSA in tris buffered saline containing 0.5% tween (TBS-T) and incubated with primary antibody anti-GSH (Virogen, Watertown, USA) using a dilution of 1 : 1500. Membranes were washed with TBST and incubated with secondary goat anti-mouse (Sigma) at a concentration of 1 : 4000 and the chemiluminescent signal was detected by using a LAS-3000 camera (Fujifilm, Tokyo).

Free thiol content of proteins was estimated using Ellman's reagent (5,5-dithiobis-2-nitrobenzoic acid, DTNB) at 412 nm in Tris buffer pH 8.0 [32]; measurements were performed from three independent preparations. MS/MS analysis of recombinant proteins was performed as described

Table 1: Label-free MS quantification of reversibly oxidised Cys residues of Hem12p and Tkl1p using Progenesis. Peptides detected in a shotgun proteomic screen of reversibly oxidised Cys residues using the redox affinity enrichment approach in WT and ΔGrx2 yeast strains ±1 mM H_2O_2. Units are arbitrary for intensity of parent ions.

Protein and Cys peptide	Peak intensity of oxidized Cys peptide (arbitrary units)			
	WT	WT + H_2O_2	ΔGrx2	ΔGrx2 + H_2O_2
Tkl1p (Cys622)				
LSVLPDNVPIMSVEVLATT**C**WGK	2.3	22.9**	9.5	58.5**
Hem12p (Cys26)				
VERPP**C**WIMR	5.0	7.0	30.0*	23.2

*Hem12p had a sixfold increase in the detection of reversibly oxidised Cys26 in the ΔGrx2 strain compared to WT ($P = 0.0042$). **Tkl1p was increased in both strains after H_2O_2 treatment and more significantly in the ΔGrx2 strain; this peptide was detected with $z = 2$ ($P = 0.00471$) and $z = 3$ ($P = 0.0109$). Peak intensities are given in arbitrary units $\times 10^4$ (Tkl1p) and $\times 10^3$ (Hem12p).

with separate aliquots of the protein mixtures digested with sequencing grade trypsin (Promega) and stored at −70°C.

2.6. Fluorescent Deglutathionylation. DiEGSSG was from IMCO Ltd (Stockholm, Sweden) and a kind gift from Professor Arne Holmgren, Karolinska Institute, Sweden. This glutathione disulfide derivative has low fluorescence due to self-quenching, while the reduced eosin-glutathione (eosin-GSH) has high fluorescence. Protein concentrations of recombinant proteins were determined using absorbance at 280 nm and the appropriate molar extinction coefficient for each protein (BSA = 43824 M^{-1} cm^{-1}, Hem12p = 58900 M^{-1} cm^{-1}, and Tkl1p = 88240 M^{-1} cm^{-1}). Proteins were incubated with excess DiEGSSG and labelling with eosin-GSH was monitored using the molar extinction coefficient of eosin isothiocyanate (EITC) at 525 nm (=56000 M^{-1} cm^{-1}). 1 μM of fluorescently labelled protein was incubated with "Grx2p mix" as above for over 5 min. Kinetic measurements were recorded over 5 min in a Synergy HT (Bio-Tek) 96-well fluorescence plate reader with excitation at 485 nm and emission 528 nm. Positive control used was BSA labelled with eosin-GSH with complete Grx2p system (IMCO, Sweden) and negative control was a duplicate but lacking Grx2p system. Deglutathionylation activity by Grx2p was determined from three independent redox interconversion preparations for each recombinant protein and also measured in duplicate.

2.7. Transketolase Activity. Activity was determined by oxidation of NADH at 340 nm over 5 min in a coupled reaction as described previously [33]. Briefly the reaction mixture containing xylulose 5-phosphate (2 mM), TPP (10 μM), $MgCl_2$ (1.2 mM), triosephosphate isomerase (1 unit), glyceraldehyde phosphate dehydrogenase (1 unit), NADH (10 μM), and ribose 5-phosphate (10 mM) was allowed to equilibrate before the addition of 1.5 μM of transketolase treated with or without different sulfhydryl reagents. When Tkl1p ± GSSG treated with 1 mM NEM was analysed, the reagent was carried over into the assay mixture at a final concentration of 0.01 mM, but this concentration of NEM had minimal effect on the activity of the enzyme. Duplicate preparations were performed for Tkl1p and Tkl1p + GSSG, activity was measured in triplicate, and statistics were performed using two tailed paired Student's t-test.

3. Results

3.1. Redox Analysis of the Proteome: Relative Quantification of the Reversibly Oxidized Cys Residues from Protein Extracts of Cell Cultures Reveals that Hem12p and Tkl1p Are Redox Sensitive Proteins. Reversibly oxidized Cys containing tryptic peptides of cell extracts from both WT and ΔGrx2 and after exposure to 1 mM H_2O_2 for 30 min were affinity purified, analysed, identified by MS/MS, and relatively quantified using the label-free quantification programme Progenesis LC-MS (Table 1). In the case of Hem12p, only Cys26 was detected as reversibly oxidized in cell extracts and there was no significant change in the signal intensity of the parent ion of the peptide containing Cys26 after H_2O_2 treatment, yet there was a sixfold increase in the amount of reversibly oxidized Cys26 parent ion in the ΔGrx2 strain.

In the case of Tkl1p only one of the two Cys residues, Cys622, could be detected. The tryptic peptide containing reversibly oxidized Cys622 was detected with a higher abundance in the ΔGrx2 strain but more significantly in both strains after H_2O_2 treatment. We relatively quantified the proteins between strains using SRM to confirm that the increase in the detection of the Cys redox peptides was due to oxidation of the Cys residue and not to an increase in the protein concentrations. Table 2 lists the proteotypic peptides, the appropriate transitions used for each peptide, and the ratio of detection between strains. Despite some variability on the behaviour of the proteotypic peptides and transitions selected, it is clear that a change in protein total concentration cannot account for the significant increase in abundance of the oxidized Cys peptides detected in the ΔGrx2 strain compared to WT. According to these results, both Hem12p and Tkl1p showed a true redox response on their Cys residues upon H_2O_2 treatment and/or Grx2p depletion.

A striking increase in the oxidized form of Cys-peptides was the common response of both enzymes to the absence of Grx2p, suggesting they could be prone to glutathionylation [11]. To check this possibility, we prepared the recombinant forms of Hem12p and Tkl1p and studied the glutathione dependent redox interconversion *in vitro* by both redox proteomic and biochemical strategies. A scheme for the strategy employed is outlined in Figure 2. Proteins were initially reduced using a trace of the thiol reductor TCEP and glutathionylated using a high concentration of oxidized

Table 2: SRM quantification of Hem12p and Tkl1p in WT and ΔGrx2 yeast strains. Proteotypic peptides and transitions used for SRM analysis and relative quantification are shown. Peak intensity is given in arbitrary units $\times 10^4$. SRM was performed with two independent biological replicates.

Proteotypic peptide	Q1 (m/z)	Q3 (m/z)	Fragmentation	Peak intensity	
				WT	ΔGrx2
Uroporphyrinogen decarboxylase					
VTLQGNLDPGVMYGSK	839.93	838.41	2+/y8	2.35	1.66
DAEIASEITIQPVR	771.41	1113.63	2+/y10	1.87	ND
YIVNFGHGTHPFMDPDVIK	1094.04	1061.53	2+/y9	3.32	ND
NPEDLQTVLDYK	717.86	979.55	2+/y8	5.16	6.33
QMIEAFGGGK	519.26	665.33	2+/y7	2.42	ND
Transketolase					
FFGFTPEGVAER	678.83	757.39	2+/y7	9.70	4.10
QNLPQLEGSSIESASK	844.43	1332.66	2+/y13	0.63	0.18
SFVVPQEVYDHYQK	580.29	653.81	2+/y10	9.41	6.63
ANSGHPGAPLGMAPAAHVLWSQMR	819.41	919.49	2+/y7	0.22	0.23
SLPNIQVWRPADGNEVSAAYK	772.40	938.46	2+/y9	0.28	0.21

ND not detected.

glutathione (GSSG), a strategy widely employed by many groups [34, 35]. The proteins were desalted to remove excess GSSG and subsequently incubated with the Grx2p system (Grx2p, glutathione reductase (GR), NADPH, GSH) to monitor deglutathionylation. Aliquots are taken at each stage with remaining free thiols blocked with NEM before analysis by MS/MS.

3.2. Hem12p: Cys52 of Hem12p Can Be Glutathionylated and Subsequently Deglutathionylated by Grx2p In Vitro. Treatment of Hem12p with GSSG produced a glutathionylated version of the protein as detected initially in a preliminary analysis by Immunoblotting (not shown). Following the scheme outlined in Figure 2, we obtained 3 samples of the protein: (1) fully reduced, (2) GSSG treated (glutathionylated), and (3) incubated with a Grx2p system (theoretically deglutathionylated). Tryptic digestion of these samples, analysis by MS/MS, and quantification of the total protein and individual peptides containing Cys confirmed the identification of the glutathionylated Cys residues (Figures 3 and 4). In this analysis, the most susceptible identifiable residue to glutathionylation is Cys52 and incubation with the Grx2p system resulted in almost complete deglutathionylation of the residue. Hem12p contains 6 Cys residues within 5 tryptic peptides, where 1 peptide contains 2 Cys residues (Figure 5). We detected 4 of the 5 peptides, the remaining peptide containing 2 Cys residues being nonamenable to MS/MS detection due to size or amino acid composition (peptide containing Cys126 did not fragment well and was not included in analysis). Reduced Hem12p had an average free thiol content of 4.5 μM/μM protein and Hem12p treated with GSSG had an average free thiol content of 1.25 μM/μM protein as determined by titration with DTNB, indicating that ≈3 Cys residues were oxidized per protein molecule. Therefore, we also cannot rule out (de)glutathionylation of Cys270/271 or Cys126.

Inspection of the extracted ion chromatograms for the Cys52 peptide confirmed that the parent ion containing

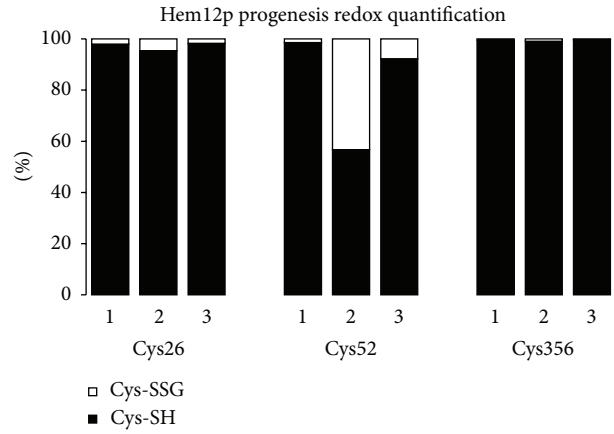

Figure 3: Redox interconversion of Hem12p. Hem12p was initially reduced with TCEP followed by either incubation with NEM (sample 1), incubation with GSSG followed by NEM (sample 2), incubation with GSSG followed by Grx2p system, and then NEM (sample 3). Progenesis quantification of modified thiol groups was carried out using the signal intensity of parent ions for the treated recombinant protein. Recombinant protein quantification for each treatment is normalized to all peptides detected and quantified for the recombinant protein (see Supplementary Information available online at http://dx.doi.org/10.1155/2013/932472 for further description of the method).

the glutathione moiety is almost completely reduced after incubation with Grx2p system (Figure 4).

In a separate assay to confirm deglutathionylation by Grx2p, we used a fluorescent GSSG moiety (DiEGSSG), where fluorescence is quenched when it is part of a disulfide and fluorescence is liberated in the form of eosin-GSH [36]. We labelled Hem12p with this reagent and calculated, using appropriate molar extinction coefficients, that for every mole of Hem12p, there was ~1.5 moles of fluorescent glutathione

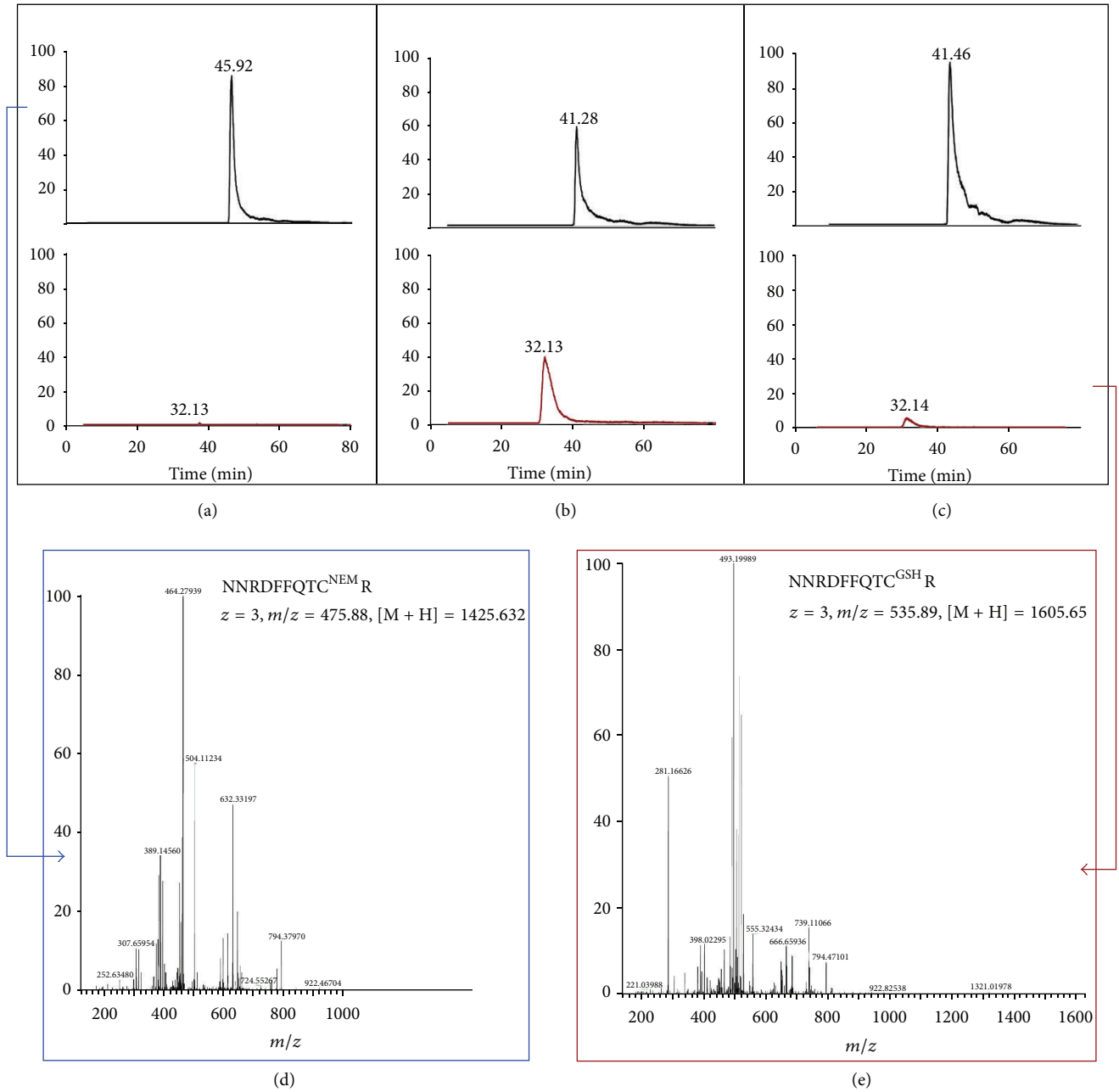

Figure 4: MS analysis of recombinant Hem12p. (a) Representative extracted ion chromatograms (XIC) of peptide NNRDFFQTCR with Cys52 of Hem12p (a) reduced, (b) +GSSG, (c) +Grx2p system. Traces in the upper panels correspond to the reduced peptide followed by alkylation with NEM (+125); traces in red in the lower panel correspond to the peptide glutathionylated (+305). (d) Fragmentation spectra of the parent ion in reduced state (+NEM) and (e) with GSH are presented.

attached. We monitored the activity of the deglutathionylation of Hem12p in the presence of the Grx2p system by the increase in fluorescence, showing the same rate as the reference protein, glutathionylated BSA (Figure 6). These results demonstrate that glutathionylated Cys52 in uroporphyrinogen decarboxylase is a substrate for Grx2p.

Unfortunately, we were unable to source or produce the reagents necessary to measure the activity of this enzyme, but from previous studies it was shown that the activity of Hem12p from *S. cerevisiae* is at a maximum in the presence of reducing agents such as dithiothreitol, and inhibited by sulfhydryl agents [37]. Together these results would suggest that the glutathionylation and subsequent reversible redox dependent control would provide an excellent means for the cell to protect this constitutively expressed enzyme and provide a mechanism for the control of heme biosynthesis dependent on the prevailing redox environment.

3.3. Tkl1p: Reversible Oxidation of Cys622 of Tkl1p Is an Oxidative Stress Response. Tkl1p contains two Cys residues.

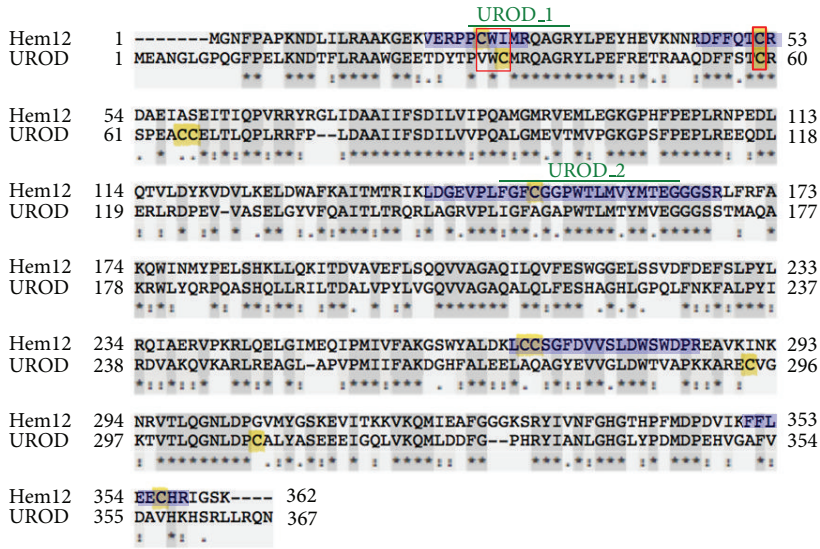

Figure 5: Alignment of uroporphyrinogen decarboxylase from *S. cerevisiae* and human. Hem12p is the enzyme from *S. cerevisiae* UniProt P32347 and UROD is from human, UniProt P06132. Cysteines are highlighted in yellow; dark grey shadowed residues indicate identical positions; tryptic Cys-peptides in Hem12p are highlighted in blue; thin red square marks Cys26 and its equivalent Cys35 in UROD; thick red square marks the conserved cysteine, Cys52 in Hem12p and Cys59 in UROD, respectively; green lines indicate the sequence signatures for Uroporphyrinogen decarboxylase UROD_1 and UROD_2 (PS00906 and PS00907, resp., according to ProSite). The sequences have been aligned using the program Clustal-ω and share 49.60% identity.

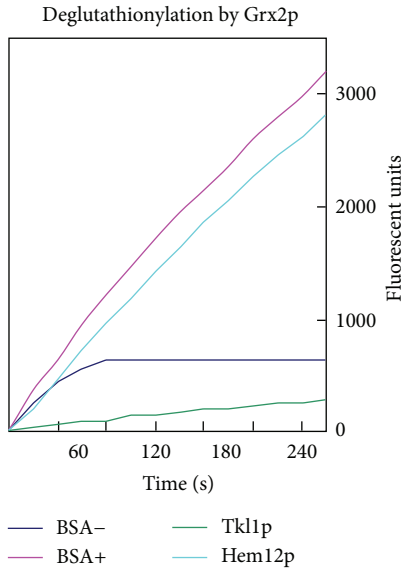

Figure 6: Deglutathionylation of fluorescently labelled proteins (with eosin-GSH) by Grx2p system. Increase in fluorescence emission by free eosin-GSH is given in arbitrary units. BSA labelled with eosin-GSH and then incubated with complete Grx2p system or not are used as the positive (BSA+) and negative (BSA−) controls, respectively.

Cys159 is part of the active site with a role in TPP binding and highly conserved across different species [38]. As shown in Table 1, the relative abundance of the peptide containing reversibly oxidized Cys622 was highest in H_2O_2 treated cells, with the ΔGrx2 strain having the highest signal intensity.

When recombinant Tkl1p was analysed it was not detected as glutathionylated in a preliminary analysis by western blotting following the same scheme outlined in Figure 2 (not shown). The tryptic peptide containing Cys159 is 77 amino acids long and we were unable to detect this peptide, either by electron spray MS/MS or MALDI-TOF/TOF. We also attempted to detect this Cys residue using alternative proteases and again were unable to detect a peptide containing Cys159. Cys622-containing peptide was only detected in its reduced state, with a tenfold lower intensity of the reduced peptide after GSSG treatment than when it was treated with TCEP. Extracted ion chromatograms of the reduced peptide are presented in Figure 7(a) and their quantitative analysis in Figure 7(b). The decrease in the amount of reduced peptide is quantitatively comparable to the increase in the oxidized peptide in extracts of cell cultures after H_2O_2 exposure (see Table 1). However, the oxidized form of the peptide could not be identified at this point.

The published structure of *S. cerevisiae* Tkl1p (PDB: 1GNS) with TPP cofactor, E4-P and Ca^{2+}, indicates it is a homodimer and that the Cys622 detected by our redox proteomic approach is accessible in the dimer (Figure 8(a)). Incubation of the enzyme with TPP is necessary for correct folding and activity, with the number of accessible free thiol groups dependent on TPP binding [39]. Intersubunit contacts are confined to the N-terminal and intermediate domains, whereas C-terminal domains have few contacts and their packing is very loose with a large "tunnel" at the interface. Moreover, the C-terminal domain does not contribute to TPP and substrate binding, but a possible regulatory role for this domain was proposed [40]. Cys622 of both subunits is in a loop at the interface, with their –SH side chains pointing away

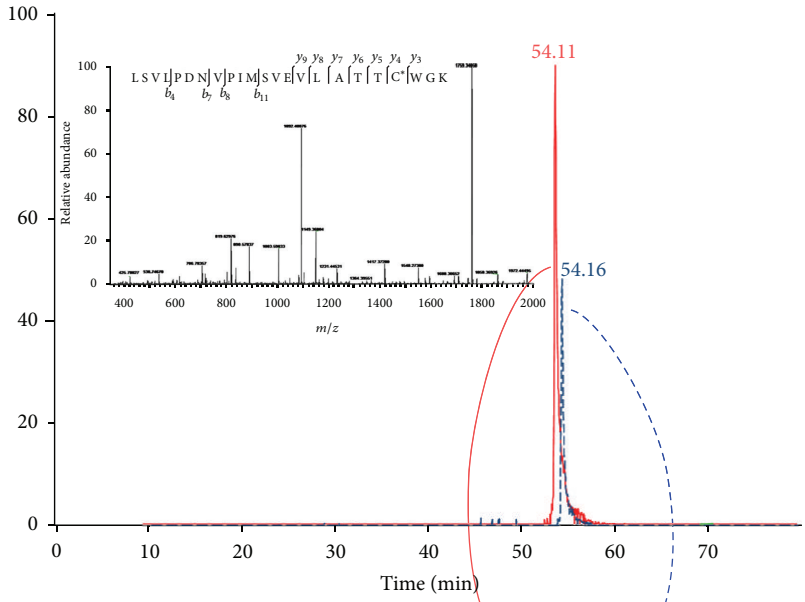

(a)

Reduced Cys peptide of Tkl1p	+TCEP	+GSSG	+GSSG +Grx2 system
LSVLPDNVPIMSVEVLATT**C**WGK	92.8	6.7	7.7

(b)

	—	DTT (1 mM)	NEM (1 mM)*
Tkl1p	30.54 ± 12.3	32.54 ± 2.09	7.39 ± 3.18
Tkl1p + GSSG	57.34 ± 21.1	52.94 ± 15.8	31.51 ± 3.18

(c)

Figure 7: Redox interconversion and activity of Tkl1p. (a) Representative extracted ion chromatogram and fragmentation (inset) of tryptic peptide from Tkl1p containing Cys622 (reduced) after treatment with TCEP (red) or GSSG (blue), followed by NEM. (b) Progenesis quantification of reduced peptide after treatments in the presence of Grx2p system (values in arbitrary units $\times 10^6$). (c) Transketolase activity after redox treatments, ≈80% inhibition of enzyme activity after pretreatment with NEM, significance $P < 0.05$. *The final concentration of NEM in the assay was 0.01 mM; this concentration had little effect on activity. Units are μmol min^{-1}/μg protein.

from each other and separated by ≈9 Å [41]. In the crystal structure, the Cys622 residue is surrounded by positively charged amino acids. According to the structure of the dimer, the distance between the nonconserved Cys622 and the active site is >30 Å, which would normally prohibit a direct influence on the catalytic mechanism. Cys622 is ~4 Å from Arg491 (Figure 8(b)), which could stabilize a possible thiolate at Cys622 and is preceded by two Thr residues (Thr620 and Thr621), favourable to the formation of a stable sulfenic acid on Cys622 [42].

Using electron spray ionisation and MS/MS we were unable to detect the Cys622 tryptic peptide with glutathione or as a sulfenic acid (or further oxidation states). However, analysis by MALDI-TOF/TOF allowed the detection of the peptide containing Cys622 in the sulfenic acid form (+16 Da), and with a mass difference of +305 Da, corresponding to glutathionylation after GSSG treatment (Figure S2).

Comparison of the enzymatic activity of reduced Tkl1p and treated with GSSG surprisingly resulted in higher activity of the enzyme after GSSG treatment (Figure 7(c)). Treatment of the reduced Tkl1p with NEM resulted in a significantly lower activity of the enzyme indicating that free thiols are needed for activity. However, pretreatment of the enzyme with GSSG protected against almost complete inactivation as compared to NEM alone. Preincubation of the enzyme with DTT did not significantly alter the activity of the enzyme and had little effect on the activity of Tkl1p treated with GSSG (Figure 7(c)). Consistent with this result, estimation of the free thiol content of the reduced protein and of that subsequently treated with GSSG failed to show any significant differences (not shown). Moreover, incubation of the enzyme with DiEGSSG resulted in partial glutathionylation with ~ 0.35 moles of the fluorescent moiety for every mole of Tkl1p. As to be expected the fluorescent deglutathionylation of the

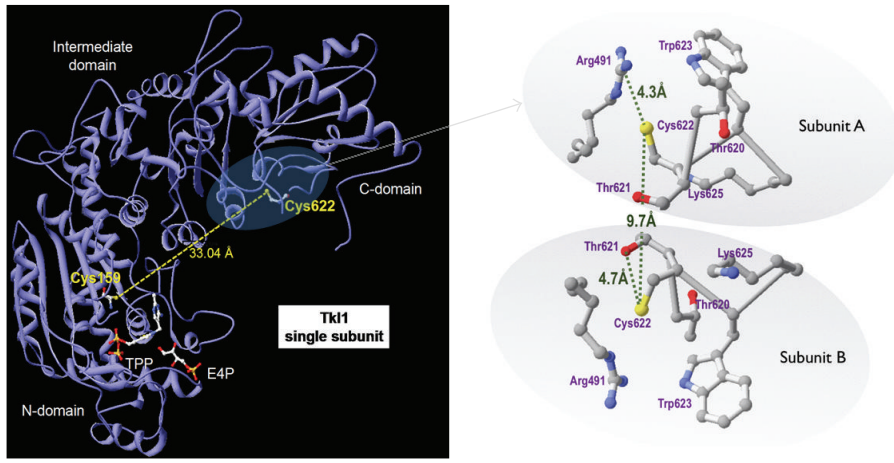

(a) (b)

FIGURE 8: Positioning of Cys622 in the structure of the Tkl1p molecule. Structure of Tkl1p with bound TPP, E4P, and Ca^{2+}. (a) Subunit of homodimer, distance between cys622 and cys159 of active site from either subunit is too large for intradisulfide. (b) Interphase between subunits of homodimer, distance between cys622 of homodimers is 9.68 Å; Cys622 is close to both Thr and Arg residues, which can favour a thiolate and formation of sulfenic acid. Figures were prepared from structure PDB 1NGS using the free software DeepView [26].

treated enzyme by the Grx2p system as measured by an increase in fluorescence was ~10-fold lower than for Hem12p or the positive control BSA (Figure 6).

Together these results suggest that treatment of the enzyme with GSSG results in a conformational change accompanied by limited glutathionylation of Cys622 and marked enhancement of the enzymatic activity. This indicates that glutathionylation is probably not a natural redox modification of this enzyme. However, the plant orthologue of this enzyme has previously been identified as a Trx target [43] and our results would suggest that the protein is involved in a thiol disulfide exchange mechanism.

4. Discussion

Cys residues due to their various oxidation states can influence the activity of enzymes, whether they form part of the catalytic site, involved in cofactor binding or allosteric modulation [9, 44]. Proteomics has developed into a powerful tool not only for the detection and identification of proteins, but recent advances have allowed the identification and quantification of posttranslational modifications on specific residues of redox proteins [45]. In a previous shotgun proteomic screen to detect potential Grx2p protein targets two proteins, Hem12p and Tkl1p, were identified as containing reversibly oxidized Cys residues in a ΔGrx2 strain but not in the corresponding WT [18]. Both proteins function at critical junctions in iron regulation and biosynthetic metabolism, respectively. In this study we applied proteomic approaches to characterise the redox properties of these proteins and confirm targets of thiol disulfide exchange with Grx2p.

Cys26 of Hem12p is located inside a characteristic uroporphyrinogen decarboxylase sequence signature, UROD_1, which, according to the literature and modelling, is placed near the catalytic site and involved in substrate binding [46] (see Figure 5). In the ΔGrx2 yeast strain there was a 6-fold increase in the abundance of reversibly oxidized Cys26, yet SRM showed that overall protein abundance did not change significantly between strains, indicating the reversible oxidation was a true redox posttranslational modification in response to the lack of Grx2p. However, this cysteine residue was not sensitive to GSSG treatment of the enzyme *in vitro*, suggesting that the redox change observed *in vivo* could follow a different mechanism. Whether another thiol oxidoreductase is involved would be an interesting matter for further research.

Hem12p-Cys52 is involved in substrate binding and is highly conserved across species but is not essential for catalytic activity [28]. In the recombinant protein, Cys52 could be glutathionylated and deglutathionylated *in vitro*, indicating it is a model substrate for deglutathionylation by Grx2p. These results further strengthen the links between glutaredoxins and the tight control of iron homeostasis within the cell. Hem12p is a constitutive protein that catalyses the 5th step in heme biosynthesis in the cytosol before synthesis is completed within the mitochondria. Heme biosynthesis needs to be tightly regulated within the cell to prevent overproduction of toxic porphyrins and is correlated to oxygen tension within the yeast cell [23]. The biosynthesis of Fe/S clusters is also tightly coordinated with that of heme, and in yeast deletion of genes important for Fe/S assembly negatively affects heme synthesis [47]. The glutaredoxin family of proteins has been clearly implicated in iron control with the monothiols Grx3p, Grx4p, and Grx5p playing key roles in iron regulation [27, 48, 49]. We previously detected changes in iron homeostasis in strains lacking Grx2p [18]. The potential covalent regulation of the activity of the constitutive enzyme Hem12p by thiol disulfide exchange would provide a rapid means to control heme biosynthesis as a function

of cytosolic or mitochondrial redox state as compared to a slower control mechanism carried out by transcriptional regulation at other points in the pathway.

Cys622 of Tkl1p is highly sensitive to redox changes; its oxidized form increases > 4-fold induced by the lack of Grx2p and > 6-fold by H_2O_2 *in vivo*, without any increase in the total amount of the protein. Only a relatively low proportion of the recombinant protein could be glutathionylated *in vitro* and we could only detect one of the two Cys containing tryptic peptides within the protein. Interestingly, preincubation of the protein with GSSG affects the activity of the enzyme and protects deactivation by the sulfhydryl reagent NEM, indicating a thiol protective effect. These results support a thiol disulfide exchange mechanism controlling the activity of the protein, but our results suggest that it is not a natural direct target of Grx2p. Transketolase is an ideal node for redox control within the cell. Its activation under oxidative conditions would be coherent with diversion of metabolic flux toward the PPP to provide reducing power for antioxidant defense systems. Moreover, the products of transketolase reaction form starting points for several other biosynthetic pathways, thus redistributing the fate of glucose derived metabolites towards macromolecular building blocks for cellular proliferation (see Figure 1(a)).

Using a redox proteomics approach we have shown that Cys296 of yeast pyruvate kinase, located at the allosteric activator domain, was sensitive to oxidative conditions and we suggested a role in adaptation to oxidative stress [14]. Similar behaviour of the equivalent Cys358 in human pyruvate kinase PKM2 was subsequently demonstrated to be the basis of a redox regulatory mechanism for metabolic remodelling that allowed cancer cells to resist oxidative stress and proliferate [13]. In the same way, the redox sensitivity of human uroporphyrinogen decarboxylase and transketolase may be worthy of study. The two cysteines of Hem12p identified here as being redox sensitive, Cys26 and Cys52, have their counterpart residues Cys35 and Cys59 in UROD, the human orthologue (see Figure 5). Similarly, the human transketolase is rich in cysteine residues some of which may be prone to reversible oxidation with influence on enzyme functionality. Incidentally, overexpression of the human orthologue UROD has been associated with diseases involving porphyrin metabolism and cancer [25] and enhancement in the activity and concentration of TKLT1 are highly correlated with rate of tumour growth in a variety of cancers [50].

The redox properties of yeast Hem12p and Tkl1p described here could have an impact on the knowledge of redox regulatory mechanisms in all life kingdoms. For instance, the plant orthologues of these two enzymes have been identified as Trx targets in chloroplasts and *Chlamydomonas* [43]. Regulation of plant enzymes by thiol-disulfide exchange mediated by thioredoxin pioneered the work in the field [51]. Recently, glutathionylation and nitrosylation have also been demonstrated to operate in plants, with "redoxins" performing a crucial role [52]. In the case of uroporphyrinogen decarboxylase, redox regulation would have an influence on the biosynthetic pathways for siroheme and chlorophyll where the later has to be regulated by light/darkness fluctuations through the redox state of the chloroplast [53].

5. Conclusions

The results presented herein demonstrate that Tkl1p and Hem12p from yeast are sensitive to changes in the cellular redox homeostasis and uncover striking redox properties of these important enzymes involved in iron homeostasis and antioxidant and biosynthetic metabolism. These findings could reach beyond yeast to enlighten metabolic remodelling mechanisms involving their human counterparts. The door is now open to further work in this direction to describe the molecular, physiological, and pathological insights in depth.

Acknowledgments

The authors thank Lourdes Laura Muñoz for excellent technical assistance and Dr. John Mulligan for helpful discussions. Mass spectrometry was performed at the Proteomics Facility, SCAI, University of Córdoba, node 6 of the ProteoRed Consortium financed by ISCIII. This work was supported by Grants P06-CVI-01611 from the Andalusian Government and BFU2009-08004 and BFU2012-32056 from the Spanish Government.

References

[1] D. A. Tennant, R. V. Durán, and E. Gottlieb, "Targeting metabolic transformation for cancer therapy," *Nature Reviews Cancer*, vol. 10, no. 4, pp. 267–277, 2010.

[2] L. H. Hartwell, "Yeast and cancer," *Bioscience Reports*, vol. 24, no. 4-5, pp. 523–544, 2004.

[3] R. Diaz-Ruiz, S. Uribe-Carvajal, A. Devin, and M. Rigoulet, "Tumor cell energy metabolism and its common features with yeast metabolism," *Biochimica et Biophysica Acta*, vol. 1796, no. 2, pp. 252–265, 2009.

[4] O. Warburg, "On the origin of cancer cells," *Science*, vol. 123, no. 3191, pp. 309–314, 1956.

[5] H. G. Crabtree, "Observations on the carbohydrate metabolism of tumours," *The Biochemical Journal*, vol. 23, no. 3, pp. 536–545, 1929.

[6] D. Hanahan and R. A. Weinberg, "Hallmarks of cancer: the next generation," *Cell*, vol. 144, no. 5, pp. 646–674, 2011.

[7] W. Xu, T. Barrientos, and N. C. Andrews, "Iron and copper in mitochondrial diseases," *Cell Metabolism*, vol. 17, no. 3, pp. 319–328, 2013.

[8] C. N. Roy and N. C. Andrews, "Recent advances in disorders of iron metabolism: mutations, mechanisms and modifiers," *Human Molecular Genetics*, vol. 10, no. 20, pp. 2181–2186, 2001.

[9] C. Klomsiri, P. A. Karplus, and L. B. Poole, "Cysteine-based redox switches in enzymes," *Antioxidants and Redox Signaling*, vol. 14, no. 6, pp. 1065–1077, 2011.

[10] R. Brigelius-Flohé and L. Flohé, "Basic principles and emerging concepts in the redox control of transcription factors," *Antioxidants and Redox Signaling*, vol. 15, no. 8, pp. 2335–2381, 2011.

[11] J. J. Mieyal, M. M. Gallogly, S. Qanungo, E. A. Sabens, and M. D. Shelton, "Molecular mechanisms and clinical implications of reversible protein S-glutathionylation," *Antioxidants and Redox Signaling*, vol. 10, no. 11, pp. 1941–1988, 2008.

[12] E. M. G. Allen and J. J. Mieyal, "Protein-thiol oxidation and cell death: regulatory role of glutaredoxins," *Antioxidants & Redox Signaling*, vol. 17, no. 12, pp. 1748–1763, 2012.

[13] D. Anastasiou, G. Poulogiannis, J. M. Asara et al., "Inhibition of pyruvate kinase M2 by reactive oxygen species contributes to cellular antioxidant responses," *Science*, vol. 334, no. 6060, pp. 1278–1283, 2011.

[14] B. McDonagh, S. Ogueta, G. Lasarte, C. A. Padilla, and J. A. Bárcena, "Shotgun redox proteomics identifies specifically modified cysteines in key metabolic enzymes under oxidative stress in *Saccharomyces cerevisiae*," *Journal of Proteomics*, vol. 72, no. 4, pp. 677–689, 2009.

[15] C. M. Grant, K. A. Quinn, and I. W. Dawes, "Differential protein S-thiolation of glyceraldehyde-3-phosphate dehydrogenase isoenzymes influences sensitivity to oxidative stress," *Molecular and Cellular Biology*, vol. 19, no. 4, pp. 2650–2656, 1999.

[16] V. Ravichandran, T. Seres, T. Moriguchi, J. A. Thomas, and R. B. Johnston Jr., "S-thiolation of glyceraldehyde-3-phosphate dehydrogenase induced by the phagocytosis-associated respiratory burst in blood monocytes," *Journal of Biological Chemistry*, vol. 269, no. 40, pp. 25010–25015, 1994.

[17] I. Schuppe-Koistinen, P. Moldeus, T. Bergman, and I. A. Cotgreave, "S-Thiolation of human endothelial cell glyceraldehyde-3-phosphate dehydrogenase after hydrogen peroxide treatment," *European Journal of Biochemistry*, vol. 221, no. 3, pp. 1033–1037, 1994.

[18] B. McDonagh, C. A. Padilla, J. R. Pedrajas, and J. A. Barcena, "Biosynthetic and iron metabolism is regulated by thiol proteome changes dependent on glutaredoxin-2 and mitochondrial peroxiredoxin-1 in *Saccharomyces cerevisiae*," *Journal of Biological Chemistry*, vol. 286, no. 17, pp. 15565–15576, 2011.

[19] B. Comín-Anduix, J. Boren, S. Martinez et al., "The effect of thiamine supplementation on tumour roliferation: a metabolic control analysis study," *European Journal of Biochemistry*, vol. 268, no. 15, pp. 4177–4182, 2001.

[20] J. Watson, "Oxidants, antioxidants and the current incurability of metastatic cancers," *Open Biology*, vol. 3, no. 1, Article ID 120144, 2013.

[21] C. I. Kobayashi and T. Suda, "Regulation of reactive oxygen species in stem cells and cancer stem cells," *Journal of Cellular Physiology*, vol. 227, no. 2, pp. 421–430, 2012.

[22] I. U. Heinemann, M. Jahn, and D. Jahn, "The biochemistry of heme biosynthesis," *Archives of Biochemistry and Biophysics*, vol. 474, no. 2, pp. 238–251, 2008.

[23] L. Zhang and A. Hach, "Molecular mechanism of heme signaling in yeast: the transcriptional activator Hap1 serves as the key mediator," *Cellular and Molecular Life Sciences*, vol. 56, no. 5-6, pp. 415–426, 1999.

[24] G. H. Elder and A. G. Roberts, "Uroporphyrinogen decarboxylase," *Journal of Bioenergetics and Biomembranes*, vol. 27, no. 2, pp. 207–214, 1995.

[25] E. Ito, S. Yue, E. H. Moriyama et al., "Uroporphyrinogen decarboxylase is a radiosensitizing target for head and neck cancer," *Science Translational Medicine*, vol. 3, no. 67, p. 67ra7, 2011.

[26] N. Guex and M. C. Peitsch, "SWISS-MODEL and the Swiss-PdbViewer: an environment for comparative protein modeling," *Electrophoresis*, vol. 18, no. 15, pp. 2714–2723, 1997.

[27] M. T. Rodríguez-Manzaneque, J. Tamarit, G. Bellí, J. Ros, and E. Herrero, "Grx5 is a mitochondrial glutaredoxin required for the activity of iron/sulfur enzymes," *Molecular Biology of the Cell*, vol. 13, no. 4, pp. 1109–1121, 2002.

[28] K. A. Neilson, N. A. Ali, S. Muralidharan et al., "Less label, more free: approaches in label-free quantitative mass spectrometry," *Proteomics*, vol. 11, no. 4, pp. 535–553, 2011.

[29] P. Picotti, H. Lam, D. Campbell et al., "A database of mass spectrometric assays for the yeast proteome," *Nature Methods*, vol. 5, no. 11, pp. 913–914, 2008.

[30] B. McDonagh, R. Requejo, C. A. Fuentes-Almagro, S. Ogueta, J. A. Bárcena, and C. A. Padilla, "Thiol redox proteomics identifies differential targets of cytosolic and mitochondrial glutaredoxin-2 isoforms in *Saccharomyces cerevisiae*. Reversible S-glutathionylation of DHBP synthase (RIB3)," *Journal of Proteomics*, vol. 74, no. 11, pp. 2487–2497, 2011.

[31] J. R. Pedrajas, P. Porras, E. Martínez-Galisteo, C. A. Padilla, A. Miranda-Vizuete, and J. A. Bárcena, "Two isoforms of *Saccharomyces cerevisiae* glutaredoxin 2 are expressed in vivo and localize to different subcellular compartments," *Biochemical Journal*, vol. 364, no. 3, pp. 617–623, 2002.

[32] G. L. Ellman, "Tissue sulfhydryl groups," *Archives of Biochemistry and Biophysics*, vol. 82, no. 1, pp. 70–77, 1959.

[33] N. J. Veitch, D. A. Maugeri, J. J. Cazzulo, Y. Lindqvist, and M. P. Barrett, "Transketolase from Leishmania mexicana has a dual subcellular localization," *Biochemical Journal*, vol. 382, no. 2, pp. 759–767, 2004.

[34] J. W. Park, J. J. Mieyal, S. G. Rhee, and P. B. Chock, "Deglutathionylation of 2-Cys peroxiredoxin is specifically catalyzed by sulfiredoxin," *Journal of Biological Chemistry*, vol. 284, no. 35, pp. 23364–23374, 2009.

[35] M. Zaffagnini, L. Michelet, C. Marchand et al., "The thioredoxin-independent isoform of chloroplastic glyceraldehyde-3- phosphate dehydrogenase is selectively regulated by glutathionylation," *FEBS Journal*, vol. 274, no. 1, pp. 212–226, 2007.

[36] A. Raturi and B. Mutus, "Characterization of redox state and reductase activity of protein disulfide isomerase under different redox environments using a sensitive fluorescent assay," *Free Radical Biology and Medicine*, vol. 43, no. 1, pp. 62–70, 2007.

[37] F. Felix and N. Brouillet, "Purification and properties of uroporphyrinogen decarboxylase from *Saccharomyces cerevisiae*. Yeast uroporphyrinogen decarboxylase," *European Journal of Biochemistry*, vol. 188, no. 2, pp. 393–403, 1990.

[38] C. E. Bobst and F. R. Tabita, "The role of cysteine 160 in thiamine diphosphate binding of the Calvin-Benson-Bassham cycle transketolase of Rhodobacter sphaeroides," *Archives of Biochemistry and Biophysics*, vol. 426, no. 1, pp. 43–54, 2004.

[39] G. A. Kochetov and G. F. Lutovinova, "Sulfhydryl groups and transketolase activity," *Biochemical and Biophysical Research Communications*, vol. 22, no. 1, pp. 129–134, 1966.

[40] Y. Lindqvist, G. Schneider, U. Ermler, and M. Sundstrom, "Three-dimensional structure of transketolase, a thiamine diphosphate dependent enzyme, at 2.5Å resolution," *EMBO Journal*, vol. 11, no. 7, pp. 2373–2379, 1992.

[41] M. Nikkola, Y. Lindqvist, and G. Schneider, "Refined structure of transketolase from *Saccharomyces cerevisiae* at 2.0 Å resolution," *Journal of Molecular Biology*, vol. 238, no. 3, pp. 387–404, 1994.

[42] S. M. Marino and V. N. Gladyshev, "Redox biology: computational approaches to the investigation of functional cysteine residues," *Antioxidants and Redox Signaling*, vol. 15, no. 1, pp. 135–146, 2011.

[43] Y. Balmer, A. Koller, G. Del Val, W. Manieri, P. Schürmann, and B. B. Buchanan, "Proteomics gives insight into the regulatory function of chloroplast thioredoxins," *Proceedings of the*

National Academy of Sciences of the United States of America, vol. 100, no. 1, pp. 370–375, 2003.

[44] D. P. Jones, "Radical-free biology of oxidative stress," *American Journal of Physiology*, vol. 295, no. 4, pp. C849–C868, 2008.

[45] M. Lindahl, A. Mata-Cabana, and T. Kieselbach, "The disulfide proteome and other reactive cysteine proteomes: analysis and functional significance," *Antioxidants and Redox Signaling*, vol. 14, no. 12, pp. 2581–2642, 2011.

[46] F. G. Whitby, J. D. Phillips, J. P. Kushner, and C. P. Hill, "Crystal structure of human uroporphyrinogen decarboxylase," *EMBO Journal*, vol. 17, no. 9, pp. 2463–2471, 1998.

[47] H. Lange, U. Mühlenhoff, M. Denzel, G. Kispal, and R. Lill, "The heme synthesis defect of mutants impaired in mitochondrial iron-sulfur protein biogenesis is caused by reversible inhibition of ferrochelatase," *Journal of Biological Chemistry*, vol. 279, no. 28, pp. 29101–29108, 2004.

[48] N. Pujol-Carrion, G. Belli, E. Herrero, A. Nogues, and M. A. de la Torre-Ruiz, "Glutaredoxins Grx3 and Grx4 regulate nuclear localisation of Aft1 and the oxidative stress response in *Saccharomyces cerevisiae*," *Journal of Cell Science*, vol. 119, no. 21, pp. 4554–4564, 2006.

[49] G. Bellí, M. M. Molina, J. García-Martínez, J. E. Pérez-Ortsín, and E. Herrero, "*Saccharomyces cerevisiae* Glutaredoxin 5-deficient Cells Subjected to Continuous Oxidizing Conditions Are Affected in the Expression of Specific Sets of Genes," *Journal of Biological Chemistry*, vol. 279, no. 13, pp. 12386–12395, 2004.

[50] S. Langbein, M. Zerilli, A. Zur Hausen et al., "Expression of transketolase TKTL1 predicts colon and urothelial cancer patient survival: Warburg effect reinterpreted," *British Journal of Cancer*, vol. 94, no. 4, pp. 578–585, 2006.

[51] R. A. Wolosiuk and B. B. Buchanan, "Thioredoxin and glutathione regulate photosynthesis in chloroplasts," *Nature*, vol. 266, no. 5602, pp. 565–567, 1977.

[52] K. van der Linde, N. Gutsche, H.-M. Leffers et al., "Regulation of plant cytosolic aldolase functions by redox-modifications," *Plant Physiology and Biochemistry*, vol. 49, no. 9, pp. 946–957, 2011.

[53] A. Stenbaek and P. E. Jensen, "Redox regulation of chlorophyll biosynthesis," *Phytochemistry*, vol. 71, no. 8-9, pp. 853–859, 2010.

Hindawi Publishing Corporation
Oxidative Medicine and Cellular Longevity
Volume 2013, Article ID 139491, 6 pages
http://dx.doi.org/10.1155/2013/139491

Review Article

Roles of Mitochondrial Dynamics under Stressful and Normal Conditions in Yeast Cells

Dmitry A. Knorre,[1,2] Konstantin Y. Popadin,[3] Svyatoslav S. Sokolov,[1,2] and Fedor F. Severin[1,2]

[1] *Belozersky Institute of Physico-Chemical Biology, Moscow State University, Vorobyevy Gory 1, Moscow 119992, Russia*
[2] *Institute of Mitoengineering, Moscow State University, Vorobyevy Gory 1, Moscow 119992, Russia*
[3] *Department of Genetic Medicine and Development, University of Geneva Medical School, 1 rue Michel-Servet, 1211 Geneva, Switzerland*

Correspondence should be addressed to Fedor F. Severin; severin@belozersky.msu.ru

Received 7 May 2013; Accepted 25 June 2013

Academic Editor: Cristina Mazzoni

Eukaryotic cells contain dynamic mitochondrial filaments: they fuse and divide. Here we summarize data on the protein machinery driving mitochondrial dynamics in yeast and also discuss the factors that affect the fusion-fission balance. Fission is a general stress response of cells, and in the case of yeast this response appears to be prosurvival. At the same time, even under normal conditions yeast mitochondria undergo continuous cycles of fusion and fission. This seems to be a futile cycle and also expensive from the energy point of view. Why does it exist? Benefits might be the same as in the case of sexual reproduction. Indeed, mixing and separating of mitochondrial content allows mitochondrial DNA to segregate and recombine randomly, leading to high variation in the numbers of mutations per individual mitochondrion. This opens a possibility for effective purifying selection-elimination of mitochondria highly contaminated by deleterious mutations. The beneficial action presumes a mechanism for removal of defective mitochondria. We argue that selective mitochondrial autophagy or asymmetrical distribution of mitochondria during cell division could be at the core of such mechanism.

1. Introduction

Almost all eukaryotic cells harbor mitochondria—the distant descendants of endosymbiotic alphaproteobacteria (see [1] for review). In most types of eukaryotic cells, mitochondria are organized in complex reticular structures with dynamically changing topology. Changes of the structures are usually referred to as mitochondrial dynamics. These changes include events of mitochondria fission and fusion, as well as active transport of individual filaments. Importantly, defects of mitochondrial dynamics are associated with defects in mechanisms of mitochondrial DNA (mtDNA) maintenance [2]. This makes the baker's yeast *Saccharomyces cerevisiae* a useful tool for studies of mitochondrial dynamics mechanisms. Importantly, in contrast to most of animal cells, yeasts are able to proliferate without a functional respiratory chain and ATP-synthase. Such cells still have basal mitochondrial morphology, membrane potential, and metabolic activities. Moreover, yeast cells lacking mitochondrial DNA can be easily cultivated in medium containing a fermentable carbon source (e.g., glucose). This allowed performing several large-scale screenings aimed at identification of genes involved in mitochondrial dynamics and maintenance of reticular mitochondrial morphology [2, 3]. It was found that proteins involved in the molecular mechanisms of mitochondrial fusion and fission in yeast have many similarities to such mechanisms in animals (see [4] for review). The molecular mechanisms of mitochondrial fusion, fission, and movement were reviewed in detail recently [4–8].

In this review we briefly discuss these mechanisms focusing on the role of mitochondrial dynamics in cell physiology under stressful and normal conditions using an example of *Saccharomyces cerevisiae* yeast cells.

2. Mitochondrial Dynamics: Mechanisms and Stress Response

Mitochondrial fission is an active process organized by several proteins (see [9] for review). The key role is played by GTPase Dnm1p, which is capable of oligomerization on the lipid surface: it was shown that Dnm1p forms ~80 nm spirals on liposomes [10, 11]. A subsequent GTP hydrolysis results in a conformational change of Dnm1p, constriction of the spirals, and fission of the lipid vesicles [11]. Fis1p is localized at the outer membrane of mitochondria and recruits Dnm1p on the mitochondrial surface by means of adaptor proteins: Caf4p and its paralog Mdv1p [12]. It was shown that during membrane scission Dnm1p-dependent constriction is accompanied by longitudinal tension of lipid vesicles [13]. This implies that mitochondrial movement along the cytoskeleton could be an important factor for mitochondrial fission. Interestingly, for some stressful conditions fission of mitochondrial reticulum was observed even in the absence of the *DNM1* gene. Kitagaki and colleagues [14] have shown that high (15%) concentration of ethanol facilitates fission of yeast mitochondria even on Δ*dnm1* background. Possibly, severe changes in ion composition of cytoplasm and mitochondrial matrix or significant change in mitochondrial lipid composition leads to mechanical division of mitochondria into small compartments. Indeed, most of the protocols of mitochondria isolation do not allow preserving native structure of mitochondrial reticulum.

Mitochondrial fusion in yeast is orchestrated by another set of proteins including Fzo1p, Mdm30, Ugo1p, and Mgm1p. Studies on isolated mitochondria show that the process of fusion occurs in several stages [15, 16]: docking of mitochondria and fusion of the outer membranes followed by fusion of the inner membranes (Figure 1). Docking of mitochondria in yeast is controlled by outer membrane protein Fzo1p. Fzo1p is a GTPase [17] that forms trans-dimers allowing anchoring of separate mitochondrial vesicles. According to the model of Anton and colleagues [16], this process requires GTP binding, whereas hydrolysis of GTP allows moving to the next stage—fusion of the outer membranes. While mitochondrial fusion requires GTP, Meeusen and McCaffery [15] have shown that the rate of mitochondrial fusions could be as high as 50% of the maximum level with energy regeneration system in the absence of exogenous GTP. This indicates that low concentration of endogenous GTP is sufficient to maintain physiological rates of mitochondrial fusion. At the same time, the uncoupler FCCP (Carbonyl cyanide-4-(trifluoromethoxy)phenylhydrazone) and the ionophore valinomycin were found to be effective inhibitors of fusion of isolated yeast [15] and human [18] mitochondria. Accordingly, FCCP [19] and also other uncouplers and inhibitors of respiratory chain were found to induce mitochondrial reticulum fission in various human cell lines (see [20] for review). Another important factor regulating mitochondrial fusion is cellular redox state. Very recently, it was shown that docking of mitochondria is regulated by the ratio of reduced/oxidized glutathione: GSSG induces the generation of disulphide-mediated mitofusin oligomers and in this way promotes fusion [21]. It was found that C684A mutation

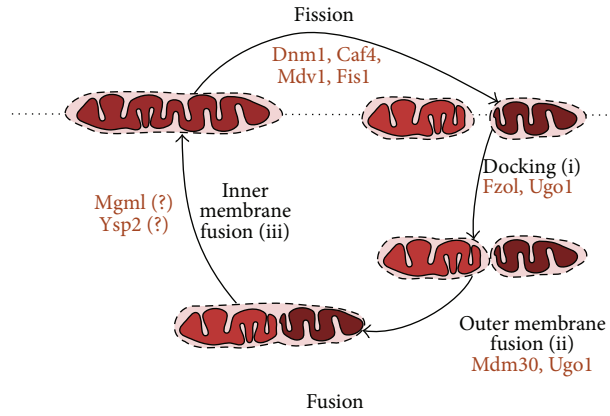

Figure 1: Proteins driving the cycle of mitochondrial fusion and fission. Mitochondrial fusion starts with the docking mediated by Fzo1 and Ugo1. Docking is followed by the outer membrane fusion mediated by Mdm30 and Ugo1. The inner membrane fusion is likely to be dependent on Mgm1 and Ysp2. Caf4, Mdv1 and Fis1 make a platform for fission which is being executed by Dnm1 oligomers.

of cysteine in Mfn2 inhibits mitochondrial fusion, pointing to a role of this residue in oligomerization of mitofusin and docking of mitochondria [22]. As *S. cerevisiae* genome contains a homolog of Mfn2, FZO1, the redox-dependent mechanism of regulation is likely to be conserved also in yeast. At the same time, treatment of human cells with hydrogen peroxide [22] or treatment of yeast cells with the drug amiodarone that induces endogenous formation of reactive oxygen species [23] causes mitochondrial fission. This apparent contradiction could be explained by the fact that high concentration of hydrogen peroxide inhibits the respiratory chain, thus counteracting the stimulating effect on mitochondria fusion [24]. Another explanation is based on the importance of the lipid composition for mitochondrial fusion; the inactivation of genes encoding enzymes of mitochondrial biosynthesis of lipids, phosphatidylethanolamine and cardiolipin (*PSD1* and *CRD1*, correspondingly), inhibits mitochondrial fusion [25, 26]. Therefore, peroxidation of cardiolipin induced by hydrogen peroxide could also retard mitochondrial fusion.

To conclude this part, it should be noted that stresses generally tip the mitochondrial dynamics towards fission. This is not surprising; local damage to fused mitochondria might depolarize the whole cellular mitochondrial content [27]. In other words, cells with fissed mitochondria seem to be more resistant to stresses; at least a minor fraction of the mitochondrial vesicles might be lucky to escape the damage. In theory, a cell with fragmented mitochondria is as resistant as the one with separated mitoplasts surrounded by an intact outer membrane. We have recently shown that such morphology can be observed in Δ*ysp2* cells in stationary phase [28]. The *YSP2* gene was previously discovered as a genetic factor that decreases resistance to amiodarone and acetic acid [29]. This is consistent with a possible role of Ysp2p in mitochondrial inner membrane fusion (Figure 1).

3. Role of Mitochondrial Dynamics under Normal Conditions

It must be noted that mitochondrial fusion and fission not only happen under stress, but also constantly occur under normal conditions. This is true not only for yeast cells, but also for cells of higher organisms. Both processes consume energy. Thus the question arises about the biological role of these processes under stress-free conditions.

It has been suggested that fusion-fission cycle can maintain high quality of mitochondrial protein components, keeping mitochondrial vesicles with low membrane potential out of the process of fusion into the mitochondrial reticulum and their consequent elimination by mitophagy (mitochondria-specific autophagy; see [30] for review). This filtering will keep the average quality of the mitochondrial respiratory chain on a constant level and work against ROS-induced protein damage but will not affect mtDNA quality if segregation of proteins and mtDNA is independent during fusion-fission process. However, since mtDNA is a subject to high mutation rate [31], the effective purifying selection which eliminates *de novo* deleterious mutations is required to maintain the quality of mtDNA. Thus, it has been proposed that the fusion-fission process can not only select mitochondria on the level of phenotypes (proteins), but also contribute to preferential elimination of mtDNA with deleterious mutations [32]. However, the functional link between mitochondrial phenotypes (protein components) and genotypes (mtDNA) is necessary for establishment of this kind of selection on a genetic level. For example, low mitochondrial membrane potential needs to be determined by deleterious mutations in mtDNA. There are two not mutually exclusive ways to develop such phenotype-genotype linkage. The first is purely mechanistic and based on passive membrane colocalization of mtDNA and proteins encoded by the mtDNA. Indeed, the inner membrane proteins were shown to have significantly lower mobility than proteins localized in the outer membrane [33]. Thus the local quality of the mitochondrial membrane is expected to be linked to the quality of the neighboring mtDNA attached to the membrane. This membrane linkage will lead to the formation of fissed mitochondria with correlated quality of phenotypes and genotypes, making a "fusion quality filter" effective in elimination of mtDNA with deleterious mutations (see [34] for review).

The second mechanism is based on active expression of mtDNA in fissed mitochondria and subsequent incorporation of newly synthesized proteins into mitochondrial membrane, so that genotype fitness influences phenotype fitness. This scenario does not depend on passive inheritance of mtDNA in complex with their protein products but requires long periods of existence of fissed mitochondria sufficient for incorporation of newly synthesized proteins into the mitochondrial membrane. The mechanism of purification of mitochondria from mutant copies of DNA during the fusion-fission process resembles the mechanism proposed to explain the existence of sexual reproduction (mutational deterministic hypothesis; [35, 36]). The fusion-fission process (as well as genetic recombination) restores high variability in the numbers of mutant mtDNAs per mitochondrial vesicle (number of deleterious mutations per offspring), making selection more effective (Figure 2). Indeed, elimination of the minimal numbers of mitochondrial vesicles maximally contaminated by mutant mtDNA will keep the heteroplasmy level low and will be energetically less expensive than elimination of large numbers of moderately contaminated mitochondria. The mutational deterministic hypothesis depends on high mutation rate and a negative epistasis between deleterious mutations [35–37]. Since both parameters are poorly known for the mitochondrial genome, future experimental studies are required to test the importance of the mechanism.

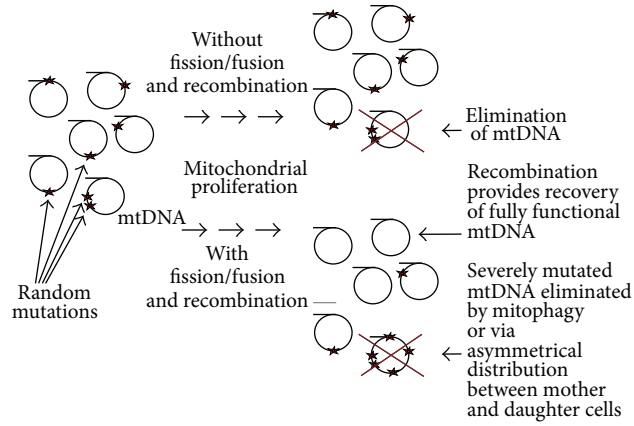

Figure 2: Hypothetical scheme illustrating how the mitochondrial fusion-fission cycle helps to maintain mitochondrial DNA. Rearrangements of the DNA induced by mitochondrial fission-fusion and recombination result in appearance of mutation-free mitochondrial genomes. Removal of genomes with high levels of deleterious mutations inhibits the high rate of mtDNA damage (see text for details).

The relative influence of the first (passive) and the second (active) mechanisms on the maintenance of the mtDNA quality during the fusion-fission process depends on the frequency of fusion-fission events and the rate of mtDNA transcription and translation, and thus they can be different in various cells.

Is there any experimental evidence that mitochondrial dynamics counterbalance the high rate of deleterious mutation accumulation in yeast? It was recently shown that the *FIS1* and *MDV1* genes appear to be involved in maintenance of heteroplasmy in diploid yeast cells acquired after mating of haploids cells with different mitochondrial markers [38]. Although the authors did not observe this effect in Δ*dnm1*/Δ*dnm1* diploid, the results indicated that mitochondrial dynamics affect redistribution of different variants of the mitochondrial genome. The knockouts of genes involved in mitochondrial dynamics increase the chance of *petite* mutation in yeast. *Petite* mutation refers to inability of growth on medium with a nonfermentable carbon source (ethanol, glycerol, etc.), and it is usually associated with deletions or complete loss of mtDNA (see [39] for review). The inactivation of a fusion protein-encoding gene (*FZO1*) results in quick degradation of the mitochondrial genome [40], whereas the deletions of fission genes *DNM1* or *FIS1*, while increasing rate

of petite mutation, still allow maintenance of the functional copies of mtDNA in the cells.

To draw parallels between sexual reproduction and fusion-fission dependent recombination of mtDNAs one should consider the ways of elimination of nonfunctional mitochondria. Apparently, the functional mtDNA could outcompete the damaged one by advantages in replication. Although the opposite situation is described in the literature as suppressive petite mutation [41], the latter is not a common case. An alternative explanation comes from experiments with human cell lines. In 2008, Twig and colleagues [42] showed that after fission mitochondria can depolarize and get targeted to an autophagosome. The process of selective elimination of mitochondria unable to maintain their own transmembrane potential was called mitophagy. Mitophagy attracted a lot of attention because the mutations in PINK1 and Parkin (involved in marking the malfunctioning mitochondria for mitophagy) were found to be linked to Parkinson disease (see [43, 44] for review). It was suggested that mitophagy is necessary for quality control of mitochondria, to remove damaged protein complexes [8] or damaged mtDNA [32]. There are no homologs of PINK1 or Parkin in *Saccharomyces cerevisiae*. However, certain conditions, including nitrogen starvation or rapamycin treatment, induce selective mitochondrial autophagy in Atg32-dependent manner. Atg32 is located on the outer mitochondrial membrane and initiates the assembly of the autophagic complex which includes several ubiquitin ligases and adaptor proteins [45, 46]. Moreover, treatment of cells with mitochondrial respiratory chain inhibitors Antimycin A or KCN triggers a general increase of autophagy [47]. Intriguingly, this increase was shown to be Atg32 dependent [47]. Recently, it was shown that mitophagy indeed plays a role in maintaining mitochondrial quality in yeast [48].

Interestingly, it was shown that mitochondrial fission is not a necessary prerequisite for mitophagy in yeast [49]. This underscores the importance the "futile" fission-fusion cycle; the mitophagy of fully fused mitochondria can be lethal for the cells (yeast cannot live without mitochondria).

Another possible way to remove mtDNA with deleterious mutations relies on asymmetrical division of yeast cells (see [50] for review). It was shown that a complex molecular mechanism (based on the polarisome) fulfills bud-to-mother transport of damaged macromolecules in yeast cells [51]. Moreover, it was recently reported that mitochondria with higher rate of superoxide production are retained in the mother cells [52]. Such selective retention is not surprising because actin cables anchor mitochondria via Mmm1p and Mdm10p [53], which in turn form a protein complex spanning both mitochondrial membranes and being capable of binding mtDNA (see [54] for review). The machinery responsible for mother-bud distribution of mitochondria also includes mitochondrial anchor in the mother cell (cortical protein Num1 [55] and myosin-related motor which moves mitochondria towards the bud (Myo2, [56]). Possibly, multiple rounds of asymmetrical distribution of malfunctioning mitochondria lead to a decrease of mtDNA stability in replicatively old cells. In accordance with this hypothesis, it was shown that the chances of *petite* mutation significantly increased with replicative age [57].

Replicatively old yeast cells demonstrate slower growth and increased chance of viability loss [58]. Some authors argue that the death of a replicatively old mother cell could be an active process similar to apoptosis of mammalian cells [59]. Therefore, if asymmetrical redistribution of mitochondria indeed exists, damaged mtDNA is constantly eliminated by replicative aging.

Is there any evidence linking yeast replicative aging and mitochondrial dynamics? Recently it was found that replicatively old yeast cells harbor fissed mitochondria with decreased transmembrane potential [60]. Earlier Scheckhuber and colleagues [61] showed that replicatively aged yeast cells have fissed mitochondria and that the deletions of either *DNM1* or *FIS1* genes provide a certain increase in *S. cerevisiae* lifespan. Indeed, mitochondrial dynamics appear to be necessary for asymmetrical redistribution of mitochondria. Theoretically, if the dynamics are lost due to mutations, then the old mother cells of the mutants gain some advantage over the wild type ones carrying accumulating copies of damaged mtDNA. However, this benefit is obviously canceled by a moderate decrease in competitive fitness of the mutant cells; high-throughput screening [62] has shown a decrease in competitive fitness of strains lacking *FIS1, CAF4, DNM1,* or *FZO1* compared to the wild type strain.

4. Conclusions

To conclude, it appears that mitochondrial dynamics in yeast play different roles under stress and under normal conditions and normal aging. A single onset of fission followed by recovery of the reticulum seems to be required for the stress-resistances. Alternatively, multiple "futile cycles" of fusion and fission contribute to maintenance of mitochondrial genomes in the long term under stress-free conditions.

Acknowledgment

This work was supported by the Russian Foundation for Basic Research Grant 12-04-01412.

References

[1] M. W. Gray, G. Burger, and B. Franz Lang, "The origin and early evolution of mitochondria," *Genome Biology*, vol. 2, no. 6, pp. 1018.1–1018.5, 2001.

[2] T. Hanekamp, M. K. Thorsness, I. Rebbapragada et al., "Maintenance of mitochondrial morphology is linked to maintenance of the mitochondrial genome in Saccharomyces cerevisiae," *Genetics*, vol. 162, no. 3, pp. 1147–1156, 2002.

[3] K. S. Dimmer, S. Fritz, F. Fuchs et al., "Genetic basis of mitochondrial function and morphology in Saccharomyces cerevisiae," *Molecular Biology of the Cell*, vol. 13, no. 3, pp. 847–853, 2002.

[4] J. Zhao, U. Lendahl, and M. Nistér, "Regulation of mitochondrial dynamics: convergences and divergences between yeast and vertebrates," *Cellular and Molecular Life Sciences*, vol. 70, no. 6, pp. 951–976, 2013.

[5] H. Otera and K. Mihara, "Molecular mechanisms and physiologic functions of mitochondrial dynamics," *Journal of Biochemistry*, vol. 149, no. 3, pp. 241–251, 2011.

[6] R. J. Braun and B. Westermann, "Mitochondrial dynamics in yeast cell death and aging," *Biochemical Society Transactions*, vol. 39, no. 5, pp. 1520–1526, 2011.

[7] J. R. Lovas and X. Wang, "The meaning of mitochondrial movement to a neuron's life," *Biochimica et Biophysica Acta*, vol. 1833, no. 1, pp. 184–194, 2013.

[8] B. Westermann, "Mitochondrial fusion and fission in cell life and death," *Nature Reviews Molecular Cell Biology*, vol. 11, no. 12, pp. 872–884, 2010.

[9] L. L. Lackner and J. M. Nunnari, "The molecular mechanism and cellular functions of mitochondrial division," *Biochimica et Biophysica Acta*, vol. 1792, no. 12, pp. 1138–1144, 2009.

[10] E. Ingerman, E. M. Perkins, M. Marino et al., "Dnm1 forms spirals that are structurally tailored to fit mitochondria," *Journal of Cell Biology*, vol. 170, no. 7, pp. 1021–1027, 2005.

[11] J. A. Mears, L. L. Lackner, S. Fang, E. Ingerman, J. Nunnari, and J. E. Hinshaw, "Conformational changes in Dnm1 support a contractile mechanism for mitochondrial fission," *Nature Structural & Molecular Biology*, vol. 18, no. 1, pp. 20–26, 2011.

[12] Q. Guo, S. Koirala, E. M. Perkins, J. M. McCaffery, and J. M. Shaw, "The mitochondrial fission adaptors Caf4 and Mdv1 are not functionally equivalent," *PloS One*, vol. 7, no. 12, Article ID e53523, 2012.

[13] A. Roux, K. Uyhazi, A. Frost, and P. De Camilli, "GTP-dependent twisting of dynamin implicates constriction and tension in membrane fission," *Nature*, vol. 441, no. 7092, pp. 528–531, 2006.

[14] H. Kitagaki, Y. Araki, K. Funato, and H. Shimoi, "Ethanol-induced death in yeast exhibits features of apoptosis mediated by mitochondrial fission pathway," *FEBS Letters*, vol. 581, no. 16, pp. 2935–2942, 2007.

[15] S. Meeusen, J. M. McCaffery, and J. Nunnari, "Mitochondrial fusion intermediates revealed in vitro," *Science*, vol. 305, no. 5691, pp. 1747–1752, 2004.

[16] F. Anton, J. M. Fres, A. Schauss et al., "Ugo1 and Mdm30 act sequentially during Fzo1-mediated mitochondrial outer membrane fusion," *Journal of Cell Science*, vol. 124, no. 7, pp. 1126–1135, 2011.

[17] G. J. Hermann, J. W. Thatcher, J. P. Mills et al., "Mitochondrial fusion in yeast requires the transmembrane GTPase Fzo1p," *Journal of Cell Biology*, vol. 143, no. 2, pp. 359–373, 1998.

[18] A. C. Schauss, H. Huang, S.-Y. Choi et al., "A novel cell-free mitochondrial fusion assay amenable for high-throughput screenings of fusion modulators," *BMC Biology*, vol. 8, article 100, 2010.

[19] F. Legros, F. Malka, P. Frachon, A. Lombès, and M. Rojo, "Organization and dynamics of human mitochondrial DNA," *Journal of Cell Science*, vol. 117, no. 13, pp. 2653–2662, 2004.

[20] C. Sauvanet, S. Duvezin-Caubet, J.-P. di Rago, and M. Rojo, "Energetic requirements and bioenergetic modulation of mitochondrial morphology and dynamics," *Seminars in Cell and Developmental Biology*, vol. 21, no. 6, pp. 558–565, 2010.

[21] T. Shutt, M. Geoffrion, R. Milne, and H. M. McBride, "The intracellular redox state is a core determinant of mitochondrial fusion," *EMBO Reports*, vol. 13, no. 10, pp. 909–915, 2012.

[22] V. P. Skulachev, L. E. Bakeeva, B. V. Chernyak et al., "Thread-grain transition of mitochondrial reticulum as a step of mitoptosis and apoptosis," *Molecular and Cellular Biochemistry*, vol. 256-257, no. 1-2, pp. 341–358, 2004.

[23] A. I. Pozniakovsky, D. A. Knorre, O. V. Markova, A. A. Hyman, V. P. Skulachev, and F. F. Severin, "Role of mitochondria in the pheromone- and amiodarone-induced programmed death of yeast," *Journal of Cell Biology*, vol. 168, no. 2, pp. 257–269, 2005.

[24] A. C. Nulton-Persson and L. I. Szweda, "Modulation of mitochondrial function by hydrogen peroxide," *The Journal of Biological Chemistry*, vol. 276, no. 26, pp. 23357–23361, 2001.

[25] A. Joshi, M. Thompson, N. Fei, M. Huttemann, and M. L. Greenberg, "Cardiolipin and mitochondrial phosphatidylethanolamine have overlapping functions in mitochondrial fusion in Saccharomyces cerevisiae," *The Journal of Biological Chemistry*, vol. 287, no. 21, pp. 1–20, 2012.

[26] E. Y. L. Chan and G. A. McQuibban, "Phosphatidylserine decarboxylase 1 (Psd1) promotes mitochondrial fusion by regulating the biophysical properties of the mitochondrial membrane and alternative topogenesis of mitochondrial genome maintenance protein 1 (Mgm1)," *The Journal of Biological Chemistry*, vol. 287, no. 48, pp. 40131–40139, 2012.

[27] A. A. Amchenkova, L. E. Bakeeva, Y. S. Chentsov, V. P. Skulachev, and D. B. Zorov, "Coupling membranes as energy-transmitting cables. I. Filamentous mitochrondia in fibroblasts and mitochondrial clusters in cardiomyocytes," *Journal of Cell Biology*, vol. 107, no. 2, pp. 481–495, 1988.

[28] D. A. Knorre, S. M. Ojovan, V. B. Saprunova, S. S. Sokolov, L. E. Bakeeva, and F. F. Severin, "Mitochondrial matrix fragmentation as a protection mechanism of yeast Saccharomyces cerevisiae," *Biochemistry*, vol. 73, no. 11, pp. 1254–1259, 2008.

[29] S. Sokolov, D. Knorre, E. Smirnova et al., "Ysp2 mediates death of yeast induced by amiodarone or intracellular acidification," *Biochimica et Biophysica Acta*, vol. 1757, no. 9-10, pp. 1366–1370, 2006.

[30] R. Youle and A. van der Bliek, "Mitochondrial fission, fusion, and stress," *Science*, vol. 337, no. 6098, pp. 1062–1065, 2012.

[31] C. Richter, J.-W. Park, and B. N. Ames, "Normal oxidative damage to mitochondrial and nuclear DNA is extensive," *Proceedings of the National Academy of Sciences of the United States of America*, vol. 85, no. 17, pp. 6465–6467, 1988.

[32] S. Vidoni, C. Zanna, M. Rugolo, E. Sarzi, and G. Lenaers, "Why mitochondria must fuse to maintain their genome integrity," *Antioxidants & Redox Signaling*, vol. 19, no. 4, 2013.

[33] V. M. Sukhorukov, D. Dikov, K. Busch, V. Strecker, I. Wittig, and J. Bereiter-Hahn, "Determination of protein mobility in mitochondrial membranes of living cells," *Biochimica et Biophysica Acta*, vol. 1798, no. 11, pp. 2022–2032, 2010.

[34] A. Kowald and T. B. L. Kirkwood, "Evolution of the mitochondrial fusion—fission cycle and its role in aging," *Proceedings of the National Academy of Sciences of the United States of America*, vol. 108, no. 25, pp. 10237–10242, 2011.

[35] A. S. Kondrashov, "Selection against harmful mutations in large sexual and asexual populations," *Genetical Research*, vol. 40, no. 3, pp. 325–332, 1982.

[36] A. S. Kondrashov, "Deleterious mutations and the evolution of sexual reproduction," *Nature*, vol. 336, no. 6198, pp. 435–440, 1988.

[37] A. S. Kondrashov, "Classification of hypotheses on the advantage of amphimixis," *Journal of Heredity*, vol. 84, no. 5, pp. 372–387, 1993.

[38] E. Bradshaw, M. Yoshida, and F. Ling, "Mitochondrial fission proteins Fis1 and Mdv1, but not Dnm1, play a role in maintenance of heteroplasmy in budding yeast," *FEBS Letters*, vol. 586, no. 8, pp. 1245–1251, 2012.

[39] V. Contamine and M. Picard, "Maintenance and integrity of the mitochondrial genome: a plethora of nuclear genes in the budding yeast," *Microbiology and Molecular Biology Reviews*, vol. 64, no. 2, pp. 281–315, 2000.

[40] D. Rapaport, M. Brunner, W. Neupert, and B. Westermann, "Fzo1p is a mitochondrial outer membrane protein essential for the biogenesis of functional mitochondria in Saccharomyces cerevisiae," *The Journal of Biological Chemistry*, vol. 273, no. 32, pp. 20150–20155, 1998.

[41] B. Ephrussi, H. de Margerie-Hottinguer, and H. Roman, "Suppressiveness: a new factor in the genetic determinism of the synthesis of respiratory enzymes in yeast," *Proceedings of the National Academy of Sciences of the United States of America*, vol. 41, no. 12, pp. 1065–1071, 1955.

[42] G. Twig, A. Elorza, A. J. A. Molina et al., "Fission and selective fusion govern mitochondrial segregation and elimination by autophagy," *EMBO Journal*, vol. 27, no. 2, pp. 433–446, 2008.

[43] M. Müller and A. S. Reichert, "Mitophagy, mitochondrial dynamics and the general stress response in yeast," *Biochemical Society Transactions*, vol. 39, no. 5, pp. 1514–1519, 2011.

[44] G. Twig and O. S. Shirihai, "The interplay between mitochondrial dynamics and mitophagy," *Antioxidants & Redox Signaling*, vol. 14, no. 10, pp. 1939–1951, 2011.

[45] I. Bhatia-Kiššová and N. Camougrand, "Mitophagy in yeast: actors and physiological roles," *FEMS Yeast Research*, vol. 10, no. 8, pp. 1023–1034, 2010.

[46] K. Suzuki, "Selective autophagy in budding yeast," *Cell Death and Differentiation*, vol. 20, no. 1, pp. 43–48, 2013.

[47] M. Deffieu, I. Bhatia-Kissová, B. Salin et al., "Increased levels of reduced cytochrome b and mitophagy components are required to trigger nonspecific autophagy following induced mitochondrial dysfunction," *Journal of Cell Science*, vol. 126, part 2, pp. 415–426, 2013.

[48] Y. Kurihara, T. Kanki, Y. Aoki et al., "Mitophagy plays an essential role in reducing mitochondrial production of reactive oxygen species and mutation of mitochondrial DNA by maintaining mitochondrial quantity and quality in yeast," *The Journal of Biological Chemistry*, vol. 287, no. 5, pp. 3265–3272, 2012.

[49] N. Mendl, A. Occhipinti, M. Müller, P. Wild, I. Dikic, and A. S. Reichert, "Mitophagy in yeast is independent of mitochondrial fission and requires the stress response gene WHI2," *Journal of Cell Science*, vol. 124, no. 8, pp. 1339–1350, 2011.

[50] K. A. Henderson and D. E. Gottschling, "A mother's sacrifice: what is she keeping for herself?" *Current Opinion in Cell Biology*, vol. 20, no. 6, pp. 723–728, 2008.

[51] B. Liu, L. Larsson, A. Caballero et al., "The polarisome is required for segregation and retrograde transport of protein aggregates," *Cell*, vol. 140, no. 2, pp. 257–267, 2010.

[52] J. R. McFaline-Figueroa, J. Vevea, T. C. Swayne et al., "Mitochondrial quality control during inheritance is associated with lifespan and mother-daughter age asymmetry in budding yeast," *Aging Cell*, vol. 10, no. 5, pp. 885–895, 2011.

[53] I. Boldogh, N. Vojtov, S. Karmon, and L. A. Pon, "Interaction between mitochondria and the actin cytoskeleton in budding yeast requires two integral mitochondrial outer membrane proteins, Mmm1p and Mdm10p," *Journal of Cell Biology*, vol. 141, no. 6, pp. 1371–1381, 1998.

[54] J. C. Xin and R. A. Butow, "The organization and inheritance of the mitochondrial genome," *Nature Reviews Genetics*, vol. 6, no. 11, pp. 815–825, 2005.

[55] T. Klecker, D. Scholz, J. Förtsch, and B. Westermann, "The yeast cell cortical protein Num1 integrates mitochondrial dynamics into cellular architecture," *Journal of Cell Science*, vol. 126, no. 13, pp. 2924–2930, 2013.

[56] J. Förtsch, E. Hummel, M. Krist, and B. Westermann, "The myosin-related motor protein Myo2 is an essential mediator of bud-directed mitochondrial movement in yeast," *Journal of Cell Biology*, vol. 194, no. 3, pp. 473–488, 2011.

[57] J. R. Veatch, M. A. McMurray, Z. W. Nelson, and D. E. Gottschling, "Mitochondrial dysfunction leads to nuclear genome instability via an iron-sulfur cluster defect," *Cell*, vol. 137, no. 7, pp. 1247–1258, 2009.

[58] D. Sinclair, K. Mills, and L. Guarente, "Aging in Saccharomyces cerevisiae," *Annual Review of Microbiology*, vol. 52, pp. 533–560, 1998.

[59] P. Laun, A. Pichova, F. Madeo et al., "Aged mother cells of Saccharomyces cerevisiae show markers of oxidative stress and apoptosis," *Molecular Microbiology*, vol. 39, no. 5, pp. 1166–1173, 2001.

[60] A. L. Hughes and D. E. Gottschling, "An early age increase in vacuolar pH limits mitochondrial function and lifespan in yeast," *Nature*, vol. 492, no. 7428, pp. 261–265, 2012.

[61] C. Q. Scheckhuber, N. Erjavec, A. Tinazli, A. Hamann, T. Nyström, and H. D. Osiewacz, "Reducing mitochondrial fission results in increased life span and fitness of two fungal ageing models," *Nature Cell Biology*, vol. 9, no. 1, pp. 99–105, 2007.

[62] A. Baryshnikova, M. Costanzo, Y. Kim et al., "Quantitative analysis of fitness and genetic interactions in yeast on a genome scale," *Nature Methods*, vol. 7, no. 12, pp. 1017–1024, 2010.

Hindawi Publishing Corporation
Oxidative Medicine and Cellular Longevity
Volume 2013, Article ID 636287, 13 pages
http://dx.doi.org/10.1155/2013/636287

Research Article

Maintenance of Mitochondrial Morphology by Autophagy and Its Role in High Glucose Effects on Chronological Lifespan of *Saccharomyces cerevisiae*

May T. Aung-Htut,[1] Yuen T. Lam,[1] Yu-Leng Lim,[1] Mark Rinnerthaler,[2] Cristy L. Gelling,[1] Hongyuan Yang,[1] Michael Breitenbach,[2] and Ian W. Dawes[1]

[1] *School of Biotechnology and Biomolecular Sciences, University of New South Wales, Sydney, NSW 2052, Australia*
[2] *Department of Genetics, University of Salzburg, Hellbrunnerstrare 34, 5020 Salzburg, Austria*

Correspondence should be addressed to Ian W. Dawes; i.dawes@unsw.edu.au

Received 13 May 2013; Accepted 21 June 2013

Academic Editor: Joris Winderickx

In *Saccharomyces cerevisiae*, mitochondrial morphology changes when cells are shifted between nonfermentative and fermentative carbon sources. Here, we show that cells of *S. cerevisiae* grown in different glucose concentrations display different mitochondrial morphologies. The morphology of mitochondria in the cells growing in 0.5% glucose was similar to that of mitochondria in respiring cells. However, the mitochondria of cells growing in higher glucose concentrations (2% and 4%) became fragmented after growth in these media, due to the production of acetic acid; however, the fragmentation was not due to intracellular acidification. From a screen of mutants involved in sensing and utilizing nutrients, cells lacking *TOR1* had reduced mitochondrial fragmentation, and autophagy was found to be essential for this reduction. Mitochondrial fragmentation in cells grown in high glucose was reversible by transferring them into conditioned medium from a culture grown on 0.5% glucose. Similarly, the chronological lifespan of cells grown in high glucose medium was reduced, and this phenotype could be reversed when cells were transferred to low glucose conditioned medium. These data indicate that chronological lifespan seems correlated with mitochondrial morphology of yeast cells and that both phenotypes can be influenced by factors from conditioned medium of cultures grown in low glucose medium.

1. Introduction

Mitochondria are important organelles whose primary function is to synthesize ATP, but they also play important roles in many cellular processes including apoptosis and aging [1–4]. Due to their dynamic nature, the number and shape of mitochondria in a cell are variable depending on the growth conditions of the cell [5–7].

In *Saccharomyces cerevisiae*, the morphology of mitochondria is under the influence of the availability of oxygen and the nature of the carbon source for growth. Under anaerobic conditions, very small mitochondria known as promitochondria are observed. These are devoid of respiratory pigments and import ATP to perform the remaining essential metabolic functions [8]. On the other hand, enlarged tubular structures are found in aerobically grown cells [9]. *S. cerevisiae* cells respire in the absence of glucose, and these cells have a similar mitochondrial morphology to those observed in stationary phase cells where many small, round mitochondria are the dominant form [6, 10]. High glucose concentrations promote calcium and mitogen protein kinase-mediated activation of mitochondrial fission and stimulate reactive oxygen species production [11].

Restriction of glucose intake extends the cellular lifespan in a manner similar to caloric restriction [12, 13]. Alternatively, inhibition of nutrient signaling pathways by deletion of the *TOR1* gene or addition of rapamycin to growth media also extends both replicative and chronological lifespan (CLS) in *S. cerevisiae* [14, 15]. One of the downstream processes under regulation by the TOR pathway is autophagy, which is activated upon starvation or inhibition of TOR signaling [16]. Autophagy is conserved in all eukaryotic cells [17, 18] and it

is important during starvation because it not only removes damaged organelles, but it also provides nutrients by recycling cellular constituents [19–21]. There is also increasing evidence that autophagy may play a role in lifespan extension in *Caenorhabditis elegans*, *Drosophila melanogaster,* and *S. cerevisiae* [22–24], especially during caloric restriction [25].

In neonatal rat ventricular myocytes, a high glucose concentration induced cell death via mitochondrial fragmentation possibly due to increased production of reactive oxygen species (ROS) [1]. Despite this interest in ageing, nutrients, and mitochondrial morphology, it remains to be determined whether there is any correlation between mitochondrial morphology and chronological ageing in *S. cerevisiae* over a wide range of glucose concentrations. We, therefore, investigated the mitochondrial morphology of yeast cells grown in different concentrations of glucose and sought to identify functions that are important in maintaining mitochondrial structure at elevated levels of glucose.

2. Materials and Methods

2.1. Yeast Strains, Media, and Growth Conditions. All *S. cerevisiae* strains used were derived from BY4743 (*MATa/MATα his3Δ1/his3Δ1 leu2Δ0/leu2Δ0 met15Δ0/MET15 LYS2/lys2Δ0 ura3Δ0/ura3Δ0*). Yeast strains were grown aerobically at 30°C in YPD (1% yeast extract, 2% peptone, and 2% glucose) or in synthetic complete medium SC (0.17% Difco yeast nitrogen base without amino acids and ammonium sulfate, 0.5% ammonium sulfate and 0.79 g/L amino acids mixture) supplemented with the indicated concentration of carbon source. The concentrations of amino acids used were according to [26]. For visualization of mitochondria, strains were transformed with the plasmid pUC35-*ACO1*-GFP and pUC35-*CIT1-Dsred* (gift from Professor Trevor. Lithgow, Monash University, Melbourne, VIC, Australia). Yeast strains harboring the plasmid pUC35-*ACO1*-GFP were grown in SC medium lacking uracil. For antibiotic selection, nourseothricin (ClonNAT, Werner BioAgents) or hygromycin B (Sigma-Aldrich) were added to a final concentration of 100 mg/L and 300 mg/L, respectively. Starter cultures were prepared by inoculating a single colony into 1.5 mL SC medium and incubating overnight at 30°C. The starter culture was then diluted to OD_{600} 0.1–0.15 in 2 mL fresh SC medium in a 10 mL tube for microscopic examination or 10 mL in a 50 mL tube for CLS and incubated at 30°C with shaking throughout the experiment. At the indicated intervals, 20 μL culture was removed for microscopic examination and 100 μL for serial dilution and spotting on a YPD plate. Five μL of undiluted culture and of each dilution was spotted onto a YPD plate and incubated for 2-3 d at 30°C. Conditioned medium was prepared by growing the cells in SC medium containing different concentrations of glucose for 48 h and collecting the supernatant by centrifuging at 1800 ×g for 5 min. For media exchange experiments, the cells were grown for 6 h before pelleting and resuspending in the indicated conditioned media unless otherwise stated. The morphology of mitochondria was observed 2 h after media exchange.

2.2. Measurement of Oxygen and Glucose Consumption. The rate of oxygen consumption was monitored using a standard 3 mL Clark-type oxygen electrode. The system was connected to a PowerLab data acquisition and analysis system (ADInstruments). Culture (2 mL) at the indicated time points was transferred to the chamber maintained at 30°C with constant stirring, and oxygen content was monitored for at least 10 min. For glucose consumption, the concentration of glucose in the supernatant was measured at 6, 24, 48, and 72 h after inoculation using an automated glucose analyzer (YSI 2300 STAT Plus Glucose & Lactate Analyzer).

2.3. Microscopy. Mitochondrial morphology was observed using an Olympus BX60 fluorescence microscope at 100× magnification. An aliquot 5–10 μL of sample was taken at indicated times, and micrographs of the cells with representative morphology were taken at room temperature. The images were acquired using IP lab software, and Adobe Photoshop was used to adjust the image size and the brightness and contrast. To determine the percentage of cells with total mitochondrial fragmentation within a population, the cells were grown for three days. An aliquot of sample was examined at indicated time points. The percentage of cells showing no visible tubular mitochondrial structure was determined by direct microscopic examination. For each assay at least 350 cells were counted, and the data are the mean of three independent experiments.

2.4. Gas Chromatography-Mass Spectrometry (GC-MS) Analysis. The GC-MS analysis was carried out using the Thermo Scientific DSQ II Single Quadrupole GC/MS at the Bioanalytical Mass Spectrometry Facility (BMSF), University of New South Wales. The samples were analyzed by GC-MS with the split injection mode and split ratio of 1 : 10. Carrier gas was helium at a constant flow rate of 1.5 mL/min. The inlet temperature was maintained at 240°C. GC oven temperature was held at 70°C for 1 min and then ramped to 140°C at 15°C/min where it was held for a further min. Mass spectrometry was carried out in positive ion mode using electron ionization and the mass spectra recorded within 41–74 amu.

2.5. Measurement of Intracellular pH. Intracellular pH was determined by the method of Brett et al. [27]. Strain BY4743 was transformed with pCB901YpHc containing the pHluorin gene (gift from Professor Rajini Rao, Johns Hopkins University School of Medicine, Baltimore) and pUG35 (non-pH sensitive GFP). The cells were grown in different glucose concentrations for 24 hours, and the intracellular pH was analyzed using a FACSCanto II (BD Biosciences). The fluorescent signals were collected at two different channels: Alexa Fluor 488 (488 nm) and AmCyan (405 nm). A calibration curve of the ratio of fluorescent intensities of 405/488 nm versus pH was obtained as follows. Sample (50 μL) was diluted in 1 mL of medium containing 50 mM MES, 50 mM HEPES, 50 mM KCl, 50 mM NaCl, 0.2 M ammonium acetate, 10 mM NaN_3, 10 mM 2-deoxyglucose, 75 μM monensin, and 10 μM nigericin, titrated to eight different pH values within the

range of 5.0–8.0. The background was subtracted using the cells with pUG35, and the value of 405/488 was calculated using FlowJo software for each individual pH. The intracellular pH of the cells growing in different concentrations of glucose was estimated by comparing the ratio of fluorescent intensities of 405/488 nm obtained for the cells with the calibration curve.

2.6. Measurement of Intracellular Acetate. The intracellular acetate concentration was measured for cells of the wild type and the Δ*atg1* mutant grown in different concentrations of glucose for 24 hours using the commercial kit from R-Biopharm (Cat. no. 10148261035) according to the manufacturer's instructions.

2.7. Dihydroethidium (DHE) Staining and FACS Analysis. Staining with DHE (Molecular Probes) was performed as described by [28]. Briefly, cells (500 μL) were stained with 5 μg/mL final concentration of DHE for 10 min and analyzed using a FACSort (BD Bioscience). Analysis was performed for 20,000–30,000 cells per sample. All analyses were performed twice independently.

3. Results

3.1. Mitochondrial Morphology Changes in Response to Different Glucose Concentrations. In order to determine whether increasing glucose concentration also has an effect on mitochondrial structure and how this correlates with cellular lifespan in *S. cerevisiae*, we monitored the changes in mitochondrial morphology in *S. cerevisiae* cells growing in calorie-restricted (0.5%) and high glucose conditions (2% and 4%). *S. cerevisiae* cells were transformed with an aconitase-GFP fusion construct, *ACO1*-GFP, and expression of GFP was used to visualize mitochondrial structure. The use of this construct has been verified in [29].

To ensure that mitochondrial morphology was examined at a similar growth phase, the growth of wild-type cells expressing *ACO1*-GFP in the different levels of glucose was monitored (Figure 1). A similar growth rate was observed for all glucose conditions and cells reached stationary phase at a comparable time. The final yields of these three levels of glucose culture were also similar.

Having determined the growth states of the cultures in the three glucose conditions, changes of mitochondrial morphology were examined. Cells were grown in synthetic medium (SC) containing 0.5%, 2%, or 4% glucose, and after 17 h growth, as cells entered the diauxic shift, mitochondrial morphology was examined using fluorescence microscopy. Remarkable differences in mitochondrial morphology were observed in response to changing glucose concentrations (Figure 2(a)). Under the standard laboratory condition with 2% glucose as a carbon source, mitochondria appeared as elongated tubular structures. However, in media containing 0.5% glucose, mitochondria displayed a highly branched, short-rod morphology similar to that observed in cells growing by respiration in ethanol medium [3]. In the highest level of glucose tested (4%), mitochondria displayed a partial bead-thread structure with very few connections and branches.

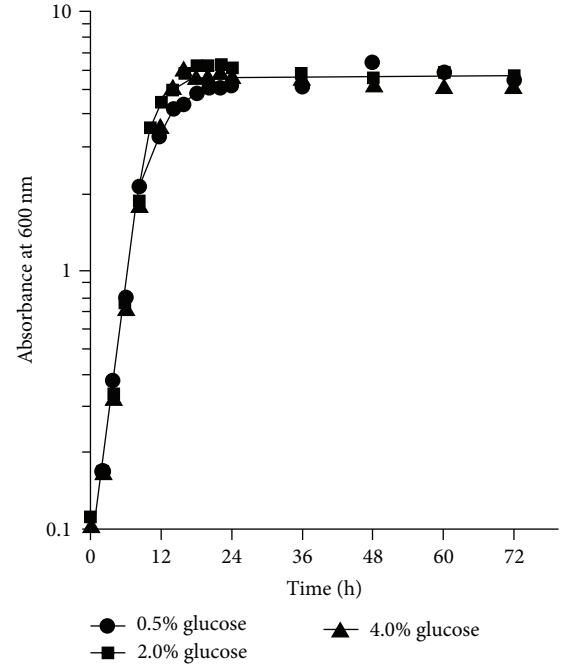

Figure 1: Growth of BY4743 overexpressing *ACO1*-GFP plasmid in SC medium supplemented with different concentrations of glucose. An overnight culture of cells in SC medium was diluted to an initial absorbance at 600 nm of 0.1 in fresh SC medium containing the glucose concentration indicated and the cultures incubated at 30°C with shaking. The cell concentration was estimated at intervals. Data are from a single experiment.

Observations using a *CIT1*-DsRed construct instead of the *ACO1*-GFP construct also produced the same result, indicating that the effect of glucose concentrations on mitochondrial morphology was independent of the use of the aconitase-GFP fusion (data not shown).

The difference in mitochondrial morphologies between cells grown in 2% glucose and 4% glucose was independent of osmotic stress, since addition of an equivalent molar concentration of sorbitol to 2% glucose medium did not affect the mitochondrial appearance (data not shown).

Having observed the characteristic mitochondrial morphology associated with glucose levels, we monitored the change of mitochondrial morphology in cells grown in 0.5%, 2% or 4% glucose media for 24, 48 and 72 hours (Figure 2(a)). Furthermore, to assess the structural changes of mitochondria, the percentage of cells in the population displaying total mitochondrial fragmentation, in which only punctate mitochondria with complete absence of tubular mitochondria within an individual cell, was determined (Table 1).

Cells grown in 2% or 4% glucose displayed an increased heterogeneity in mitochondrial morphology with time, showing a progression towards punctate fragmented structures over 72 hours (Figure 2(a)). After 24 hours of growth, the culture grown in 4% glucose had the highest number of cells with totally fragmented mitochondria (10%) followed by those grown in 2% glucose (7%) and 0.5% glucose (2%)

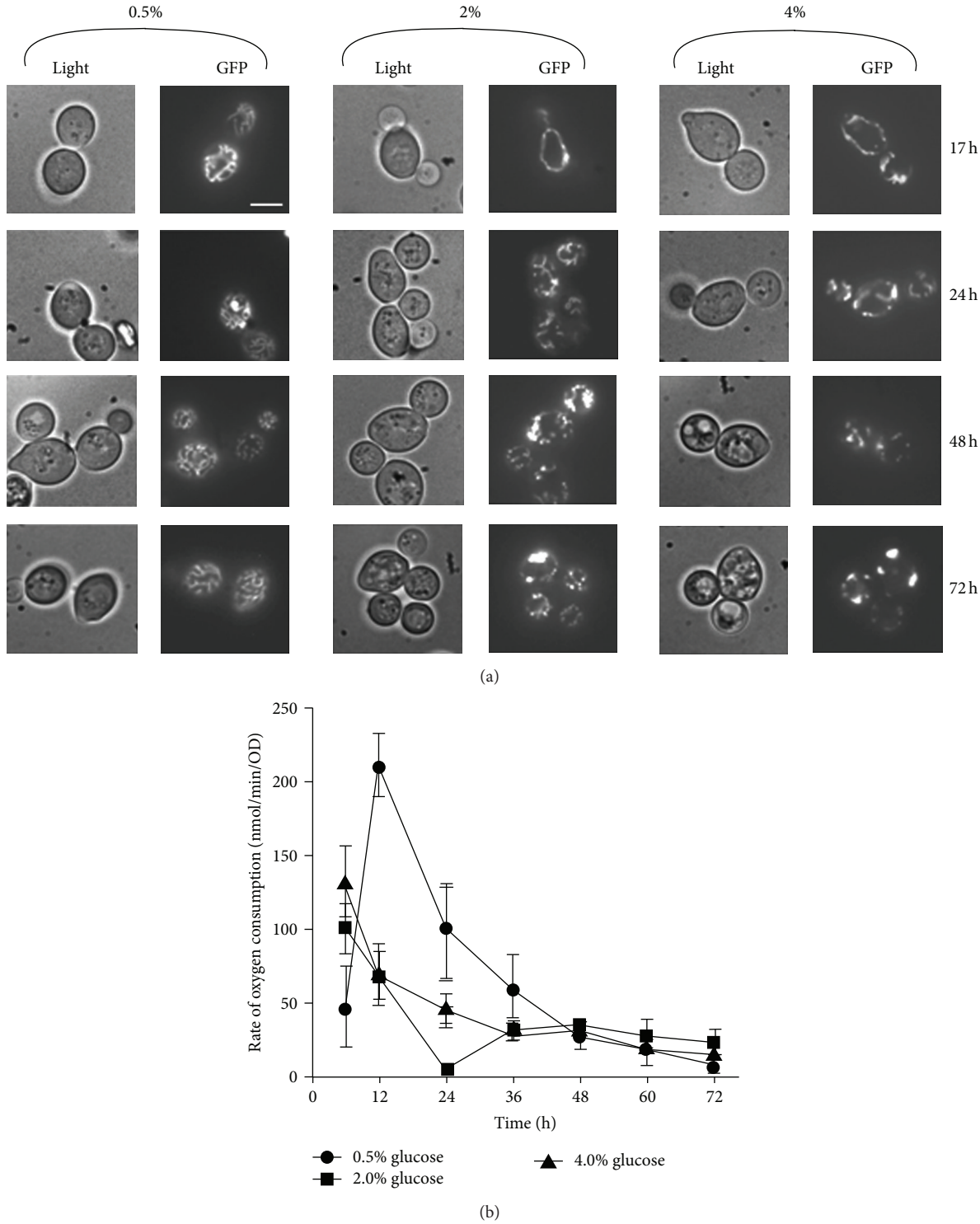

Figure 2: Mitochondrial morphologies of *S. cerevisiae* grown in different concentrations of glucose. (a) BY4743 wild-type cells transformed with an *ACO1*-GFP fusion construct were grown for 72 hours in three different concentrations of glucose (0.5%, 2%, and 4%), and the morphology of mitochondria was observed at the indicated times using a fluorescent microscope. The micrographs shown are representative of the population. Scale bar: 5 μm. (b) The rates of oxygen consumption of these cells were also measured at the initial 6 hours after inoculation and at 12 hours intervals throughout the 72 hours time course. Data are the mean of three separate cultures in parallel. Error bars indicate the standard deviation.

Table 1: The percentage of wild-type and mutant cells showing completely fragmented mitochondrial morphology in cultures incubated in three different concentrations of glucose (0.5%, 2%, and 4%) at the times indicated.

Strain	0.5% glucose			2% glucose			4% glucose		
	24 h	48 h	72 h	24 h	48 h	72 h	24 h	48 h	72 h
Wild type	1.6 (0.7)	2.4 (0.9)	2.2 (1.2)	6.5 (0.8)	36.0 (1.1)	63.6 (4.3)	10.7 (2.1)	38.2 (7.5)	66.2 (6.7)
Δ*dnm1*	0.8 (1.3)	0.8 (0.9)	2.9 (1.2)	1.3 (1.5)	22.4 (1.0)	45.1 (1.3)	3.6 (1.5)	29.5 (2.2)	67.5 (1.9)
Δ*fis1*	n.d.	n.d.	n.d.	1.8 (1.1)	7.3 (2.1)	30.2 (1.5)	6.3 (0.8)	13.3 (1.2)	63.2 (5.7)
Δ*tor1*	1.0 (1.0)	0.9 (0.3)	1.5 (0.7)	6.1 (0.3)	8.2 (1.1)	36.7 (0.9)	11.3 (1.2)	27.0 (1.0)	41.4 (1.0)
Δ*gpa2*	1.7 (0.6)	1.2 (0.4)	4.9 (0.6)	6.3 (0.6)	39.7 (3.7)	67.7 (1.7)	5.6 (1.6)	34.7 (1.0)	54.8 (1.0)
Δ*snf3*	1.9 (0.4)	3.8 (0.5)	6.0 (0.7)	5.5 (0.7)	32.9 (3.1)	47.7 (2.3)	8.5 (1.9)	71.2 (4.2)	75.4 (5.4)
Δ*rgt2*	n.d.	n.d.	n.d.	5.3 (1.9)	28.8 (3.6)	50.7 (2.6)	8.3 (2.2)	22.7 (2.9)	72.4 (6.2)
Δ*pde1*	0.8 (0.7)	1.0 (0.4)	1.3 (1.2)	11.9 (1.5)	60.0 (2.0)	78.4 (1.6)	16.3 (3.1)	61.7 (2.2)	70.5 (2.9)
Δ*pde2*	4.8 (0.1)	3.8 (0.9)	9.3 (4.3)	6.8 (1.5)	56.1 (5.4)	84.6 (1.7)	16.6 (4.8)	48.0 (8.4)	68.1 (2.9)
Δ*uth1*	3.1 (1.7)	2.9 (0.4)	6.8 (3.0)	7.5 (2.2)	37.0 (4.4)	54.9 (2.6)	14.0 (3.3)	34.0 (7.5)	63.0 (5.1)
Δ*atg32*	n.d.	n.d.	n.d.	8.2 (1.7)	27.6 (2.8)	50.1 (4.2)	9.3 (1.5)	60.2 (1.6)	68.4 (4.3)
Δ*atg1*	14.8 (5.2)	8.0 (0.7)	12.0 (1.7)	14.4 (1.4)	57.7 (1.0)	74.6 (0.8)	13.0 (2.2)	60.5 (7.2)	74.4 (0.5)
Wild type + rapamycin[1]	2.8 (0.2)	3.2 (0.3)	4.2 (0.7)	3.9 (0.6)	6.2 (1.3)	12.0 (0.9)	5.6 (1.5)	7.6 (1.0)	14.9 (0.9)
Δ*uth1* + rapamycin[1]	2.5 (0.6)	2.6 (0.8)	2.1 (0.4)	2.5 (0.7)	3.6 (0.5)	5.9 (0.7)	3.8 (0.9)	6.1 (0.5)	17.2 (1.6)
Δ*atg1* + rapamycin[1]	7.4 (0.5)	10.1 (1.5)	13.5 (1.6)	9.0 (0.4)	30.8 (1.4)	62.5 (0.9)	12.9 (0.8)	31.1 (1.8)	67.4 (0.7)

[1]Wild-type cells or mutants were grown in the presence of 10 nM rapamycin.
*The *fis1*Δ strain used in these experiments has been shown to also carry a mutation in the *WHI2* gene which rescues the mitochondrial respiratory defect caused by *FIS1* deficiency, but which also causes a failure to suppress cell growth during amino acid deprivation [29].

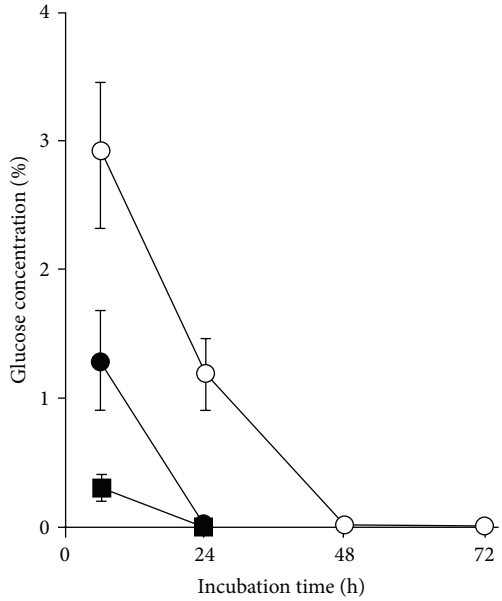

Figure 3: Glucose consumption of *S. cerevisiae* growing in 0.5%, 2%, and 4% glucose. Glucose in the culture medium was measured at intervals after incubation of the cells in SC medium containing glucose at 0.5% (closed squares), 2% (closed circles), or 4% (open circles). The measurements were performed on three separate cultures grown in parallel, and error bars indicate the SEM.

(Table 1). The percentages of cells with totally fragmented mitochondria grown in 4% and 2% glucose increased to 64% and 66%, respectively, after 72 hours. However, cells under caloric restriction showed an average of less than 3% of the population with total mitochondrial fragmentation at that time.

We monitored respiratory rate under the above conditions to determine whether this affected the morphology of mitochondria. Maximal respiratory activity was observed in cells after 12 hours of growth in 0.5% glucose medium (Figure 2(b)). This respiration peak coincided with the presence of highly branched mitochondrial morphology observed in 0.5% glucose-grown cells. However, respiratory activity in these cells decreased from 24 hours to a low level at 72 hours, yet the highly branched mitochondrial morphology was maintained throughout the 72 hours time course. Therefore, a high rate of respiration was not required to maintain the highly branched mitochondrial morphology in these cells. On the other hand, the respiratory activity of 4% glucose-grown cells was relatively low and underwent a gradual decrease throughout the 72 h incubation. Since total mitochondrial fragmentation was observed in 4% glucose-grown cells as early as 24 hours of growth, decreasing the respiratory activity could not be the cause of the onset of mitochondrial fragmentation in the presence of high glucose levels.

Glucose concentrations were measured in the supernatant collected from the different media at intervals throughout growth. The level of glucose was close to zero after 24 hours of growth in medium originally supplemented with 0.5% and 2% glucose, while cells consumed approximately half of the glucose in 4% glucose medium (Figure 3). These data indicate that there was no correlation between the concentration of glucose remaining in the medium and the progression of mitochondrial fragmentation.

Together, the above data showed that neither growth state nor respiratory rate, and the rate of glucose consumption

correlated with mitochondrial fragmentation observed in high glucose concentrations. We then further investigate the cause of early mitochondrial fragmentation in cells grown at high glucose concentrations (2% and 4%) by analyzing the mitochondrial morphology of cells lacking genes involved in maintaining mitochondrial morphology.

3.2. Progression of Mitochondrial Fragmentation in High Glucose Is Independent of Mitochondrial Fission. Mitochondrial morphology is modulated by a delicate balance between mitochondrial fission and fusion, and in *S. cerevisiae,* deletion of the *DNM1* gene involved in mitochondrial fission increases replicative lifespan [4]. We therefore determined whether the mitochondrial fragmentation observed in cells grown in a high level of glucose was regulated by factors affecting mitochondrial fission by examining mutant strains (*dnm1*Δ and *fis1*Δ) with known defects in the fission process. The *fis1*Δ strain used in these experiments has been shown to also carry a mutation in the *WHI2* gene which rescues the mitochondrial respiratory defect caused by FIS1 deficiency, which also causes a failure to suppress cell growth during amino acid deprivation [30]. The mutant cells were transformed with the *ACO1*-GFP construct and grown in 2% or 4% glucose medium under the same condition described above.

The *dnm1*Δ mutant defective in mitochondrial fission was expected to show a reduced level of mitochondrial fragmentation [4]; however, when grown in 4% glucose, it displayed fragmentation comparable to that of the wild type (Table 1, see also Supplementary Figure S1 available online at http://dx.doi.org/10.1155/2013/636287). A slight reduction in the percentage of *dnm1*Δ cells that harbored fragmented mitochondria was observed when cells were grown in 2% glucose. Nevertheless, mitochondrial fragmentation progressed in the *dnm1*Δ strain under the high glucose conditions. Cells lacking *FIS1* also showed a reduction in the percentage of cells containing mitochondrial fragmentation when grown in 2% glucose. However, similarly to *dnm1*Δ, mitochondrial fragmentation was observed when *fis1*Δ cells were grown in 4% glucose, resulting in 63% of cells containing completely fragmented mitochondria. These results indicated that mitochondrial fragmentation was unavoidable when cells were grown in 4% glucose, even in cells defective in mitochondrial fission. Hence, mitochondrial fragmentation observed in high glucose levels was independent of mitochondrial fission.

Cells deleted for the mitochondrial fusion gene *FZO1* lack mitochondrial DNA and had severely deformed mitochondria in both glucose concentrations examined, and it was therefore difficult to determine whether there was any involvement of mitochondrial fusion in the fragmentation of mitochondria using this mutant.

3.3. Inhibition of TOR Signaling Pathway Reduces Mitochondrial Fragmentation. Since nutrient availability might play a greater role than mitochondrial fission processes in modulating mitochondrial fragmentation when cells were grown at high glucose concentration, we examined mutant strains lacking genes involved in glucose sensing (*SNF3*, *RGT2*), glucose metabolism (*HXK2, GPA2*, *PDE1*, and *PDE2*), and general nutrient sensing (*TOR1*). Mutant cells transformed with the *ACO1*-GFP construct were grown in 2% or 4% glucose medium as described above.

Mutants with a deletion affecting glucose sensing or glucose metabolism showed 50% to 84% of cells with totally fragmented mitochondria morphology after 72 hours of growth in either 2% or 4% glucose (Table 1). Among the mutants screened, only cells lacking the *TOR1* gene showed a substantial reduction in the percentage of cells with totally fragmented mitochondria when grown in 2% or 4% glucose (Table 1; Supplementary Figure S2). Mitochondrial fragmentation of *tor1*Δ mutant cells was 42% and 37% when cells were grown in 4% glucose and 2% glucose, respectively, after 72 hours. As an alternative approach to genetic manipulation of the TOR pathway, the wild-type cells were treated with 10 nM rapamycin to inhibit both *TOR1* and *TOR2* gene products. Cells treated with rapamycin showed an even greater reduction in total mitochondrial fragmentation than in the *tor1*Δ strain, with only 12% to 15% of the cells showing totally fragmented mitochondria when the cells were grown for 72 hours in 2% or 4% glucose media containing 10 nM rapamycin, respectively (Table 1; Supplementary Figure S3). Hence, deletion of *TOR1* only partially suppressed mitochondrial fragmentation while inhibition of the TOR pathway by rapamycin, which also inhibits *TOR2,* further repressed the extent of mitochondrial fragmentation during cell growth in high glucose levels.

3.4. Autophagy Is Required to Resist Mitochondrial Fragmentation Caused by Volatile Glucose Metabolites. Since mitochondrial fragmentation occurred after cells had grown in media, we tested whether cells grown in different concentrations of glucose excreted metabolites are capable of stimulating mitochondrial fragmentation. In order to test this hypothesis, conditioned medium (in which cells had been grown in 0.5% or 4% glucose for either 24 hours or 48 hours) was collected and then used to replace the growth medium of cells grown either to exponential (6 hours) or stationary phase (48 hours).

The conditioned medium that was initially supplemented with 4% glucose (4% glucose, 48 hours) contained substances that caused mitochondrial fragmentation in exponential phase cells, regardless of the glucose concentration of the medium in which the cells were pregrown (Figure 4). Mitochondrial fragmentation was observed as early as 2 h after transfer into this medium. Fragmentation also occurred for stationary phase cells pregrown in medium containing 2% and 4% glucose. In contrast, stationary phase cells pregrown in 0.5% glucose were resistant to mitochondrial fragmentation induced by the same medium. It was hypothesized that mitochondrial fragmentation was prevented in these cells because nutrients became depleted, and autophagy was activated earlier than in the other growth regimes.

In order to investigate the involvement of autophagy in resistance to conditioned medium-induced mitochondrial fragmentation, the autophagy mutant strains Δ*uth1*, Δ*atg1*, and Δ*atg5* were grown to stationary phase in medium containing 0.5% glucose and then transferred into the conditioned medium (4% glucose, 48 hours). The mitochondria

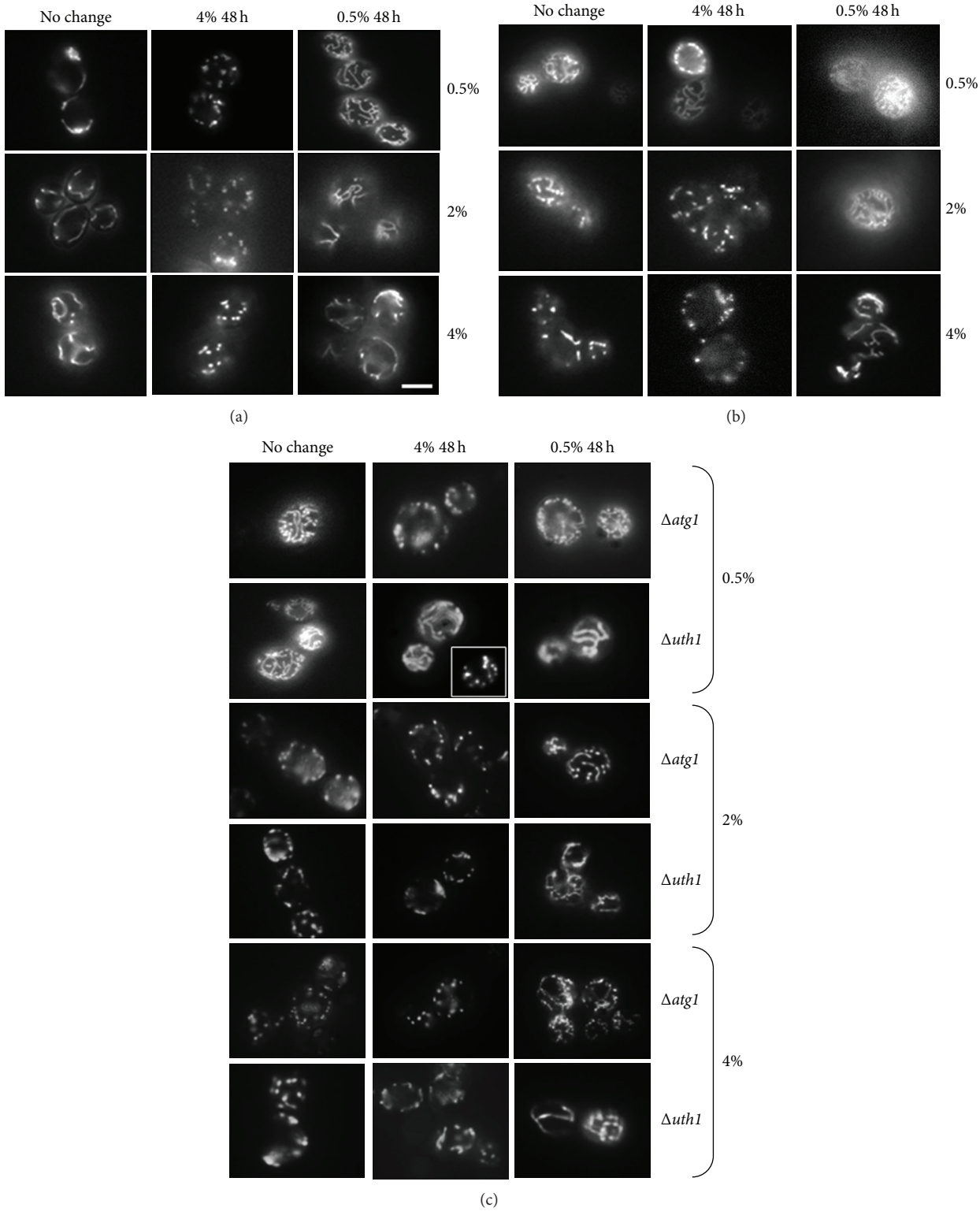

Figure 4: Conditioned medium from *S. cerevisiae* grown in 4% glucose triggered mitochondrial fragmentation, which was delayed by autophagy. (a) The wild-type cells pregrown to exponential phase for 6 hours in 0.5%, 2%, and 4% glucose to exponential phase were transferred to the 4% conditioned medium (4% 48 h) or 0.5% conditioned medium (0.5% 48 h), and mitochondrial morphology was observed. (b) The wild-type cells grown to stationary phase for 48 hours in 0.5%, 2%, and 4% glucose, then transferred to the 4% conditioned medium (4% 48 h) or 0.5% conditioned medium (0.5% 48 h), and mitochondrial morphology was observed. (c) Mutants affected in autophagy (Δ*atg1* and Δ*uth1*) were grown to stationary phase as under (b), and mitochondrial morphology was observed. Scale bar: 5 μm. The micrographs shown are representative of the populations. Note: the micrograph for the Δ*uth1* mutant transferred into 4% 48 h represents the morphology of half the population of the cells, and the inset represents that of the other half of the population.

of the Δ*atg1* and Δ*atg5* mutants became fragmented, but not those of the mitophagy mutant Δ*uth1*. These results indicated that general autophagy was important for conferring resistance to the metabolites that stimulated mitochondrial fragmentation and that starvation may be able to delay mitochondrial fragmentation. Indeed, delayed fragmentation was observed in the cells growing in 10-fold diluted SC medium containing 2% glucose compared to the cells growing in normal SC medium with 2% glucose (data not shown).

Since conditioned medium (4% glucose, 48 hours) appeared to contain a substance that stimulated fragmentation of mitochondria, it was analysed further. Treatment with diluted spent medium did not cause mitochondrial fragmentation in *S. cerevisiae* pregrown in any of the glucose concentrations (Figure 5(a)), indicating that the effect was probably not due to the physical disturbance of changing the medium but due to the concentration of the glucose metabolites present. These cells maintained tubular mitochondrial structure for at least 62 hours after the medium was exchanged. In addition, vacuum evaporation of the conditioned medium rendered it unable to stimulate mitochondrial fragmentation (Figure 5(a)) indicating that the stimulatory substance/s were volatile. Interestingly, mitochondrial fragmentation stimulated by the conditioned medium was found to be reversible once the medium was removed (Figure 5(b)).

3.5. The Observed Mitochondrial Fragmentation Was Not due to Intracellular Acidification. Since the metabolite(s) responsible for mitochondrial fragmentation was(were) volatile, we analysed all of the 48 hours conditioned media (0.5% glucose, 2% glucose, and 4% glucose) by gas chromatography-mass spectrometry. Three volatile substances with higher concentrations in the 4% glucose-conditioned medium were detected: acetic acid, ethanol, and 2,3-butanediol (Supplementary Table S1). Of the three compounds, acetic acid was the only one that resulted in mitochondrial fragmentation when separately added to the cells (Supplementary Figure S4).

Mitochondrial fragmentation triggered by acetic acid treatment could be due to intracellular acidification caused by release of protons or to accumulation of acetate. In addition to acetic acid, benzoic acid and 2,4-dinitrophenol (2,4-DNP) also triggered mitochondrial fragmentation (Figure S1). One feature that is common to these three compounds is their ability to lead to acidification within the cells, and therefore we analyzed the intracellular concentration of acetate and intracellular pH of cells grown in different glucose concentrations. The intracellular level of acetate was higher in the wild-type cells growing in 2% and 4% glucose than those growing in 0.5% (See Supplementary Table S2). The intracellular pH of the cells grown in different concentrations of glucose was measured using the pH-sensitive GPF probe pHluorin. No significant correlation between intracellular pH and mitochondrial fragmentation was found (Supplementary Figure S5). Although mitochondrial fragmentation was already established in 2% and 4% glucose-grown cells within 24 hours of inoculation (Table 1), the intracellular pH of these cells was similar to that of 0.5% glucose-grown cells at that time. These results indicated that intracellular acidification was unlikely to be responsible for triggering mitochondrial fragmentation and that acetate or some metabolite derived from it is more likely to be responsible.

3.6. Autophagy Is Required to Reduce Mitochondrial Fragmentation. One of the many cellular processes regulated by the TOR pathway is autophagy, which recycles damaged proteins and organelles and makes amino acids and other essential metabolites to the cell [31] available. To determine whether autophagy plays a role in the reduction of mitochondrial fragmentation under high glucose conditions, a mutant strain defective for initiation of autophagy (*atg1*Δ) was transformed with *ACO1*-GFP construct to examine mitochondrial fragmentation (Table 1).

Cells deleted for *ATG1* displayed higher percentages (approximately 75% after 72 hours incubation) of mitochondrial fragmentation than the wild type, indicating that autophagy acts to reduce the onset of mitochondrial fragmentation in 2% and 4% glucose-grown cells. Since autophagy was important in maintaining mitochondrial morphology under these conditions, cells lacking genes affecting mitochondrial-specific autophagy, *ATG32* [32, 33], and *UTH1* [34] that is also affected in cellular ageing [35], were analyzed. Surprisingly, deletion of *UTH1* or *ATG32* did not affect mitochondrial fragmentation compared to that in the wild-type cells, indicating that mitochondrial-specific autophagy alone did not substantially suppress mitochondrial fragmentation. However, general autophagy, involving *ATG1* appears to play a vitally important role for reducing mitochondrial fragmentation under higher glucose conditions since deletion of *ATG1* elevated the fragmentation of mitochondria seen in cells grown on higher glucose levels.

Subsequently, we checked whether the TOR pathway regulated the function of autophagy in reducing mitochondrial fragmentation. The autophagy mutants were treated with rapamycin, and total mitochondrial fragmentation was examined. A reduction of mitochondrial fragmentation in rapamycin-treated *uth1*Δ was observed (Table 1), which was consistent with the finding that deletion of *UTH1* did not have an impact on mitochondrial fragmentation and that the suppression effect of rapamycin observed was independent of *UTH1*. In the *atg1*Δ mutant, although treatment with rapamycin reduced mitochondrial fragmentation compared to the untreated mutant cells, the level of mitochondrial fragmentation remained much higher than in rapamycin-treated wild-type cells. Hence, rapamycin inhibition of the TOR pathway led to suppression of mitochondrial fragmentation, but this was largely dependent on the presence of a functional autophagy pathway. Therefore, it is likely that autophagy functions downstream of the TOR pathway in maintaining mitochondria in a nonfragmented state.

3.7. Role of Autophagy in Mitochondrial Fragmentation Induced by Glucose Metabolites. Having identified a cellular process that is able to prevent mitochondrial fragmentation in cells grown in high glucose concentrations, we next examined what triggered mitochondrial fragmentation in these cells.

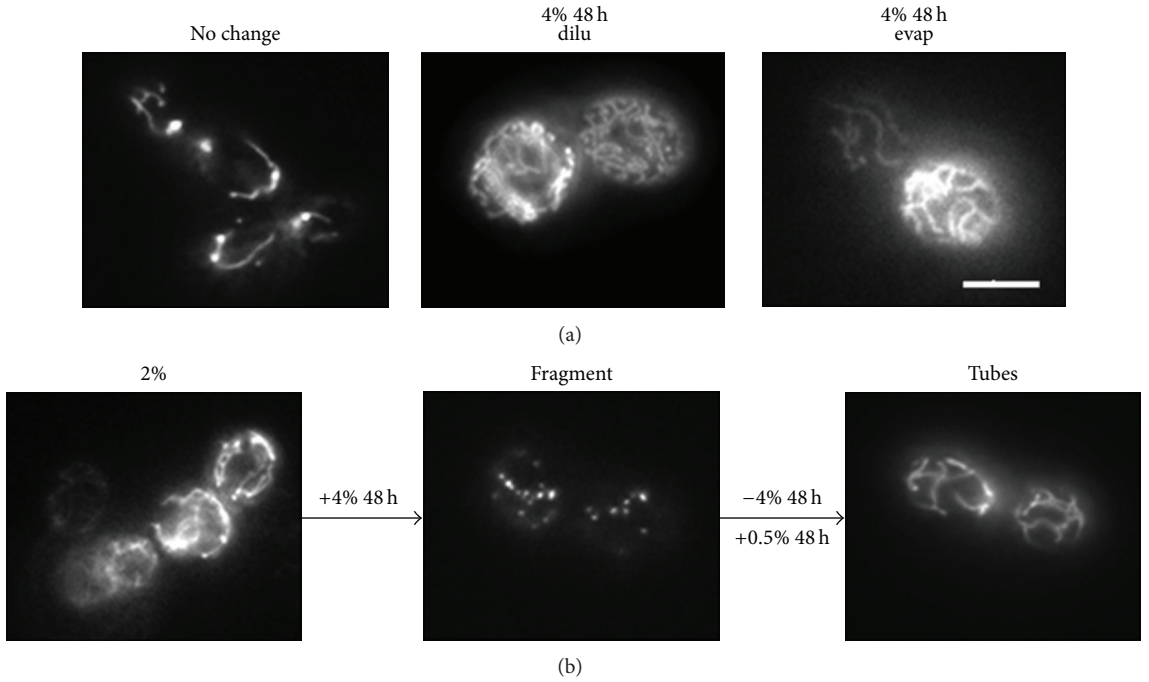

Figure 5: Reversibility of conditioned medium-induced mitochondrial fragmentation. (a) The mitochondria of the wild-type cells grown in 2% glucose did not fragment when they were transferred into diluted (4% 48 h dilu) and evaporated (4% 48 h evap) conditioned media (4% glucose, 48 hours). Mitochondria were observed at 2 hours, 20 hours, and 62 hours after media exchange. Only the micrographs taken at 20 hours after medium exchange are shown. (b) Mitochondrial fragmentation of the wild-type cells grown in 2% glucose was triggered by the 4% conditioned medium (+4% 48 h). Cells were grown in the 4% conditioned medium for 24 hours before transferring into the 0.5% conditioned medium (+0.5% 48 h). The morphology of mitochondria was observed 2 hours after transfer. Scale bar: 5 μm. The micrographs shown are representative of the populations.

Mitochondria are the major site of reactive oxygen species (ROS) production, and an elevation of ROS could be one of the causes of mitochondrial fragmentation. We examined the levels of superoxide anion by DHE staining of cells growing in 0.5%, 2%, and 4% glucose over a 72 h time course and flow cytometry analysis to determine whether elevation in superoxide levels was correlated with the occurrence of mitochondrial fragmentation.

Cellular superoxide levels increased over time regardless of the concentration of glucose, as shown in Figure 6. Cells grown in 0.5% glucose had the highest superoxide level after 24 hours growth, which is consistent with the fact that respiratory activity was the highest for these cells at that time (Figure 2(b)). After 72 h incubation, cells grown in 4% glucose had the highest level of superoxide followed by those grown in 2% glucose and then those grown in 0.5% glucose. It is therefore unlikely that an increase in ROS level triggered mitochondrial fragmentation during cell growth, since the onset of elevated levels of ROS in 0.5% glucose-grown cells did not lead to mitochondrial fragmentation.

Since fragmentation occurred 24 hours after inoculation in media, we analyzed whether the glucose metabolites accumulated in the medium during growth stimulated mitochondrial fragmentation. To test this hypothesis, conditioned medium (in which cells were grown for either 24 hours or 48 hours) originating from 4% glucose or 0.5% glucose medium was collected and then was used to replace the growth medium of cells grown to either exponential (6 hours) or stationary phase (48 hours).

The 48 hours conditioned medium that was initially supplemented with 4% glucose (4% conditioned medium) contained substances that caused mitochondrial fragmentation in wild-type cells in exponential phase, regardless of the glucose concentration of the medium in which cells were pregrown (Figure 4(a)). For instance, mitochondrial fragmentation was observed as soon as two hours after transferring cells into the 4% conditioned medium. This fragmentation was also found for stationary phase wild-type cells pregrown in medium containing 2% or 4% glucose (Figure 4(b)). In contrast, the stationary phase cells pregrown in 0.5% glucose did not display fragmented mitochondria after transfer into the 4% conditioned medium (Figure 4(b)). We hypothesized that the early nutrient depletion in 0.5% glucose-grown cells activated autophagy leading to resistance to induction of mitochondrial fragmentation.

In order to investigate the involvement of autophagy in this mitochondrial fragmentation process, the *atg1*Δ and *uth1*Δ autophagy mutants were grown for 48 hours in 0.5%, 2%, and 4% glucose and then transferred into the conditioned media (Figure 4(c)). Mitochondrial fragmentation was observed in the *atg1*Δ mutant cells, including those pregrown in 0.5% glucose, after transfer into the 4% glucose conditioned medium. On the other hand, *uth1*Δ cells pregrown in 0.5% glucose medium were partially resistant to 4%

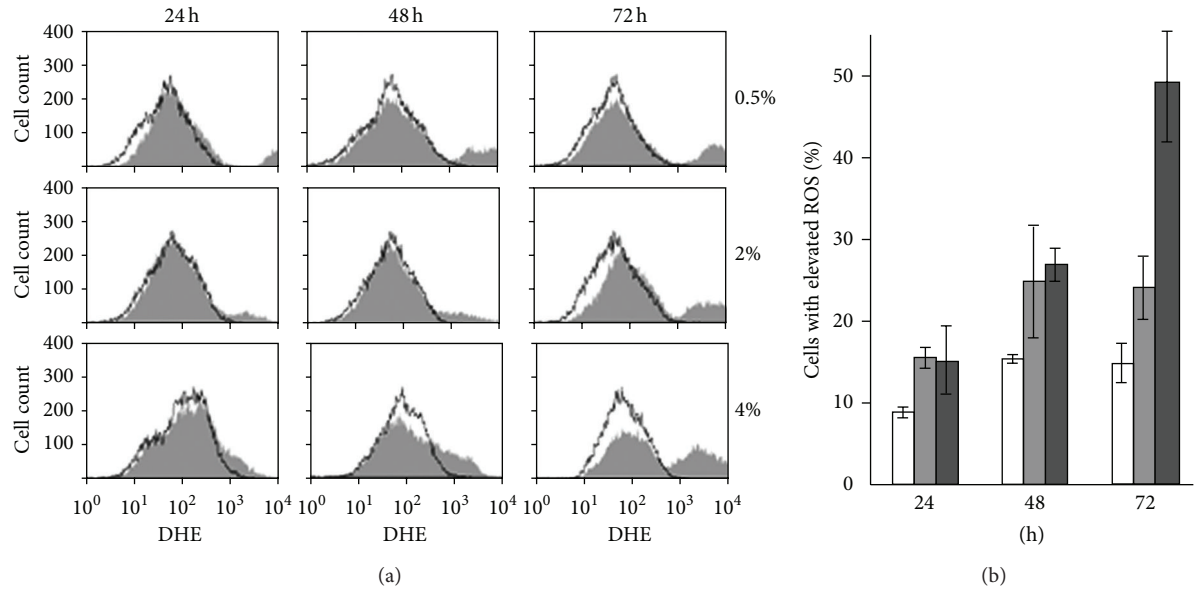

Figure 6: ROS levels in *S. cerevisiae* at 24 h, 48 h, and 72 h of growth. Wild-type cells grown in 0.5%, 2%, and 4% glucose were collected at the indicated times and stained with 5 μg/mL DHE to detect superoxide radicals. Fluorescence intensities were analyzed by flow cytometry. (a) The clear and filled histograms represent the cells without and with DHE, respectively. (b) Percentage cells showing elevated ROS levels at each incubation time for cells grown in 0.5% glucose (clear rectangles), 2% glucose (lighter grey rectangles), and 4% glucose (darker grey rectangles). Data are the averages from two independent experiments; bars indicate the range of data obtained.

conditioned medium-induced mitochondrial fragmentation (approximately 50% of the total population displayed tubular mitochondria). These results indicated that activation of general autophagy during starvation played an important role in conferring resistance to those metabolites present in the conditioned medium that stimulated mitochondrial fragmentation.

Conversely, wild-type cells transferred into 0.5% conditioned medium displayed tubular mitochondria independent of the growth phase and the level of glucose in which the cells were pregrown (Figure 4(c)). The fragmented mitochondria in the *atg1*Δ, and *uth1*Δ mutants also returned to a tubular structure after cells were transferred into 0.5% conditioned medium, although these cells required a longer time for recovery.

The effects seen using 4% conditioned medium to stimulate fragmentation of mitochondria were not due to the physical disturbance of changing the medium. When conditioned medium was removed and fresh medium was supplemented to cells, there was no fragmentation in cells pregrown in any of the glucose concentrations used. Interestingly, mitochondrial fragmentation stimulated by the 4% conditioned medium was found to be reversible once the medium was replaced by the 0.5% conditioned medium (Figure 5). The reversible nature of the process indicated that the cells were not yet committed to any deleterious effects that may result from mitochondrial fragmentation.

3.8. Mitochondrial Fragmentation and Chronological Lifespan. The above results demonstrated that *S. cerevisiae* cells grown in high glucose concentrations not only possessed fragmented mitochondria but also showed higher levels of oxidative stress than those grown in calorie-restricted conditions. It is well known that *S. cerevisiae* cells that are restricted in their calorie intake have longer chronological and replicative lifespans [36, 37], that maintenance of the morphology of mitochondria is important for cell survival since the mutants that preserve tubular mitochondrial structure (such as Δ*dnm1*) live longer than the wild-type cells [4], and the mutants that progress early to mitochondrial fragmentation have shorter lifespan [38]. This led us to investigate whether reversing fragmentation of mitochondria of cells grown in 2% and 4% glucose would extend their lifespan.

Since mitochondrial fragmentation in 4% or 2% glucose-grown cells could be reversed in 0.5% conditioned medium (Figure 5(b)) and vice versa (Figure 5(a)), we determined whether chronological lifespan (CLS) could also be reversed in the same way. Cells were grown in 0.5%, 2%, or 4% glucose for 48 hours and then transferred into conditioned media as shown in Figure 6, and their CLS were assessed.

As expected, cells grown in 0.5% glucose had an extended CLS compared to those grown in higher glucose concentrations (Figure 7). Interestingly, their lifespan was shortened when these cells were transferred into 4% conditioned medium. On the other hand, the lifespan of cells grown in 4% glucose medium was extended following their transfer into 0.5% conditioned medium. Burtner et al. [39] have also shown that the CLS was reversible by substituting spent growth medium in a similar way. Here, we show that the CLS of *S. cerevisiae* varied depending on the type of medium into which cells were exchanged and that this correlated with the reversible changes in mitochondrial morphology.

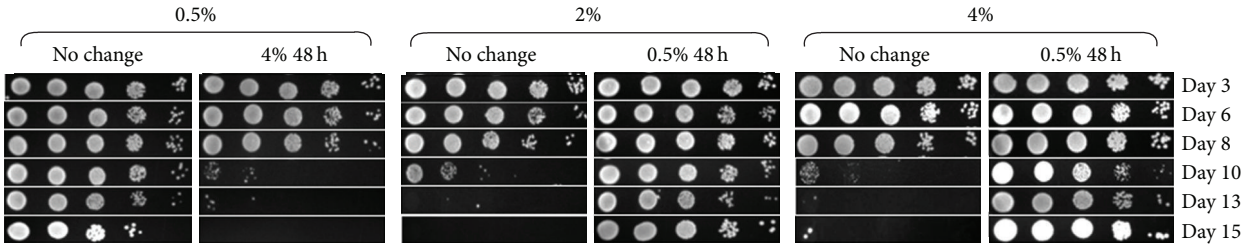

Figure 7: The shortened chronological lifespan of *S. cerevisiae* cells grown in higher concentrations of glucose can be reversed without genetic manipulation. Wild-type cells were grown in media containing 0.5%, 2%, and 4% glucose for 48 hours and exchanged into the conditioned media originally supplemented with 0.5% (0.5% 48 h) or 4% (4% 48 h) glucose. Cell viability was assessed by spotting diluted cultures onto YPD plates at indicated times and compared with that of the cells without any media exchange (no change).

4. Discussion

Mitochondrial morphology is dynamic and responds to changes in a cell's physiology and metabolism. This morphology is modulated by the balance between fusion and fission processes [5, 40, 41]. However, factors such as apoptotic signals or oxidative stress cause an imbalance between these two processes resulting in fragmentation of mitochondria to a punctate morphology [6, 26, 42, 43], and this altered morphology occurs on induction of cell death and during ageing of cells [44]. Here, we have shown that mitochondrial morphology of *S. cerevisiae* changes depending on the concentration of glucose in the medium and that high glucose availability triggers mitochondrial fragmentation in yeast. This process is largely independent of mitochondrial fission or mitochondrial respiratory activity, instead reflecting nutrient sensing mechanisms involving the TOR pathway via the general autophagy process that it modulates. Early onset of respiratory activity correlated with an increased level of ROS in cells grown in low glucose levels as expected, but it is unlikely that mitochondrial damage caused by an increasing level of ROS is a trigger for mitochondrial fragmentation since cells grown in low glucose were respiring, producing relatively high levels of ROS (superoxide anion) yet maintained their mitochondrial structure during prolonged incubation.

To investigate possible mechanisms involved in maintaining the mitochondrial structure, a set of deletion mutants was examined for the phenotype of reduced mitochondrial fragmentation in the presence of higher concentrations of glucose. The mutant lacking *TOR1* was the only one examined that repressed mitochondrial fragmentation under higher glucose levels (2% and 4%). Wild-type cells treated with rapamycin also displayed nonfragmented mitochondria for a prolonged period under these conditions. Together, these results demonstrated that regulation of the TOR pathway plays a major role in the maintenance of mitochondrial structure. Both caloric restriction and inhibition of TOR delayed fragmentation in an autophagy-dependent manner since deletion of the *ATG1* gene led to an increased fragmentation under both conditions. Interestingly, selective elimination of damaged mitochondria by mitophagy in response to mitochondrial dysfunction [36] by mutating the *UTH1* or *ATG32* genes did not affect the fragmentation of mitochondria observed in higher glucose-grown cells. Hence, the protective effect of autophagy is most likely by modulation of nutrient status, or elimination of cellular damage to components other than mitochondria, since they are degraded only by selective autophagy [45]. It is possible that the early low level of ROS observed in respiring cells in 0.5% glucose condition may have activated autophagy to maintain mitochondrial structure under this condition [46].

The importance of autophagy in cellular lifespan extension is highlighted by the demonstration of its importance in *C. elegans* during dietary restriction [25] and that autophagy and amino acid homeostasis are required for extended CLS in *S. cerevisiae* [24]. Autophagy is necessary for rapamycin-induced lifespan extension [47]. Induction of autophagy by spermidine also increases longevity in yeast, flies, and human cells [48]. Based on our data, the prevention or delay of the onset of mitochondrial fragmentation by autophagy may play an important role in lifespan extension.

It is interesting that both the fragmentation of mitochondria and the shortening of CLS of cells grown in high glucose condition are reversible. Fragmented mitochondria in cells were able to return to a tubular morphology, and the cellular lifespan was extended when high glucose medium was replaced by the conditioned medium originating from cells grown on low glucose. The reversibility with respect to CLS has also been shown [39]. For mitochondrial morphology this change occurred within 2 hours of replacement. This reversibility of mitochondrial fragmentation is dependent on general autophagic processes. Further study on the composition of the conditioned media and comparison between the one that shortens lifespan and the one that lengthens may reveal which factor(s) present in the medium cause early cell death. These results further point to the correlation between mitochondrial morphology and chronological lifespan in *S. cerevisiae*, which has relevance to the effects of glucose and/or caloric restriction on cell aging.

Acknowledgments

This work was supported by grants from the Australian Research Council. Yuen T. Lam was supported by the Australian Postgraduate Award. The authors are grateful to Professor Trevor Lithgow for his kind donation of pUC35-*CIT1-Dsred* plasmid and thank Gabriel Perrone for the help with flow cytometry analysis.

References

[1] G. A. Cortopassi and A. Wong, "Mitochondria in organismal aging and degeneration," *Biochimica et Biophysica Acta*, vol. 1410, no. 2, pp. 183–193, 1999.

[2] D. R. Green and J. C. Reed, "Mitochondria and apoptosis," *Science*, vol. 281, no. 5381, pp. 1309–1312, 1998.

[3] D. Arnoult, "Mitochondrial fragmentation in apoptosis," *Trends in Cell Biology*, vol. 17, no. 1, pp. 6–12, 2007.

[4] C. Q. Scheckhuber, N. Erjavec, A. Tinazli, A. Hamann, T. Nyström, and H. D. Osiewacz, "Reducing mitochondrial fission results in increased life span and fitness of two fungal ageing models," *Nature Cell Biology*, vol. 9, no. 1, pp. 99–105, 2007.

[5] G. J. Hermann and J. M. Shaw, "Mitochondrial dynamics in yeast," *Annual Review of Cell and Developmental Biology*, vol. 14, pp. 265–303, 1998.

[6] B. J. Stevens, "Variation in number and volume of mitochondria in yeast according to growth conditions. A study based on serial sectioning and computer graphics reconstruction," *Biologie Cellulaire*, vol. 28, pp. 37–56, 1977.

[7] J. Bereiter-Hahn and M. Voth, "Dynamics of mitochondria in living cells: shape changes, dislocations, fusion, and fission of mitochondria," *Microscopy Research and Technique*, vol. 27, no. 3, pp. 198–219, 1994.

[8] H. Plattner and G. Schatz, "Promitochondria of anaerobically grown yeast. III. Morphology," *Biochemistry*, vol. 8, no. 1, pp. 339–343, 1969.

[9] H. P. Hoffmann and C. J. Avers, "Mitochondrion of yeast: ultrastructural evidence for one giant, branched organelle per cell," *Science*, vol. 181, no. 4101, pp. 749–751, 1973.

[10] W. Visser, E. A. van Spronsen, N. Nanninga, J. T. Pronk, J. G. Kuenen, and J. P. Van Dijken, "Effects of growth conditions on mitochondrial morphology in Saccharomyces cerevisiae," *Antonie van Leeuwenhoek*, vol. 67, no. 3, pp. 243–253, 1995.

[11] T. Yu, S. S. Sheu, J. L. Robotham, and Y. Yoon, "Mitochondrial fission mediates high glucose-induced cell death through elevated production of reactive oxygen species," *Cardiovascular Research*, vol. 79, no. 2, pp. 341–351, 2008.

[12] E. J. Masoro, "Overview of caloric restriction and ageing," *Mechanisms of Ageing and Development*, vol. 126, no. 9, pp. 913–922, 2005.

[13] J. C. Jiang, E. Jaruga, M. V. Repnevskaya, and S. M. Jazwinski, "An intervention resembling caloric restriction prolongs life span and retards aging in yeast," *The FASEB Journal*, vol. 14, no. 14, pp. 2135–2137, 2000.

[14] M. Kaeberlein, R. W. Powers III, K. K. Steffen et al., "Cell biology: regulation of yeast replicative life span by TOR and Sch9 response to nutrients," *Science*, vol. 310, no. 5751, pp. 1193–1196, 2005.

[15] R. W. Powers III, M. Kaeberlein, S. D. Caldwell, B. K. Kennedy, and S. Fields, "Extension of chronological life span in yeast by decreased TOR pathway signaling," *Genes and Development*, vol. 20, no. 2, pp. 174–184, 2006.

[16] J. R. Rohde, R. Bastidas, R. Puria, and M. E. Cardenas, "Nutritional control via Tor signaling in *Saccharomyces cerevisiae*," *Current Opinion in Microbiology*, vol. 11, no. 2, pp. 153–160, 2008.

[17] F. Reggiori and D. J. Klionsky, "Autophagy in the eukaryotic cell," *Eukaryotic Cell*, vol. 1, no. 1, pp. 11–21, 2002.

[18] C. W. Wang and D. J. Klionsky, "The molecular mechanism of autophagy," *Molecular Medicine*, vol. 9, no. 3-4, pp. 65–76, 2003.

[19] W. Droge, "Autophagy and aging-importance of amino acid levels," *Mechanisms of Ageing and Development*, vol. 125, no. 3, pp. 161–168, 2004.

[20] W. A. Dunn Jr., J. M. Cregg, J. A. K. W. Kiel et al., "Pexophagy: the selective autophagy of peroxisomes," *Autophagy*, vol. 1, no. 2, pp. 75–83, 2005.

[21] J. J. Lemasters, "Selective mitochondrial autophagy, or mitophagy, as a targeted defense against oxidative stress, mitochondrial dysfunction, and aging," *Rejuvenation Research*, vol. 8, no. 1, pp. 3–5, 2005.

[22] G. Juhasz, "Atg7-dependent autophagy promotes neuronal health, stress tolerance, and longevity but is dispensable for metamorphosis in *Drosophila*," *Genes & Development*, vol. 21, pp. 3061–3066, 2007.

[23] M. L. Tóth, T. Sigmond, É. Borsos et al., "Longevity pathways converge on autophagy genes to regulate life span in Caenorhabditis elegans," *Autophagy*, vol. 4, no. 3, pp. 330–338, 2008.

[24] A. L. Alvers, L. K. Fishwick, M. S. Wood et al., "Autophagy and amino acid homeostasis are required for chronological longevity in *Saccharomyces cerevisiae*," *Aging Cell*, vol. 8, no. 4, pp. 353–369, 2009.

[25] K. Jia and B. Levine, "Autophagy is required for dietary restriction-mediated life span extension in *C. elegans*," *Autophagy*, vol. 3, no. 6, pp. 597–599, 2007.

[26] N. Alic, V. J. Higgins, and I. W. Dawes, "Identification of a Saccharomyces cerevisiae gene that is required for G1 arrest in response to the lipid oxidation product linoleic acid hydroperoxide," *Molecular Biology of the Cell*, vol. 12, no. 6, pp. 1801–1810, 2001.

[27] C. L. Brett, D. N. Tukaye, S. Mukherjee, and R. Rao, "The yeast endosomal Na+(K+)/H+ exchanger Nhx1 regulates cellular pH to control vesicle trafficking," *Molecular Biology of the Cell*, vol. 16, no. 3, pp. 1396–1405, 2005.

[28] T. Drakulic, M. D. Temple, R. Guido et al., "Involvement of oxidative stress response genes in redox homeostasis, the level of reactive oxygen species, and ageing in *Saccharomyces cerevisiae*," *FEMS Yeast Research*, vol. 5, no. 12, pp. 1215–1228, 2005.

[29] H. Klinger, M. Rinnerthaler, Y. T. Lam et al., "Quantitation of (a)symmetric inheritance of functional and of oxidatively damaged mitochondrial aconitase in the cell division of old yeast mother cells," *Experimental Gerontology*, vol. 45, no. 7-8, pp. 533–542, 2010.

[30] W.-C. Cheng, X. Teng, H. K. Park, C. M. Tucker, M. J. Dunham, and J. M. Hardwick, "Fis1 deficiency selects for compensatory mutations responsible for cell death and growth control defects," *Cell Death and Differentiation*, vol. 15, no. 12, pp. 1838–1846, 2008.

[31] D. J. Klionsky and S. D. Emr, "Autophagy as a regulated pathway of cellular degradation," *Science*, vol. 290, no. 5497, pp. 1717–1721, 2000.

[32] T. Kanki, K. Wang, Y. Cao, M. Baba, and D. J. Klionsky, "Atg32 is a mitochondrial protein that confers selectivity during mitophagy," *Developmental Cell*, vol. 17, no. 1, pp. 98–109, 2009.

[33] K. Okamoto, N. Kondo-Okamoto, and Y. Ohsumi, "Mitochondria-anchored receptor Atg32 mediates degradation of mitochondria via selective autophagy," *Developmental Cell*, vol. 17, no. 1, pp. 87–97, 2009.

[34] I. Kiššová, M. Deffieu, S. Manon, and N. Camougrand, "Uth1p is involved in the autophagic degradation of mitochondria,"

Journal of Biological Chemistry, vol. 279, no. 37, pp. 39068–39074, 2004.

[35] N. M. Camougrand, M. Mouassite, G. M. Velours, and M. G. Guerin, "The 'SUN' family: UTH1, an ageing gene, is also involved in the regulation of mitochondria biogenesis in *Saccharomyces cerevisiae*," *Archives of Biochemistry and Biophysics*, vol. 375, no. 1, pp. 154–160, 2000.

[36] J. C. Jiang, E. Jaruga, M. V. Repnevskaya, and S. M. Jazwinski, "An intervention resembling caloric restriction prolongs life span and retards aging in yeast," *The FASEB Journal*, vol. 14, no. 14, pp. 2135–2137, 2000.

[37] D. L. Smith Jr., J. M. McClure, M. Matecic, and J. S. Smith, "Calorie restriction extends the chronological lifespan of *Saccharomyces cerevisiae* independently of the Sirtuins," *Aging Cell*, vol. 6, no. 5, pp. 649–662, 2007.

[38] R. Sugioka, S. Shimizu, and Y. Tsujimoto, "Fzo1, a protein involved in mitochondrial fusion, inhibits apoptosis," *Journal of Biological Chemistry*, vol. 279, no. 50, pp. 52726–52734, 2004.

[39] C. R. Burtner, C. J. Murakami, B. K. Kennedy, and M. Kaeberlein, "A molecular mechanism of chronological aging in yeast," *Cell Cycle*, vol. 8, no. 8, pp. 1256–1270, 2009.

[40] J. M. Shaw and J. Nunnari, "Mitochondrial dynamics and division in budding yeast," *Trends in Cell Biology*, vol. 12, no. 4, pp. 178–184, 2002.

[41] B. Westermann, "Mitochondrial fusion and fission in cell life and death," *Nature Reviews Molecular Cell Biology*, vol. 11, pp. 872–884, 2010.

[42] P. Ludovico, F. Rodrigues, A. Almeida, M. T. Silva, A. Barrientos, and M. Côrte-Real, "Cytochrome c release and mitochondria involvement in programmed cell death induced by acetic acid in *Saccharomyces cerevisiae*," *Molecular Biology of the Cell*, vol. 13, no. 8, pp. 2598–2606, 2002.

[43] S. Matsuyama and J. C. Reed, "Mitochondria-dependent apoptosis and cellular pH regulation," *Cell Death and Differentiation*, vol. 7, no. 12, pp. 1155–1165, 2000.

[44] R. J. Braun and B. Westermann, "Mitochondrial dynamics in yeast cell death and aging," *Biochemical Society Transactions*, vol. 39, no. 5, pp. 1520–1526, 2011.

[45] T. Kanki and D. J. Klionsky, "Mitophagy in yeast occurs through a selective mechanism," *Journal of Biological Chemistry*, vol. 283, no. 47, pp. 32386–32393, 2008.

[46] R. Scherz-Shouval, E. Shvets, E. Fass, H. Shorer, L. Gil, and Z. Elazar, "Reactive oxygen species are essential for autophagy and specifically regulate the activity of Atg4," *The EMBO Journal*, vol. 26, no. 7, pp. 1749–1760, 2007.

[47] A. L. Alvers, M. S. Wood, D. Hu, A. C. Kaywell, W. A. Dunn Jr., and J. P. Aris, "Autophagy is required for extension of yeast chronological life span by rapamycin," *Autophagy*, vol. 5, no. 6, pp. 847–849, 2009.

[48] T. Eisenberg, H. Knauer, A. Schauer et al., "Induction of autophagy by spermidine promotes longevity," *Nature Cell Biology*, vol. 11, no. 11, pp. 1305–1314, 2009.

Hindawi Publishing Corporation
Oxidative Medicine and Cellular Longevity
Volume 2013, Article ID 760629, 9 pages
http://dx.doi.org/10.1155/2013/760629

Review Article

The Benefits of Humanized Yeast Models to Study Parkinson's Disease

V. Franssens, T. Bynens, J. Van den Brande, K. Vandermeeren, M. Verduyckt, and J. Winderickx

Functional Biology, KU Leuven, Kasteelpark Arenberg 31, 3001 Heverlee, Belgium

Correspondence should be addressed to V. Franssens; vanessa.franssens@bio.kuleuven.be and J. Winderickx; joris.winderickx@bio.kuleuven.be

Received 8 May 2013; Accepted 18 June 2013

Academic Editor: Paula Ludovico

Over the past decade, the baker's yeast *Saccharomyces cerevisiae* has proven to be a useful model system to investigate fundamental questions concerning the pathogenic role of human proteins in neurodegenerative diseases such as Parkinson's disease (PD). These so-called humanized yeast models for PD initially focused on α-synuclein, which plays a key role in the etiology of PD. Upon expression of this human protein in the baker's yeast *Saccharomyces cerevisiae*, the events leading to aggregation and the molecular mechanisms that result in cellular toxicity are faithfully reproduced. More recently, a similar model to study the presumed pathobiology of the α-synuclein interaction partner synphilin-1 has been established. In this review we will discuss recent advances using these humanized yeast models, pointing to new roles for cell wall integrity signaling, Ca^{2+} homeostasis, mitophagy, and the cytoskeleton.

1. Introduction

Parkinson's disease (PD) is the most prevalent neurodegenerative movement disorder in elderly people. The clinical features of this disease include motor deficits such as resting tremor, rigidity, bradykinesia, and postural instability. These symptoms result from the selective and progressive loss of dopaminergic neurons in the substantia nigra pars compacta and the presence of fibrillary cytoplasmic inclusions called Lewy bodies. Although early studies mainly addressed environmental factors as the cause of neuronal demise, these days the involvement of genetic risk factors is the main focus of many studies. At present 18 genetic loci (designated PARK1-18) have been associated with the development of PD, including the autosomal dominant α-synuclein, LRRK2, and Omi/Htra2 and the autosomal recessive Parkin, PINK1, DJ-1, and ATP13A2 [1]. α-Synuclein was the first gene that was found to play a role in the pathogenesis of PD. Beside the missense mutations A53T, A30P, and E46 K [2–4], duplications and triplications of this gene have been shown to result in parkinsonism [5–7]. In addition, aggregated α-synuclein was identified as the major component of Lewy bodies in the brains of sporadic PD patients [8]. The presynaptic protein synphilin-1, which has been identified as an α-synuclein interaction partner using the yeast-two-hybrid system [9], was also found to be a Lewy body constituent [10]. Since the discovery of α-synuclein as a key player in PD, a diverse research community has evolved, focusing on the molecular properties of this protein, and its interaction partner synphilin-1, and the cellular dysfunction that underlies α-synuclein-mediated pathology. A whole range of model systems have been developed to study the different levels and aspects of α-synuclein and synphilin-1 dysfunction. Studies in the classical animal models, like transgenic mice, *Drosophila melanogaster*, and *Caenorhabditis elegans*, have been able to model the *in vivo* aspects of the disease. However, mechanistic aspects of a disease often emerge from studies at the cellular and subcellular level. To this end, usually, mammalian cell lines are used, but recently also the budding yeast *Saccharomyces cerevisiae* has manifested itself as a valuable model to provide insight into the mechanisms of PD. Recent new findings in yeast models expressing α-synuclein led to new roles for cell wall integrity signaling, intracellular Ca^{2+} buildup, and mitophagy, underscoring the usefulness

and power of a yeast model to uncover new aspects of PD pathology.

2. Humanized Yeast Models

At first sight it might not seem very obvious to use a simple and unicellular organism such as yeast to study a complex brain disorder like PD. Indeed, the budding yeast has its limitations, as it cannot recapitulate the complex cellular interactions occurring in the human brain. Likewise, proteins and pathways required for the development of multicellular organisms, are not represented in yeast. Still, yeast cells possess strong similarities to human cells. Around 60% of the yeast genes show sequence homology to a human orthologue [11], and of the human disease-related genes, over 25% have a close homologue in yeast [12]. Importantly, yeast and human cells share fundamental aspects of eukaryotic cell biology. In many cases, yeast has even been the model system where these cellular processes and the genetic components comprising them have been elucidated. This allows a number of key processes, which are of particular interest to PD pathology, to be efficiently investigated in the well-understood yeast model. These include the mechanisms of protein folding, quality control and degradation, the components involved in the secretory pathway and vesicular trafficking, the study of mitochondrial dysfunction and oxidative stress, and even the mechanisms of cell death and survival. Finally, yeast models also possess several clear advantages compared to higher model organisms [13]. Budding yeast cultures show a rapid growth, with a doubling time of 1,5 to 3 hours. This allows a fast and easy scale-up, which is profitable for high-throughput genetic and small-molecule screens. Yeast is readily amenable to many different genetic modifications. Easy DNA transformation and the availability of a host of selectable markers allow the introduction of multiple self-replicating plasmids. Moreover, stable and highly specific introduction of genes, modifications, and markers in the genome, through introduction of DNA sequences by homologous recombination, is highly efficient in yeast. Finally, what makes yeast especially attractive is an extensive set of high-throughput tools that lend themselves to a systematic and genome-wide analysis of particular cellular processes or screenable phenotypes. These include not only comprehensive collections of yeast mutants with gene deletions [14], hypomorphic alleles, and conditionally repressible promoters [15], but also plasmid libraries that allow the study of gene overexpression [16] or systematic localization studies using the yeast GFP-fusion collection [17]. Using these high-throughput techniques in combination with recombinant expression of components implicated in the development of PD, the yeast model can be used to identify genes that positively and negatively regulate important processes linked to PD pathology, like protein aggregation and cellular toxicity.

3. Yeast Models for α-Synuclein and Synphilin-1

It has already been a decade since yeast was used for the first time as a model to study α-synuclein toxicity [18]. In this study, the intracellular localization of wild type and mutant α-synuclein fused to green fluorescent protein was visualized in yeast cells. At low expression levels, the wild type and A53T mutant fusion proteins accumulate at the plasma membrane, consistent with the affinity of α-synuclein for phospholipids [19]. However, upon increased expression, their localization shifted from the plasma membrane towards cytoplasmic aggregates (Figure 1(a), left panel). This coincided with an increase in toxicity reflected in a reduced growth of the yeast cells expressing these human proteins. A30P mutant α-synuclein on the other hand displayed a cytosolic localization, and a minor toxic effect could only be seen upon multicopy expression. Since the description of this initial model, several other groups have taken advantage of the potential that the yeast model system offers to study PD-related features. Beside studies concentrating on a specific cell biological process, also genome-wide screens have been conducted to identify genes and processes that modulate α-synuclein-induced toxicity in yeast. These studies demonstrate that α-synuclein interferes with a broad range of processes to exert its toxicity, like membrane binding, protein quality control and autophagy, Ca^{2+} and Mn^{2+} transport, protein phosphorylation, vesicular trafficking and recycling, and cell death and aging [20–23].

The protein-protein interaction between α-synuclein and synphilin-1 has originally been described using the yeast-two-hybrid system. Hence, the yeast model can probably also be used to study the functional interactions between these two proteins. In a humanized yeast model, a dsRed-synphilin-1 formed aggregates in about 30% of the cell population (Figure 1(a), right panel) [24]. This is much more than an α-synuclein-eGFP fusion, which induces aggregate formation in only 2% of the cells. However, when coexpressed, synphilin-1 induced a sixfold increase in the amount of cells with α-synuclein aggregates. When fluorescently tagged synphilin-1 and α-synuclein formed inclusions in the same cell, they would often colocalize, still, aggregates containing only one of the two proteins could also be found. The pathways leading to synphilin-1 or α-synuclein aggregates however seem quite different. While soluble synphilin-1 is localized mainly in the cytoplasm, its aggregates would form at lipid droplets and detergent resistant membranes (DRMs). In contrast, α-synuclein localizes mainly at the plasma membrane, where its inclusions also initiate [18, 25], but it interacts less with DRMs as compared to synphilin-1 [24].

3.1. The Reciprocal Relation between α-Synuclein and the Ubiquitin-Proteasome System. Healthy cells rely on quality control mechanisms that monitor the proper folding of native proteins and respond to damaged and misfolded proteins. These include molecular chaperones that stabilize and refold abberrant and damaged proteins and proteolytic systems that eventually remove proteins beyond repair. Despite the description of a decrease in proteasomal function in the substantia nigra in PD [26] and an accumulation of ubiquitin in Lewy bodies [27, 28], the precise role for the ubiquitin-proteasome system (UPS) (dys)function in the development of PD remains to be elucidated. For this reason the relationship between the ubiquitin-proteasome system and α-synuclein was also studied in more detail in the yeast models

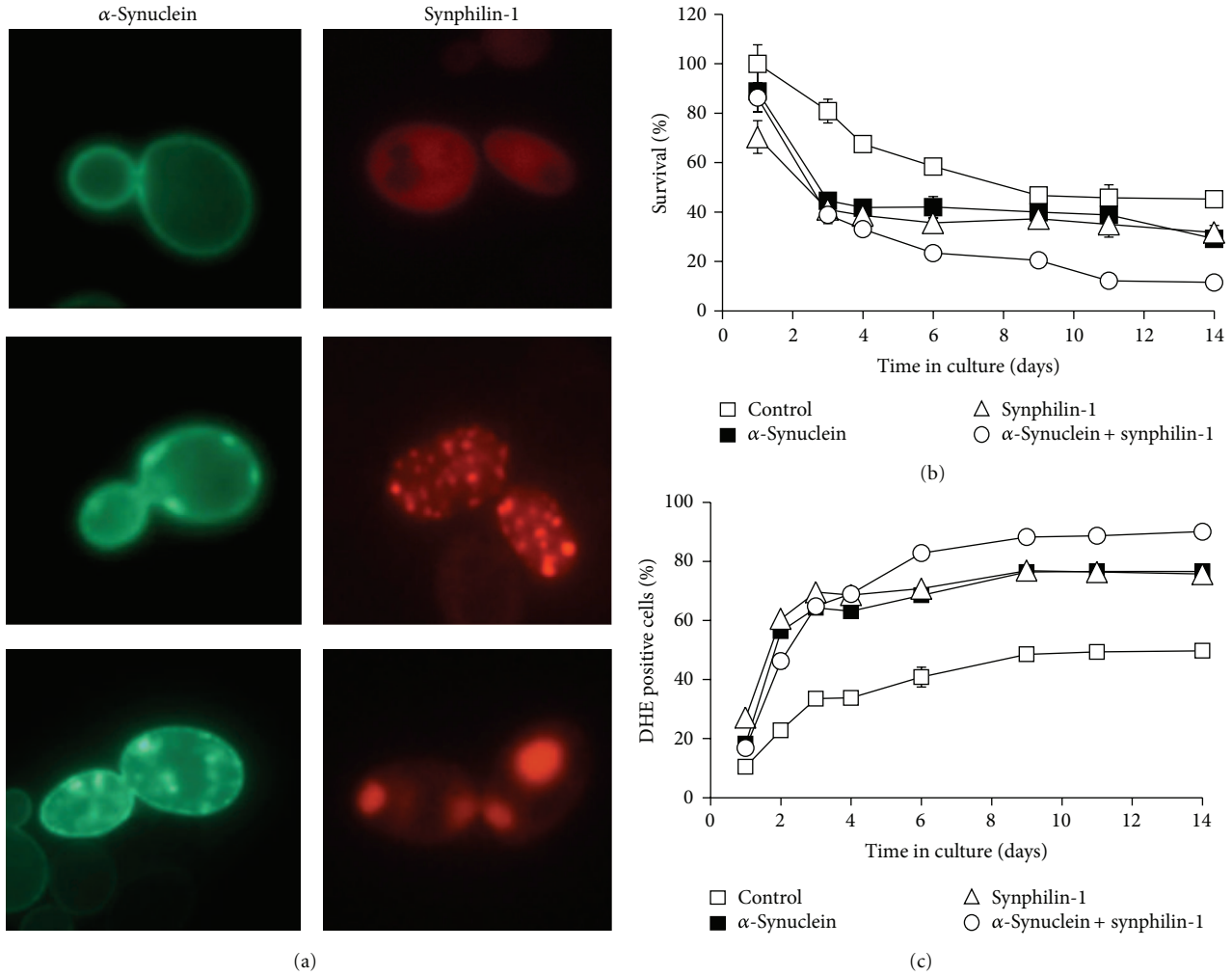

Figure 1: Expression of α-synuclein and synphilin-1 in *Saccharomyces cerevisiae*. (a) Fluorescence microscopic visualization of wild type α-synuclein-eGFP (left panels) and dsRed-synphilin-1 (right panels) fusion proteins expressed separately in wild type yeast cells. (b) and (c) Quantification of viable cells (b) and DHE positive cells (c) in wild type yeast cells expressing wild type α-synuclein and synphilin-1 alone or together. The strains were kept in culture for two weeks [24].

for PD. In their pioneering PD yeast model, Outeiro and Lindquist [18] reported about the link between α-synuclein toxicity and the ubiquitin-proteasome system by showing an increase in ubiquitin accumulation and decreased proteasomal function in yeast cells expressing α-synuclein. This α-synuclein-mediated proteasome impairment in yeast is not caused by changes in the individual peptidase activities of the proteasome or by the amount of available proteasome complexes [29]. Instead, impairment of the proteasome coincided with an altered proteasome composition. Next to the effect of α-synuclein expression on proteasomal function, also the inverse relation has been studied. The effect of proteasome activity on α-synuclein behaviour was investigated using the proteasomal inhibitor, lactacystin, or by the analysis of yeast mutants deleted for proteasomal components. These approaches demonstrated that malfunctioning of the proteasome increases the accumulation of α-synuclein inclusions [25, 30] and enhances α-synuclein toxicity [30, 31], indicating a role for the proteasome in α-synuclein degradation. Such proteasomal degradation of α-synuclein most likely occurs on the soluble form, since clearance of α-synuclein aggregates by the yeast proteasome is negligible [32].

3.2. Autophagic Clearance of α-Synuclein Aggregates. When the activity of the proteasome becomes compromised or overwhelmed, misfolded proteins are directed to the autophagic pathway for degradation. This pathway is well conserved among eukaryotic cells and involves the lysosome in mammalian cells and the vacuole in yeast. The observation in higher eukaryotes that α-synuclein aggregates can be removed by autophagy suggested a connection between autophagy and the pathogenesis of PD [33–35].

Autophagy induction in both mammals and yeast has previously been achieved by treatment with rapamycin, leading to the inhibition of the TOR kinase. Treating α-synuclein expressing yeast cells with this autophagy-inducing drug resulted in a significant decrease of α-synuclein inclusions [25]. In a recent study, yeast cells expressed multiple copies

of α-synuclein-GFP under an inducible *GAL1*-promotor, allowing the study of the formation of α-synuclein aggregates on galactose-containing medium subsequent repression of α-synuclein expression, and a chase of the aggregates on glucose-containing medium [32]. This clearly showed that, once neosynthesis of α-synuclein is switched off, yeast cells can rid themselves of the formed aggregates within hours, which also rescues the α-synuclein cellular toxicity. This aggregate clearance seems to be mainly mediated by autophagy, as evidenced by pharmacologic inhibition with PMSF, which blocks vacuolar serine proteases, or via genetic blockade in a yeast mutant for Atg1, a kinase essential for the induction of autophagy. Furthermore, yeast Ypk9, the ortholog of a lysosomal P-type ATPase (ATP13A2) was identified as a suppressor of α-synuclein toxicity, and overexpression of Ypk9 was shown to reduce intracellular α-synuclein inclusions [22, 36]. In contrast with these studies reporting on clearance of α-synuclein inclusions via the autophagic-lysosomal pathway, it was observed that fluorescently tagged wild type and A53T mutant α-synuclein are not able to enter the vacuolar lumen in yeast and that expression of the native proteins causes a defect in vacuolar fusion [23]. The A30P mutant, on the other hand, did not affect vacuolar fusion and was targeted to the vacuole via the endocytic pathway upon overexpression of the α-synuclein toxicity suppressor Ypp1 [37].

3.3. Role of Mitochondrial Dysfunction and Mitophagy in α-Synuclein Toxicity. Mitochondria are not only the main producers of cellular energy but are also considered to be important regulators of neuronal functioning. Small irregularities in their normal function have been implicated in the pathogenesis of various neurodegenerative diseases, including PD. Early evidence for this came from observations that administration of mitochondrial complex I inhibitors, such as MPTP, rotenone, and paraquat, resulted in changes reminiscent of those seen in PD [38–40]. Later studies showed that several of the familial PD-associated proteins are linked directly or indirectly to mitochondrial pathways including PINK1, Parkin, DJ-1 and Omi/HtrA2 as reviewed in [41]. In addition, increasing evidence suggests that mitochondrial function is also affected by α-synuclein via multiple mechanisms. Interestingly, studies in yeast models identified genes and compounds affecting mitochondrial function as being critical mediators of α-synuclein toxicity [23, 42, 43].

Zabrocki and colleagues [23] performed a genetic screening by expressing an α-synuclein-eGFP-fusion protein in a genome-wide collection of viable yeast deletion strains. This screening retrieved 15 mutants that were deleted for a gene involved in mitochondrial function or the oxidative stress response. These included genes responsible for the induction of the antioxidant response or involved in the actual removal of the oxidating agents and a series of genes mediating the degradation of misfolded mitochondrial proteins.

Subsequently, the importance of mitochondria in α-synuclein toxicity was also demonstrated in postmitotic, stationary phase yeast cells, via measurement of the so-called chronological life span (CLS) [44]. Expression of wild type and A53T mutant α-synuclein in these aged yeast cells, which rely on mitochondria for their energy production, induces a strong increase in markers for reactive oxygen species (ROS), apoptosis, and necrosis, eventually resulting in cell death. This effect is not dependent on the main apoptotic players or the unfolded protein response. Instead, in cells lacking functional mitochondria (rho^0), α-synuclein was not able to exert this toxic effect and failed to induce cell death. In a study by the group of Lindquist, a microarray analysis was performed using a yeast model with α-synuclein overexpression [43]. This revealed a decrease in transcript levels of genes involved in mitochondrial and respiratory functions and an upregulation of transcripts related to oxidoreductase activities. Phenotypically, this manifested itself in an abnormal mitochondrial morphology, which correlated with a loss of mitochondrial membrane potential and a striking increase in ROS production. As such, these data confirm that α-synuclein overexpression strongly affects mitochondrial functions.

Increasing insight in the physiological function of the familial risk genes PINK1 and Parkin has highlighted the importance of mitochondrial dynamics, more specifically their role in the regulation of the removal of damaged mitochondria via mitophagy (reviewed in Imai and Lu [45]). A recent study used the yeast PD model to examine the link between α-synuclein toxicity and mitophagy in chronologically aged yeast cells [46]. Expression of wild type and A53T mutant α-synuclein in yeast was shown to induce mitophagy. Moreover, the α-synuclein-mediated decrease in chronological life span is even dependent on mitophagy, since deletion of Atg32, a mitochondrial protein required for initiation of mitophagy in yeast, alleviated α-synuclein induced toxicity. This also correlated with lower ROS levels in these *atg32* deletion mutants upon α-synuclein expression.

Furthermore, the important role of mitochondria and ROS was also demonstrated in small-molecule screens using humanized yeast as a screening tool. A yeast strain overexpressing α-synuclein was used to screen a chemical library for compounds that are able to relieve toxicity [43]. Four 1,2,3,4-tetrahydroquinolines could reduce the α-synuclein toxicity at multiple levels, that is, by a reduction of the formation of α-synuclein aggregates, restoration of vesicular trafficking from ER to Golgi, and rescue of mitochondrial abnormalities. Earlier, a similar screen for compounds alleviating α-synuclein toxicity in yeast cells has been performed by Griffioen et al. [42]. From a library of about 10.000 small molecules, two could rescue the growth defect caused by α-synuclein overexpression, that is, epigallocatechin-3-gallate (EGCG) and quercetin. These two compounds are flavonoids with antioxidant properties, which are found in large amounts in green tea.

3.4. α-Synuclein and Synphilin-1 Toxicity Is Sirtuin Dependent. Sirtuins or Silence Information Regulators (SIRs) have originally been discovered in yeast. They possess NAD-dependent protein deacetylase activity, which plays a key role in transcriptional silencing at genomic loci including the mating-type locus, telomeres, and ribosomal DNA (rDNA) [47, 48]. In yeast, Sir2 was shown to be required for the increased mitotic life-span, that is, the number of times a cell

can divide, upon calorie restriction [49]. This is in contrast with its role in nondividing cells, where deletion of *SIR2* extends chronological life span (CLS), that is, the cell viability of a batch culture over a period of several weeks. Being evolutionary conserved from bacteria to humans, sirtuins were also found to modulate aging in multicellular organisms such as nematodes, fruit flies, and mice [50–52]. The association of sirtuins with aging made these proteins of great interest for researchers because of their potential as therapeutic targets for age-related diseases such as Parkinson's disease.

The CLS model is typically used to study aging in yeast. In such cultures, expression of α-synuclein and synphilin-1 both induced a strong increase in ROS accumulation and a concomitant decrease in cell survival (Figures 1(b) and 1(c)) [24]. However, in a *sir2* deletion mutant, the toxicity induced by α-synuclein expression was lowered while for synphilin-1 it was largely absent. This suggests that these disease-associated proteins exert their effect via a Sir2-dependent process, possibly involving the segregation of these proteins.

More recently, it was reported that Sir2 is an essential mediator of α-synuclein toxicity in aged yeast cells via its control of mitophagy [46]. The process of mitophagy, which is required for wild type and A53T mutant α-synuclein to execute its toxic effect, is blocked in a *sir2* deletion mutant.

3.5. Phosphorylation of α-Synuclein. Most of the α-synuclein found in Lewy bodies of PD patients is phosphorylated at Ser129 [53]. A large amount of research has gone into the elucidation of the role of Ser129 phosphorylation in the processes of α-synuclein localization, aggregation, and toxicity. Still, there is no clear consensus since studies in animal models of PD have yielded conflicting results on the role of Ser129 phosphorylation [54–56]. It has been shown that Ser129 can be phosphorylated by several kinases, like the polo-like kinases (PLK) 1 to 3, casein kinases (CK) 1 and 2, and the leucine-rich repeat kinase 2 (LRRK2) [57–59]. The polo-like kinases and casein kinases possess yeast orthologues, allowing their study in this simple model system. Zabrocki and coworkers [23] expressed α-synuclein in yeast mutants deleted for the yeast casein kinases. Deletion of the plasma membrane localized CK-1 kinases, Yck1 or Yck2, resulted in decreased Ser129 phosphorylation and reduced toxicity in yeast cells. Deletion of Yck3, a CK-1 kinase localized at the vacuolar membrane influenced neither the α-synuclein phosphorylation level nor its toxicity. However, Yck3 was picked up as a component that, when overexpressed, reduced the α-synuclein toxicity in yeast, indicating that the influence of α-synuclein phosphorylation on toxicity might depend on the subcellular localization of the kinase and the α-synuclein substrate [22]. It should be noted however that biochemical evidence that these yeast CK-1 kinases directly phosphorylate α-synuclein is still lacking. On the other hand, a recent study also showed that deletion of Yck1 or Yck2 increased the α-synuclein toxicity, while, similar to Yck3, overexpression of Yck1 could partially alleviate the α-synuclein induced growth defect [60].

Overexpression of Cdc5, the yeast polo-like kinase 2, also rescues α-synuclein toxicity [22]. However, a detailed analysis of the relationship between the Cdc5 kinase and α-synuclein toxicity in yeast gave quite surprising results [61]. For this kinase, good biochemical evidence was provided that it directly phosphorylates the Ser129 residue. However, α-synuclein was shown to be toxic to yeast cells but not because it was phosphorylated at this residue. Instead, α-synuclein inhibits the Cdc5 kinase from binding and activating Tus1, a guanine nucleotide exchange factor for the small GTPase Rho1, and thus disrupts the signaling cascade it controls, the so-called cell wall integrity pathway. This MAP kinase pathway is not only regulated through the cell cycle but is also responsive to a number of external stressors that act upon the cell wall [62]. These results could be confirmed in mammalian cells that, unlike yeast cells, do not have cell walls but do contain similar PLK-Rho/Ras-MAPK signaling modules that are activated upon cell stress. In a neuroblastoma cell line, α-synuclein expression was shown to cause an attenuated stress-induced activation of the p38 and JNK MAP kinases, resulting in reduced cell viability [61]. These effects of α-synuclein toxicity and impaired MAPK signaling were abolished in an α-synuclein mutant that cannot bind the mammalian polo-like kinase 2.

3.6. Increased Intracellular Ca^{2+} Mediates α-Synuclein Toxicity. Ca^{2+} is an important intracellular messenger that regulates a variety of vital cell functions. Therefore, its levels are tightly controlled in the cytoplasm, ER, and mitochondria. Accumulating evidence points towards an important role for Ca^{2+} imbalance in the pathogenesis of neurodegenerative diseases such as PD [63, 64]. Although several of these studies linked Ca^{2+} to α-synuclein toxicity and aggregation, the underlying mechanisms remain unclear [65–67]. Given the high conservation of the regulation of Ca^{2+} homeostasis between yeast and humans, yeast models were recently used to investigate this matter [68]. Heterologous expression of α-synuclein in yeast elicited an increase in cytosolic calcium levels, which preceded a rise in oxidative radicals and eventually cell death. Systematic deletion of the calcium channels, buffering proteins, and sensors known from the yeast genome pointed to a role for the Golgi-resident Ca^{2+}/Mn^{2+} ATPase *PMR1* (plasma membrane-related Ca^{2+}ATPase1). Its deletion decreased the α-synuclein-induced elevation in cytoplasmic Ca^{2+} levels and also led to a strong decrease in ROS production and subsequent cell death. Furthermore, in the study of Büttner et al. [68], the *PMR1* orthologues in flies and nematodes were also shown to be required for an α-synuclein induced Ca^{2+} increase, leading to loss of dopaminergic neurons. A similar intracellular Ca^{2+} buildup has recently been described in a transgenic mouse model, where overexpression of α-synuclein seems to interfere with cytosolic calcium clearance and buffering mechanisms [69]. Increased Ca^{2+} levels, leading to mitochondrial oxidative stress, could provide an explanation for the preferential loss of dopaminergic neurons of the substantial nigra pars compacta in PD. Work by the group of Surmeier has shown that, because of their specific dependence on L-type Ca^{2+} channels for autonomous pacemaking, higher intracellular Ca^{2+} levels render these cells specifically vulnerable to oxidative damage [70, 71].

3.7. Segregation of α-Synuclein and Synphilin-1 Aggregates. Although aggregation of disease-associated misfolded proteins such as α-synuclein and synphilin-1 has already been scrutinized in a large number of studies, many fundamental questions remain. Recently, the use of yeast to study the role of the cytoskeleton as a transport route directed towards large protein aggregates has become an important area of focus. This research revealed that protein aggregates are not random deposits of insoluble material but are formed via an active and regulated process, involving transport of small deposits along components of the cytoskeleton, that is, microtubuli and actin cables. In this respect, it has been observed that the so-called aggresomes are formed by the convergence of small inclusions at the centrosome via microtubuli-based transport [72]. These aggresomes are thought to be cytoprotective since they can easily be removed via autophagy. Other studies provided data suggesting that during yeast cell division, damaged and aggregated proteins are asymmetrically segregated between mother and daughter cells in a Sir2, polarisome, and actin-cytoskeleton-dependent manner [73, 74].

When expressed in yeast, α-synuclein has been shown to be initially localized at the plasma membrane [18, 25]. At this site, the protein starts to form small aggregates, which later evolve to larger cytoplasmatic inclusions. Synphilin-1, on the other hand, starts out being dispersed in the yeast cytoplasm and forms a number of small cytoplasmatic aggregates, which evolve into one or a few large cytoplasmic inclusions [24]. Interestingly, screening the genome-wide collection of yeast deletion strains to identify mutants that display enhanced inclusion formation of α synuclein eGFP, retrieved 24 mutants that are affected in genes involved in tubulin, actin, and cytoskeleton functions. These include the major components of the polarisome (Bni1, Pea2, Spa2, and Sph1), which is a focal point of actin polymerisation during yeast cell division as well as the GimC/prefolding complex, which is required for efficient transfer and folding of newly synthesized actin and tubulin by the chaperonin TriC/CCT [23]. The outcome of this screen suggests that the transport of α-synuclein aggregates might also be dependent on the actin/polarity machinery [75]. Analysis of the synphilin-1 inclusions in yeast demonstrated that the large inclusions, which were observed in stationary phase cells, correspond to aggresomes [24]. In addition, it was found that synphilin-1 inclusions localized to actin cables and actin patches. Moreover, selective drug-induced disruption of the structure of actin filaments and microtubuli by addition of, respectively, Latrunculin-B and Benomyl, revealed that the transport of synphilin-1 inclusions along actin cables is equally important to prevent synphilin-1 toxicity as aggresome formation via microtubuli-mediated transport. Furthermore, the observation that Sir2 is required for synphilin-1 to exert its toxic effect together with its role to retain damaged and aggregated proteins in the yeast mother cell suggests that Sir2 might also be important for the segregation of synphilin-1 aggregates in the described yeast PD model. Together, these findings strengthen the role of the cytoskeleton and Sir2 in the transport of synphilin-1 aggregates and point towards a possible role of the elements of the cytoskeleton in the segregation of α-synuclein aggregates.

4. Concluding Remarks

Over the past ten years, several research groups have developed great expertise in uncovering the cellular aspects of α-synuclein toxicity using humanized yeast models. More recently, a yeast model was also designed to study the presumed pathobiology of the α-synuclein interaction partner synphilin-1.

Despite its limitations as a unicellular eukaryote, yeast can faithfully reproduce key features of PD pathology. Moving on from studying mere protein aggregation and growth inhibition, these models now start to provide a tool to study new features of the α-synuclein induced-cellular toxicity. One of the new advances that has been studied in yeast addresses the role of an intracellular Ca^{2+} buildup upon α-synuclein expression, mediated by the plasma membrane-related Ca^{2+} ATPase1. This Pmr1-induced Ca^{2+} increase appears to be essential for α-synuclein toxicity from yeast to flies and nematodes. Furthermore, the yeast polo-like kinase 2, Cdc5, which was thought to induce α-synuclein toxicity by phosphorylating Ser129, appears to be inhibited itself by α-synuclein, leading to reduced cell wall integrity signaling. Similarly, an α-synuclein-induced reduction of PLK2 signaling, resulting in inhibition of MAPK signaling, was also shown to increase stress sensitivity in mammalian cells. Finally, yeast has given some clues that α-synuclein-induced toxicity is dependent on the process of mitophagy, which has recently also been implicated in the PD pathology mediated by human PINK and Parkin-1. These results demonstrate the usefulness of humanized yeast models in uncovering new molecular and cellular attributes of α-synuclein and synphilin-1 toxicity.

Acknowledgments

This work was supported by IWT Vlaanderen, the KU Leuven Research Fund, and the Fund of Scientific Research of Flanders (FWO).

References

[1] L. M. Bekris, I. F. Mata, and C. P. Zabetian, "The genetics of Parkinson disease," *Journal of Geriatric Psychiatry and Neurology*, vol. 23, no. 4, pp. 228–242, 2010.

[2] M. H. Polymeropoulos, C. Lavedan, E. Leroy et al., "Mutation in the α-synuclein gene identified in families with Parkinson's disease," *Science*, vol. 276, no. 5321, pp. 2045–2047, 1997.

[3] R. Krüger, W. Kuhn, T. Müller et al., "Ala30Pro mutation in the gene encoding α-synuclein in Parkinson's disease," *Nature Genetics*, vol. 18, no. 2, pp. 106–108, 1998.

[4] J. J. Zarranz, J. Alegre, J. C. Gómez-Esteban et al., "The new mutation, E46K, of alpha-synuclein causes Parkinson and Lewy body dementia," *Annals of Neurology*, vol. 55, no. 2, pp. 164–173, 2004.

[5] M.-C. Chartier-Harlin, J. Kachergus, C. Roumier et al., "α-synuclein locus duplication as a cause of familial Parkinson's disease," *Lancet*, vol. 364, no. 9440, pp. 1167–1169, 2004.

[6] P. Ibáñez, A.-M. Bonnet, B. Débarges et al., "Causal relation between α-synuclein gene duplication and familial Parkinson's disease," *Lancet*, vol. 364, no. 9440, pp. 1169–1171, 2004.

[7] A. B. Singleton, M. Farrer, J. Johnson et al., "alpha-Synuclein locus triplication causes Parkinson's disease," *Science*, vol. 302, no. 5646, p. 841, 2003.

[8] M. Baba, S. Nakajo, P.-H. Tu et al., "Aggregation of α-synuclein in Lewy bodies of sporadic Parkinson's disease and dementia with Lewy bodies," *American Journal of Pathology*, vol. 152, no. 4, pp. 879–884, 1998.

[9] S. Engelender, Z. Kaminsky, G. Xin et al., "Synphilin-1 associates with α-synuclein and promotes the formation of cytosolic inclusions," *Nature Genetics*, vol. 22, no. 1, pp. 110–114, 1999.

[10] K. Wakabayashi, S. Engelender, M. Yoshimoto, S. Tsuji, C. A. Ross, and H. Takahashi, "Synphilin-1 is present in Lewy bodies in Parkinson's disease," *Annals of Neurology*, vol. 47, pp. 521–523, 2000.

[11] D. Botstein, S. A. Chervitz, and J. M. Cherry, "Yeast as a model organism," *Science*, vol. 277, no. 5330, pp. 1259–1260, 1997.

[12] D. E. Bassett Jr., M. S. Boguski, and P. Hieter, "Yeast genes and human disease ," *Nature*, vol. 379, no. 6566, pp. 589–590, 1996.

[13] F. Sherman, "Getting started with yeast," *Methods in Enzymology*, vol. 350, pp. 3–41, 2002.

[14] E. A. Winzeler, D. D. Shoemaker, A. Astromoff et al., "Functional characterization of the *S. cerevisiae* genome by gene deletion and parallel analysis," *Science*, vol. 285, no. 5429, pp. 901–906, 1999.

[15] S. Mnaimneh, A. P. Davierwala, J. Haynes et al., "Exploration of essential gene functions via titratable promoter alleles," *Cell*, vol. 118, no. 1, pp. 31–44, 2004.

[16] Y. Hu, A. Rolfs, B. Bhullar et al., "Approaching a complete repository of sequence-verified protein-encoding clones for *Saccharomyces cerevisiae*," *Genome Research*, vol. 17, no. 4, pp. 536–543, 2007.

[17] M. R. Martien, S. M. McCraith, S. L. Spinelli et al., "A biochemical genomics approach for identifying genes by the activity of their products," *Science*, vol. 286, no. 5442, pp. 1153–1155, 1999.

[18] T. F. Outeiro and S. Lindquist, "Yeast cells provide insight into alpha-synuclein biology and pathobiology," *Science*, vol. 302, no. 5651, pp. 1772–1775, 2003.

[19] E. Jo, J. McLaurin, C. M. Yip, P. St. George-Hyslop, and P. E. Fraser, "α-Synuclein membrane interactions and lipid specificity," *Journal of Biological Chemistry*, vol. 275, no. 44, pp. 34328–34334, 2000.

[20] S. Willingham, T. F. Outeiro, M. J. DeVit, S. L. Lindquist, and P. J. Muchowski, "Yeast genes that enhance the toxicity of a mutant huntingtin fragment or alpha-synuclein," *Science*, vol. 302, no. 5651, pp. 1769–1772, 2003.

[21] J. Liang, C. Clark-Dixon, S. Wang et al., "Novel suppressors of α-synuclein toxicity identified using yeast," *Human Molecular Genetics*, vol. 17, no. 23, pp. 3784–3795, 2008.

[22] E. Yeger-Lotem, L. Riva, L. J. Su et al., "Bridging high-throughput genetic and transcriptional data reveals cellular responses to alpha-synuclein toxicity," *Nature Genetics*, vol. 41, no. 3, pp. 316–323, 2009.

[23] P. Zabrocki, I. Bastiaens, C. Delay et al., "Phosphorylation, lipid raft interaction and traffic of α-synuclein in a yeast model for Parkinson," *Biochimica et Biophysica Acta*, vol. 1783, no. 10, pp. 1767–1780, 2008.

[24] S. Büttner, C. Delay, V. Franssens et al., "Synphilin-1 enhances a-synuclein aggregation in yeast and contributes to cellular stress and cell death in a sir2-dependent manner," *PLoS One*, vol. 5, no. 10, Article ID e13700, 2010.

[25] P. Zabrocki, K. Pellens, T. Vanhelmont et al., "Characterization of α-synuclein aggregation and synergistic toxicity with protein tau in yeast," *FEBS Journal*, vol. 272, no. 6, pp. 1386–1400, 2005.

[26] K. S. McNaught and P. Jenner, "Proteasomal function is impaired in substantia nigra in Parkinson's disease," *Neuroscience Letters*, vol. 297, no. 3, pp. 191–194, 2001.

[27] V. Manetto, G. Perry, M. Tabaton et al., "Ubiquitin is associated with abnormal cytoplasmic filaments characteristic of neurodegenerative diseases," *Proceedings of the National Academy of Sciences of the United States of America*, vol. 85, no. 12, pp. 4501–4505, 1988.

[28] P. G. Galloway, I. Grundke-Iqbal, K. Iqbal, and G. Perry, "Lewy bodies contain epitopes both shared and distinct from Alzheimer neurofibrillary tangles," *Journal of Neuropathology and Experimental Neurology*, vol. 47, no. 6, pp. 654–663, 1988.

[29] Q. Chen, J. Thorpe, and J. N. Keller, "α-synuclein alters proteasome function, protein synthesis, and stationary phase viability," *Journal of Biological Chemistry*, vol. 280, no. 34, pp. 30009–30017, 2005.

[30] N. Sharma, K. A. Brandis, S. K. Herrera et al., "α-synuclein budding yeast model: toxicity enhanced by impaired proteasome and oxidative stress," *Journal of Molecular Neuroscience*, vol. 28, no. 2, pp. 161–178, 2006.

[31] C. Dixon, N. Mathias, R. M. Zweig, D. A. Davis, and D. S. Gross, "α-Synuclein targets the plasma membrane via the secretory pathway and induces toxicity in yeast," *Genetics*, vol. 170, no. 1, pp. 47–59, 2005.

[32] D. Petroi, B. Popova, N. Taheri-Talesh et al., "Aggregate clearance of alpha-synuclein in *Saccharomyces cerevisiae* depends more on autophagosome and vacuole function than on the proteasome," *The Journal of Biological Chemistry*, vol. 287, pp. 27567–27579, 2012.

[33] J. L. Webb, B. Ravikumar, J. Atkins, J. N. Skepper, and D. C. Rubinsztein, "Alpha-Synuclein is degraded by both autophagy and the proteasome," *Journal of Biological Chemistry*, vol. 278, no. 27, pp. 25009–25013, 2003.

[34] T. Pan, S. Kondo, W. Le, and J. Jankovic, "The role of autophagy-lysosome pathway in neurodegeneration associated with Parkinson's disease," *Brain*, vol. 131, no. 8, pp. 1969–1978, 2008.

[35] M. Deleidi and W. Maetzler, "Protein clearance mechanisms of alpha-synuclein and amyloid-Beta in lewy body disorders," *International Journal of Alzheimer's Disease*, vol. 2012, Article ID 391438, 9 pages, 2012.

[36] A. D. Gitler, A. Chesi, M. L. Geddie et al., "α-Synuclein is part of a diverse and highly conserved interaction network that includes PARK9 and manganese toxicity," *Nature Genetics*, vol. 41, no. 3, pp. 308–315, 2009.

[37] T. R. Flower, C. Clark-Dixon, C. Metoyer et al., "YGR198w (YPP1) targets A30P α-synuclein to the vacuole for degradation," *Journal of Cell Biology*, vol. 177, no. 6, pp. 1091–1104, 2007.

[38] R. Betarbet, T. B. Sherer, G. MacKenzie, M. Garcia-Osuna, A. V. Panov, and J. T. Greenamyre, "Chronic systemic pesticide exposure reproduces features of Parkinson's disease," *Nature Neuroscience*, vol. 3, no. 12, pp. 1301–1306, 2000.

[39] J. W. Langston, P. Ballard, J. W. Tetrud, and I. Irwin, "Chronic parkinsonism in humans due to a product of meperidine-analog synthesis," *Science*, vol. 219, no. 4587, pp. 979–980, 1983.

[40] H.-H. Liou, M. C. Tsai, C. J. Chen et al., "Environmental risk factors and Parkinson's disease: a case-control study in Taiwan," *Neurology*, vol. 48, no. 6, pp. 1583–1588, 1997.

[41] H. Büeler, "Impaired mitochondrial dynamics and function in the pathogenesis of Parkinson's disease," *Experimental Neurology*, vol. 218, no. 2, pp. 235–246, 2009.

[42] G. Griffioen, H. Duhamel, N. Van Damme et al., "A yeast-based model of α-synucleinopathy identifies compounds with therapeutic potential," *Biochimica et Biophysica Acta*, vol. 1762, no. 3, pp. 312–318, 2006.

[43] L. J. Su, P. K. Auluck, T. F. Outeiro et al., "Compounds from an unbiased chemical screen reverse both ER-to-Golgi trafficking defects and mitochondrial dysfunction in Parkinson's disease models," *Disease Models and Mechanisms*, vol. 3, no. 3-4, pp. 194–208, 2010.

[44] S. Büttner, A. Bitto, J. Ring et al., "Functional mitochondria are required for α-synuclein toxicity in aging yeast," *Journal of Biological Chemistry*, vol. 283, no. 12, pp. 7554–7560, 2008.

[45] Y. Imai and B. Lu, "Mitochondrial dynamics and mitophagy in Parkinson's disease: disordered cellular power plant becomes a big deal in a major movement disorder," *Current Opinion in Neurobiology*, vol. 21, no. 6, pp. 935–941, 2011.

[46] B. Sampaio-Marques, C. Felgueiras, A. Silva et al., "SNCA (alpha-synuclein)-induced toxicity in yeast cells is dependent on sirtuin 2 (Sir2)-mediated mitophagy," *Autophagy*, vol. 8, pp. 1494–1509, 2012.

[47] S.-I. Imai, C. M. Armstrong, M. Kaeberlein, and L. Guarente, "Transcriptional silencing and longevity protein Sir2 is an NAD-dependent histone deacetylase," *Nature*, vol. 403, no. 6771, pp. 795–800, 2000.

[48] G. Blander and L. Guarente, "The Sir2 family of protein deacetylases," *Annual Review of Biochemistry*, vol. 73, pp. 417–435, 2004.

[49] S.-J. Lin, P.-A. Defossez, and L. Guarente, "Requirement of NAD and SIR2 for life-span extension by calorie restriction in *Saccharomyces cerevisiae*," *Science*, vol. 289, no. 5487, pp. 2126–2128, 2000.

[50] H. A. Tissenbaum and L. Guarente, "Increased dosage of a sir-2 gene extends lifespan in *Caenorhabditis elegans*," *Nature*, vol. 410, no. 6825, pp. 227–230, 2001.

[51] B. Rogina and S. L. Helfand, "Sir2 mediates longevity in the fly through a pathway related to calorie restriction," *Proceedings of the National Academy of Sciences of the United States of America*, vol. 101, no. 45, pp. 15998–16003, 2004.

[52] T. Finkel, C.-X. Deng, and R. Mostoslavsky, "Recent progress in the biology and physiology of sirtuins," *Nature*, vol. 460, no. 7255, pp. 587–591, 2009.

[53] J. P. Anderson, D. E. Walker, J. M. Goldstein et al., "Phosphorylation of Ser-129 is the dominant pathological modification of α-synuclein in familial and sporadic lewy body disease," *Journal of Biological Chemistry*, vol. 281, no. 40, pp. 29739–29752, 2006.

[54] X. Chen, M. G. Garelick, H. Wang, V. Li, J. Athos, and D. R. Storm, "PI3 kinase signaling is required for retrieval and extinction of contextual memory," *Nature Neuroscience*, vol. 8, no. 7, pp. 925–931, 2005.

[55] M. Wakamatsu, A. Ishii, Y. Ukai et al., "Accumulation of phosphorylated α-synuclein in dopaminergic neurons of transgenic mice that express human α-synuclein," *Journal of Neuroscience Research*, vol. 85, no. 8, pp. 1819–1825, 2007.

[56] S. A. da Silveira, B. L. Schneider, C. Cifuentes-Diaz et al., "Phosphorylation does not prompt, nor prevent, the formation of α-synuclein toxic species in a rat model of Parkinson's disease," *Human Molecular Genetics*, vol. 18, no. 5, pp. 872–887, 2009.

[57] M. K. Mbefo, K. E. Paleologou, A. Boucharaba et al., "Phosphorylation of synucleins by members of the polo-like kinase family," *Journal of Biological Chemistry*, vol. 285, no. 4, pp. 2807–2822, 2010.

[58] M. Okochi, J. Walter, A. Koyama et al., "Constitutive phosphorylation of the Parkinson's disease associated α-synuclein," *Journal of Biological Chemistry*, vol. 275, no. 1, pp. 390–397, 2000.

[59] H. Qing, W. Wong, E. G. McGeer, and P. L. McGeer, "Lrrk2 phosphorylates alpha synuclein at serine 129: Parkinson disease implications," *Biochemical and Biophysical Research Communications*, vol. 387, no. 1, pp. 149–152, 2009.

[60] V. Sancenon, S. A. Lee, C. Patrick et al., "Suppression of alpha-synuclein toxicity and vesicle trafficking defects by phosphorylation at S129 in yeast depends on genetic context," *Human Molecular Genetics*, vol. 21, pp. 2432–2449, 2012.

[61] S. Wang, B. Xu, L. C. Liou et al., "Alpha-synuclein disrupts stress signaling by inhibiting polo-like kinase Cdc5/Plk2," *Proceedings of the National Academy of Sciences of the United States of America*, vol. 109, pp. 16119–16124, 2012.

[62] D. E. Levin, "Cell wall integrity signaling in *Saccharomyces cerevisiae*," *Microbiology and Molecular Biology Reviews*, vol. 69, pp. 262–291, 2005.

[63] D. J. Surmeier and P. T. Schumacker, "Calcium, bioenergetics, and neuronal vulnerability in Parkinson's disease," *The Journal of Biological Chemistry*, vol. 288, pp. 10736–10741, 2013.

[64] T. Calì, D. Ottolini, and M. Brini, "Mitochondria, calcium, and endoplasmic reticulum stress in Parkinson's disease," *BioFactors*, vol. 37, no. 3, pp. 228–240, 2011.

[65] N. T. Hettiarachchi, A. Parker, M. L. Dallas et al., "α-Synuclein modulation of Ca^{2+} signaling in human neuroblastoma (SH-SY5Y) cells," *Journal of Neurochemistry*, vol. 111, no. 5, pp. 1192–1201, 2009.

[66] S. Nath, J. Goodwin, Y. Engelborghs, and D. L. Pountney, "Raised calcium promotes α-synuclein aggregate formation," *Molecular and Cellular Neuroscience*, vol. 46, no. 2, pp. 516–526, 2011.

[67] S. Nath, J. Goodwin, Y. Engelborghs, and D. L. Pountney, "Raised calcium promotes α-synuclein aggregate formation," *Molecular and Cellular Neuroscience*, vol. 46, no. 2, pp. 516–526, 2011.

[68] S. Büttner, L. Faes, W. N. Reichelt et al., "The Ca^{2+}/Mn^{2+} ion-pump PMR1 links elevation of cytosolic Ca^{2+} levels to alpha-synuclein toxicity in Parkinson's disease models," *Cell Death & Differentiation*, vol. 20, pp. 465–477, 2012.

[69] L. Reznichenko, Q. Cheng, K. Nizar et al., "*In vivo* alterations in calcium buffering capacity in transgenic mouse model of synucleinopathy," *The Journal of Neuroscience*, vol. 32, pp. 9992–9998, 2012.

[70] C. S. Chan, J. N. Guzman, E. Ilijic et al., "'Rejuvenation' protects neurons in mouse models of Parkinson's disease," *Nature*, vol. 447, no. 7148, pp. 1081–1086, 2007.

[71] J. N. Guzman, J. Sanchez-Padilla, D. Wokosin et al., "Oxidant stress evoked by pacemaking in dopaminergic neurons is attenuated by DJ-1," *Nature*, vol. 468, no. 7324, pp. 696–700, 2010.

[72] R. R. Kopito, "Aggresomes, inclusion bodies and protein aggregation," *Trends in Cell Biology*, vol. 10, no. 12, pp. 524–530, 2000.

[73] B. Liu, L. Larsson, A. Caballero et al., "The polarisome is required for segregation and retrograde transport of protein aggregates," *Cell*, vol. 140, no. 2, pp. 257–267, 2010.

[74] B. Liu, L. Larsson, V. Franssens et al., "Segregation of protein aggregates involves actin and the polarity machinery," *Cell*, vol. 147, no. 5, pp. 959–961, 2011.

[75] E. Swinnen, S. Büttner, T. F. Outeiro et al., "Aggresome formation and segregation of inclusions influence toxicity of α-synuclein and synphilin-1 in yeast," *Biochemical Society Transactions*, vol. 39, no. 5, pp. 1476–1481, 2011.